

MODELLING
PLANFORM CHANGES OF
BRAIDED RIVERS

Samenstelling promotiecommissie:

prof. dr. ir. F. J. A. M. van Houten	Universiteit Twente, voorzitter / secretaris
prof. dr. ir. H. J. de Vriend	Universiteit Twente, promotor
prof. dr. S. J. M. H. Hulscher	Universiteit Twente
prof. dr. ir. E. W. C. van Groesen	Universiteit Twente
prof. dr. ir. A. W. Heemink	Technische Universiteit Delft
prof. dr. ir. A. E. Mynett	UNESCO-IHE Delft
prof. dr. C. Paola	University of Minnesota
dr. ir. E. Mosselman	WL Delft Hydraulics

Cover: Landsat satellite image of the Jamuna River, February 25 1995. Figures on the back cover: initial, intermediate and final bed and water levels of a two-dimensional morphological simulation of a bend cutoff.

Copyright © 2003 by H. R. A. Jagers
Printed by PrintPartners Ipskamp B.V.

ISBN 90-9016879-6

MODELLING
PLANFORM CHANGES OF
BRAIDED RIVERS

PROEFSCHRIFT

ter verkrijging van
de graad van doctor aan de Universiteit Twente,
op gezag van de rector magnificus,
prof. dr. F. A. van Vugt,
volgens besluit van het College voor Promoties
in het openbaar te verdedigen
op vrijdag 6 juni 2003 om 16:45 uur

door

Hendrik Reinhard Albert Jagers
geboren op 22 december 1970
te Enschede

Dit proefschrift is goedgekeurd door de promotor:

prof. dr. ir. H. J. de Vriend

Summary

Rivers with multiple channels, splitting and rejoining around islands, are called braided rivers. The Jamuna River in Bangladesh, shown on the cover of this thesis, is an example of such a river. Every year, substantial erosion occurs along the banks of this river; it is not uncommon to observe bankline shifts of several hundreds of metres. Before intervening with the natural behaviour of such a river, one should be aware of the consequences in both the near future and the long run. However, planform changes of the Jamuna River cannot be predicted with sufficient accuracy for three to five years ahead. This is the result of limitations in process knowledge, modelling techniques and sensitivity to initial and boundary conditions. This study has focused on modelling techniques to predict planform changes of braided rivers and their relation with state-of-the-art knowledge on the physical processes and the availability of model input data.

The dynamic nature of braided rivers combined with the size of the Jamuna River (total width 5–17 km) complicates the collection of the model input data. Field surveys offer the most comprehensive data on the local characteristics of a river, but these surveys are time consuming for a river as large as the Jamuna River. This is a problem in periods of the rapid morphological change. Remote sensing techniques can help to keep track of large-scale planform changes. However, the remote sensing techniques applied to study the Jamuna River cannot provide us with accurate elevation data; this poses a large restriction on the range of modelling techniques that can be applied.

Braiding results from a fundamental instability of wide, shallow channels (the characteristic multi-channel planform only emerges during low flow). The interaction of morphological processes in a wide range of scales can be aggregated into six types of large-scale planform changes: channel migration, channel width change, mid-channel bar growth, channel formation, channel abandonment and deformation of confluences and bifurcation. These processes are influenced by the often highly variable discharges in braided rivers, variations in vegetation, varying sediment composition, and tectonic and human influences. A general overview of the research in this field is provided.

A variety of numerical models has been developed for meandering rivers: from kinematic formulations, via dynamic one-dimensional models using linearised equations for flow (and morphology), to two-dimensional non-linear models using adaptive grids. The dynamics of a braided river is, however, far more complicated than that of a meandering river due to the numerous channel bifurcations and the large morphological changes during flood. A comparison of the modelling approaches for meandering and braided rivers indicates that

the modelling of braided river morphodynamics is still in its infancies. Generic process-based models form the basis for future models of braided rivers, however, restrictions in computational time, input data availability and process descriptions limit their suitability for such large scale applications today.

Three modelling techniques have been analysed with respect to their suitability for predicting planform changes of braided rivers: a neural network, a cellular model (Murray and Paola, 1994) and an object-oriented approach (Klaassen *et al.*, 1993).

A multi-layer perceptron network has been trained to predict bank erosion based on a limited amount of geometrical information: the location (distance and direction) relative to the nearest channel, the local width of the nearest channel, and the fraction of water in the neighbourhood. Based on these data the neural network was able to learn a number of simple rules, such as: erosion is more likely along wide channels. Furthermore, the output of an appropriately trained network can be used as an indication of the probability that erosion will occur. Thus it is possible to get a probabilistic statement without requiring extensive and time-consuming computations. Although the results show that a neural network approach can be applied, they also indicate the importance of a large amount of representative training data and an appropriate representation of the initial planform by the input parameters. One of the major disadvantages of this approach is that the neural network is a black box approach: the empirical knowledge represented by the network cannot be extended easily.

The cellular model is based on a simplified water routing scheme, formulae for alongstream and lateral sediment transport, and mass conservation for water and sediment. The model is able to reproduce the general behaviour of braided rivers, but suffers from an oversimplified water routing scheme. An alternative scheme is presented that solves some of the problems at the expense of a significant increase in simulation time. Both water routing schemes are too simplified to be of use for predicting planform changes of actual rivers. Furthermore, the model relies on topographic data that, as indicated above, may not be readily available.

The object-oriented approach is based on a subdivision of the braided planform into separate branches (the objects); therefore, this approach is also referred to as the branches model. The dynamics of each individual branch is governed by four possible processes: branch migration, branch widening and narrowing, branch abandonment, and branch splitting due to mid-channel island growth. Computer simulations using this model display a behaviour that is less dynamic than an actual braided river. The advantage of this model approach is that the individual planform changing processes are well defined; this allows for incremental improvement of the model. Furthermore, the simple kinematic process formulations are well suited for a Monte Carlo approach in an overall stochastic model concept.

Based on a comparison of the advantages and disadvantages of the various models, it has been concluded that the branches model is the most promising approach for the short-term development of a model for medium- to long-term predictions. Although cutoffs play an important role in the dynamics of braided rivers, the branches model does not yet include a submodel for this process: the algorithm relies on the expert judgement of the user. The second part of the study has, therefore, focused on the formation of new channels as a result of cutoffs.

Channel incision results from erosion caused by an alongstream increase in the sediment transport rate. The direction of the channel forming process is determined by the location of the largest gradient: headward erosion (or backcutting) starting at downstream end or

gradual incision starting at the upstream end. The former process is encountered on hillslopes where discharge and shear stresses increase downslope due to an increase in rainfall runoff. New channels across a mature part of the flood plain during flood are generally also formed by this process. Headward erosion has also been observed in flume experiments of gravel-bed streams and under various circumstances in prototype streams. The incision from the upstream side has on the other hand been observed in the Jamuna River. This provides us with a second reason for investigating this topic further by means of computer simulations.

Two-dimensional depth-averaged morphological simulations of sharp bends have been carried out to improve the understanding of the processes involved. The results of those simulations indicate that cutoff formation is accelerated by a low water level downstream, a large (alluvial) roughness, a low threshold for sediment transport, and a small value for the exponent c of the Shields parameter θ (or of the velocity u) in the sediment transport relation if the average sediment transport rate remains constant. An additional sensitivity analysis has shown that the numerical aspects (such as the resolution of the spatial discretisation and quasi-steady flow approximation) have not significantly influenced the outcome of the simulations. Neither has the depth-averaged approach had a decisive influence on the results of the simulations.

In all simulations, the cutoff channel started forming at the upstream end, which agrees with the observations of the Jamuna River. Non-hydrostatic effects and vegetation, which have not been included in the numerical simulations, may play a role. Furthermore, only uniform non-cohesive sediments have been considered. Based on a more detailed analysis of the processes, it is expected that cohesion or non-uniformity of the bed composition plays an important role in the formation of bend cutoffs via headcut erosion. A simple model concept for simulating headward erosion has been presented and tested. Further analysis and validation are needed to improve the modelling of this type of erosion.

Finally, an algorithm for formation of new channels has been presented that can be implemented as a new module in the branches model. The actual implementation, calibration and testing of the new module was beyond the scope of the present study. The algorithm is conceptually similar to the model of Howard (1996) for cutoffs in meandering rivers. However, in line with the other modules of the branches model, the algorithm has been formulated using geometric parameters only: cutoff ratio, bifurcation angle, vegetation cover, and relative curvature. Furthermore, the effect of flow convergence/divergence is included based on geometric properties of the cutoff channel. If topographic steering must be taken into account, a rough estimate of the flood plain elevations is required.

Samenvatting

Rivieren bestaande uit een netwerk van zich telkens weer splitsende en samenvloeiende geulen worden vlechtende rivieren genoemd. Op de omslag van dit proefschrift staat een voorbeeld van zo'n rivier: de Jamuna in Bangladesh. Jaarlijks erodeert deze rivier grote hoeveelheden oevermateriaal, waardoor de oeverlijn lokaal regelmatig met enkele honderden meters landinwaarts verschuift. Voordat men ingrijpt in het natuurlijk gedrag van een dergelijke rivier, dienen de gevolgen van een dergelijke ingreep voor zowel de korte als de lange termijn duidelijk te zijn. Echter de natuurlijke veranderingen van het geulenpatroon van de Jamuna zijn niet voldoende nauwkeurig drie tot vijf jaar vooruit te voorspellen. Dit is het gevolg van lacunes in de proceskennis, beperkingen van de bestaande numerieke modellen en gevoeligheid voor begin- en randcondities. Deze studie heeft zich gericht op de ontwikkeling en vergelijking van modelleringstechnieken voor dit soort situaties in relatie tot de huidige stand der proceskennis en de beperkte beschikbaarheid van invoergegevens.

Het dynamisch gedrag van vlechtende rivieren gecombineerd met de afmetingen van de Jamuna (totale breedte 5–17 km) bemoeilijkt het verzamelen van voldoende invoergegevens. Veldobservaties vormen de belangrijkste bron van gedetailleerde informatie, maar deze wijze van gegevensverzameling is tijdrovend voor rivieren zo groot als de Jamuna. Dit is een probleem wanneer de morfologische ontwikkelingen snel verlopen. Aardobservatietechnieken kunnen helpen bij het volgen van de grootschalige veranderingen in het geulenpatroon, maar de op de Jamuna toegepaste technieken leveren geen nauwkeurige hoogtegegevens; dit is een belangrijke beperking voor het type model dat in zo'n geval toegepast kan worden.

Het vlechtgedrag komt voort uit een fundamentele instabiliteit van brede, ondiepe rivieren (het karakteristieke geulenpatroon is alleen zichtbaar tijdens laagwater). De interactie van morfologische processen op verschillende schalen leidt tot zes basistypen van veranderingen in het geulenpatroon: geulmigratie, breedteverandering, bankvorming midden in een geul, geulvorming, geulaanzanding en de vervorming van samenvloeiingen en splitsingspunten. Deze processen worden beïnvloed door de meestal grote afvoervariaties in vlechtende rivieren, ruimtelijke variaties in begroeiing en bodemsamenstelling, en tektonische en menselijke invloeden. Een algemeen overzicht van het onderzoek op dit gebied wordt gegeven.

Rivierenonderzoek heeft geleid tot de formulering van een groot aantal modellen voor meanderende rivieren: van kinematische formuleringen, via dynamische eendimensionale modellen gebaseerd op gelineariseerde vergelijkingen voor de beweging van water (en zand), tot tweedimensionale niet-lineaire modellen met bewegend rooster. Het gedrag van vlechtende rivieren is echter (als gevolg van de splitsingspunten en de grote morfologische veranderingen tijdens hoogwater) vele malen complexer dan dat van meanderende rivieren. Een vergelijking

van de beschikbare modelleringstechnieken voor meanderende en vlechtende rivieren toont aan dat het modelleren van vlechtende rivieren nog in de kinderschoenen staat. Generieke procesmodellen vormen de basis van toekomstige modellen voor vlechtende rivieren, maar de toepasbaarheid van deze modellen op korte termijn wordt beperkt door restricties ten aanzien van rekentijd, beschikbaarheid van invoergegevens en lacunes in de procesbeschrijvingen.

Drie modelleringstechnieken zijn vergeleken in de context van hun toepasbaarheid voor het voorspellen van veranderingen in het geulenpatroon van vlechtende rivieren: een neurale netwerk, een cellulair model (Murray and Paola, 1994) en een object-georiënteerde aanpak Klaassen *et al.* (1993).

De neurale-netwerkaanpak maakt gebruik van een meerlaags perceptron netwerk met als uitvoerparameter de kans op — of gediscretiseerd: het wel of niet optreden van — erosie van een bepaald punt. Als invoerparameters zijn een beperkt aantal geometrische kenmerken van de omgeving van het beschouwde punt gebruikt: de plaats (afstand en richting) ten opzichte van de dichtsbijzijnde geul, de lokale breedte van de betreffende geul, en de relatieve hoeveelheid water in de omgeving. Het neurale netwerk blijkt in staat om, op basis van deze informatie, een aantal eenvoudige vuistregels te leren zoals: erosie is aannemelijker nabij brede geulen. Het voordeel van deze neurale-netwerkaanpak is dat een probabilistische uitspraak over het al dan niet optreden van erosie kan worden verkregen zonder langdurige berekeningen. De resultaten tonen aan dat de gevolgde aanpak in principe werkt. Echter, een grote hoeveelheid representatieve gegevens is nodig voor het trainen van het netwerk; verder is een juiste keuze van de invoerparameters van wezenlijk belang. Een van de grootste beperkingen van de neurale-netwerkaanpak is het blackboxkarakter: de empirische kennis vergaard tijdens het trainen van het netwerk kan niet eenvoudig worden uitgebreid.

Het cellulaire model is gebaseerd op een vereenvoudigde schematisatie van de waterbeweging gecombineerd met formules voor sedimenttransport in langs- en dwarsrichting, en massa-balansen voor water en zand. Het model vertoont dynamisch gedrag dat op grote schaal lijkt op het gedrag van vlechtende rivieren, maar in detail afwijkt ten gevolge van de vereenvoudiging van de waterbeweging. Naast deze standaard versie is een alternatieve schematisatie van de waterbeweging geformuleerd. Deze aanpassing lost een aantal van de problemen op, maar gaat echter gepaard met een grote toename van de rekentijd. Beide schematisaties van de waterbeweging zijn te eenvoudig voor gebruik ten behoeve van het voorspellen van de morfologische veranderingen van echte rivieren. Bovendien is deze aanpak gebaseerd op hoogte-informatie welke, zoals al eerder aangegeven, niet altijd beschikbaar is.

De object-georiënteerde aanpak is gebaseerd op de opsplitsing van het geulenpatroon in de afzonderlijke geulen (de objecten) en wordt daarom ook wel aangeduid als het geulenmodel. De dynamica van de individuele geulen wordt gegeven door een viertal elementaire processen: geulmigratie, breedteverandering, geulaanzanding, geulsplitsing ten gevolge van bankvorming in het midden van de geul. Numerieke simulaties gebaseerd op dit concept vertonen een gedrag dat minder dynamisch is dan dat van vlechtende rivieren. Het voordeel van deze aanpak is dat de elementaire processen afzonderlijk en duidelijk herkenbaar zijn gemodelleerd; hierdoor is het mogelijk om het model mee te laten groeien met de zich geleidelijk ontwikkelende inzichten. Bovendien leent de eenvoudige, kinematische schematisatie van de processen zich voor een Monte-Carloaanpak in een algeheel stochastisch modelconcept.

De vergelijking van de voor- en nadelen van de verschillende modelleringstechnieken heeft geleid tot de conclusie dat het geulenmodel het meest geschikt is voor de ontwikkeling

van een praktisch bruikbaar model ten behoeve van voorspellingen voor de middellange en lange termijn. Hoewel geulvorming een belangrijke rol speelt in de algehele dynamica van vlechtende rivieren, bevat het geulenmodel geen submodel voor dit proces: het algoritme is afhankelijk van het deskundige oordeel van de gebruiker. Het tweede deel van dit onderzoek betreft daarom een nadere bestudering van het fysische proces van geulvorming.

Geulvorming is het resultaat van een toename in de sedimenttransportcapaciteit in stroomrichting. De richting waarin de geul zich vormt is afhankelijk van de plaats van de grootste gradiënt: een stroomopwaarts migrerende bodemstap (headcut) beginnend aan de benedenstroomse zijde, of een geleidelijke insnijding beginnend van bovenstrooms. Het eerste proces komt voor op hellingen waar afvoer en schuifspanningen toenemen in benedenstroomse richting ten gevolge van een zich verzamelende regenval. Dit proces treedt ook op wanneer zich een nieuwe geul vormt door een ontwikkeld deel van het hoogwaterbed (bijvoorbeeld, bochtafsnijding door een uiterwaard). Terugschrijdende erosie is ook waargenomen tijdens laboratoriumexperimenten van grindrivieren en onder verschillende prototype omstandigheden. Daar staat tegenover dat insnijding van bovenstrooms waargenomen wordt in de Jamuna. Dit verschil vormt de tweede reden om dit onderwerp nader te bestuderen met behulp van computer simulaties.

Tweedimensionale dieptegemiddelde morfologische simulaties van scherpe rivierbochten zijn uitgevoerd om het inzicht in de optredende processen te vergroten. De resultaten van deze simulaties laten zien dat de vorming van een bochtafsnijding wordt versneld door: een lage benedenstroomse waterstand, een grote (alluviale) ruwheid, een lage drempelwaarde voor het sedimenttransport, en een kleine macht voor de Shields parameter (of snelheid) in de sedimenttransportrelatie, wanneer de gemiddelde grootte van het sedimenttransport gelijk blijft. Een extra gevoeligheidsanalyse heeft aangetoond dat numerieke aspecten (zoals de fijnheid van de ruimtelijke discretisatie en de quasi-stationaire stromingsbenadering) geen significante invloed hebben gehad op de uitkomst van de simulaties. Evenmin heeft de dieptegemiddelde benadering een doorslaggevende invloed gehad op de resultaten.

Alle simulaties wijzen op de vorming van de bochtafsnijding aan de bovenstroomse zijde, hetgeen in overeenstemming is met de waarnemingen in de Jamuna. Het ontbreken van niet-hydrostatische effecten en begroeiing in de modellen kan bijgedragen hebben aan deze uitkomst. Bovendien zijn alleen simulaties uitgevoerd met uniform, niet-cohesief materiaal. Op basis van een nadere procesanalyse wordt verwacht dat cohesieve eigenschappen en niet-uniformiteit van het sediment een belangrijke rol speelt bij de vorming van bochtafsnijdingen door middel van terugschrijdende erosie. Een eenvoudig modelconcept voor het simuleren van terugschrijdende erosie is geformuleerd en getest. Nadere procesanalyse en modelvalidatie zijn nodig voor de verdere modelontwikkeling van dit erosieproces.

Tenslotte is er een algoritme voorgesteld waarmee de vorming van nieuwe geulen gemonitoreerd kan worden als submodel van het geulenmodel. Het implementeren, calibreren en testen van het submodel valt buiten deze studie. Het gepresenteerde algoritme is conceptueel vergelijkbaar met het submodel voor bochtafsnijdingen in het meandermodel van Howard (1996). In overeenstemming met de overige procesbeschrijvingen van het geulenmodel is het nieuwe algoritme alleen gebaseerd op geometrische parameters: afsnijdingsratio, splitsingshoek, begroeiingsgraad, en relatieve kromtestraal. Bovendien wordt het effect van stroomconvergentie respectievelijk -divergentie in rekening gebracht op basis van geometrische eigenschappen van de nieuw te vormen geul. Indien rekening gehouden dient te worden met topografische effecten is een ruwe schatting van de terreinhoogtes benodigd.

Preface

This study on the behaviour of braided rivers has been carried out from July 1995 until January 2000 as a Ph.D. study at the department of Civil Engineering at the University of Twente in cooperation with WL | Delft Hydraulics. Finally, almost three and a half years after the end of the official research period, the work has finished. During this period, I tried to reconcile my theoretical background as a mathematician and my fundamental background as a physicist with the empirical ‘rules of thumb’ approach of civil engineering and the descriptive style of geomorphologists. This thesis is an amalgamation of these approaches.

Before starting with the acknowledgements, I would like to point your attention to the CD that accompanies this thesis. It contains a digital version of this thesis (with colour figures), animations, internet links, and the slides of presentations held at conferences in 1997, 1999, and 2001. Furthermore, it contains a selection of the output files of the numerical simulations described in Chapter 7 together with a program to interactively inspect them.

The FAP21/22 project consortium provided data for this research. The consortium consisted of RRI (Rhein-Ruhr Ing.-GmbH, Dortmund, Germany) / Prof. D. Lackner & Partners (Bremen, Germany) / CNR (Compagnie Nationale du Rhône, Grenoble, France) / WL | Delft Hydraulics (The Netherlands) / BETS (Bangladesh) for the FPCO (Flood Plan Coordination Organization, Bangladesh). The FAP21/22 project was funded by KfW (Kreditanstalt für Wiederaufbau, Germany) and CFD (Caisse Française de Développement, France). WL | Delft Hydraulics supported this research and NWO co-funded my field visits to the Jamuna River in Bangladesh and the Allier River in France, both in 1996, and my visit to the 6th International Conference on Fluvial Sedimentology in Cape Town in 1997.

Although this study has been carried out as a Ph.D. study at the department of Civil Engineering at the University of Twente, I have rarely been at the university during the past few years. I thank my former colleagues at the Civil Engineering department for those moments that we shared, in particular, some unforgettable trips with good and bad weather.

Far away from the university, reorganisations of faculties and research groups have gone by with little notice. I am grateful to Prof. Suzanne Hulscher for helping when, in the end, it turned out that the remaining part of the Ph.D. research budget had been reallocated. Major changes have also occurred at WL | Delft Hydraulics since the start of this research in July 1995. I am also grateful to the department of Civil Engineering for supporting my relocation from ‘De Voorst’ to Delft.

I thank my present and former colleagues of WL | Delft Hydraulics for the pleasant atmosphere at the office (all departments). I thank the following colleagues in particular: Henk

van de Boogaard for discussing neural networks and commenting on a draft version of Section 5.1, Dano Roelvink and Giles Lesser for their enthusiasm to get the 3D morphology simulations of Appendix D.6 working, and Cor Flokstra for elucidating the sometimes unexpected behaviour of Delft3D. Furthermore, I thank Gerrit Klaassen for bringing various relevant reports and papers to my attention, Henk Verheij for commenting on Section 7.4, and Maarten van der Wal for the discussions about various processes in the Jamuna River.

I am grateful to my supervisor Erik Mosselman and my promotor Huib de Vriend for their valuable input during discussions and for their comments on the draft version of this thesis. I thank Brad Murray for providing background information on the cellular model. I thank the members of the graduation committee for their participation. I thank my colleagues Hanneke van der Klis, Astrid Blom, Mark van Koningsveld and Stefan Aarninkhof for the discussions about the ups and downs of doing Ph.D. research.

Over the past eight years, I have shared my office room with many people from Johan Crebas in 1995/6 (if he was in the office and not abroad) to Tillmann Baur (during the past two years). I thank them all for the pleasant time that we had. I have asked two of these people to be my paronyms, to assist me on the day of the defence of my thesis: Astrid Blom and Ron Agtersloot. Astrid and I shared an office room during her M.Sc. work at WL | Delft Hydraulics in 1996/7. Astrid, your return to WL | Delft Hydraulics with the message that you had selected a date for the defence of your Ph.D. thesis, has significantly accelerated the finishing of this thesis. Whenever Ron and I met after he left WL | Delft Hydraulics in 1999, he has been asking whether I had selected a date. Ron, finally you can plan your holidays without checking it against the progress of my research. Astrid and Ron, I thank you both for your assistance.

Finally, I thank my parents for all the support that they have given me in so many ways during the past thirty-two years. I hope to spend more time with you, now this thesis has finished. Thank you!



Delft, April 2003

Contents

Summary	v
Dutch summary	ix
Preface	xiii
1 Introduction	1
1.1 Research background	2
1.2 What is braiding?	4
1.3 Problem description	9
1.4 Outline of the thesis	14
2 Case study: the Jamuna River	17
2.1 Geophysical setting	18
2.1.1 The upper reaches	18
2.1.2 The middle reaches	21
2.1.3 The lower reaches	23
2.2 Main characteristics	25
2.2.1 Hydrodynamics	25
2.2.2 General morphology	26
2.2.3 Planform and bed topography	28
2.3 Summary	36
3 Braiding processes	39
3.1 Micro-scale morphodynamics	40
3.1.1 The occurrence of bedforms	41
3.1.2 The shape of bedforms	44
3.1.3 The effect of bedforms on the flow	45
3.1.4 Sediment transport	48
3.2 Macro-scale morphodynamics	53
3.2.1 Alternate bars	54
3.2.2 Braid bars	56
3.2.3 Bars and flow patterns	57
3.3 Mega-scale morphodynamics	60
3.3.1 Islands	60
3.3.2 Confluences and bifurcations	61
3.3.3 Large scale erosion and sedimentation	62

3.4	Sources of uncertainty	66
3.5	Planform dynamics of braided rivers	69
3.5.1	Field studies	70
3.5.2	Laboratory experiments	74
3.5.3	Theoretical studies	79
3.6	Discussion	80
3.6.1	Channel migration	80
3.6.2	Channel widening and narrowing	81
3.6.3	Mid-channel bar growth	81
3.6.4	Channel formation	81
3.6.5	Channel abandonment	82
3.6.6	Node deformation	82
4	Planform models: an introduction	83
4.1	Models for meandering rivers	83
4.1.1	Kinematic models	84
4.1.2	Dynamic models using linearised equations for flow	87
4.1.3	Dynamic models using linearised equations for flow and morphology	89
4.1.4	Dynamic model using non-linear equations	94
4.2	Simple models for braided rivers	96
4.2.1	Markov chain	96
4.2.2	Random walk models	98
4.2.3	Turbulence analogy	100
4.3	Generic models	101
4.3.1	Time series extrapolation	101
4.3.2	Generic process-based model	103
4.3.3	Lattice gas models	106
4.4	Summary	108
5	Some planform models in detail	111
5.1	Neural network	112
5.1.1	Model description	113
5.1.2	Results	116
5.1.3	Discussion	122
5.2	Cellular model	125
5.2.1	Model description	125
5.2.2	Results	128
5.2.3	Discussion	131
5.3	Branches model	132
5.3.1	Model description	132
5.3.2	Extraction of channel network from satellite image	140
5.3.3	Results	143
5.3.4	Discussion	146
5.4	Discussion	147
5.4.1	Comparison	148
5.4.2	Conclusion and research direction	151
5.4.3	Summary	153

6 Channel formation	157
6.1 Types of channel formation and cutoffs	157
6.2 Channel incision and chute cutoffs	160
6.2.1 Channel formation on hillslopes	160
6.2.2 Cutoff descriptions	162
6.3 Modelling chute cutoff stability	165
6.4 Discussion	173
7 Numerical modelling of cutoffs	177
7.1 Overview of the simulation program	178
7.2 Model description	179
7.2.1 Initial topography and boundary conditions	179
7.2.2 Reference simulation	183
7.3 Simulations	185
7.3.1 Upstream boundary: discharge	186
7.3.2 Downstream boundary: water level	188
7.3.3 Roughness	190
7.3.4 Sediment transport relation	195
7.3.5 Geometry	199
7.4 Direction of channel formation	203
7.4.1 Analysis of processes	203
7.4.2 Numerical modelling of headcuts	206
7.5 Discussion	211
7.5.1 Adaptation of the branches model	213
8 Conclusions	217
8.1 The Jamuna River	217
8.1.1 General characteristics	217
8.1.2 Model input data	218
8.2 Planform changes	218
8.2.1 Physical processes in braided rivers	218
8.2.2 Sources of uncertainty	219
8.2.3 Planform changes in braided rivers	220
8.3 Modelling planform changes	221
8.3.1 Existing models	222
8.3.2 Neural network	222
8.3.3 Cellular model	223
8.3.4 Branches model	223
8.3.5 Model comparison: suitability	224
8.4 Channel formation	225
8.4.1 Processes	225
8.4.2 Modelling concepts	226
8.4.3 2D simulations	226
8.5 Cutoff submodel for the branches model	227
Bibliography	229

A Tables and figures	251
A.1 Overview FAP24 reports and data	251
A.2 Results of Delft3D simulations	254
B Program details	271
B.1 Programs related to neural network	271
B.1.1 Pre-processing	271
B.1.2 Back-propagation algorithm	272
B.2 Implementation branches model	273
B.3 Extract channel network from satellite image	279
C Model details	285
C.1 Analytical cutoff criterion	285
C.2 Dynamics of bifurcations	288
C.3 Delft3D description	291
C.3.1 Flow equations	291
C.3.2 Morphological equations	292
C.3.3 Staggered definition of variables	296
D Simplifying assumptions of the 2D simulations: a verification study	299
D.1 Gridcell size	299
D.2 Hydrodynamics of drying and flooding	300
D.3 Boundary conditions	301
D.4 Spiral flow	303
D.5 Suspended sediment	304
D.6 Integrated model	307
Index	311
About the author	313

Chapter 1

Introduction

The term ‘braided river’ refers to a system of channels, splitting and rejoining around islands. The Jamuna River in Bangladesh, shown on the cover of this thesis, is an example of such a river. Every year, substantial erosion occurs along the banks of this river and parts of the flood plain are reworked intensively. These changes have a strong impact on the local inhabitants and the planning and design of infrastructural and protection works. A simple solution seems to be constraining the dynamic nature of this river by protecting the banks with dikes and groynes, just as the western society has done along their rivers for the last two centuries. However, the building and maintenance costs of several hundreds of kilometres of protection works are too high for a developing country like Bangladesh. Moreover, there is a growing notion that there are limits to the extent to which large rivers can be controlled. The 1993 flood of the Mississippi River and the recent floods in Europe have once again shown that nature is difficult to control. Before intervening with the natural behaviour of a river, one should be aware of the consequences in both the near future and the long run. For this, we need to be able to predict the effects of human intervention. Such a prediction requires a certain degree of understanding of the behaviour of the river in natural and disturbed conditions. The understanding of the evolution of braided rivers like the Jamuna River is increasing, but it is not yet sufficient to foresee all effects. Uncertainty in initial and boundary conditions and sensitivity to small changes limit the predictability. Changes in the channel pattern of the Jamuna River cannot be predicted with sufficient accuracy for three to five years ahead.



Figure 1.1: An eroding bank along the Jamuna River.

This chapter fills in the details of the problem sketched above. The first section describes the background of the research which led to the initial research question. The above-mentioned definition of a braided river, as basically a river with islands, is rather general and needs some refinement, which is given in Section 1.2. Subsequently, the research questions addressed in this thesis are introduced in Section 1.3 followed by an outline of the thesis in the last section.

1.1 Research background

The Jamuna River in Bangladesh is a braided sand-bed river characterised by substantial planform changes during individual floods. The average discharge during flood amounts about 60,000 m³/s which, combined with the flooding caused by the other large rivers, results in an inundation of 20–30% of the country. However, in 1987 and 1988 extreme floods occurred which led to the flooding of 40% and 60% of the country, respectively (Thorne and Russel, 1993). The peak discharge of 1988 was more than 90,000 m³/s and it coincided with the flood peak of the Ganges River (Thorne *et al.*, 1993). Since the people in Bangladesh are used to the yearly flooding, it is generally not considered a large threat for the population itself.¹ However, the floods cause more damage to property of individuals, to infrastructural works, and to society as a whole, thereby retarding (or even stopping) the socio-economic development of the rural areas. For this reason a number of internationally funded projects — jointly known as the Flood Action Plan (FAP) for Bangladesh — were started in 1990/1991 to investigate the problems associated with the flooding and to find ways to solve them.

Furthermore, the small and densely populated country of Bangladesh² is split into four parts by the Jamuna, Ganges, Padma and Meghna Rivers. There are only a few bridges across these rivers and, therefore, goods and people cross the river generally by ferry as shown in Figure 1.2. Only the Ganges River and the Upper Meghna River were crossed by railroad bridges when in the 1980s an international project was started to build a multi-purpose bridge

¹ A comprehensive comparison of the viewpoints and knowledge of the local population and the international engineering community working on the Jamuna River is given by Schmuck-Widmann (2001).

² Bangladesh is about 3.6 times larger than The Netherlands and it has 8 times as many inhabitants. The resulting population density of about 875 people per square kilometre in 2000 makes it one of the world most densely populated countries.

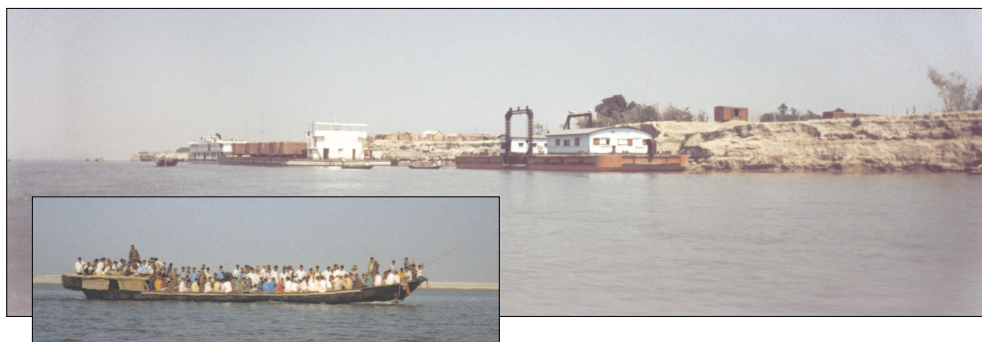


Figure 1.2: Pictures of wagons and people crossing the Jamuna River near Bahadurabad.



Figure 1.3: People in action to shift the flood-defence embankment near Kamarjani. On the left hand side one of the permeable groynes (consisting of a set of piles) that was tested as part of the Bank Protection and River Training Pilot Project (FAP21/22).

across the Jamuna River. The active bed of this river, which consists of multiple branches of up to 2 km wide during low flow, is between 5 and 17 km wide. Bank erosion may attain a rate of several hundreds of metres per year and the locations of maximum erosion shift rapidly over the years (Coleman, 1969; Klaassen and Masselink, 1992). Local erosion may result in scour holes of up to 40 m deep. Obviously, thorough understanding of the river behaviour is essential when one starts building a bridge across (or river training works in or along) such a river.

Finally, the morphological activity of the river does not only affect the construction of bridges and training works, but it also directly influences the lives of the people living along the river and on its islands. Erosion causes loss of land at one location, while land is gained by sedimentation at other places. Some people see their land disappear in the river, while others see their land re-emerge after several years (cadastral maps keep track of land ownership). Extensive protection works have fixed the courses of the rivers in western countries. The Jamuna River, however, is much larger and more dynamic than those rivers, which makes a similar approach much more expensive and less appropriate. Although a continuous earthen flood-defence embankment exists along most of the western bankline, it is not intended to protect the land from ongoing erosion. Whenever the river comes close to it, it is shifted inland (see Figure 1.3). The Bank Protection and River Training Pilot Project, also known as FAP21/22, was set up as a framework within which cheap yet effective river training methods had to be developed to prevent large-scale erosion. For this purpose some test structures (groynes and revetments) were designed and constructed along the braided Jamuna River, and their performance was monitored.

For the decision where to build such test structures, one needs good insight into the future planform changes. On the one hand no erosion should occur at the construction site during the building of the structure, but on the other hand for testing it is absolutely necessary

that the site will be attacked by the river once the structure is completed. For the project in Bangladesh this led to the need to predict planform changes at least 2–3 years in advance. For the rapidly changing, braided Jamuna River with its sensitive dependence on small perturbations, a prediction span of two to three years is too long to be covered adequately by either simple extrapolation or detailed two-dimensional mathematical modelling. For the other two applications (flood management and building bridges and other infrastructural works) slightly less detailed yet long-term predictions are needed to make sure that the investments are cost-effective.

From this starting point the current line of research was started with the following two basic questions:

- In which way and to what extent are we able to predict the time-evolution of the braided pattern in time, based on the observed behaviour of braided rivers and the main principles of flow and sediment transport?
- To what extent are we able to predict the changes caused by a change in exogenic parameters (e.g. discharge) or by human interference (e.g. bridges and dikes)?

Over time these questions have been adapted as the research progressed. In particular halfway the project a new research direction has been chosen. Section 1.3 describes the whole line of research, but first the concept of braiding is defined for a non-specialist audience.

1.2 What is braiding?

In the introduction a braided river was defined as a system of channels, splitting and rejoining around islands. This definition is sufficient for the concept of braiding but for practical purposes one should have a more precise definition. The Jamuna River clearly satisfies the conditions as shown by Figure 1.4, and so does the Amur River shown in Figure 1.5. But,

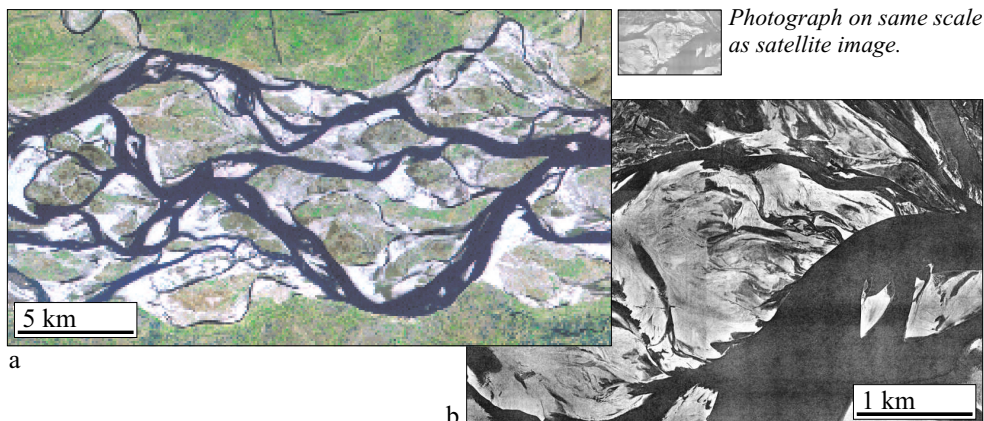


Figure 1.4: On the left: a Landsat satellite image of the Jamuna River showing the braided planform during low flow in 1995. On the right: an aerial photograph of a smaller section of the Jamuna River in 1991. The river flows from left to right. The white areas are unvegetated sand bars.

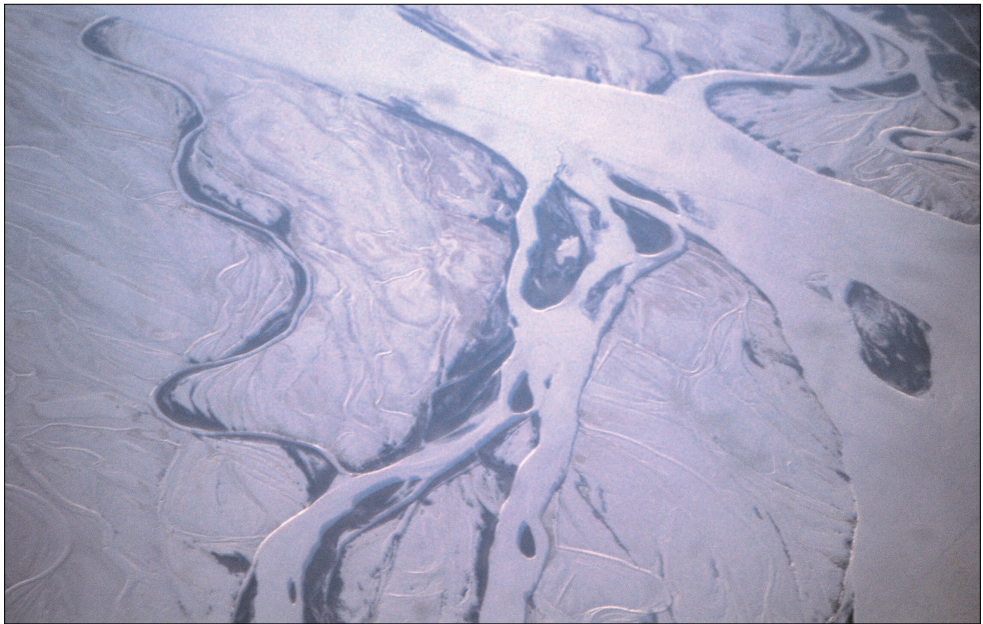


Figure 1.5: Photograph of a snow- and ice-covered braided reach of the Amur River near Khabarovsk (Feb. 2003). The river flows from bottom right to top left.

should a river with a single island also be called braided? And what about the network of rivers in the southern part of the Netherlands, do they together form one braided river? As the answers to both questions should be negative, a closer look at the distinguishing characteristics of the various river types is required.

The river types are distinguished based on their planform, that is, the shape of the stream as seen from above. *Meandering* and *braided* are the two main planform types described in classical literature (Leopold and Wolman, 1957). All Dutch rivers are, for instance, individually characterised by a single channel with flood plains on one or both sides. Although some of the rivers have been straightened artificially by removing the largest bends, their meandering nature is still clearly recognizable on the maps. Besides braided and meandering river reaches Leopold and Wolman distinguish also *straight* river segments which, as they indicated, are seldom longer than 10 channel widths. Many intermediate types exist from strongly meandering with one or more islands to almost straight with vegetated stable or bare regularly-shifting islands. Various classification schemes have been proposed to structure the diverse continuum of river types.

Kellerhals *et al.* (1976) propose a classification based on channel sinuosity (from straight to tortuous meandering) and the presence of islands (from none to fully braided). Whereas sinuosity is consistently defined as the length along the river from point A to B divided by the distance between A and B along a straight line, various definitions are in use as index for the braiding intensity (Bridge, 1993). All these definitions include in some way the number of islands or channels per cross-section. Since these numbers change when the water level (and thus the discharge) varies, the braiding indexes undergo seasonal changes. This makes it difficult to uniquely and consistently identify their values. Chalov and Alabyan (1994) and

Alabyan and Chalov (1998) distinguish straight, sinuous and branched planforms at three different scales or structural levels: the low water channel, the flood channel, and the valley bottom (see Figure 1.6). Now, we see islands and bars splitting the river into multiple parallel channels at three scales. For the largest (valley) scale the term anabranching is used.³ Although Alabyan and Chalov reserve the label ‘braided’ only for the scale of the flood channel, it is often also used for rivers with a branched planform at low water levels. It should be remarked that, contrary to what Figure 1.6 may suggest, sinuous and branched are not always mutually exclusive planform types: sinuous flood channels with islands exist and are generally referred to as wandering (Alabyan and Chalov, 1998).⁴

Although the classification scheme in Figure 1.6 provides enough flexibility to describe the planforms of most rivers, it is not sufficient for characterising the behaviour of the rivers. Whether the sinuous planform of a river is stable or actively migrating depends on the yearly variation in discharge combined with the type and availability of sediment, the presence of vegetation and the geomorphological activity in the region (and, of course, river training works). Nanson and Knighton (1996), for example, distinguish six types of anabranching rivers of which four can be classified anabranched rivers with more or less straight, stable channels; the two remaining types can be classified as anabranched with meandering and braided channels, respectively. Of the four types with stable, straight channels two can be described as multichannel systems with large, relatively stable, vegetated islands made of sand and gravel, respectively. The two remaining types are anastomosing rivers and ridge-forming rivers. Anastomosing rivers were extensively studied by Makaske (1998). Following

³ At this scale one can also see tributive (drainage pattern, merging channels) and distributive (river delta, splitting channels) river systems.

⁴ The term incomplete meandering is used when the islands result from cutoffs occurring before meanders reach their maximum curvature.

structural level	plan outline			limiting conditions
	straight	sinuous	branched	
valley bottom				
flood channel				
low water channel				

Figure 1.6: Classification of river channel patterns by Alabyan and Chalov (1998) distinguishing straight, sinuous and branched planforms at three different scales.



Figure 1.7: Images of the Waimakariri River, New Zealand, on April 5, 2000 and April 15, 2000 (Hicks et al., 2000). The river flows towards the camera.

the concepts introduced by Smith and Smith (1980) and Nanson and Knighton (1996), he concludes that it is the nature of the islands rather than their size that distinguishes anastomosing rivers from braided rivers: an *anastomosing* river is characterised by laterally stable (sand/clay) levees which enclose convex muddy/swampy floodbasins, whereas the islands of a braided river consist of unprotected, non-cohesive sand/gravel concave deposits. Ridge-forming rivers are characterised by narrow, elongated islands stabilised by trees. So, there are many different types of islands and it is not only the presence of islands (at any discharge) that makes a river braided.

Islands in braided rivers, sometimes called braids, are relatively small (that is, generally shorter than a few times the river width) and often not, or only sparsely, vegetated. In an actively braiding river, the islands are continuously formed, reshaped and removed (Hicks et al., 2000) as illustrated by Figure 1.7. Leopold and Wolman (1957) identified one mechanism that should lead to a braided planform: central bar growth. A variation in the river width will cause a disequilibrium in the sediment transport rate: when the channel widens the sediment transport capacity of the river reduces and sediment is deposited, and vice versa.⁵ When the river is sufficiently wide the deposited sediments may form a bar in the middle of the river (indicated as a medial bar in Figure 1.6) which may over time grow to become a quasi stable island that gives the river a braided appearance at higher discharges. For a more extensive description of this and other braiding mechanisms the reader is referred to Chapter 3 about braiding processes.

Why are some rivers braided while others are meandering? Theoretical analyses have shown that both meandering and braiding result from instabilities in the basic set of equations governing the motion of water *and* sediment (Engelund and Skovgaard, 1973; Parker, 1976; Fredsøe, 1978)⁶. It has been shown that wide, shallow channels lead in theory to braiding via

⁵This relation holds most clearly for sediment transported near the river bed and less so for suspended sediments which require a longer distance to adapt.

⁶That meandering can also be observed in dynamical systems without sediments such as the Gulf Stream (Pinet, 1992), supraglacial melt-water streams (Parker, 1975) and on glass and plastic plates (Gorycki, 1973a) such as windscreens of cars is attributed to contributions of the Coriolis acceleration, heat differences and surface tension effects, respectively (Parker, 1976; Gorycki, 1973b). When in a meandering river over time — as the meanders become more extended — a cutoff (that is, a short cut) occurs, the begin and end sections of the old channel become clogged with sediments and an oxbow lake is formed. In the systems without sediment the behaviour is quite different: old parts of the Gulf Stream drift off as eddies of cold or warm water, while old stream courses in the

the growth of one or more bars per cross-section. So, channels with large ratios of width to depth tend to be braided, but then the question should be rephrased to: why are some rivers wide and shallow while others are narrow and deep? One can think of several reasons why a river may be wide and shallow:

1. *Insufficient sediment transport capacity for channel initiation.* Extensive floods over wide plains, such as flash floods in flat, arid areas and melt water flows over the sandur plains of Iceland, may not last long enough or be sufficiently concentrated to initiate the formation of large channels.
2. *Easily erodible banks.* Non-cohesive banks that are made of sands or gravels and that are not protected by vegetation are easily eroded. Once the channel is wide enough for braiding the only requirement for maintaining the braided planform is that the planform changes fast enough (or the climate is extreme enough) to prevent vegetation from stabilising the bars. Note that once the river has attained its braided character, it is not necessary for the outer banks to be easily erodible. Many lowland rivers in cultivated areas remain their braided appearance within a channel confined by dikes.
3. *Aggradational area.* If the sediment supply from upstream is larger than the local sediment transport capacity, sedimentation will occur resulting in a continuous shallowing of the river.
4. *Discharge reduction.* When climates and rainfall patterns change, the average yearly discharge transported by the river may decrease (or the discharge distribution over the year may change) resulting in an adaptation of the river planform. The transition to the new planform will take time and during this period often a braided planform is observed.

The last two reasons (and, depending on one's point of view, also the first two) suggest some kind of disequilibrium whereas field observations suggest (and theory indicates) that rivers with a braided pattern may be as close to equilibrium as rivers with a meandering or other planform (Leopold and Wolman, 1957; Parker, 1976). Interpreted differently, braiding may be considered to be the fundamental pattern of alluvial rivers; only vegetation and/or cohesive sediments can prevent it from developing (Paola, 2001).

Characteristic features of an active braided river are a wide and shallow channel (caused by any of the reasons mentioned above), an alluvial bed of non-cohesive sediments and a limited amount of vegetation within the channel. The planform changes result from spatial variations in the sediment transport rate which is in general large for braided rivers. The energy needed for transporting water and sediment along a slope by a river originates from the reduction in potential energy caused by the transport downhill. The energy needed by a braided river for continuously reshaping the river bed originates from the same source. The larger amount of energy dissipation by braided rivers is correlated with the observation that braided rivers are found on steeper slopes than meandering rivers (see Figure 1.8) since the release of potential energy per metre river length is larger for steeper slopes. Phrased differently, larger slopes cause higher flow velocities which lead to more erosion of bars and banks than the lower velocities observed of rivers on gentler slopes.

supraglacial streams remain active until they become exposed by further incision of the stream into the ice or when they become blocked by other processes.

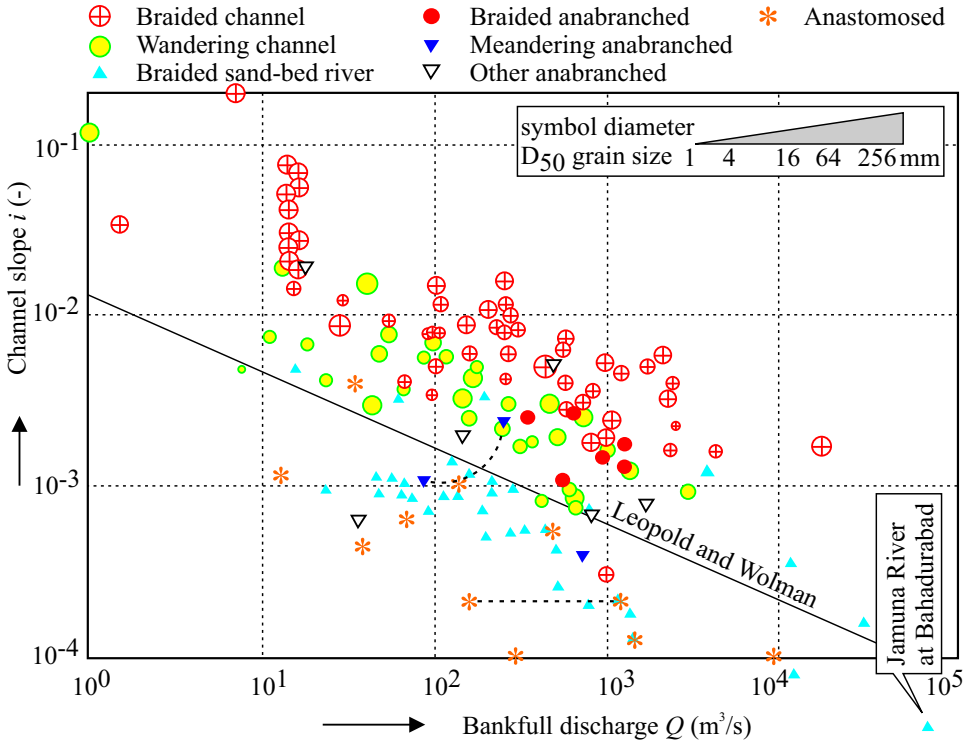


Figure 1.8: Discharge-gradient-grainsize plot of braided rivers of Ferguson (1984b) reproduced from Struiksma and Klaassen (1988) with added data on anabranching rivers by Nanson and Knighton (1996) and Knighton (1998).

1.3 Problem description

Section 1.1 about the research background ended with two basic questions regarding the predictability of planform changes in braided rivers that may or may not be influenced by man. The questions asked depend on the degree of detail that is required. Depending on this required degree of detail and the relevant processes in the river, one must choose the appropriate aggregation level of the model. For explanation of this let us look at a braided river at various levels of aggregation.

From a very large distance, islands and bars of the braided river become invisible and all channels can be combined into one wide, shallow channel (Paola, 1996, and Section 4.2.3). What remains visible, is a straight or meandering flood plain that develops on long time scales. A meander model (see Section 4.1) or simple extrapolation of observed bankline movement (see Section 4.3.1) can be used for predicting its future development. Such a prediction of large scales requires the input of (or at least assumptions about) the long term behaviour of related dynamic systems. For the prediction of river migration over long time spans this includes tectonic and climatic influences in the region during the prediction period, as illustrated by Section 2.1 about the geophysical setting of the Jamuna River.

If one needs a more detailed prediction of the future behaviour, one has to include the spatial characteristics of the braided pattern into the model. However, such an extension of the model requires also more input data. So, the usefulness of the extension depends not only on the gained detail of the model, but also on the accuracy with which the additionally required input data can be obtained. Upon increasing the detail of our conceptual model of the river one comes across the scale of the largest islands, the flow confluences and bifurcations, the scale of the smaller islands and the slightly smaller channel divisions, and the scale of the bars and the large-scale flow structures. Continuing even further one sees the sediment clouds and the effects of variations in suspended sediment concentrations, the dunes and other bed-forms, the large-scale turbulence, the sediment grains, until one, finally, reaches the smallest scales of turbulence. And all scales are, of course, interrelated, such that processes on the smaller scales influence the larger scales and vice versa. Mixed with these hydrodynamical and (geo)morphological processes are interactions with vegetation, wildlife, humans and their technology. Do we need to include all these processes in order to be able to accurately predict the planform changes of the braided river?

No, it is generally not required to model every detail of a complex dynamical system to be able to make useful predictions regarding its future behaviour. The growth of a tree, for example, can be predicted without the modelling of cell growth; neither does predicting the weather require the modelling of each and every cloud. Implicitly included in these questions about predicting the dynamics of a system is the required degree of detail of the prediction. If one needs a more detailed prediction of the future behaviour then a correspondingly refined model has to be used. The questions raised during the FAP21/22 studies on the Jamuna River concern the major planform changes on the scale of the islands with possible extension to the bar scale, which may already be considered to be quite detailed, given the difficulties of obtaining spatial data for a dynamic river of that size (see Section 2.2).

Model results cannot always be improved by increasing the modelled detail of the internal dynamics of the system, because the interaction of the system with its surroundings is often more important. For example, the external influences on a tree (such as wind, sun and soil

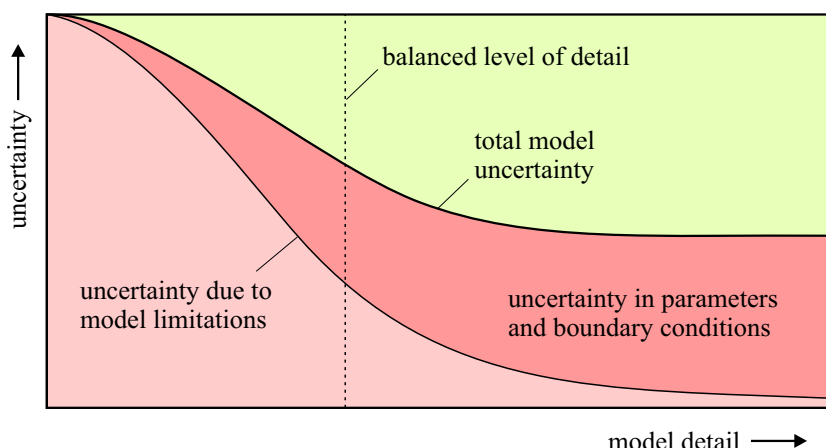


Figure 1.9: The total uncertainty in the model output decreases as the model detail is increased, but the importance of accurate model input increases.

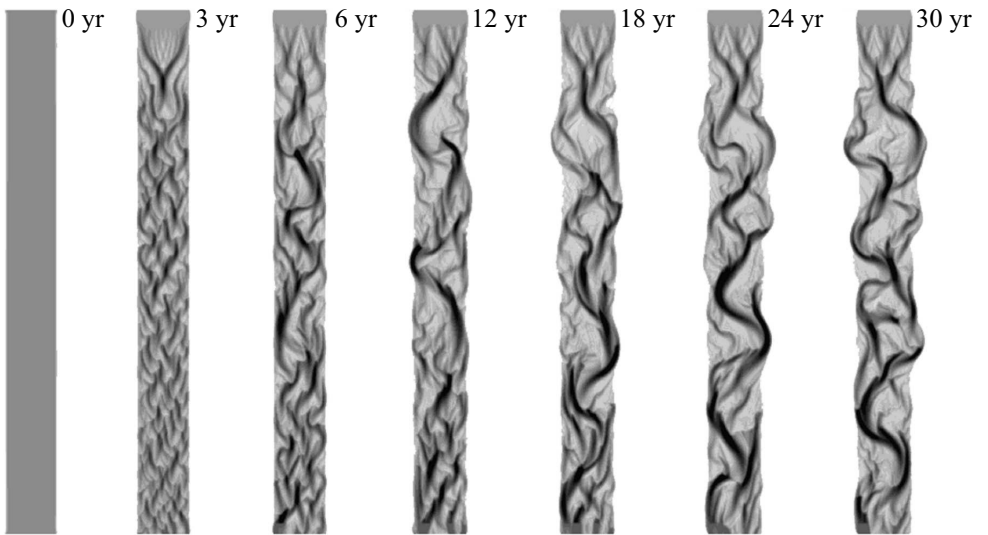


Figure 1.10: Bed level development of a braided sand-bed river as simulated by Enggrob and Tjerry (1999).

type) are more important for the prediction of its growth than the exact way in which its cells grow. So, a more refined model, as indicated in the previous paragraph, does not necessarily mean a more detailed one. Therefore, a good, useful model is obtained by balancing the description levels of the internal dynamics and the external conditions. Improved understanding of the internal processes of the system can only lead to better predictions if it is matched by better input data providing the external forcings and the boundary and initial conditions (see Figure 1.9). This holds for both deterministic and stochastic models. Other aspects for the selection of an optimal model are an economic analysis of model development costs and extra (e.g. construction) costs due to a larger uncertainty, and an analysis to balance the uncertainty caused by the various submodels (Booij, 2002).

For the rapidly changing, braided Jamuna River with its sensitive dependence on small perturbations, a prediction span of two to three years is too long to be covered by either simple extrapolation or detailed two-dimensional mathematical modelling. Two-dimensional mathematical models can be used to predict short-term planform changes. The long-term chaotic behaviour of braiding may also be studied in a statistical sense by using long-term, two-dimensional numerical simulations, which as such are valuable for improving the understanding of braided river dynamics (Enggrob and Tjerry, 1999, and Figure 1.10). Other, more simplified models can also be used in that case (Murray and Paola, 1994, and Section 5.2), which shows that the accuracy of the modelled detail is not of crucial importance here. In between the short-term changes, which may be predicted using a deterministic model, and the long-term behaviour, which can only be predicted in some statistical sense, there is an intermediate range, here indicated as medium-term, in which some deterministic element remains but where uncertainty becomes also important.⁷

⁷The medium-term period is associated with a prediction span of 2–5 years for the Jamuna River. For other types of rivers this can be quite different. For example, in the case of meandering rivers, deterministic models can often be used for a much longer period (up to decades).

Given the need for accurate predictions and the knowledge that these could not be obtained by means of two-dimensional mathematical model simulations, a prediction method was developed based on mostly geometrical information that can be obtained from satellite images and maps (Klaassen *et al.*, 1993). This prediction method is illustrated in Figure 1.11. The method is based on the understanding that there is some degree of uncertainty in every single step of the prediction. Starting from an initial planform (here, the planform of the river observed after the 1992 flood) several predictions are made for one year later (1993-A, B, C, etc.) and appropriate probabilities are assigned to them. Based on each prediction new predictions are made that are again one year further into the future (1994-BA, BB, etc. based on 1993-B) and appropriate probabilities are assigned to them, again. When all options have been considered, the results can be lumped together to answer questions about the predicted planform changes in 1994. This prediction method has been applied manually in the FAP21/22 project where it performed well. The analysis becomes, however, more and more complicated and time-consuming as the number of possible events and the number of years considered increase. Therefore, a computer implementation of this method has been constructed as a part of this study. The implementation and testing of this approach are described in Section 5.3. Furthermore, a new neural network approach has been attempted as described in Section 5.1 and some research along the lines described by Murray and Paola (1994) has been carried out (see Section 5.2). The neural network approach and the automated prediction method following the approach of Klaassen *et al.* (1993) have been compared with a general two-dimensional finite-difference model.

To summarise, the following questions are addressed in the first five chapters:

- What are the general characteristics of the Jamuna River? → *Chapter 2*
- What data are available for usage as input data for models of the Jamuna River? → *Chapter 2*
- What basic physical processes are active in braided rivers? → *Chapter 3*
- What are the primary sources for uncertainty and unpredictability given the current state of knowledge (that is, without making additional simplifying assumptions)? → *Chapter 3*
- What are the main types of planform changes observed in braided rivers? → *Chapter 3*
- Which models for predicting planform changes in (meandering and braided) rivers exist? → *Chapter 4*
- How can a neural network be used to predict planform changes in braided rivers and how well does it perform? → *Chapter 5*
- To what extent can the cellular model of Murray and Paola (1994) be used to predict planform changes in braided rivers? → *Chapter 5*
- How can the approach of Klaassen *et al.* (1993) be used as an automated approach for the prediction planform changes in braided rivers and how well does it perform? → *Chapter 5*
- Which of the described models is best suited for predicting planform changes and what is needed to improve that model? → *Chapter 5*

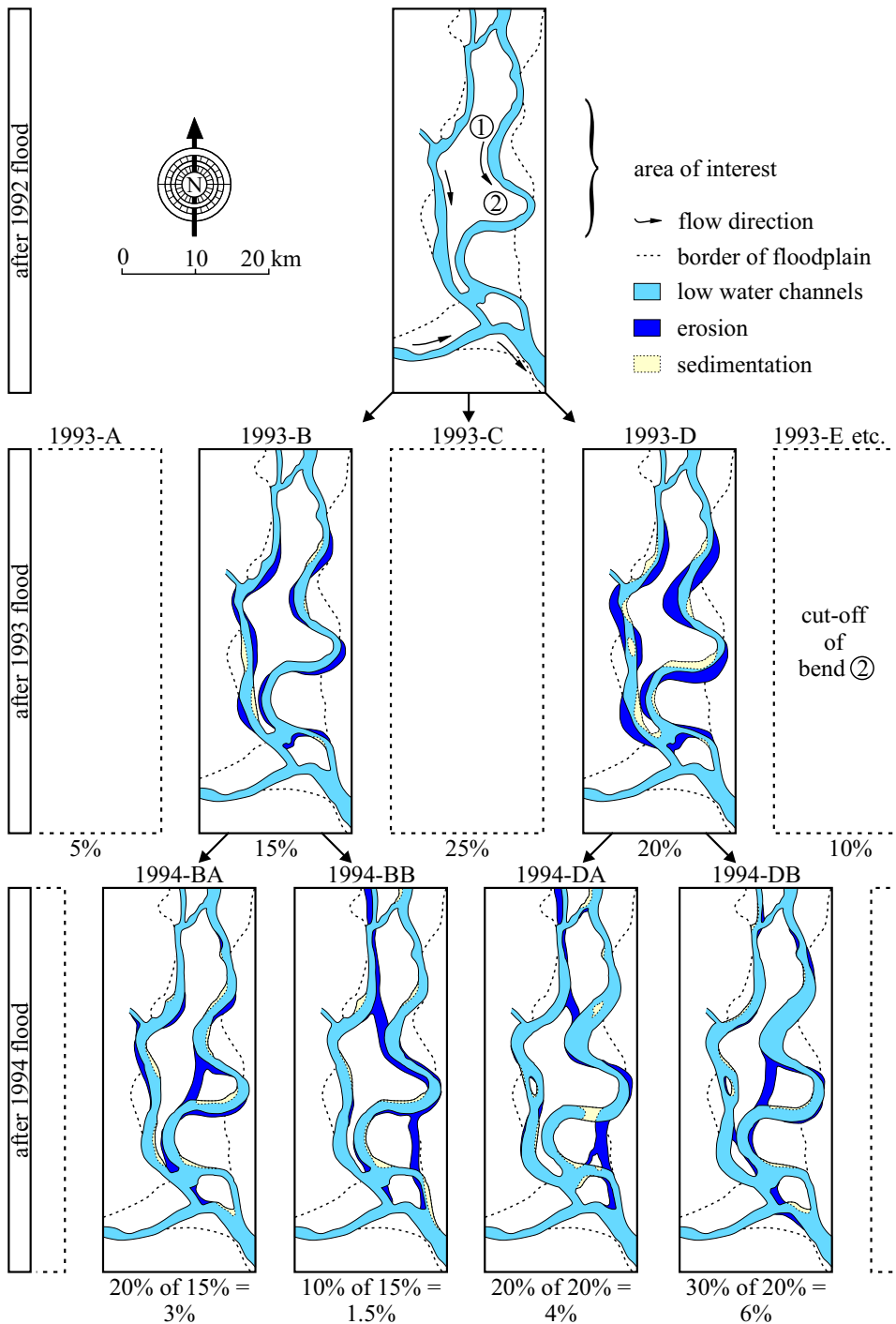


Figure 1.11: Sample application of the prediction methodology described by Klaassen et al. (1993) to a reach of the Jamuna River just upstream of the confluence with the Ganges River coming in from the left.

From the comparison it follows that although the framework described by Klaassen *et al.* (1993) is an attractive alternative for more computational intensive modelling techniques, some processes are not included adequately. For instance, the formation of new channels (cutoffs) has been left to the expert judgement of the modeller. As can be seen in the sample application of the approach by Klaassen *et al.* (1993) in Figure 1.11, predicting cutoffs is important for predicting large-scale planform changes. The added value of an automated approach is limited if these cutoff events are part of the model input. Therefore, the second part of the thesis focuses the modelling of cutoffs.

Theoretical studies concerning the formation of new channels have been very limited, so far, and descriptions of cutoffs in meandering rivers are rare. Although new channels are constantly being formed in braided rivers, little attention has been paid to the formation processes. There are two difficulties when trying to obtain field observations for the channel formation process. Firstly, channels form generally under flood conditions which make site access and data recording difficult or impossible. Secondly, there is no standardised way to predict the occurrence of cutoffs in braided rivers, so, planning a measurement campaign can be difficult. After an overview of the literature on this subject, the algebraic work of Klaassen and Van Zanten (1989) is extended by using the Delft3D computing system to investigate the influence of a number of parameters on the dynamical 2D behaviour of cutoff formation in river bends. This work addresses just one of the aspects of braiding on a much more detailed spatial scale and on a much shorter time scale than the first part of the study. The following questions are addressed in the second part of the thesis:

- What information is available in the literature on the physical processes involved in channel formation? → *Chapter 6*
- How are cutoffs dealt with in the existing numerical models? → *Chapter 6*
- How sensitive are the results of 2D morphological simulations of bend cutoffs for changes in roughness, boundary conditions and sediment transport formula? → *Chapter 7*
- How can the new knowledge be used in the approach of Klaassen *et al.* (1993)? → *Chapter 7*

1.4 Outline of the thesis

Although the chapter titles should be self-explanatory, the following describes in short the contents of the various chapters. It is recommended to read Sections 1.1 and 1.3 of this introductory chapter first, as they explain the background of the study and describe the problems addressed in this thesis.

The remaining chapters can be divided into two groups. The first group, Chapters 2 through 5, deals with planform changes in braided rivers. The second group, Chapters 6 and 7, addresses the occurrence of cutoffs. Within each of these groups the following topics are addressed: review of the relevant physical processes (Chapters 3 and 6), review of the state-of-the-art computer models related to the subject (Chapters 4 and 6), a description of the new research and conclusions (Chapters 5 and 7). The overall conclusions are summarised in Chapter 8.

The first group of chapters addresses the mathematical modelling and prediction of planform changes in braided rivers like the Jamuna River from an engineering point of view. The main problem when using models is the lack of appropriate data. Concerning predictions this is obviously true for the boundary conditions (for instance, next year's maximum discharge is unknown), but also the current planform of the river may not always be known with sufficient detail. One may, for instance, obtain the width of a channel from a satellite image, without knowing how deep the river is at that particular location and what kind of sediments the river banks consist of. Therefore, the usefulness of a prediction method is not only limited by the conceptual foundations from which the method was derived, but it is also limited by the amount and reliability of the input data. Chapter 2 describes the Jamuna River and addresses the question as to what kinds of data are available or could be obtained for this river. The conclusions regarding the availability of data can be assumed to hold for other braided rivers of similar size. Subsequently, the processes playing a role in braided rivers are described in Chapter 3; without a good understanding of the fundamental processes at the various levels of aggregation one cannot build a good model. The state-of-the-art numerical modelling of both meandering and braided rivers is described in Chapter 4. Chapter 5 describes the models investigated in this study (a neural network, a cellular model, and an object-oriented model) and the results obtained with them are discussed and compared.

The second group of chapters addresses the mathematical modelling and prediction of cutoffs in meandering and braided rivers. Chapter 6 (in particular Section 6.2) describes both the physical processes dominating channel incision and the state-of-the-art modelling of cutoffs. Chapter 7 describes investigations of channel formation using the software package Delft3D and Chapter 8 draws the final conclusions.

Chapter 2

Case study: the Jamuna River

Jamuna River is the official name of the Bangladeshi reach of the river that is often referred to by its Indian name: the Brahmaputra River. The 3000 km long river springs in the western part of the Tibet Autonomous Region [Xizang] of China not far from the sources of the Ganges River and Indus River (see Figures 2.1 and 2.2). It springs at an altitude of 5100 m from the Chemayungdung glacier near mount Kailas in the Himalayas. It flows for about 1400 km in an easterly direction across the Tibetan plateau, which is bordered by the Himalayas in the south and the Gandisê Mountains in the north, while it descends to 3000 m. In this reach the river is known as the Tsang Po or Yarlung Zangbo (Jiang) River. Not far from Nyingchi at mount Namche Barwa the river enters one of the world's largest canyons; meanwhile rapidly descending. At an altitude of 200 m above sea level it leaves the Himalayan range as the Dihang River. The canyon is the main access route for the moist air currents from the Indian Ocean as a result of which the annual average precipitation varies on the Tibetan plateau from 200 mm at the western end to 900 mm at the eastern end. It was not before 1880

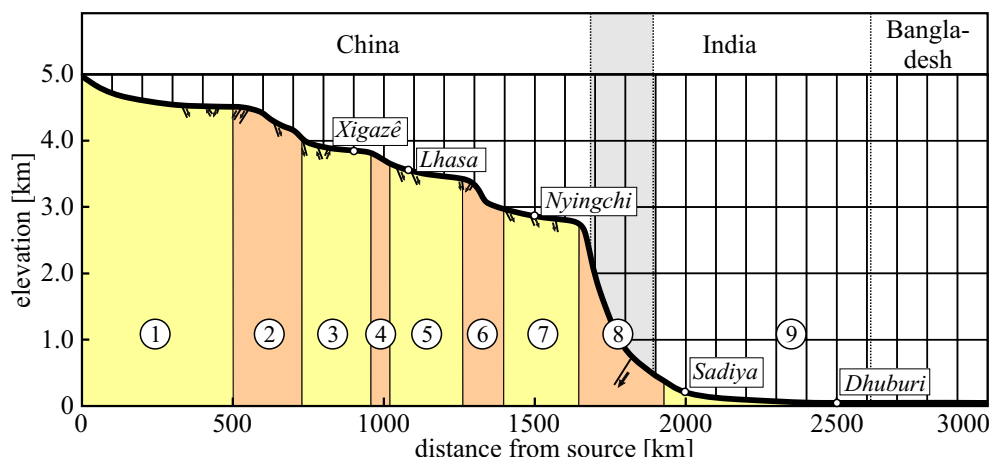


Figure 2.1: Longitudinal profile of the Brahmaputra River (Zhang, 1998). The odd-numbered reaches are characterised by relatively wide valleys and braided planforms.

that the connection between the Yarlung Zangbo and the Brahmaputra was finally confirmed by the exploration of Pandit Kishen Singh (Montgomerie, 1885) and still, its narrow canyon through the eastern part of the Himalayas remains one of world's least explored regions (Bian, 1998; National Geographic, 1999).

Just west of the town of Sadiya in the Indian province Assam the Dihang River joins with the Lohit River and Dibang River, after which it flows west through the plains of the Indian province Assam as the Brahmaputra River. As the river reaches the ninety degrees east meridian it makes a sharp left turn, goes south and enters Bangladesh. After a while, the river splits into the Old Brahmaputra River and the Jamuna River, the latter currently being the main branch. The Jamuna River merges with the Ganges River and continues as the Padma River, which merges with the Upper Meghna River to form the Lower Meghna River before discharging into the Gulf of Bengal.

The combined delta of Brahmaputra River and Ganges River ($59,000 \text{ km}^2$) is twice as large as the second largest delta in the world (the one of the Niger River). Their combined average discharge ($32,000 \text{ m}^3/\text{s}$) ranks third after the Congo River and the Amazon River, while the combined drainage area of the Ganges River ($1,100,000 \text{ km}^2$) and Brahmaputra River ($924,000 \text{ km}^2$) ranks only ninth. The river serves as an important inland waterway on both the Tibetan plateau and the Indian and Bangladeshi plains. The following two sections describe the geological development of the region and its influence on the river (Section 2.1), and the general characteristics of the dynamics of this river (Section 2.2).

2.1 Geophysical setting

The Jamuna River lies in one of the tectonically most active zones in the world. Every year India migrates to the north into Asia by approximately 5 cm. A part of this convergence is taken up in the Himalayas (1 cm/year rise); the remainder is expected to be absorbed in the Altun Tagh Mountains (West China), the Tien Shan Mountains (Northwest China), and the eastward motion of China and Mongolia (Molnar and Tapponier, 1977; Pendick, 1996). This tectonic motion has been and will be an important factor in the evolution of the river by influencing its sediment load, planform and course. From upstream to downstream we will now discuss the effects that it has (had) on the river.

2.1.1 The upper reaches (China/Tibet)

Along its course on the Tibetan plateau the river changes regularly between a braided planform (see Figures 2.4 and 2.5a) and entrenched meanders. Variations in erodibility of bed and bank materials do not explain the alternation of gorges and wide valleys, and of gentle and steep gradients. The reason for these planform changes can be found in the history of the Tibetan plateau that can be divided into three phases (Zhang, 1998):

- The thrust and north-south shortening phase started in the Eocene with the collision of the Indian Plate and the Eurasian Plate. The contact between the two continents was probably well established between 55 and 50 million years ago along the Indus-Zangbo Suture. This period is associated with volcanic activity along the border of the Eurasian Plate.

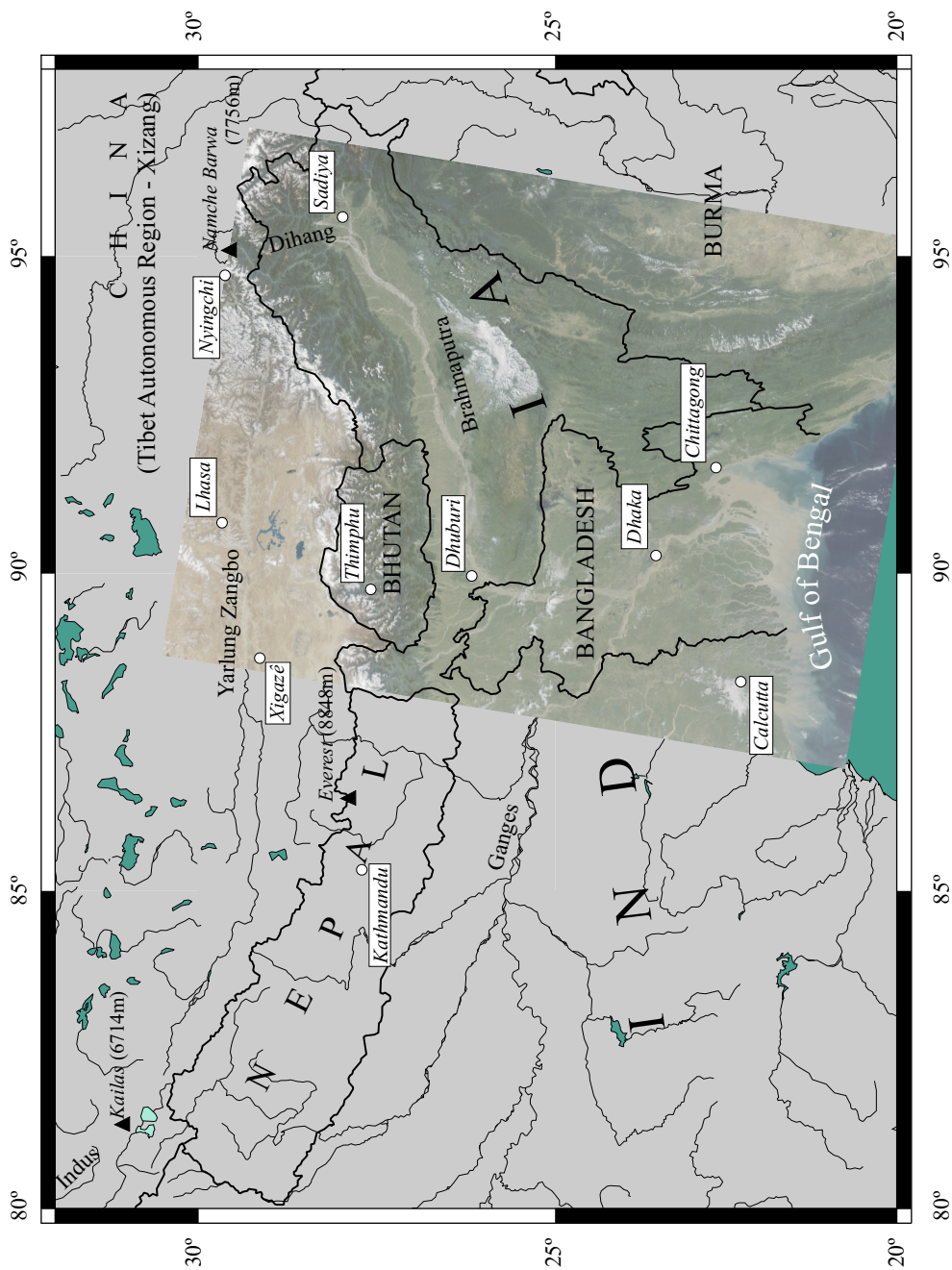


Figure 2.2: Map of the drainage area of the Brahmaputra River. Satellite image by NASA (2001b).

- The strike-slip phase started in the Miocene (between 5 and 23 million years ago) with the breaking of the Indian subcontinent along the Main Central Thrust, followed by the subduction of Indian continental crust along this fault.
- The last phase, which is associated with fast uplift and east-west extension, started in the Pliocene (between 1.6 and 5 million years ago). Sediments deposited on the south slopes of the Himalayas imply that uplift has been accelerated for the last 800 thousand years.

During the third phase, which still continues today, many normal (north-south) faults were formed. Most boundaries between gorges and wide valleys along the Yarlung Zangbo River seem to be related to these active faults. The relative lifting and subsiding of the separate blocks causes changes in the river planform. A typical example is found near Xietongmen, which lies slightly upstream of Xigatsé, where the river crosses a graben (Figure 2.3). Developing alluvial fans along the fault lines reflect the fact that the relative movement is very rapid. In the relative subsiding reaches the gradient is low, the planform is braided, and the alluvial deposits (in the valley near the Tibetan capital Lhasa up to 480 m thick) cover the whole valley including old terraces. In the relative lifting reaches the river flows in general in entrenched meanders while early Pleistocene terraces can be found high above the current flood plain.

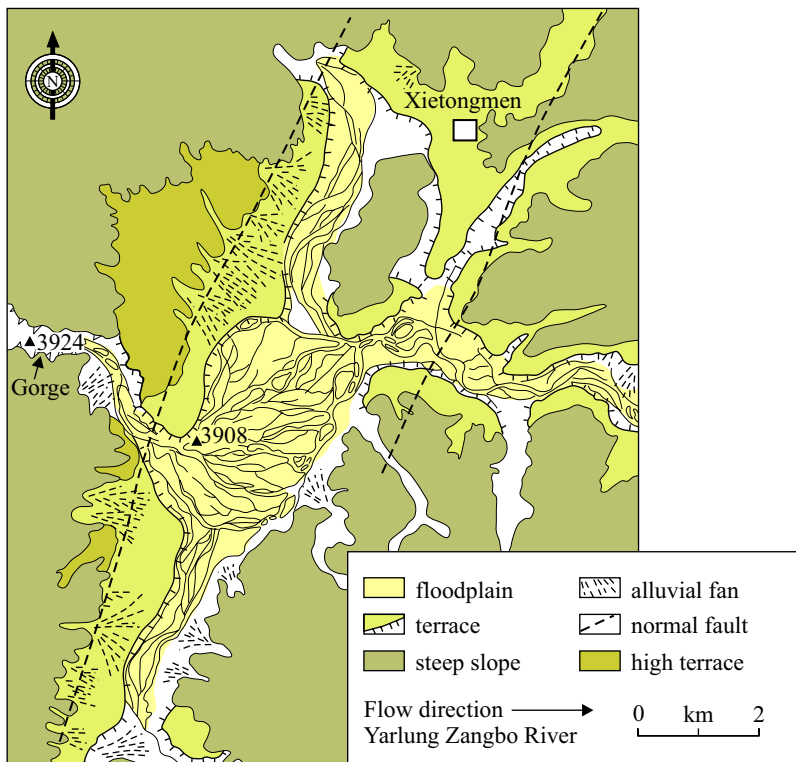


Figure 2.3: A sketch of the Yarlung Zangbo River crossing the Xietongmen graben after Zhang (1998).

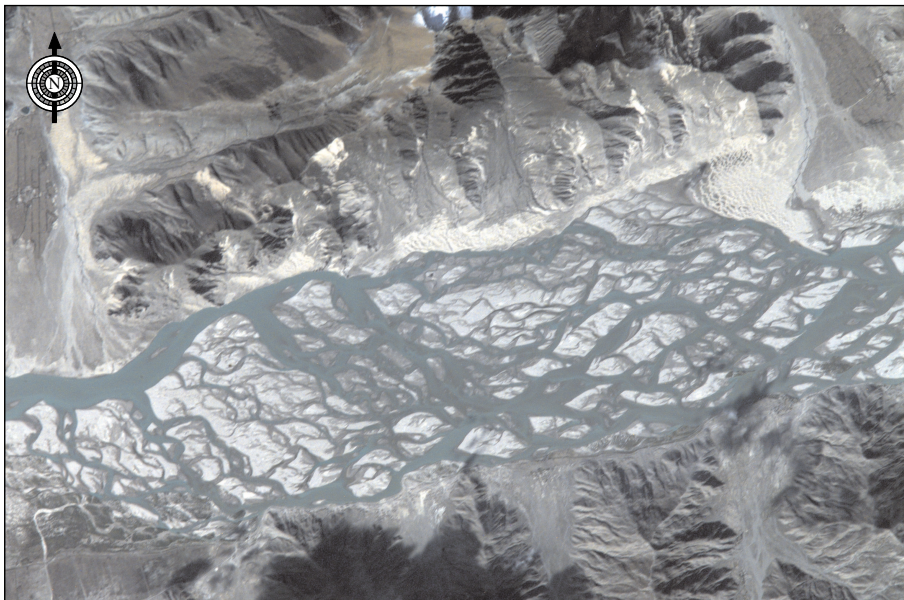


Figure 2.4: Photograph of a braided reach of the Yarlung Zangbo south of Lhasa (NASA, 2001a).

2.1.2 The middle reaches (India/Assam)

From the point at which the Brahmaputra River leaves the Himalayas (see Figure 2.5b) it flows as a braided river in its own alluvial sediments or the sediments of other rivers with Himalayan origin. Alluvial sediments form a 200–300 m thick layer of clay, silt, sand, and pebbles (Goswami, 1985). These sediments cover the active faults, which, therefore, have a less pronounced impact on the river course and planform than in the upstream reaches. Being quite close to the Main Central Thrust fault, the area regularly experiences large earthquakes. Two well-recorded earthquakes of 8.7 on the Richter's scale have occurred in the recorded history (June 12 1897 and August 15 1950). The fine sand and silt, which make up the riverbed, can easily lead to liquefaction during an earthquake. Pioneering seismologist R. D. Oldham, happened to be in the area at the time of the 1897 earthquake, and gathered many eyewitness reports. In many places riverbeds were filled up with sand; at other locations 1 m high jets of water appeared. A 3 m high wave was generated in the Brahmaputra River destroying several buildings in its path. At many places steep banks collapsed, resulting in an increased sediment load; many rivers formed new channels during the following flood season. The 1950 earthquake caused a temporary blockage of the narrow gorge upstream and a few tributaries, which led to floods a few days later (Tillotson, 1951; Poddar, 1952; Goswami, 1985). These large earthquakes have large influences on the local morphology (especially if the faultline happens to cross the river). Rapid aggradation was observed at Pandu (about 400 km downstream of Sadiya) from 1955 until 1963, which may be associated with the earthquake of 1950 (Goswami, 1985). The influence of the earthquake on the river morphology extends in downstream direction not only as a result of an increase in the amount of sediment available for transport, but also due to a possible cascade of channel realignments and associated changes in discharge distribution over the various channels.

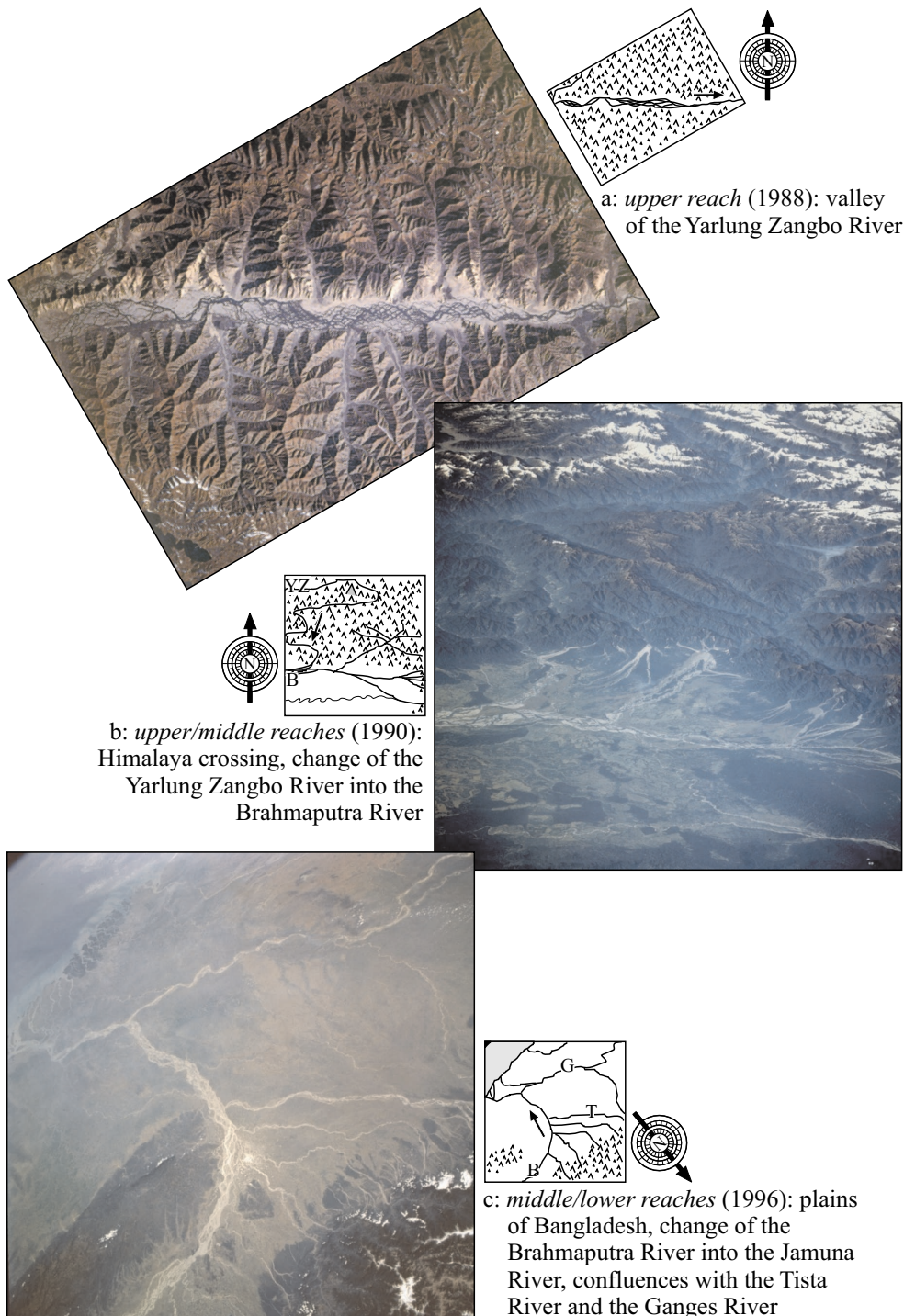


Figure 2.5: Photographs of the Tsangpo/Brahmaputra/Jamuna River taken during various space shuttle missions by NASA (1988, 1990, 1996).

2.1.3 The lower reaches (Bangladesh)

On the Bengal plains the gradients are small and relatively minor changes in land elevation are sufficient to cause dramatic changes in the river course. Natural causes for such changes can be tectonic movements, severe floods caused by tropical monsoons, and extreme sediment loads. The long-term patterns of river migration indicate that the Ganges River has been migrating eastward, whereas the preferred migration of the Jamuna River is westward. Prior to the 16th century most of the flow of the Ganges River discharged directly into the Bay of Bengal near Calcutta. The geomorphic map published by Coleman (1969), shown in Figure 2.6, illustrates the dynamic history of the central Bengal region. Holocene alluvial deposits cover the region except for three areas:

- The *Madhupur* lies on the eastern side of the Jamuna River. From its highest point (21 m above sea level) at the north-west corner the surface dips east and south and finally passes beneath the flood plain deposits of the Meghna River. The surface of the terrace is dissected and elevation differences in the order of 10 m are common.
- The *Barind* lies on the western side of the Jamuna River. Its tilting is similar to the tilting of the Madhupur with a maximum elevation of 30 m in the north.
- The *Tippera* surface covers the area around the confluence of the Upper Meghna River and Padma River. It is of unknown date with sediments that are not as deeply weathered as the Pleistocene sediments of the Madhupur and Barind, but with extensive human modification for agriculture.

The oldest known maps with an accurate indication of the river courses date back to about 1785. These maps, which were made by Major James Rennell, show the Brahmaputra River following the course currently taken by the Old Brahmaputra River.¹ Buchanan Hamilton remarked in 1810 that the Brahmaputra River threatened to shift its course to the course of the Jennai/Konnai River. By 1836 it had shifted and the Jamuna River was formed. During the first decades it was flowing as a meandering stream with a wavelength of approximately 11 km (Fergusson, 1863). These changes led to the following statement by Fergusson (1863) when he addressed the Geological Society in London:

“It may also be mentioned that the city of Sirajgange — the largest and most important mart in that part of the country — is somewhere in that neighbourhood now, but not where marked on the map, of course, as it is annually obliged to accommodate itself to the vagaries of the stream, and changes its locality. It may be ten miles further up the stream, or ten miles further down, or five miles further east or west; but it is somewhere thereabout; and that is all the information geographers can hope for in a country where land can only be classed with floating capital.”

The cause of the major shift of the river is not known, but at about the same time other changes occurred. When surveyed by Major Rennell, the Tista River took a course due south

¹Even at that time, the combined flow of the Brahmaputra River and the Meghna River downstream of their confluence in east Bengal, was known under the name of the smaller Meghna River. According to Fergusson (1863) this could indicate that the Brahmaputra River had only shifted its course towards the Meghna River after the land had been settled. This would imply that the Brahmaputra had shifted its course significantly at least once before. This is also suggested by Umitsu (1993).

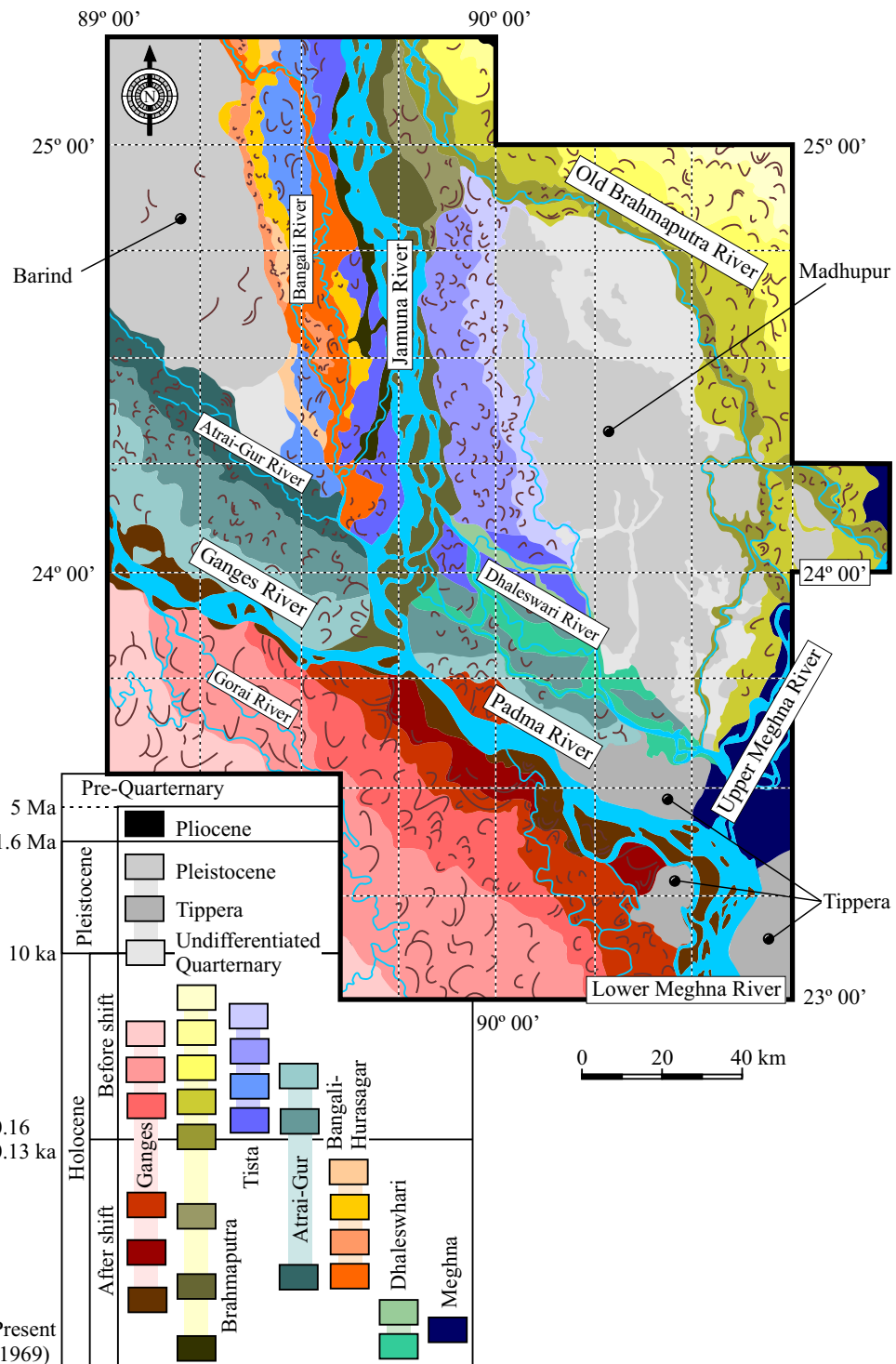


Figure 2.6: Geomorphic map after Coleman (1969).

and joined the Atrai River on its course to the Ganges River. During a flood a few years later, a large amount of debris dammed its junction with the Atrai River, deflecting the flow in south-east direction towards the Brahmaputra River. It might have followed that same course before since the downstream part of it was already indicated on Major Rennell's maps as 'Teesta Creek'. The capturing of the Tista River or even the Tsangpo River has been proposed as a possible cause for the major shift of the river (LaTouche, 1910), alternatively both changes may be attributed to tectonic tilting (Fergusson, 1863; Hirst, 1916; Morgan and McInitire, 1959).² C. R. Thorne (FAP21/22, 2001) has argued that backwater effects caused by the building of an alluvial fan in the Sylhet basin (at the eastern side of the Madhupur) may have had more impact than the tectonical processes.

With an increased discharge and a heavy silt load (resulting in part from the capture of the Tista River as a tributary), the Jamuna River gradually changed from meandering to a braided channel such as exists now (see Figure 2.5c). In the meantime the river has widened and shifted to the west, a trend that seems to continue until this day. It must be recognised, however, that a catastrophic event, such as an earthquake, could completely alter such present-day trends as it did before.

2.2 Main characteristics

A large amount of data on the Bengal rivers has been obtained by international research in particular during the River Survey Project (1996), also indicated as FAP24. The data set contains daily water level records, regular cross-section surveys, and several special bathymetric and hydrodynamic surveys at a number of interesting locations. The results of all FAP24 measurements on the Bengal rivers are published in the final report, its five annexes, twenty-four special reports and twenty compact discs of data. See Table A.1 in the appendix for an overview of the topics addressed by the various reports. The following subsections describe the river characteristics on the scale of the river. Some characteristics of the river on the channel scale, such as observations on bedforms, sediment transport and individual planform changes, are addressed in Chapter 3.

2.2.1 Hydrodynamics

The average annual flood of the Jamuna River is about 60,000 m³/s, and the discharge during low flow lies between 4,000 and 12,000 m³/s; the water level slope gradually decreases from 10 cm/km at the Indian border to 6 cm/km near the confluence with the Ganges River with a mean of 7 cm/km. The slopes of the other major Bengal rivers are even smaller (Ganges River 5.5 cm/km, Padma River 4 cm/km, and Upper Meghna River 2 cm/km and decreasing³) in agreement with the observation that braided rivers have a steeper gradient than meandering rivers (Leopold and Wolman, 1957). The Jamuna River is up to 20 m deep in the large

²The large earthquakes of 1762, 1775 and 1812 (Morgan and McInitire, 1959) may have played a role either by gradually releasing some tension by increased tilting or by (temporarily) blocking a river's course resulting in a redirection or accumulation of water which may upon release may have caused a shift.

³The Upper Meghna River is still adjusting to the decrease in discharge that was caused by the formation of the Jamuna River (currently it only takes the flow of the Kushiara and the Surma Rivers and some rivers draining the Shilong Hills) and little sediment is transported downstream due to the high subsidence rate of the Sylhet depression.

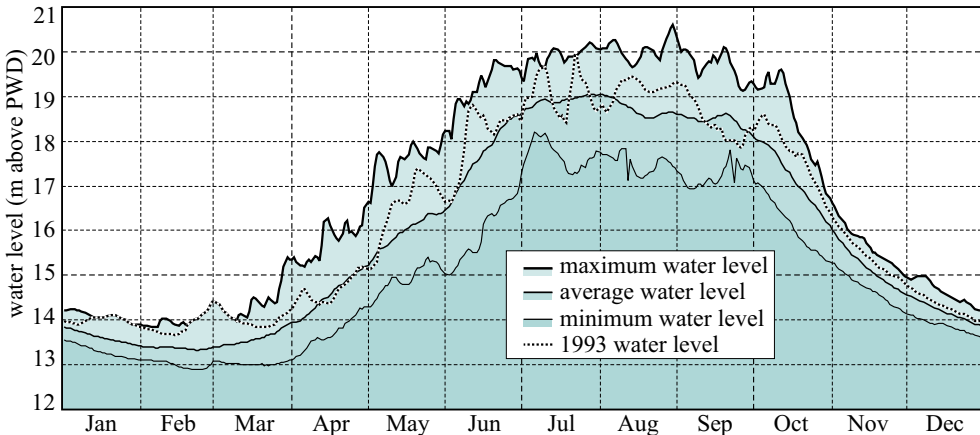


Figure 2.7: Water level variation in metres above PWD at Bahadurabad. Minimum, average, maximum over the period 1963–1995 (excluding April 1971–March 1972) and the hydrograph of 1993 are indicated.

channels, and local scour holes may reach depths of up to 45 m. Depth-averaged velocities of 3 m/s are commonly observed during flood (FAP24, 1994).

The major part of the discharge of the Jamuna River results from snow melt, but rainfall in Assam and in the northern part of Bangladesh contributes significantly. An almost continuous set of daily water level records since 1964 is available for the gauging station at Bahadurabad from the Bangladesh Water Development Board. The yearly hydrograph at Bahadurabad is shown in Figure 2.7. The water level rises rather abruptly during April–June, fluctuates slightly during the next three months, and falls rapidly during October–November. Several discharge peaks can often be observed due to the dependence on rainfall and the distribution of the tributaries along the river in Assam and Tibet. The relative timing of the floods of the Jamuna and Ganges Rivers at their confluence has significant influence on the extent of the flooding and the local morphological changes. For instance the extreme flooding of 1988 was partly caused by the concurrence of the flood peaks of the Jamuna and Ganges Rivers (Thorne *et al.*, 1993).

2.2.2 General morphology

Although most of the flood plain sediments along the Jamuna River have been deposited by other rivers (before the major diversion early in the 19th century), their composition is similar to the sediment transported by the Jamuna River today. It mainly consists of fine sands and a generally small percentage of silt/clay which is characteristic for the very young and unweathered sedimentary rocks that make up the drainage basin of the Brahmaputra River. The banks are in general made of 85% sand and 15% silt (diameter less than 0.063 mm) except for localised deposits that contain up to 55% silt and 35% clay. The sand fraction consists of 44% quartz, 18% rock fragments, 18% mica, 12% heavy minerals, and 8% feldspar (Annex 4 of River Survey Project (1996)). The bed material fines in downstream direction from 0.25 mm near the Indian border to 0.16 mm at the confluence with the Ganges River which transports a slightly finer load (see Table 2.1). The major part of the downstream fining

River	Gauging station	D_{16}	D_{35}	D_{50}	D_{84}	D_{90}
Jamuna	Bahadurabad	0.13	0.16	0.22	0.29	0.34
Ganges	Hardinge Bridge	0.10	0.12	0.15	0.18	0.21
Padma	Baruria	0.10	0.12	0.14	0.18	0.22

Table 2.1: Grain size (mm) of bed material collected in 1993–1994 by FAP24 (1996)

is probably the result of abrasion of the relatively soft mica particles of which a large amount originates from the Tista River (FAP24, 1996). Borings done within the framework of the River Survey Project have indicated that at least down to 40 m the sediments are similar to the sediments typical of the present-day Jamuna River. The sediment in the Old Brahmaputra River, however, is in general finer than the sediment in the Jamuna River near its offtake (D_{50} is 0.16 mm); downstream of Mymensingh the river crosses a coarse reach in which the mean diameter increases up to 0.25 mm.

The combined Bengal Basin rivers transport 13 million tons of sediment *a day* during flood conditions, and a total of approximately 1 milliard tons per year.⁴ Each year the floods inundate vast areas of Bangladesh, leaving behind about the half of this volume of sediment. The lightest sediment particles — clay and fine silt — are deposited on the flood plains as a thin layer of on average about 1 cm thick; the coarser materials — fine sands and silts — are predominantly deposited as crevasse splays adjacent to the river channel forming natural levees. This sedimentation compensates the high subsidence rate of Bangladesh, thereby keeping the river courses and the Bengal coastline relatively stable. The development of the Bengal Delta over the last 18000 yrs is sketched in Figure 2.8. During this period, the Brahmaputra River has switched its course several times between its present course and the pre-1800 course (see Section 2.1.3). According Allison (1998), 21% of the annual sediment budget (mostly sand and silt) is deposited at the river mouth, thereby enlarging the subaerial delta with an average of 4–7 km² of new land over the last 150–200 years. Another 12.5% (mud) is deposited further seaward as a subaqueous mud delta. Whereas the delta extends in the eastern part, the shoreline and shallow offshore areas of the western front are in a net erosional state (Allison, 1998). Net sediment transport along the coast is in westward direction for about 100 km, from where the sediment is transported via the ‘Swatch of No Ground’ (a large submarine canyon) to the Bengal fan in the deeper parts of the Indian Ocean (Coleman, 1969; Kuehl *et al.*, 1989; Goodbred and Kuehl, 2000b).

The levees consist almost entirely of overlapping crevasse-splay deposits of fine sands (up to 3 m thick) interlaced with thin layers of silt and clay. The fine sand crevasse-splays are deposited during flood when water and sediment leaves the main channel via overbank flow. Coleman (1969) observed that there is a slight change in the type of overbank flow along the Jamuna River from well separated channelised flows in the upstream area to more closely spaced broader flows in the downstream area. As the flood recedes a thin layer of silt and clay is left behind. Quite often, local rice farmers rapidly cultivate this bare land, and within a year the crevasse splays are hard to detect on aerial photographs because of cultural modification. The high sediment load of the Jamuna River not only leaves its traces on the flood plain, but it also causes the rapid planform changes of the river.

⁴Estimates based on ^{14}C dating deltaic deposits indicate that the sediment supply has been at least 2.3 milliard tons per year during the early Holocene (7–11 ka before present). A difference in climate (a stronger than present southwest monsoon in South Asia) has been proposed as the reason for the higher sediment load by Goodbred and Kuehl (2000a).

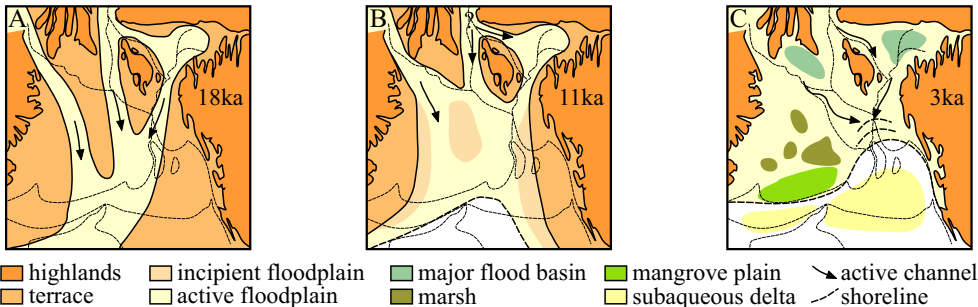


Figure 2.8: Development of the Bengal Delta from (A: 18000 yr BP) a system with incised alluvial valleys via (B: 11000 yr BP) a phase of delta growth initiated by global sea level rise to (C: 3000 yr BP) the modern system with an extensive subaqueous delta (Goodbred and Kuehl, 2000b).

Sedimentation does not only occur outside the rivers on the flood plain, but also inside the channels. The backwater effect of flood of the Jamuna River causes sedimentation in the Ganges River just upstream of their confluence (Fergusson, 1863) during the first month of the floods. The Ganges River normally reaches its maximum discharge at the end of August or the beginning of September after the main peak of the Jamuna River, its flood clears out most of the deposited sediments. When the third flood peak of the Jamuna River is low or late, deposition can be expected in the lower reaches of the Jamuna River near Aricha (Coleman, 1969).

2.2.3 Planform and bed topography

Tracking planform changes in detail for a dynamic river like the Jamuna River is a challenging task (see Figure 2.10). The size of the Jamuna River and the extent of the surrounding flood plain make field surveys very time consuming. Therefore, whenever a field survey is carried out, only a limited area is covered. The development of remote sensing techniques has, on the other hand, made it possible to obtain relatively detailed data by means of contemporary remote sensing satellite systems because of the size of this river. The resolution of satellite images — and thereby the level of detail that can be obtained from them — varies among the various satellite systems. The most commonly used images, from the SPOT and Landsat TM satellites, have resolutions of approximately 15 and 30 m, respectively. The resolution of the slightly older Landsat MSS images is about 80 m, while MOS images have a resolution of 50 m. The satellite image sensors collect data in the infra red and visible part of the spectrum.

Based on different combinations of signal strengths over the detection bands, different types of landuse can be detected. Classifications made by the National Aerospace Laboratory (NLR) in cooperation with WL | Delft Hydraulics distinguished four classes: water, sand, vegetated and other. These classes are indicated by black, white, light grey, and dark grey pixels, respectively, in Figure 2.9 for the area near Bahadurabad. Both gradual and sudden shifting of the thalweg can be observed in these images; the bend in the eastern channel, for example, increases gradually in size over the period 1990 until 1993 (gradual shift) resulting in the subsequent cutoff during the flood period in 1993 (sudden shift).

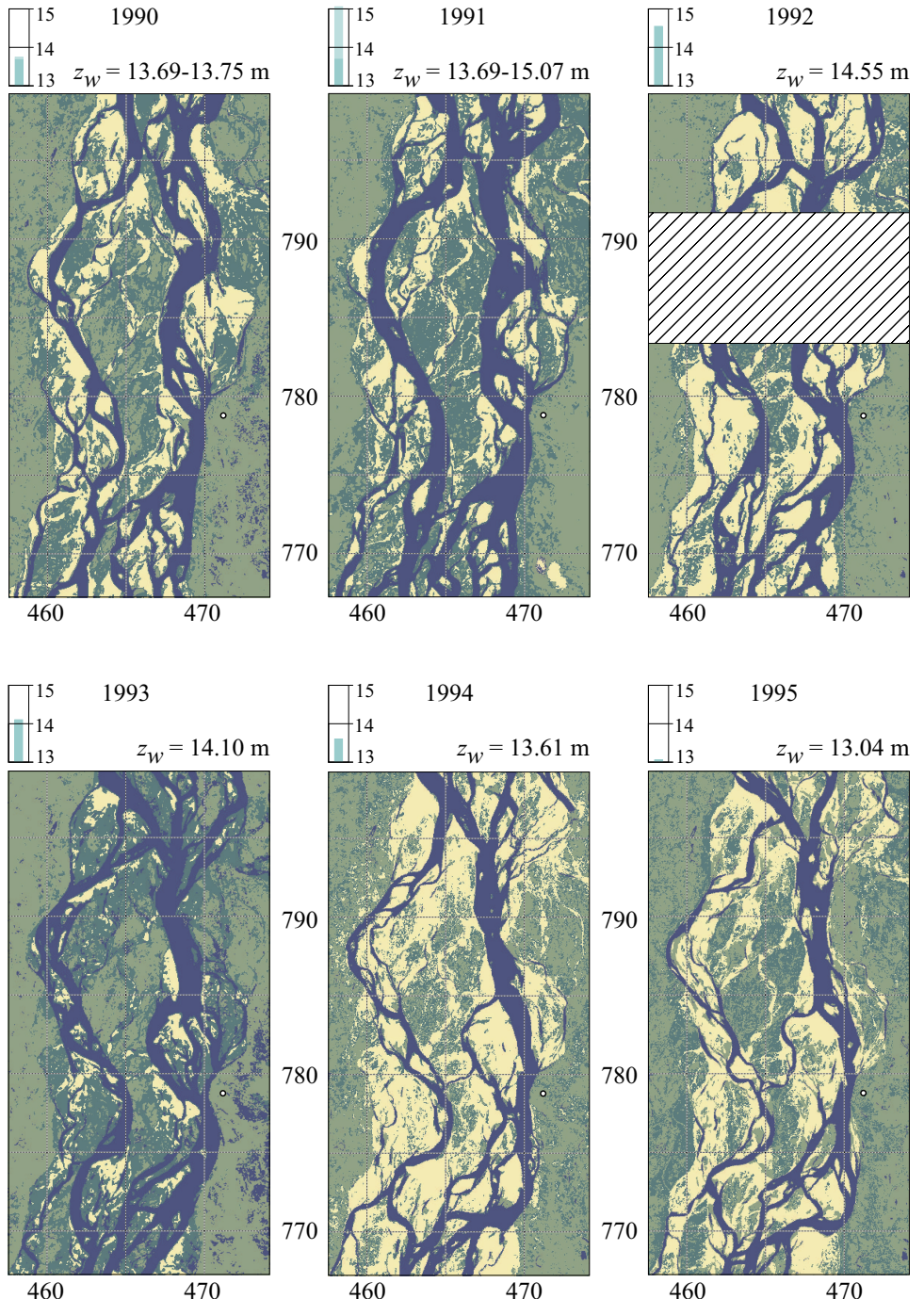


Figure 2.9: Low-stage planforms near (and associated water level range z_w at) Bahadurabad derived from satellite data 1990–1995. The images were taken during the dry season (i.e. November–March) preceding the flood period of the indicated year.

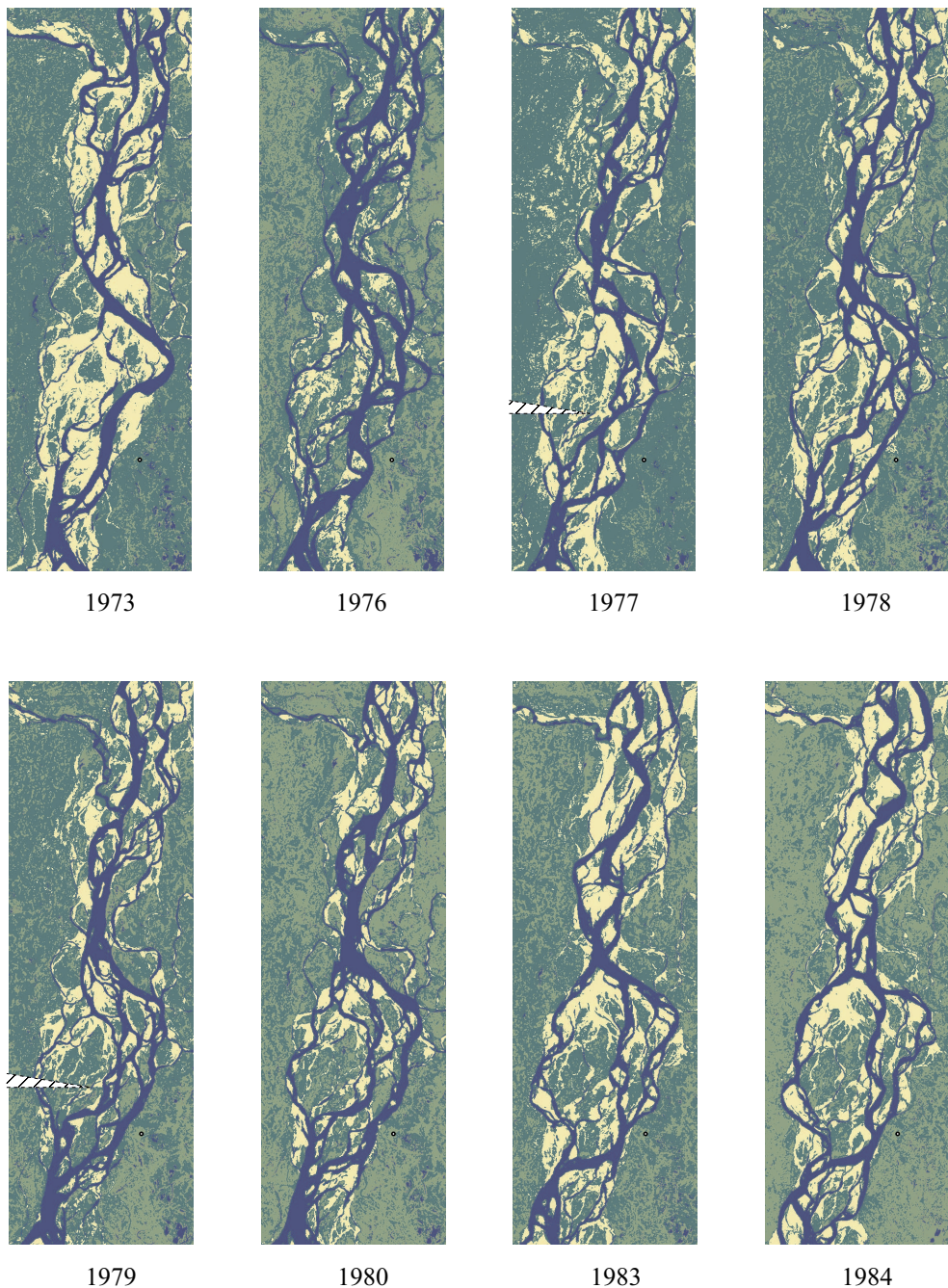


Figure 2.10: Low-stage planforms of the Jamuna River derived from satellite data 1973–1995. Flow from top to bottom. Continued on next page.

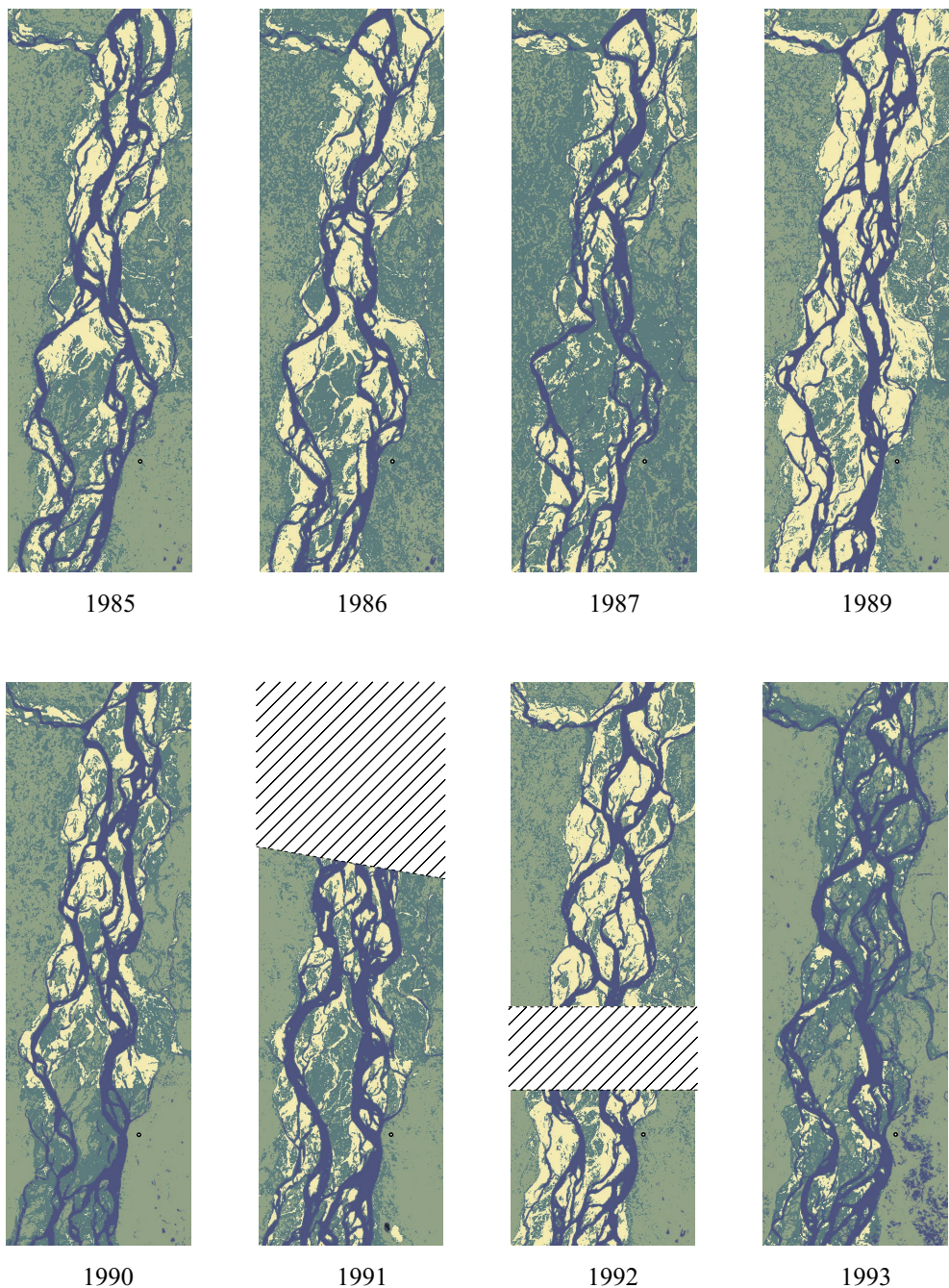


Figure 2.10 continued: Hatched areas indicate missing data.

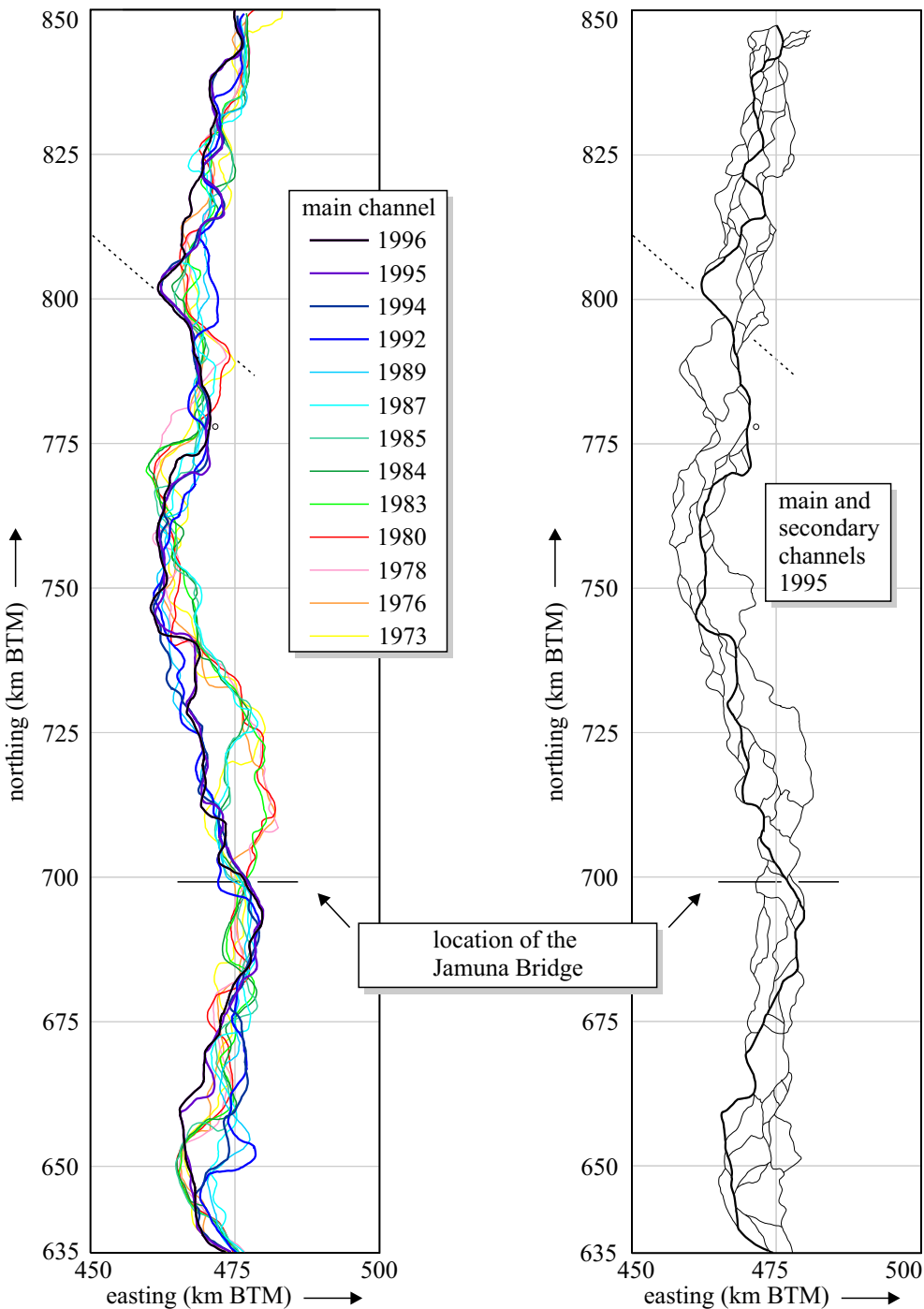
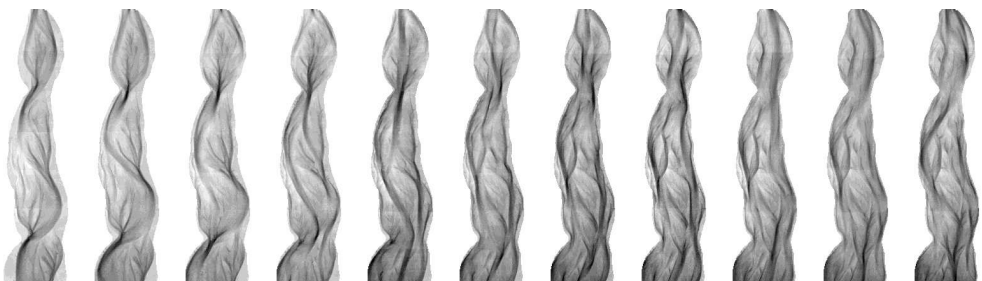


Figure 2.11: In the left axes the movement of the main channel is indicated for the period 1973–1995. In the right axes the planform in 1995 is shown. The channel centreline data was digitised by EGIS (1997) from low-stage satellite images.

For further analysis of the planform changes, EGIS (1997) digitised the channel centrelines from satellite images for 13 years between 1973 and 1995; the result of 1995 is shown on the right hand side in Figure 2.11. They have distinguished one main branch (in general the widest) and several secondary branches. An overlay of the main branches of the all available years is shown on the left hand side of the figure. One should note that some lines are regularly revisited; in particular the northwest-southeast line at northing 790 is remarkable. At that location the main branches of 1973, 1978 and 1980 (flowing out to the southeast) are in almost perfect alignment with the main branches of 1994, 1995 and 1996 (coming in from the northwest). The underlying cause may be related to tectonic influence; there are more of such indications as Mosselman *et al.* (1995) showed. At other locations the main channel seems to be able to shift its direction but not its location (for instance at the Jamuna Bridge site). These locations, generally referred to as stable or nodal points of the braided planform, are sometimes characterised by a different composition of the bank material resulting in smaller erodibility. Although the migration rate may be reduced locally, these ‘stable points’ have shown to be transient on longer time scales. Satellite imaging systems are very useful for quickly determining landuse and channel planform over vast areas, but accurate elevation data are less easily obtained by remote sensing techniques. Traditional field surveying techniques are, although very time consuming, often still the best source for elevation data. Remote sensing methods for obtaining elevation data are (Klees *et al.*, 1997a,b)

- *Stereo photogrammetry.* This technique derives the elevation data from relative shifts in the position of objects in a pair of aerial photographs or satellite images from two sufficiently separated viewpoints. The accuracy of the elevation data is between 10 and 60 m when using satellite images and in the order of a few decimetre for aerial photographs. Two unclouded daytime images are required for this approach. This technique has been applied for data acquisition during flume experiments of braiding by Stojic *et al.* (1998) and Ashmore *et al.* (2000); some results are shown in Figure 2.12.
- *Radar interferometry.* This technique works by sending out a series of pulses and measuring the strength, time lag, frequency shift and phase shift of reflected signal. In the case of synthetic aperture radar (SAR) the frequency shift detected at various locations along the flight path is used to obtain a reasonable resolution in flight direction. The strength of the reflected signal can be used for landuse classification. Combining the phase shift data of two radar recordings of the same area taken from different observation angles results in an interference pattern, from which one can determine elevation differences with an accuracy of a few metres. The sensitivity for elevation differences



*Figure 2.12: Elevation data obtained from flume experiments by means of stereo photogrammetry (Ashmore *et al.*, 2000). Greyness indicates height (range approximately 50 mm); flow from top to bottom.*

can be improved by either using a large angle between the two recordings (although relatively steep changes in elevation and variations in reflectivity depending on viewing angle will increasingly complicate the derivation of elevation data), or by combining multiple interference patterns, requiring more recordings. *Changes* in elevation can, however, be detected with a far greater precision by combining the time lag data of the two data sets mentioned above into an interference pattern similar to that of the phase. Detection of elevation changes of 2.8 cm are possible with the current ERS-1 and ERS-2 satellites (Klees *et al.*, 1997a). This approach is relatively insensitive to weather conditions; it works under both clouded and unclouded conditions.

- **Laser altimetry.** This technique is based on measuring the time lag and scatter of reflected laser pulses. The elevation can be derived from the time lag data; the scatter in the reflected signal gives an indication of the local vegetation. The accuracy of this relatively new method lies between 0.1 and 1 m. The width of the track scanned during one passage of the satellite or plane is just 0.5–1 km, requiring a large number of tracks to cover a large region. Unclouded weather (up to flight height) is required for this approach.

A completely different way of obtaining elevation data has recently been used by EGIS (1997). Based on satellite images, they distinguished three types of landuse: water, sand, and other land. Sand pixels correspond in the densely populated Bangladesh to recently deposited (low lying) sand flats. The average elevation of sand covered areas was — based on elevation data obtained from cross-section surveys at several locations along the Jamuna River — determined to be 3.5 ± 1.0 m above SLW. For the other land areas the elevation was correlated to the uninterrupted period that the area had been classified as ‘other land’ immediately preceding the date at which the latest satellite images and elevation data were obtained.⁵ They found the following relation between the average elevation in metres above SLW and the land age in years

$$\text{elevation} = 5.6 - 1.9e^{-\text{age}/3} \quad (2.1)$$

which is also plotted in Figure 2.13. This relation predicted three quarters of the calibration set within 1 m of the measured height. Using this relation a DEM (digital elevation model) was created for the flood plains in 1994 from which subsequently the planforms at various characteristic discharges were determined (see Figure 2.14).

Elevation data obtained in this way can also be used as a rough estimate of the initial condition for a two-dimensional computer model (dry areas only). One problem associated with this approach occurs whenever a water area is bordered by a sand area. On the boundary between these areas (which will in general occur at a subpixel level) pixels will have a characteristic spectral distribution in between those of pure ‘water’ and ‘sand’ pixels, often leading to the incorrect classification of those pixels as (young) ‘other land’. This classification error leads to the occurrence of small spurious dikes along the low stage channels in the DEM.⁶ This is one case in which the conventional *hard* classification, i.e. each pixel is assigned to exactly

⁵One should note that from this definition of age, it follows that even a classification as ‘sand’ resets the counting of the years.

⁶This problem becomes even more pronounced due to the rapid cultivation of emerged land along the Jamuna River in October/November shortly after the flood period. In this case the classification as ‘other land’ (in the sense of ‘not sand’) is basically correct, but the actual elevation of the land differs little from that of the surrounding sand covered areas in contrast to the abrupt change in elevation that may be derived from the change in classification.

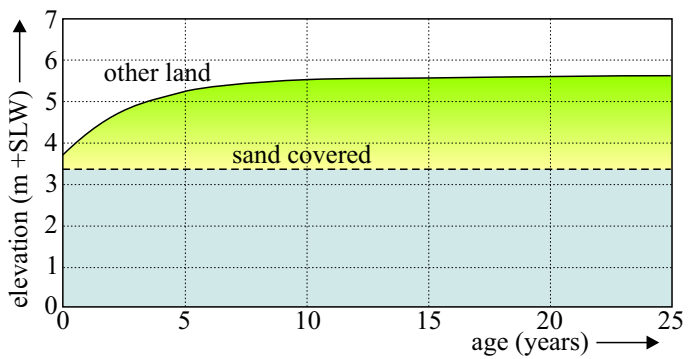


Figure 2.13: Relation between the elevation and the age of the land along the Jamuna River according to EGIS (1997).

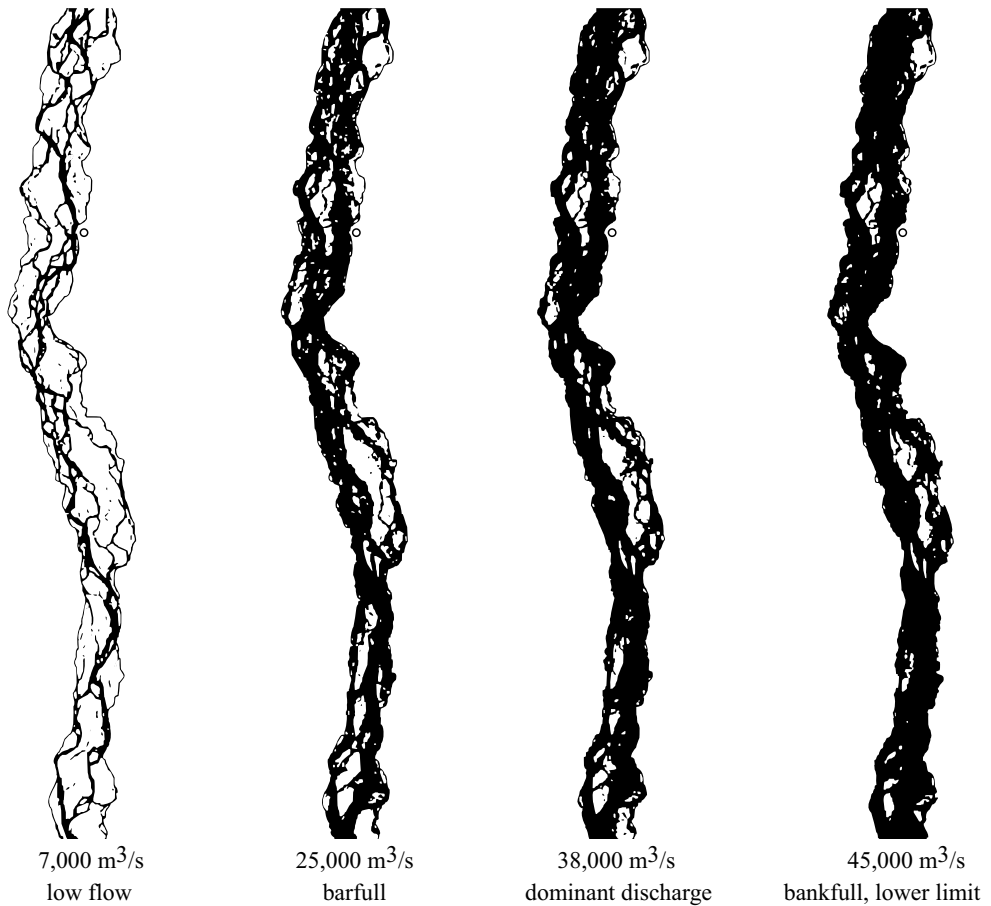


Figure 2.14: Low flow, barfull, dominant, and minimum bankfull as defined by FAP1 and FAP24 for the Jamuna River at the beginning of 1994. The planforms have been constructed by EGIS (1997) using low-stage satellite images and field data by the River Survey Project (1996).

one class, is not the best choice. *Fuzzy* classification (Foody, 1996) does not force a pixel to be a member of just one class. If, for example, a pixel corresponds to a ground area that covers for fifty percent water and fifty percent sand, a fuzzy classification algorithm can assign it for a factor 0.5 to water and for the same amount to sand. For pixels on the edge of a channel the assigned water area will neighbour the channel pixels and can as such be used to improve the estimation of the channel width and local terrain elevation.

The remote sensing methods described above may give sufficient information about the elevation of the flood plains surrounding the river, but the bed of the low stage channels cannot be determined by any of these methods. Within the framework of the River Survey Project several bathymetric surveys were carried out at various discharges. The bed of the eastern channel near Bahadurabad was surveyed seven times over the period 1993–1995 (see Figure 2.15) during both dry (water level still 3.5 m above SLW) and flood seasons. Due to limitations of the measurement technique the bed topography was obtained only for areas where the water depth was at least 2.5 m. These data can be used as input for a local two-dimensional model, although one should keep in mind that near the banklines significant errors may be introduced due to the lack of data. Unfortunately, the topography of the islands and the surrounding flood plain was not surveyed during the measurement campaigns at low stages. That would have given a more complete picture of the planform throughout the period and it could have filled in the gap in the data in areas where the flooding depth remains below the sensory threshold of 2.5 m.

At 1 m+SLW a contour is indicated for all seven bathymetries using a thin line. Note that at northing 785, in the upper half of the August 1993 image, the entrance to the right branch — which was still the major branch in June — is raised above the 1 m+SLW level. During the remaining part, probably during the falling of the flood, the entrance of the branch is eroded and in the low stage image of November 1993 the branch is open again; although it was at that time no longer the major branch. A similar situation occurred on a smaller scale at northing 777 in the lower part of the July 1995 image, where the channel bottom of the small branch connecting the left and right branches is temporarily raised during flood.

Even during bathymetric surveys of relatively small areas, significant morphological changes can be expected. The bed topography of July 1995 (an area of just over 90 km²) was for example obtained by a surveying campaign of three weeks (from July 4th until July 25th) using three boats — one from northing 790 to 782, one from 782 to 775, and one from 775 to 770. The sharp transitions in bed levels at northings 775 and 782 result from morphological development during the measurement period. Therefore, surveys requiring periods longer than a few days (maybe even hours) during rising and falling stage might be influenced by migrating bedforms and must be considered with the utmost care.

2.3 Summary

The Jamuna River is a large sand-bed braided river in Bangladesh. Along the course of the whole river from Tibet to Bangladesh, it is significantly influenced by tectonics. The relative movement of the various segments of the earth's crust clearly influences the channel planform in the upper reaches. Earthquakes may cause sudden planform changes resulting in a temporary increase in the channel dynamics moving in downstream direction through the river system during the following years. In the middle and lower reaches the alluvial deposits

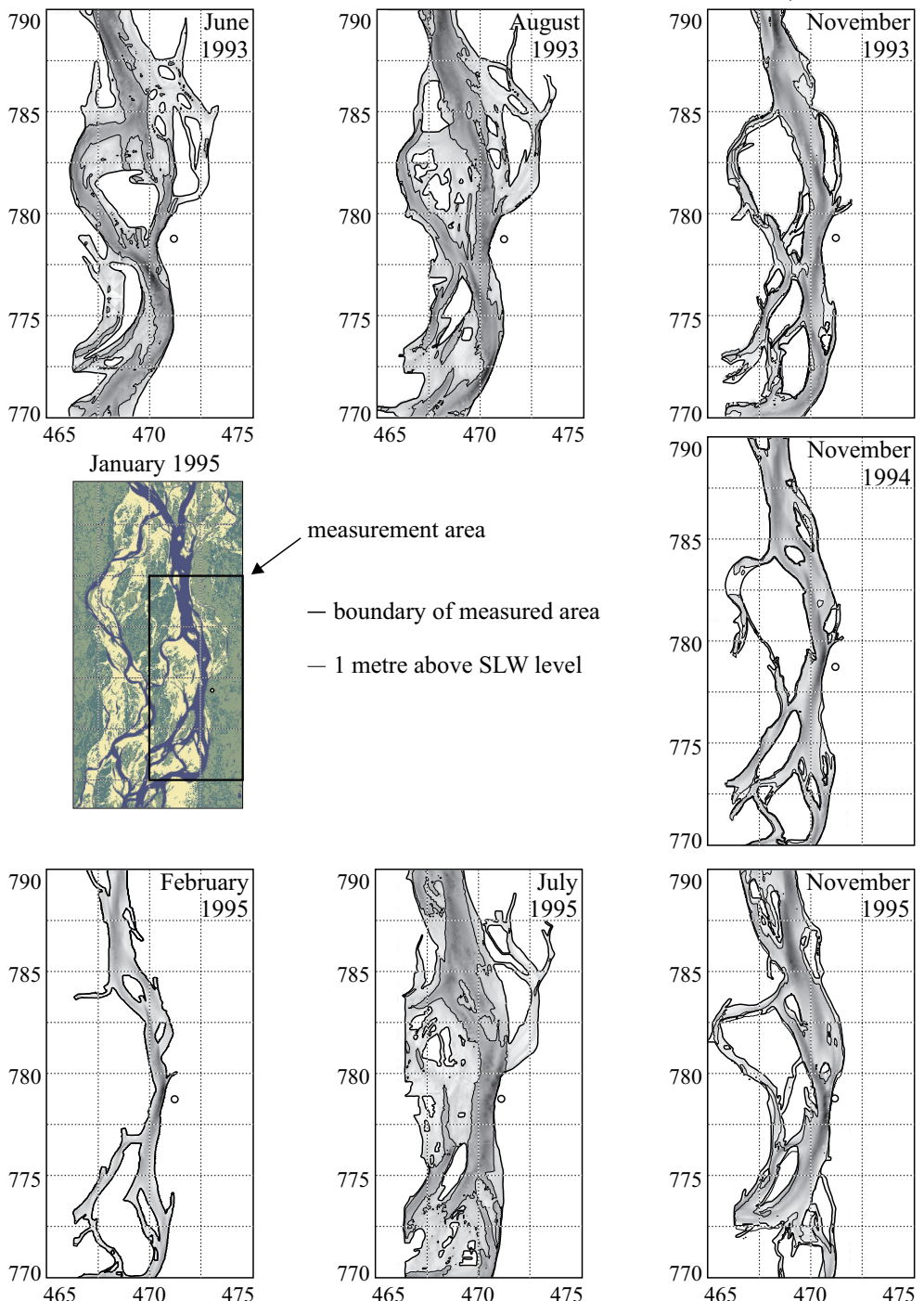


Figure 2.15: Bathymetric maps of the channels near Bahadurabad based on data obtained by River Survey Project (1996).

are much thicker than in the upper reaches and the tectonic influence is less obvious. It reveals itself through the dramatic shift in the course of the river across the Bengal plains in recent history, the alignment of individual braid channels with faultlines and channel realignments triggered by tectonic influences on the reaches upstream (e.g. changes in sediment supply).

It is difficult to get a sufficient amount of useful data for analysis from field surveys because of the size of this river. Furthermore, the river is so dynamic that the collected data become rapidly outdated for prediction purposes by channel realignments under varying flow conditions. Remote sensing techniques help to keep track of planform changes and to study the behaviour of the river, but the data (derived from aerial photographs and satellite images) are limited in type and accuracy. Especially the lack of bathymetric data and the limited accuracy of elevation data significantly reduce the value of satellite images for modelling purposes. The analysis of the large scale dynamics captured in the satellite images requires a thorough understanding of the physical processes. For the build up of this understanding, repeated, accurately planned, large scale field surveys are extremely important.

Chapter 3

Braiding processes

The series of planforms of the Jamuna River shown in Figures 2.9 and 2.10 prove that the planform of a braided river can change drastically in a relatively short period. A closer inspection of the differences between two of these planforms, shown in Figure 3.1, indicates that six elementary planform changes can be distinguished: channel migration, channel width change, mid-channel bar growth, channel formation, channel abandonment and node deformation. This chapter describes the underlying physical processes and explains why these changes occur.

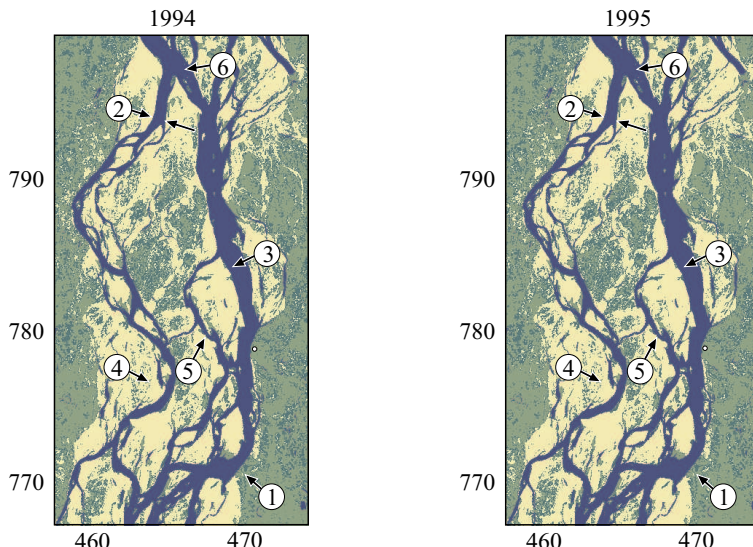


Figure 3.1: Six types of elementary planform changes identified: (1) channel migration, (2) channel width change, (3) mid-channel bar growth , (4) channel formation, (5) channel abandonment and (6) node deformation.

Although rivers flowing through endless lowlands are often considered to be symbols of everlasting tranquillity and slow change, the description of the Jamuna River in Chapter 2 shows that the evolution of lowland rivers can be quite dynamic with sometimes dramatic consequences. The dynamics of the river bed — and, therefore, of the complete river — is determined by the continuous interaction of water and sediment. Even though lowland rivers may give the impression of being a calm and slowly evolving system, the small-scale flow structure is turbulent. This turbulence influences the distribution of sediment throughout the flow. The larger-scale flow structures and the overall flow pattern of the river direct the sediment transport. The water motion indirectly affects via the sediment transport the shape of the river bed. The river bed itself, on the other hand, influences both the local and overall structure of the flow. This interaction between water motion and river bed on a range of spatial scales results in an always adjusting dynamic system of varying complexity and, to some extent, scale-invariant behaviour.

The term morphology generally refers to the study of shapes. In civil engineering and earth sciences, its meaning is usually narrowed down to the study of sedimentary shapes sculpted in the earth surface by water and wind motion and the processes involved in the self-adjusting nature of these shapes.¹ River morphodynamics addresses the evolution of these shapes in time ranging from the smallest scale (sediment particle size) to the largest scale (river basin scale). Within a river stretch, one can distinguish three types of morphological units: bedforms, bars, and islands. This section describes their occurrence in braided rivers, and the conditions under which they form. Braided rivers are, depending on the definition used (see Section 1.2), characterised by the presence of islands and/or braid bars. The addition ‘braid’ in case of the bars indicates that there are different kinds of bars. The most commonly distinguished bar types are addressed in Section 3.2. Bars are sometimes called macroforms; they may be formed by the remnants of bedforms (microforms and mesoforms) in an aggrading river reach. Eventually, braid bars may grow further and stabilise, in which case they become islands. This is, however, not the only way in which islands can be formed, as we will see in Section 3.3.1. Both sections describe the interaction of hydrodynamics and morphology on the scale considered (macro and mega, respectively). Although braiding is characterised by the large-scale interaction of bars and islands, its dynamics is determined by spatial variations in sediment transport. The general interaction of sediment transport, turbulence and bedforms (micro scale) is, therefore, described in Section 3.1 for reference.

The sources of uncertainty in theoretical and numerical models of the physical processes involved are considered in Section 3.4. Section 3.5 gives an overview of the results obtained from previous field studies, laboratory experiments, and theoretical studies on braiding processes. Finally, Section 3.6 describes six characteristic planform changes in braided rivers that have been distinguished on the basis of the results of these previous studies.

3.1 Micro-scale morphodynamics

Separate sediment particles combine under the influence of flowing water into bedforms which form patterns on the river bed (see Figures 3.2 and 3.3). Bedforms occur in a wide range of sizes, from small ripples and bedload sheets (in the order of a few centimetres thick)

¹The term morphology is also used for the momentary shape of the system.

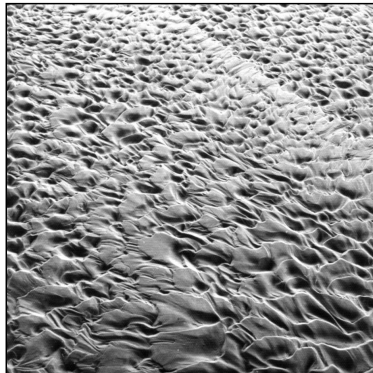


Figure 3.2: Ripples formed in a scale model. Source: photo archive of Jamuna Bridge Study, WL | Delft Hydraulics (1988–1990).

to large dunes (which, in a large river, can become several metres high). In general, bedforms are distinguished from bars by their scaling. Bedforms scale with characteristic turbulent length scales, which may vary from the thickness of the viscous sublayer near the bed (microforms) to the water depth (mesoforms); bars scale with the river or channel width (macroforms). Because the size of mesoforms depends on the water depth, and therefore on the discharge, no absolute size ranges can be given for specific mesoforms that are valid throughout the year, let alone for rivers of different magnitude.

3.1.1 The occurrence of bedforms

Which type of bedform is present in a river at a certain place and time depends — apart from the sediment type and the availability of sediment — on the local flow conditions in general and the bed-shear stress in particular (Van Rijn, 1993; Best, 1996). Up to flow velocities just above the threshold of motion, the sediment transport will be limited to a few grains transported as bedload; the bed will remain flat (lower plane bed). At somewhat higher velocities the sediment transport is intermittent and it induces (quasi-)periodic oscillations in the bed, which grow larger as velocity increases. These are ripples, bedload sheets and two- and three-dimensional dunes (see Figure 3.4). Particle (or pebble) clusters form instead of ripples if the sediment diameter is larger than about 0.7 mm. Dunes and bedload sheets² are formed at somewhat higher velocities (Best, 1996). These latter bedforms are just a few grain diameters thick but are of a significant horizontal extent. For all of these bedforms, the variation in the water level is out of phase with the oscillations in the river bed. The river is said to be in the lower flow regime.

At high flow velocities, the Froude number $Fr = u/\sqrt{gh}$ becomes important. The Froude number relates the relative velocity with which small disturbances in the water level move (being approximately \sqrt{gh}) to velocity u of the main current. As the Froude number increases, the interaction between water and sediment gradually changes. At a certain velocity — in the Jamuna River at depth-averaged velocities of 3 m/s or higher (FAP24, 1994) — the sediment is in continuous (mostly suspended) motion and the bedforms become longer,

²Bedload sheets form in poorly sorted coarse-grained sands (Best, 1996).

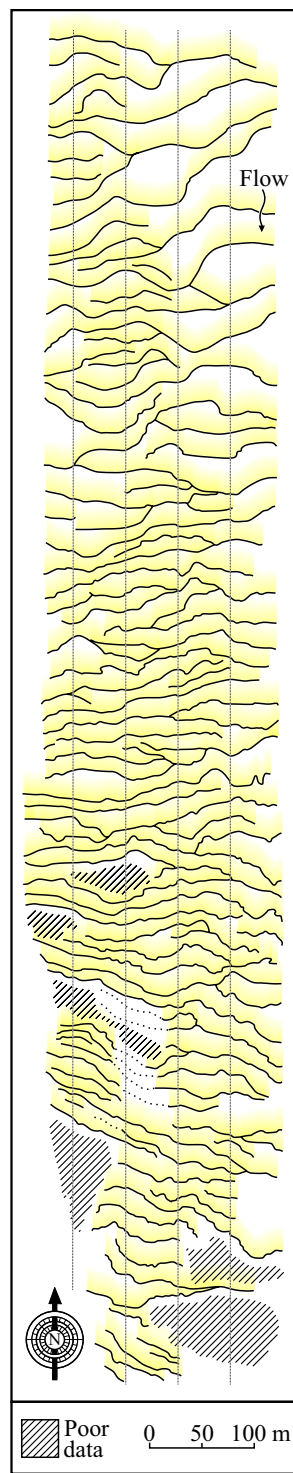


Figure 3.3: Dune crest pattern in the Jamuna River (FAP24, 1996).

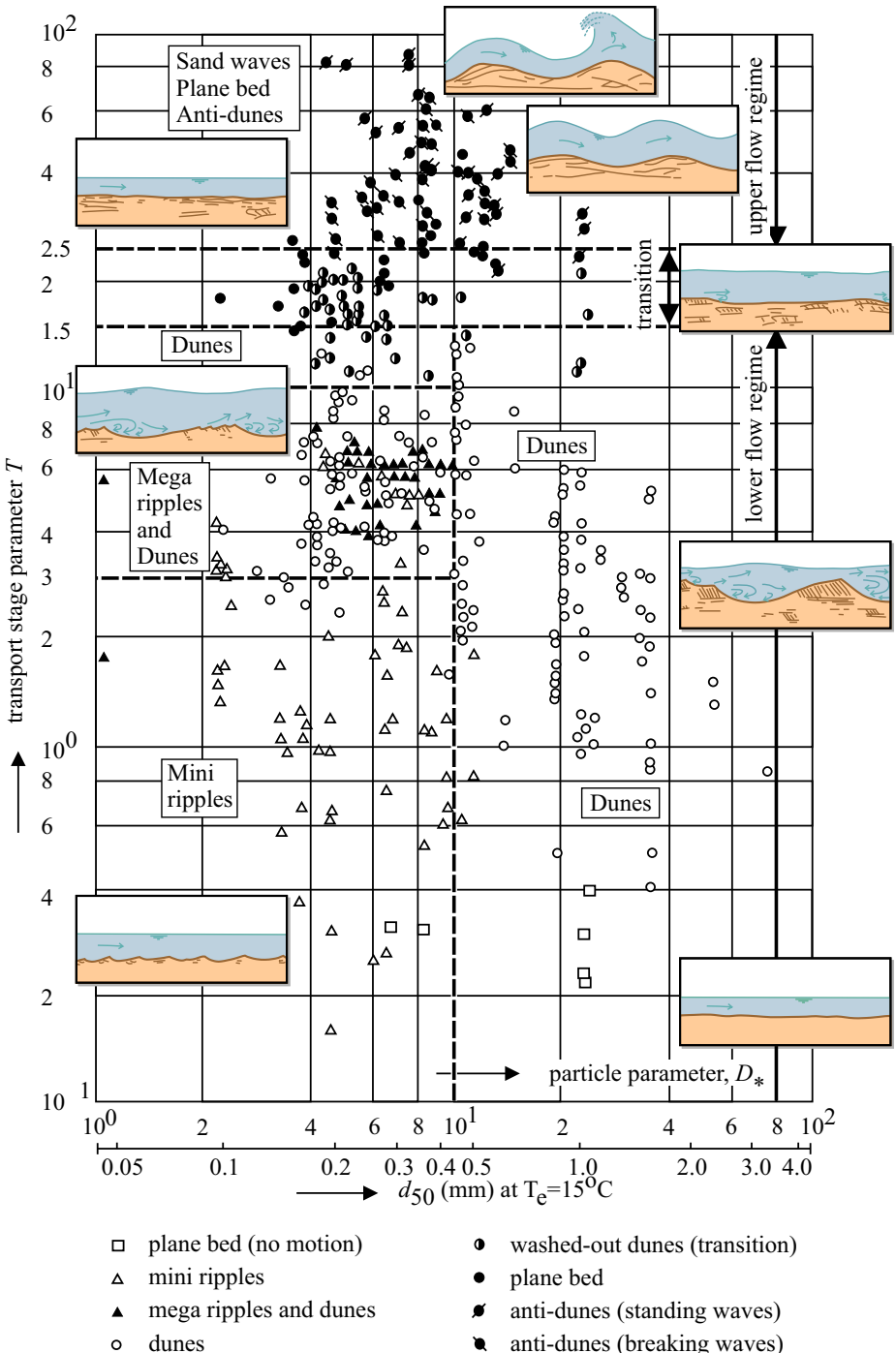


Figure 3.4: Bedform types after Simons and Richardson (1961) and conditions under which they occur according to Van Rijn (1984c, 1993). The transport stage parameter T is the grain-related excess bed-shear stress for currents $(\tau'_{b,c} - \tau_{b,cr})/\tau_{b,cr}$.

lower and more symmetrical, which results in a smoother bed (Van Rijn, 1993). This is the so-called upper plane bed or transitional phase. At still higher speeds, well defined bedforms (antidunes and transverse ribs) will form; the variations in the water level are now in phase with the oscillations in the bed (standing waves). The river is said to be in the upper flow regime. This happens when the Froude number approaches or exceeds one. At Froude numbers greater than one (rapid, supercritical flow), no disturbance can travel upstream and, thus, water movement is determined by the local and upstream channel shape (and bedforms) only. The Froude number at which the transition from lower to upper flow regime takes place depends on the sediment size. The transition starts in sand-bed rivers at Froude numbers of 0.2 to 0.4, depending on the size of the bed material (Simons and Simons, 1987). In the case of very coarse bed material and shallow streams, Froude numbers higher than one may be needed to exceed the threshold of motion and there will be no lower flow regime. Kennedy (1963) has theoretically proven that the Froude number must be at least 0.84 for antidunes to form.

In gravel-bed braided rivers and flume models (Boothroyd and Ashley, 1975; Church and Gilbert, 1975; Williams and Rust, 1969) often high flow velocities occur and bedforms associated with the upper flow regime are found. In sand-bed rivers like the Jamuna River, where the Froude number varies under normal conditions between 0.1 and 0.2 averaged over a cross-section (Klaassen, 1992), the lower flow regime is more important. The upper range of the average Froude numbers observed in the Jamuna River matches the lower bound for the transitional stage mentioned in the previous paragraph, such that the upper stage plane bed may form in the Jamuna River. Indeed, Coleman (1969) describes the overnight disappearance of all transverse bedforms in a channel of approximately fifteen metre depth as discharge increased, indicating a transition from the lower to the upper regime. Combined with the transition velocity of 3 m/s mentioned by FAP24 (1994), a Froude number of about 0.25 is obtained, which lies in the transition range mentioned in the previous paragraph. Recent investigations on the Jamuna River have indicated that Froude numbers higher than one are attained locally. This happens mainly during the falling stage when a relatively thin layer of water overflows a bar or island. Due to the fine sediment and the strongly increased sediment transport capacity, these areas of supercritical flow can only exist for periods of a few hours. After that time the erosion will have removed the cause of the supercriticality, or the water level has fallen so far, that the bar emerges (Van der Wal, 1998, pers. comm.).

3.1.2 The shape of bedforms

Ripples and dunes have in general an asymmetric shape with a gentle stoss (upstream) side and a steeper downstream face (or lee side). They both move downcurrent by the erosion of the stoss side and deposition on the lee side. Their dimensions can, however, be completely different, since ripples scale with the viscous sublayer (microforms) and dunes scale with the water depth³ (mesoforms). Within the FAP24 studies ripples are defined as asymmetric bedforms with height less than 5 cm and wavelength less than 60 cm. Dunes may on the other hand reach a height of about a quarter of the flow depth and a wavelength that is five to seven times the flow depth. If the water is deep enough, one often finds smaller dunes on the back of larger ones; such features are called ‘compound dunes’. Ripples are typically linguoid in plan shape, which is curved with its end points pointing upstream. Dunes are mostly barchan (also

³Based on measurements in the Jamuna River Coleman (1969), however, indicates that the dune height does not depend on the water depth, whereas dune length and rate of movement do.

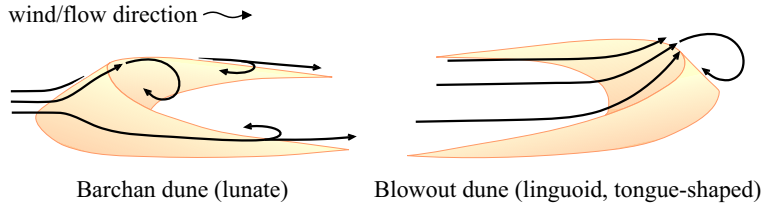


Figure 3.5: Flow over aeolian dunes (Press and Siever, 1994, after Bagnold, 1941).

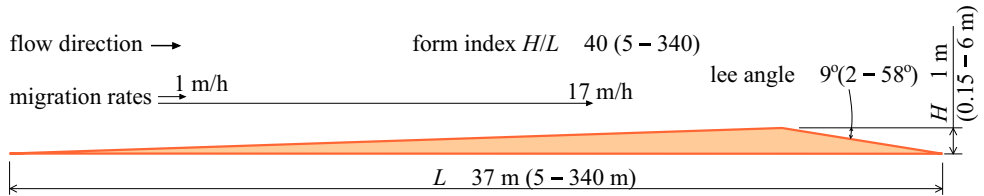


Figure 3.6: Minimum, maximum and average values for some dune properties in the Jamuna River (FAP24, 1996).

called lunate) in plan shape, that is curved with its end points pointing downstream (Fig. 3.5). Neighbouring dunes may melt together to form more or less straight-crested two-dimensional dunes spanning the major part of the channel width.

Dunes cover 40–95% of the bed of the Jamuna River at all times. Their height averages about 1 m and the average wavelength is about 37 m, the mean lee side angle is 9 degrees (see Figure 3.6). The mean lee side angle is much smaller than the characteristic angle for general dunes which is in the order of 30–45 degrees. Dune migration rates between 1 and 17 m/h have been observed in the Jamuna River. Within the category of dunes, sometimes, three further subgroups are distinguished, being — from small to large — megaripples, (normal) dunes, and megadunes or sandwaves. Coleman (1969) describes a sandwave near Aricha of 13 m high and 900 m wide which travelled over 600 m per day. Later studies (Klaassen *et al.*, 1988; River Survey Project, 1996) indicate that this morphological unit was probably an avalanche face of a moving (tributary) bar. Such a morphological unit may form when a large amount of sediment is eroded, for instance when a new channel is incised. The eroded sediment will be transported as bedload in the form of a straight-crested transverse bar or tongue-shaped linguoid bar (sometimes also called lobate transverse bar). Some authors tend to classify these solitary bedforms as bars whereas others classify them as dunes/sandwaves.

3.1.3 The effect of bedforms on the flow

The turbulence patterns and small-scale flow structures are largely determined by the effective roughness of the bed topography. The shear stress exerted on the flow by the alluvial river bed causes a characteristic logarithmic velocity profile, $u(z) = (u_*/\kappa) \ln(z/z_0)$, where u_* is the shear velocity, κ is the Von Kármán constant, z is the vertical coordinate relative to the bed, and z_0 is a measure for the height of the bedforms (Jansen, 1979). The *depth-averaged* flow velocity u is approximately equal to $C\sqrt{hi}$ where h equals the local water depth and

i is the slope. The Chézy value C represents the combination of particle roughness and form roughness. The form roughness may be split further into bedform roughness (bed friction) and, depending on the level of aggregation in the model, wall friction, bar, island and bend roughness.⁴ For wide, shallow channels the bedform (or alluvial) roughness is dominant.⁵ The roughness of the Jamuna River decreases from $C = 50 \text{ m}^{1/2}/\text{s}$ during low stage to $C = 70 \text{ m}^{1/2}/\text{s}$ (Enggrob and Tjerry, 1999) during flood. The width-averaged roughness may be as low as $C = 80–100 \text{ m}^{1/2}/\text{s}$ during flood (Klaassen *et al.*, 1988). Note that the Chézy value increases when the roughness decreases.

Even if the bed is fairly smooth, three-dimensional coherent structures form in the turbulent flow. It has been established that symmetric hairpin vortices (also known as arch or horseshoe vortices) and asymmetric hockey stick vortices play a central role in the turbulent dynamics in the near-wall regions (Smith, 1996; Rashidi, 1997). The downstream migration of a hairpin vortex may lead to unsteady separation of the boundary layer thereby bursting into the main flow. The ejected part of the boundary layer can roll up under the influence of the local shear stresses and form a secondary hairpin vortex (See Fig. 3.7). Concurrently the wall layer is replenished by a ‘sweep’ of faster moving fluid from immediately upstream. Multiple hairpin vortices may amalgamate to form larger structures which can eventually reach the surface (boils).

The presence of bedforms leads to the formation of preferred separation points and the turbulence patterns may become quasi-periodic in time and space. In recent years research has started to study the effect of these turbulent patterns on the sediment transport in two (Hansen *et al.*, 1994) and three dimensions (Blondeaux *et al.*, 1999). These studies illustrate the complexity of the fluid and sediment dynamics under idealised conditions (see Fig. 3.8).

In the lower regime turbulence and roughness will increase as the water depth and, therefore, all bedform dimensions increase.⁶ When during a prolonged period of high flow velocities a quasi-stable dune field forms, regularly spaced rows of boils transverse to the flow direction can be observed above these dunes. In the Jamuna River the average diameter of these boils is 15–45 m, while diameters of more than 200 m have been observed by Coleman (1969). When such a boil breaks the surface, the water level can be raised by more than 0.5 m. Boils are mostly observed some distance downstream of well developed dune crests. The boils result from the turbulent interaction between the water and large bedforms as described above (Jackson, 1976). Coleman (1969) observed two distinct types of boils.

- The first, and most common, type is characterised by an upwelling of water in the centre of the boil and flow towards the edges. In the area of rising water, many small boils (0.5–1 m in diameter) are present and sediment concentration is extreme ('cauliflower' type termed by Babakaiff and Hickin (1996)). These boils, which appear just for a period of 10–30 seconds, can be linked to an amalgamated group of turbulent bursts (See Fig. 3.7).
- The second type is characterised by a vortex structure, that is, a whirling flow from the outer edges to the centre; the sediment concentration is again highest where the water

⁴Other causes of energy loss (such as, weirs, vegetation and confluence mixing processes) may be represented by an increase of the effective roughness.

⁵Vegetation resistance is the main factor retarding the flow on the flood plains of natural, freely meandering rivers.

⁶In the transitional regime, the form index (or, aspect ratio) of the bedforms changes. Although the length of the bedforms still increases, the height remains more or less constant and the roughness and turbulence decrease.

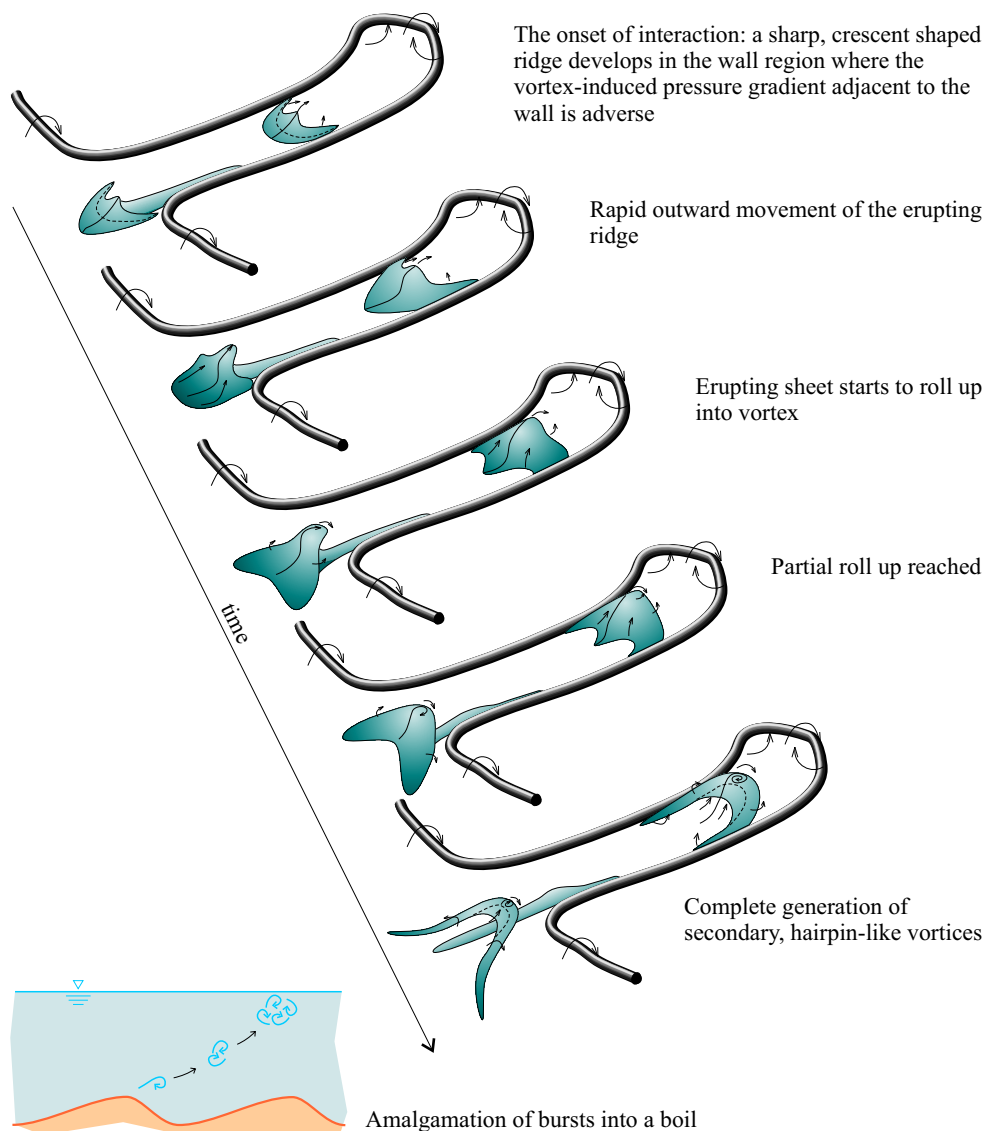


Figure 3.7: The generation of secondary vortices via boundary layer interaction for a symmetric hairpin vortex (Smith, 1996).

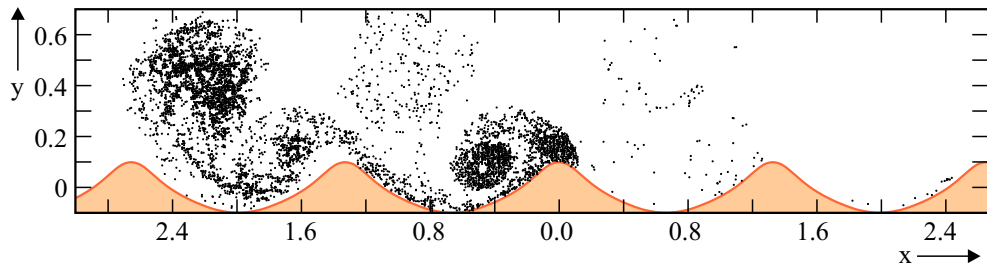


Figure 3.8: Side view of a 3D sediment distribution in an oscillating flow over a bed with symmetrical ripples at the time of flow reversal (Blondeaux et al., 1999). Sediment is released at the crest of the third ripple only ($x = 0$).

rises, which is in this case along the margins. These boils occur less often and are on average smaller than the boils of the first type; however, once formed, they exist longer — up to 50–60 seconds. Field observations indicate that they are associated with the occurrence of bedforms in very shallow water and the existence of large scour pools. Coleman (1969) observed that floating organic debris that disappeared in the centre of the boil, generally reappeared upstream from the cell after a few seconds. This suggests that this type of boil has an elongated curved shape under water, possibly related to one or more legs of horseshoe vortices reaching the water surface in the shallow flow.

Babakaiff and Hickin (1996) describe 'roller' type boils. These boils consist of an initial elongated (sediment rich) boil oriented transverse to the flow direction (with upstream upwelling and downstream downwelling) followed by the formation of two vortices at either end of the initial boil. This structure can be interpreted as a large horseshoe vortex (as sketched in Fig. 3.7) reaching the surface. The initial elongated boil corresponds to the surfacing of the head of the vortex. The two eddies can be associated with the legs of the vortex.

When at higher velocities during flood the transition stage is reached, the dunes disappear and the roughness reduces. The bed does not become completely flat but large, elongated scour holes form parallel to the flow (Coleman, 1969, Fig. 36). In this case also the pattern of turbulent cells becomes oriented parallel to the flow (Best, 1996).⁷ The associated alignment of boils in flow direction was found to be very common on large-scale aerial photographs, especially in narrow reaches where the flow velocity was large (Coleman, 1969, Fig. 37).

3.1.4 Sediment transport

A current flowing over a bed of non-cohesive sediment (i.e., sand or gravel) induces — when its speed exceeds the threshold of motion — sediment transport. The sediment can be transported near the bed as bedload or higher in the water column as suspended load. The type of transport depends on the sediment characteristics and the flow conditions. Shields (1936) has specified a relation between the critical dimensionless shear stress and the particle Reynolds

⁷The same alignment of turbulent cells can also be caused by a wind blowing in (or opposite to) the flow direction in which case the phenomenon is called Langmuir circulation (Hardisty et al., 1996; Pinet, 1992). This phenomenon is associated with white streaks on the water surface in the downwelling region on the border between two counter circulating cells.

number.⁸ One can distinguish between the minimum critical value needed to keep the grains in transport and the maximum critical value necessary for erosion. The former value increases with increasing grain diameter, whereas the latter has a local minimum due to presence of a laminar sublayer that shields fine sediments from the turbulence in the main flow. Cohesion leads to a further reduction of the erodibility for very fine sediment fractions (such as clay), which, once eroded, may remain in suspension under almost all flow conditions. This type of transported material is called wash load.

Wash load does not play a role in the reshaping of the bed and deposits of the sediment can only be found in stagnant areas within the channel system. For the Jamuna River the wash load consists of silt particles finer than $50 \mu\text{m}$, settling at velocities less than 0.4 m/s , which in general only occurs in the wake of bars and on the flood plain. Wash load does, therefore, not significantly contribute to the short-term morphological activity, but consolidated, erosion resistant deposits may influence the planform on longer time scales. It also plays an important role in the build-up of the flood plain. These finest particles may in general not be ignored in estuarine environments because flocculation and, thus, the settling velocity increases if the salinity increases (Winterwerp, 1999). Silt transport in rivers is generally capacity limited, that is, the transport capacity for silt is so large that the sediment transport rate depends mainly on the upstream availability.

The sediment transport rate is determined by

1. the interaction of the turbulent flow structure and the sediment particles (as described in the previous section),
2. the interactions between the sediment particles themselves (especially in case of sediment mixtures),
3. the interaction of the sediment particles with objects in their neighbourhood (mostly vegetation), and
4. the interaction of the sediment particles with bio-chemical processes (e.g. the effect of salinity described above).

The following subsections summarise some observations of the sediment rate in the Jamuna River, other braided rivers and flume experiments of braided streams.

Uniform sediment

Local variations in the sediment transport rate cause bed level changes. Erosion and sedimentation continue until the transport rate is in equilibrium with the hydrodynamic and morphological conditions. This equilibrium will almost never be attained, due to variations in the forcing conditions (for instance, discharge variations) or changes in boundaries (bank erosion). The sediment transport rate varies, therefore, with time, space and sediment type. Various researchers have derived sediment transport formulae under uniform flow conditions. For fine sands the critical shear stress can be neglected and the sediment transport rate can be

⁸Hjulström (1935) (Sundborg, 1956) has formulated a similar relation between the critical flow velocity and sediment diameter. Such a relation may, however, only be expected to valid if the flow is approximately uniform, i.e., in case of a logarithmic distribution of the velocity.

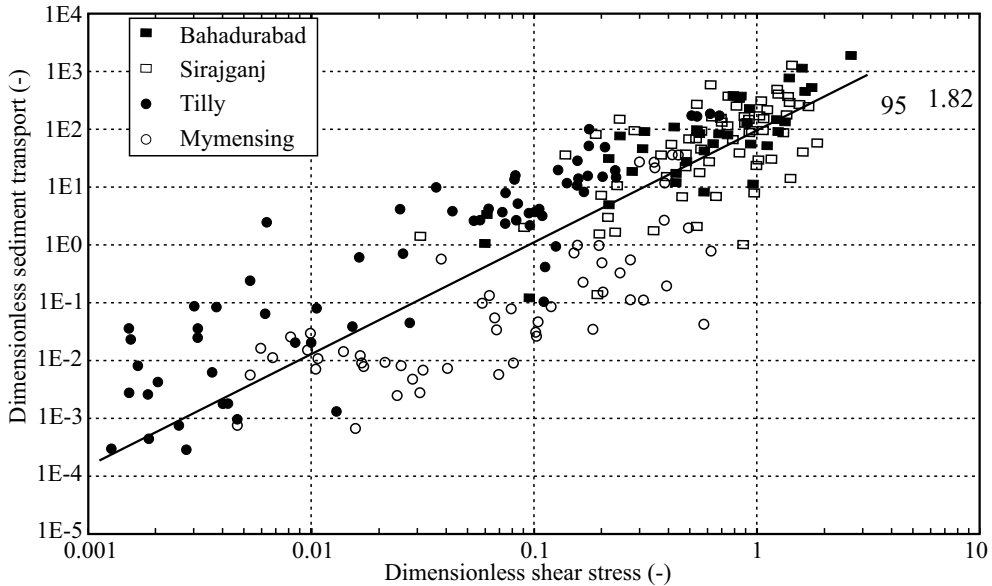


Figure 3.9: Sediment transport rate (River Survey Project, 1996, Annex 4)

assumed proportional to some power of the flow velocity u . The sediment transport formula of Engelund and Hansen (1967) is an example of this type of transport formulae. The following transport formula, which is also of this type, has been derived from data by the River Survey Project (1996, Annex 4) for the major Bangladeshi rivers,

$$\psi = s \frac{1 - \varepsilon}{\sqrt{g \Delta D_{50}^3}} = 0.165 \theta^{1.82} \frac{C^2}{g} \quad (3.1)$$

where the Shields parameter θ , defined as $(u/C)^2/(\Delta D_{50})$, is used as the characteristic quantity for particle mobility. The quadratic dependence in Equation 3.1 on the Chézy value C was taken from the Engelund-Hansen formula. The main features of this transport formula are the power of about 3.64 for the velocity (or 1.82 for θ) and a resulting transport rate that is three times the value predicted by Engelund-Hansen formula for $\theta = 1$, and twice the value for $\theta = 2$. The latter result agrees with the observation by Klaassen *et al.* (1988) that the sediment transport rate in the Jamuna River was about twice the value predicted by Engelund-Hansen.

For relatively coarse sediments the critical shear stress cannot be neglected and a critical shear stress or critical velocity is introduced. The sediment transport formula of Meyer-Peter and Müller (1948) is a typical example of this type of formulae. These coarse types of sediment are mostly transported as bedload. Ashmore (1988) conducted flume experiments with varying slopes and discharges to determine the bedload transport rate in gravel-bed braided streams. He observed that bedload transport was limited to a small section of the larger channels and little or no movement occurred across braid bars. In these shallow areas, the bed shear stress (velocity) was not large enough to bring the coarse sediment into motion; this was also observed by Davoren and Mosley (1986), whereas Leopold and Wolman (1957) observed that individual grains continued to roll across the bar top even when their diameter

was larger than the locally remaining water depth. Momentum of the grains in transport and a smooth (closely packed) bed surface may prevent a grain from settling, whereas the flow strength may not be enough to erode other particles.

Local variations in the bed shear stress may cause significant fluctuations in the alongstream sediment transport rate and, therefore, local erosion and sedimentation. From observations of these erosion and sedimentation patterns, it is possible to estimate the magnitude of variations in the sediment transport rate. For example, Sarker (1996) analysed the bathymetric data obtained by FAP24 (1996). He shows that local erosion and deposition processes may cause alongstream variations in the total sediment transport rate of up to 40 percent. Based on the characteristic dimensions of dunes and their migration rate mentioned in Section 3.1.2, FAP24 (1996) concludes that for an average transporting width of 3 km the near-bed transport amounts 0.1–2.6 million tons a day. So, this may be a substantial part of the estimated total of 5 million tons of suspended sediment assumed to be transported per day by the river during flood. One should note that the 0.1–2.6 million tons a day mentioned above are an estimate for the *near-bed* sediment transport rate and not for the *bedload* transport rate. Bedload can make up as little as 5 percent of the sediment involved in dune migration according to Kostaschuk and Ilersich (1995). Klaassen *et al.* (1988) indicate that the bedload transport in the Jamuna River is just 10% of the suspended transport. The combination of these findings indicates that suspended sediment also plays an important role in local morphological changes in the Jamuna River. These spatial variations in the sediment rate may have significant influence on the estimation of the overall sediment transport rate.

Variations in the bedload transport rate occur not only as a result of variations in the hydrodynamic conditions. Even at a constant discharge, large fluctuations in bedload transport rate occur with some regularity. In flume models the period may range from 2 to 10 hours, but the period may be several tens of hours in prototype (Ashmore, 1988; Church, 1985). These sediment pulses — called ‘autopulses’ by Goff and Ashmore (1994) — originate from various upstream erosive events. The presence of these long-period fluctuations combined with the spatial variations in sediment transport rate mentioned above and rapid changes in discharge and planform make field measurements of sediment transport rates in braided streams very difficult (Ferguson and Ashworth, 1992). Variations in bedload transport on a longer timescale are hypothesised by Griffiths (1993). He refers to observations of sediment translation waves up to 0.5 m high migrating in downstream direction with an assumed average speed on the order of 600 m per year based on a characteristic hydrograph.

Suspended sediment may, if present in very high concentrations, influence the hydrodynamics and the settling velocity of the sediment itself. The sediment concentration in the Yellow River during flood can, for instance, become so high (35 vol%) that it significantly reduces the turbulence and the height of the generated bedforms (Wan, 1983). Although the total amount of suspended sediment transported by the Jamuna River is huge, its concentration — at most 0.1 vol% during flood based on data by Hossain (1992) — remains relatively low. Based on this knowledge, FAP24 (1996, Annex 4) expects that the influence of the suspended sediment on the turbulence and on the formation of dunes in the Jamuna River is negligible. However, Best (1996) suggests that suspended sediment plays a crucial role in the transition from a dune-covered bed to the upper stage plane bed, because the latter has only been observed for fine grained sediments. Since this transition has been observed at certain locations in the Jamuna River during flood, the influence of suspended load on the bedform generation in the Jamuna River may not be completely negligible, after all.

Sediment mixtures: ‘graded sediment’

If a mixture of sediment sizes is available for transport, selective entrainment and deposition starts to play a role. Small grains hide among the larger ones, whereas the large grains are more exposed to the turbulent fluctuations of the main flow. This causes a tendency towards equal mobility (Wilcock, 1992): relative to uniform sediment conditions small grains are less easily entrained from mixtures, and coarse sediments are more easily transported. The dynamics of graded sediments is one of the main topics in morphology at this moment, physical experiments are carried out and new model concepts are tested for both sand-gravel mixtures (Kleinhans, 2002; Blom, 2003) as well as sand-mud mixtures (Van Ledden and Wang, 2001). Discrete particle models can help to study the dynamics of sand-gravel mixtures in detail (McEwan *et al.*, 1999). The hiding and exposure effects in graded sediment mixtures lead to a correction factor on the sediment transport rate in numerical models (Egiazaroff, 1965). The general picture of graded sediment dynamics is complicated further by the migration of bedforms, introducing a selective vertical mixing of various sediment fractions (Blom and Ribberink, 1999; Blom *et al.*, 2003) and possibly the formation of a coarse armour layer. When such a layer has formed — either due to selective deposition of coarse sediment or due to selective entrainment of fine sediment by winnowing — it will shield the underlying fine sediments from the flow.⁹ The most effective armouring is formed by flattened grains which under influence of the flow align and lead to an imbricate structure (see Figure 3.10). Above armour layers and other non-erodible layers the sediment transport rate is reduced below the sediment transport capacity, whereas the celerity of bed disturbances across the armour layer is increased relative to the situation without armour layer (Struiksma, 1999). In the case of a limited supply of sediment from upstream, bedload transport across the armour layer will take the form of barchan dunes (Bagnold, 1941; Wasson and Hyde, 1983; Nishimori *et al.*, 1998) as illustrated in Figure 3.5.

Within a river the mean grain diameter becomes generally smaller in downstream direction (Paola *et al.*, 1992).¹⁰ In Section 2.2.2 we have seen that the mean sediment diameter of the Jamuna River decreases from 0.25 mm at the Indian border to 0.16 mm at the confluence with the Ganges River. Abrasion of the relatively soft mica particles seems to play

⁹Note that if cohesive sediments are included, it can be the fine sediment that forms the protective layer. The time scale for compaction is however much longer than the time scale at which an armour layer of coarse sediment can be formed.

¹⁰The opposite of the downstream fining of sediment, downstream coarsening, has been observed and reproduced in flume experiments for mixtures of sand and pea-sized gravel. Parker (1996) hypothesises that the downstream coarsening may result from selective protrusion of sediment through a partial viscous sublayer.

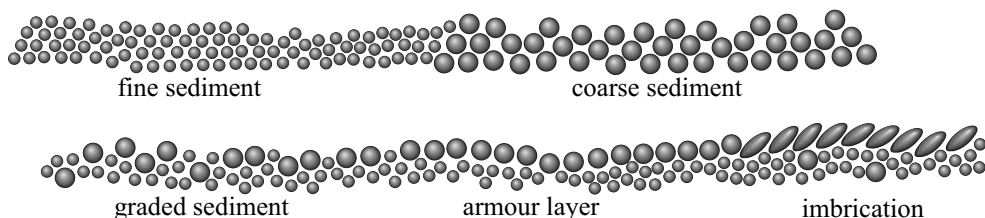


Figure 3.10: Hiding, exposure and the formation of an armour or imbrication layer in a graded sediment mixture (side view).

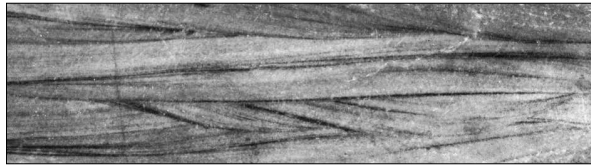


Figure 3.11: Photograph illustrating cross-bedding of ripples (scale 1:1).

an important role here. Selective deposition of the coarsest sediments will in general also contribute to downstream fining (Chein, 1961). In distinctly bi-modal sediment mixtures a sudden transition from gravel-bed to sand-bed river may occur (Parker, 1996). Besides the overall tendency for downstream fining, selective entrainment, transport and deposition of the various grain sizes (graded sediment) cause spatial variations in sediment composition. The variations in sediment composition will result in different roughnesses and it may result in different types of bedforms (see Section 3.1.1).

The migration of ripples, dunes, and bars during a period of aggradation results in thinly laminated sedimentary deposits (stratigraphy) in the river bed (see Figure 3.11); these patterns form even in fairly homogeneous sediments due to variations in density of the packing of the grains. From an economical point of view, this is one of the most interesting topics in geomorphology, because some of the world largest oilfields are contained in the ancient deposits of braided rivers. The sedimentary structure of the deposits determines the shape of oil and gas reservoirs. Due to the intricate network of remnant channels, accurate estimation of the reservoir potential and reservoir management is difficult (Martin, 1993). Understanding the general dynamics of braided rivers and the sorting mechanisms (from bedform to channel scale) in particular can give valuable information about the possible internal structure of existing reservoirs. Furthermore, heavy minerals often accumulate downstream of confluences (Ashmore, 1993; Ashworth *et al.*, 1994), whereas relatively high concentrations of gold have been found in deposits associated with diagonal bars (Karpeta, 1993).

3.2 Macro-scale morphodynamics

Bars occur in various shapes as shown in Figure 3.12. Any disturbance in a channel of sufficient width will cause the flow to meander and alternate bars to form (Leopold and Wolman, 1957). Straight, uniform flow over a flat bed is in that case an unstable equilibrium (Blondeaux and Seminara, 1985) as shown by the neutral stability curve presented in Figure 3.13. When the channel width increases more bars will form in transverse direction (Leopold and Wolman, 1957; Engelund and Skovgaard, 1973). These bars, which are not attached to the side walls, are called braid bars. When a constant forcing is applied to the river (for instance a flow obstruction or a bend) forced alternate bars may form downstream (Struiksma and Crosato, 1989) or upstream (Guala *et al.*, 1999; Zolezzi and Seminara, 2001) of the forcing location. In a bend the channel deepens along the outer bank and becomes shallower at the inner bank: a point bar develops (Einstein, 1926; Van Bendegom, 1947). Flow conditions and bed slope play an important role here. The sediment transport pattern on the bar scale is significantly influenced by bed slope and spiral flow (Koch and Flokstra, 1980). When, however, the bend is too sharp, flow separation can occur and a bar may form at the outer bend: a

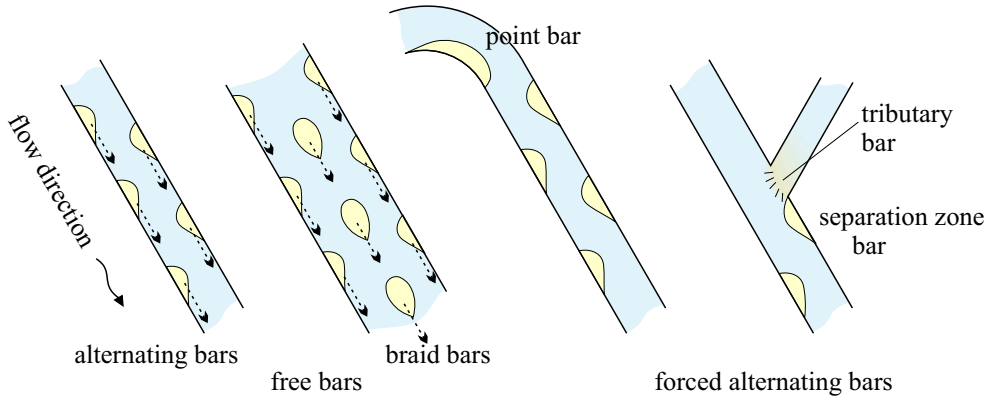


Figure 3.12: Sketches of the most commonly distinguished bar types.

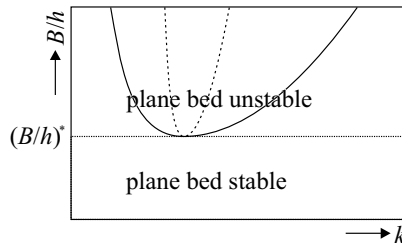


Figure 3.13: Instability of bars as a function of their wavelength and the width-depth ratio of the channel. The continuous line indicates the neutral stability curve (for $m = 1$), that is, it connects the width-depth ratios for which the alternate bars with the various wave numbers k do not grow; above the line they will grow, below it they will disappear. Below the critical width-depth ratio $(B/h)^*$ bars of all wavelengths will disappear and the plane bed is stable, above it bars will form with wavelengths in a certain characteristic range. Only within the inner (dashed) curve the bed oscillations themselves are stable. Figure after Schielen et al. (1993); Schielen (1995).

concave (bank) bench (Hickin, 1979; Nanson and Page, 1983; Parker, 1996) or counterpoint bar (Smith, 1987). A related type of forced bar forms when flow separation occurs downstream of a confluence due to a large confluence angle (Best, 1987, 1988). Such a bar is called a separation zone or confluence bar. A tributary bar is a shallow area at a confluence; when discharge from the tributary increases, it may become detached and continue to migrate downstream through the river.

3.2.1 Alternate bars

Over the last decades, the dynamics of alternate bars has been studied by several researchers using an analytical approach. It has been shown by Struiksma and Crosato (1989) that the growth rate and migration speed (in downstream direction) of alternate bars depend on their wavelength as indicated in Figure 3.14. It has for some time been assumed that the free alternate bars would under appropriate conditions initiate meandering. However, the initial

meander wavelength is 2–3 times larger than the length L_f of the fastest growing bars. Blondeaux and Seminara (1985) showed that a mildly sinuous channel of appropriate wavelength triggers a resonant response with respect to the formation of stationary bars with a wavelength that matches the meander wavelength. As meanders develop the alternate bars become forced bars and the free bars will be suppressed (Kinoshita and Miwa, 1974; Colombini *et al.*, 1987; Tubino and Seminara, 1990).

De Vriend and Struiksma (1983) and Struiksma *et al.* (1985) have shown that the adjustment of the depth-averaged main velocity distribution in a river has a characteristic length scale of

$$\lambda_w = \frac{C^2 h}{2g} \quad (3.2)$$

and that the transverse redistribution of the sediment transport has a length scale given by

$$\lambda_s = \frac{1}{(m\pi)^2} h \left(\frac{B}{h} \right)^2 f(\theta) \quad (3.3)$$

where

- B channel width,
- C Chézy roughness value,
- $f(\theta)$ Shields parameter θ dependent bed slope effect taken to be 1.5θ by Struiksma *et al.* (1985) but these days generally taken to be $0.85\sqrt{\theta}$ following Odgaard (1981) and Struiksma and Crosato (1989) or $9(D_{50}/h)^{0.3}\theta^{0.5}$ following Talmon *et al.* (1995),
- g gravitational acceleration,
- h water depth,
- m lateral mode (for alternate bars equal to 1),
- θ dimensionless shear stress or Shields parameter, equal to $(u/C)^2/(\Delta D_{50})$, where u is the local velocity, Δ is the relative submerged density of the sediment and D_{50} is the median grain diameter,

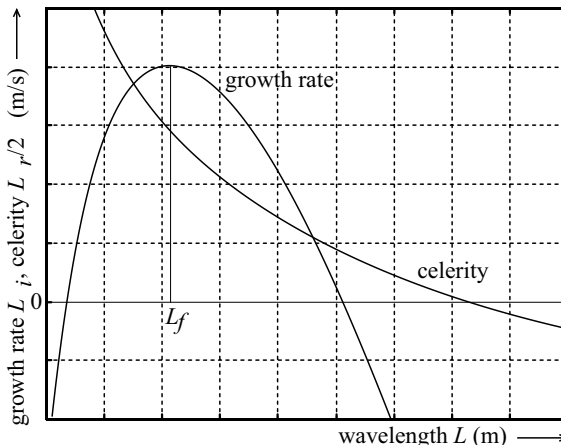


Figure 3.14: Growth rate and celerity of free alternate bars as a function of their wavelength L as obtained from a linear analysis by Struiksma and Crosato (1989).

The characteristic wavelength and damping of alternate bars in the equilibrium bed topography is largely determined by the ratio λ_s/λ_w for $m = 1$, also referred to as the interaction parameter IP by Struiksma and Crosato (1989):

$$\text{IP} = \frac{\lambda_s}{\lambda_w} = \frac{2g}{(m\pi)^2} \left(\frac{B}{h}\right)^2 \frac{f(\theta)}{C^2} \quad (3.4)$$

This ratio plays an important role in the retarded response of the channel bed to disturbances of the channel geometry (for instance, at bend entrances/exits) which results in an overshoot phenomenon. Also the power b of the sediment transport formula has a profound influence on the bed deformation: for example, as the value of b increases, the damping of bars decreases (Struiksma *et al.*, 1985). If the interaction parameter is large, higher order lateral modes ($m > 1$) will form and the channel will be braided (Fredsøe, 1978; Struiksma and Crosato, 1989).

3.2.2 Braid bars

Large shallow areas in the middle of a river (that is, not connected to the banks) are called braid, medial or mid-channel bars. Leopold and Wolman (1957) describe one process that can lead to the formation of such a bar. It starts due to the stalling of a group of coarse particles (bedload sheet), which forms the nucleus of a bar that grows by successive addition at its downstream end. Downstream of a braid bar (not necessarily emergent) a pool, or scour hole, may form due to the rejoining of the currents which flow around the bar. The sediment that is eroded during the formation of the pool is often deposited slightly downstream where it starts the initiation of a new bar, which in this case is referred to as a post confluence bar (see also Sections 3.3.3 and 3.5 on erosion and sedimentation, and the dynamics of braided rivers, respectively).

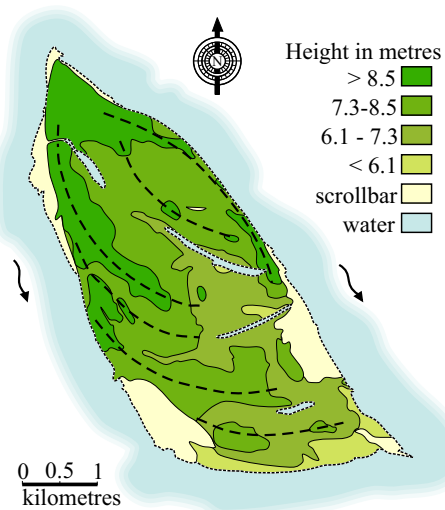


Figure 3.15: Bar topography illustrating lateral and downstream accretion (Bristow, 1987).

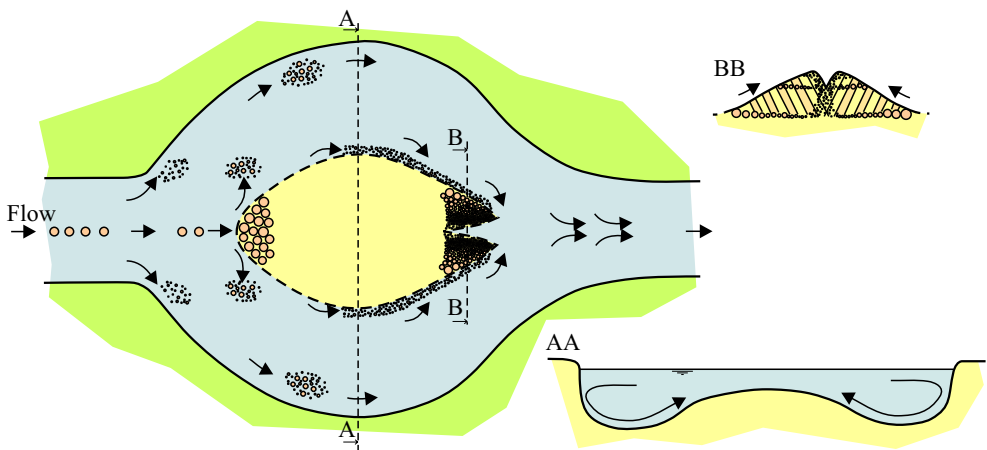


Figure 3.16: Sediment sorting processes and resulting grain size distribution within a braid bar as observed by Ashworth *et al.* (1992).

The sorting of sediment mentioned for bedforms in Section 3.1.4, continues on the macro-scale of bars. In the relatively simple case of a meandering channel, the coarsest sediment is found along the outer bend, whereas the finest sediment forms the point bar (Jansen, 1979). Sediment sorting has also been observed during the formation of braid bars. Stalling of bedload sheets in gravel-bed rivers starts with the coarsest particles; thereafter, more coarse particles are trapped at the upstream side of the initial nucleus, while finer grains deposit on the downstream side in the lee of the coarser particles (Ashmore, 1991). This process continues, resulting in a bar in which the sediments have been sorted on average from coarse (at the upstream side and along the outer rim) to fine (at the downstream side and inside the bar) as indicated in Figure 3.16 (Ashworth *et al.*, 1992).

3.2.3 Bars and flow patterns

Alternate bars and braid bars will often grow due to lateral accretion. Periodic variations in discharge and sedimentation rate result in the formation of a characteristic scrollbar topography with alternate high (ridges) and low (swales) lying areas as illustrated by Figure 3.15. Furthermore the upstream end of a bar is on average higher than the downstream end although the downstream end might emerge first during falling discharge (Krigström, 1962). If multiple bars grow together forming one large bar¹¹, this shape may be less clear.

The lateral and downstream accretion of sediments will sometimes form bar tails; these tails are often one of the few characteristics in a picture from which one can derive in which direction the braided river flows as the bar tails always point downstream.¹² Using a characteristics analysis of the depth-averaged flow equations and a sediment transport rate proportional to the local flow speed (no bed slope effect on direction or magnitude), De Vriend (1987) has

¹¹In case of mid-channel bars the compound (or mosaic) bar is called a medial bar complex. In cases where one wants to emphasise that a bar is *not* a compound bar it is generally referred to as a unit (braid) bar.

¹²In estuaries where the rising and falling flows follow different channels, the tails at the left and right side of the bars may have opposite directions.

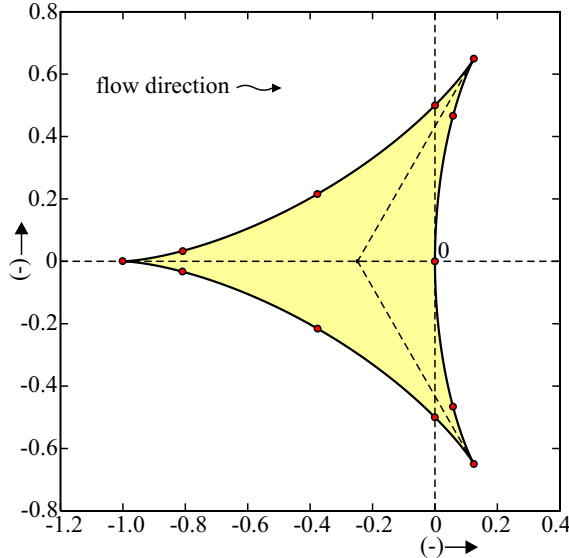


Figure 3.17: Basic form of the morphological wave-front generated by a point disturbance. The shape is given by equation 3.7 which has been derived from a characteristics analysis by De Vriend (1987). The values along the wavefront represent the local value of the parameter ϕ .

shown that an infinitely small bedform migrates and expands in alongstream direction s and normal direction n as

$$\frac{ds}{dt} = c_0 + c_1 \xi \text{ and } \frac{dn}{dt} = c_1 \eta \quad (3.5)$$

in which

$$c_0 = \left(\frac{u_{\text{tot}}}{S_{\text{tot}}} \frac{\partial S_{\text{tot}}}{\partial u_{\text{tot}}} - \frac{h}{S_{\text{tot}}} \frac{\partial S_{\text{tot}}}{\partial h} \right) \frac{S_{\text{tot}}}{h} \text{ and } c_1 = \left(\frac{u_{\text{tot}}}{S_{\text{tot}}} \frac{\partial S_{\text{tot}}}{\partial u_{\text{tot}}} - 1 \right) \frac{S_{\text{tot}}}{h} \quad (3.6)$$

and the normalised velocity components are

$$\xi = \frac{1}{2} \cos \phi (1 - \cos \phi) \text{ and } \eta = \frac{1}{2} \sin \phi (1 + \cos \phi) \quad (3.7)$$

where ϕ is a parameter running from $-\pi$ to π .

These formulae indicate that the initial bed disturbance migrates downstream with a velocity c_0 , meanwhile expanding into a triangular shape with two tails in downstream direction (see Fig. 3.17). Krigström (1962) describes indeed that bars on sandar¹³ in the earlier stages of their development show a characteristic indentation in the middle of their downstream side. As the disturbance grows the bedforms starts to influence the flow: the streamlines become curved and they wrap around the forming bar. When this happens the triangular shape becomes distorted into the typical barchan shape (Fig. 3.18) and separation occurs at the step which develops at the downstream side, leading to various kinds of vortices (Fig. 3.5). The relative size of the two tails gives also an indication of the morphological activity in the neighbouring channels — the longer tail corresponding with the channel that is more active.

¹³A sandur (plural: sandar) is an outwash plain in front of a glacier.

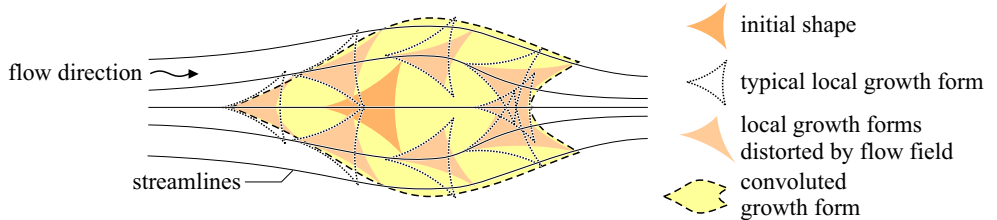


Figure 3.18: Tentative relation between the basic form of the wave-front and the actual dune/bar shape.

A second aspect, from which the flow direction can be derived, is the fact that the angle of two confluencing channels is rarely larger than ninety degrees. So, when a braid bar has an obtuse ($\alpha > 90^\circ$) angle, it marks in general the upstream side of the bars (see Figure 3.19).

Secondary flow (or spiral flow) plays an important role in dynamics of point bars. Flow in river bends has a transverse component that is directed to the inner bend near the channel bed and to the outer bend near the water surface (Van Bendegom, 1947; Rozovskii, 1961; De Vriend, 1981a). Near the water surface at the steep bank of the outer bend, a second helical cell may form which rotates in the opposite direction. The flow near the bed directs the near-bed sediment transport towards the inner bend, which results in the build-up of the pointbar. The heightening of the pointbar causes a gradual increase in the transverse bed slope. In the absence of erodible side-walls, the increasing downslope gravity component will eventually counteract the inward-directed force exerted on the sediment by the helical flow and an equilibrium condition is established. A similar secondary flow structure was proposed for the curved channels on both sides of an island in a braided river (Richardson *et al.*, 1996; Richardson and Thorne, 1998; River Survey Project, 1996, vol. 16). However, in many cases the secondary flow is too weak to be detected conclusively by state-of-the-art measuring techniques, or the secondary flow structure is more complicated due to the presence of large bars, multiple islands, and confluences. Lane *et al.* (2000) show that the interpretation of relevant measurement data is sensitive to the plane of observation. Secondary flows generated by these morphological units generally interact. The flow structure generated

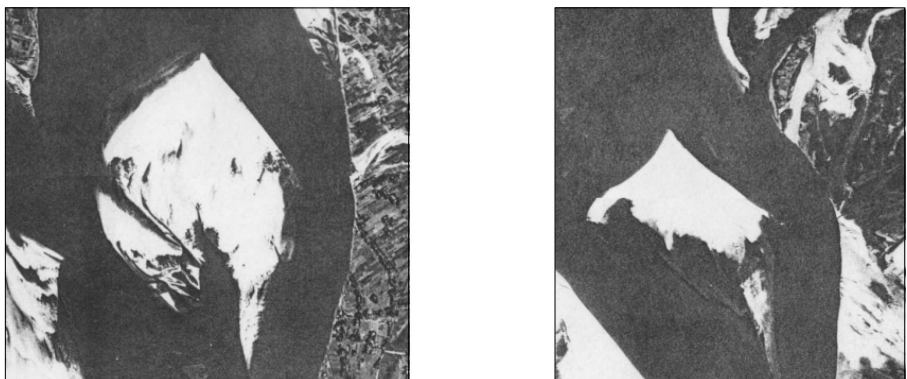


Figure 3.19: Two examples of braid bars in the Jamuna River from which flow direction can be derived (in both cases from top to bottom).

by a scour pool in confluences consists of two helical cells back-to-back with convergence at the surface, downwelling in the mixing zone and divergence at the bed. In reality this simplified image is complicated by complex confluence geometries, the formation of Kelvin-Helmholtz instabilities in the shear layer at the boundary between the merging flows, and the presence of horizontal separation vortices in the lee of the avalanche faces at the confluence entrance (Ashmore, 1993).

Examination of aerial photographs by Coleman (1969) showed that the upstream (bifurcation) angles of bars mirror the spatial variation in the local flow direction. A large variation in flow direction, a wide and shallow channel with a large number of bars and islands, rapid bank erosion and fast migration of the thalweg appear to be correlated, as do the opposite extremes. Rising stage can be associated with adjustment of channel alignment by erosive action. Coleman found that the flow direction during the rising stage was significantly influenced by bank erosion (slumping). The falling stage, on the other hand, is associated with deposition and the formation of new low-stage channels. The flow direction during this stage is, according to Coleman, predominantly controlled by deposition and formation of sand bars.

3.3 Mega-scale morphodynamics

Islands have the same scale as bars. So, what defines these two types of morphological units as being two separate groups? Section 3.3.1 addresses this question. Inextricably linked with islands are channel confluences and bifurcations. The behaviour of these nodes in the channel network is the topic of Section 3.3.2. The last section is about erosion (bank erosion, scour) and sedimentation on the scale of islands, channels and rivers.

3.3.1 Islands

Islands may be distinguished from braid bars based on their size, age, elevation and the presence of vegetation or cultivation. The distinction of the morphological units based on only one of these properties fails in general. For example, distinction between bars and islands based on the presence of vegetation alone is not very useful in Bangladesh as most land that is exposed after the flood is quickly occupied by the local inhabitants and immediately put under cultivation. The generalising concept behind the characteristics mentioned above is stability: islands are more stable than braid bars. However, stability cannot be quantified and, therefore, researchers have sought for a quantifiable replacement among the related island properties. The stability of a bar or an island depends mostly on its dimensions (surface area and height) and the sediment properties (cohesive or non-cohesive), but also on the presence of vegetation. The presence of cultivated land does not increase the stability of the land¹⁴ but it is in general an indicator of for the natural stability of the island. A single universal and quantifiable indicator seems not to exist.

An island can be formed either by the growth of a large stable braid bar, or by the river cutting a new channel through the flood plain. In the case of an alluvial river, both islands and flood

¹⁴The inhabitants may however construct protection works or plant protective vegetation (catkin) and thereby contribute to the stability of the land, which may eventually lead to the change of a bar into an island.

plains are created by river deposits and their heights will, therefore, in the case of a non-degrading and non-dying river (i.e., excluding causes 3 and 4 for braiding listed on page 8) always be lower than the highest possible flood level.¹⁵ Even when an island is excised from the flood plain, naming is not always unambiguous: a large island formed in this manner may be interpreted either as a part of the flood plain that splits the previously single-threaded river into an anabranching river, or as an island within a river. The large islands in the Jamuna River are of such a size that this debate is held (see the discussion by Bridge, 1993). Contrary to the building of an island by coalescence of bedforms and bars — which is a process leading to increasingly stable morphological units — the formation of a new island by excision from the flood plain is in general the starting point of a period of continued erosion.

3.3.2 Confluences and bifurcations

The planform of a confluence in a braided river can vary significantly over time due to variations in the discharge ratio and the flow directions of the converging channels. Their dynamics has been studied by Ashmore (1993). The observed behaviour can be summarised as a combination of migration, rotation, resizing and obliteration (abandonment of one of the confluencing channels). Ashmore (1993) also distinguishes two more complex changes. First, one of the confluencing channels may split (due to partial emergence of the tributary bar) and thereby split the confluence into two closely spaced confluences. Second, a bar may emerge in the area immediately downstream of the confluence, resulting in a combined confluence-bifurcation point.¹⁶ The latter process was more extensively studied by Ashworth (1996) for a simplified geometry. Observations by Ashmore and Parker (1983) indicate that confluence scour holes may be up to six times deeper than the average channel (see also the subsection on scour in Section 3.3.3); other researchers have found scour holes that were less deep (Best, 1986), which might be attributed to finer sediment and even suspended load (Klaassen and Vermeer, 1988). The local secondary flow is characterised by two counter-rotating flow cells with plunging flow in the centre (Mosley, 1976; Ashmore *et al.*, 1992). This image is complicated by three dimensional flow effects (Best and Roy, 1991; Best *et al.*, 1991).

Bifurcations are less dynamic, because there is only one inflow from upstream which may migrate, rotate or change in magnitude. The distribution of water and sediment at a bifurcation is, however, of crucial importance for the downstream channels. The sediment distribution depends heavily on the local bed topography, the mode of sediment transport (bedload or suspended load) and the three-dimensional flow field. Sediment distribution problems can be difficult to solve if the upstream geometry is complex and large amounts of sediment are involved (for example in the case of the Gorai river). Modelling the behaviour of such bifurcations using one-dimensional models is not useful since the outcome is completely determined by the sediment distribution relation (nodal point relation) prescribed by the modeller (Wang *et al.*, 1995). We will come back to this topic in Section 6.3.

¹⁵In non-alluvial rivers (such as bedrock rivers) and degrading alluvial rivers, islands may be higher than the highest possible flood level, but bars will always be lower.

¹⁶Basically this process does not change the confluence and it should be excluded from the list of confluence changes.

3.3.3 Large scale erosion and sedimentation

Changes in the flow velocity and, therefore, in the sediment transport rate, cause erosion and deposition of sediment. Two types of erosion may be distinguished: bank erosion (horizontal direction) and scour of the channel bed (degradation, vertical direction), whereas deposition of sediment occurs mainly on the channel bed (aggradation, vertical direction).¹⁷ The lack of a significant physical mechanism for bank accretion indicates that a channel can only be stable if the (maximum) shear stress exerted on the channel bank is less than the critical shear stress τ_c necessary for the initiation of motion. This has been suggested by Parker (1978) for bedload rivers. Parker shows that this condition (for a bedload dominated non-cohesive channel) results in a maximum of $(1+\varepsilon)\tau_c$ for the bed shear stress in the centre of the channel with a theoretical value of 0.2 for ε . Therefore, the sedimentary composition of the channel banks control the channel dimensions and, thereby, also the channel type (see cause 2 for braiding listed on page 8). Bank protection measures stop the supply of sediment from the bank, but the resulting surplus in the sediment transport capacity will be compensated by increased erosion of the channel bed. This process may affect the large scale morphology by attracting a larger part of the flow. Other human interferences with braided rivers (such as bridge piers, groins and vanes) affect via their influences on the hydrodynamics also the large scale erosion and sedimentation patterns (Mosselman and Sloff, 2002).

Bank erosion

Under alluvial conditions, bank erosion occurs continuously along the outer bank of a channel bend (by the flow scraping along the bank) and at the upstream end of an island or an emerged bar (by a current impinging on it from upstream). In case of non-cohesive sediments (dry sand or gravel), bank slopes are restricted to 30–45° and erosion takes place by intermittent shallow slides of a few grains thick. Banks made of more cohesive sediments are prone to gradual undercutting and the destabilised (possibly even overhanging) bank will sooner or later collapse locally and fall into the channel. The newly created bankline will match the local flow direction better, and the adaptation of the bankline will progress with the adjacent reaches (Coleman, 1969). As this example already indicates, bank erosion can happen continuously by direct erosion (the sediment removed from the bank is directly transported by the stream) or by discrete events (collapse).

There are basically three causes to initiate the collapse of banks. First, as already mentioned above, the bank may destabilise due to gradual undercutting or toe erosion. Second, the strength of the bank may be reduced by saturation with water during flood or heavy rainfall, and the bank may collapse under the additional weight of the absorbed water (liquefaction). This will often occur only when the water level drops to a lower level. Third, the flow of water in the sediments that make up the banks may cause rearrangement of the sediments and erode channels within the sediment. This process, which is called piping in case of concentrated flows or sapping in case of larger outflow areas, leads to the destabilisation of certain sedimentary layers which make the banks more prone to large scale bankslides (Hagerty, 1991a,b). Once erosion has been initiated, erosion may continue due to relatively shallow slides; this process is referred to as ‘breaching’ by Van de Berg *et al.* (2002).

¹⁷Biochemical processes may result in a small amount of sedimentation in horizontal direction. These processes may result in a narrowing of the channel comparable to the narrowing of pipes due to corrosion.

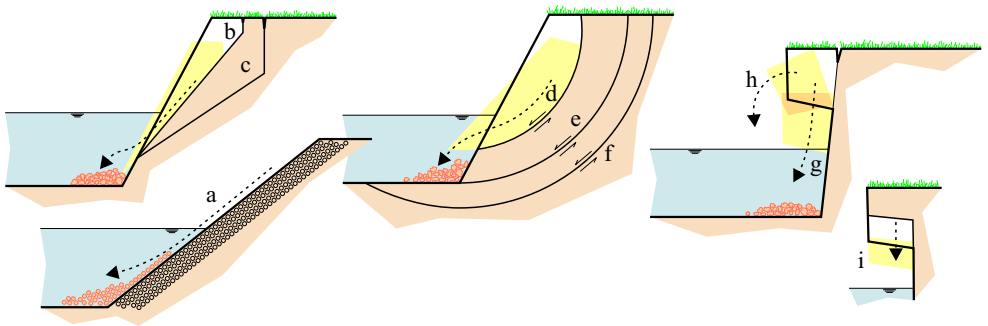


Figure 3.20: Bank failure types: shallow slip (a), plane slip (b) and slab type (c) failures with plane shear surfaces, slope (d), toe (e) and base (f) rotational slides with concave shear surfaces, and shear (g), beam (h) and tensile (i) cantilever failures.

The subsequent mass movement of bank material can be caused by either a bankslide (with either a planar or concave shear surface) or a cantilever failure (Thorne, 1982). The mass movement of sediment leads in all cases to the relocation of sediment towards the toe of the bank, from where the sediment is gradually removed. The types of mass movement will be discussed now in somewhat more detail (see also Figure 3.20):

- **Bankslides with plane shear surfaces.** The section of the bank that fails slides down the plane surface to cover the toe of the bank. The motion is mainly a translation. Depending on the ratio of their thickness d_s and length L_s , these slides are called: shallow slip failures (d_s/L_s small), plane slip failures (d_s/L_s medium), and slab type failures (d_s/L_s large). Shallow slip failures have a shear plane that is in general parallel to the bank slope. The thicker slides occur in more cohesive sediment, when the critical shear stress — which is higher in cohesive soils — is exceeded by the shear stress exerted on the failure plane by a large block of soil. The probability of a slide occurring is highest during the falling stage, when the banks are saturated and the counteracting pressure of the water in the channel disappears.
- **Bankslides with concave shear surfaces.** These slides are — contrary to the previous type of mass movement — characterised by a rotating motion of a section of the bank along a more or less circular-shaped shear surface; this type of erosion is generally indicated as rotational slip failure. The probability of the occurrence of these slides is also highest during the falling stage. Depending on the start of the shear surface, the failure type may be further specified as being a rotational slope, toe, or base failure.
- **Cantilever failure of overhanging cohesive sediment blocks.** Overhanging sediment blocks are in general caused by erosion of more easily erodible soil (undercutting) from under a more cohesive top layer. The name of the cantilever failure depends on which force fails to keep the block in place: a shear failure occurs when the shear stresses in a vertical plane connecting the block with the remainder of the bank fail and the block falls down vertically. In case of a beam failure the block tears off when the horizontal tensile stresses become too large. Finally, when the vertical tensile stresses become too large in a horizontal plane, a tensile failure occurs and the block falls straight down again, but now leaving another part of the soil protruding from the bank.



Figure 3.21: Photographs of eroding banks composed fine and coarse sediments along the Allier River. In the case of non-cohesive coarse sediments, the bank slope is approximately 45 degrees.

In braided rivers, characterised by mainly non-cohesive sediments and little vegetation, shallow slip and plane slip failures will be most common. Large scale slumping (slab type or rotational failure) due to liquefaction of the underlying sediments during the falling of the discharge has been observed along the Jamuna River by Coleman (1969). The fraction silt/clay in the sediments of the Jamuna River is large enough that eroding banks can become almost vertical as shown in Figure 1.1. Similarly steep banks composed of fine sediments can be observed along the Allier River, France, whereas eroding banks composed of coarser sediments are more gentle (see Figure 3.21).

Scour

During the rising stage, the cross-sectional area may significantly increase due to scour; however, the largest scour depths occur in general during the last part of the flood, as the adaptation of the bed level lags behind. When the channels become wider due to bank erosion and when the flow velocity decreases during the falling stage, deposition starts to fill in the scour holes again. Four types of local channel scour related to planform characteristics can be distinguished (Galay *et al.*, 1987; Klaassen and Vermeer, 1988; Hoffmans and Verheij, 1997):

- *Bend scour.* The secondary flow generated in channel bends induces a net sediment transport towards the inner bend. This transport results in the accumulation of sediment at the inner bend, thus extending the pointbar (Van Bendegom, 1947). At the outer bend a scour hole forms, which is in general deepest just downstream of the apex of the bend. In a long bend with constant radius of curvature the deepest scour is located at the upstream side due to overdeepening (Struiksmma and Crosato, 1989). The scour causes a steepening of the bank, thereby increasing the probability of bank erosion. Similar scour holes (although somewhat deeper) are formed when the channel bank is protected or naturally stabilised by some non-erodible element.
- *Confluence scour.* When two (or more) channels meet, a scour hole forms (see also Section 3.3.2 on confluences and bifurcations). This confluence scour hole is spoon-shaped and the most pronounced if two large channels meet at a relatively large angle; at sharp-angle confluences of small channels the scour is much smaller. The shape

of the scour hole is maintained by two back-to-back helicoidal vortices which are of similar origin as the secondary flow in a channel bend (Ashmore and Parker, 1983).¹⁸ Often one, or both, of the confluent channels builds an avalanche face (Ashmore, 1993) or tributary bar (Krigström, 1962) into the confluence. When the channels are unequal in size, the avalanche face of the largest channel often progrades further into the confluence; this may cause a lateral shift and reorientation of the scour hole. The sediment eroded from the scour hole at a symmetric confluence is often deposited in the middle of the channel immediately downstream of the confluence. This may form the initial disturbance from which a new island (or bar) and a new scour hole may form, possibly leading to the onset of braiding. Alongside the scour hole a separation zone bar may form when one of the channels joins the other at a high angle (Best, 1986, 1987, 1988). A comparison of prediction formulae for the depth of a confluence scour hole is given by Best (1986).

- *Constriction scour.* When a channel is constricted to a narrow bed, due to human intervention or due to the presence of less erodible sediment types in the banks, constriction scour will result in a deepening of the channel. The presence of clay deposits in the banks in the downstream reaches of the Jamuna River may cause the change in channel pattern that was observed by Coleman (1969): from wide and shallow when it enters Bangladesh and narrow and deep in the lower reaches near its confluence with the Ganges River.
- *Obstruction scour.* Closely related to constriction scour is obstruction scour. This occurs when the flow encounters a fixed non-erodible point, such as a groyne head or bridge pier. This type of scour is sometimes subdivided further into: protrusion scour (at the upstream edge) and local scour (at the downstream edge). Obstruction scour is in general more localised scour than constriction scour.

¹⁸Besides the resemblance to bend scour, confluence scour can also be seen to be analogous to constriction scour (Ashmore and Parker, 1983).

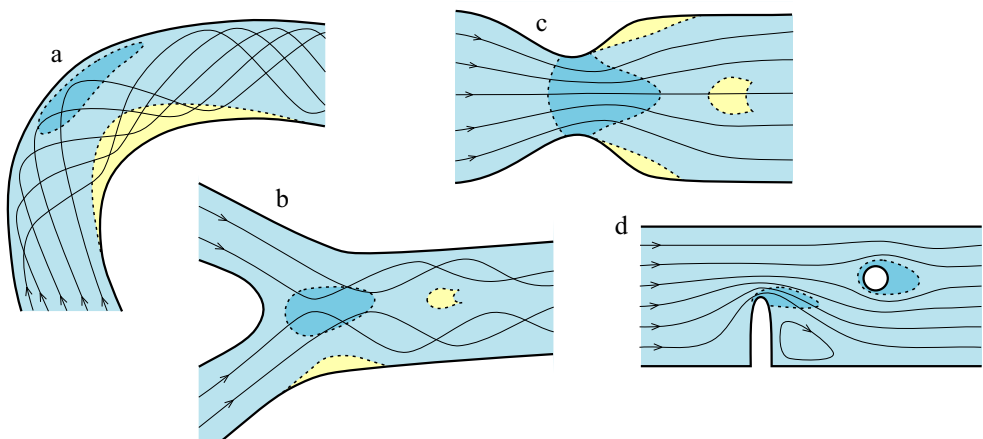


Figure 3.22: Scour types: (a) bend scour; (b) confluence scour; (c) constriction scour; (d) obstruction scour.

Two negative effects are associated with bend scour: first, a destabilization of the (possibly protected) outer bank, and second, the growth of a pointbar at the inner bend. The latter effect may hinder shipping. Artificial non-erodible layers can be used to counteract these effects. The effect of such measures and similar natural controls (e.g. bedrock outcrops) is a local reduction in the transport capacity and the formation of a scour hole downstream (Struiksma, 1999). Similar phenomena can occur under alluvial conditions with sediment mixtures (see the subsection on sediment mixtures of Section 3.1.4). Constriction and obstruction scour are associated with the most common forms of river training works, therefore, they or their effects on the overall planform have to be included in the model that is used to predict the effects of such human interference.

Sedimentation

The sediment eroded from the banks and scoured from the channel bed in a bend is deposited as soon as the transport capacity reduces downstream. Large scale erosion in a river dominated by bedload transport is generally associated with significant sedimentation in a downstream area nearby. This relation holds only to a lesser degree for suspended sediment. Sedimentation may be wide-spread during a flood (on the flood plain) or during the falling stage of a flood (throughout the channel system). During flood, suspended sediments are transported onto the flood plain. Relatively coarse sediments are generally deposited as crevasse splays close to the river channel, whereas the clay and silt are deposited in a thin layer across the whole flood plain. The splay deposits build up natural levees of coarse material interlined with thin layers of finer grained clay and silt deposits (see also Section 2.2.2).

Localised deposition occurs either as a result of a persistent flow pattern or mixing processes. An example of the first case is the formation of a pointbar due to the spiral flow in a meander bend. An example of the second case is the sedimentation of relatively fine sediments in a slack water zone, downstream of a braid bar, due to a continuous supply of sediment due the mixing caused by eddies on the edge of the recirculation zone. Pointbar deposits are generally characterised by coarser sediments than the fillings of oxbow lakes. These differences in sediment composition can have a significant effect on the planform of the whole river as is illustrated by recent numerical simulations of meandering rivers (see Section 4.1.2). Localised erosion and deposition may have a large effect on the local transport rates (see Section 3.1.4).

3.4 Sources of uncertainty

Whenever a (numerical, analytical or conceptual) model is used for predictions, there will always be some uncertainty. Uncertainty enters the model prediction wherever there are boundaries — be it physical or conceptual boundaries. Four types of boundaries can be distinguished, each with its own kind of uncertainty.

Boundary in space (large scale)

The physical boundaries of a hydrodynamic model are not only the inflow (discharge) and outflow (downstream water level) boundaries, but also the banks (side walls), the water

surface and the bed. The discharge that will enter the study area from upstream is not known in advance. Based on historical data one can predict what the hydrograph for the simulation period will look like on average, but there is generally a large uncertainty margin around it (Van der Klis, 2000; Van Vuren *et al.*, 2002). Will the flood be high or low, and how long will it last? Also, the speed with which the flood will recede has to be known for an accurate prediction. If one tries to circumvent these problems by extending the model to include the upstream catchment area and maybe even a hydrological model, the problems remain basically unanswered: they are only shifted upstream or converted into other types of uncertainty. Also the downstream boundary, which may depend on the runoff of other regions and other rivers, is impossible to predict accurately a long time ahead. At the water surface one again encounters the influence of the weather: wind, precipitation, and pressure — although they are generally of less importance than the accuracy of the upstream boundary condition.

Besides the often ignored interaction with groundwater at the channel bed and banks, another element of uncertainty is found at these locations; it is the roughness of the banks and the channel bed. Detailed understanding of the interaction of bedforms and water motion is required to predict the formation of bedforms and the associated (alluvial) roughness, which is of crucial importance to the accurate prediction of the flow field. The depth dependence of the Chézy value is often simply parametrised using Manning's n as $C = h^{1/6}/n$, or using the roughness height k_s as $C = 18 \log(12h/k_s)$.¹⁹ Within the River Survey Project (1996) a new empirical relation between the Chézy value and the water depth has been derived: $C \approx 15.2h^{0.69}$. Considering the variability in these relations, this result was considered to be reasonably close to $C = 25h^{0.5}$ by FAP24 (1996). The latter relation is obtained for an average water depth h_{mean} of 5.8 m from the formula $C = 60(h/h_{\text{mean}})^{0.5}$ used by DHI in their numerical models for the Jamuna River (Enggrob and Von Lany, 1994; Enggrob and Tjerry, 1999). Further resistance can be caused by the presence of vegetation (along the banks and on the flood plain).²⁰ It is obvious that the flow resistance due to vegetation is influenced by time-varying characteristics such as vegetation height and density, but an accurate expression for the roughness as function of these quantities for various vegetation types has yet to be found.

In the case of morphodynamics, the area of interest, that is, the interface between the water and the subsoil, is a boundary plane itself. So, while hydrodynamic studies may address the internal mechanics of the flow far away from any physically active boundary, this is not possible for morphology. Most aspects of sediment transport and morphology are directly related to boundary/interface processes.

At the flow side of the morphologically active layer one has to consider sediment entrainment and deposition. The sediment actively transported by the flow is subject to the same uncertainties as the flow itself (such as the upstream boundary condition — how much washload/suspended sediment is entering the model area?). Sediment transport essentially involves the dynamic interaction of a large number of particles (grains) with the flow and each other. It is generally modelled in terms of mean sediment fluxes. The interaction of physical and chemical forces leads to selective transport of grains, but accurate models to describe all these processes at the level of the individual grains have yet to be found (limits to

¹⁹This relation holds only for $12h \gg k_s$. For small values it is often clipped to a minimum Chézy value of about $10 \text{ m}^{1/2}/\text{s}$.

²⁰Since both physical objects (bedforms) and ecological elements (trees, bushes) contribute to the local flow resistance the general term trachytype (based on the Greek word τραχύτης for roughness) has been introduced as a label for any characteristic set of roughness elements.

the knowledge). Variations in velocity distribution, turbulence characteristics and vegetation also play a role. The influx of sediment (and its distribution over the vertical) determines the capacity of the flow to pick up additional sediment.

Below the morphologically active layer there is a natural, usually incomplete archive of all previous morphological and geological activity. Variations in sediment composition (non-cohesive coarse grained or cohesive, compacted clayey deposits) combined with biological influence may have a strong impact on the erodibility, on the type of bank erosion (see also Section 3.3.3), and hence on the channel planform (see Section 1.2). Coleman (1969), for instance, indicates that, due to inhomogeneous bank composition, a spatial variation in the bank erosion rate may occur. This can (at least temporarily) cause a change in the local flow direction, thereby possibly changing the downstream pattern of erosion and deposition. Variations in bed material may cause similar adaptations in the river morphodynamics, although the influence is often more localised.

Boundary in space (small scale)

The second type of boundary deals with the internal or subgrid boundaries. With respect to hydrodynamic modelling this includes often neglected 3D effects and turbulence characteristics. Many of the so-called large-scale flow structures are too small to be resolved by the large-scale numerical simulation models. If the underlying physical mechanisms are still not fully understood, these boundaries correspond to the conceptual boundaries described below. An empirical subgrid closure model is used for the energy dissipation / viscosity. The use of these turbulence models and large eddy simulation (LES) techniques significantly improves the predictive capabilities of the numerical models in this respect — as illustrated in Figure 3.23 — but a large part of the non-isotropic flow structure at the sub-grid scale remains a matter of empiricism and expert judgement. The validity of the empirical subgrid closure models has to be assessed. In morphological models, the dynamics of bedforms and the resulting mixing of sediments (Blom, 2003) are phenomena on a subgrid scale. Numerical (discretisation, rounding, approximation) errors may be considered also to be part of this category as they generally show up on the smallest scales first.

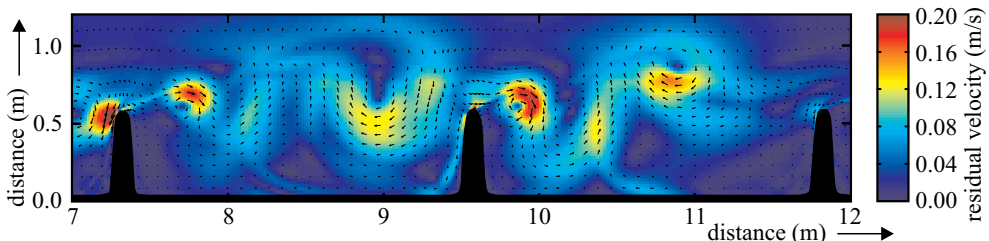


Figure 3.23: An application of Delft3D with Large Eddy Simulation to determine the time-varying behaviour of a globally constant flow along a series of groynes (Van Schijndel and Jagers, 2003). The figure shows the residual velocity at a certain timestep, i.e. the momentary velocity minus the time-averaged velocity.

Boundary in knowledge (modelling concepts)

The restraints of the state-of-the-art knowledge form the third type of boundary (conceptual boundaries). There are many processes that are not fully understood. Simplifying assumptions included either deliberately (to reduce computational time) or due to a lack of process understanding, add to the uncertainty in the prediction. Two-dimensional graded sediment numerical models that include the effects of spatial variations in sediment composition in the subsurface have been developed over recent years. Although first results look promising (Slooff *et al.*, 2001) much research on the interaction of the sediment fractions, and the formulations used (Blom, 2003), is needed. Research on the interaction of vegetation and morphology is just starting in the relatively new field of biogeomorphology (Baptist and Mosselman, 2002).

Boundary in time

Finally, there is one important boundary left, namely the one in *time*. The initial state of the dynamical system to be modelled is only known exactly in theoretical situations; in practical applications only an estimate of the initial state is available. The uncertainty of the initial condition combined with the non-linearities in the model limit the predictability of the model (even without the uncertainty entering into the model through the other boundaries mentioned above). Chaotic phenomena observed in the atmospheric sciences (Lorenz, 1963) also play a role in hydrodynamics, although the larger viscosity and unidirectional forcing of the flow in rivers (that is, downhill flow) limit its effects. On a global scale the hydrodynamic and atmospheric system interact to produce complex phenomena like El Niño (Cane, 1983).

Morphological studies are also sensitive to the relatively poorly known initial condition. A small depression on a bar may grow to become a new channel or it may become filled with clayey sediment during flooding. An island head slightly left or right from the centre of the approaching flow determines whether the left or the right bank is attacked in the following period and, thereby, it determines the overall migration pattern of the channels downstream and eventually upstream. A morphological system like a braided river is susceptible to inherent limitations of predictability due to its internal dynamics. The predictive success depends on the timescale that we are considering (Church, 1996). Extension of predictive models with new processes requires the availability of data on the relevant parameters. For example, in the case of graded sediment models this comes down to information about the spatial variation in the sediment distribution throughout the relevant part of the subsurface. In many prototype cases little information will be available and a large amount of uncertainty remains.

3.5 Planform dynamics of braided rivers

The previous sections of this chapter have focused on the elementary processes involved in morphological change. This section addresses the more aggregate level of planform changes in braided rivers based on field (prototype) studies, laboratory (flume) experiments and theoretical analyses. A thorough understanding of the mechanics of planform changes is a first step in the development of a reliable model for braiding. Due to the complexity of braided

rivers, detailed observations and measurements in the field are difficult and the limited number of theoretical studies that has been done considers only extremely simplified geometries. Fortunately, it has been demonstrated that laboratory models and prototype gravel braided streams agree in the descriptive aspects of channel form and bar development mechanisms (Ashmore, 1982; Ashmore and Parker, 1983; Southard *et al.*, 1984), although one should check the influence of the changing ratio of characteristic hydrodynamic and morphologic length scales (Struiksmma, 1980; Struiksmma *et al.*, 1985). Furthermore, Ashmore (1993) indicates that there is a limit to the utility of laboratory experiments in elucidating the dynamics of confluences, because he notices that in many cases the models are too small (or the instruments too large), and the confluences too unstable, to allow detailed measurements of flow and sediment transport.

3.5.1 Field studies

Bridge and Gabel (1992) studied the sediment dynamics of the Calamus River: a low sinuosity, braided river in Nebraska. From their observations they describe the typical evolution of bars and channels using three stages (see Figure 3.24). Braid bar development starts with the emergence of a part of an alternate bar. The emergent area grows over several years (with varying discharge) by lateral and downstream accretion and the channel banks erode. Asymmetric bar growth and the formation of a scrollbar complex at the upstream end of one the outflanking channels causes the filling in, and subsequent abandonment, of one of the parallel channels. This description of the braiding processes, switching between a one and two channel system, indicates that this river is barely above the threshold for braiding.

The university of Leeds carried out an interesting study within the framework of FAP24 (1996) concerning the behaviour of the Jamuna River at the bar scale (see River Survey Project, 1996, Special Report 9). Based on their observations as shown in Figure 3.25 they propose a six-stage model for mid-channel bar growth:

1. The model starts describing a suitable initial condition: a ‘Y’ shaped planform. This is indicated by the arrows in the upper left subplot of Figure 3.25.

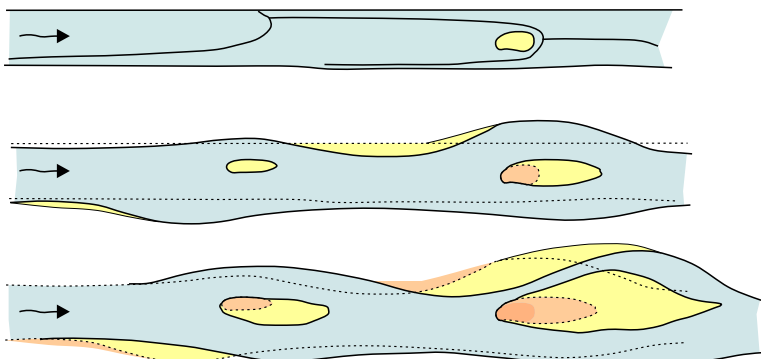


Figure 3.24: Typical evolution of bars and channels in the Calamus River, Nebraska (Bridge and Gabel, 1992).

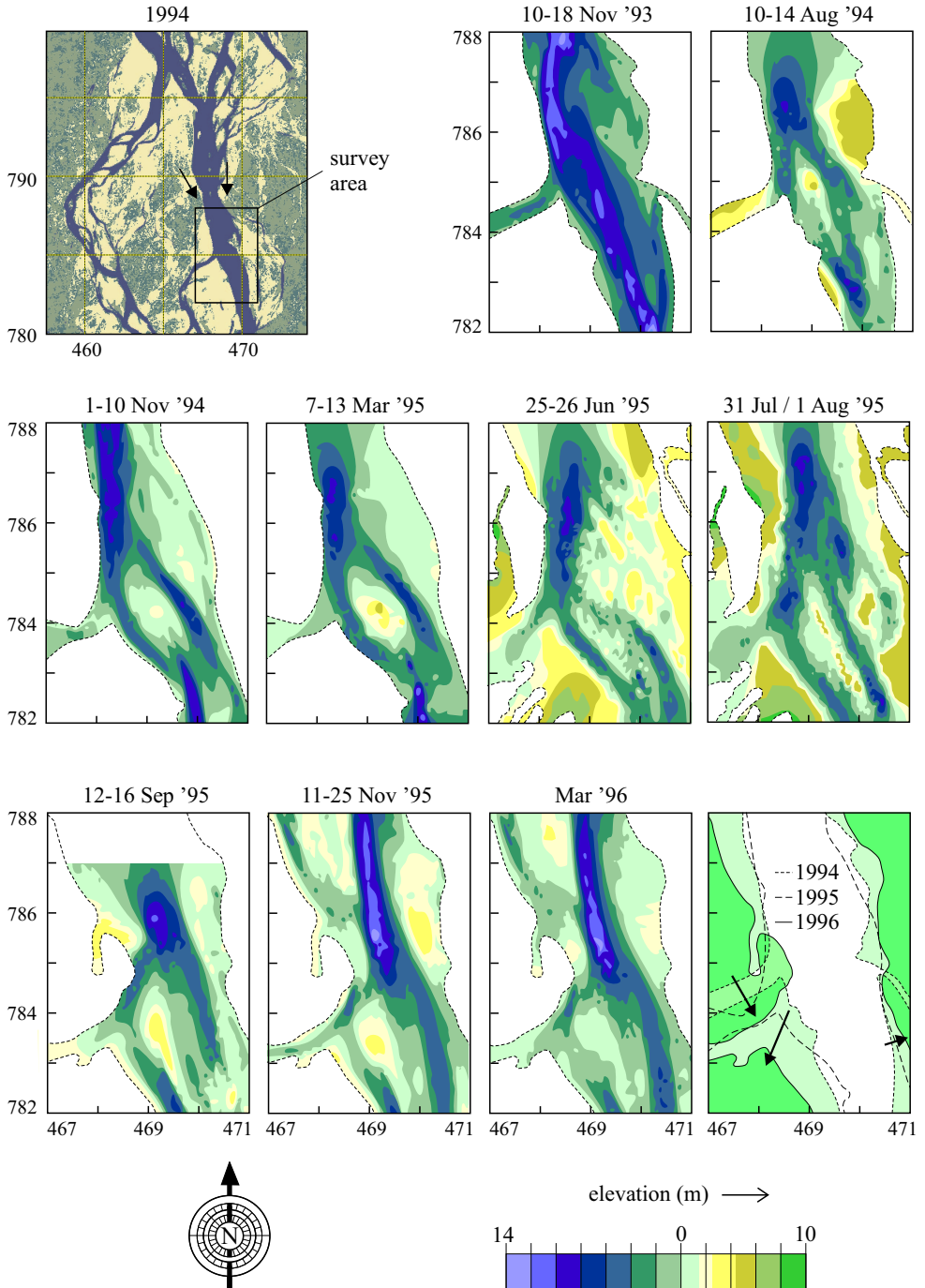


Figure 3.25: Bar behaviour underlying the six-stage model (River Survey Project, 1996, Annex 4 and Special Report 9).

2. Downstream of the flow convergence, a flow divergence (initiated for instance by bank widening) forms. At this stage, initial sediment deposition occurs and the growth of a symmetric mid-channel bar is initiated (November 1993, August 1994).
3. The bar grows through lateral accretion and aggradation of the bar top; this leads in combination with the deepening of the channels eventually to bar emergence (November 1994, March 1995).
4. Bar growth develops asymmetrically due to external factors (June–August 1995).
5. Planform sinuosity (of one of the channels) increases. Note that, as in the Calamus River case described by Bridge and Gabel (1992), upstream sedimentation (here, north-west of the considered bar) plays an important role in the reshaping of the western channel (September 1995).
6. Finally, one of the minor channels is abandoned and the bar coalesces with a neighbouring bar or flood plain (November 1995, March 1996). Note that, the bar in Figure 3.25 also reached this state in June 1995.

Again this describes the formation of new bar in the centre of a channel, a process referred to as central bar braiding or mid-channel bar formation. This process, which is covered by just the second and third step, was also observed by Leopold and Wolman (1957) and reported by Coleman (1969). The first step (describing the initial planform) was not identified as such by Coleman (1969), although he remarks that according to his observations islands have often a relatively deep scour pool immediately upstream. The causal relationship that downstream of a scour hole a bar may form, was not yet identified. The third and following steps described above deal with channel shifting, bar type conversion and feedback effects resulting in braiding.

Regarding the channel shifting, Coleman (1969) observed variations in the processes during the year, which results in two different types of channel shifting.

- At low stage, when the river is subdivided into numerous small channels, there is often just one branch per cross-section serving as the main channel. At that time, the main channel follows in general a meandering course from the left to right bank and back. When the discharge increases, the channel widens and deepens to accommodate the increased discharge. In the meantime, it gradually straightens its path and causes thereby lateral erosion and migration of the thalweg. This shifting of the thalweg takes place gradually over a time span of several weeks.
- During falling stage (September/October), at the end of the flood peak, large amounts of sediment are deposited and bars growth rapidly grow in size. The thalweg shifts induced by these deposits are often sudden and erratic.

So, there is a seasonal variation in the rate of thalweg shifting, with the maximum amount taking place during rising and falling stages. During the falling stage, the movement is more erratic and sudden. Similar observations were reported by Chein (1961) for the braided Yellow River, China. He indicates that the channel shifting is most intense when (1) a large amount of easily erodible sediment is available, (2) there is a large variation in the discharges and sediment concentrations, (3) the rise and fall of the flood are rapid, (4) the channel is

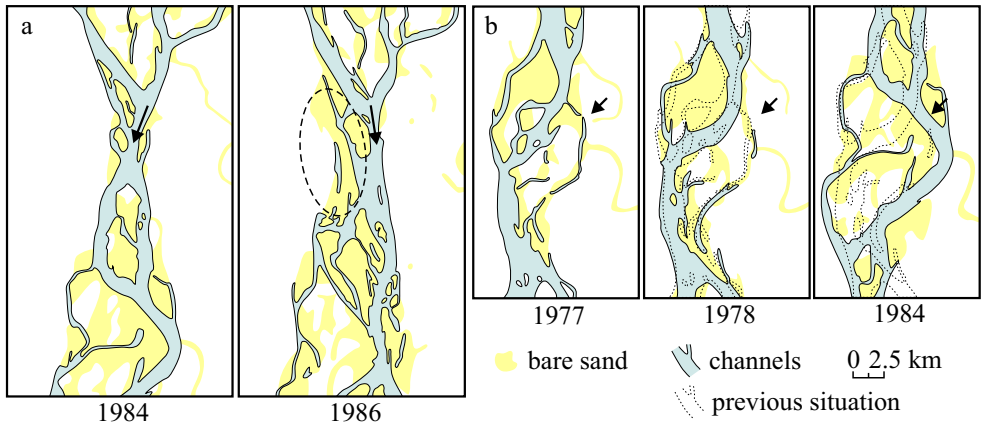


Figure 3.26: Processed satellite images of the Jamuna River illustrating the processes causing channel shifting (Klaassen and Masselink, 1992). a: Bar-induced shifting: due to the growth of the bar complex at the right bank (indicated by the dashed ellipse) the direction of the flow changes as indicated by the arrows and the downstream planform changes drastically. b: Outer bend overflow channel formation: the arrows indicate the reuse of a previously abandoned channel.

steep and the flow speed is high, and (5) the river consists of a wide, shallow non-restrictive channel belt.

Based on satellite images of the Jamuna River, Klaassen and Masselink (1992) distinguished three types of processes responsible for the sudden channel shifts, namely

- *bar-induced shifting.* A rapid shift in thalweg position may result when a large sand bar migrates to a position where it (partially) blocks the main channel, meanwhile forcing a larger part of the flow through another existing channel that was less important up to that moment (see Figure 3.26a). The main element of the bar-induced shifting is the reorientation of the bifurcation leading to a redistribution of water and sediment. This process has no immediate influence on the general topology of the planform, that is, the process itself does not form new channels or abandon others, but the shifted discharge distribution may cause more changes further downstream.
- *development of a cutoff.* If there is no other channel available to take over the flow when the transport capacity of a curved main channel is reduced, a new, straighter channel may be created. This may also happen if — due to some planform changes upstream — the discharge through the channel increases beyond the capacity of the channel. The formation of the new, straighter channel is the most important aspect of this process.
- *outer bend overflow channel formation.* This third process leads to the formation of a new channel that bifurcates from the old channel in an outer bend (see Figure 3.26b). The new channel is in this case not necessarily straighter and shorter than the old channel; this suggests that the channel is not created to increase the overall transport efficiency, but that it should instead be looked upon as solving a local disequilibrium in the momentum balance during flood. This disequilibrium may be caused by an increased discharge imposed upstream or an increased curvature due to migration during previous years. Klaassen and Masselink (1992) indicate that this process is often associated with the reoccupation of an old channel near the outer bend — a process called ‘secondary anastomosis’ by Church (1972).

The latter two processes are related to the chute cutoff process described by Ashmore (1991) for flume studies.

3.5.2 Laboratory experiments

Although flume and scale models are widely used in the study of braiding, relatively little is reported on the braiding processes. Flume studies of confluence scour (Ashmore and Parker, 1983), sediment transport rates (Ashmore, 1988; Hoey and Sutherland, 1991; Warburton and Davies, 1994) and sediment sorting (Ashworth *et al.*, 1992) in braided rivers and flume studies of depositional structures by braided rivers (Ashworth *et al.*, 1994) will not be discussed here. This section focuses on the planform dynamics of braided rivers.

Ashmore (1991) describes eleven flume experiments with varying slopes and discharges in which the processes leading to braiding were studied. The streams were generic models of gravel-bed braided streams. Each of the experiments started from a straight trapezoidal channel. He observed the following four phenomena which led to braiding (sketched in Figure 3.27):

1. *Formation of a chute cutoff.* In most cases alternate bars formed within the initially straight channel, followed by slight meandering and pointbar accretion. From the theoretical analyses mentioned in the previous section we know that the alternate bar mode forms initially when the width-depth ratio is relatively small. Subsequently, the meandering led to a slight widening of the channel and braiding was initiated by the development of chute channels across the point bars formed by the initial meandering. The cutoff process often started when a pulse of bedload (bedload sheet or transverse bar) migrated into the neighbouring main channel. The cutoff channels formed from an initial depression by headward erosion (that is, erosion proceeding in upstream direction), meanwhile capturing an increasing volume of water, and rapid enlargement. At the downstream end of the cutoff channel a large transverse bar prograded out into the confluence downstream of the newly formed braid bar; the change in flow direction that this caused downstream led in some cases to the erosion of braid or point bars located immediately downstream of the confluence.

Bedload streams, which are unable to build up the inner point bar to bank-full elevation (or, alternatively, to fill the chute with fine sediment) in the absence of fine-grained suspended sediment transport (Carson, 1986), are most likely to form chute cutoffs. The role of suspended sediment in stabilizing point bars and preventing chute cutoff in laboratory streams has been demonstrated experimentally by Schumm and Khan (1972). A change in flow direction immediately upstream of the point bar head, a (possibly related) pulse of bedload causing a reduction in the flow capacity of the main channel, combined with the absence of fine-grained bar tail and bar top deposits, triggers the initiation of braiding by chute cutoff. Alternate bars forming in straight flumes have been observed many times, but those bars seldom led to braiding. A complete description of the conditions at which chute cutoffs develop must include considerations regarding bank stability and associated bend widening and/or scour. In a later stage of the braiding process new channels may not only be formed by incision of new channels, but also by ‘secondary anastomosis’: reoccupation of previously abandoned channels (Ashmore, 1991; Church, 1972).

2. *Growth of a mid-channel bar.* During experiments with a low stream power, alternate bars were barely formed and braiding developed very slowly. In that case a bedload sheet stalled at a short distance downstream of an artificial confluence caused by the arrangement of the flume entrance conditions. This artificial convergence and subsequent divergence of streamlines must have been associated with a local increase, respectively decrease, in the shear stress and sediment transport rate. These spatial variations in the sediment transport rate cause the generation and stalling of the bedload sheet. Ashmore (1991) indicates that the coarse downstream margin of the stalled bedload sheet became the sedimentary nucleus of the braid bar that formed at that location. Furthermore, he notes that almost all braid bars that formed following this mechanism were solitary braid bars in an otherwise unbraided channel, and that this may be typical of streams barely above the threshold for braiding.

Although the initial confluence was an artefact of the model setup, similar stalling of bedforms has been observed in flow expansions in prototype streams. The process has been described extensively in the literature starting with Leopold and Wolman (1957)

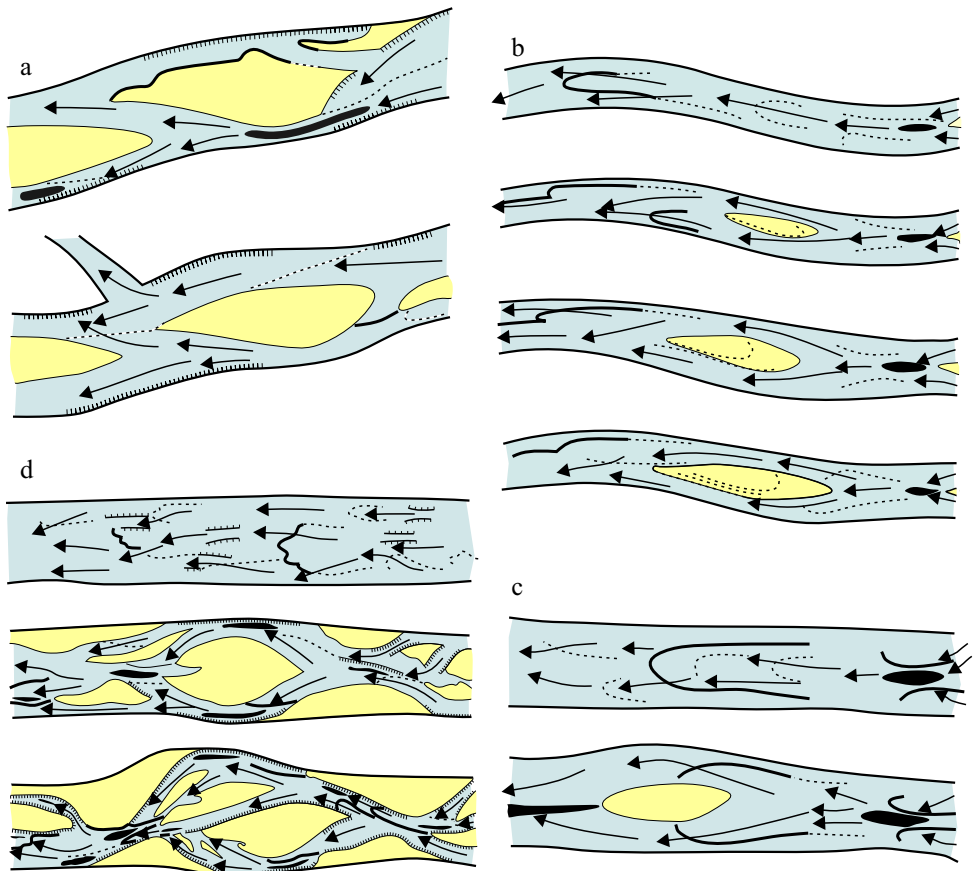


Figure 3.27: Sketches by Ashmore (1991) of the four braiding processes that he observed. a: formation of a chute cutoff. b: growth of a mid-channel bar. c: conversion of a transverse bar. d: simultaneous growth of multiple bars.

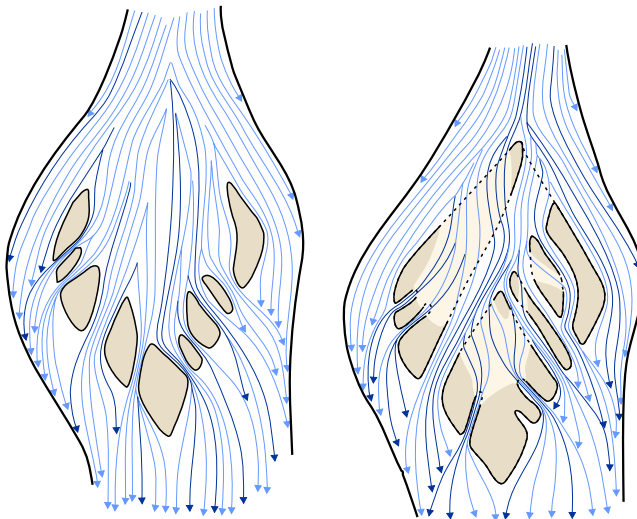


Figure 3.28: Dissection of the head of a spool bar at two different water levels as observed by Krigström (1962) on the sandur plains of Iceland. Over time the scars at the downstream end of the bar enlarge in upstream direction by headward erosion.

and it is the most often quoted mechanism for the initiation of braiding. The absence of pronounced bed scour, the low confluence angle, and the low bank erosion rates all characterise the mid-channel braiding process.

3. *Dissection of a linguoid bar*, originally called ‘Conversion of a transverse bar’ by Ashmore (1991). Linguoid bars, which were called lobate transverse bars by Ashmore, were common in all his experiments, but they were more numerous and better developed in those with higher discharge and slope. In some experiments braiding was initiated by flow division around the downstream end of a stalled, symmetrical linguoid bar. The linguoid planshape (with the points in upstream direction) is quickly converted into the braid-type bar shape (with the points in downstream direction) when the central part of the bar stalls. The other parts of the bar continue to migrate downstream (at both sides of the bar) and they result in lateral accretion of the bar while the upstream end accretes due to the arrival of subsequent bedload sheets. This process is different from the central bar braiding process, in that the sediment transport rate is much higher in this case, but in both cases the stalling of the migrating bedform occurs in a reach where the channel widens. The process may also be initiated by two or three bedload sheets overriding each other.

Krigström (1962) describes a similar process, namely the dissection of the head of a spool bar. Ashmore (1991), however, indicates two differences between the two process descriptions. First, in his experiments multiple dissections of the bar front did not occur, whereas it was described by Krigström (see Figure 3.28). Second, Ashmore indicates that the experiments show that the braid bar gradually grows by lateral accretion rather than it being formed entirely by falling-stage modification of the initial bedform (Church and Jones, 1982). However, Krigström (1962) also mentions that the drop in water level that causes the erosive action is initially caused by downcutting

of the channels alongside the bar.²¹ Changes in discharge may contribute. The influence of a falling discharge on the formation of multiple chutes has also been noted by Rundle (1985). Field studies of proglacial outwash in the upper reaches of the Kicking Horse River (Hein and Walker, 1977; Smith, 1974) have also shown the influence of a drop in discharge. The experiments of Ashmore (1991) have shown that, although the falling-stage may speed up the process, it is not a necessary condition for the dissection process to occur. One should note that theoretical analyses had already proven that discharge variations are not necessary for braiding to develop by the growth of central or multiple bars (see Section 3.5.3).

Ashmore (1991) observed flow divergence around the bar (leaving the central part undisturbed), but Lewis and Lewin (1983) observed the opposite: the dissection of the central part of the bar by one channel instead of two channels being formed or maintained at the left and right bar margins. They refer to this process as a mobile bar cutoff. So, the bar dissection process seems to consist of a range of processes all acting on a large — stalled or slowly migrating — bar, which is reshaped by the formation of one or more new channels. One should note however that the process described by Lewis and Lewin (1983) does not lead to braiding, as it forms only one new channel.

4. *Simultaneous growth of multiple bars.* In a steep but wide and shallow channel, bed disturbances may form at several locations at the same time as predicted by theory (see Section 3.5.3). Based on an experiment with such a wide, shallow channel Ashmore (1991) remarks that the instability manifests itself initially by local, isolated flow accelerations marked by pronounced waves on the water surface and antidunes on the bed. The sediments eroded in these areas were deposited as stacks of bedload sheets downstream of the flow accelerations. The resulting morphological pattern was similar to, but less regular than the multiple-row bars described by Fujita (1989) which corresponds to the initial emergence of a high transverse morphological mode ($m \gg 1$) (see Figure 3.29).

²¹The downstream end of a bar emerges often first although the upstream end of the bar is higher; this results from a water level slope that is larger than the slope of the bar surface.

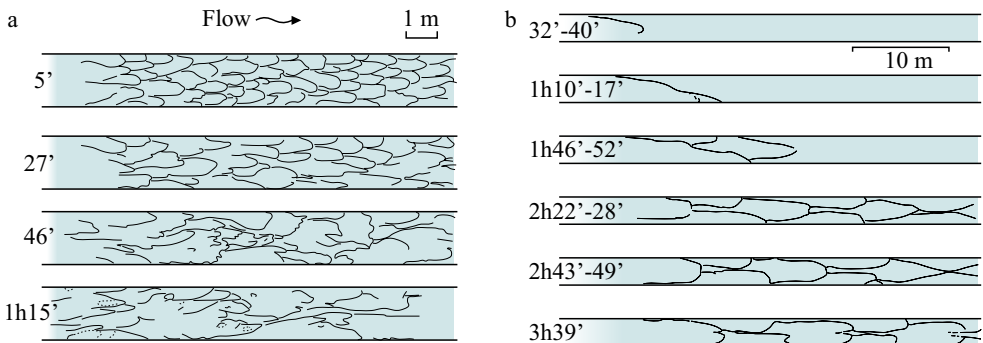


Figure 3.29: Flume experiment observations by Fujita (1989). a: multiple bar braiding with an initially very high transverse mode throughout the model reach which is later on largely replaced by a much lower mode. b: gradual downstream progress of a low order braiding instability.

The initiation of braiding from multiple bars occurs only in channels with very high width-depth ratio and it was not observed later on during the experiments; once braiding had been established none of the channels became wide and shallow enough to allow for this process to occur again. Ashmore (1991) suggests that the multiple bar dissection process might be more common in sand-bed than gravel-bed streams; however, it can be expected that in general one of the other braiding processes will be triggered, due to natural disturbances in the prototype, before the channel reaches a sufficiently high width-depth ratio for multiple-bar braiding to occur. The process might be important on large outwash fans, where frequently new shallow channels are formed; at those locations multiple-row braid bars can often be observed (Boothroyd and Nummedal, 1978).

Underlying these four braiding processes, there appears to be one common feature, being the stalling and vertical accretion of bedforms, in this case mostly bedload sheets, in a flow expansion. In the cases of mid-channel bar growth, linguoid bar dissection, and multiple bar growth the braiding is a direct consequence of the stalling of the bedforms. In these cases the stalled bedforms become the nucleus of the new braid bar. Although the stalled bedforms do not directly contribute to the size of the braid bar in the case of the chute cutoff mechanism, that process is also triggered by the stalling of bedforms. The sediment transport rate and the local geometry determine which braiding process occurs. The processes described above are the end members of a continuum of possible processes that all result from a local reduction in the local transport capacity due to a decrease of the bed shear stress. Repetto and Tubino (1999) show that variations in channel width may inhibit the formation of free bars and lead to the formation of forced central bars. The divergence of the flow and the related reduction in the bed shear stress result in a gradual sedimentation. This sedimentation is the result of gradients in the sediment transport rate/capacity. So, contrary to the emphasis on the stalling of bedforms by the description of Ashmore (1991), bar formation does not require shear stresses to drop below a critical shear stress.

The supply of bedload sediments from upstream plays an important role in all of these braiding processes. In the case of the central bar mechanism, where the transport rate is relatively low, isolated braid bars form. But also in the other cases — where the braiding is more dynamic and sediment transport rate is higher — is the braid bar formation still closely related to the arrival of pulses of bedload material from immediately upstream. The source of such a pulse might be bank erosion, or scour. Bend scour by secondary currents around a newly formed braid bar, and confluence scour downstream of a braid bar contribute to the propagation of the braiding process in downstream direction. Regular variations in the bedload transport rate under laboratory conditions have been observed by Ashmore (1988), see Section 3.1.4 on sediment transport. Once braiding was established in the experiments, increased braiding activity was often associated with the passage of these ‘waves’ of bedload material. This autogenic, periodic behaviour can maintain active braiding without the necessity for overall aggradation in the braided river even under conditions of steady flow and steady sediment supply.

The role of the nodes (confluences and bifurcations) of the channel network is crucial in the redistribution of the sediment transport over the various channels. The distribution of suspended sediment is in first approximation proportional to the discharge distribution. The bifurcation angle and the local bed slopes have a significant influence on the distribution of the bedload transport. The geometry of a bifurcation is constantly reshaped by the local flow

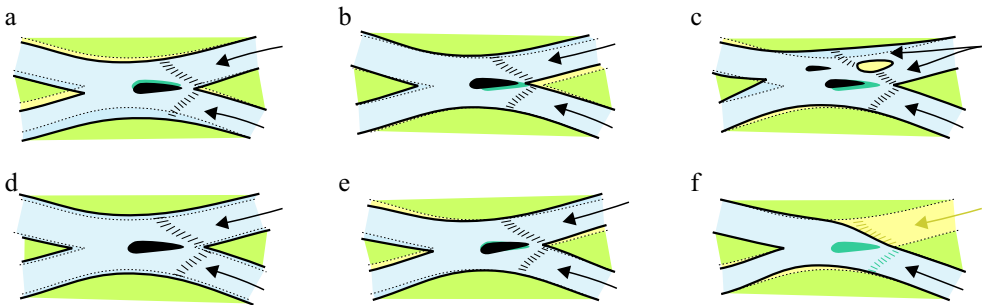


Figure 3.30: Six modes of confluence kinetics distinguished by Ashmore (1993).

conditions which vary in time due to discharge variations and upstream planform changes. The upstream planform changes can be either gradual and systematic (for instance due to the migration of an upstream meander bend) or sudden and irregular. The latter can be expected when the flow conditions are determined by more than one channel due to the presence of a confluence upstream. Experiments by Ashmore (1993) show that confluences often adapt rapidly under the influence of upstream changes, and their dynamics can be very erratic. Ashmore discerns six modes of confluence kinetics (see Figure 3.30):

- a) lateral migration following changes in upstream channel configuration or discharge;
- b) upstream and downstream shifting caused by relocation or gradual migration of the confluent channels;
- c) avulsion or bifurcation in the neighbourhood of the confluence, thereby increasing the complexity of the confluence;
- d) changes in the scale of the confluence (enlargement or reduction) caused by changes in discharge;
- e) rotation of the scour axis, due to redistribution of flow upstream, relative migration of the confluent channels, or prograding of a transverse bar into the confluence; and
- f) obliteration of the confluence due to abandonment of one of the confluent channels.

The changes in the confluence will cause subsequent changes in the planform of the downstream channels. The combination of a confluence and a bifurcation (a scour pool and a downstream braid bar) is often recognised as a fundamental building block of braided stream morphology from which larger bar complexes grow. The connection between confluence kinetics and braid bar sedimentation is a key element of braided river mechanics and must according to Ashmore (1993) be incorporated into conceptual and mathematical models of braided river sedimentation.

3.5.3 Theoretical studies

Most theoretical studies of braiding have been limited to linear stability analyses of straight channels (Engelund and Skovgaard, 1973; Parker, 1976; Fredsøe, 1978). Non-linear stability

analyses have mainly focused on the behaviour of alternate bars in straight (Colombini *et al.*, 1987; Tubino, 1991) or mildly meandering channels (Seminara and Tubino, 1989; Schielen, 1995). Linear stability analyses have shown that beyond a certain threshold for the width-depth ratio alternate bars will form (see Figure 3.13). If the width-depth ratio increases further, multiple rows of bars form, and at even higher ratios there is a tendency towards braiding. These studies have demonstrated that under appropriate conditions multiple bar braiding is an inherent property of the dynamical morphological system, even at a constant discharge. Recent studies on bar formation in channels with periodic, alongstream variations in width have shown that the formation of central bars may be forced upon a channel by width variations (Repetto and Tubino, 1999). Pittaluga *et al.* (2001) indicate that secondary flow and momentum play an important role in this process. The formation of bars at a channel widening is similar to the forcing of a point bar geometry by the sinuosity of a channel (Seminara and Tubino, 1989) and a phenomenon related to overdeepening (Struiksma *et al.*, 1985) may be involved (Mosselman, 2000, pers. comm.).

3.6 Discussion

Summarising the previous sections, the range of processes that characterise braiding includes: formation of single (or multiple) mid-channel bars by deposition in wide channels and flow expansions; dissection of large bedforms (often during falling stage); formation of new channels by avulsions/chute cutoffs and abandonment of other channels; lateral migration of channels and associated accretion of point bar complexes; longitudinal translation, rotation, expansion or contraction and obliteration of confluences and associated formation or erosion of downstream bar complexes. Furthermore, these processes are influenced by the often highly variable discharges in braided rivers, variations in vegetation, and varying sediment composition. In the discussion, tectonic and human influences have been largely ignored.

At the beginning of this chapter, six characteristic planform changes were identified based on satellite images of the Jamuna River. Two of those (channel migration and changes in channel width) are not unique to braided/anabranching rivers. The remaining four processes are unique to rivers with multiple branches; they are: (mid-channel) bar growth, channel formation (cutoff), channel abandonment, node (confluence, bifurcation) deformation. In the following sections, these six planform changes are discussed individually in the context of the physical processes and observations described in this chapter.

3.6.1 Channel migration

Two types of channel migration can be distinguished. The first type of migration is the lateral channel migration due to channel curvature, which has been studied extensively for meandering rivers: the outer bend is eroded and accretion of the pointbar takes place. Bank erosion and secondary flow are the dominant processes. The second type of migration occurs during flood when — in a river with a large difference between low-stage and high-stage discharges, as for example the Jamuna River — bars that have a fixed location during low stages become mobile during high stages. The migration of the bars results in a net downstream migration of the low-stage channels, which cannot be explained based on low-stage processes alone. In this case, the adaptation of the velocity profile due to flow acceleration and deceleration, or

(depending on the steepness of the bank) erosion due to overbank flow with flow separation, are important. In many cases low-stage channels disappear almost completely during the flood. New low-stage channels are subsequently cut into the bed topography when the flood falls; this process can cause erratic shifts of low-stage channels over a flood period.

3.6.2 Channel widening and narrowing

Bank erosion processes may lead to channel widening, but there is no equally powerful accretion process that balances the (horizontal) bank erosion. Gradual narrowing of a channel can occur due to any of the following four processes. First, if enough sediment is available, a meandering channel may show a net accretion by building the pointbar faster than eroding the outer bend. Second, in cases with abundant vegetation, a channel can become narrower due to gradual invasion of vegetation into the channel. Sediment is trapped more effectively by the vegetation, which eventually leads to a narrower channel. Third, degrading rivers, which incise into bedrock or alluvial deposits, can become narrower when there is not enough flow strength available to erode the bed in all places to a sufficient degree. Fourth, rivers with a varying discharge may deposit sediments during flood, up to such heights that the low-stage channels become narrower. Since large morphological changes occur in the Jamuna River during the yearly flood, the low-stage channels of this river can become narrower in this manner. Mosselman *et al.* (1995) indicate, however, that channel abandonment occurs as a result of shallowing rather than narrowing.

3.6.3 Mid-channel bar growth

A mid-channel bar/island can form in the centre of a channel if the sediment supply exceeds the local sediment transport capacity; this may for instance occur in a flow expansion. Such a bar may suddenly appear in the low-stage planform after a flood after being present below the low-stage water surface in the preceding years. In theory, multiple rows of bars could form at once in this way, but the width-depth ratio required for multiple bars to form are attained only under rare circumstances (e.g., during the initial stages of channel formation after an avulsion). In the Jamuna River and other braided rivers with a similar high sediment load, it is more likely that mid-channel bars are formed by the dissection of large migrating bars.

Changes in bar size after its formation (i.e., either growth due to accretion or shrinking due to erosion) can be attributed to migration of the neighbouring channels or to changes in the bed of the high-stage channel during following floods. Vegetation can — once the bar has emerged — help to stabilise the newly formed island. However, based on the series of planforms shown in Figure 2.10 it is concluded that this process does not play an important role in the dynamics of the low-stage planforms of the Jamuna River because the small mid-channel bars generally disappear after one year.

3.6.4 Channel formation

To maintain the braided appearance, new channels and islands must be formed to compensate for abandoned channels. This occurs mainly due to the formation of new channels across braid- or pointbars or parts of the flood plain. This conclusion is similar to the observation

by Ashmore (1991) that braiding started in most of his experiments due to chute cutoff formation. The formation of new channels across large bars, can be also be interpreted as the large-scale equivalent of the dissection of stalled linguoid bars. The formation of a chute cutoff or, more generally, the formation of a new channel may be triggered by an obstruction of the flow due to sedimentation at another location in the river cross-section. For a more extensive discussion of this process, see Chapter 6 and further.

3.6.5 Channel abandonment

Channels are abandoned as a result of an increase in the sediment supply relative to the sediment transport capacity (depending on the discharge). This change is often triggered by the realignment of the channels at the bifurcation upstream, which in turn occurs due to on-going migration of the bifurcating channel or the passage of a large dune or migrating bar. The latter event may lead to partial or complete blockage of the channel entrance and, therefore, to channel abandonment. The abandoned channel will be gradually filled in by overbank deposits, or it can be reopened after having been dormant for several years. Mosselman *et al.* (1995) indicate that a large percentage of the channels with a rather oblique offtake is abandoned within a few years (see Section 5.3.1 about the concepts underlying the branches model for braided rivers). The abandonment of a single branch upstream will result in the re-distribution of discharge of multiple branches downstream. This may trigger further channel abandonments.

3.6.6 Node deformation

Confluence dynamics is strongly influenced by the changes in the relative discharges and sediment transport rates of the confluent channels; such changes result from discharge variations (flood or low stage) and planform changes upstream. Since the relative discharges and sediment transport rates cannot be determined easily from the planform, reorientation and translation of a confluence — due to changes in these parameters — will often occur unexpectedly and may, therefore, seem to occur randomly. The discharge ratio and the confluence angle determine the dimensions and orientation of the confluence scour hole. In the flow expansion downstream of this scour hole, a mid-channel bar and, thus, a bifurcation may form. If this occurs, any adjustment of the confluence will immediately lead to a reshaping of the bifurcation point and a redistribution of discharge at the downstream bifurcation with yet more changes downstream. The migration and rotation can be predicted reliably if the confluence migrates consistently for a longer period of time. This occurs, for instance, if the confluence is dominated by one of the two confluencing channels.

Chapter 4

Planform models: an introduction

In the previous chapter we have discussed the processes involved in river morphology in general and those involved in braiding in particular. Starting with this chapter the emphasis shifts to the mathematical modelling of planform changes of these rivers. In the next chapter three models for planform changes in braided rivers will be described that have been implemented and tested as part of this study. In order to be able to place these models in an appropriate context, this chapter describes the developments in the mathematical modelling of planform changes. These developments have mainly occurred during the last few decades, triggered by the increasing capabilities of computers. The first section describes several models for the simpler case of meandering rivers. The first one of these models forms the basis for one of the braided river models to be discussed in the next chapter. The other models indicate the state-of-the-art modelling for meandering rivers. The second section describes several simple models that reproduce one or more aspects of braiding although they cannot be used for predicting planform changes. The last section describes two general purpose modelling methods that can be applied to any river.

4.1 Models for meandering rivers

While modelling braided rivers is still in its infancy, modelling meandering rivers has received a lot of attention over the last decades. The planform of a meandering channel is — contrary to the general braided pattern — often relatively simple; this makes the meandering channel the first candidate for basic morphological research beyond the straight-channel case. In spite of the relative simplicity, making detailed predictions for channel migration of meandering rivers is often still quite difficult, due to the uncertainties in the boundary conditions, such as discharge variations and inhomogeneities in bank composition. Most meander models are no longer valid when significant (point-bar) flooding occurs or when a cutoff is on the brink of occurring, since the lateral variations in the river are generally assumed to be given by some simple theoretical relation. General 2D aspects are not included in the meander models besides the one described by Mosselman (1991, 1992). In the first subsection a very simple, empirical model of meandering is described, which was developed by Ferguson (1984a), Howard (1984) and Howard and Knutson (1984). This model, which uses a

kinematic approach, has been used as one of the building blocks for the branches model for braided rivers that is described in Section 5.3. A model based on geometry and time only is called kinematic, contrary to a model that includes also momentum equations, which is called dynamic.

Dynamic models can be based on the nonlinear equations for flow and morphology or on appropriately linearised versions of these equations. Within the group of dynamic models using linearised equations one can distinguish two subgroups. First, models that include (linearised) equations for flow which are combined with formulations for bank erosion and channel migration. Second, models that include equations for both flow and morphological development again combined with formulations for bank erosion and channel migration. A model within the first group has been developed by Ikeda *et al.* (1981); it was used by Parker *et al.* (1982) and Sun *et al.* (1996). This model and its applications are described in the second subsection. The models developed by Johannesson and Parker (1989) (and extended by Howard (1992, 1996)), Crosato (1990) belong to the second group; they are described in the third subsection. The last subsection describes a model that was developed about a decade ago by Mosselman (1991, 1992). It combines a 2D non-linear depth-averaged model with a quasi-steady approach for the adaptation of its non-orthogonal mesh between its gradually shifting left and right bank.

4.1.1 Kinematic models

One of the most important steps in the modelling of meandering rivers was the development of the kinematic meander model of Ferguson (1984a), Howard (1984) and Howard and Knutson (1984). Field measurements by Nanson and Hickin (1983) on the Beatton River, British Columbia, had indicated that the lateral migration rate ζ of the bend apex increased with increasing (bend-averaged) curvature until some critical curvature above which the migration rate dropped sharply. Ferguson (1984a) modelled this relation with the following equation

$$\frac{\zeta}{B} = \begin{cases} k \left(\frac{cB}{R} \right)^{-2} & \text{if } R < cB \\ k \left(\frac{cB}{R} \right)^2 & \text{if } R > cB \end{cases} \quad (4.1)$$

where

- B channel width,
- c critical R/B ratio (equal to 3) associated with the maximum migration rate,
- k partially non-dimensionalised migration rate equal to 0.02 yr^{-1} ,
- R local radius of curvature.

This relation is plotted in Figure 4.1a together with the measurement data of Nanson and Hickin (1983). The assumption that the migration rate ζ can be normalised using the channel width B is remarkable. If there would really exist such a unique relation between ζ/B and B/R then two rivers of different magnitude with (except for scale) identical planforms would have after one year still exactly the same planform (again except for scale). This indicates that the time scale would be independent from the size of the river, which is not the case in reality. If the relation is assumed to apply locally to all points of a meandering channel — and

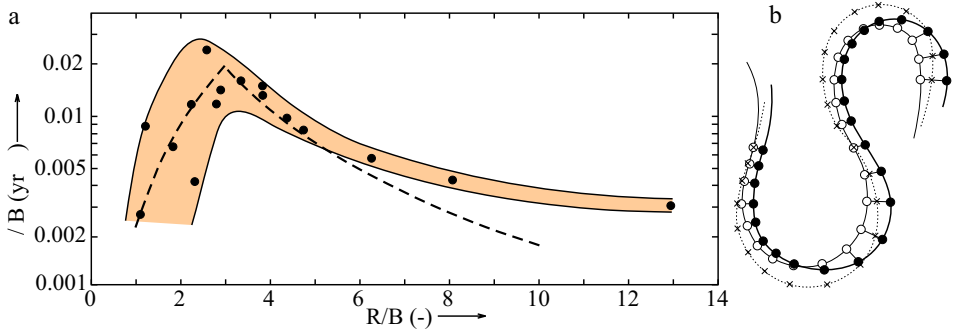


Figure 4.1: a: Migration rates measured by Nanson and Hickin (1983) (dots) and the relation modelled by Howard (1984) (dashed line). b: The influence of the lag effect on meander development. The thin line indicates the initial channel alignment, the dotted line would form without the lag effect, the thick line indicates the new course when the lag effect is included.

not only to the bend apex for which it had been obtained — the resulting migration pattern is characterised by lateral migration and extension of bends only (as indicated by the dotted line in Figure 4.1b). The typical asymmetry observed in physical meanders (the thick line in Figure 4.1b) is not reproduced.

It was soon realised that some lag effect was needed to reproduce the natural lag between the bend apex and the point of maximum shear stress. Ferguson (1984a) implemented this lag effect by computing the adjusted migration rate ζ in point i from the curvature at point $i - 1$; the direction of migration was taken perpendicular to the chord $i, i + 1$. The same approach was recently used by Gilvear *et al.* (2000). Note that with this method the lag effect depends on the discretisation used. Howard and Knutson (1984) suggested to compute the adjusted bend migration rate ζ_a by means of an integral of the nominal bend migration rates ζ_n (that is the rates as computed directly from the local curvatures) over the total upstream reach

$$\zeta_a(s) = \Omega \zeta_n(s) + \left[\Gamma \int_0^\infty \zeta_n(s - \xi) G(\xi) d\xi \right] \left[\int_0^\infty G(\xi) d\xi \right]^{-1} \quad (4.2)$$

for some weighting parameters Ω and Γ and weighting function $G(\xi)$. This type of relation is in line with the outcome of a theoretical study by Parker (1984) which is based on the model for flow in a meandering channel by Ikeda *et al.* (1981) that will be described in the next section. Parker (1984) shows that — given a linear relationship $\hat{\zeta} = E_0 \hat{u}_b^*$ between the dimensionless lateral migration rate $\hat{\zeta} = \zeta / u_0$ and the local near-bank velocity deviation \hat{u}_b^* — the normalised lateral migration rate follows from an exponential weighting of the upstream curvatures

$$\hat{\zeta}(\hat{s}) = -\chi E_0 \hat{c}(\hat{s}) + c_f [(A + 2)\chi + F_0^2 \chi^4] \int_0^\infty \chi E_0 \hat{c}(\hat{s} - \xi) e^{-2\chi c_f \xi} d\xi \quad (4.3)$$

where the meaning of the variables is as defined in Section 4.1.2. The relationship shown in Figure 4.1 is now assumed to indicate the relation between the *adjusted* migration rate and the bend curvature. However, Nanson and Hickin (1983) did not explicitly take the upstream reach of influence into account while determining the characteristic bend curvatures.

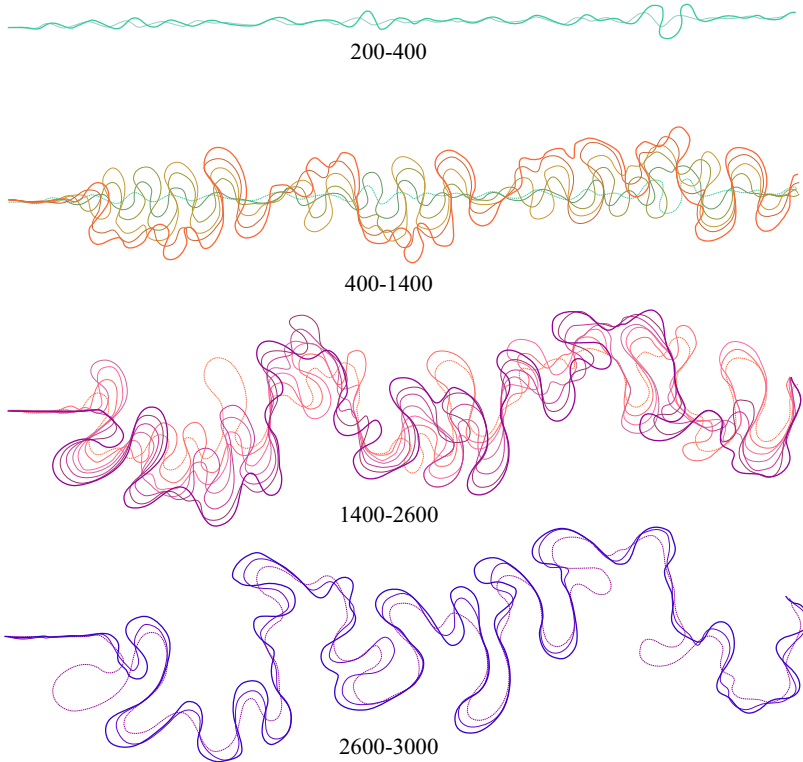


Figure 4.2: Simulation results by Howard and Knutson (1984).

In any case, the exact form of the relation between the (uncorrected) nominal bend migration rate ζ_n and the local curvature is not known. Based on simulations with varying relations $\zeta_n/B = f(B/R)$, Howard and Knutson (1984) conclude that there are not enough data available to determine the real shape of $f(B/R)$. Notwithstanding this fact any relation similar to the original one seems to work reasonably fine. Howard and Knutson found that, when both migration rates are plotted, the adjusted migration rate curve is almost equal to the curve of the nominal migration rate except for small values of R/B (strongly curved bends). This observation can be explained by the fact that strongly curved bends are generally the shortest; therefore, the influence of the upstream reach is the largest in that case. Note that the erosion rate ζ in Equation 4.3 is normalised using u_0 rather than B , unlike Figure 4.1a and Equation 4.1.

If a prolonged period of migration is simulated, a meander migration model should also incorporate the effect of chute and neck cutoffs. A chute cutoff occurs when the river cuts a new channel through recently deposited point bar sediments in a relatively sharp bend. This process is not explicitly included in the model of Howard and Knutson (1984) but it is to some extent represented by the fact that upstream weighting of the channel curvatures may lead to erosion of the inner bend. Ferguson (1984a) remarks that the combination of upstream weighting of channel curvatures and the decrease in nominal migration rate for sharp bends ($R < cB$ in Equation 4.1) may cause the development of double-headed meanders. Neck cutoffs, the second type of cutoffs, occur when local sinuosity becomes so large that adjacent

loops touch each other. This process is included in the model by the rule that a neck cutoff occurs whenever the distance between two channel sections becomes less than one channel width. The sharp bend in the river that remains after the shortening of the channel by a neck cutoff is in general smoothed by erosion of the inner bend, which in that case does not represent chute cutoff because of the probable age of the deposits. The remainder of the old channel (the horseshoe or oxbow lake) is not taken into account during the remainder of the simulation. Some of the very realistically looking results of long-term meander development obtained by Howard and Knutson (1984) are shown in Figure 4.2.

This approach (without the cutoffs) has been used in the branches model of braided rivers described in the next chapter. As already mentioned above, the mathematical equations governing this modelling approach are basically identical to those obtained by linearising the one-dimensional flow equations. This approach is discussed in the next section.

4.1.2 Dynamic models using linearised equations for flow

A dynamic model that is based on the linearised equations for depth-averaged flow assuming an equilibrium bed profile in meander bends has been developed by Ikeda *et al.* (1981) and used further by the same authors in 1982. This model also forms the basis for the analysis by Parker (1984) mentioned in the previous section. This section describes this model and its recent application by Sun *et al.* (1996).

Ikeda *et al.* (1981) and Parker *et al.* (1982)

Ikeda *et al.* (1981) consider two channels as illustrated in Figure 4.3. The first one is meandering with a small amplitude and width B . The channel length is L , its slope is i and the reach averaged flow velocity and water depth are u and h , respectively. The second channel is straight and follows the maximum valley slope. The width, discharge and roughness of the straight channel are equal to the corresponding quantities in the meandering channel. Due to the shorter length L_0 of the straight channel, the slope i_0 and the velocity u_0 are larger whereas its water depth h_0 is smaller. The near-bank velocity deviation \hat{u}_b^* is defined as

$$\hat{u}_b^* = \frac{u_b - u}{u_0} \quad (4.4)$$

where u_b is the naturally occurring near-bank depth averaged streamwise velocity. By neglecting the coupling between the flow and sediment equations Ikeda *et al.* (1981) theoretically derive that the near-bank velocity deviation due to curvature-induced bed topography

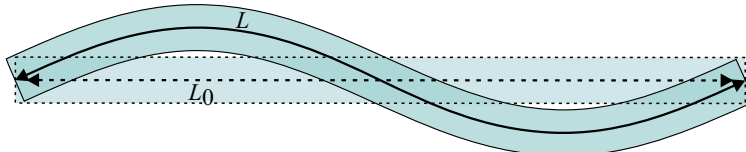


Figure 4.3: Meandering and straight channels compared by Ikeda *et al.* (1981).

— which they assume to be in equilibrium with the local curvature — satisfies the following equation

$$\frac{\partial \hat{u}_b^*}{\partial \hat{s}} + 2\chi c_f \hat{u}_b^* = -\chi \frac{\partial \hat{c}}{\partial \hat{s}} + c_f (F_0^2 \chi^5 + A \chi^2) \hat{c} \quad (4.5)$$

where

- A constant representing the influence of secondary flow on bend scour,
- \hat{c} dimensionless curvature, b/R , where b is half of the channel width $b = B/2$,
- c_f equals i_0/F_0^2 or g/C^2 , a friction factor / drag coefficient,
- F_0 equals $u_0/\sqrt{gh_0}$, the Froude number of the straight channel,
- \hat{s} dimensionless alongstream coordinate s/h_0 ,
- χ equals u/u_0 , the ratio of mean flow speed in the meandering and straight channels (decreases for increasing sinuosity).

Ikeda *et al.* (1981) use this model as a starting point for the analysis of the origin of meandering. This analysis was extended by a nonlinear analysis by Parker *et al.* (1982) using the same model. The latter analysis quantified the initial tendency for meanders to ‘fatten’ and grow asymmetrically.

Sun *et al.* (1996)

Sun *et al.* (1996) have used the model described above¹ in a numerical program for the planform of meandering rivers and the development of meander belts. For this study they have superimposed the one-dimensional meander model on a lattice consisting of square gridcells. Each cell has a certain erodibility and age assigned to it. When the river migrates through a gridcell the erodibility of that particular gridcell is changed into a user defined erodibility of relatively coarse grained pointbar deposits. After a cutoff has occurred, the erodibility of the gridcells in which the abandoned reach was positioned decreases in time from the average flood plain erodibility to the low erodibility of clay deposits. The simulations confirm that the time required for filling the oxbow lakes with inerodible clay deposits has significant influence on the formation of meander belts. If the oxbow lakes become quickly filled in with erosion resistant sediments, river migration will be irregular and the river migration seems not to be confined to a limited section of the flood plain. If, on the other hand, the oxbow lakes remain easily erodible a period in the order of the time required for bends to migrate downstream by one wavelength, a stable meander belt is formed (Figure 4.4).

In the models described in this section, flow and morphology have been decoupled. It is assumed that the morphology adapts instantaneously to the changing curvature. The interaction between flow and sediment transport was taken into account in the models that appeared one decade after the work of Ikeda *et al.* (1981). These dynamic models based on the linearised equations for both flow and morphology are presented in the following section.

¹Based on work by Johannesson and Parker (1988, 1989) they replaced A by $A + A_s - 1$ where A_s indicates the lateral momentum exchange due to secondary flow.

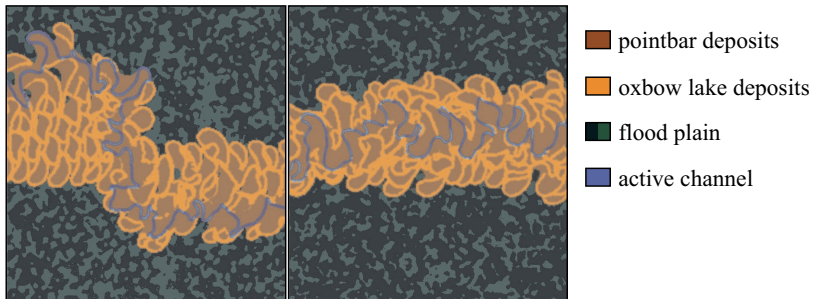


Figure 4.4: Meander belt simulations by Sun et al. (1996). Left: Oxbow lake sediments solidify quickly, no meander belt is formed. Right: Oxbow lake sediments solidify slowly, a stable meander belt is formed.

4.1.3 Dynamic models using linearised equations for flow and morphology

Several years after the model by Ikeda *et al.* (1981), Johannesson and Parker (1989) formulated a new model based on a linearisation of the coupled system of flow and sediment transport in meander bends. At the same time a similar model was developed by Struiksmma and Crosato (1989) and Crosato (1990). The main difference between the model by Johannesson and Parker (1989) and the latter model is the use of a (co)sine shaped perturbation in transverse direction by the latter authors and a linear transverse profile by the former ones. This section describes these models and the extension of the former model by Howard (1992, 1996).

Johannesson and Parker (1989)

Johannesson and Parker (1989) formulate a model that is based on the model by Ikeda *et al.* (1981), which has been described in the previous section. The new model includes two important processes neglected in the derivation of the model by Ikeda *et al.* (1981). First, the convective transport of primary flow momentum by the secondary flow in bends. Second, the interaction of flow and sediment transport in the shaping of the channel bed. The importance of the latter aspect had been indicated previously by Blondeaux and Seminara (1985) and Struiksmma *et al.* (1985). The former process had been described among others by De Vriend (1981b).

Using the same meandering channel as in the previous section — that is, a meandering channel with a small amplitude and width B , length L , slope i , roughness c_f , flow velocity u and water depth h — Johannesson and Parker (1989) derive the following equation for the dimensionless secondary current strength σ_s as

$$a \frac{d\sigma_s}{ds} + \delta\sigma_s = \delta\sigma \quad (4.6)$$

where

$$\delta = \frac{\chi_1^2(\chi + \frac{1}{4})}{\frac{1}{12}\chi^2 + \frac{11}{360}\chi + \frac{1}{504}} \quad (4.7)$$

and where

- a equals $2H/(Bc_f)$,
- s dimensionless downstream coordinate (normalised by division by $B/2$),
- σ local normalised dimensionless curvature (normalised by division by the minimum radius of curvature r_m),
- χ equals $\chi_1 - \frac{1}{3}$,
- χ_1 equals α/c_f with α a constant equal to 0.077.

The parameters χ and χ_1 originate from the zeroth order dimensionless velocity shape function $T(\hat{z})$ in the central portion of the channel given by Engelund (1974) as

$$T(\hat{z}) = \frac{1}{\chi_1} (\chi + \hat{z} - \frac{1}{2} \hat{z}^2) \quad (4.8)$$

where \hat{z} is the normalised vertical coordinate. Subsequently Johannesson and Parker (1989) determine the dimensionless excess velocity u_C near the left bank due to curvature-induced bed topography using

$$a \frac{du_C}{ds} + 2u_C = n[-a\chi_{20} \frac{d\sigma}{ds} + (F^2\chi_{20} - 1)\sigma] + (A + A_s)n\sigma_s \quad (4.9)$$

and the dimensionless excess depth h_C near the left bank due to curvature-induced bed topography using

$$h_C = n(F^2\chi_{20}\sigma + A\sigma_s) \quad (4.10)$$

where the first part of the term on the right hand side results from the slope in the water level and the second part stems from the variation in the channel bed level. Furthermore the following notation has been used

- A parameter indicating the effect of the bed slope on the transverse bed topography, given by $A = \frac{2}{45\alpha^2\beta}(\chi + \frac{2}{7})/(\chi + \frac{1}{3})$ where β is a parameter indicating the effect of the transverse bed slope on the sediment transport direction

$$\frac{q_n}{q_s} = \frac{v(0)}{u(0)} - \frac{\beta}{\gamma} \frac{\partial \eta}{\partial n} \quad (4.11)$$

where

- q_s, q_n dimensionless volumetric streamwise and transverse sediment transport components per unit width,
- $u(0)$ streamwise velocity near the bed (normalised by division by U),
- $v(0)$ transverse velocity near the bed including contribution of secondary flow (normalised by division by U),
- γ equals $B/(2H)$, half of the width-depth ratio,
- η bed level (normalised by division by H),
- A_s equals $181(2\chi^2 + \frac{4}{5}\chi + \frac{1}{15})/(\gamma^2\chi_1)$, parameter indicating the lateral momentum exchange due to secondary flow,
- F equals U/\sqrt{gH} , the Froude number,
- n normalised transverse coordinate (normalised by division by $B/2$),

$$\chi_{20} \text{ equals } \frac{1}{\chi_1^3} (\chi^3 + \chi^2 + \frac{2}{5}\chi + \frac{2}{35}).$$

Finally the dimensionless excess velocity u_F near the left bank ($n = 1$) due to the response of the free system to the forcing using

$$a^2 \frac{d^2 u_F}{ds^2} + a(3 - b - \frac{\pi^2}{4}\Gamma) \frac{du_F}{ds} + \frac{\pi^2}{2}\Gamma u_F = a[(b-1) \frac{du_C}{ds} - \frac{dh_C}{ds}] \quad (4.12)$$

and the associated dimensionless excess depth h_F using

$$h_F = -\eta_F = a \frac{du_F}{ds} + 2u_F \quad (4.13)$$

where

b power of the sediment transport relation,

Γ equals $\beta/(\gamma^2 c_f^2)$, coefficient of gravitational diffusion,

η_F change in bed level due to the response of the free system to the forcing.

The total velocity is given by $u[1 + \Psi_0(u_C + u_F)]$ and the total water depth is given by $h[1 + \Psi_0(h_C + h_F)]$ where $\Psi_0 = B/(2r_m)$ and r_m is the minimum radius of curvature used for normalising the curvature.

Howard (1992, 1996)

Howard (1992, 1996) has used this model and combined it with formulations for cutoffs and overbank sedimentation. The erosion rate ζ is in general given by

$$\zeta = 2E[e_1(u_C + u_F) + e_2(h_C + h_F)] \quad (4.14)$$

For the simulations Howard (1992, 1996) uses $e_1 = 1$ and $e_2 = 0$, thereby switching off the influence of the water depth. The flood plain is modelled in the same way as Sun *et al.* (1996) using a lattice consisting of square gridcells. Contrary to them Howard uses a spatially constant erodibility. In the model by Howard (1992, 1996) each cell has a certain elevation



Figure 4.5: Flood plain elevation as simulated by Howard (1996).

and age assigned to it. When the river leaves a gridcell the elevation of that particular gridcell is assigned the near-bank bed level within the channel. The elevation of the (dry) gridcell increases during the simulation due to overbank sedimentation. The deposition rate $\Phi(i, j)$ in a gridcell (i, j) is modelled as a function of the relative flood plain height and the distance to the active channel:

$$\Phi(i, j) = [z_{\max} - z(i, j)](\nu + \mu e^{-D(i, j)/\lambda}) \quad (4.15)$$

where

$D(i, j)$	distance to active channel,
$z(i, j)$	local flood plain height,
z_{\max}	maximum flood plain height,
λ	characteristic length scale for coarse sediment deposition,
μ	deposition rate of coarse sediment,
ν	deposition rate of fine sediment.

Figure 4.5 indicates the variation in the flood plain elevation after a long simulation that started with an almost straight channel. The model of Howard (1992) has also been used by Stølum (1996). He indicates that meandering is characterised by chaotic dynamics which leads to a state of self-organised criticality around a state characterised by an averaged sinuosity of π . Spatial and temporal clustering of cutoffs leads to the creation and destruction of ordered and chaotic river segments.

Other models based on Johannesson and Parker (1989)

The model of Johannesson and Parker (1989) has been extended by Sun *et al.* (2001c) to investigate the effect of lateral flood plain tilting on meander development. Sun *et al.* (2001a,b) have extended the model further to include multiple bedload fractions. With this model they study the effect of the within-channel sorting of coarse sand fractions on the composition of the flood plain sediments (compare their study on the effect of sand clay sorting due to cutoffs described in the previous section). Imran and Parker (1999) have generalised the work of Johannesson and Parker (1989) to a non-linear model which remains valid for larger channel curvatures.

Crosato (1990): MIANDRAS

The meander model MIANDRAS developed by Crosato (1990) can be used to predict the future migration of a constant-width meandering river by solving three differential equations, for water depth, downstream velocity and bank erosion, respectively. The model is based on the following assumptions:

- the channel width B is constant in space and time,
- the vertical pressure distribution is hydrostatic,
- the shallow-water flow approximation is appropriate,
- the channel curvature and the bed slope are relatively small,

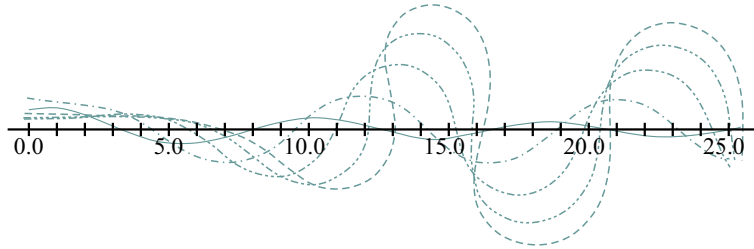


Figure 4.6: Successive centre-lines in a MIANDRAS simulation by Crosato (1990).

- the spatial variations in roughness and grain sorting are negligible,
- the sediment transport rate can be determined from local conditions only (dominant bed-load), and
- the Froude number is small enough for the rigid lid approximation to apply.

Under these conditions the full set of equations can be linearised and a transverse (co)sine-shaped solution can be imposed², which in the end gives the following equation for the equilibrium water depth $h_1(s)$

$$\frac{\partial^2 h_1}{\partial s^2} + \left(\frac{1}{\lambda_s} - \frac{b-3}{2\lambda_w} \right) \frac{\partial h_1}{\partial s} + \frac{h_1}{\lambda_s \lambda_w} = - \frac{h_0}{k_B} (b-1) \frac{\partial^2 \Gamma}{\partial s^2} + \left(A h_0^2 k_B - \frac{(2-\sigma)(b-1)h_0}{2\lambda_w k_B} \right) \frac{\partial \Gamma}{\partial s} + \frac{A h_0^2 k_B}{\lambda_w} \Gamma \quad (4.16)$$

with

- | | |
|---------------|---|
| A | equals $2\alpha_1 \kappa^{-2} [1 - \sqrt{g}/(\kappa C)]$, |
| B | channel width, |
| b | exponent of the sediment transport law, |
| C | Chézy value, |
| D_{50} | median grain size, |
| E | calibration coefficient in the order of 0.5 for flume till 1 for rivers, |
| $f(\theta_0)$ | weighting function $0.85\sqrt{\theta_0}/E$ for the transverse bed slope effect, |
| g | gravitational constant, approximately 9.81 m/s^2 , |
| h_0 | zero order solution for the water depth given by $[Q/(BC\sqrt{i})]^{2/3}$, |
| h_1 | first order solution for the water depth (to be computed), |
| i | water surface slope, |
| k_B | equals $m\pi/B$, the wave number of the perturbation in the transverse bed profile, |
| m | transverse oscillation mode, $m = 1$ for a meandering channel (the perturbation in the transverse direction equals half a cosine with extremes near the banks), |
| Q | discharge, |

²The models derived by Ikeda *et al.* (1981) and Johannesson and Parker (1989) are based on linear functions for the perturbation in the transverse direction.

R_c	radius of curvature of the centreline,
u_0	zero order solution for the stream wise velocity given by Q/Bh_0 ,
α_1	calibration coefficient on the order 0.4–1.2 (secondary flow effect on sediment transport direction),
Γ	equals $m\pi/(2R_c)$,
Δ	relative submerged density of the sediment,
θ_0	equals $u_0^2/(C^2 \Delta D_{50})$, the Shields parameter based on the zero order solution,
κ	Von Kármán's constant, being 0.4,
λ_s	equals $f(\theta_0)/(k_B^2 h_0)$, the adaptation length of bed deformations,
λ_w	equals $C^2 h_0/(2g)$, the adaptation length of main flow,
σ	calibration coefficient in the order of 2–4 (convection of momentum due to secondary flow),

where the curvature due to non-uniformity of the flow has been ignored. Given the old water depth $h(t_i)$ and the equilibrium water depth h_1 obtained from Equation 4.16, the water depth at the next timestep t_{i+1} is computed as

$$h(t_{i+1}) = h(t_i) + [h_1 - h(t_i)](1 - e^{-(t_{i+1} - t_i)/T}) \quad (4.17)$$

with $T = \lambda_s h_0/s_0$ the characteristic time scale for the transition period. Subsequently, a quasi-steady approximation of the streamwise velocity u is computed using

$$\frac{\partial u}{\partial s} + \frac{u}{\lambda_w} = h \frac{1}{2\lambda_w} \frac{u_0}{h_0} - \frac{u_0}{k_B} \frac{\partial \Gamma}{\partial s} - \frac{2 - \sigma}{2\lambda_w} \frac{u_0}{k_B} \Gamma \quad (4.18)$$

and, finally, the lateral channel migration rate is computed according to the following formula

$$\frac{\partial n}{\partial t} = E_u u + E_h h \quad (4.19)$$

in which E_u and E_h are spatially varying coefficients for the dependence of the bank erodibility on flow speed and water depth. From the erosion rate a new centreline is computed, thereby changing R_c and thus Γ for the next timestep. Because the computation is limited to only one transverse mode m ($m = 1$) the applicability of the model is limited to narrow, deep channels with a relatively low bank erosion rate. In channels with a high width-depth ratio or a high bank erosion rate, the cross-sectional channel shape will generally deviate too much from the assumed sine shape. For these cases a more general modelling approach has to be followed as described by Mosselman (1992).

4.1.4 Dynamic model using non-linear equations

In order to circumvent the restriction of a channel of constant width and predefined cross-sectional profile the development of RIPA was started (Mosselman, 1991, 1992). That model is based on the 2D shallow water equations (more extensively described in Section 4.3.2) with a rigid lid approximation; the non-linear equations are solved on a non-orthogonal curvilinear grid. What distinguishes this model from the general purpose 2D models is the inclusion of a bank erosion module and an adaptive grid. Unfortunately, the consequences of these extensions are so far-reaching that they basically restrict the application of the model to meandering rivers only. The rate of bankline retreat is given by

$$\left| \frac{\partial n_B}{\partial t} \right| = E_\tau \frac{\tau_w - \tau_{wc}}{\tau_{wc}} H(\tau_w - \tau_{wc}) + E_{hB} \frac{h_B - h_{Bc}}{h_{Bc}} H(h_B - h_{Bc}) \quad (4.20)$$

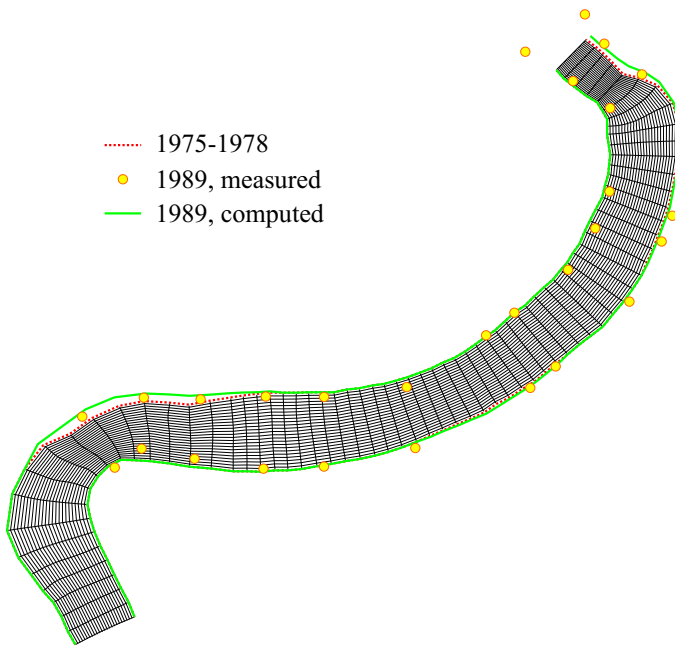


Figure 4.7: Application of the RIPA model to the migration of the Ohře River, Czech Republic (Mosselman, 1992).

where

- E_τ erodibility coefficient for bank erosion due to excess bank shear stress,
- E_{h_B} erodibility coefficient for bank erosion due to excess bank height,
- $H(x)$ Heaviside function, being zero for $x < 0$ and one for $x \geq 0$,
- h_B total bank height, given by the sum of local water depth h and ‘free board’ height h_{fb} being the elevation difference between bank top and water surface
- h_{Bc} critical total bank height,
- n_B transverse location of the bankline,
- τ_{bs} bed shear stress,
- τ_w flow shear stress of bank, $\tau_w \approx \alpha_L \tau_{bs}$, with α_L the ratio of bank shear stress to bed shear stress, taken equal to 0.75,
- τ_{wc} critical bank shear stress.

Figure 4.7 shows some results of this model for the Ohře River, Czech Republic.

Because there is no physical mechanism that leads to bankline accretion, the channel can only become wider in this model. This tendency for continuous widening can be limited by introducing an artificial narrowing mechanism that removes areas from the computational grid at which the water depth drops below some arbitrary threshold, say, ten centimetres. Although this methodology might give reasonable results for simulations with a constant discharge, problems arise if it is applied in situations where the discharge varies significantly. Permanent removal of (almost) dry model areas during low flow could block important flow paths during high flow. Whereas the eroding outer bends would be suited best with a dedicated

curvilinear meander model, the drying/flooding problem at the inner bend and the associated impossibility of defining a clear border of the channel require a more general 2D approach. This has led to the gradual development of bank erosion modules for general 2D numerical models over the last decade (see also Section 4.3.2 about general purpose shallow water models).

4.2 Simple models for braided rivers

As indicated in the previous section, the modelling of meandering rivers is far from being complete; the models are, however, sufficient to predict a large part of the planform changes for meandering rivers with a uniform width if the flow is mainly within the main channel and if the variation in erodibility of the banks is limited. In this section a number of simple models is described that — although not suitable for prediction of planform changes — reproduce or describe some aspects of braided patterns. The first subsection describes a Markov chain that can be characterised as a one dimensional, statistical approach to modelling a braided river. The second subsection continues with two dimensional, statistical models constructed by Howard *et al.* (1970), Krumbein and Orme (1972) and Rachocki (1981). The final model mentioned in that section includes some basic physical relationships (Webb, 1994, 1995). The last subsection discusses the viewpoint of Paola (1996), which leads to a procedure for averaging variables over the width of the braid plain. The width averaged equations for braided rivers turn out to be identical to those for a single threaded river (although the precise meaning of the parameters has changed).

4.2.1 Markov chain

A Markov chain has been constructed to model the alongstream variations in the number of channels per cross-section in a statistical sense. The state of the Markov chain is given by the number of channels per cross-section and the type of transition in the previous segment: c(onfluence), b(ifurcation) or n(o change). Whenever a confluence occurs at a certain cross-section the number of branches is decreased by one, while at a bifurcation the number of parallel branches increases by one. The possibilities of multiple confluences or bifurcations occurring at the same cross-section and of confluences and bifurcations involving more than two in- and outflowing channels, respectively, have been excluded from this model. In the

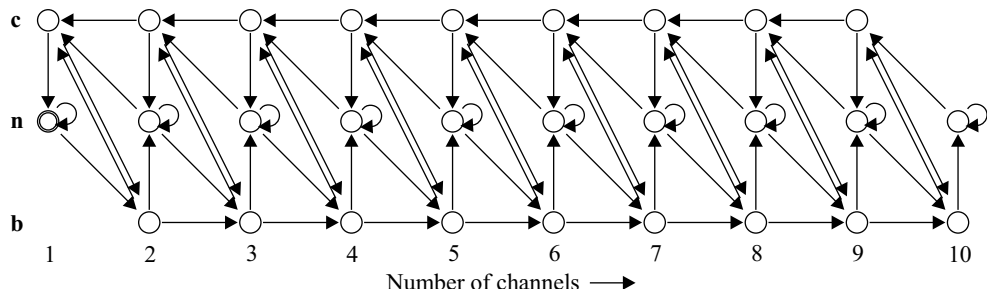


Figure 4.8: Graphical representation of the Markov chain

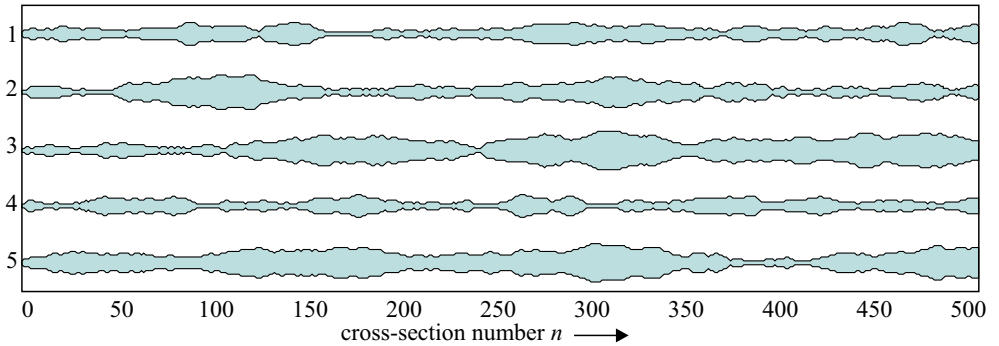


Figure 4.9: Five realisations of the Markov chain model. The variation in the width of the shaded area between the two banklines indicates the variation in the number of parallel branches.

previous chapter we have seen that a confluence is often followed by a bifurcation within a short distance; this observation has been included in the model by distinguishing between cross-sections with n parallel branches just after a confluence, just after a bifurcation and ‘far away’ from the last change. The state at a certain cross-section is, therefore, given by the number of parallel branches n and the indication **c** for a reach just downstream of a confluence, **b** just downstream of a bifurcation and **n** for other ‘normal’ reaches. The number of branches is limited to at most ten. The resulting model can be depicted as a directed graph as shown in Figure 4.8.

The behaviour of the Markov chain will depend on the transition probabilities. If the total probability of increasing the number of branches is larger than or equal to the probability of a reduction of the number of branches, the model will result in a gradual but persistent increase in the number of channels: a pattern characteristic of a river delta. If on the other hand the probability of a confluence is larger than the probability of a bifurcation, a narrow river with little or no islands will form, resembling a drainage network leading to a single channel. In the other cases cross-sections with a limited number of branches will be (quasi-)stable and a braided pattern will form. Figure 4.9 shows five realisations of the Markov-chain model with the following transition probabilities, which were independent of n .

to	from		
	c [n]	n [n]	b [n]
c [$n - 1$]	0.05	0.18	0.00
n [n]	0.90	0.70	0.97
b [$n + 1$]	0.05	0.12	0.03

For these settings the average expected number of channels per cross-section is 3.6, while the distribution of the number of channels per cross-section will be on average

number of channels n	1	2	3	4	5	6	7	8	9	10
average occurrence	13%	27%	19%	13%	9%	6%	5%	3%	2%	2%

One should note that quite often nodal points, i.e. reaches with a small number of parallel branches, are generated when the transition probabilities are suitably chosen, although a large

variety of patterns is obtained, as is shown in Figure 4.9. Coleman (1969) observed several narrow sections in the planform of the Jamuna River, which seemed to be quite stable. This example shows that even a very simple model is able to reproduce these narrow sections, so the occurrence of these sections is not remarkable; it may be coincidence. Whether these narrow sections are stable (forced by flood plain or geological conditions) or of a temporal nature (indeed just coincidence) cannot be predicted by this or any other model without proper knowledge of the influencing conditions.

4.2.2 Random walk models

One step higher in the cascade of models for braided rivers, but still stochastic, are the random walk models. Several of those models have been described for both braided rivers and alluvial fans (Howard *et al.*, 1970; Krumbein and Orme, 1972; Rachocki, 1981). The general description of these models is that a flow starts at one end of a regular lattice and progresses across the lattice by making one step at a time; at each step a channel can either continue as a single channel or split into two branches, which will follow independent paths until they happen to split again or join. The choice for either splitting or continued flow in a certain direction is purely determined by chance. The channel pattern that is constructed in this way consists of a number of interconnected nodes and vertices of the lattice, which is either rectangular (Howard *et al.*, 1970) or diamond shaped (Krumbein and Orme, 1972; Rachocki, 1981). Some results are shown in Figure 4.10.

Rachocki (1981) added, although in an extremely simplified manner, the aspect of discharge distribution over the branches: the discharge was divided into two equal parts at each bifurcation. When the pattern obtained by Krumbein and Orme (Figure 4.10b) is interpreted in this way, it consists of one large meandering channel with a few small side channels (Figure 4.10c). Furthermore, he considers the time evolution of the braided pattern by generating multiple patterns starting from the same inflow but otherwise completely independent. Channels that are active in two successive patterns are so purely by chance (although slightly helped by the limited width of the grid). Liverpool *et al.* (1995) describe a similar type of model for meandering rivers. In their model time evolution is modelled by selecting an arbitrary point next to the channel and rerouting the channel along the other side of the point (Figure 4.11). This approach gives a gradual transition from one pattern to the next, but it

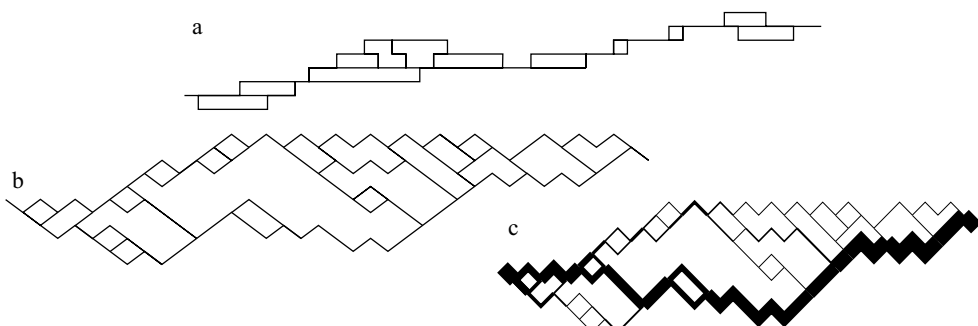


Figure 4.10: Some results of the random walk models: a by Howard *et al.* (1970), b by Krumbein and Orme (1972), and c the same pattern as b, but now as Rachocki (1981) would have interpreted it.

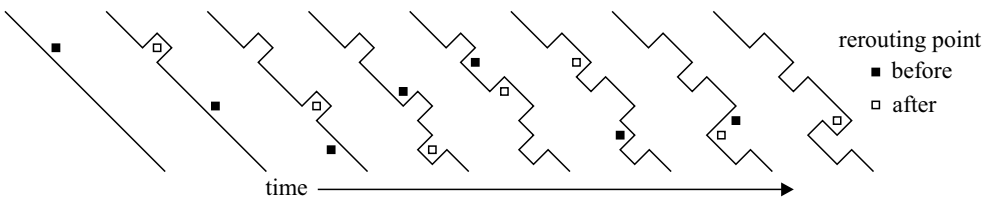


Figure 4.11: Dynamics of the lattice based meander model of Liverpool et al. (1995).

requires that flow may occur in any direction on the lattice. For the purpose of having a simple model that reproduces the channel patterns of braided rivers, these models have been succeeded by the more physics-based, dynamic, cellular model of Murray and Paola (1994) described in Section 5.2.

Webb (1994, 1995) describes a random walk model that has been developed for the simulation of the internal structure of stratigraphical deposits. The channels in that model are no longer laterally constrained by a grid, but there is still a discretisation in the streamwise direction. Although the occurrence of bifurcations and the sizes of the downstream channels are stochastic variables, mass conservation is guaranteed. Channels are assigned width B , depth h , and velocity u on the basis of their individual discharge Q and user-specified geometrical relations ($B = aQ^b$, $h = cQ^f$, $u = kQ^m$). Furthermore, empirical physical knowledge has been incorporated into the model by the fact that the individual channels are attracted laterally by low-lying areas in the terrain. The river is assumed to be steadily aggrading³, such that each braided pattern in a sequence contributes a certain amount of sediment to the flood plain, thereby differentiating between within-channel and flood plain deposits. The deposits of the previous iteration form the top layer of the terrain that influences the formation of the next braided pattern. Layer by layer this builds a stratigraphy similar to that left behind by an aggrading braided river (Figure 4.12). The model for planform changes is, however, still very simple and not useful for river engineering purposes. In the near future we may expect more physics-based models for stratigraphy based on the concepts as proposed by Murray

³ Aggradation is not necessary for braiding (Parker, 1976; Xu, 1996), it is, however, necessary for creating these three dimensional deposits, which require the preservation of a stack of channel courses.

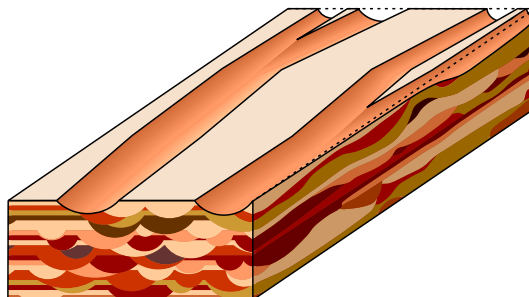


Figure 4.12: Stratigraphy obtained from the braided channel simulator by Webb (1994). The lateral extent of the channel deposits is small, whereas a longitudinal section shows extended, in thickness varying channel deposits.

and Paola (1994), or Tetzlaff and Harbaugh (1989), which eventually may be replaced by graded sediment models based on the current state-of-the-art modelling tools.

4.2.3 Turbulence analogy

The stochastic nature of turbulence resembles in some respects the stochastic nature of stream braiding. In both cases coherent structures have been observed in the otherwise chaotic looking patterns. From this viewpoint Paola (1996, 2001) describes a width-averaged model for braiding.

Turbulence is characterised by a hierarchy of scales of eddies, while braiding is characterised by a cascade of bedforms, bars and islands; moreover, both turbulence and braiding exhibit fractal behaviour within this hierarchy of scales (Foufoula-Georgiou and Sapozhnikov, 1998; Nykanen *et al.*, 1998; Sapozhnikov and Foufoula-Georgiou, 1996, 1997; Paola and Foufoula-Georgiou, 2001). Furthermore, Paola remarks that, in both systems, interactions between coherent structures give rise to short-lived events that contribute disproportionately to the overall net transport. In this respect he mentions confluences as being the braiding equivalent of sweeps and ejections in turbulence; deep confluences are, however, sometimes interpreted as the stabilizing elements in a braided river, which is the opposite of being a short-lived event. Therefore, the transverse and linguoid bars emerging from the constantly changing confluences might be better candidates for these short-lived events.

Besides these similarities there are two main differences. Firstly, braiding is a two dimensional phenomenon, whereas turbulence is essentially three dimensional. Secondly, there is a smallest scale (Kolmogorov fine-scale) in turbulence that plays a different role (dissipation of kinetic energy to heat) from the larger scales (extraction of kinetic energy from the mean flow). Paola mentions that there does not seem to be such an energy cascade in braiding. However, braiding can be seen as another way of extracting kinetic energy from the main stream, supplementary to turbulence. In that case there is no need for a clearly defined smallest scale, since the increased friction and increased turbulence lead to the required dissipation.

Paola (1996) considers a section of a braided stream as shown in Figure 4.13. When the lateral variations within a braided river are not of interest, averaging over the width of the braid plain is possible. In the case of turbulent flow the physical quantities are averaged over flow cells of certain fixed dimensions. In a braided stream, however, several quantities

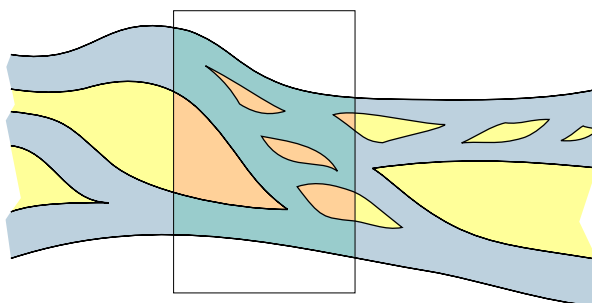


Figure 4.13: Definition of the averaging area.

(such as water depth and flow velocity) are only well defined within the branches, so the averaging over the cross-section should be limited to averaging only over the wetted part of the cross-section, that is the part corresponding to the channels. Variations in extent of the wetted part along the river can cause severe problems in the numerics. Therefore, the average is also taken over a certain distance in streamwise direction. This distance is chosen in such a way that it is long enough to take care of variations in the cross-sectional area, so that the effective average area (indicated by the cross-hatched area) is a constant fraction of the total averaging area (indicated by the dotted area). The river is assumed to exhibit a, statistically speaking, uniform pattern over distances larger than the averaging distance. Paola (1996) assumes furthermore that at length scales greater than the averaging distance, the sinuosity is small enough for the cross-stream momentum balance to be ignored. Temporal variations in the quantities are also neglected.

The analysis by Paola (1996) confirms the usual assumption that on a spatially averaged scale the relations that govern braiding are similar to those for single-channel rivers. Since braided rivers exhibit self-similarity in a certain range of scales, it may also be assumed that these same relations hold on a partly averaged scale (averaging over all channels except the major anabranches). Although this analysis does not directly help to predict planform changes in braided rivers, its conclusion indicates that averaging over medium scales is allowed. It should, however, be remarked that the smallest scales will influence the planform changes in the long run: limiting the detail of the model limits also the prediction horizon.

4.3 Generic models

We will end this chapter by mentioning briefly some generic models that can (at least theoretically) be used for all rivers: meandering, braided or other. The first is not a model for river planform changes, but rather a generic method to obtain a prediction: time series extrapolation. The second one is the generic morphological model based on process descriptions formulated using partial differential equations (PDEs). Finally, we will have a look at the recent developments in the field of lattice gas models as an alternative for PDE-based modelling.

4.3.1 Time series extrapolation

Whenever there is no model available or when the application of a large detailed model would be too expensive, one can try to extrapolate past behaviour derived from maps or surveys. This method is best described by an example taken from one of the FAP studies.

Overlay plots of bankline positions of the Jamuna River since 1830 indicate a gradual widening and a migration to the west. Based on this observation the migration rate of the centreline of the Jamuna River was estimated within the FAP1 project at fifty metres per year (Halcrow *et al.*, 1991). Recent studies of EGIS (1997) have indicated that the right bankline has migrated about 1500 metres to the west over the last 23 years (1973-1996). The left bankline has meanwhile migrated 1500 metres to the east, resulting in an overall average widening of three kilometres. The variation in the migration rate of the left bankline is, however, large and in several reaches the left bank has not eroded, locally resulting in a net westward migration

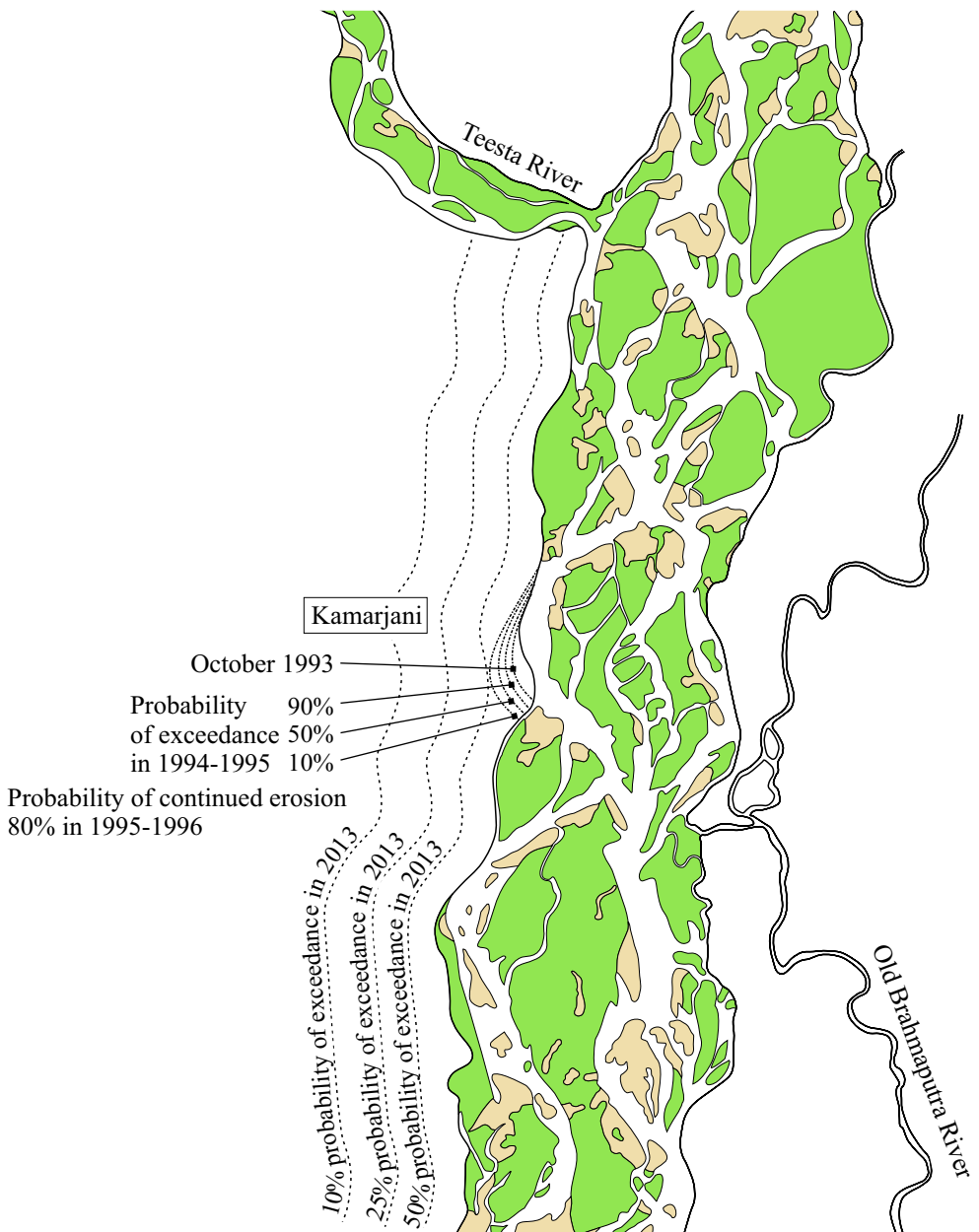


Figure 4.14: Long-term prediction of bankline migration along the Jamuna River near Kamarjani by FAP21/22 (1994).

of the river centreline. The migration rate derived by FAP1 was used in 1994 in the FAP21/22 (1994) project to make a long term prediction of the migration of the right bankline at several locations (among others at Kamarjani, see Figure 4.14). Basically this approach can be summarised into the following trend equation

$$x(s, t) = x_0(s) + \zeta(s)t \quad (4.21)$$

where x is the lateral coordinate of the bankline, x_0 is its initial position, $\zeta(s) = \zeta_0$ is the observed constant migration rate per year, s is the streamwise coordinate, and t the prediction span in years. In discrete time this model can per location s also be interpreted as a simple autoregressive time series model

$$x_t = \zeta_0 + x_{t-1} + \varepsilon_t \quad (4.22)$$

where ε_t indicates a random variation in the erosion rate ζ_0 and t indicates time expressed in years. Contrary to standard time series models, the random variation is not normally distributed, since it is restricted to $\varepsilon_t > -\zeta_0$ unless some form of bank accretion is taken into account. To improve long-term prediction one can try to determine a location dependent value of ζ which varies with the local bank properties and tectonic motion. For prediction of seasonal variations in erosion rates (due to flooding) one could switch to a model based on monthly data using a higher-order autoregressive model. This latter model is only useful for predictions not too far into the future. Yearly variations in the hydrograph may, however, severely limit the prediction capability of such a model. Although, in many cases the application of such a simple method can be quite effective, little physical insight is gained by applying it. Therefore, we will not consider this option any further.

4.3.2 Generic process-based model

The last section of this chapter describes the generic shallow water models; the description is kept brief, as we will come back to this kind of model in Chapter 7. The classical depth-averaged shallow water model consists of three equations for the water motion. First, the equation of mass conservation, which is given by

$$\frac{dh}{dt} + h \frac{\partial u}{\partial x} + h \frac{\partial v}{\partial y} = 0 \quad (4.23)$$

where h is the flow depth, and u and v are the depth averaged velocities in the x and y directions, respectively. Note that we have used the following shorthand notation

$$\frac{d\xi}{dt} \doteq \frac{\partial \xi}{\partial t} + u \frac{\partial \xi}{\partial x} + v \frac{\partial \xi}{\partial y} \quad (4.24)$$

Second and third, the momentum equations in the x and y directions, given by

$$\frac{du}{dt} = -g \frac{\partial z_w}{\partial x} - u \frac{g \sqrt{u^2 + v^2}}{hC^2} \quad (4.25)$$

and

$$\frac{dv}{dt} = -g \frac{\partial z_w}{\partial y} - v \frac{g \sqrt{u^2 + v^2}}{hC^2} \quad (4.26)$$

where C is the Chézy coefficient for bed roughness and z_w is the water level. These equations are based on the hydrostatic pressure assumption, $p(z) = p_0 + \rho g(z_w - z)$. Several extensions to these equations have been made such as the incorporation of correction factors for secondary flow in channel bends (Rozovskii, 1961; De Vriend, 1981a; Struiksma *et al.*, 1985). Similarly, the description of sediment transport and morphology requires a mass balance equation for the sediment and a model of the sediment dynamics. The latter may be implemented as either total load transport by means of an empirical transport formula or as two separate components representing bedload and suspended load. The resulting changes in the bed level are computed from the mass conservation of sediment, given by the Exner equation

$$(1 - \varepsilon) \frac{\partial z_b}{\partial t} + \frac{\partial S_x}{\partial x} + \frac{\partial S_y}{\partial y} = 0 \quad (4.27)$$

where ε represents the porosity of the bed, z_b is the bed level, and S_x and S_y are the total sediment transport rates per unit width in x and y direction. The numerical model solves these equations on a discretised domain. The right hand side of this equation can be extended with terms for the concentration c of suspended sediment in the water column

$$-\frac{\partial(hc)}{\partial t}$$

sediment supply and dredging (human interference) per gridcell,

$$\frac{V_{\text{supply}} - V_{\text{remove}}}{\Delta x \Delta y}$$

and bank erosion

$$\frac{z_{\text{bank}} - z_b}{\Delta n} \frac{\partial n}{\partial t}$$

where z_{bank} is the elevation of the bank, Δn is the gridcell size perpendicular to the bank, and $\partial n / \partial t$ is the bank erosion rate.

Bank erosion is often excluded from these models because correct simulation of long-term morphological development in combination with bank erosion requires either on-line adaptation of the grid, or a procedure to prevent the spatially fixed discretisations from influencing the spatial distribution of bank erosion.

- On-line adaptation of the grid complicates the solution procedure (especially if the adapted grid must obey certain orthogonality and smoothness conditions). The RIPA model described in Section 4.1.4 combines the full shallow water equations with bank erosion, but this model has been developed especially for meandering rivers. The DHI model used by Enggrob and Tjerry (1999) for predicting the short-term planform changes in the Jamuna River uses an adaptive grid solution to include the bank erosion process in a generic model. This approach has also been studied by Shimizu (2002) and WL | Delft Hydraulics (see Figure 4.15).
- A solution procedure that uses a spatially fixed discretisation has been used by Enggrob and Tjerry (1999) for their long-term simulations reproduced in Figure 1.10. A similar approach is recently been used to model the breaching of a barrier island by WL | Delft Hydraulics (Roelvink, pers. comm.). Olsen (2000, 2002) has developed a 3D model that by means of a cut-cell technique should be able to follow the shifting banklines more closely (see Figure 4.16).

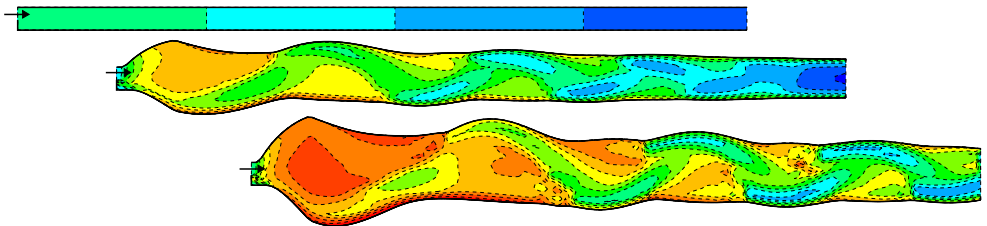


Figure 4.15: Development of a meandering channel using on-line grid adaptation in Delft3D due to flow at low Froude number starting from straight channel. Flow from left to right.

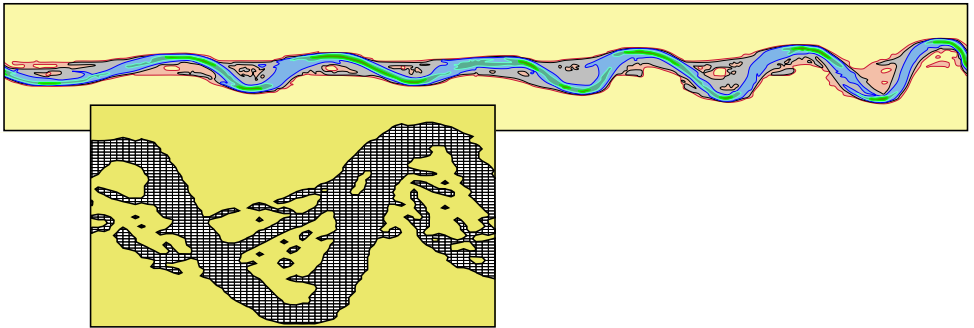


Figure 4.16: Top image: meander pattern as computed by Olsen (2001) for almost supercritical flow starting from a straight channel with slightly oblique inflow. Bottom image: plot of the grid for one bend illustrating cut-cell technique. Flow from left to right.

The consequences of omitting the bank erosion term are obviously that phenomena related to that process, such as meander migration, cannot be simulated. Furthermore, the depth of bend scour is overpredicted if the sediment supply for an alluvial bank is ignored (Darby and Delbono, 2002).

Another disadvantage of these 2D models is the long simulation time that is often required to obtain a single morphological prediction. As indicated in Section 3.4, there are many sources of uncertainty. If the researcher wants to assess the influence of those uncertainties, multiple — possibly, hundreds of — simulations are necessary. The combination of a long simulation time for a single model run and a large number of cases to be considered, leads inevitably to an even longer total simulation time. In view of the increasing demand for sensitivity studies, fast, yet adequate, modelling tools should be maintained.

In nature, irregularities of the bed often develop into dunes and bars. Due to artificial smoothing and lack of detail in the process description, these phenomena may not occur in the numerical model. In the extreme case, all channels and bars may disappear during a long term simulation. Enggrob and Tjerry (1999) have shown with their model that large bars and channels can persist or even form in models with complex geometries as shown in Figure 4.17. This has been achieved by making the Chézy coefficient C strongly dependent on the local water depth h . This was necessary because a more uniform roughness distribution resulted in flow velocities across the shallow bars that were too large, which led to locally unrealistic erosion of the bars. As described in Section 3.4, C was taken proportional to the square root

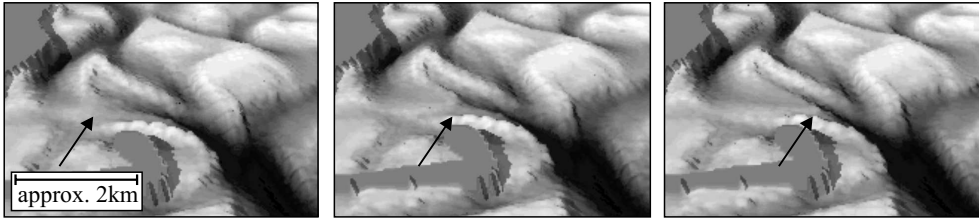


Figure 4.17: Large sand bar moving through channel on the left. Three frames taken from an animation by DHI (2001).

of h in the predictions of the planform changes near the Jamuna Bridge Site. This dependence is probably too strong as is indicated in the project evaluation report (Section 3.3 of DHI and SWMC, Jan. 1997), although the same relationship is still in use today.

4.3.3 Lattice gas models

Most process based morphological and/or hydrodynamic models are based on solving coupled sets of partial differential equations. Each step of the hydrodynamic simulation consists of finding a solution of a large system of equations in which all points of the spatially discretised model area are coupled. This coupling is the result of the implicit solution procedure, which is used to improve the numerical stability and to increase the maximum allowed timestep. The basic equations relate, however, only local quantities. The local hydrodynamics is determined by the local velocity components, pressure (water level) differences, resistance and gravity forces. The local morphodynamics is determined by the local variations in the bed shear stress and sediment availability. Since morpho- and hydrodynamics often evolve on completely different timescales, the hydrodynamics can, in the context of morphodynamics, often be interpreted as a part of the system that instantaneously adjusts to changes throughout the model area. The hydrodynamics acts, therefore, in a quasi-steady modelling approach as a non-local force on the morphology. In a hydrodynamic simulation, which is used to determine the equilibrium flow field, or — when the processes act on similar timescales — in a combined hydro- and morphodynamic simulation, local forces will be dominant. Based on the concept of only local interactions, cellular automata and associated cellular models like the one described in Section 5.2, have been developed that exhibit complex behaviour that has also been observed in nature. Research in the field of cellular automata has resulted in an alternative for the conventional approach using partial differential equations, namely lattice gas models. Because the dynamics of these models is defined by local relations only, simulations can be easily distributed over multiple processors. The following paragraphs introduce the concepts of these models and sketches some of the possibilities offered by this approach (See also Boghosian, 1999; Chopard *et al.*, 2002).

The first lattice gas models describe the movement of individual particles over a lattice (or grid). The particles should not be interpreted as water molecules but as water volumes. At each grid segment either one or zero particles can be present. All particles move with the same speed: from one gridpoint to the next in one timestep. Particles collide when they meet at a node; in which case the resulting situation is given by a set of local collision rules that obey conservation of momentum and mass. The first models used a rectangular lattice,

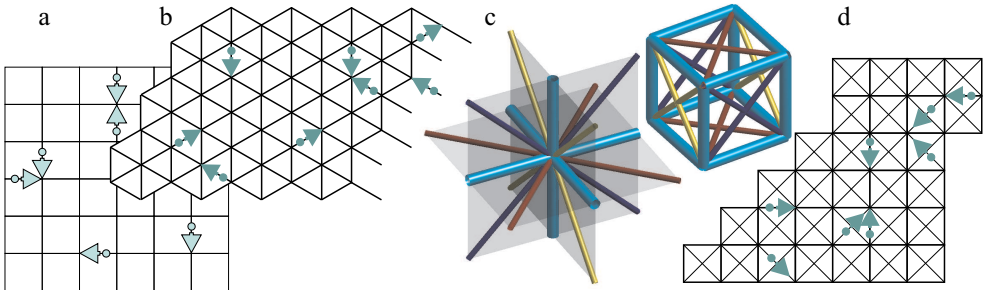


Figure 4.18: The rectangular, two-dimensional lattice (a) used by the first lattice gas models was because of non-isotropy succeeded by the hexagonal lattice (b) of the FHP model of Frisch et al. (1986). The three-dimensional lattice (c) that allows for an isotropic schematisation of the fluid motion was obtained by projecting a four-dimensional regular grid into three-dimensions (Frisch et al., 1987). A similar approach was later followed to define a rectangular lattice (d) in 2D (Qian et al., 1996).

which resulted in non-isotropic effects on the flow. Frisch *et al.* (1986) showed that isotropy could be obtained (for 2D simulations) by using a hexagonal lattice (see Figure 4.18). A three-dimensional lattice that allows for an isotropic schematisation of the fluid motion was obtained by projecting a four-dimensional regular grid into three-dimensions. This model is indicated by FCHC (face centred hyper cubic) lattice (Frisch *et al.*, 1987). The geometry of the FCHC lattice consists of a regular 3D grid with the diagonals of the cube faces added; the connections of the regular grid have multiplicity 2, the others 1. A similar grid was constructed for 2D applications; it consists of a regular grid with weight 4 and diagonals with weight 1 (Qian *et al.*, 1996). The particulate character of the model manifests itself when small scale phenomena on the grid are considered. Macroscopic physical quantities can only be obtained by averaging over large portions of the grid and over multiple simulations (space and ensemble averaging).

The ensemble averaging can effectively be done before the simulations when the correlations between the particles are neglected (the Boltzmann molecular chaos hypothesis). The discrete approach is thereby converted into a real-valued approach whereby the variables are no longer binary but floating point values between 0 and 1 (McNamara and Zanetti, 1988). This type of model is indicated as a Lattice Boltzmann model. The discrete collision rules of the lattice gas models were initially converted into non-linear functions, using a procedure similar to the one used in fuzzy logic. Although efficiency was gained by reducing the number of simulations to be averaged during the post-processing, the computational complexity of the non-linear collision term became too large for practical applications. A solution was found in relaxing the relation with the lattice gas models and to use linearised versions of the collision terms and formulations unrelated to lattice gas models (Higuera and Jiménez, 1989; Higuera *et al.*, 1989). This development has led to the Bhatnager-Gross-Krook (BGK) modelling approach (Qian *et al.*, 1992; Bhatnager *et al.*, 1954) that can be used in cases with relatively high Reynolds numbers.⁴ when a Smagorinski subgrid model is applied (Hou *et al.*, 1988). As a result of the switch from lattice gas to lattice Boltzmann models the binary arithmetic, which was ideal for computer implementation, is lost and round-off errors are introduced⁵

⁴Simulations for Reynold numbers in the order of 500,000 have been recently done by Shock *et al.* (2002).

⁵Alternative formulations have been developed that use integer arithmetic with large numbers as a compromise.

Lattice gas and lattice Boltzmann models have been used to solve several two- and three-dimensional problems in fluid dynamics, see for instance Lowe *et al.* (1996). Numerical simulations of fluids with large particles in suspensions are described in detail by Ladd (1994a,b). Simulations with transport, erosion and sedimentation of snow flakes are described by Masselot and Chopard (1998, 1999). Dupius and Chopard (2000) have carried out lattice gas simulations concerning the erosion and sedimentation under submarine pipes. Dupius (2002) presents the results of a 3D lattice gas model for two meander bends. Building on the success of cellular automata to reproduce complex behaviour using simple rules, the range of applications of lattice gas models has increased significantly over the last decade. It is expected that — although lattice gas methods, just like other cellular models, are valuable research tools for the detailed and/or fundamental, process-oriented studies — they will not be applied to large scale morphological modelling of rivers in the foreseeable future.

4.4 Summary

Over the last decades research on the meandering of rivers has contributed substantially to the understanding of the interaction of processes of flow, sediment transport, shaping of the channel bed, and channel migration. The kinematic approach used by Ferguson (1984a), Howard (1984) and Howard and Knutson (1984) made it possible to illustrate the long term evolution of the planform of meandering rivers. The spatial lag between channel curvature and near bank flow velocity turned out to be of crucial importance for the development of realistic looking meanders. The theoretical analyses by Ikeda *et al.* (1981), Parker *et al.* (1982) and Parker (1984) led to a physics-based justification for the handling of the lag effect in the kinematic model by Howard and Knutson (1984). Furthermore, these analyses showed the importance of the bend instability phenomenon in the development of meanders. In the meantime studies regarding the flow in river bends led to a better understanding of the dynamics involved (De Vriend, 1981b). It turned out to be necessary to include corrections for the exchange of momentum due to secondary flow. Subsequent studies by Blondeaux and Seminara (1985) and Struiksma *et al.* (1985) showed the importance of the interaction of flow, sediment transport and morphology. The usually assumed transverse bed profile in equilibrium with local curvature turned out to be invalid; a lag effect was needed, once again. This led to the development of combined flow and morphodynamic models by Johannesson and Parker (1989) and Crosato (1990). This is basically where the development of one-dimensional meander models ends (except for sedimentological extensions by Sun *et al.* (1996) and further analysis by Howard (1992, 1996) and Stølum (1996)). The next step in meander modelling will lead to two- and three-dimensional models, as first formulated by Mosselman (1991, 1992). Significantly increased computational costs and implementation difficulties with respect to new phenomena such as bank accretion, overbank flow and mesh adaptation have slowed down the development of new meander models.

Due to the nature of braided rivers, models of such rivers need to be two-dimensional in some sense. The one dimensional, statistical Markov chain approach uses the width as a dependent variable. The random walk models by Howard *et al.* (1970), Krumbein and Orme (1972), Rachocki (1981) and Webb (1994, 1995) use a two-dimension lattice with multiple parallel branches. Paola (1996) tries to deal with the second spatial dimension by averaging over the width of the braid plain.

One can find generally applicable models only in the extremes. These models are either so generic that anything can be modelled (time series models are an example of these models), or they include descriptions of the relevant physical processes (that is, a generic two or three dimensional model). A generic physics-based model offers the best perspectives in the long run, but the construction of such a model requires still a significant amount of research with respect to both physical processes and numerical modelling.⁶ Practical solutions have to be found for the immediate future.

Basically there are only two options to deal with planform changes of braided rivers in physics-based models. The first option is to treat the branches of the braided channels as separate channels. Each channel can, in that case, be modelled using any one of the meander concepts described in Section 4.1. A model based on the kinematic approach is discussed in more detail in Section 5.3. Of crucial importance for the success of such a model, are the physical foundation for the definition of the individual channels and their interaction at the bifurcations and confluences. The second option is to deal with all branches within a two-dimensional model covering the entire braid plain. Simulation time and numerical treatment of low-stage channel migration are two important aspects of this approach.

⁶Although in some respects similar to the quest for a grand unified “Theory of everything” by physicists there is one important difference. Basically all equations necessary for modelling a river are known at a microscopic level, but the appropriate way of spatial integration to a macroscopic scale is not yet known.

Chapter 5

Some planform models in detail

Coleman (1969) indicates that planform changes of the Jamuna River over a short period (one, two, in some cases perhaps three years) can probably be (manually) predicted with reasonable accuracy, based on comparative studies of the migration patterns over several preceding years. He suggested that — for this task to be accomplished — aerial photographs should be available on an annual basis. Basically it is this method that has been used during the FAP studies which started two decades later. In these projects, which continue until the present day, an expert predicts the most likely planform changes based on a series of satellite images of successive years and local field observations. One should note that the aerial photographs suggested by Coleman contain much more detailed information than the best satellite images available in the FAP projects. The supplementary field data contribute in many cases significantly to the success of predictions.

In this chapter we will focus on the question whether an automated alternative for this manual prediction method can be developed that is as good as that method or even better. Three computer models for the dynamic behaviour of braided rivers have been developed. The models are based on a neural network approach (Section 5.1), a cellular approach (Section 5.2) and a geometric object-oriented approach (Section 5.3), respectively. After describing the models and the simulation results obtained with them, these models are compared with a generic depth-averaged PDE approach in Section 5.4. The approaches are compared with respect to the quantification of the uncertainty in the prediction, their computational speed, their physical foundation, their applicability to new cases in the future, their resolution, the ease with which new insight can be included, and the amount of data required to run the models.¹

¹A summary of the Sections 5.1 (neural network), 5.3 (object-oriented approach) and 5.4 (discussion) has been presented by Jagers (2001).

5.1 Neural network

Since the 1980s, research on and application of artificial neural networks² have strongly increased. Today neural networks are widely used as modelling and analysis tools in data-rich environments. It has been shown that neural networks are able to learn a large variety of geometrical relations that for humans are hard to describe in simple rules. A good example is the use of neural networks for character recognition (Hertz *et al.*, 1991). Hence it seems logical to investigate how neural networks can be of use in predicting planform changes in (large) braided rivers. Within the present framework a neural network approach has been used to relate remote sensing images of low-stage planforms of two successive years.

It is assumed that morphological changes are mainly determined by the local and upstream flow pattern, bed topography and planform. This is not true for sedimentation or degradation due to backwater effects, but it is a reasonable assumption planform changes such as bend migration in meandering rivers where the local migration rate is determined by a weighting of the local and upstream channel curvature. The only downstream influence results from the determination of the local curvature that requires a downstream channel point. More in general the bank erosion rate depends on the angle at which the flow approaches the bank. Similarly, the distribution of the discharge over multiple branches is determined by the geometry of the bifurcation and the upstream channel alignment although backwater effects play a role in determining the exact distribution. Furthermore, it is assumed that a particular channel planform is accompanied by a, for that geometry, characteristic flow pattern and bed topography (such as the pool/point bar combination in bends). Based on these assumptions one may tentatively conclude that the planform may to some extent contain sufficient information for a prediction of planform changes. For meandering rivers this idea leads to the kinematic meander models described in Section 4.1.1. Braided rivers like the Jamuna River are often associated with large variations in discharge although in general some kind of characteristic flood can be defined. Although the exact height and duration of the flood are important for estimating the extent of the erosion, they generally don't significantly influence the location at which erosion occurs. Whether the location can be identified from a satellite image depends on the amount of relevant information contained in the image: is it enough to estimate the flow conditions during the dominant period of erosion? For the time being, it is assumed that a satellite image of the low-stage planform contains enough information.

For the usage of a neural network a parametrisation of input and output planforms is needed. The parametrisation should be selected such that there are sufficient data available to train the network. That is, there must be enough independent input output combinations to determine the parameters in the neural network. Predicting a planform basically boils down to determining for every point whether it will be land or water. The present neural network is based on this viewpoint by relating for every point in the vicinity of the river its neighbourhood and the land/water situation in the next year. The parametrisation of the neighbourhood of a point is based on a land/water classification of a satellite image. A description of neural networks in general and the applied one in particular is given in Section 5.1.1. The results are discussed in Section 5.1.2.

²Since in this text only artificial neural networks are considered, the adjective ‘artificial’ — which is generally used to distinguish them from biological neural networks, such as the brain — is omitted henceforth.

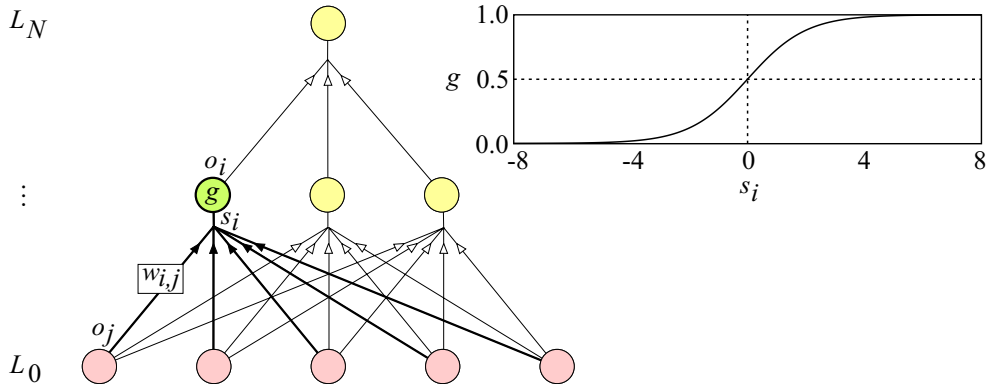


Figure 5.1: The structure of a multi-layer perceptron or multi-layer feed-forward network.

5.1.1 Model description

A neural network is basically a set of interconnected neurons (or processing units) which all perform the same simple operation on their inputs. The neural network is often constructed in a layered manner as indicated in Figure 5.1: each row of neurons receives its inputs only from the neurons in the previous layer; such a network is called a multi-layer feed-forward network. Each neuron i in a layer L_n is connected to all the neurons j in the previous layer L_{n-1} , and it computes the weighted sum s_i of their outputs o_j minus an offset (often referred to as threshold) θ_i as

$$s_i = \sum_{j \in L_{n-1}} w_{i,j} o_j - \theta_i \quad (5.1)$$

where $w_{i,j}$ represents the weight with which the output o_j of neuron j contributes to the internal state s_i of neuron i . The output o_i of the neuron is determined by a non-linear activation function g of the neuron's state s_i . This non-linear function is generally a sigmoid function, as for example

$$o_i = g(s_i) = \frac{1}{1 + \exp(-s_i)} \quad (5.2)$$

A graph of this function is shown in Figure 5.1. Variations on this function are used depending on the field of application.³ The offset θ_i and the weights $w_{i,j}$ determine the range of values that can be assumed by the state s_i . This range determines which part of the non-linear function is effectively used by the neuron and thereby it determines the kind of operation that the neuron represents. For sufficiently large negative values of s_i , where $\exp(-s_i) \gg 1$, g takes on the form of an exponential function. In this range, Equations 5.1 and 5.2 can be combined to give

$$o_i \approx e^{s_i} = e^{-\theta_i} \prod_{j \in L_{n-1}} e^{w_{i,j} o_j} \quad (5.3)$$

which indicates that the operation of the neuron is of a multiplicative nature. In the neighbourhood of $s_i = 0$ the function is linear and the operation performed by the neuron is additive. For positive values of s_i in the order of 2–6, g resembles a logarithmic function. Weighting

³Sometimes a periodic function (for example a sine function) is used. In that case the offset θ_i is limited to the range of 0 to 2π .

that takes the state s_i into both extremes (either a large positive or negative state) uses the function as a logical switch.

The bottom layer L_0 of neurons in Figure 5.1 is the input layer and it contains the input neurons, which are only used for (often predefined) input scaling. The top layer L_N is the output layer, which generates the final result of the network. The intermediate layers (of which there is just one in the figure) are called hidden layers.⁴ One set of known input-output combinations M_{train} is used repeatedly during the training of the network — that is the calibration phase during which the values of the parameters (weights $w_{i,j}$ and offsets θ_i) are determined. A second set of known input-output combinations M_{test} is used to test whether further calibration of the parameters actually improves the prediction power of the network or only results in overfitting the training set.

The fit of the network on a set $M = \{\xi^\mu, \zeta^\mu | 1 \leq \mu \leq m\}$ is generally measured by the cost function E given by

$$E[\underline{w}, \underline{\theta}] = \frac{1}{2} \sum_{\substack{i \in L_N \\ 1 \leq \mu \leq m}} (\zeta_i^\mu - o_i^\mu)^2 \quad (5.4)$$

where the summation of residual errors — that is, differences between the output o_i^μ of output neuron i given the input vector ξ^μ and network parameters $w_{i,j}$ and θ_i and the target value ζ_i^μ — is taken over all input-output combinations in the set M and all output neurons i . This approach is based on the assumption that the residual errors (for varying μ and i) are independent and Gaussian distributed. In each training step the network parameters are adjusted using a conjugated gradient method, which leads to a reduction of this error on the training set M_{train} . The parameters can be adjusted after each evaluation of a single input-output combination ξ^μ, ζ^μ (incremental updating) or after all combinations in the training set M_{train} have been evaluated (batch updating). The latter approach was used in this project and, therefore, the cost function E given in Equation 5.4 is includes a summation over all combinations in the training set M_{train} . The gradient of the cost function E is determined by the (error) back-propagation algorithm (see Appendix B.1.2).

Now, let us consider the setup of the neural network used for the prediction of the erosion locations from the planform geometry as derived from a satellite image taken during the preceding low-water season. A small neural network with five input neurons, one or two hidden layers, and one output neuron has been used for predicting whether a land pixel will be classified as a water pixel after one year. The five inputs that were supplied to the neural network are indicated in Figure 5.2. They are:

1. the distance to the nearest channel,
2. & 3. the sine and cosine of the angle α_{nc} between the direction to the nearest channel and the flood flow direction,
4. the local width of the nearest channel, and
5. the fraction of the 11×11 pixels neighbourhood (centred around the point of interest) that is covered by water.

⁴It has been proven that in theory just one hidden layer with sufficient neurons is needed to approximate any continuous function, while two hidden layers are needed for representing any function. References can be found in Hertz *et al.* (1991).

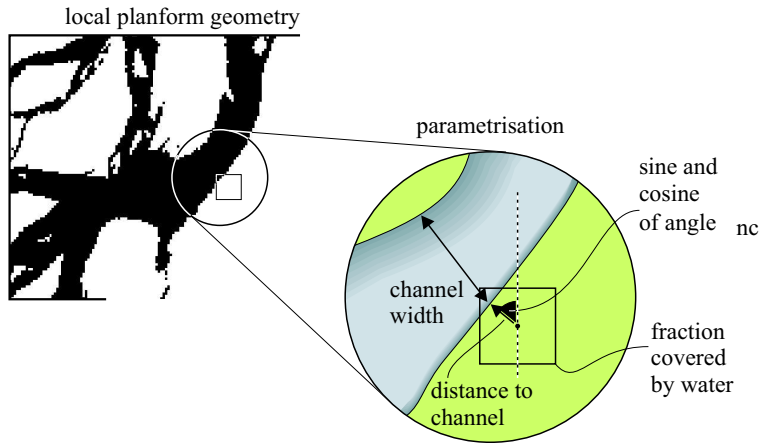


Figure 5.2: Definition of input variables for neural network.

Appendix B.1 describes the way in which these parameters have been derived from the satellite image. The angle α_{nc} of the direction to the nearest channel relative to the flood flow direction is approximated by the angle relative to the north-south direction because the overall river direction (that is, the dominant overall flow direction during flood) is oriented north-south in the studied reach of the Jamuna River. The reason why the sine and cosine are specified as two input variables instead of the angle itself is that the angle changes abruptly when going through a full circle. Depending on your definition this discontinuity occurs when turning from 2π to 0 or from π to $-\pi$ radians. A small change in flow direction would, therefore, have a large effect on the angle α_{nc} , whereas it is expected that the net effect of such a small change on the probability of erosion should be small. Better results are obtained when there are no discontinuities in input variables and, therefore, the sine and cosine have been used instead.⁵ Furthermore, all five input variables were normalised separately such that the average over the training set was zero and the variance in the training set equals one. In this way, the training of the network is based on the variations of the parameter values and not influenced by their absolute magnitudes. This procedure, which is similar to the preconditioning of a system of equations before solving, helps to get a good convergence during the training phase of the network.

The number of neurons in the hidden layers has been varied between one and seven, resulting in eight to forty-three parameters (weights and thresholds) that had to be fitted during the training phase. All network configurations are shown in Figure 5.3. The number of neurons in the hidden layers is indicated between brackets. So, 5(3)21 refers to a network with 5 input neurons (all networks had this), 3 neurons in the first hidden layer, 2 neurons in the second hidden layer and 1 output neuron (all networks had this). The configuration of the network shown in Figure 5.2 would be indicated as 5(3)1. The networks have been trained on and applied to pixels within a distance of seven pixel units from the land-water boundary. For the image used, this corresponds to a maximum distance of 350 m because each pixel represented an area of 50 m \times 50 m.

⁵The sine and cosine are only partially independent input variables. Their magnitudes are obey the formula $\sin^2 + \cos^2 = 1$, but their signs are independent.

Only five variables have been used to characterise the local planform. The list of variables can, of course, be extended with other quantities and this may have a positive effect on the performance of the neural network. One should, however, take care that the input quantities are well-defined for all points. The distance to the closest upstream bifurcation has for instance a completely different meaning for points on a bar (related to bar migration in downstream direction) than for points on the edge of the flood plain (mainly relevant for the lateral erosion rate). Therefore, this parameter is not a good input quantity for the network. Another example is the node type (confluence or bifurcation) of the nearest upstream node. An upstream confluence may, for instance, trigger the formation of a new bifurcation due to mid-channel bar growth near the point of interest, and consequently an increased probability of erosion, as described in Section 3.5. On the other hand, an upstream bifurcation can, depending on the bifurcation angles, result in either decreased erosion (when the nearest branch is abandoned) or increased erosion (when the other branch is abandoned) as shown by Moselman *et al.* (1995). Besides the requirement that the quantities should have a well-defined meaning, the inclusion of the various input variables (such as the upstream node type mentioned above) depends on our insight in the relevant processes. So, choosing an optimal set of input variables requires a good understanding of the braiding processes involved. A number of possible extensions will be addressed in the discussion of the neural network approach in Section 5.1.3.

5.1.2 Results

Ten different neural network configurations were tested with a varying number of neurons in the hidden layer(s). The training of the neural networks started with randomly chosen weights and thresholds. For each configuration twenty different initial parameter settings were tried. The same training and testing data sets were used for all configurations and they both consisted of 2500 randomly selected input-output combinations. Figure 5.3 shows for each network configuration evolution of the cost function $E[\underline{w}, \underline{\theta}]$ as defined by Equation 5.4 for the training run that ended in the best fit to the training data. The network configuration is indicated in each graph. The numbers indicate the number of neurons in the input layer (always 5), the number of neurons in the hidden layer(s) (between the brackets) and the number of output neurons (always 1). The thick lines indicate the evolution of the cost function for the training set and the thin lines refer to the cost function for the test set. From these graphs it is easily observed that all configurations lead to a minimum of just over 135 for the cost function for the test set. Once that value is reached further adjustments lead to overfitting which is indicated by an improving fit to the training set and a generally deteriorating fit to the test set.

For one of the trained configurations the performance of the neural network was assessed in some more detail. This is the 5(3)1 configuration with one hidden layer containing three neurons. The weights and threshold were not taken from the end result of the training, but rather after the 75th iteration, marked with a circled asterisk \circledast in Figure 5.3, at which moment the performance of the neural network is similar for both the training and the test set. The network can be described by

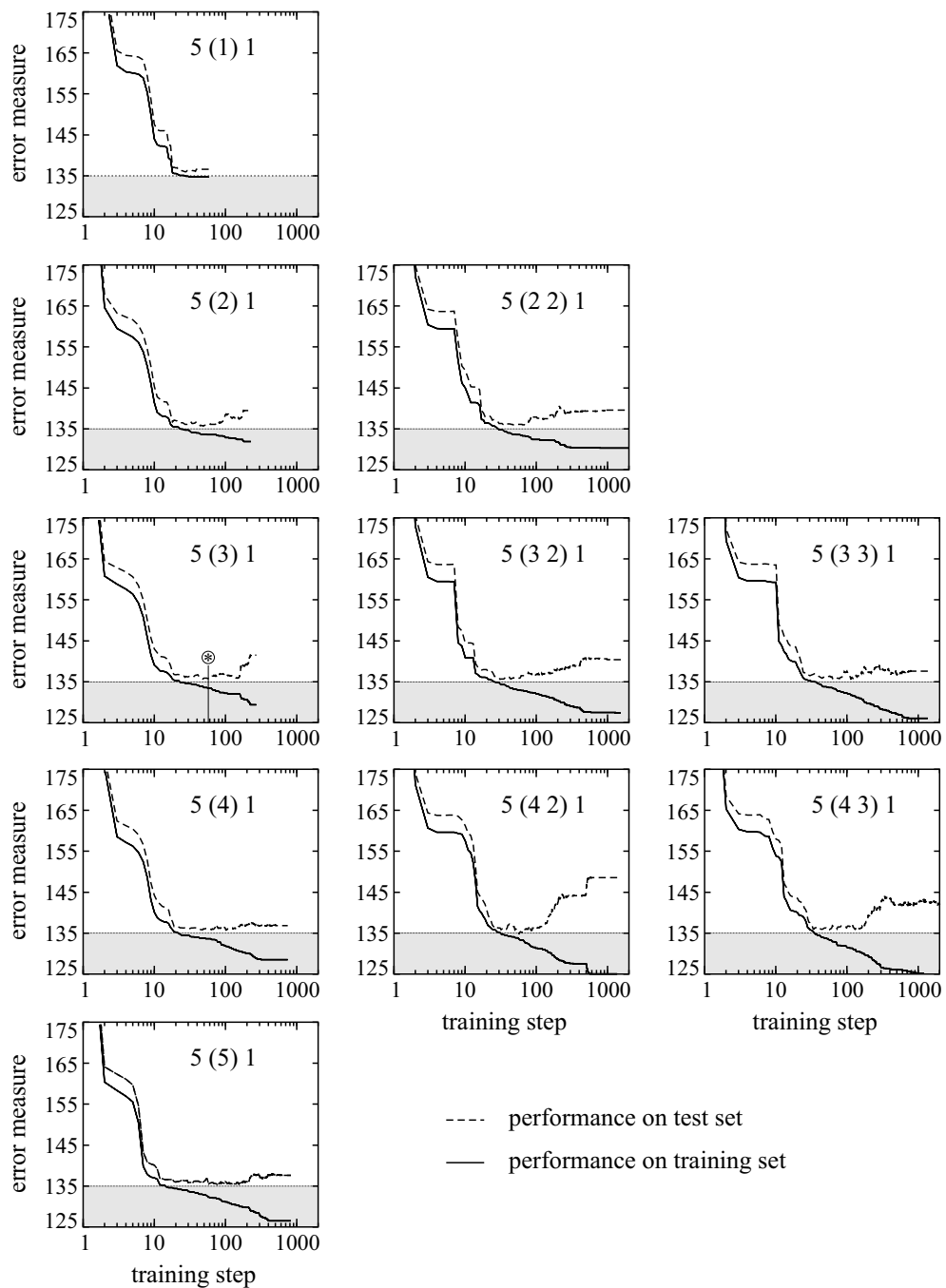


Figure 5.3: Convergence of the neural network training for ten different network configurations: five inputs, a varying number of neurons in the hidden layer(s), and one output. The number of neurons in the hidden layers is indicated between brackets, e.g. 5(3 2) 1. Continuous and dashed lines indicate the performance of the networks on the training and test data respectively.

- Five input scaling operations

$$\begin{aligned}
 o_1 &= 0.54(\text{distance to channel} - 3.55) \\
 o_2 &= 1.75(\cosine - 0.02) \\
 o_3 &= 1.22(\sin + 0.02) \\
 o_4 &= 0.17(\text{channel width} - 6.51) \\
 o_5 &= 5.85(\text{water fraction} - 0.19)
 \end{aligned} \tag{5.5}$$

- Three operations by the neurons in the hidden layer

$$\begin{aligned}
 o_6 &= g(-0.46o_1 - 0.68o_2 - 0.29o_3 - 0.85o_4 - 1.85o_5 - 0.81) \\
 o_7 &= g(-0.12o_1 - 1.40o_2 + 1.26o_3 - 0.47o_4 - 0.82o_5 + 2.05) \\
 o_8 &= g(-0.31o_1 - 0.98o_2 + 0.34o_3 - 0.84o_4 - 3.40o_5 - 2.20)
 \end{aligned} \tag{5.6}$$

- One operation by the output neuron

$$\text{prediction} = o_9 = g(-0.64o_6 - 1.41o_7 - 1.52o_8 + 0.37) \tag{5.7}$$

Although the geometric information comprised by the input variables is limited, the neural network was able to give reasonable predictions regarding bank erosion at several locations. This is shown in Figure 5.4. Reasonably correct predictions are marked with white numbers in black circles, whereas incorrect predictions are marked with black numbers in white circles. When comparing the predicted probability of erosion and the observed erosion sites one should keep in mind that the prediction is limited to the points within seven pixels of the channels. From this figure it can be observed that most of cases with a correct prediction (❷, ❸, ❹, ❻) are situated along the east bank of the main channel, whereas most errors (❼–⫽) are located along the secondary channels and in the bar complex in the lower right of the figure where flooding occurs and planform changes are large. This observation can be explained by noting that the planform changes in the latter (relatively low-lying) areas result to a large extent from bed level changes during flood. The planform changes along the main branches result, on the other hand, from bank erosion; the input variables of the neural network are better suited for the latter approach. Exceptions to this rule are incorrect predictions ❸ and ❹ along the main channel and the correctly predicted erosion at location ❸ along a secondary channel. Along the western channel correct predictions (❶, ❻) are alternated with incorrect predictions (➋, ⑃, ⑆, ⑈). The formation of a new channel as indicated by ⑊ in the lower left of the figure was not predicted by the network since it had only been trained on and applied to points within a distance of seven pixels from the land-water boundary. However, even if the network had been used for other points as well⁶, the network is unlikely to predict new channels like this, since the amount of data to learn from is too limited.

The average performance and the contribution of the various input variables have been analysed in some more detail. The results are shown in the Figures 5.5 and 5.6. This analysis was based on all the 5000 input-output combinations in the training and test sets, not including

⁶After appropriate training, of course, as it is easy to see that the network given by Equations 5.5 till 5.7 incorrectly predicts a relative large probability of $g(0.37) \approx 0.59$ on erosion anywhere far away from the river ($o_1 \rightarrow \infty$).

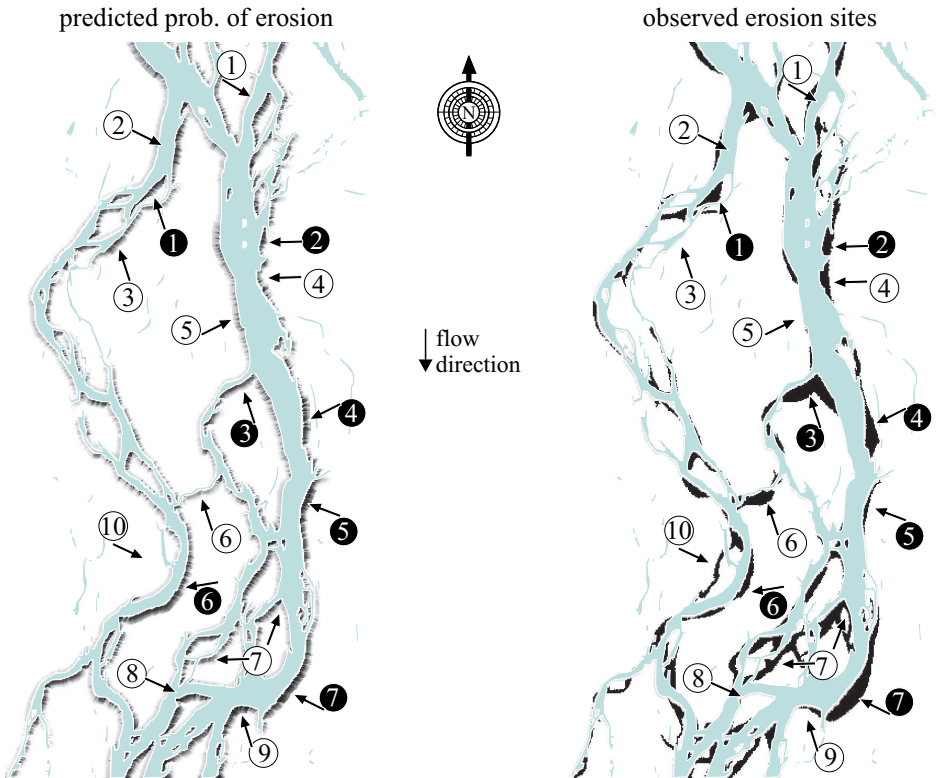


Figure 5.4: Prediction test of the neural network with three neurons in the hidden layer. Reasonably correct predictions are marked with white numbers in black circles; incorrect predictions are marked with black numbers in white circles.

any unused input-output combinations. Figure 5.5 contains five graphs in which the predicted probability of erosion P_{pred} is plotted against the value ξ_i of one of the input variables (distance to nearest channel, cosine and sine of α_{nc} , width of nearest channel, and water fraction). Input-output combinations that correspond to locations that were actually eroded are plotted in black dots, while combinations related to locations that were not eroded are plotted in grey dots.⁷ From these graphs it is clear that most black dots are located above the grey dots, indicating that the predicted probability of erosion P_{pred} is on average higher for the eroded sites than for the non-eroded sites.

A better comparison can be carried out using the average probabilities of erosion. Therefore, two lines have been added to each of the five graphs of Figure 5.5. The line marked with circles indicates — as a function of the selected input variable — the average probability of erosion predicted by the model, whereas the line marked with stars indicates the fraction of the sites that was actually eroded. In all five graphs the two lines match quite well, which shows that at least the average prediction by the neural network is good. The distance between the two lines is largest for input values for which very few data points were available in the

⁷A majority vote has been applied when multiple input-output combinations would have to be plotted at the same location.

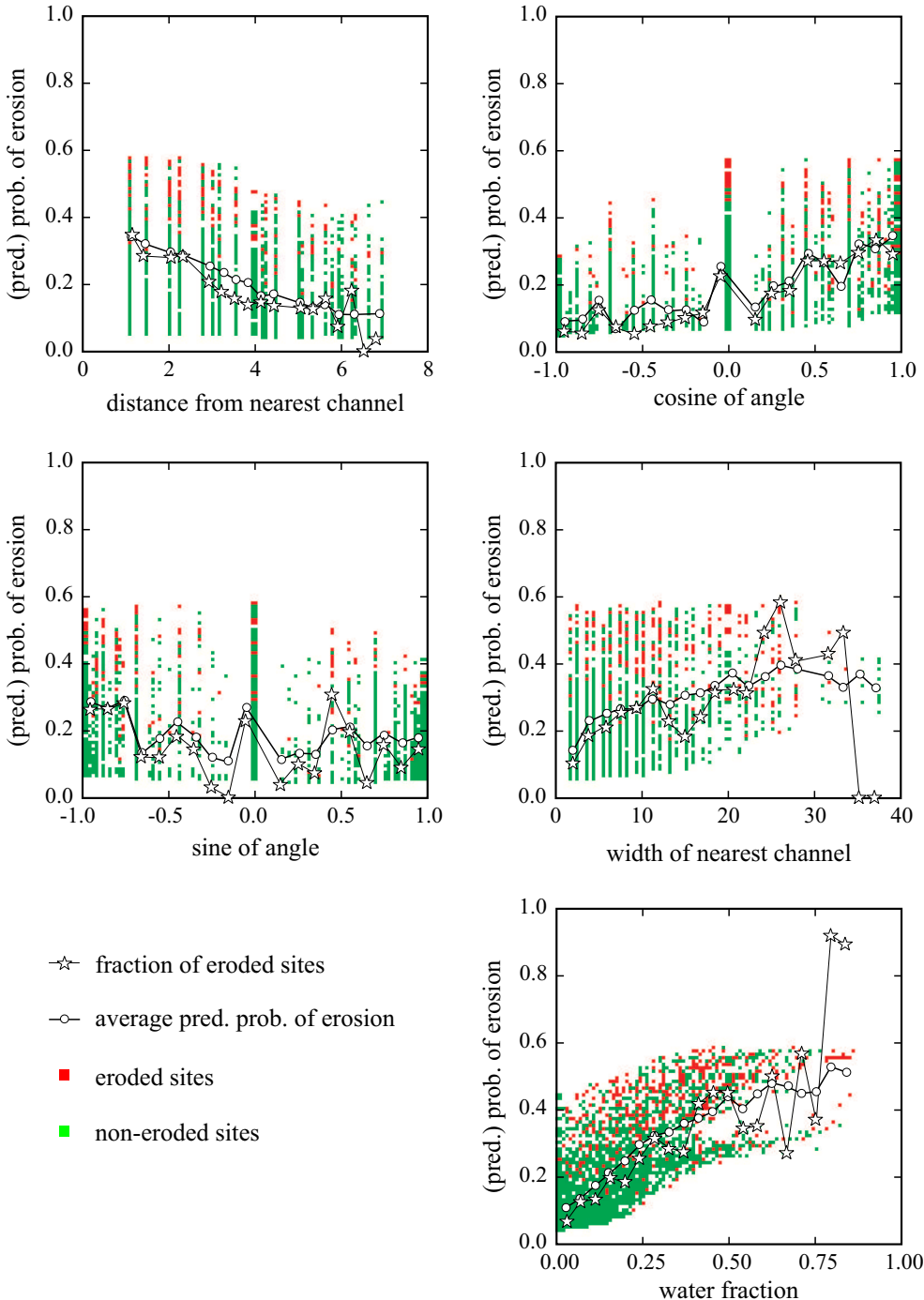


Figure 5.5: Dependence of the predicted probability of erosion on the value of the input variables.

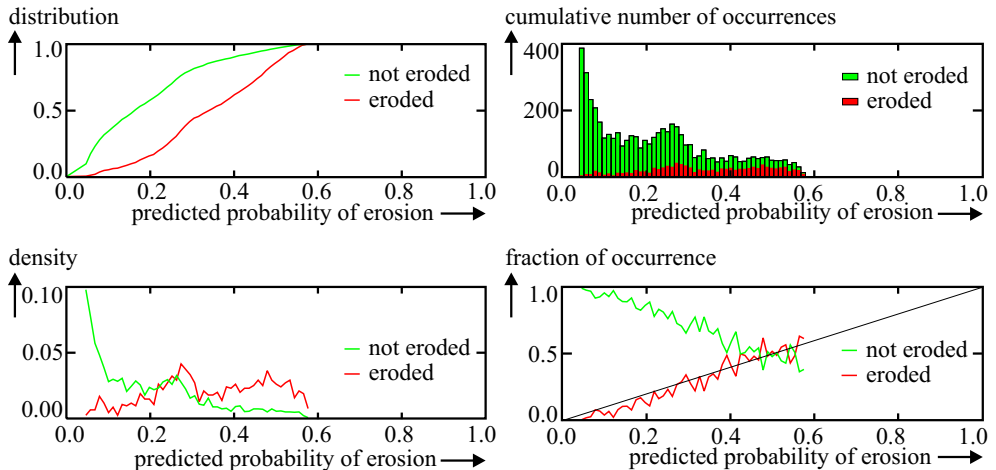


Figure 5.6: A comparison of the predicted probability of erosion and the observed average probability of occurrence.

training set. A large part of the scatter can thus be attributed to the limited amount of data for those cases; it is not necessarily related to shortcomings of the neural network. The first graph of Figure 5.5 indicates that there is a negative correlation between the probability of erosion and the distance between the point of interest and the channel, that is, points further away from a channel have a smaller probability of being eroded than points close to a channel. The second graph shows that points downstream (south) of a channel (cosine equal to 1) have a higher probability of erosion. This is caused by the overall southward flow direction during flood. The third graph does not show any clear relation between the sine of the angle towards the nearest channel and the probability of erosion. So, there is not a large difference in the probability of erosion along an east or west bankline. The fourth graph indicates that when the nearest channel is wide, the probability of erosion is larger than when it is narrow. The fifth and last graph indicates a clear relation between the water fraction of the neighbourhood and the probability of erosion: land pixels surrounded by a large amount of water are more likely to be eroded than pixels with less water in their neighbourhood.

Some of these results have been presented in a slightly different way in Figure 5.6. The lower left graph of this figure shows the estimated probability density function $p_e(o_9)$ of the actual occurrence of erosion as function of the predicted probability o_9 of erosion by the neural network. The estimated probability density function $p_{ne}(o_9)$ of no erosion is also plotted in this graph. Fortunately, $p_{ne}(o_9)$ is larger than $p_e(o_9)$ for small predicted probabilities of erosion $o_9 \lesssim 0.3$, and smaller for larger values of o_9 . The same conclusion can also be drawn from the estimated cumulative density functions shown in the upper left graph. There is a quite large overlap in the two distributions, so, the predicted probability of erosion is not sufficient to clearly distinguish between erosion and non erosion. The receiver operator characteristic (ROC) curve for this neural network is plotted in Figure 5.7. The ROC curve is obtained by plotting the true positive rate (or, sensitivity) against the false positive rate (or, $1 - \text{specificity}$) for varying threshold value for the predictor o_9 . The true positive rate is the fraction of the predicted erosion cases that were actually eroded; the false positive rate is the fraction of predicted non-erosion cases that were actually eroded. The area under the

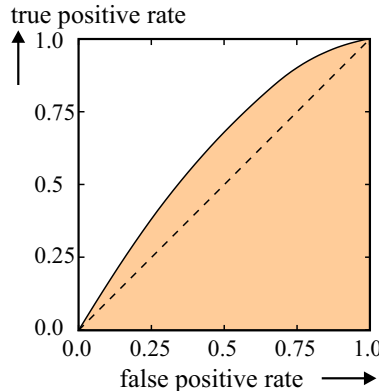


Figure 5.7: Receiver operator characteristic curve of the neural network defined by Equations 5.5 to 5.7.

ROC curve, here 62%, is a measure for the performance of the variable o_9 to distinguish between erosion and non-erosion: a value of 50% would indicate that the variable is non-distinguishing (for instance, a random guess), a value of 100% would indicate that the erosion and non-erosion cases could be distinguished perfectly based on the variable. The upper right graph of Figure 5.6 shows the cumulative number of eroded and non-eroded pixels in the analysis, again as a function of the predicted probability of erosion. About 20% of the sites in the training and test sets were locations at which erosion did actually occur. Finally, the lower right graph of Figure 5.6 indicates that, of all sites at which the predicted probability of erosion P_{pred} equals p , approximately a fraction p was actually eroded for this data set. Also note that the neural network never predicts a probability of erosion higher than 0.6. This can also be derived from the Equation 5.7, since the maximum value of o_9 is equal to $g(0.37) \approx 0.59$ because the outputs o_6 , o_7 and o_8 of the hidden neurons will always lie between 0 and 1. As the last graph showed, this is in almost perfect agreement with the fraction of actually eroded sites that are assigned this maximum predicted probability of erosion. It is not absolutely clear from the data whether it should be possible to identify locations with a significantly higher probability of erosion from the five input variables available to the neural network.

5.1.3 Discussion

The results show that, based on the limited set of five input values, the simple neural network was able to learn the following three rules.

1. Points near a channel have a higher probability of erosion than points further away (as far as the trained networks are concerned only up to 7 pixels away).
2. Channels tend to migrate down-valley, expressed by the fact that erosion rate is highest for points at which the cosine of α_{nc} is close to one.
3. Wide channels migrate faster and erode more land.

So, one can conclude that a neural network, when applied this way, can learn certain rules based on satellite images of braided rivers.

Whether or not neural networks will become a useful prediction tool depends on several aspects. The two most important points are the availability of training data and the selection of suitable parameters for the schematisation of the initial planform. Regarding the availability of training data there are two major limitations.

- *The larger neural network, the more data is needed for training.* Hertz *et al.* (1991) describe an example of a neural network for the seemingly simple task of recognising handwritten digits. It consisted of four layers with 256 input neurons (representing a 16×16 bitmap⁸ of the digit), 768 neurons in the first hidden layer, 192 in the second, 30 in the third, and 10 neurons in the output layer representing the ten digits 0–9. If all connections would have been used, 351124 parameters would have to be calibrated. By giving the network an internal structure, the number of independent parameters was reduced to 9760. The network was calibrated using 7300 digits in the training set and 2000 digits in the test set. Note that the total number of cases used in the training process was smaller than the number of independent parameters. The example illustrates that neural networks — larger than the 5(3)1 network used herein — have been used in other fields dealing with pattern recognition. So, a much larger network might be needed for more accurate predictions of the planform changes in the Jamuna River. And, even in that case the question remains whether such a network can be applied to other braided rivers without recalibration.

One should note that in the case described above the outcome is largely deterministic in nature: handwritten digits can generally be identified as representing a certain number except for some indeterminate boundary cases of, for example, 1 and 7. Whereas, in our case the erosion of a location depends not only on the five input variables but also on external factors like flood magnitude, erodibility, elevation and channel curvature. So, there may be locations characterised by the same values for the five input variables, of which some fraction is eroded while the remainder is not. This means that we need a much larger data set to obtain a well-defined average probability. Part of this uncertainty will remain even if the number of input variables is increased. The amount of data needed for calibrating such a model would be huge and seldom available. This can be a problem, since a lack of suitable training data cannot be compensated by incorporating established empirical relationships into the network.

- *There is little or no data for special cases.* The lack of training data becomes more pronounced when a network is to be trained for cases where human impact plays a role. It is not possible to apply a neural network when the effect of new kinds of river training works are to be predicted, since there will be no data available to train the network. Moreover, it is hardly ever possible to predict the effect of human impact when a large network is used, since the amount of training data that is available for these cases is extremely limited.

⁸When a similar approach is applied to the braided river one would cover, given a satellite image with a resolution of 50 metres (as was used here), an area of just 800 m × 800 m. Compared to channels in the order of 1 km wide, this is still a small area. A coarser satellite image could be used further away from the immediate vicinity of the point of interest, making the covered area a bit larger. Using a much coarser overall grid such that the area becomes substantially larger would reduce both the detail of the prediction and the amount of training data available.

As has been postulated a few times in this section, the schematisation of the initial planform is important. The number of input variables used here is rather limited and could be extended with other quantities, such as the state of all points in the neighbourhood, the fraction of water in a larger area, the curvature of the channel, the size of the landmass on which the point is located, the fraction of sand-covered area in the neighbourhood of the pixel, the distance to the nearest channel at a different stage, and other information about the local and upstream river section. The question is whether those extensions would help to improve the prediction. In the following, the some extensions are discussed.

- Including the initial state of all points in the neighbourhood as input variables would probably help to improve the prediction in some cases, but the number of network parameters to be determined increases rapidly when a large area is included.
- One of the inputs now included in the model is the fraction of the 11×11 neighbourhood covered by water. Similar fractions determined for different areas could already give some more information while the number of parameters remains limited. However, a large part of this information is already included via the other input variables: distance, width and angle of nearest channel.
- The characteristics of a second channel in the neighbourhood is for very few points of crucial importance.
- Including the size of the landmass on which the point is located would help to identify the large erosion on the ‘small’ braid bars in the eastern channel. However, this will also lead to an undesirable increase in the predicted probability of erosion for the bars in the less active western channel.
- Including the channel curvature seems a logical extension since the curvature plays a crucial role in case of meandering rivers. One should note that, unlike the presently used inputs the channel curvature cannot be derived simply from the satellite image; a spatially averaged representation of the channel centreline is needed for this purpose. For the studied case channel curvature would not substantially contribute to the accuracy of the prediction since the locations where the curvature is most dominant in the main channels are already correctly dealt with (locations ⑥ and ⑦), whereas along the smaller channels no correlation between the curvature and eroding banks appears to exist. Furthermore, the question arises whether the low or high stage channel curvature should be used. The latter one seems more appropriate.

One might be tempted to think that the planform at a higher stage, when all small bars have been flooded, is simpler in geometry, and that its annual changes are therefore easier to predict. At ‘barfull’ discharge (defined as $25,000 \text{ m}^3/\text{s}$ for the Jamuna River) the number of parallel branches is indeed reduced considerably, as shown in Figure 2.14. However, the application of a neural network to such a planform does not seem to be feasible, because at a higher stage less information is available on the courses of the thalwegs. The bends along the western bankline (in particular at the top end of the image) are at that stage all flooded. Some of these bends correspond to actual deep areas, whereas others correspond to lateral bars as can be seen in the low stage ($7,000 \text{ m}^3/\text{s}$ discharge) image, completely left in the same figure. If only the information of the ‘barfull’ discharge is used, the two cases cannot be distinguished, whilst the low stage image can at least give some information about the location of those bars by means of the classification of the land as sand or vegetated. A combination

of low and high stage planform information may help to improve the predictions, but this approach is limited to the banklines of the mainland only, since the land-water transition at the islands generally shifts when the water level rises. If only the movements of the banklines of the mainland have to be predicted, there are alternative prediction methods that are much easier to use (such as the trend extrapolation method described in Section 4.3.1).

The foregoing discussion indicates that, although the neural network was able to correctly identify several locations where erosion did occur, there are also several limitations to its applicability. The amount of data required for training the network and the definition of a suitable schematisation of the initial planform characteristics are the two most important issues. For a comparison of the neural network approach with two other prediction methods, the reader is referred to Section 5.4.1.

5.2 Cellular model

In recent years an increasing number of researchers has used cellular computer models to study naturally occurring patterns. In these models the cells of a lattice interact according to local rules based on abstractions of the (physical) relations describing a dynamic system. Examples of such models are the ‘Game of Life’ by John Conway (Berlekamp *et al.*, 1982), and models for wind ripples formation by Anderson (1994) and Forrest and Haff (1992), for dune formation by Nishimori *et al.* (1998), and for landscape and drainage pattern evolution by Chase (1992), Howard (1994), and Willgoose *et al.* (1991). A cellular model of stream braiding was presented by Murray and Paola (1994, 1997), which was shown to result in planforms similar to actual rivers (Sapozhnikov *et al.*, 1998). A description of that model is given in Section 5.2.1. As part of the study reported here, the model was implemented and several test runs were carried out. The results of these runs are described in Section 5.2.2.

5.2.1 Model description

The model area consists of a rectangular $N \times M$ grid with some prescribed initial topography, which was in general a tilted surface with a uniform slope in N direction with small, random elevation perturbations; the perturbations had an amplitude in the order of the mean downhill elevation difference between adjacent rows of cells. In each computational step a certain amount of water is released at the upstream boundary ($N = 1$), its path across the grid and the resulting morphological changes are computed, and finally the topography is updated. How the water flows over the grid and how much sediment is transported is determined by the local elevation differences. For these computations only two quantities are needed per cell (i, j) , being the topographical height z_{ij} and an amount (volume or flow) of water Q_{ij} . Furthermore, S_{ijd} is the directional slope from cell (i, j) to $(i + 1, j + d)$ defined by

$$S_{ijd} = \frac{z_{ij} - z_{(i+1)(j+d)}}{\Delta_{ijd}} \quad (5.8)$$

where d can be either $-1, 0$ or 1 and Δ_{ijd} equals 1 for $d = 0$ and $\sqrt{2}$ for $d = \pm 1$.

Let us now follow the flow more in detail (see for reference Figure 5.8). A certain amount of water Q_{ij} that has entered a cell (i, j) from upstream is always distributed to one or more

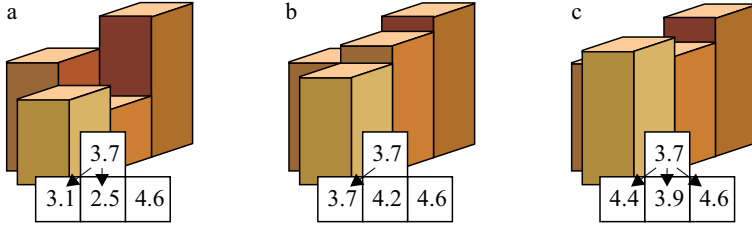


Figure 5.8: Dependence of the flow direction on the local elevation differences in the cellular model of Murray and Paola (1994).

of the three downstream neighbours. The amount Q_{ijd} going to its downstream neighbours $(i+1, j+d)$ depends on the relative heights of those neighbours. If possible, water is routed to only those cells that are lower than the current cell (case a). In that case the amount going to each lower-lying neighbour is proportional to $(S_{ijd})^n$ where the exponent n is a value between 0.5 and 1. If none of the downstream points lies lower, water is distributed equally over the downstream cells that have the same elevation as the current cell (case b). If such cells do not exist either, the water will flow uphill and the amount of water received by each of the downstream cells is proportional to $(-S_{ijd})^{-n}$, where the slope S_{ijd} is negative (indicating uphill flow) for all cells and n is the same exponent between 0.5 and 1 (case c). Summarising, the flow is determined by

$$Q_{ijd} = \begin{cases} Q_{ij} \frac{S_{ijd}^n}{\sum_{\{\delta | S_{ij\delta} > 0\}} S_{ij\delta}^n} & \text{if } S_{ijd} > 0 \\ Q_{ij} \frac{1}{\sum_{\{\delta | S_{ij\delta} = 0\}} 1} & \text{if } S_{ijd} = 0 \text{ and } S_{ij\delta} \leq 0 \text{ for all } \delta \\ Q_{ij} \frac{(-S_{ijd})^{-n}}{\sum_{\delta} (-S_{ij\delta})^{-n}} & \text{if } S_{ij\delta} < 0 \text{ for all } \delta \\ 0 & \text{otherwise.} \end{cases} \quad (5.9)$$

This simple water routing scheme does not include backwater effects, thus preventing information to propagate in upstream direction, which, according to Murray and Paola (1994), implies supercritical flow everywhere in the braided stream. The dependence of the flow distribution on the downstream slope can be reconciled with the lack of information propagating in upstream direction by field and flume experiments that supercritical flow locally responds to differences in slope (Murray and Paola, 1997). If the morphological length scale and the cell size are large compared to the characteristic length scale of the backwater curve, equilibrium flow conditions may be assumed to be satisfied locally (Cui and Parker, 1997; Jansen, 1979). Under this condition the same local flow distribution rule can be applied for subcritical rivers. The Froude number is generally less than one for sand-bed braided streams and only locally above one for gravel-bed streams (see also Section 3.1 on micro-morphology and hydrodynamics in braided rivers). Flow up adverse bed slopes, represented by the third case of Equation 5.9, may be caused by the momentum of the flow or it may be associated with an adverse bed gradient at the upstream side of a submerged bar. An unfortunate side effect of this formulation is that non-local uphill flow is also possible. This non-physical effect can only be prevented by significantly different water routing scheme (see Section 5.2.2).

The total sediment flux Q_{ijd}^{sed} transported by the water flowing from cell (i, j) to $(i + 1, j + d)$ is assumed to be equal to

$$K[Q_{ijd}(S_{ijd} + S_0)]^m \quad (5.10)$$

where

- m constant larger than 1, mostly equal to 2.5,
- K calibration constant, such that the elevation changes are at most a few percent of the mean elevation difference between two consecutive rows in each morphological step⁹,
- Q_{ijd} amount of water flowing from cell (i, j) to $(i + 1, j + d)$ as computed above, and
- S_0 constant representing momentum effects,
- S_{ijd} local slope.

This corresponds to sediment transport rule (3) of Murray and Paola (1994). Murray and Paola (1994, 1997) indicate that the value of 2.5 for m is based on field and flume observations by Ashmore (1985). If one tries to derive the relation using the sediment transport formula by Engelund and Hansen (1967), which basically states that the sediment transport rate is proportional to the fifth power of the local flow velocity, and the Chézy relation $u = C\sqrt{hs}$ for uniform equilibrium flow, one obtains that $Q_{\text{sed}} \propto u^5 \propto (hs)^{5/2}$ when a constant Chézy roughness is assumed. This would suggest that the variable Q_{ij} is proportional to the water depth h , which, however, not make sense in combination with the water distribution Equation 5.9. Murray and Paola (1997) continue by writing $(hs)^{5/2}$ as $(h^{3/2}s^{1/2})^{5/3}s^{5/3}$ and thus they obtain — using $q = Ch\sqrt{hs}$ — $Q_{\text{sed}} \propto (qs)^{5/3}$, so $m \approx 1.67$ and Q_{ij} represents, as could have been expected, the discharge flowing through cell i, j . The braided pattern that forms using this slightly lower value of m is a bit more regular and less realistic according to Murray and Paola (1997), and therefore they prefer to use a value of 2.5 or above for m . The higher value of m corresponds to a power of 7.5 in the sediment transport relation. This value can be obtained for gravel near the threshold of motion, but it is high for sand bed rivers and gravel bed rivers well above the threshold of motion. A value of m larger than 1 is required for braiding to develop (Paola, 2001).

A second type of sediment transport that has been included in the model is lateral, gravitational sediment transport (which represents bank erosion). The lateral sediment transport rate is assumed proportional to the sediment transport out of the channel cell and the lateral slope: $FS_{ijd^*}\sum_d Q_{ijd}^{\text{sed}}$ where S_{ijd^*} is the lateral slope from cell (i, j) to $(i, j + d^*)$ with d^* either plus or minus one. This term contributes obviously only to the calculation if S_{ijd^*} is positive, that is, if the flow transporting cell (i, j) lies lower than the cell next to it. Given these sediment fluxes the elevation of each cell is changed based on the local sediment balance; the elevation of the cells on the boundary remain unchanged (that is, equilibrium transport conditions are assumed).

In the program made by Murray and Paola (1994) the water and sediment motion was confined by high walls along the sides of the grid. Because water can flow uphill when all three downstream points have elevations higher than h_{ij} , these high walls cannot guarantee that the flow stays away from the boundaries and that no sediment is fed to the stream from these side walls. Therefore, in the current implementation these side walls have been removed and

⁹Alternatively, one may define K as a physical constant and introduce a timestep Δt such that the condition is satisfied.

the algorithm relies on an adaptation¹⁰ of the water and sediment routing schemes along the boundary points to contain the flow.

One should note that this model is not a cellular automaton, since that label requires that the five following conditions are satisfied: space is discrete (the spatial unit is called a cell), time is discrete, the state of each cell is part of a (discrete and) finite set, changes in state occur based on local update rules, and the whole automaton updates synchronously. The model described in this section does not satisfy the conditions of synchronous update and a finite state. Of course one could argue that any implementation on a computer automatically satisfies the condition that the state of each cell is part of a discrete, finite set, since in the end it is represented by a certain fixed number of bits. The range of possible values is, however, so large that it is effectively non-finite. The original model implemented by (Murray, 1995, pers. comm.) used integer arithmetic, hence the states were discrete, whereas the implementation used here was implemented using floating point arithmetic resulting in non-discrete states.

5.2.2 Results

Starting from a uniformly sloping plane with small irregularities, a braided pattern evolves within a few thousand iterations. Figure 5.9 illustrates some of the patterns that emerge. If the contribution of the lateral sediment flux is sufficiently large, it prevents the channels from incising deeply into the bed (Murray and Paola, 1997); meanwhile it creates a wider channel, which in turn will promote the formation of new bars. The non-linearity in the dependence of the sediment transport on the discharge causes relative high points in the terrain, which receive flow from one upstream cell and distribute it to several downstream cells, to aggrade further. Similarly, holes that attract flow from the three upstream cells and pass the discharge on to mainly one of the downstream cells will deepen. This ‘natural’ tendency for the bed level variations to increase is partly counteracted by the lateral sediment flux and the gravitational component in flow direction by the dependence on the local bed slope S_{ijd} . When K and S_0 are large the diffusive effect of these two processes is relatively small and this may lead to excessively deep holes and associated high islands. If S_0 is relatively small, the channels remain relatively wide and undefined (Murray and Paola, 1997).

The colouring of the plot seems to significantly influence the visual impression that is obtained from the simulation. A smooth transition in the colours from ‘dry’ areas to flooded areas results in a braided pattern with unchannelled reaches, which gives a rather artificial impression. A much sharper transition is needed for the best looking result; in the simulations described here, where the average discharge was 0.05 per cell, the best result was obtained by having 70% of the colour change between 0.025 and 0.05.

Due to the simplification that water can only flow towards the three neighbouring cells on the next line, the behaviour of the model can sometimes be unrealistic as illustrated by the following example. Figure 5.10 shows a river reach of which the bed lies much lower than the surrounding flood plains. The water enters the computational domain at the two gridcells in the upper right corner and it flows through the river as indicated by the arrows. Irrespective of the bed topography, the water is not able to follow the main channel in the downstream reach, where it follows a course of 60 degrees relative to the positive i direction. The water in the

¹⁰Basically it is the same algorithm but for border cells the water is now distributed over the two downstream cells that fall inside the grid.

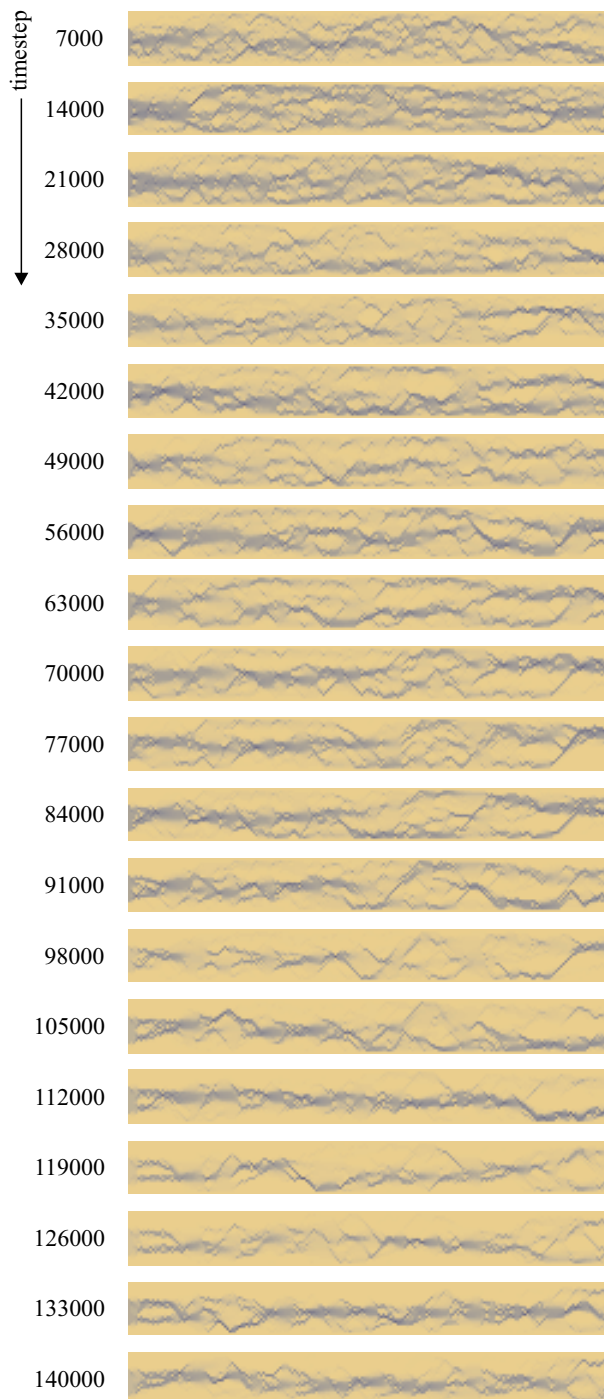


Figure 5.9: Flow pattern variation at various timesteps during a run of the cellular model on a 200×20 grid with $n = 0.5$, $m = 2.5$, $S_0 = 3$, $K = 0.1$, and $F = 0.01$ and an inflow of 0.1 in each of the cells in the range 5–15. Flow is from left to right.

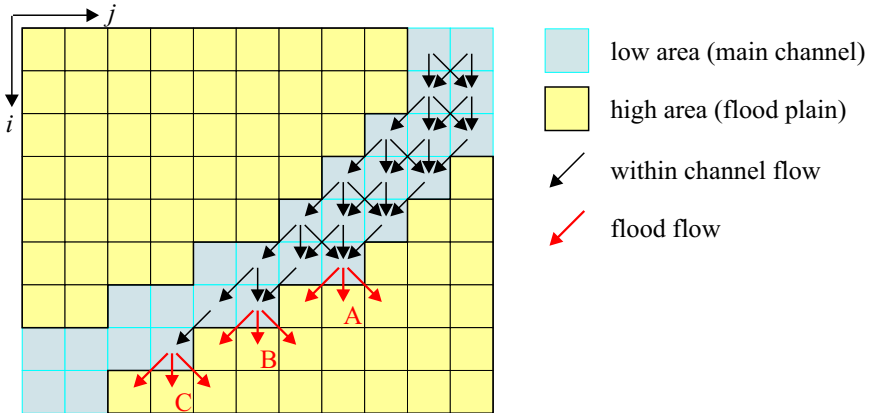


Figure 5.10: Water cannot follow a channel at an angle larger than 45 degrees in the cellular model.

model will always leave the main channel at the locations A, B and C, while the distribution depends on the exact bed topography.

- uniform slope in negative j direction: 100% at C
- horizontal bed: 91% at A, 8% at B and 1% at C
- uniform slope in positive i direction: 94% at A, 6% at B and < 1% at C

Murray and Paola (1997) indicate that uphill flow is locally possible in braided rivers. Due to the form of the flow distribution function given in Equation 5.9 it is possible to have uphill flow on a model wide scale. In this case the factor S_0 in the sediment transport makes also uphill sediment transport and braided behaviour on reverse slopes possible. Uphill flow on a large scale is clearly unrealistic. It is, however, unavoidable as long as one maintains the assumption that water always flows in positive i direction. The same restriction that led to the results described in the previous paragraph. Therefore, an alternative flow routing scheme has been constructed.

The new routing scheme does not restrict to the positive i direction, but it can be any of the eight grid directions (horizontal, vertical and diagonal). The local flow direction in a certain cell is determined by a weighted average of the flow directions of the discharges entering the cell. Given the local flow direction, the water is allowed to flow out of the cell in the indicated direction and the two neighbouring directions. The distribution of flow over these three directions is carried out analogous to Equation 5.9. This scheme still allows for uphill flow locally, but the probability of uphill flow is greatly reduced.¹¹ However, as a result of this change in the flow routing scheme, it is no longer possible to solve the flow by one sweep through the grid from $i = 1$ to N . The flow may eventually reverse direction or even follow a path that forms a loop (resembling Escher's waterfall, see Figure 5.11), therefore, only a fraction α of the water in a cell flows per timestep in the direction indicated by the inflow in the previous timestep. The fraction $\alpha < 1$ is needed for stability when water starts ponding. For a normal sloping valley in positive i direction, the resulting braided pattern

¹¹Uphill flow is still possible, for example when elevation increases uniformly in positive i direction. The flow in positive i direction will reduce with every step by about 70% but never vanish.

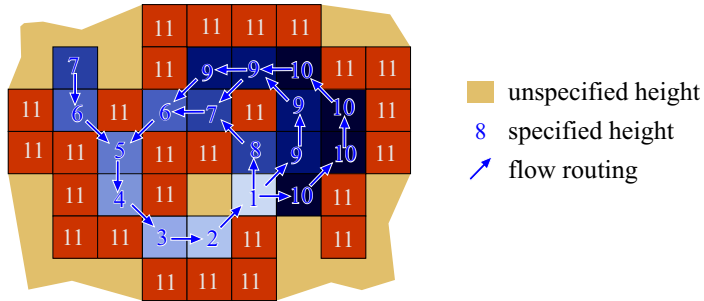


Figure 5.11: The alternative water routing scheme allows water to flow in any direction. This may cause loops in the flow pattern.

resembles the pattern obtained using the model by Murray and Paola (1994) but its channels are more rounded due to the adaptation of the local flow direction in the way described above. Furthermore, the development of the flow pattern slows down by a factor of N since now at least N computational steps are needed for the water to flow to the end of the model.

5.2.3 Discussion

One of the main assumptions underlying the cellular model is the anisotropy in flow direction, which implies that water flows in positive i direction only. This assumption can only be relaxed if a suitable way is found for computing the 2D flow over a random topography (preferably a simplification of the general 2D model discussed in Section 4.3.2). The approach using a local anisotropy based on the direction of the flow entering the cell, which was suggested in the last paragraph of the previous section, turns out to work not very well. Thomas *et al.* (2002) have adapted the flow routing two ways. First, they allow the water to move to five downstream cells ($i+1, j+d$) with $d = -2, -1, 0, 1$ or 2 .¹² Second, they base their flow routing not only on the bed slope but also on estimated water levels: The discharge is distributed based on a routing potential P_{ijd} which depends on an estimation for the downstream water depth and the local bed slope. If the initially estimated water depth is zero for all downstream points, the flow is assumed to be supercritical and the water is distributed based on water depth estimates based on a Froude number of 1. The flow pattern obtained with this adapted water routing scheme agrees well with field data (Thomas *et al.*, 2002). Furthermore, the sediment transport has been based on the general form of a bedload transport formula with critical threshold for sediment motion. The results of this approach look promising.

A different approach was recently used by Sun *et al.* (2002) for channelised flow on alluvial fans. In their model, water flows in a limited number of channels. These channels may enter and leave cells in any direction as long as the flow goes downhill. New channels, which are created if local topography is appropriate for avulsion, follow a random course downhill with a preference to continue in the flow direction taken. Eventually each channel merges with another, reaches the distal end of the alluvial fan, or reaches a local minimum in the terrain

¹²This routing scheme should only be applied in case of relatively smooth topography since one gridcell wide barriers will be permeable for this scheme.

and stops. Contrary to the model by Murray and Paola (1994), channels are assumed to have subgrid dimensions and lateral erosion is not yet included.

One can conclude that the cellular model developed by Murray and Paola (1994) is able to reproduce several characteristics of braided rivers which has been shown in more detail by Murray and Paola (1996, 1997) and Sapozhnikov *et al.* (1998). However, due to the simplifications made in deriving the model, some unphysical artefacts are included. Therefore, the model cannot be used as a simplified version of a 2D depth averaged model for prediction purposes.¹³ Recent adaptations by Thomas *et al.* (2002) seem to adequately solve most of the problems.

5.3 Branches model

The third model that has been implemented and analysed as part of this study is based on work on the Jamuna River by WL | Delft Hydraulics. The planform changes occurring in braided rivers cannot always be predicted with sufficient accuracy, as already indicated in Section 3.4. Any prediction for the medium and long term must be accompanied by an estimated probability of occurrence, and an indication of alternative developments. A single run with a normal two-dimensional model of such a river takes often a day or more, thereby making it practically impossible to do a large number of simulations in a probabilistic setting. From this point of view, a model concept was developed that could give a reasonably accurate prediction of the planform changes in a fraction of the time required for the full 2D approach. A number of studies (Klaassen and Masselink, 1992; Klaassen *et al.*, 1993; Mosselman *et al.*, 1995) had led to a basic functional design of such a model by Mosselman and Martin (1993).

In short, the model is based on a representation of the braided river as a network of channels. In software development terms, this model can be referred to an object-oriented model: the whole river is subdivided into more or less identical, relatively simple ‘objects’, namely the channels. Each individual channel can change its width, form mid-channel bars, migrate or be abandoned. These four processes all include some random aspects that vary between simulation runs. From the outcomes of many simulations the spatial distribution of erosion and sedimentation probabilities is determined. The concepts underlying the four implemented planform processes mentioned above are described in Section 5.3.1, whereas the results obtained with the model are described in Section 5.3.3. The section in between addresses the problem of obtaining the model’s channel network from a satellite image.

5.3.1 Model description

Each of the channels in a braided river can be interpreted as a short river section and can be treated as a short meandering channel that migrates according to the kinematic model of Howard and Knutson (1984) (see also Section 4.1.1 describing that model). This is the first step in obtaining the object-oriented branches model. The channels form together a network as shown in Figure 5.12 which is the basis for the model. The branches (channels) of this network are separate objects of which the behaviour is coupled by the nodes (confluences and bifurcations); the behaviour of the channels is characterised by four processes acting

¹³Murray and Paola (1994) did not intend to create a model for predicting planform changes.

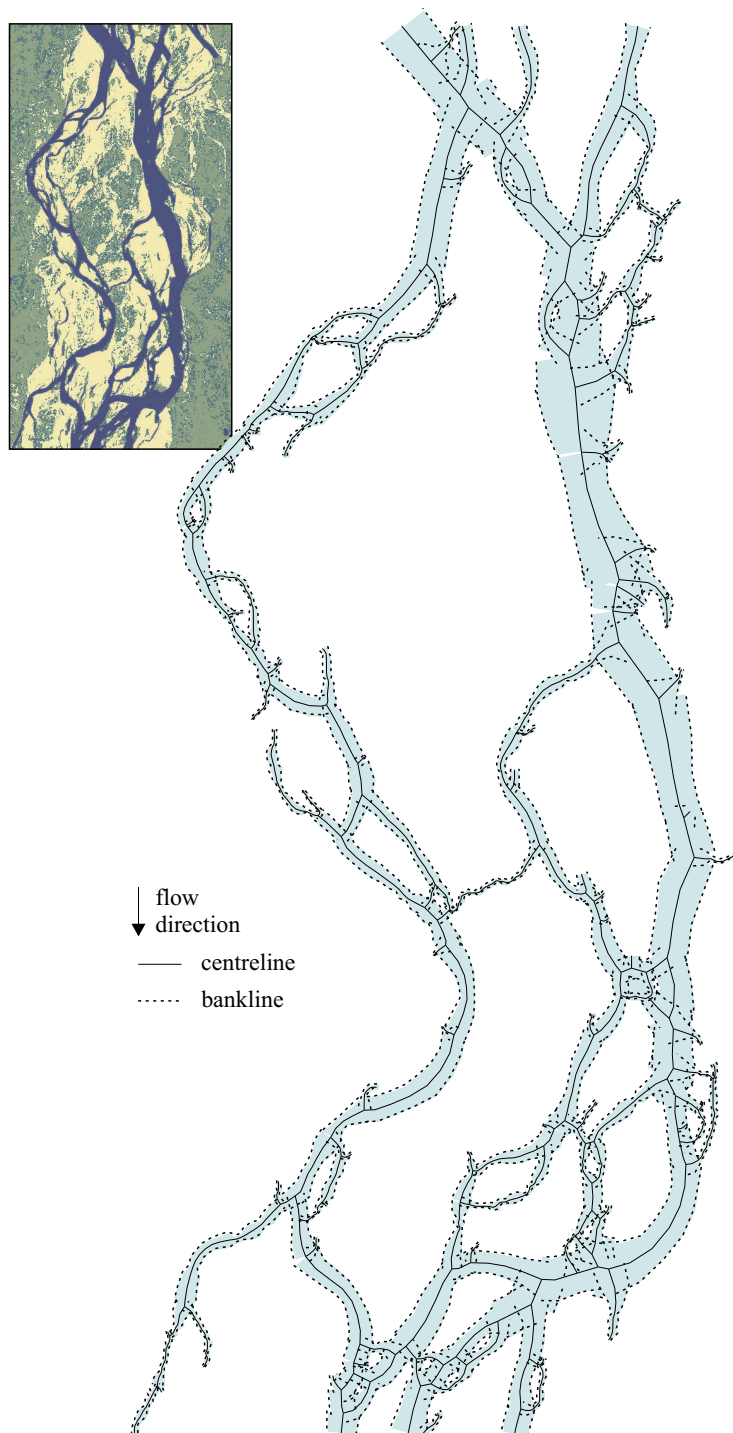


Figure 5.12: Channel network as used by the branches model and the satellite image from which it was derived.

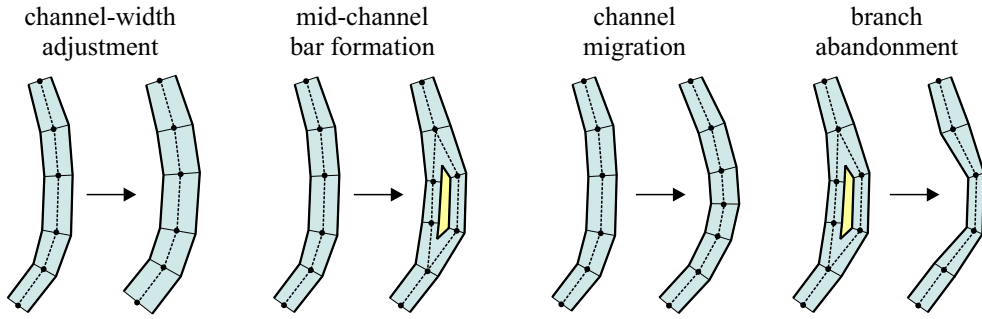


Figure 5.13: The four processes implemented in the branches model.

on them. These processes have been formulated as empirical geometric rules mixed with stochastic elements.

At the end of Chapter 3 six characteristic planform changes have been mentioned: channel migration, channel width change, bar growth, channel abandonment, channel formation, and node deformation. Modules for the first four changes have been included in the branches model. The node deformation is not included as a primary steering process, but only as secondary effect caused by the migration of upstream and downstream channels. A new channel that might form during the following flood season can only be included in the model by manually adding it to the channel network before the start of the simulation.

The last step in predictive modelling is correctly interpreting the results. Since the four processes included are partly determined by random processes, the result of one model run represents just one realisation of an ensemble of planforms that may have formed at the end of the prediction period. Repeated simulations based on the same initial planform and different stochastic influences result in a set of possible planforms (Monte Carlo simulation). These planforms are combined into an image in which the shade or colour of a pixel indicates the frequency with which the site has been part of the predicted channel networks at the end of the individual runs. This frequency may be interpreted as a probability of erosion.

Now, let us describe the model in more detail. Each branch consists of two or more (computational) points, as indicated by the small dots in Figure 5.13. Together, the connections between these points form the centrelines of the channel network. In each of these points a local curvature c_i , width B_i (perpendicular to the local centreline) and depth h_i are defined. The depth cannot be derived directly from the satellite image and, therefore, must be estimated in another way. Furthermore, it should be noted that the depth varies significantly with the discharge. Since the depth has only a limited influence on the processes, it has been assumed to be equal to 25 m throughout the network shown in Figure 5.12. In the following the four processes are described for an arbitrary point i somewhere in the network.

Channel width adjustment

Width adjustment is included in the model as a completely stochastic process because so far no clear correlation with any geometrical quantity has been found (Mosselman *et al.*, 1995). The new width of a channel at point i is given by $B_i(1 + [\Delta B_i / B_i]_{\text{corrected}})$ where the

relative width change $\Delta B_i/B_i$ is initially determined by a random selection from a normal distribution with zero mean and a user-specified standard deviation. It is assumed that for sediment with a certain reference erodibility E_{ref} the standard deviation of the relative width change is proportional to some power of the local channel width: $\sigma_B = \alpha_1 B_i^{\beta_1}$. Mosselman and Martin (1993) suggest to use $\alpha_1 = 0.46$ and $\beta_1 = 0$ for the Jamuna River, so no width dependence is observed.

Two corrections are applied to this randomly selected width change $\Delta B_i/B_i$: a limitation for the change in channel width such that the channel width remains always positive and a multiplication factor for spatially varying erodibility.

1. The channel width can only be larger than zero, so values of $\Delta B_i/B_i$ less than -1 are not acceptable. However, the random selection method described above may lead to such values. In fact, the probability $p\{\Delta B_i/B_i < -1\}$ of a channel getting a negative width is equal to the probability $p\{\Delta B_i/B_i > 1\}$ that the width of the channel increases by a factor of 2 or more since

$$p\{\Delta B_i/B_i = -x\} = p\{\Delta B_i/B_i = x\} \quad (5.11)$$

holds for the normal distribution. Furthermore, it is assumed that the initial channel has a more or less stable width in the case of the reference erodibility E_{ref} . This means that there should be no net tendency to widen for the river as a whole. Both issues are solved by correcting values of $\Delta B_i/B_i$ less than zero as indicated by the following formula

$$[\Delta B_i/B_i]_{\text{corrected}} = \frac{\Delta B_i/B_i}{1 - (\Delta B_i/B_i)} \quad \text{if } \Delta B_i < 0 \quad (5.12)$$

This correction has been chosen in such, that branches have a net tendency to neither widen nor narrow, i.e. the probability of channel widening by a factor x equals the probability of channel narrowing by a factor $1/x$

$$p\{1 + [\Delta B_i/B_i]_{\text{corrected}} = 1/x\} = p\{1 + [\Delta B_i/B_i]_{\text{corrected}} = x\} \quad (5.13)$$

Note, however, that there are hardly any physical mechanisms that allow straight channels to become narrower by accretion of the channel banks. They can only become narrower by incision into sediments that have been deposited during a flood or by meandering.

2. The erodibility may vary spatially, whereas we have assumed that the standard deviation is only valid for the reference erodibility E_{ref} . The channel widening is influenced

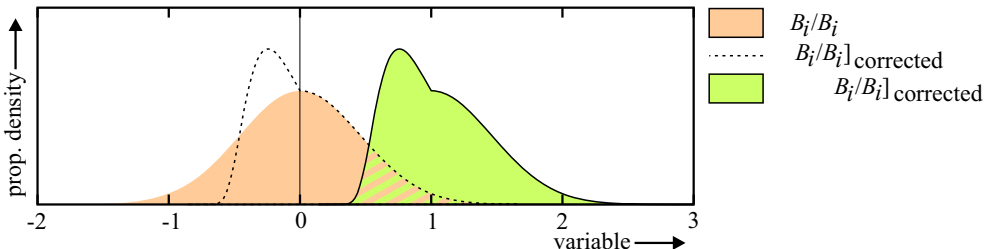


Figure 5.14: The probability density function of the width change.

by the erodibilities of left E_{left} and right E_{right} banks. This influence is assumed to be linear in the erodibility, so the previously computed values of $\Delta B_i/B_i$ are multiplied by the average relative erodibility $(E_{\text{right}} + E_{\text{left}})/(2E_{\text{ref}})$. This factor is only applied when the channel widens (i.e. positive $\Delta B_i/B_i$), which results in a net tendency for channels to widen in sediments with an erodibility above the reference value and a net tendency to narrow for channels in sediments with a smaller erodibility.¹⁴

Summarising, the new width of the channel is given by $B_i(1 + [\Delta B_i/B_i]_{\text{corrected}})$ where

$$[\Delta B_i/B_i]_{\text{corrected}} = \begin{cases} \frac{E_{\text{right}} + E_{\text{left}}}{2E_{\text{ref}}} \frac{\Delta B_i}{B_i} & \text{if } \Delta B_i > 0 \\ \frac{\Delta B_i/B_i}{1 - (\Delta B_i/B_i)} & \text{if } \Delta B_i < 0 \end{cases} \quad (5.14)$$

It is assumed that this width change is accompanied by a change in channel depth. Furthermore, it is assumed that under equilibrium conditions the depth is related to the width as a power function: $h_{i,\text{new}} = \alpha_1 B_{i,\text{new}}^{\beta_2}$. Various effects may result in deviations from this value. Therefore, the depth in the model is only partly adjusted to the new width using the following relation

$$[h_{i,\text{new}}]_{\text{corrected}} = \alpha_h h_{i,\text{new}} + (1 - \alpha_h) h_{i,\text{old}} \quad (5.15)$$

The relaxation factor α_h is assumed to be variable, and is drawn from a uniform distribution between 0 and α_{hm} , where the maximum value α_{hm} has to be specified by the user. When data on the channel depth are scarce — such as in our case where we have derived all data from a satellite image — the added value of including Equation 5.15 in the model is limited. Therefore, the change in depth has been excluded from the current model by setting α_{hm} and hence α_h to zero. This has caused the water depth to remain constant throughout the simulations. This simplification influences the width-depth ratio, which is the trigger for the mid-channel island formation process.

Branch creation by mid-channel island formation

If the width-depth ratio of a channel exceeds some threshold value, the flat channel bed becomes unstable and bars are formed. These will often be alternate bars, but sometimes, when the width-depth ratio is large, mid-channel braid bars may form. Such a braid bar may grow until it becomes an island, thereby splitting the original channel into four new channels (upstream, downstream, left and right) which are joined together by one new bifurcation and one new confluence. In the branches model an island is created with a probability P_{cr} if the quotient of local width B_i and local depth h_i exceeds the threshold value β_c , as suggested by Klaassen *et al.* (1993) on the basis of theoretical studies by Colombini *et al.* (1987), Struiksma and Crosato (1989) and Schielen *et al.* (1993). In the computer program the upstream end of the island is placed within the channel at a randomly chosen point at which the condition for island creation ($B_i/h_i > \beta_c$) is fulfilled.

¹⁴If the erodibilities for left and right bank are not the same, channel widening may lead to a relative shift of the centreline towards the more easily erodible bank. Similarly, a less easily erodible bank (e.g. in case of river protection works) may attract and deepen the channel (see also Section 3.3.3). The shifting of the centreline is not taken into account in the current version of the model.

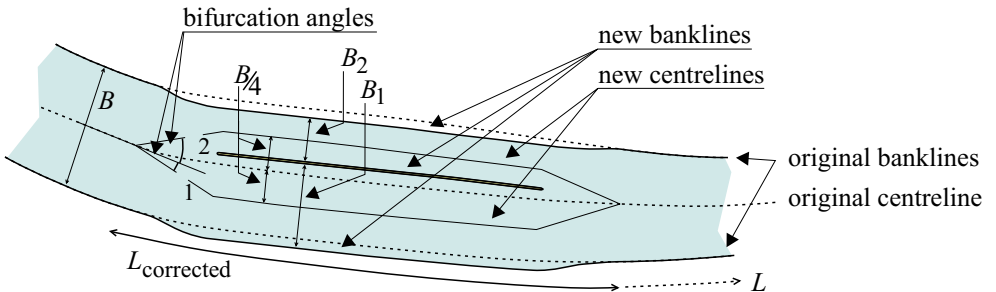


Figure 5.15: Example illustrating mid-channel island formation.

When an island is to be created, the procedure continues as follows (illustrated in Figure 5.15). The centrelines of the branches at either side of the island are located one quarter of the original channel width B_i (for clarity in the figure abbreviated to B) from the centreline of the original channel. From a negative-exponential distribution with user-specified mean L_{av} , the length L of the island is drawn. The actual length of the island that is created will be shorter ($L_{\text{corrected}}$) if the width-depth ratio becomes less than β_c at a point within the length L from the upstream end of the island, or if the remaining length of the branch in which the island is created is shorter than L . The widths of the two channels bordering the island are determined by the resulting bifurcation angles ϕ_1 and ϕ_2 , which are defined as the angles of the first sections of the two channels with the direction of the reach immediately upstream. The expressions for the channel widths are given by the following formulae $B_{i,1} = B_i \phi_1 / (\phi_1 + \phi_2)$ and $B_{i,2} = B_i \phi_2 / (\phi_1 + \phi_2)$. The sum of the widths of the two channels bordering the island is assumed to be equal to the width of the original channel. The largest channel is the one best aligned with the upstream channel, in a straight reach mid-channel bars will result in a symmetric split of the original channel.

From Figure 5.15 and the relations specified above one can derive that a channel shift of $[\max(\phi_1, \phi_2) / (\phi_1 + \phi_2) - 1/2]B/2$ is associated with the formation of the island. Furthermore, the initial width of the island is zero; only due to independent lateral migration of the two channels, the island can obtain substantial lateral dimensions. Secondary islands may be created at one or both sides of the newly formed island if the width-depth ratio of the newly created channels is still larger than β_c . Island formation by cutoff processes has not been modelled explicitly. However, when the user expects that a channel might be created in that way, it can be included in the model by specifying it manually in the initial network before the simulation starts.

Branch migration

The migration model consists of two components. The first part is similar to the kinematic model of meandering rivers by Howard and Knutson (1984). The second part is a down-valley migration caused by flooding.

- The kinematic migration model is simple, but Parker (1984) has shown that it is equivalent with the more physics-based model by Ikeda *et al.* (1981). See in this respect Sections 4.1.1 and 4.1.2. The channel migration rate normal to the flow direction based on

local variables is given by the nominal bend migration rate

$$\zeta_{n,j} = \left(\frac{\partial n}{\partial t} \right)_{n,j} = \alpha_{mg1} B_j f(c_j, B_j) \quad (5.16)$$

where $\zeta_{n,j}$ is a shorthand notation for the nominal migration rate $(\partial n / \partial t)_{n,j}$ normal to the channel centreline in point j (n is the local coordinate in normal direction), α_{mg1} a random multiplication factor with mean one and standard deviation σ_{mg1} , B_j is the local channel width as defined in the previous paragraphs, c_j is the local curvature and $f(c_j, B_j)$ is an approximation of the Hickin-Nanson relation. In the current program this relation is modelled as

$$f(c_j, B_j) = \begin{cases} k_1 (3c_j B_j)^{k_2} & \text{if } 3c_j B_j > 1 \\ k_1 (3c_j B_j)^{k_3} & \text{if } 3c_j B_j < 1 \end{cases} \quad (5.17)$$

which is inspired by the formulation used by Ferguson (1984a) (Equation 4.1 of Section 4.1.1, reproduced if $k_1 = 0.02$, $k_2 = -2$, $k_3 = 2$) and the exponential relation derived by Parker (1984) (reproduced if $k_2 = k_3 > 0$). Following Mosselman and Martin (1993), σ_{mg1} has been assigned the value 0.4.

The effective migrate rate in a meandering river is not equal to the nominal migration rate based on local variables alone; it is better approximated by a weighted average of the local and upstream nominal migration rates as shown by Howard and Knutson (1984) and Parker (1984) (see Section 4.1.1). They showed that a negative-exponential weighting with a proper adjustment length of the nominal migration rates gives a good estimate for the effective migration rate in a meandering river. It is assumed that the same approach can also be used in the channel network. The adjusted bend migration rate is obtained from the nominal migration rate $(\partial n / \partial t)_{n,j}$ by a weighted average over a reach upstream of the point i as

$$\left(\frac{\partial n}{\partial t} \right)_{a,i} = E_{loc} \frac{\sum_j \left(\frac{\partial n}{\partial t} \right)_{n,j} \exp \left(-\frac{s_j}{\lambda_a} \right)}{\sum_j \exp \left(-\frac{s_j}{\lambda_a} \right)} \quad (5.18)$$

where s_j is the distance from point j to point i along the river, λ_a is the characteristic averaging length scale, and the local erosion rate E_{loc} equals E_{left} in case of left-bank erosion and E_{right} in case of right-bank erosion. Both summations are carried out over the upstream points j within the modelled reach. At confluences within the upstream reach of point i the upstream influences of the two branches are weighted by their relative discharge, approximated — under the assumption of uniform roughness C and slope i — by the local value of $B_j h_j^{1.5}$. Straight reaches are assumed upstream of the upstream boundary points. At first only the effect of the largest branch was taken into account, but in that case the downstream channel tends to align with that branch, in order to form one continuous meandering channel with a side channel often joining the main channel at an almost right angle.

- The channels migrate not only due to the flow within the channel of non-zero curvature, but also due to the overbank flow in the direction of the valley slope during flood. This

is called migration due to cross-channel overbank flow, and is given by

$$\frac{\partial x_{\text{valley}}}{\partial t} = \alpha_{\text{mg2}} \chi |\sin(\psi - \psi_{\text{val}})| \quad (5.19)$$

where $\psi - \psi_{\text{val}}$ denotes the angle between the channel and the valley slope (Mosselman *et al.*, 1995), χ is an effective cross-stream erosion factor, α_{mg2} is a random multiplication factor with mean one and standard deviation σ_{mg2} and x_{valley} is the spatial coordinate in down-valley direction. The cross-channel migration contributes only a shift in the direction of the valley slope, whereas the bend migration results in a migration normal to the local channel direction. Migration due to overbank flow is according to this relation largest at locations where the river flows perpendicular to the valley (and flood) direction.

Confluence locations are defined as the intersection of the centrelines of the two channels upstream of the confluence; the location of a bifurcation is determined by the intersection of the two channels downstream. The nodes move as dictated by these definitions, and the third channel is adjusted to connect to the new position of the node. Although the migration of a bifurcation is determined by the migration of the two channels downstream, it is still influenced by the curvature of the channel upstream, namely through the weighting of the local and upstream nominal bend migration rates.

Branch abandonment

Investigation of satellite images of the Jamuna River has shown that branches may be abandoned if the (upstream) bifurcation angle ϕ_i as indicated in Figure 5.16 is large (Klaassen *et al.*, 1993; Mosselman *et al.*, 1995). Based on this empirical knowledge the probability that a branch i will be abandoned is modelled as being zero below a critical bifurcation angle $\phi_{i,c}$, and linearly increasing for larger angles. The probability that a branch is abandoned is given by

$$P_{i,\text{ab}} = \begin{cases} 0 & \text{if } \phi_i < \phi_{i,c} \\ \min(1, \alpha_\phi (\phi_i - \phi_{i,c})) & \text{if } \phi_i > \phi_{i,c} \end{cases} \quad (5.20)$$

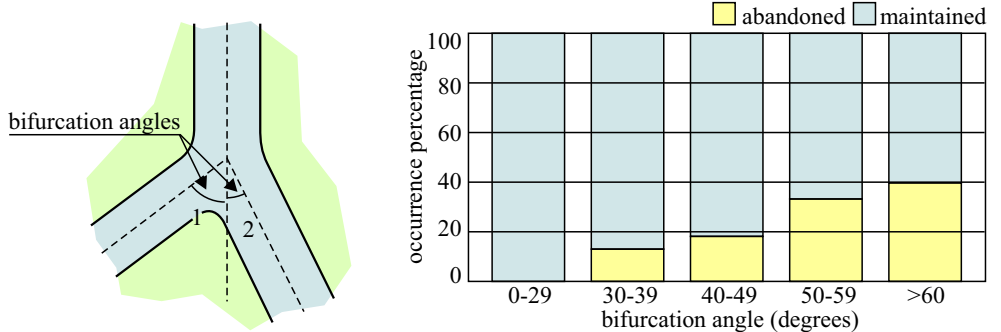


Figure 5.16: Definition of bifurcation angle and its influence on channel abandonment (Mosselman *et al.*, 1995).

where α_ϕ is a user-specified constant. The critical angle $\phi_{i,c}$ for a branch i consists of a constant critical angle ϕ_c and a branch dependent modification angle $\Delta\phi_{i,c}$. The modification angle will in general be zero, but it allows for modelling cutoffs and human interference to keep a branch open. A possible cutoff channel may be added manually by the user; the probability of it being formed — in the model inversely modelled as the probability that it is not immediately abandoned — can be influenced using the modification angle. When recurrent measures are taken to keep a branch open, their effect can be taken into account by raising the critical angle using the modification angle.

5.3.2 Extraction of channel network from satellite image

The model described in the previous section requires a channel network. An automated process has been developed that constructs a channel network (comprising centreline, channel width, and information about confluences and bifurcations) from a satellite image of which each pixel has been classified as representing either land or water. The automated process that extracts the channel network consists of eight steps, which are outlined below; a more detailed description can be found in Section B.3. The process is illustrated in Figure 5.17 using a 1994 satellite image of a section of the Jamuna River near Bahadurabad.

Step 1. Either by supervised or unsupervised classification of a satellite image one obtains a thematic image. In a thematic image each pixel has a value which indicates that it belongs to a particular class of pixels that have a certain property in common — often the spectral distribution in the original satellite image. In the example case four classes were initially distinguished: water, bare (sand covered) land, vegetated land, and other types of landuse (indicated by black, white, light grey, and dark grey in image 1 of Figure 5.17).

Step 2. For the construction of the network one only needs the classes that correspond to water, so, one reclassifies the original image by giving all classes which correspond to water surfaces a value 1 and the other classes a value 0. When the image satisfies the following three conditions this step can be automated:

- the classification has resulted in a sufficiently patchy classification of the land area,
- the water area is grouped into one class, and
- the river runs from the top of the image to the bottom.

Under these conditions, which apply to the example case, the water class will be the only class containing an uninterrupted sequence of pixels connecting top and bottom of the image, and as such it can be selected automatically. This step in the algorithm could be improved by extending it with an algorithm that tries to connect separate water areas to the network (e.g., the second channel in the upper part of the left branch in Figure 5.17).

Step 3. The class of all water pixels contains in general, besides the river itself, all kinds of small ponds, lakes, and possibly even some pixels incorrectly classified as water. These areas are not relevant to the extraction of the channel network and can therefore be removed. This can be done by selecting only the largest body of water, which

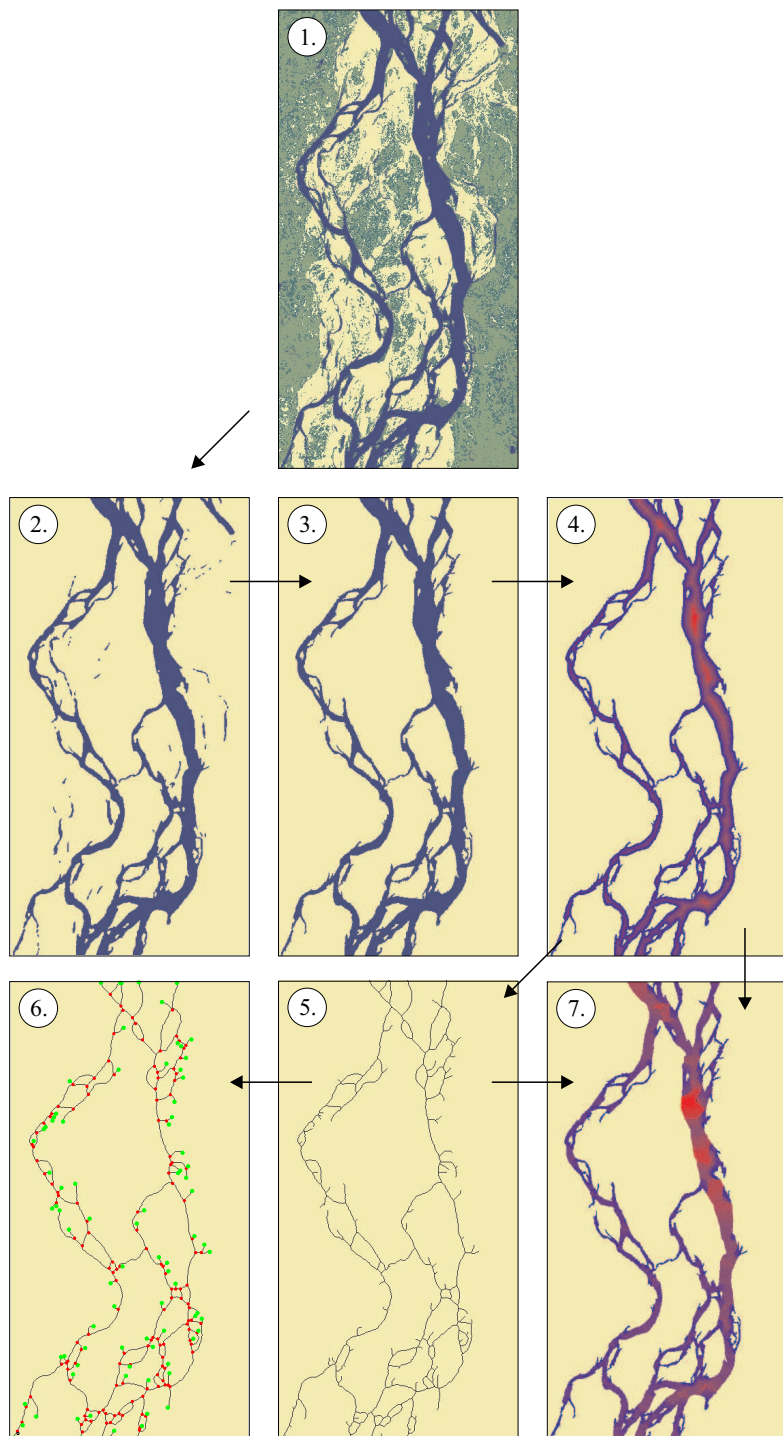


Figure 5.17: Example illustrating the results of the various steps in the extraction process to obtain from a satellite image a channel network as shown in Figure 5.12.

is the main channel. One should note that by removing all small water areas also all partially dry channels and oxbow lakes, which are disconnected from the main channel system, are removed. These areas might nevertheless be relevant to the model, since they may also indicate high-water channel courses. Yet, it has not been attempted to reconnect them to the main channel system: all of these elements have been removed. Similarly, islands of just a few pixels in size have been removed.

Step 4. In preparation of the extraction of the centrelines, the distance of all water pixels to the nearest bankline has been determined. This data set is used again later on in the process, when computing the local channel width.

Step 5. The main step in the channel extraction process is the determination of the centreline from the image. Although this is a relatively simple operation for the human eye, it is difficult to implement correctly on a computer. Taking the pixels locally furthest from the banks is not a well-defined operation when the channel width varies. Therefore, the process has been implemented as a ‘guided’ skeletonising operation. The skeletonising operation used in digital image processing is an iterative algorithm which removes pixels from all edges of an area, thereby slowly reducing it in size. The algorithm works in such a way that the homotopy of the area remains unchanged (i.e. holes remain holes, islands remain islands), but branches that are connected to the main channel at just one end may be removed and spurious branches may form due to irregularities in the channel bankline. Furthermore, the remaining skeleton is not necessarily a good representation of the channel centrelines. Therefore, the implemented algorithm is an adaptation: the procedure is guided by the distance information computed in the previous step. Furthermore, the channel connections to the edge of the image (the upstream and downstream boundaries) are fully preserved.

Step 6. Subsequently the nodes, endpoints, and channels have been distinguished based on the local connectivity of the network of centrelines.

Step 7. The local channel width has been determined as the smallest distance between two bankline pixels for which the distance to the centreline pixel is smaller than their mutual distance. This definition gives a value that is in general approximately equal to twice the distance of the centreline pixel to the bank, but it can be significantly smaller than that value near nodes.

Step 8. Now the nodes, endpoints, and channels have all been identified separately in the image, making it possible to trace the courses of the individual branches. And finally the connections between these elements can be derived, thus completing the extraction of the channel network. The end result of this step was shown in Figure 5.12.

This procedure gives an *undirected* channel network, i.e. it does not tell which way the water flows through each of the channels; for the branches model, however, a directed channel network is needed since it is important to know the flow direction for computing the weighted migration rates and for computing the bifurcation angles. Furthermore, sometimes complex nodal points occur, where more than two channels come together, where a channel bifurcates into more than two channels, or where a confluence and a bifurcation occur in the same node. The branches model is unable to deal with these situations. These problems have been solved interactively, using a program that allowed the user to reverse the suggested flow direction in

a channel and that made it easy to split a complex node by shifting one of the constituting confluences or bifurcations slightly upstream or downstream.

5.3.3 Results

The model was first applied to a meandering channel, in order to get an impression of how the various parameters relating to the lateral and down-valley migration processes influence the channel pattern. The other three processes were switched off in these computations. The initial planform is sine-shaped with a wavelength of 6000 spatial units (along the channel centreline one meander is initially 8800 units long) and the channel width equals 1000 units. Figures 5.18a–c show the effect of the characteristic length for upstream averaging λ_a on the lateral migration rate. From these results one can observe that for $\lambda_a = 0$ no weighting takes place and bends evolve symmetrically (Figure 5.18a). The meander development in the straight reaches depends on numeric truncation errors. Due to the lack of upstream weighting this simulation is extremely sensitive to small changes in local curvature. For larger λ_a (in the order of 3000) a more natural pattern emerges, showing the characteristic asymmetric development of the bends (Figure 5.18b). For still larger values of λ_a (in the order of 30000, Figure 5.18c) opposite bends begin to cancel each other's influences on the local migration rate and only slight changes in the planform occur. If the simulation were to continue for a long time, meander bends with a much larger wavelength would develop. If, on the other hand, the lateral migration is switched off and the channel is allowed to migrate in down-valley direction, a pattern (Figure 5.18d) emerges that resembles the meander pattern observed in meandering rivers of which the lateral migration is restricted by non-erodible banks.

The lateral migration process is driven by an instability phenomenon: meander amplitudes grow until cutoff processes or obstructions limit further growth and the net downstream migration of the meanders is relatively small. Even without disturbances entering the reach from upstream, meanders will keep developing as illustrated by the simulations of Howard and Knutson (1984) (Figure 4.2). The down-valley migration on the other hand is a marginally stable process since the lateral extent of the meanders is neither increased nor decreased. The numerical procedure of adaptively adding and removing channel points causes a small net decrease in the lateral extent of the meanders and a slow down-valley shift of the sections parallel to the valley direction $\psi = \psi_{\text{val}}$ which normally would not shift due to Equation 5.19.

The evolution of an initially random channel under the influence of the two migration processes is shown in Figure 5.18e. Relatively high-frequency oscillations in the meander pattern quickly vanish due to the upstream weighting of the curvature, whereas lower frequencies are amplified. The down-valley migration due to overbank flow causes a straightening in the upstream reach. The effect of mid-channel island formation averaged over 100 simulations is indicated in Figure 5.18f (the migration rate is kept deterministic in these simulations). In this figure an overlay is made of all simulation results and for every point the number of channels is indicated that encompasses it. The average length of the islands that were created was 1000 spatial units, that is of the same order as the channel width. The process results in a tendency for the river to widen and there is a small probability of a significantly different planform. The effect of the stochastic variation of the lateral migration rate $\alpha_{\text{mg}1}$ and down-valley migration rate $\alpha_{\text{mg}2}$ on the migration of the meandering channel is shown in

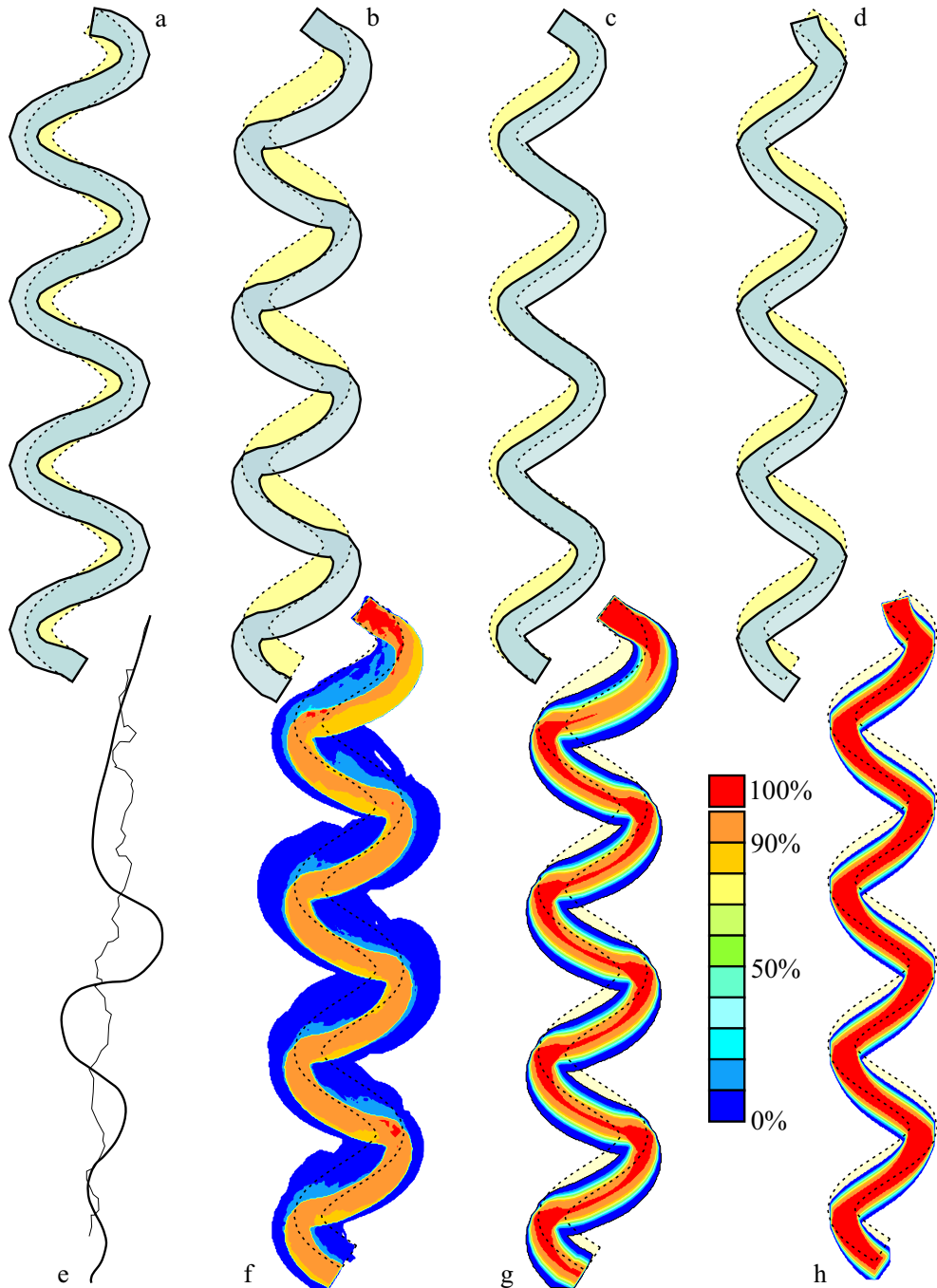


Figure 5.18: Results of the branches model when applied to a single branch meandering channel. The initial planform is sine-shaped with a wavelength of 6000 spatial units (along the channel centreline one meander is initially 8800 units long), the width equals 1000 units. a: $\lambda_a = 0, \chi = 0$, b: $\lambda_a = 3000, \chi = 0$, c: $\lambda_a = 30000, \chi = 0$, d: $k_1 = 0, \chi > 0$, e: initial random lateral deviation from a straight line, f: $\lambda_a = 3000, \chi = 0, P_{re} = 0.5$, g: $\lambda_a = 3000, \chi = 0, \sigma_{mg1} = 0.5$, h: $k_1 = 0, \chi > 0, \sigma_{mg2} = 0.5$.

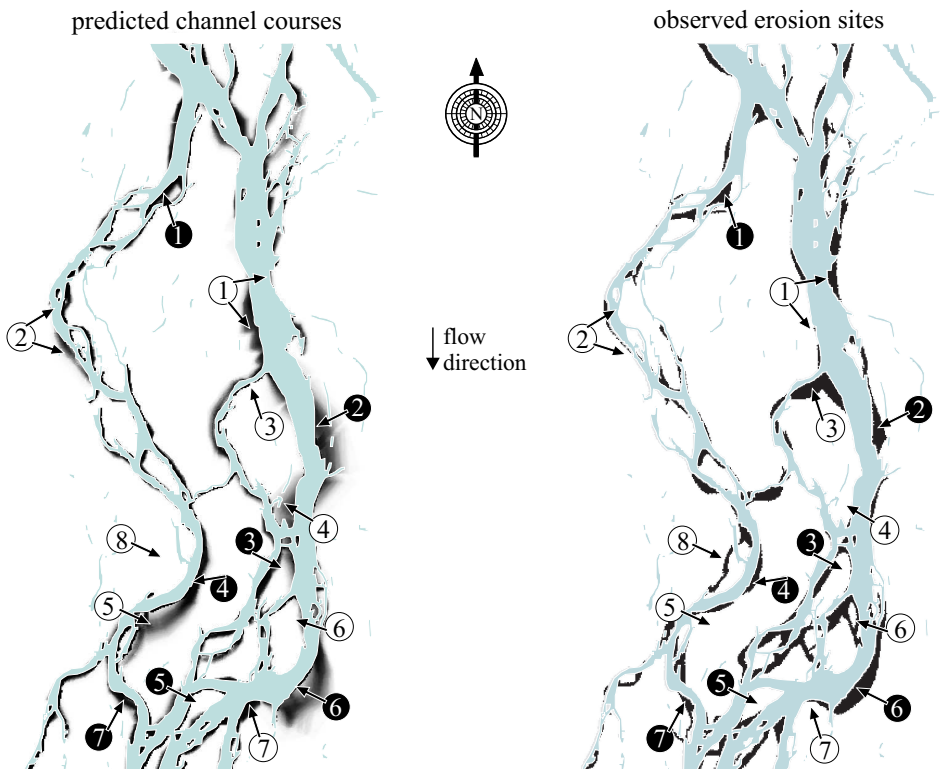


Figure 5.19: Comparison of branch model results and actual changes. Reasonably correct predictions are marked with white numbers in black circles; incorrect predictions are marked with black numbers in white circles.

Figures 5.18g and h respectively. The spatial uncertainty in the predicted planform is largest where migration rates are largest.

The predicted planform (and the spatial distribution of the uncertainty) for a short section of the Jamuna River near Bahadurabad is shown in Figure 5.19. In some reaches the prediction is quite good, but in other places significant errors are found; some of these errors may be removed by calibrating the spatial distribution of the erodibility, which was kept constant in this simulation. Correct predictions occur both along the major channels (❷, ❾) and the minor channels (❸, ❽, ❿). However, incorrect predictions of meandering and erosion occur also throughout the model (❶, ❻–❽). Although the bank erosion in the low-lying bar complex is quite well predicted (❸, ❽), some features of this dynamical region are not reproduced such as at location ❾ — although this is partly because of channel formation processes on a small scale and cutoffs are not automatically formed. The new channel ❾ could only have been predicted by the model if it had been specified by the user. Although the prediction of erosion at ❷ is reasonably correct, the tendency of the eastern channel to meander is overpredicted: no erosion occurred along the right bank at locations ❶ and ❻ and erosion was overpredicted at ❽. Although erosion occurred along the left bank at ❶ no significant erosion was observed in the model.

During flood, when most changes occur, the branches are merely deep areas in the main channel, at least if we assume that they have not been filled in by the increased sediment transport. The reasonably correct prediction of the bankline changes of the bar complex is, therefore, remarkable. Is that coincidence? Based on the satellite images of 1994 and 1995 shown in Figure 3.1, we must conclude that the planform changes in that area between the 1994 and 1995 planforms are largely concealed by the 1994 planform. The predicted planform is basically equal to the original 1994 planform with some slight shifting and meandering of the channels. So, the seemingly correct prediction of the erosion locations in the bar complex is mainly an optical illusion; the actual planform changes in that area were much larger than suggested by the right hand side of Figure 5.19.

The spatial distribution of the uncertainty in the planform plotted in Figure 5.19 is essentially different from the probability of erosion as computed by the neural network (Figure 5.4). However, the results should be the same if the planform changes are relatively small, because in that case an eroded stretch of land will be part of the river. If, on the other hand, the planform changes are so large that channels shift over distances in the order of the channel width — such as at location ⑥ in the lower right part of Figure 5.19 — points near the initial bankline may well be eroded, although they have a negligible probability of belonging to the channel network *after* the prediction period: there is a high probability that the channel will migrate over a larger distance than the channel width. At the end of the prediction period there will probably be land again at those locations, but they will lie at the other side of the channel: the probability of erosion is high.

5.3.4 Discussion

The application of this model to rivers like the Jamuna River, where the flood period covers an important part of the year, is complicated by the fact that the branches as included in the model do not represent the flood-flow paths. Therefore, this model is — just as the neural network — not capable of correctly predicting changes in bar complexes. Although the whole pattern of erosion is quite different from that obtained from the neural network, the average quality of the prediction is comparable: correct in some locations, completely wrong at others. Incremental improvement using more knowledge about the river is, however, possible using the branches model described here. EGIS (2002) has extended the conceptual approach of Klaassen *et al.* (1993) by correlating the four processes with sedimentary features (bar shapes).

The process of island formation contributes little to the prediction of the erosion; islands formed by mid-channel bar formation have to grow for several years before they become important. This conclusion is in line with the observation in Section 3.6 that mid-channel bar formation does not significantly influence the dynamics of the low-stage planform of the Jamuna River. Abandonment of a major branch is followed by realignment of the downstream branches and will be important in general. However, it did not play a role in the test case. Width change should only be of importance when there is a clear cause for channel widening or narrowing, for instance during a realignment of channels after a channel abandonment or a cutoff; in that case width change should be structural and not stochastic. Migration is the dominant process in many cases.

This model is well-suited for anabranching rivers, where the islands are large and the flood period is absent or less important. Improvement of the meander model following the approach

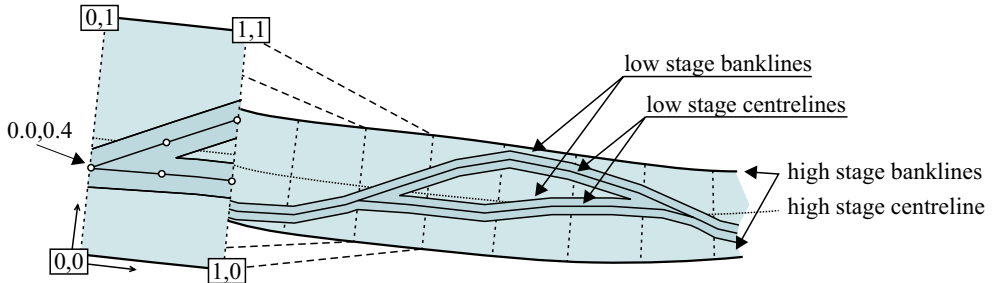


Figure 5.20: Two-stage channel network.

used by Johannesson and Parker (1989) or Crosato (1990) (see Section 4.1.3) might be desirable in that case. Treatment of bifurcations and confluences should then also be changed. One may wonder whether this model can be improved, such that it applies better to flood-dominated, braided rivers. Improvements are possible. One may for instance couple two channel networks — one for low stages and one for high stages — by using the channel migrations during high stage to warp the low stage channels. To achieve this, the low stage channels must be specified in local coordinate systems connected to the high stage channels as indicated in Figure 5.20. The low-stage channel points should be able to move freely within the high stage channel boundaries. Low-stage migration would lead to widening of the high-stage channel if the low-stage channel attempts to migrate out of the main channel. The erodibility within the high-stage channels should be smaller (smaller bank height) than outside the high-stage channels. The processes of mid-channel island formation and branch abandonment are not so relevant at the scale of the high-stage planform. This approach, which would require an enormous effort with regard to the development of the bookkeeping system, would be able to deal with two stages; all flood waves should have the same magnitude. A probably easier solution would be to extend the branches model with a coarse two-dimensional flow model. Using the coarse two-dimensional model the flow pattern during flood could be determined. This flow pattern could subsequently be used to shift the low-stage channel network by adapting, for instance, the downvalley migration approach. During the low flow period lateral migration would cause planform changes that would affect the next flood period. The computational effort and the amount of input data required to run such models would both increase significantly.

5.4 Discussion

In this chapter and the previous one we have discussed several models that have helped us to understand the behaviour of meandering and braided rivers, although about the latter much remains still unknown. If we focus on *predicting* in practical situations, the number of applicable models is significantly reduced. This section compares the neural network approach and the branches model with the more traditional shallow water model with respect to their ability to handle practical engineering situations. Furthermore, some directions for further research are indicated. The cellular model has been excluded from this analysis because in its present form it is not suited for modelling an actual river, primarily because of the anisotropy in the flow routines and the possibility of unlimited uphill flow. The attractiveness of that model lies in the ability to model a braided river with a few (relatively simple) rules, which

is very interesting from a theoretical viewpoint. But for engineering practice, where reliable predictions have to be made, it would be necessary to operate such a model using gridcells that are at least one order of magnitude smaller than the width of the major channels. This is necessary to obtain sufficient accuracy for estimating the planform changes. Section 5.4.1 compares the three models based on speed, handling of uncertainty, physical basis, general applicability (to other braided rivers), detailed prediction, extendability with new knowledge, and input requirements. Subsequently, Section 5.4.2 discusses some research directions that may lead to improvements for the branches model; one of these directions (the formation of new channels) is addressed more extensively in the second part of this thesis.

5.4.1 Comparison

Before comparing the models, we first have to determine which properties of the models we want to compare. In Chapter 3 a large number of processes is mentioned that plays a role in the continuous reshaping of a braided river. The interaction of flow structures at various scales, sediment transport, formation of bars, fed by a varying rate of bank erosion and upstream boundary conditions, leads to a complex system that may completely transform its appearance when a certain threshold is exceeded or when the flow distribution over the upstream channels changes slightly. Varying influences from inhomogeneous soil composition and fluctuating vegetation and uncertainty about coming hydrographs lead to a limited predictability of the planform changes. The ideal model should be able to handle this uncertainty and make it explicit in its output.

The accuracy of a prediction can be assessed by including several stochastic elements, either by means of a Monte Carlo approach, or by explicitly computing the (approximate) characteristics of the probability distributions of the output variables. In the case of Monte Carlo simulations many (deterministic) simulations are done to determine the variability in the output variables. Therefore, a single simulation should not take too long. Thus, computational speed is also important here. This is less of a problem when other (more direct) methods are used to determine the distribution of the variables, but non-linearities in the equations significantly complicate the application of such methods (Van der Klis, 2001). Preferably, the model should be physically based (as opposed to purely empirical) to provide a solid framework for further extension. Furthermore, it should be easy to generalise to other cases (other rivers), and the model should give reasonably detailed predictions. In view of future research, it should be possible to extend the model using newly obtained insights, and it should require as little input data as possible.

Although it is always difficult to compare essentially different approaches, the general results support the conclusions summarised in Table 5.1. In the following, we will discuss the ratings in detail.

neural network

The most important advantages of the neural network approach are:

1. *Uncertainty.* A single run of the neural network provides information on the probability of erosion; no repeated simulations are necessary. This approach does, however, not provide any information on the correlation of events.

	Neural Network	Branches model	Conventional 2D
Uncertainty	+	o	-
Speed	+	+	-
Physics	-	+	+
New cases	-	o	+
Detail	-	-	+
Extendability	-	+	+
Data required	+	+	-

Table 5.1: Comparison of the capabilities of three modeling approaches

2. *Speed.* Once it has been constructed and trained, a prediction can be made by applying the neural network to a satellite image of the initial condition.
3. *Data required.* In the current setup of the network all geometric information can be derived automatically from a satellite image, so little manual data processing is needed. Extensions to the network may alter this. The derivation of a parameter indicating the upstream weighted curvature, for instance, will require manual assistance for determining the flow direction in a number of channels. Furthermore, many sets of satellite images (pairs of initial and final conditions) are needed for the training of the network.

However, there are also a number of important disadvantages:

1. *Physics.* The model is not based on the physical principles governing hydrodynamics and morphology. One may argue that knowledge of these processes is included in the data used for training the network and, therefore, in the calibrated network itself. However, this physical knowledge is not present in any identifiable form: it is not accessible to the user.
2. *New cases.* Planform changes in other rivers might be successfully predicted by a neural network with the same structure, but in general a network trained for one river cannot be applied as it is to another river. Obvious reasons are differences in flood characteristics and differences in relative erodibility. If there are not enough historic data available for training the network for a new river, the network cannot be applied. The lack of training data cannot be compensated using expert judgement or theoretical knowledge. This complicates the application of a neural network to new cases.
3. *Detail.* Starting from geometric satellite data, one cannot expect accurate predictions at small scales. The resolution of a prediction is less than that of the input.
4. *Extendability.* New aspects of river planform changes are difficult to incorporate, because the required input variables must be sensibly defined for all points. The distance to the upstream confluence might be relevant in some cases (e.g. for the process of mid-channel bar formation), but it is not well for all channel geometries (e.g. in case the first upstream node is a bifurcation). Alternatively one could train multiple networks, one for every condition; however, formulating simple empirical models for the various conditions would then be preferable.¹⁵

¹⁵A neural network could be used to fill in knowledge gaps as an alternative for other data fitting methods.

branches model

The most important advantages of the branches model are:

1. *Uncertainty.* The probability of erosion can be computed for every point. Although multiple simulations are required, which may be considered a disadvantage relative to the neural network approach, this approach can also provide information on the correlation of events.
2. *Speed.* A prediction can be made relatively fast without any complex computations. When a 2D flooding mode is included for high-stage flows, the computational time required will increase. However, if the high-stage flow pattern is not influenced too much by the low-stage planform changes, the results of one computation can be reused several times.
3. *Physics.* Physical knowledge is included by theoretically derived relations and empirical relations based on observations. The physics in the model is identifiable and relatively easily verifiable.
4. *New cases.* The same model can be used for any braided river, although recalibration of a small number of parameters is needed. A limited amount of data suffices if the setting of a number of parameters is provided by experts. The accessibility of physical relations in the model plays an important role in this respect.
5. *Extendability.* Lacking physical processes can be added easily due to the process-based approach. The concept of a low-stage channel network may, however, turn out to be too restrictive.
6. *Data required.* All geometric information can, in principle, be derived almost automatically from a satellite image. When the role of the water depth in the model is extended, obtaining the input data will become more difficult.

The branches model has one important disadvantage and that is the inability to predict planform changes in great detail. This is caused by the resolution of the data from the satellite images and the scale at which the processes are modelled. The effects of protection works that are not visible on a satellite image can be included by manually entering them as local areas of low erodibility.

general 2/3D model

From the point of view of the present aspects of comparison, the conventional 2D and 3D models are the opposite of the neural network. The positive points of the one are the negative points of the other. The most important advantages of the branches model are therefore:

1. *Physics.* The partial differential equations that constitute these models are based on the fundamental laws of physics: conservation of mass and momentum. Less generally applicable empirical relations and concepts form the basis of the sediment transport models.

2. *New cases.* Since only the basic equations of physics are included, the model can be applied easily to other rivers. Although calibration is necessary, most parameters can be determined by experts from relatively few data.
3. *Detail.* The basic model concept allows for detailed computations if enough data, computer time and memory space are available.
4. *Extendability.* The model can be extended to include other physical processes, once they have been formulated in mathematical terms. It is relatively easy to adapt the sediment transport model or to include a subgrid model, but processes like bank erosion requiring an adaptive grid will be significantly more difficult to implement for the general case.

The conventional 2/3D models have three disadvantages:

1. *Uncertainty.* A single simulation does not give any information on the probability of erosion. Large numbers of simulations with varying boundary conditions are required, but the time needed for a single computation is still an obstacle to the Monte Carlo approach.
2. *Speed.* Solving the non-linear partial differential equations requires significantly more time than computations with the other models. More detailed computations take relatively longer due to increasingly restrictive conditions on the computational timestep when the spatial discretisation becomes finer.
3. *Data required.* Depending on the way it is used (schematically or to reproduce a prototype situation) the model requires more detailed information about the channel geometry: high-resolution data in the horizontal plane and bed topography data.

5.4.2 Conclusion and research direction

Based on the comparison in the previous section, one can conclude that the branches model is — at this moment — the most promising development approach for medium- to long-term predictions. However, computational speed increases so fast that it will be possible to run a state-of-the-art general 2D model in a Monte Carlo setting with 100 simulations within 10 years from now. Research and model development of alternative approaches must proceed quite fast to keep up with this development. It should be noted that the application of 2D models in a Monte Carlo setting, will only be possible if we do not use the extra speed to increase the resolution of the model. Although computational power has increased significantly over the last decades, the average simulation time has remained the same, or gone up, due to the increased model detail. If this trend continues, little hope exists for a process-based approach that takes into account input and model uncertainty. At this point one should recall the example of a tree given in Section 1.3 that illustrates that increasing the detail of the model does not always improve the accuracy answer. Depending on the research question an appropriate level of detail must be chosen that is in balance with the uncertainty in the specification of initial and boundary conditions and model parameter values. With the numerical models available today solutions can be found for many of the questions related

to river dynamics. Yet, there are situations that require more than a standard 2D numerical model.

Two opposite developments can be noted in the river studies: on the one hand there is a growing interest in large scale, multi-disciplinary studies (see for example Silva *et al.*, 2000), whereas on the other hand engineering studies focus more and more on design details. Therefore, the developments in the field of process-based models cover a similarly broad range of topics. Effective and efficient modelling techniques are needed for the large scale studies. This results in the application of 1D network models — possibly coupled with 2D models for the modelling of floods (Verwey, 2001; Dhondia and Stelling, 2002) — or coarse 2D models. The simulation time of large scale 2D models is kept limited by using a coarse curvilinear or unstructured grid to model only the important areas in detail. Furthermore, domain decomposition techniques are developed to distribute a single simulation over multiple processors.

On a smaller scale, bank erosion processes have been studied. Bank erosion results in changing planforms, and it requires adaptations of the grid used in the numerical simulations. Rudimentary adaptive grids are gradually incorporated into general 2D models to include the effects of bank erosion on the planform and flow pattern (analogous to the earlier work by Mosselman (1992) described in Section 4.1.4). Sediment eroded from the outer bank is transported towards the inner bank by the transverse component of the velocity in river bends. This (transverse) secondary flow effect has been parametrised and incorporated into 2D models (Rozovskii, 1961; De Vriend, 1981a; Struiksma *et al.*, 1985). The resulting quasi-3D or 2.5D models are sufficient for most river engineering studies. When other deviations from the logarithmic velocity profile occur, for instance, due to variations in salinity or strong variations in the alongstream bed-slope (acceleration and deceleration), a 3D numerical model is required. Flow over and around structures may lead to deviations from the hydrostatic pressure distribution, such that a non-hydrostatic 3D model (with an appropriately chosen turbulence model) is needed but these elements are generally of minor importance in large scale morphological studies.

The continued development of a model for braided rivers based on the branches approach, would fit in the desire to have an efficient modelling technique for studies that require only a prediction of large scale planform changes. Further research is needed to make the branches model better suited for those cases. Four important problems associated with the current version of the branches model have been identified and they are listed below:

1. Although the formation of mid-channel bars/islands is included in the current version of the branches model, there is a need for further research into the location of these islands. When the random placement of the islands, as implemented in the current version of the model, is averaged over a large number of simulations, only an additional widening effect is observed. Field observations and laboratory studies seem to indicate that mid-channel bars form preferably immediately after confluences (see Section 3.5). Is this the only preferred location? Where do they for example form in wide shallow meandering reaches, in the bends or in the transition sections? What is the influence of the flood characteristics on the formation of these and other bars?
2. The migration of the nodes (bifurcations and confluences) is currently restricted by the fact that nodes cannot slide along each other. This needs to be improved, but as yet it is not clear which of the possible outcomes sketched in Figure 5.21b-d should be selected as the most probable. This can be generalised to the question: How do

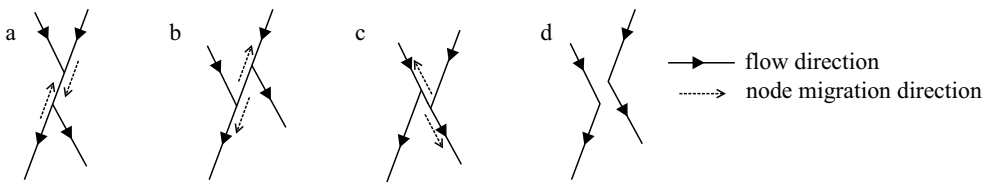


Figure 5.21: In the current implementation of the branches model nodes cannot slide along each other (b and c) and they cannot vanish (d). The topology of the initial condition (a) is maintained during the simulation.

nodes interact? Furthermore, the migration of confluences in the model follows the migration of the two merging channels. Since upstream influence can be expected to be largest, this seems quite reasonable. But, how do bifurcations migrate? The migration of bifurcations is currently implemented as the intersection of the two downstream branches, but this needs to be verified against field or experimental observations. Both downstream branches are influenced by the curvature of the upstream channel and so they will both tend to align (at least in their upstream reach) with the upstream channel, thus causing an increasingly sharp and ultimately ill-defined bifurcation angle.

3. As the flood period plays an important role in the erosion and deposition of sediments in the Jamuna River, the influence of the flow directions during high stages on the channel migration needs further investigation. In particular, what happens to branches that are oriented almost perpendicular to the local flow direction during flood? Is there a physical basis for the down-valley shift as included in the model? Can the low-stage channels be dealt with using a subgrid approach?
4. In the model, new branches can only form due to mid-channel bar growth. Field observations and laboratory studies, however, suggest that the formation of new branches by means of channel formation (chute ‘cutoff’ formation in meandering rivers) is at least as important. The physical processes behind this phenomenon are not yet well-understood. Why do some channels incise from the upstream end, whereas others cut backward from the downstream end? What influence does the geometry of the neighbouring branches have on the formation? Under which conditions are new channels formed in braided rivers?

The formation of new branches by means of cutoff channel incision has been selected as the subject of the second part of this study.

5.4.3 Summary

Three models for the planform changes of braided rivers have been studied: a neural network, a cellular model and an object-oriented approach. The neural network has been trained to predict bank erosion based on a limited amount of geometrical information. For each point near the bankline the distance to the nearest channel, the sine and cosine of the angle between the direction to the nearest channel and the overall river direction, the local width of the nearest channel, and the fraction of water in a neighbourhood were determined and presented as inputs to the neural network. Based on these inputs the neural network was able to learn

a number of very simple rules. The two most important aspects when constructing a neural network are the availability of training data and the selection of suitable parameters for the schematisation of the input. Without enough training data, a neural network cannot learn the relations; without the appropriate input variables, the network might not learn the right rules. The output of an appropriately trained network can be used as an indication of the probability that erosion will occur. Thus it is possible to get a probabilistic statement without requiring extensive and time-consuming computations. The empirical, physical knowledge represented by the network is, however, not accessible, not generic, and not easily extendable.

The cellular model by Murray and Paola (1994) uses a simplified 2D approach to study the interaction of the relevant processes in braided rivers. For basic studies this model is very useful, however, for more advanced studies the most restrictive assumption is related to the anisotropy in flow direction, which implies that water can only flow in one direction. A recent adaptation of this model seems to adequately solve most of the problems (Thomas *et al.*, 2002).

In the third model the braided river is split into separate branches (the objects). Four processes are defined to act on the branches: branch migration, branch widening and narrowing, branch abandonment, and branch splitting due to mid-channel island growth. A computer program that combines these four processes may be used to predict planform changes in anabranching rivers, but for a braided river, where the definitions of the branches varies continuously with the discharge, the concept of clearly defined channels is difficult to maintain. However, the speed of the simulations makes it possible to use a Monte Carlo approach. If the individual simulations are reasonably correct, the model can be useful in a probabilistic setting for medium-term prediction where other methods of predicting become too costly. The model approach allows for incremental improvement of separate modules, such that the model may be improved over time.

General 2/3D models, although preferable from a fundamental point of view, are too time consuming to be used in a probabilistic approach if a large number of simulations has to be carried out. These models are best applied at time spans that allow for a deterministic approach, hence short-term simulations.¹⁶

The neural network approach, the object-oriented branches model, and the general 2/3D model have been compared with respect to the modelling of the uncertainty in a prediction, their computational speed, their physical foundation, their applicability to new cases, the detail of their predictions, the ease with which the models can be extended using improved insight, and the amount of data required to run the models. Based on this comparison it has been concluded that the branches model is the most promising approach for the development of a model for medium- to long-term predictions. When computational speed becomes less of a problem, the general 2/3D model may become preferable. Regarding the development of the branches model, four directions have been indicated.

1. A more extensive study into the formation of islands is needed to improve the subroutine regarding mid-channel island formation.
2. Nodes are currently treated as the place where channels happen to meet. A study has

¹⁶General 2/3D models are also used to determine equilibria and average tendencies over very long-term spans, in which case the transitional period does not matter and may therefore be changed to accelerate the simulation.

to indicate in which way nodes influence the planform changes.

3. High stage flow should be included explicitly in the model. Its influence on channel migration should be determined from theory and/or experiments.
4. Cutoffs occur currently only at user-defined locations. The process of channel formation should be investigated to check for an automated approach.

The last topic has been addressed in the second part of this study.

Chapter 6

Channel formation

In the previous chapters we have described the processes involved in braiding and some planform models for braided (and meandering) rivers. Three models were analysed in some detail, and based on that analysis it was concluded in Section 5.4.2 that the processes leading to the formation of new channels were not fully understood. The formation of new channels is one of the key ingredients of braiding, since braided rivers are after all characterised by the dynamic behaviour of multiple intertwined branches. But also in meandering rivers the formation of new channel courses or cutoffs plays an important role. The ever increasing length of a meandering river stretch is from time to time reduced by the cutoff of meander bends.

This chapter focuses on the description of channel formation by incision (like chute cutoffs) in the literature. The first section describes the three types of channel formation, of which the incision process is one. Section 6.2 summarises what has been written about channel incision and the stability of cutoff channels. The third section focuses on the question in which direction the channel incision process travels: from upstream to downstream or from downstream to upstream. In the next chapter a 2D numerical model is used for the analysis of channel incision processes, cutoff formation and cutoff stability.

6.1 Types of channel formation and cutoffs

In general — that is, when we restrict ourselves not only to meandering and braided rivers — there exist three processes by which new channels can form (See Figure 6.1).

1. *Mid-channel bar formation.* An existing channel may split into multiple channels by the growth of one or more bars within a wide channel: bank erosion and mid-channel sedimentation often interact. The bars can be formed while submerged and emerge during low stage, thus splitting the channel. As already mentioned in Sections 3.5 and 3.6, Ashmore (1991) observed that one or more mid-channel bars only formed in his experiments with low stream power or wide channels. Ashworth (1996) has studied the formation of mid-channel bars downstream of confluences. Furthermore, this process has been studied theoretically using stability analysis for straight channels

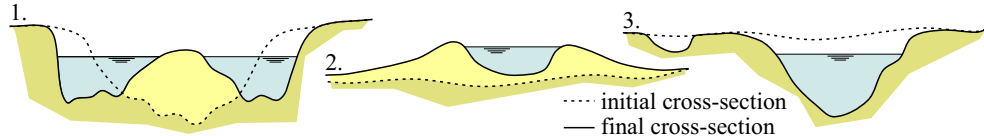


Figure 6.1: Sketches illustrating the three channel-forming processes: (1) Channel widening and mid-channel bar formation, (2) levee building, (3) channel incision.

with constant width (Engelund and Skovgaard, 1973; Fredsøe, 1978; Parker, 1976) and more recently with periodically varying width (Repetto and Tubino, 1999).

2. *Building of levees.* In the case of anastomosing rivers with low lying flood plain in between the channels (Makaske, 1998), the new channels might form due to selective deposition of splay sediments when a channel breaks through its banks and flows out onto the low-lying flood plain. Contrary to the case of mid-channel bar formation where sedimentation occurs in the middle of the flow, a new channel may now form by depositing sediments along the edges of a main flow. These deposits may form levees which subsequently further constrain the flow, thereby building a new channel. So, sedimentation is the main channel-forming process. This process is called a (first-order¹) avulsion — although one should note that the term avulsion is often used for any major change in river course. In braided rivers, where the flood plain has normally the elevation of the average flood, this process is not important.
3. *Channel incision.* Finally channels may form by incising a new course into bars/islands or flood plain during a flood or when one or more of the existing channels become partly obstructed and local flooding of shallow bars occurs. In this case, erosion dominates the channel formation. One of the best known examples of this process is the chute cutoff process, which incises a new channel across the inside of a meander bend when at high flow the river follows a shallow area between scroll bars on the point bar. The term ‘chute cutoff’ is sometimes also used to indicate any other cutoff process related to the formation of a chute, that is a (local) flow acceleration. The process is sometimes also referred to as a third-order avulsion¹ (Nanson and Knighton, 1996). Ashmore (1991) mentions that the dissection of stalled bars and the chute cutoff might be thought of as end members of a continuum of processes with a similar basic mechanism but varying geometry, ranging from symmetric bars to point bars.

The chute cutoff, which was mentioned above in relation to channel incision, is only one out of four types of cutoff distinguished by Erskine *et al.* (1992) (see Figure 6.2)

1. *Neck cutoff* There are two types of neck cutoff that differ in the process that creates the final gap. In both cases the pointbar progressively narrows in one place due to lateral migration of the upstream and downstream meander bends. Subsequently, the two limbs of the meander may either continue to migrate and finally meet leading to

¹The term ‘second-order avulsion’ is used to indicate the reoccupation of a previously abandoned channel. If the old channel has been abandoned recently little erosion may be needed to reuse the abandoned channel. Older channels which merely remain visible as shallow areas must be eroded anew, which may be more difficult than eroding a completely new channel as old infilled oxbow-lakes generally consist of deposits with a high clay fraction (Allen, 1965).

a breach (first type, bank erosion), or — in the second case — the cutoff may form during high flow by incising a new channel across the narrow meander neck (Allen, 1965; Erskine *et al.*, 1992). The latter process belongs to the third category of channel forming processes described above and it is only a formal, geometrical definition that distinguishes it from a chute cutoff. The former case (the neck cutoff by bank erosion) creates — when the old meander bend is not immediately abandoned — a new channel consisting of little more than a bifurcation and a confluence. In general, a neck cutoff is defined as a cutoff that connects two parts of the river that are separated by less than one channel width. Lewis and Lewin (1983) distinguish between neck cutoffs that lead to the abandonment of a single meander bend and those that cut off multiple bends.

According to Howard and Knutson (1984), neck cutoff (by bank erosion) is the dominant shortening process for meandering rivers with narrow channels, well vegetated banks and low gradients. The overall sinuosity of chute cutoff dominated meandering rivers is lower than that of neck cutoff dominated rivers. In braided rivers new connections may occasionally form in a way similar to neck cutoffs in meandering rivers. When two parallel branches migrate laterally towards each other, a new connection is formed when the island in between them is completely eroded at one location; this process does, however, not lead to the formation of channels of substantial length, nor does it increase the number of parallel branches. So, this process is of negligible importance for the maintenance of the braided appearance.

Matthes (1948) states that 13–15 neck cutoffs may have occurred per century along the Lower Mississippi River before human interference began. These cutoffs compensated at most 40% of the length increase due to the estimated average development of meanders; the remaining 60% must have been compensated by the other types of cutoffs. So, different cutoff types can occur in the same river.

2. *Chute cutoff* A chute cutoff is a cutoff resulting from a local flow acceleration. This may occur along the inside of a meander bend or during flood across a isthmus between two river sections. In the latter case the distance between the river sections should be more than one channel width. Lewis and Lewin (1983) make a further distinction between chute cutoffs that lead to the abandonment of a single meander bend and those that cut off multiple bends.

According to Howard and Knutson (1984) chute cutoffs occur most frequently where bend curvature is strong, during high flood discharges especially in rivers with wide channels, poorly cohesive, weakly vegetated banks, and high gradients. This refers to

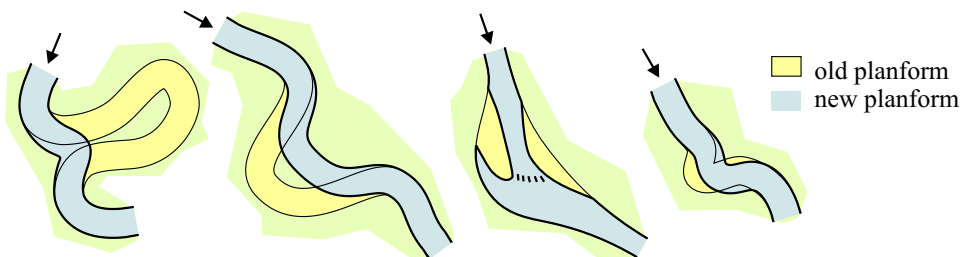


Figure 6.2: Sketches illustrating the four cutoff types: (1) neck cutoff, (2) chute cutoff, (3) mobile bar cutoff, (4) bend flattening.

the chute cutoff along the inside of a meander bend. It is associated with wandering or incomplete meandering rivers. The large-scale chute cutoffs may occur in any type of meandering alluvial river.

3. *Mobile bar cutoff* The mobile bar cutoff as described by Lewis and Lewin (1983) has already been mentioned in Section 3.5.1 when describing the initiation of braided by the dissection of linguoid bars. It can be interpreted as a submerged chute cutoff and it should be grouped with the other channel incision processes.
4. *Bend flattening* Bend flattening described by Matthes (1948) and Erskine and Melville (1982) is related to the formation of concave bank benches and the associated reduction in channel curvature due to pointbar erosion. This process is, therefore, not associated with a discrete shift in channel course, but merely a change in migration direction. It will reduce the river length, but it does not lead to a new cutoff channel. It does not belong to the channel forming processes.

The following sections give an overview of the literature on channel incision and the formation of chute cutoffs.

6.2 Channel incision and chute cutoffs

This section gives an overview of the processes involved in the formation of new channels by incision as described in the literature. First, we start with the description of the related topic of gully formation by initially unchannelised overland flow and other hillslope processes (Section 6.2.1), followed by a summary of the described observations of chute cutoffs in general and in braided rivers in particular (Section 6.2.2).

6.2.1 Channel formation on hillslopes

After a rainfall event there are basically two ways in which the rainfall runoff can reach the channel system draining the catchment:

- *overland flow*. The thickness d of the water layer flowing down the hillslope, increases due to the steady accumulation of precipitation. When the water depth d and slope angle θ increase, the shear stress τ exerted on the terrain surface by the flow increases also. When the shear stress exceeds the critical shear stress τ_c erosion starts to occur. Horton (1945) hypothesised that once overland flow becomes erosive, (periodic) rills will form parallel to the flow direction on unvegetated slopes. Analytical studies by Smith and Bretherton (1972) have, however, indicated that straight and convex surfaces are stable against small perturbations when the diffusive action of raindrops is taken into account. The rills may, therefore, only be encountered on concave surfaces. Dense vegetation protects the surface against the erosive processes (see Figure 6.3a), whereas rills and (further downhill) gullies start forming where there are small gaps in the vegetation. Izumi and Parker (1995) have obtained a realistic value of about 33 m for the initial distance between rills from an analytical study using a purely erosion model for bed evolution

$$(1 - \varepsilon) \frac{\partial z_b}{\partial t} = -E \quad (6.1)$$

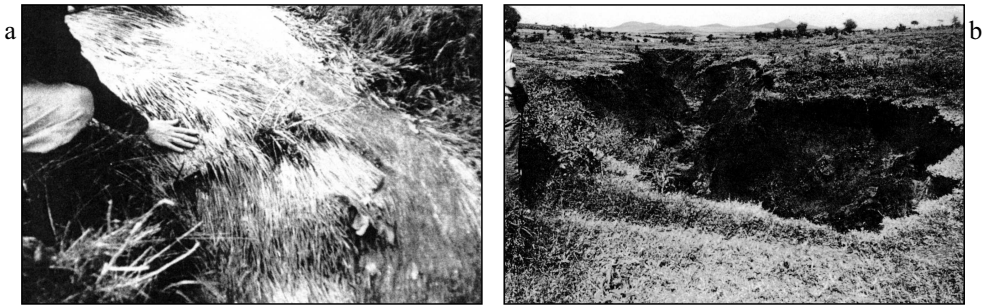


Figure 6.3: **a** (left) A mat of vegetation protects the ground surface from erosion by overland flow (Montgomery and Dietrich, 1994). **b** (right) Small headcut; headward retreat of the channel occurs mainly due to plunge-pool erosion, tunnel erosion, and collapse (Dietrich and Dunne, 1993).

where ε is the bed porosity, z_b is the bed level, t is time and the erosion rate E is given by

$$E = \begin{cases} E(\tau_b) & \text{if } \tau_b > \tau_{b,c} \\ 0 & \text{if } \tau_b \leq \tau_{b,c} \end{cases} \quad (6.2)$$

where τ_b is the shear stress and $\tau_{b,c}$ is the critical shear stress for the erosion of the cohesive sediment.

- *subsurface flow.* Two different components of subsurface flow can be distinguished: seepage and tunnel flow. Both processes may cause sediment movement in the subsoil, which may result in the formation of new surface channels by the collapse of cavities in the underground. At locations where the subsurface flow re-emerges, small cuts in the root-mat may form, from which new channels may eventually be formed (Knighton, 1998).

Once an initial channel is formed, it grows in *headward* (upstream) direction by the erosive action of the overland flow spilling into the channel and the subsurface flow undermining the banks by seepage flow and piping (see also Section 3.3.3). The head — being the most upstream end of the channel — can be either a gradual transition from undisturbed slope into channel, a step, or a headcut (see Figure 6.3b). Runoff processes and head types are summarised in Figure 6.4.

Izumi and Parker (2000) have studied the case of a flow over a (downward-)concave base profile as shown in Figure 6.5. The base profile is further restricted to be a self-preserving form that migrates in upstream direction under the influence of erosion. They indicate that a transportational formulation for the morphological changes (as in Equation 4.27) has a strongly diffusional component which does not allow for a base solution with a concave slope. Therefore, Izumi and Parker use again the erosional formulation given by Equation 6.1. They have shown that the flow will be laterally unstable if the erosion rate is sufficiently sensitive for changes in the shear stress τ_b : $E(\tau_b) = \alpha[(\tau_b/\tau_{b,c}) - 1]^\gamma$ with $\gamma \geq 1$. The characteristic transverse wavelength is of the same order of magnitude as the wavelength obtained from their 1995 model described at the beginning of this section.

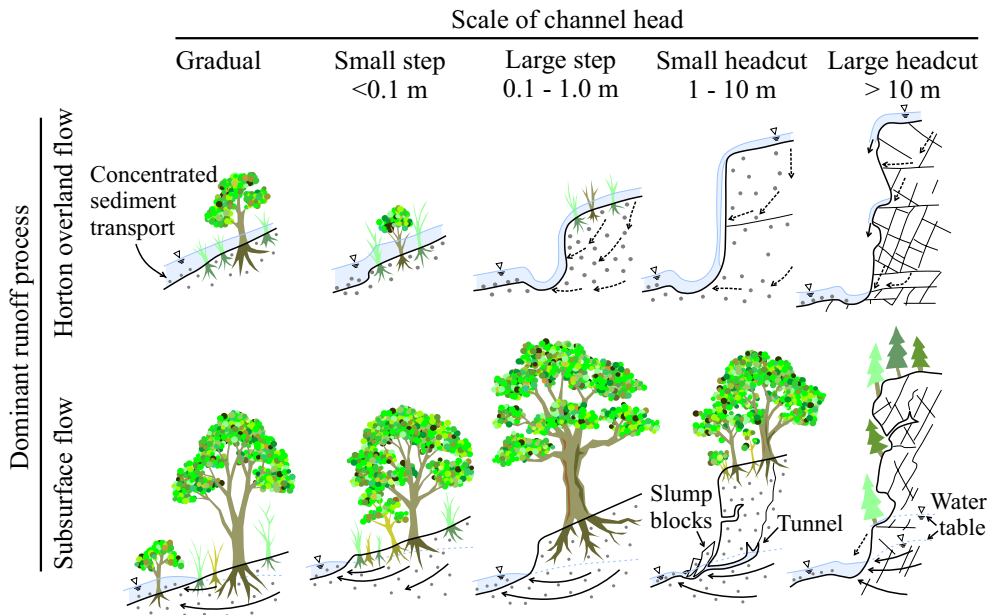


Figure 6.4: Channel head types on the basis of incision depth and dominant runoff process. Sketches indicate overland and subsurface flows. The normal arrows indicate saturated flow, and the dotted arrows indicate unsaturated flow. Figure after Dietrich and Dunne (1993).

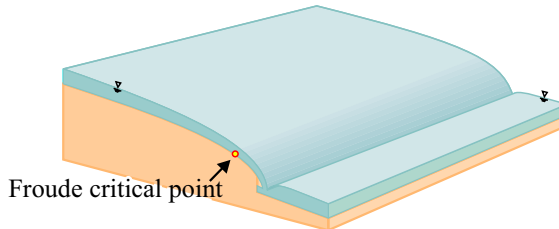


Figure 6.5: Concave slope topography used by Izumi and Parker (2000).

6.2.2 Cutoff descriptions

Documentation on the processes and mechanics of cutoffs is limited. Their infrequent occurrence makes them harder to study. Furthermore, the large variety in geomorphological conditions on the flood plains of meandering rivers makes it more difficult to draw conclusions about the occurrence criteria of cutoffs and the associated physical processes. Early studies have led to some general conclusions that cutoffs usually occur during very high stages when water scours out channels across narrow necks of overdeveloped bends and that the cutoff channel results from the gradual enlargement of a initially shallow area (Matthes, 1948). This was further generalised by Johnson and Paynter (1967) who hypothesised that a cutoff that occurred on the River Irk at Chadderton, Lancashire, formed due to a raise in water level upstream of the meander bend such that the gradient of the water surface was steepened and the stream could flow across the lowest part of the flood plain. The required water level

increase may occur due to either a combination of gradual lengthening of the channel bend and a relatively high discharge, or a sudden blockage of the flow in the bend (for instance due to a bank- or landslide or an ice jam).

Possible interactions with the morphological development of the main channel have been indicated by Joglekar (1971) who describes the development of a cutoff as enlargement of a shallow side channel due to a temporal lag in the adaptation of the channel bed during a flood. He states that when during high stages the outer bend pools become deeper and the riffles become shallower, the flow tends to flow across the flood plain, thereby partly following remnants of old channels and other depressions in the flood plain. At first when the floods begin to fall, the riffles will still be elevated, considerably reducing the flow through the main channel and forcing a relatively large amount of the discharge through the side channels. Although the flow depth on the flood plain is relatively small and velocities are small, high velocities may be reached locally at the downstream end where the flow joins the main channel. These high velocities may lead to backcutting and the formation of a new channel.

An extensive description of a chute cutoff was published by Gay *et al.* (1998). In their paper they describe the formation of chute cutoffs across meander necks in the Powder River (Montana, USA) during floods in March 1989. Photographs of the headcuts that formed at the down-river edge of meander necks are shown in Figure 6.6. Figure 6.7 shows an isometric drawing of the headcuts which progressed headward (up-river) across the necks. One can observe multiple headcuts in the lower part of the figure. These headcuts all originate from the initial phase of the cutoff process; over time one headcut became dominant. The reason why that particular one was selected is unknown. It depends not only on its location relative to the mainstream overland flow, but also on other aspects like possibly favourable conditions in erodibility and flow resistance due to the locally sparse vegetation. One can safely assume that the tributaries to the main headcut have reduced the flow into the other gullies, thereby reducing their growth rates. The maximum observed rate of upstream extension of the headcut was in the order of 10 m/h and the main gully reached a length of 150 m after the first day of flooding. Another 100 m was eroded during the next two weeks, which were characterised by a lower discharge. The cutoff finally stopped about 70 m short of completion. Gay *et al.* (1998) indicate that the headcut propagation rate strongly depends on the cross-neck flow rate and on whether or not the soil and underlying layers are frozen.

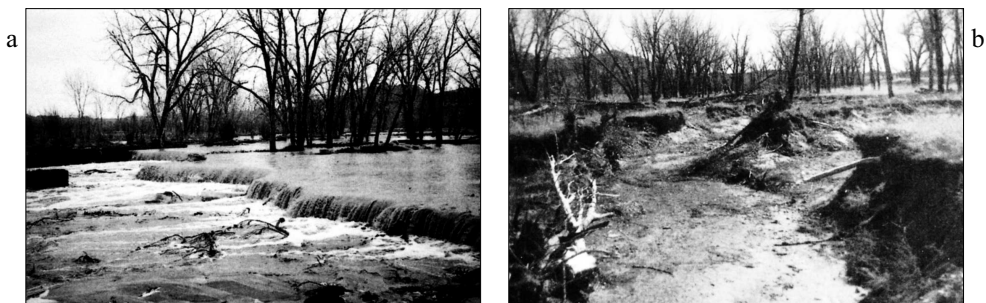


Figure 6.6: Photographs of headcuts in (a) the process of forming and (b) final state from Gay et al. (1998).

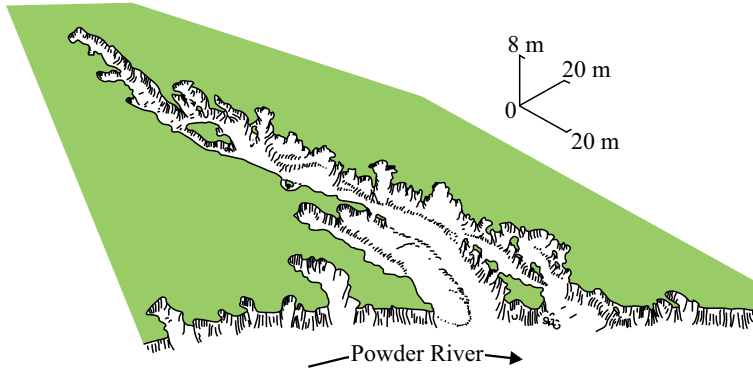


Figure 6.7: Isometric drawing of the headcut by Gay et al. (1998). Headcuts up to 2 m deep.

When a cutoff is formed (artificially or naturally) a new, shorter channel course will be established which is not in equilibrium with the rest of the river. The backwater effect leads to ongoing erosion in upstream direction (Jansen, 1979) which in the case of a completed cutoff in the Powder River resulted in a deepening of the upstream river until it came across some exposed bedrock as observed by Gay *et al.* (1998). At the same time a sedimentation wave will proceed in downstream direction. The reduced channel length and associated decrease in sinuosity also result in a reduced resistance and an increased flow velocity as observed by Erskine *et al.* (1992) (see also the notes on friction in Section 3.4). The impact of a cutoff can be quite large, or, as Joglekar (1971) phrased it:

“Whenever a river succeeds in establishing a cutoff, there follows a period of total chaos, for miles above and below the newly-formed short cut. Banks start caving, new channels are formed, some old channels get silted up, until at last, probably during low stages, there is a temporary stability for a few months. With the next floods again, the agitated period of adjustments commences, until equilibrium is finally established.”

Gay *et al.* (1998) observed in at least one completed cutoff case that a large sand-and-gravel bar was blocking the upstream end of the original meander bend; the moment at which that bar largely formed — before or after the completion of the cutoff channel — had unfortunately not been observed. It can be expected that this bar was the first step in the closing off of the original channel forming a horseshoe or oxbow lake. The typical description of the sedimentation of the old channel as reported by for example Allen (1965) entails the formation of two (relatively coarse-grained) bedload plugs at upstream and downstream end of the bend, followed by the slow, homogeneous infilling of the remaining lake by (relatively fine) sediment supplied by overbank flow (see Figure 6.8). Although the plugs indicated in Figure 6.8 are quite large, they may be hard to detect in the sedimentary record when the analysis is based on just a limited number of drillings. Erskine *et al.* (1992), for example, did not find the characteristic plugs in their measurements on the lower Hunter River, Australia. They furthermore indicate that the infilling of the old channel might not be quite as homogeneous as often suggested. They concluded that in their case the sedimentary infill of the cutoffs is not uniformly fine-grained, because the sedimentary character of a cutoff infill is determined by the interaction of three factors, namely

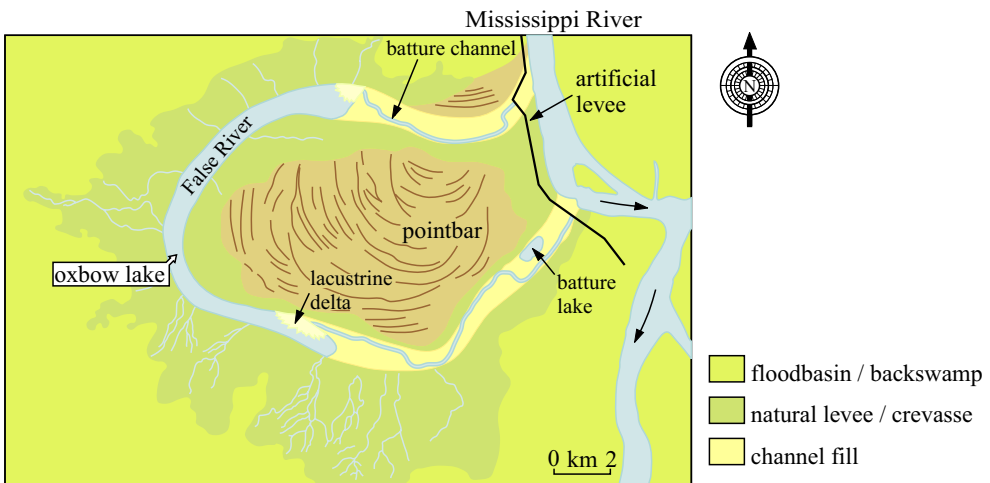


Figure 6.8: The geomorphology of an oxbow lake (False River cutoff channel, Mississippi River) after Allen (1965) and Gagliano and Howard (1984)

1. the nature and availability of sediment to be transported by high discharges,
2. the magnitude and frequency of floods which transport the available sediment, and
3. the variation in position within a cutoff with respect to distance from the present channel.

Sedimentation not only occurs in the abandoned channel once the cutoff is completed. Gay *et al.* (1998) observed that during stages less than bankfull sand and mud were also deposited in the downstream sections of gullies that had not completed the cutoff.

Ashmore (1991) observed that in most of his flume experiments a braided channel formed by the development of chute channels across alternating point bars (see also Section 3.5.2). The onset of the cutoff process often coincided with the arrival of a pulse of bed-load from upstream in the form of a bed-load sheet or migratory transverse unit bar. The steep gradient near the head of the slough channels resulted in their headward erosion, capture of progressively larger volumes of water, and rapid enlargement. Bed-load streams, which include most braided streams, are unable to build the inner point bar to bank-full elevation (or, alternatively, to fill the chutes between the scrollbars) in the absence of fine-grained suspended sediment transport; this makes them more prone to the formation of chute cutoffs (Carson, 1986). The role of suspended sediment in stabilising point bars and preventing chute cutoff in laboratory streams has been demonstrated experimentally by Schumm and Khan (1972).

6.3 Modelling chute cutoff stability

Due to the complex nature of cutoffs, few models have been published on this subject. Howard (1996) has included an empirical procedure for including chute cutoffs in a meander model. His approach will be described first. Subsequently, the subject of chute cutoff

stability is addressed. The relevant work ranges from empirical formulations by Joglekar (1971), via quasi-equilibrium models by Klaassen and Van Zanten (1989) and Biglari (1989) to a dynamical system analysis by Wang *et al.* (1995). This section is concluded with a presentation of the work by Slingerland and Smith (1998) on the distribution of sediment at a crevasse channel offtake and the healing or enlargement of the avulsion.

Howard (1996)

The meander model of Howard and Knutson (1984) which was described in Section 4.1.1, includes a procedure for neck cutoffs. These cutoffs have been programmed to occur when the river's centreline approaches itself to within a predetermined distance (of about one channel width). No separate procedure for chute cutoffs was included, but certain types of chute cutoffs may indirectly be accounted for by the model as it incorporates the possibility for pointbar erosion when the curvature of the channel becomes large (the erosion rate becomes negative for small R/B ratios). Also the improved model described by Howard (1992), which is based on the model by Johannesson and Parker (1989) described in Section 4.1.3, contains only the procedure for neck cutoffs. More recently, however, Howard (1996) extended that model with a procedure for chute cutoffs. Because a chute cutoff may develop slowly over years, no fixed condition has been specified in the model for which chute cutoffs form. Once every 50 iterations for each point i of the meandering channel it is checked whether a cutoff channel might form from i to any point j within a distance of 50 times the channel width downstream of i . This check starts by selecting for each i the most likely course for the cutoff channel based on the following expression for the probability $P(i, j)$ of a cutoff channel from i to j

$$P(i, j) = K_c R_c(i, j) e^{\min\{-K_l L_c(i, j) - K_e E(i, j) + K_a \cos[\phi(i, j)] + K_v u_{1b}(i), 0\}} \quad (6.3)$$

where

- $E(i, j)$ the average or maximum elevation encountered along the chute from i to j ,
- K_* spatially and temporally constant positive coefficients: K_a, K_c, K_e, K_l, K_v ,
- $L_c(i, j)$ the distance along the chute from i to j ,
- $P(i, j)$ indicates the probability of occurrence of a chute cutoff from i to j (its value is assumed unity if $L_c(i, j)$ is less than 1.5 times the channel width),
- $R_c(i, j)$ gradient ratio $[L_p(i, j) - L_c(i, j)]/L_p(i, j) = 1 - [1/\lambda_c(i, j)]$ where $L_p(i, j)$ is the distance along the meander from i to j and $\lambda_c(i, j) = L_p(i, j)/L_c(i, j)$ the cutoff sinuosity (similar to the cutoff ratio λ defined below),
- $u_{1b}(i)$ near bank excess velocity,
- $\phi(i, j)$ angle between the chute cutoff direction and the local flow direction in the meander.

According to this expression the maximum probability of a cutoff from i to j increases linearly with the gradient ratio between these two points: the larger the relative reduction in length due to the cutoff, the larger the probability of occurrence. The maximum probability is reduced by a factor that depends on the amount of sediment to be eroded during the formation of the cutoff (parametrised by the absolute length of the cutoff and characteristic flood plain elevation along the cutoff), the bifurcation angle and the near bank excess velocity. The schematisation is such that the initial probability is reduced the least for a short cutoff across a low-lying part of the flood plain, which bifurcates from the original channel at a small angle

at a location where the near bank excess velocity is large. Compare the effect of the bifurcation angle here with the formulation for channel abandonment in the framework of Klaassen *et al.* (1993) given by Equation 5.20.

Let $P(i)$ be the maximum value of $P(i, j)$ over all possible values of j and let j_* be the value of j for which this maximum is reached. This maximum is compared with a random number $p(i)$ selected from a uniform distribution. The cutoff from i to j_* is formed when $p(i) \leq P(i)$. From the simulations it is observed that the chute cutoff probability has a significant influence on the overall sinuosity of a meandering channel.

Joglekar (1971)

Joglekar (1971) defines the cutoff ratio λ as the length of the channel bend ACB and the length of the cutoff channel AB (see Figure 6.9). The cutoff ratio λ is always larger than 1. Joglekar indicates that a cutoff will not necessarily occur for any given value of λ , but that a cutoff becomes increasingly probable as the ratio increases and when the other conditions (like flood discharge, vegetation, and bed material) are favourable. This is in line with the stochastic approach by Howard (1996) described above. Typical values of λ at which cutoffs occur vary among rivers from 1–3 for chute cutoff dominated rivers to 8–10 and larger for rivers like the Mississippi River in which neck cutoffs dominate. Furthermore, Joglekar (1971) refers to work on the Hooghly River that indicates that R/\sqrt{Q} is another important measure for cutoff formation. The rationale behind this measure is that the critical radius of curvature R depends on the discharge Q in the sense that a small discharge can follow a sharper bend (smaller radius of curvature) than a large discharge. Analysis of field and laboratory data by Inglis (1938–39, 1947) has shown that meander wavelength L_m , meander width B_m and channel width B are all proportional to \sqrt{Q} or approximately so, according to several other researchers listed by Jansen (1979) and Knighton (1998). Therefore, the ratio R/\sqrt{Q} can be interpreted as geometric ratio of the local radius of curvature and an average characteristic length scale of the meandering river. Note that if we replace \sqrt{Q} by the channel width B , we

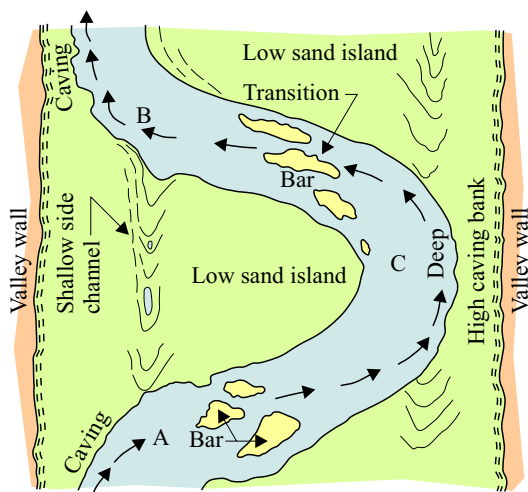


Figure 6.9: Cutoff channel geometry used by Joglekar (1971).

obtain the ratio R/B . The migration rate becomes, as indicated above and in Section 4.1.1, negative for small values of this ratio. This is associated with the occurrence of small chute cutoffs along the inside of the bend.

For the design of an artificial cutoff Joglekar (1971) gives four guidelines. First, the upstream entrance should be aligned such that the curvature of the flow lines entering the cutoff is smaller than the curvature of the existing channel — this is only possible if the cutoff entrance is located in an outer bend. Second, the upstream entrance should be made bell shaped.² Because enlargement of the cutoff starts at the outlet, there is no need to impose a particular shape there. Third, for maximum shear stress the channel should be dug as deep as possible; the width is not very important, but the side slopes should be appropriate for the sediment type. Fourth, Joglekar (1971) states that when using Lacey's regime formulae $R = 0.47(Q/f)^{1/3}$ and $I = 0.5 \cdot 10^{-3} f^{5/3} Q^{-1/6}$, the expression RI^2 depends only on the silt factor $f = 1.76\sqrt{m}$, where m is the mean particle diameter in mm, R is the hydraulic radius in feet and I is the water surface slope. Therefore, when the bed and bank material of the cutoff channel and the existing channel are the same, the values of RI^2 for the cutoff channel and the meander bend may be compared directly. Joglekar (1971) indicates that, for the completion of the cutoff, it is necessary that the value of RI^2 for the cutoff channel is larger than that of the existing bend. This raises the question why RI^2 should be a relevant parameter. What does RI^2 represent? Using another one of Lacey's formulae, which relates the velocity V to R and I as $V = 60f^{-1/4}R^{3/4}I^{1/2}$, one can write that $RI^2 \propto (VI)^{4/3}$. Comparing RI^2 is under the assumption of this formula for V identical to comparing VI . The product of V and I can be interpreted as the release rate of potential energy as a unit discharge flows down a slope I with velocity V (the streampower of a unit discharge). The higher RI^2 value for the cutoff implies that — under the assumption of the correctness of Lacey's formulae — the release rate of potential energy in the cutoff is higher. If the extra losses in the cutoff channel are limited by appropriately shaping the cutoff according to the first three points, this extra energy can be used to enlarge the cutoff further and therefore RI^2 might indeed be a relevant parameter when designing a cutoff. The same relation can be derived in a more general way, as will be shown in the next section.

Klaassen and Van Zanten (1989) and Biglari (1989)

Klaassen and Van Zanten (1989) analytically derived a criterion for the occurrence of a cutoff in meandering channels assuming the idealised situation of a clearly defined but small cutoff channel as indicated in the sketch in Figure 6.10. This analysis was later extended by Biglari (1989). Under the assumptions that

1. both the cutoff channel and the original bend are long enough for normal depth to be attained at the bifurcation,
2. the sediment distribution at the bifurcation is proportional to the discharge distribution (implying that most sediment is transported as suspended load),
3. the Engelund-Hansen formula describes the local transport capacity (mu^n with $n = 5$), and

²Although not indicated by Joglekar (1971) the reason for this bell shape is probably twofold. First, the cutoff catches a larger discharge due to the wider entrance. Second, less sediment is available at the entrance to plug the newly created cutoff channel.

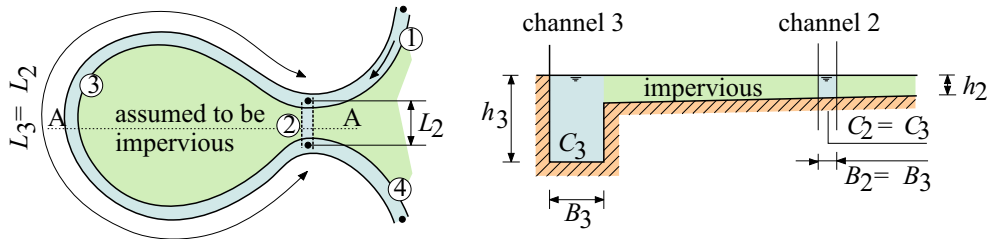


Figure 6.10: Cutoff schematisation by Klaassen and Van Zanten (1989).

4. the water depth in the channel just upstream of the bifurcation equals the local normal water depth (neglecting the drop in water level caused by the increased discharge capacity downstream due to the flow through the cutoff channel),

he derived that the cutoff channel will increase in size whenever the following condition is met

$$\eta > \frac{(1 + \beta\gamma\eta^{3/2}\lambda^{1/2})^{5/3}}{\gamma\lambda^2(\sigma + \beta\gamma\eta^{3/2}\lambda^{1/2})} \quad (6.4)$$

where

- β width ratio $B_{\text{cutoff}}/B_{\text{bend}}$,
- γ roughness ratio $C_{\text{cutoff}}/C_{\text{bend}}$ in general less than 1,
- η depth ratio $h_{\text{cutoff}}/h_{\text{bend}} < 1$,
- λ cutoff ratio $L_{\text{bend}}/L_{\text{cutoff}} > 1$ equal to the slope ratio $i_{\text{cutoff}}/i_{\text{bend}}$,
- σ multiplication factor relating the distribution of sediment transport $S_{\text{bend}}/S_{\text{cutoff}}$ to the distribution of discharge $Q_{\text{bend}}/Q_{\text{cutoff}}$. $\sigma > 1$ implies that a relatively large part of the sediment enters the existing bend.

For the derivation of this condition — and a version for a general exponent n in the transport formula — the reader is referred to Section C.1. This condition simplifies for small values of β to $\gamma\eta\lambda^2\sigma > 1$, which was first obtained by Klaassen and Van Zanten (1989) from a slightly different analysis. If one also assumes that γ and σ are both approximately equal to 1, Equation 6.4 reduces to the condition that $h\lambda^2$ should be larger for the cutoff than for the original meander bend as suggested by Joglekar (1971). From the more general condition given above one can conclude that the larger the values of γ , η , and λ the higher the probability on a cutoff is. This means that a relatively smooth flood plain, a large flood, and a large bend are favourable conditions. Furthermore, the criterion turns out to be rather sensitive with respect to the exponent n in the sediment transport relation. The smaller the value of n the easier cutoffs occur. One should, however, note that this criterion holds only during the initial stage of the cutoff as long as the flow through the cutoff has negligible influence on the main channel.

A subsequent study by Klaassen and Masselink (1992) based on the analysis of satellite images in the Jamuna River, found that cutoffs in the Jamuna River occurred at a ratio λ between 1 and 1.7 with an average value of 1.25. The cutoff ratio in the braided Jamuna River is very low in comparison to a meandering river, where a cutoff ratio of 5–30 is common, indicating that cutoffs occur very quickly in the Jamuna River. This may be explained by the

high overbank flow, the low value of $n = 3.64$ (see Section 3.1.4), the easily erodible alluvial deposits, and the relatively smooth flood plain that is only scarcely vegetated (see Chapter 2).

Analysis of satellite images of the Jamuna River by Mosselman *et al.* (1995) has indicated that channel abandonment correlated better with the bifurcation angle (see Section 5.3.1 and Figure 5.16) than with the cutoff ratio λ .³ This has led to the conclusion by FAP24 (1996) that the deviation angle of a channel from the upstream channel direction is more important than the cutoff ratio. This conclusion can be disputed, since the processes involved in channel formation and channel abandonment are different. Furthermore, it is obvious that the formation of a new channel in a braided river not necessarily means abandonment of the old channel, since otherwise one would never get a braided pattern. It is expected that the combination of λ and σ in Equation 6.4 may serve as a good predictor for the formation of a cutoff channel.

The theoretical work by Klaassen and Van Zanten (1989) and Biglari (1989) addresses the stability of a cutoff channel from a quasi-equilibrium point of view thereby for a large part ignoring the underlying dynamics. Biglari (1989) checked the analytically derived Equation 6.4 against the outcome of several simulations with a one-dimensional numerical model. The numerical model had the advantage of not requiring the assumption of normal flow (assumptions 1 and 4 mentioned above). The results agreed fairly well for a narrow ($\beta \leq 0.4$), somewhat rougher ($0.6 \leq \gamma \leq 1$) cutoff channel up to a water depth ratio η of about 0.4. For higher values of η — for which the assumption of upstream normal flow is incorrect — the numerical model indicated that the growth of the cutoff requires a larger cutoff ratio λ than predicted by Equation 6.4.

Wang *et al.* (1995)

Wang *et al.* (1995) carried out a phase-plane stability analysis of the dynamics of a single channel splitting into two parallel branches ending in a lake. A similar study was carried out by Flokstra (1985). They assume that the sediment distribution at the bifurcation varies as specified by the following, symmetrical nodal point relation

$$\frac{S_1}{S_2} = \left(\frac{Q_1}{Q_2} \right)^k \left(\frac{B_1}{B_2} \right)^{1-k} \quad (6.5)$$

for some constant k , where S_j for $j = 1, 2$ are the sediment transport rates entering the two downstream branches with discharges Q_j ($j = 1, 2$) and widths B_j ($j = 1, 2$). The sediment transport capacity $S_{j,\text{cap}}$ is assumed to be given by

$$S_{j,\text{cap}} = B_j m \left(\frac{Q_j}{B_j h_j} \right)^n \quad (6.6)$$

where h_j is the water depth in branch j and m and n are empirical constants. From these equations a system of two coupled, non-linear, first-order differential equations for water depths h_1 and h_2 is derived (a summary of which is presented in Appendix C.2). The stability of the equilibrium with both branches open turns out to depend on the values of k and n . If $k < n/3$ the equilibrium is unstable, if $k > n/3$ it is stable. For the equilibria with just one branch open the reverse holds; they are stable if $k < n/3$. Both situations are sketched in

³The effect of the bifurcation angle on the sediment distribution is represented by the parameter σ in the work of Klaassen and Van Zanten (1989).

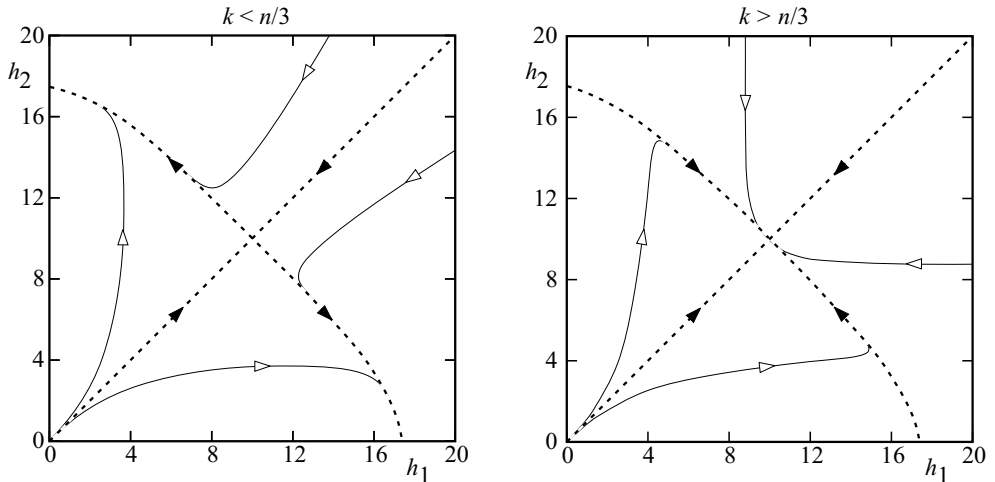


Figure 6.11: Phase diagrams indicating the changes in water depths h_1 and h_2 for a constant discharge. The equilibrium with both branches open is unstable if $k < n/3$. Symmetric case: two branches of equal length, slope, width and roughness.

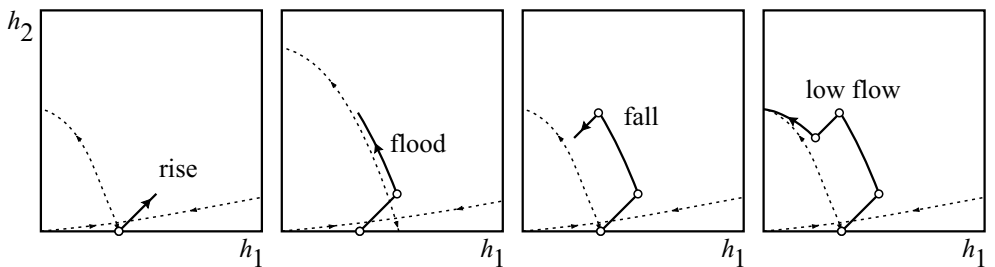


Figure 6.12: Phase diagrams indicating the development of a cutoff during and after a flood for a case with $k < n/3$. The development starts with the equilibrium situation that only the first branch is open. In the end, only the second branch, which is steeper and narrower, remains open.

Figure 6.11 for a case with two identical downstream branches. The condition for (in)stability of the equilibrium with both branches can also be derived using the approach by Klaassen and Van Zanten (1989); this has been shown in Appendix C.1.

What does this analysis learn us about the formation of a new channel? It is clear that in the case of $k > n/3$, even an initially small secondary streamlet would gradually enlarge such that a bifurcation point with two stable branches formed. In the other case ($k < n/3$) shown in Figure 6.11, the second channel cannot form. At first one might assume that this is the result of system dynamics near the equilibrium on the h_1 axis: any small deviation from the case of only channel 1 open is brought back to its original equilibrium by the system. But, in fact, it is caused by symmetry of the case considered: the phase diagrams have been plotted for two channels of equal length, slope, width and roughness. If the slope and width of the second channel is larger and smaller, respectively, the phase plane is not symmetric. Figure 6.12 shows how a rise in water levels during a flood may trigger a cutoff. The rise and fall of the flood have been assumed to be instantaneous, whereas the flood is assumed to be

significantly long on the morphological timescale. In a similar way quasi-periodic behaviour may be triggered by periodicity in the discharge variation.

One can conclude that the sediment distribution at the bifurcation point plays an important role in the channel formation process. Slingerland and Smith (1998) have formulated a physics-based model concept for determining the sediment distribution S_1/S_2 at a bifurcation. This approach has been used by them to predict whether an initially formed crevasse channel would heal or enlarge to form a complete avulsion.

Slingerland and Smith (1998)

Slingerland and Smith (1998) schematised the avulsion site using a one-dimensional numerical model of three branches as indicated in Figure 6.13. A crevasse channel has formed halfway the main channel at an elevation l (lip height) from the main channel bottom. The main mode of sediment transport is suspended load and the vertical distribution of the sediment concentration in the main channel is given by the Rouse profile

$$c(y) = c_r e^{a(y-y_r)/H} \quad (6.7)$$

where

- a the Rouse number equal to $-w_s/(kU_*)$,
- $c(y)$ suspended sediment concentration at height y ,
- c_r reference concentration for suspended sediment at height y_r , calculated using the modified Bagnold bedload transport formula given by Bridge and Bennett (1992), being proportional to the excess shear stress divided by the grain diameter,
- H water depth in the main channel at the crevasse entrance,
- k grain size parameter, assumed to have a constant value of 0.1,
- U_* bed shear velocity,
- w_s fall velocity,
- y vertical coordinate, and
- y_r reference height at which the reference concentration c_r is given, here the top of the moving bed layer ($y_r/H \approx 0$).

The sediment entering the crevasse channel originates from the upper part of the water column, which contains the lowest concentration of suspended sediment. The resulting average

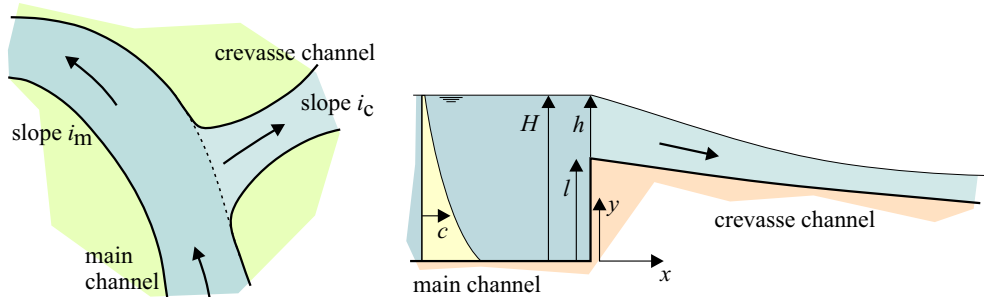


Figure 6.13: Channel and crevasse geometry as used by Slingerland and Smith (1998).

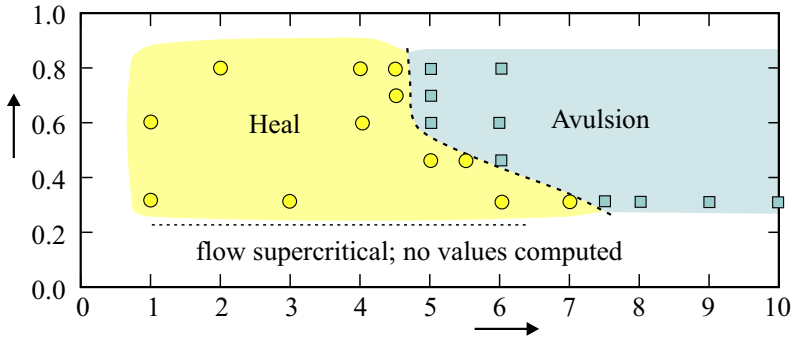


Figure 6.14: Predicted behaviour of the crevasse channel carrying very fine (0.1 mm) sand as a function of initial relative entrance height $\eta = 1 - (l/H)$ and relative bed slope λ . The circles mark the simulations that led to the closing of the crevasse; the squares mark the simulations in which the avulsion was completed. The width of the main channel and that of the crevasse were equal.

sediment concentration \bar{c} entering the crevasse channel is

$$\bar{c} = \frac{1}{h} \int_l^H c(y) dy = \frac{H c_{r0}}{a_0 h} \left(e^{a_0} - e^{a_0 l/H} \right) \quad (6.8)$$

where H , a_0 and c_{r0} are the water depth, Rouse number and reference concentration in the main channel just upstream of the offtake, and $h = H - l$ is the flow depth in the crevasse channel. If this concentration is smaller than the capacity of the crevasse channel erosion will occur, leading to deepening of the crevasse channel (the width is assumed constant) and lowering of the lip height l . This increases flow depth in the crevasse channel, but it also increases the sediment concentration entering the crevasse channel since the water from lower in the main channel has a higher sediment load, and it reduces the slope in the crevasse channel.

Numerical computations by Slingerland and Smith (1998) indicate that for coarse sand (0.4 mm diameter) the development of a crevasse channel depends on the slope of the crevasse channel while the influence of the water depth is negligible. Equation 6.4 indicates that the product $\eta \lambda^2$ is important for the development of cutoffs, a remnant of this relation is seen in the boundary between healing and avulsion for fine sand (0.1 mm) which is shown in Figure 6.14. Deviations from a threshold relation $\eta \propto \lambda^{-2}$ are caused by the depth dependence of the sediment distribution parameter σ via Equation 6.8, the large width of the crevasse channel ($\beta = 1$) and the redistribution of the discharge over the two channels.

6.4 Discussion

The documentation on the processes and mechanics of cutoffs is limited. The number of models on topics related to cutoffs is, therefore, also limited. The available models indicate that the stability of cutoffs depends on the relative dimensions of the cutoff channel, its resistance, the sediment type and the sediment distribution ratio at the upstream bifurcation.

The papers referred to in previous sections either do not specify the direction of the cutoff process or describe headward cutting of a channel. Joglekar (1971), for example, does not explicitly indicate the direction of the erosion process leading to the cutoff, but the lines indicating the shallow side channel in Figure 6.9 suggest erosion from downstream. Therefore, one might be easily tempted to conclude that channels always form by backcutting. In the case of hillslope processes this is probably true, but in rivers there might be another channel cutting process. There are at least two well documented examples from the Jamuna River where the cutoff process has occurred starting at the upstream side.

Figure 6.15 illustrates the cutting of a new channel through a braid bar complex near Bahadurabad during the flood of 1993. In March 1992 the main branch was following a slightly meandering course along the western side of the braid bar complex, while several smaller, intertwining channels broke up the braid bar complex. In March 1993 the bend of the main channel upstream of the braid bar complex had become much more acute: the channels through the bar complex had straightened and formed a finger-shaped pattern. The finger-shaped pattern at the upstream side of a bar complex is found — at least for the Jamuna River — to be an indication of the possibility that a cutoff may form (Mosselman, pers. comm. and FAP21/22, 2001). In March 1994 the cutoff had completed and the main channel has since been following a straight course through the former braid bar complex towards Bahadurabad. Meanwhile, the original main branch was reduced to a relatively small channel.

Figure 6.16 illustrates the more recent development of a cutoff channel near Kamarjani during the flood of 1999. The formation of the new channel had been expected for some time and it would probably have occurred in 1998 if it had not been that a bar migrated in front of the channel entrance. The newly formed channel is characterised by a straight, deep approach channel at the upstream side indicative of channel formation from the upstream side.

The examples above indicate that the channels may be formed from the upstream side although the process of channels forming from the downstream side (by means of backcutting) may be more common based on the literature in the previous sections. In the next chapter, a 2/3D numerical model will be used to investigate the processes involved. The purpose of these simulations is twofold: first, to determine a cutoff criterion for the branches model (see Section 5.4.3), and second, to determine the cause for either direction of channel formation.

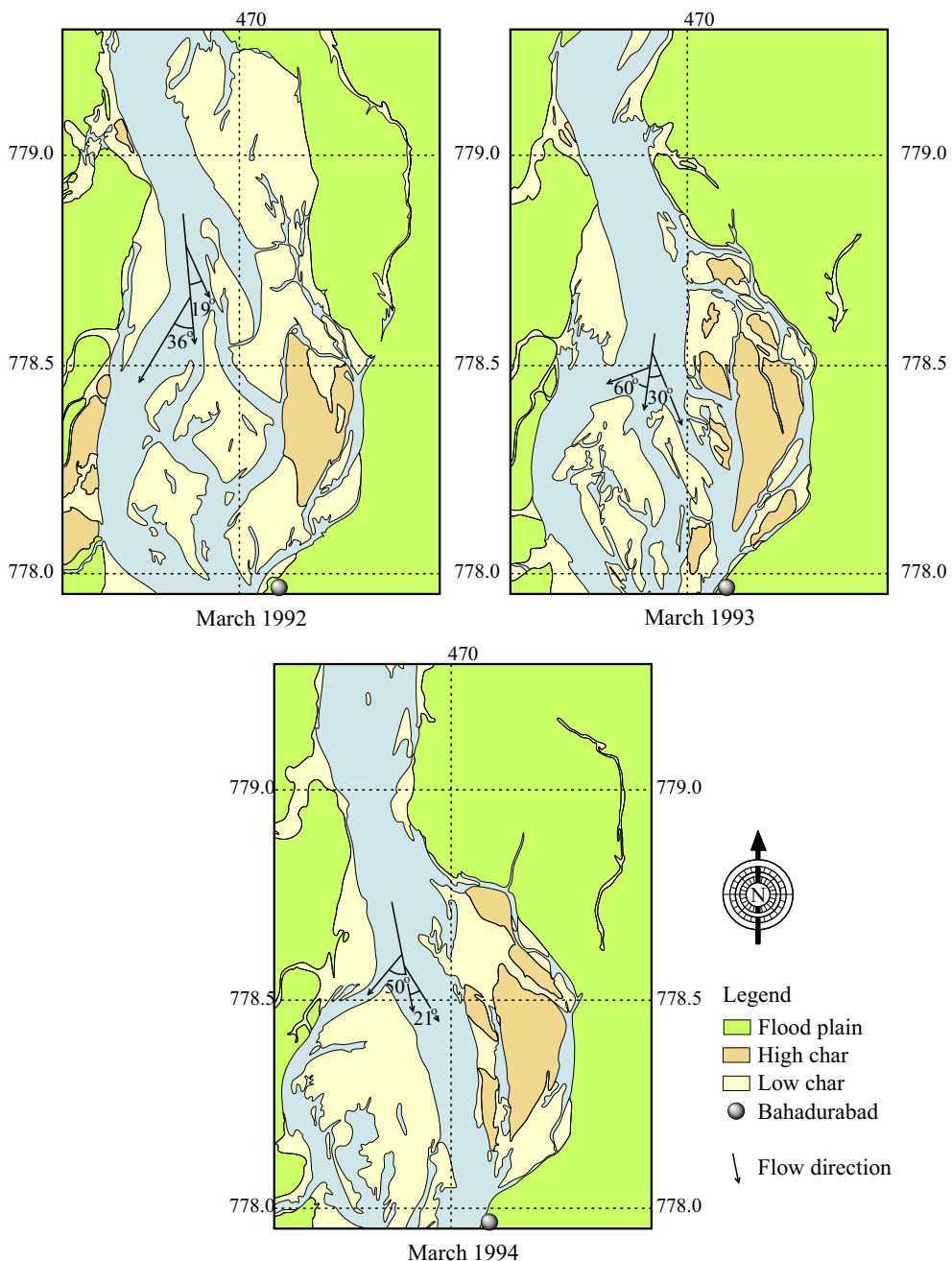


Figure 6.15: Changes of the planform of the bend and cutoff near Bahadurabad (River Survey Project, 1996).

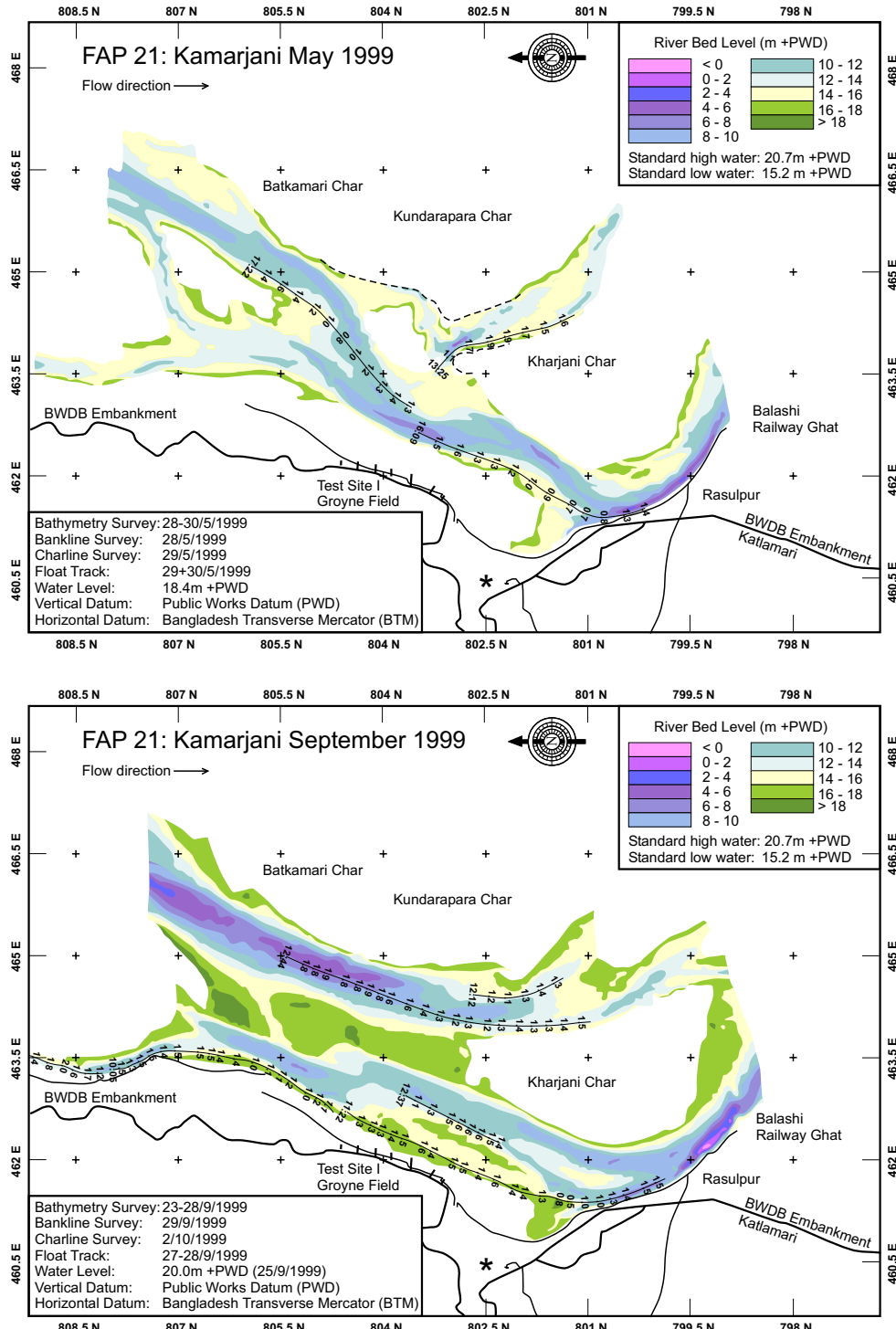


Figure 6.16: Planform changes near Kamarjani.

Chapter 7

Numerical modelling of cutoffs

The formation of a new channel is difficult to predict because it is significantly influenced by the local characteristics of the flood plain (such as elevation, sediment composition, presence of vegetation) and the unpredictability of the hydrograph. In the previous chapter, the literature was studied regarding the incision of new channels into the flood plain: both the formative processes and the mathematical modelling of cutoffs were described. We learnt that the formation process may start at either end, although backcutting (that is, the process starting at the downstream end) seems to occur more often. So far, the formation of channels has been studied using empirical relations and zero- or one-dimensional models (Section 6.2.2). These models neglect the effect of momentum and the processes selecting the location of the cutoff channel. Furthermore, the nodal point relation required for distributing the transported sediment over the two channels (the existing channel and the cutoff channel) significantly influences the behaviour of the channel system, as shown by Wang *et al.* (1995). Such a nodal point relation is not necessary in a two-dimensional model. Because of these aspects, we have used a two-dimensional approach in this study.

Morphological simulations of a bend cutoff have been carried out. The results of these simulations are presented in this chapter. The results are analysed to improve the understanding of the processes involved. The analysis is extended to determine why channels sometimes form from the downstream end and in other cases from the upstream end. Based on the dynamics observed in the simulations and the data from the literature study presented in the previous chapter, a new submodule for cutoff formation is proposed for the branches model.

This chapter starts with a short description of the morphological module of the Delft3D modelling system of WL | Delft Hydraulics that was used in the simulations. Subsequently, the model schematisation and simulation setup (such as bend geometry, discharge variation and timestepping) are described in Section 7.2. Section 7.3 presents and discusses the simulation results. The direction of channel formation is addressed in Section 7.4. The results are summarised in Section 7.5. Finally, this leads to an adaptation of the branches model with respect to the process of channel formation, which is formulated Section 7.5.1.

7.1 Overview of the simulation program

The simulations that are described in this chapter have been carried out using the Delft3D-MOR program from the Delft3D software package. Five modules can be distinguished within this program:

- **Main.** The main or steering module takes care of the switching and communication between the physical modules. Figure 7.1 shows the interaction of the various modules. This conceptual model is based on the assumption that, in general, the physical processes are sufficiently loosely coupled to allow the splitting of the dynamical system into separate modules, each addressing the dynamics of one sub-system (De Vriend, 1987). When, for instance, the hydrodynamics adapts, the bed levels are assumed to remain unchanged, and vice versa. The coupling of the processes is explicit: at every moment during the simulation only one module is active, which results in a basic decoupling of the various physical processes. The user can specify the order in which the modules are executed and the relative time frames of the various modules by means of a ‘process tree’. By selecting the number of timesteps to be spent in each module, the user may vary the coupling frequency between the processes, from an almost fully coupled approach to a quasi-steady approach.

In the latter case, the flow module iterates until the flow pattern reaches an equilibrium state, where after the sediment transport rates are determined and the bed levels are updated. As long as the bed level changes are relatively small, one can assume that the water levels and discharge distribution remain unaffected. Under these assumptions, it is possible to compute the new flow velocities using $\bar{u} = \bar{q}/h$ where \bar{q} is the local unit discharge vector and h is the local adjusted water depth. By using this approximation, generally referred to as continuity correction, one can directly continue with another morphological step (as indicated by the arrow labelled ‘constant flow pattern loop’ in Figure 7.1). In this way, the number of executions of the time-consuming flow module may be reduced significantly. In general, the quasi-steady time-stepping approach can be used when the morphological time scale is much larger than the hydrodynamic

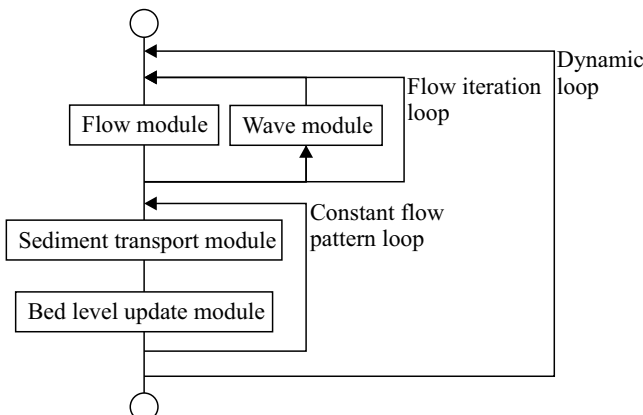


Figure 7.1: The main module of Delft3D-MOR controls the interaction of the four physical process modules.

time scale (Jansen, 1979). In our simulations we maintain a large part of the coupling between flow and morphology by frequently switching between flow and morphology modules.

- *Wave.* A wave module is part of the modelling system, but it is not used here.
- *Flow.* The flow module supports two modes: a three-dimensional mode and a two-dimensional mode with a parametrisation for the secondary flow (quasi three-dimensional). Both modes are based on the hydrostatic pressure assumption. The three-dimensional mode can be used in combination with the wave module, but it cannot be used in combination with the sediment transport module.
- *Sediment transport.* There exist two versions of the sediment transport module¹: a total transport module and a suspended transport module. The total transport module is to be used when the sediment transport rate is assumed to be given by a total transport formula depending on the local flow conditions, such as the formulae of Meyer-Peter and Müller (1948) and Engelund and Hansen (1967). Unless otherwise indicated, we will use the ‘general transport formula’, which allows the user to specify any power relation between the total sediment transport rate S and the Shields parameter θ . It is given by

$$S = \alpha D_c \sqrt{\Delta g D_c} \theta^b (\mu \theta - \theta_{cr})^c \quad (7.1)$$

where

- D_c characteristic user-specified grain size,
- g gravitational constant,
- Δ relative density of the sediment,
- α, b, c, μ various user-specified constants.

The suspended transport module distinguishes between bedload and suspended transport. This module should be used in conjunction with for example the sediment transport formula of Van Rijn (1984a), if the relaxation effect in the suspended sediment concentration cannot be neglected.

- *Bed level update.* The bed level update module implements sediment continuity. Spatial variations in the sediment transport rate result in local erosion or sedimentation.

A short description of the basic equations and the discretisation used by the flow, sediment transport, and bed level update modules of Delft3D-MOR is given in Appendix C.3.

7.2 Model description

7.2.1 Initial topography and boundary conditions

In order to keep the geometry as simple as possible, an artificial bend was used in the simulations. Its dimensions, the sediment properties and the boundary conditions were chosen to

¹ Actually, there are currently four versions; besides the ones mentioned in the text there exists a silt version and a graded sediment version. The graded sediment version of the transport module has an associated graded sediment bed level update module.

match the data from the Jamuna River. The modelled channel is 500 m wide; its depth is uniform (3.5 m) at the in- and the outlet and cosine-shaped away from the boundaries with the centre of the channel at about -7 m and the sediment size is 200 μm . The geometry was obtained in two steps. First, a curvilinear representation of the main channel was created consisting of five straight sections connected by four bends of 80 degrees each. The channel bed was imposed on this curvilinear grid. These elevation data were then combined with an elevation of +7 m around the edges of the model and interpolated onto a rectangular grid with gridcells of 50 m \times 50 m (See Figure 7.2). This gave the initial topography, to which a uniform slope of 7×10^{-5} in mean flow direction was added. At the inlet and outlet the flood plain was removed from the model to get well defined in- and outflow sections. All other bend geometries studied here have been constructed in a similar way.

Each simulation concerned a flood peak of 320 hours (that is, almost 2 weeks) during which the discharge at the upstream boundary varied as shown in Figure 7.3. The simulated period is much shorter than the yearly flood period of the Jamuna River but the total variation in simulated water levels (about 4 m) is of the same order of magnitude as the variations in the prototype (see Figure 2.7). The simulation period has been determined using a — for the Jamuna River representative — choice of parameters such that there was significant morphological development, but not a complete cutoff. Due to the extensive flooding and drying that occurs during the passage of the flood wave, it was not immediately clear that a quasi-steady approach would be acceptable. For example, non-steady phenomena during flooding or drying might be of importance for the morphological development. However, limitations of the software package prevented a completely unsteady approach, which has led to the stepped schematisation of the hydrograph: each time the boundary conditions are kept constant for

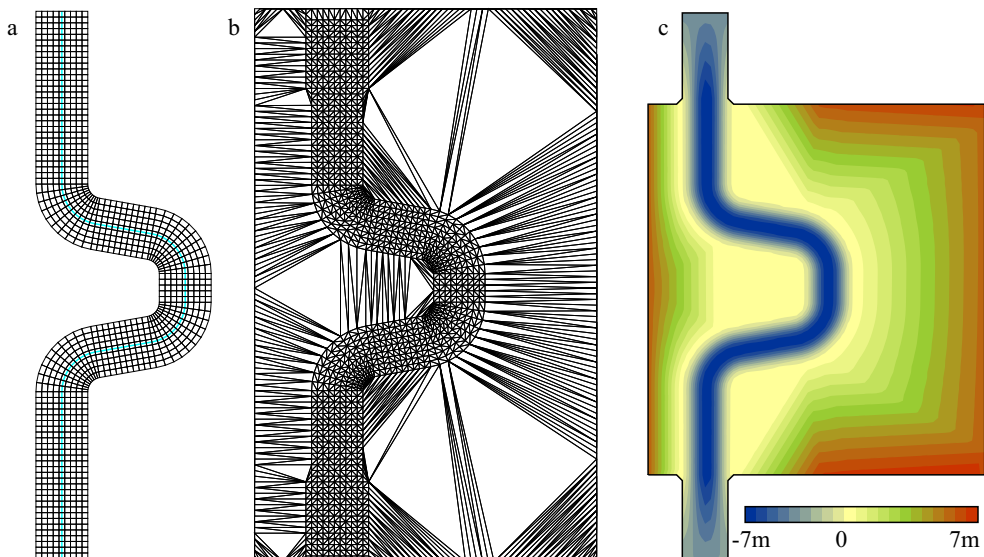


Figure 7.2: Construction method of the model topography. a: initial curvilinear model of the channel. b: triangular interpolation of the flood plain elevations. c: the final situation: the initial bed topography defined on a rectangular grid.

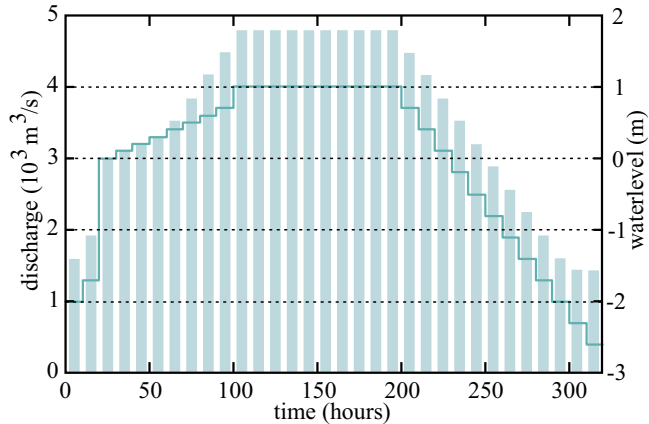


Figure 7.3: Boundary conditions for the reference simulation. Discharge variation (bars) at the upstream boundary, and the water level variation (line) at the downstream boundary.

a period of ten hours (except during the peak of the flood, when the boundary conditions remain unchanged for a period of 100 hours)².

Each step of the hydrograph was handled in the same way. After adapting the boundary conditions, the flow field was allowed to stabilise until the velocities throughout the modelling area changed less than 1 cm/s per minute ('flow iteration loop' in Figure 7.1). After this process of flow stabilisation (during which bed levels remained constant) the morphological modules were activated. The interaction between flow and morphology was taken into account by alternating executions of the flow and morphology modules for one minute each. So, referring to Figure 7.1, the 'dynamic loop' was used instead of the 'constant flow pattern loop'. The internal timestep in the flow module was 0.1 minute, so the bed levels were effectively updated every 10th timestep of the flow computations. Figure 7.4 shows this switching between modules as a process tree. Each step of the hydrograph was covered by a separate run of the simulation program, which was restarted from the end result of the previous run. This was done for two reasons. Firstly, if the complete hydrograph had been simulated using a single run, the process tree would have been much more complicated: it would have consisted of 23 subtrees of the type used now. Secondly, splitting the simulation into separate runs made the simulations less vulnerable to computer crashes. Each simulation took approximately 3 days of computer time.

The large step in the downstream boundary condition at $T = 20$ hours as shown in Figure 7.3 is an artefact, which was necessary in combination with the quasi-steady approach. During the flooding of the flood plain no stationary state could be reached unless the downstream water level was raised to approximately flood plain level. During the falling stage of the flood this problem did not occur because morphological developments had changed the terrain sufficiently to allow for a stable state.

As indicated in the previous section, the flow module can run in either three-dimensional mode or two-dimensional mode with (or without) a parametrisation for the secondary flow.

²Recent adaptations in the modelling system gave the opportunity to verify that this schematisation has not significantly affected the simulation (see Appendix D.3)

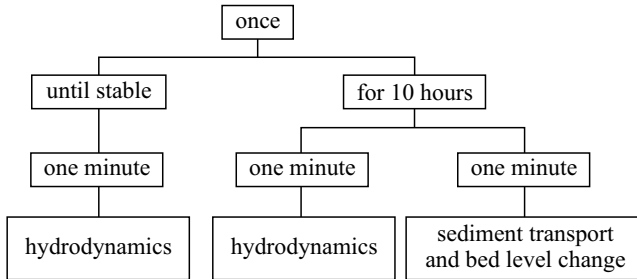


Figure 7.4: Process tree used in the simulations. Each simulation period starts with an iteration on the hydrodynamics until the flow field has sufficiently stabilised. Subsequently the sediment transport rates and bed levels are updated after each minute of the flow computation.

In the present study, the flow module has been used in two-dimensional mode. This has been done for three reasons:

1. There is no physical reason that requires a three-dimensional approach: the topography is relatively smooth, the flow accelerations and decelerations are small, and there is no stratification due to salinity or temperature.
2. A three-dimensional model would make the simulations computationally even more expensive.
3. The current version of the program does not allow the flow module running in three-dimensional mode to be combined with the morphology modules.

However, an important restriction, forced upon this study by the simulation program, was the inability to include the effects of secondary flow. Although an option for this was included in the program, severe problems were encountered when this feature was combined with the drying and flooding of the flood plain. Secondary flow effects and drying and flooding had been used extensively before in models of estuaries. There are two reasons why this did not lead to similar problems. Firstly, in tidal areas the flow field and sediment transport is averaged over a tidal period, which reduces the effect of an incidental extreme value in the spiral flow intensity. In the present simulations no significant averaging was applied. Secondly, in the estuarine areas often suspended sediment transport submodels are used, whereas the present study focused mainly on total load transport formulations. It had to be assumed that the spiral flow — although it plays an important role in the morphodynamics of river bends in general (see Section 3.2) — is not crucial for the simulation of the bend cutoff: the spiral flow plays, therefore, a smaller role in the development of the cutoff than in the shaping of the bed of the main channel bend. This assumption could be made plausible by referring to the fact that streamline curvature (the dominant quantity generating the spiral flow) is less important in the relatively straight cutoff channel. As the problems encountered have been solved since, this assumption could be verified. It turns out that the neglect of the spiral flow effect has not significantly influenced the results of the simulations. For a discussion of the verification simulations, the reader is referred to Appendix D.4.

7.2.2 Reference simulation

The reference simulation used to study the effects of these aspects is the same in all cases. The boundary conditions of this reference simulation are shown in Figure 7.3. The roughness throughout the reference model is given by a constant Manning value of $0.02 \text{ s/m}^{1/3}$ and the applied (total load) sediment transport relation reads

$$s = 1.9 \cdot 10^{-4} \theta^{1.25} \quad (7.2)$$

where θ is the Shields parameter. This transport formula is of the same type as the one derived from measurement data of Bangladeshi rivers (see Equation 3.1), but it is characterised by a lower exponent. This reference case was chosen based on the stage of development of the cutoff in an initial set of simulations for the reference hydrograph shown in Figure 7.3. An analysis of the influence of the sediment transport relation on the formation of the cutoff (Section 7.3.4) suggests that a similar morphological development could have been obtained using another combination of calibration factor α and exponent c in Equation 7.1.

Figure 7.5 shows three snapshots of the simulation of this reference case. The first frame shows the river flowing through the initially imposed artificial meander. The second frame shows the river at the end of the flood peak, where after the flood starts to recede and the last frame shows the situation as it is at the end of the simulation. The largest change in the channel pattern occurs during the peak flood and the recession period. During the flood the velocity on the flood plain reaches a magnitude of 2 m/s. Locally, a large amount of sediment is transported due to these high flow velocities. The bed levels and water levels along two sections are also shown in Figure 7.5. The lines of both sections are indicated in the three plan views.

- AA The first section (5 km long) runs in a straight line from the inflow boundary to the output boundary except for the central part where it is shifted to follow a course across the lower part of the flood plain (approximately following the course of the cutoff). The irregularities in the initial bed level along this section result from the discrete nature of the line followed by this section caused by the underlying model grid.
- BB The second section (3 km long) follows a straight, transverse line through the centre of the flood plain.

In the upstream reach most changes have taken place by the end of the flood period. At that time most of the downstream shift of the pointbar (PB) has also occurred although the downstream end of the pointbar has not significantly lowered. This suggests that the sediment transport capacity increases only slightly along section AA across the pointbar. The upstream side of the pointbar is characterised by an expansion wave, the downstream side by a shock wave. During the subsequent falling of the flood, most erosion occurs at the downstream end of the pointbar, indicating that the sediment transport capacity increases significantly across the pointbar. The lowering of the whole pointbar during this phase is clearly visible in both sections. During this phase of the simulation significant morphological changes also occur in the downstream reach. The bend in the main channel triggers the development of alternate bars (and eventually meandering) in the downstream reach. The sediment used to built up the first alternate bar originates in these simulations mainly from the reshaping of flood plain area FP2 (downstream of the pointbar). The alternate bars appear as shallow areas in the plot of section AA.

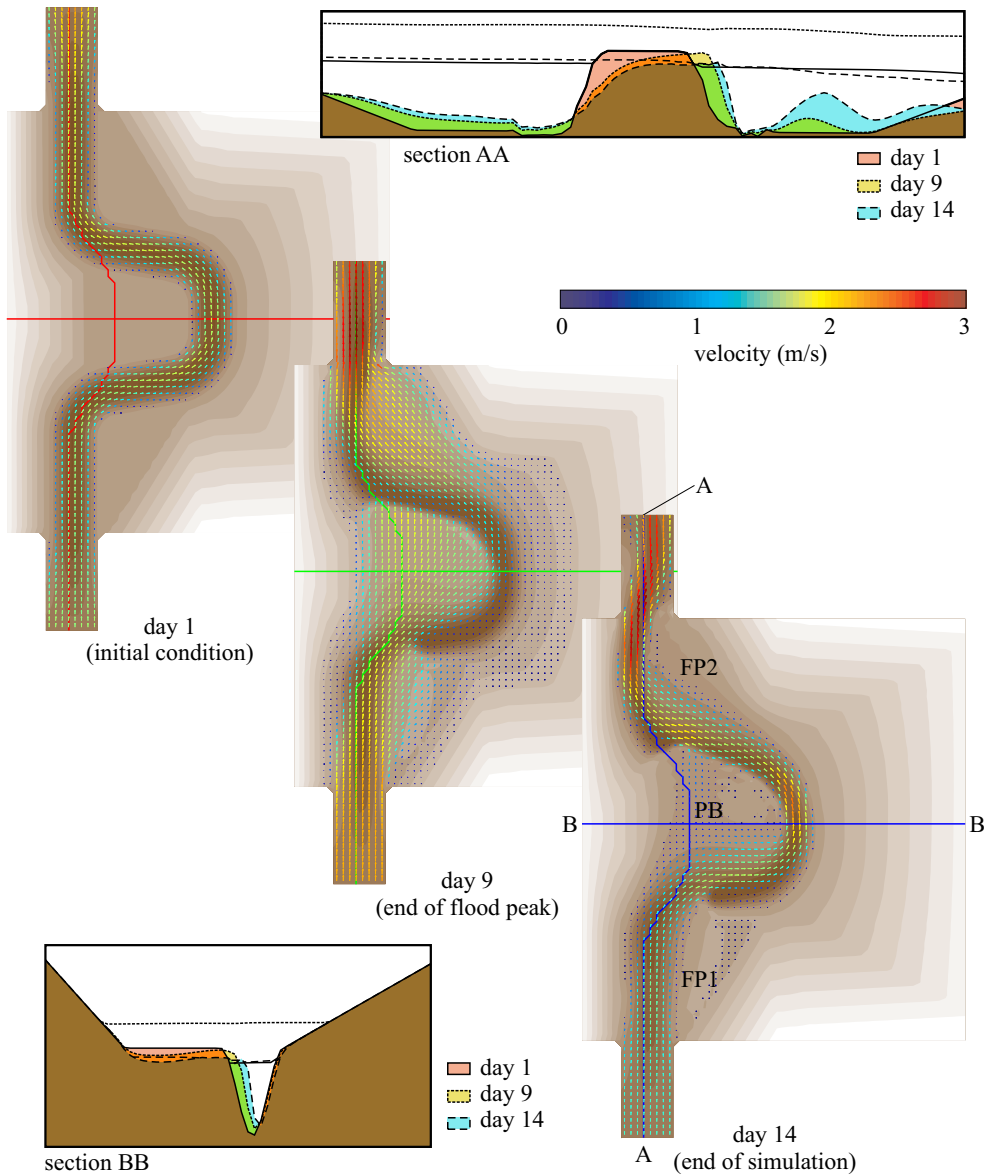


Figure 7.5: Flow field and bed topography in reference case at the start of the simulation, after the flood peak and at the end of the simulation. The bed levels and water levels along two sections AA and BB are also shown.

7.3 Simulations

There are many aspects that can influence the formation of a new channel. Roughly speaking, these aspects can be divided into three categories:

- *hydrodynamics* related, such as the imposed flow boundary conditions (characteristics of rising, peak and falling periods of the flood), the roughness and the eddy viscosity (magnitude and spatial distribution), and the assumed flow structure (secondary and more general 3D flow).
- *sediment transport* related, such as the applied sediment transport relation (bedload and/or suspended load, critical shear stress), the sediment type (sediment size, uniform or graded, (non)cohesive),
- *geometry* related, such as the shape of the bend (extent, width and approach angle of the flow) and the flood plain elevations.

In Chapter 6 it has been concluded that there are two ways in which cutoff channels form, namely, either from the upstream end or from the downstream end. The selection mechanism that leads to the formation of the channel in either way, must depend on the variation of the net sediment transport capacity (transport capacity minus sediment supply from upstream) and the local availability of sediment along the course of the cutoff channel to be formed. Without an understanding of the selection mechanism, a general description of the process of cutoff formation cannot be given. Because variations in sediment availability cannot be modelled adequately in the state-of-the-art numerical models, we will — at least initially — consider only variations in the net sediment transport capacity. These variations are determined by the water level slope across the pointbar and the sediment transport formulation. We have, therefore, selected the following aspects for a sensitivity analysis:

- *discharge Q , downstream water level z_w and roughness formulation C or n .* These three quantities are the main factors determining the water level slope across the pointbar.
- *critical shear stress θ_{cr} and exponent c of the sediment transport relation.* These quantities determine — together with the calibration factor, which only influences the time scale — the transport formula.

For each of these aspects a number of simulations has been carried out. The results of these simulations are presented and analysed in the first four subsections. The analysis consists of a qualitative comparison of the planform changes and morphological changes along section AA (as defined in Figure 7.5) and a quantitative comparison of the following variables (see Figure 7.6)

- Δs shift of the downstream end of the pointbar measured along section AA (the downstream end of the pointbar has been defined as the grid point at which the bed level gradient along section AA is largest),
- ΔA integral of the pointbar erosion in the vertical plane of section AA,
- Δz_c average pointbar erosion along section AA, determined as the quotient of ΔA and the distance $\Delta s'$ over which erosion occurred,

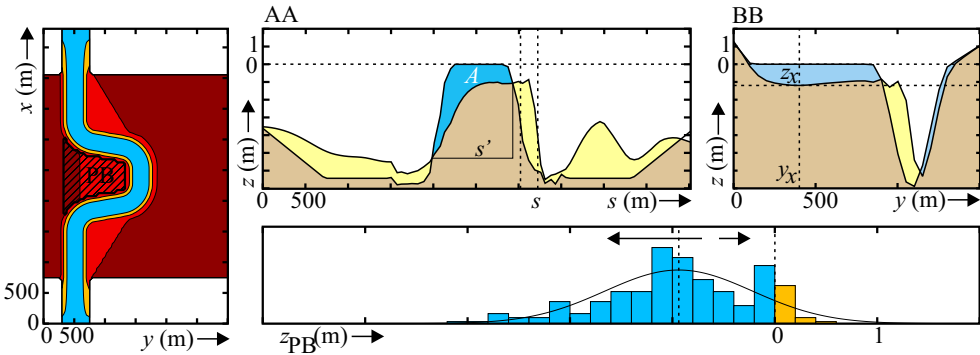


Figure 7.6: Graphical definition of the variables Δs , ΔA , y_x , Δz_x and Δz_{PB} (μ and σ) used to quantify the development of the cutoff. The leftmost plot indicates the pointbar area PB used in the computation of ΔV_{PB} , μ and σ .

- y_x location of deepest part of the cutoff channel in cross-section BB,
- Δz_x maximum erosion of the pointbar in cross-section BB (i.e. the erosion at location y_x),
- Δz_{PB} bed level change of the grid points³ on the pointbar within the area PB indicated in the leftmost plot of Figure 7.6 (quantified using mean μ and standard deviation σ), and
- ΔV_{PB} total volume eroded from the pointbar, i.e. $\sum \Delta x \Delta y \Delta z_{PB}$ where the summation is carried out over all eroded points within the area PB.

An overview of all simulations is given in Table A.3 and Figures A.1–A.3. The CD that accompanies this thesis contains data files of all simulations and a program to interactively inspect them. The last subsection discusses simulations for two other geometries. The definition of the quantities described above depends to a large extent on the initial topography and the resulting shape and location of the cutoff. Therefore, the results obtained for different geometries have only been compared qualitatively.

7.3.1 Upstream boundary: discharge

The influence of the discharge has been investigated by carrying out two simulations with a lower discharge ($\Delta Q = -10$ and -25% , respectively) and four simulations with a higher discharge ($\Delta Q = +10$, $+25$, $+50$ and $+100\%$, respectively). The resulting planforms are shown in Figure A.4. The quantitative results have been summarised in Table 7.1.

As could be expected the cutoff channel has established itself furthest during the simulation with the highest discharge. Changes in the magnitude discharge affect both the height of the pointbar and the migration distance in downstream direction. This can also be observed in the long-section plot in Figure 7.8. The shift Δs of the downstream edge of the pointbar

³Only grid points at which the bed level was changed by more than 1 cm during the simulation were included in the analysis.

nr	ΔQ %	Δs m	ΔA 10^3 m^2	Δz_c m	y_x m	Δz_x m	Δz_{PB}		ΔV_{PB} 10^6 m^3
							μ m	σ m	
1	0	202	1.42	1.51	900	1.20	0.94	0.72	0.57
2	-25	131	0.78	0.86	850	0.43	0.43	0.50	0.26
3	-10	131	1.16	1.25	900	0.88	0.74	0.64	0.45
4	+10	202	1.62	1.71	900	1.49	1.11	0.79	0.68
5	+25	262	1.90	1.98	900	1.87	1.28	0.91	0.83
6	+50	322	2.28	2.34	850	2.41	1.59	1.04	1.05
7	+100	1004	2.70	2.76	800	3.24	2.03	1.15	1.40

Table 7.1: Overview of the simulations carried out with increased/decreased discharge. All simulations use the same downstream water levels as the reference case, a Manning's roughness coefficient of $0.02 \text{ s/m}^{1/3}$, and sediment transport parameters $\alpha = 16.77$, $c = 1.25$ and $\theta_{cr} = 0$.

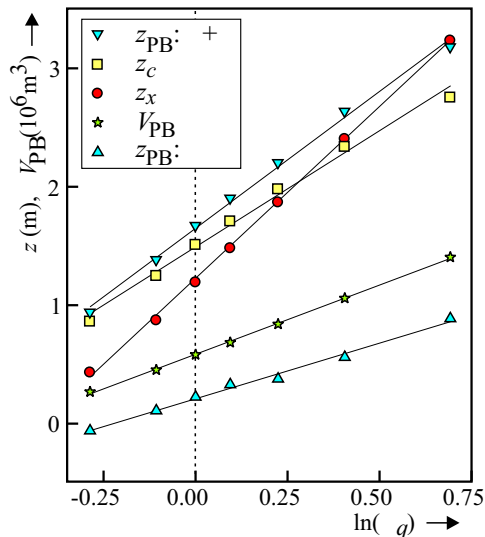


Figure 7.7: Graph of the data in Table 7.1. The magnitude of the erosion (quantified in different ways) depends linearly on the logarithm of $\alpha_q = 1 + (\Delta Q/100)$.

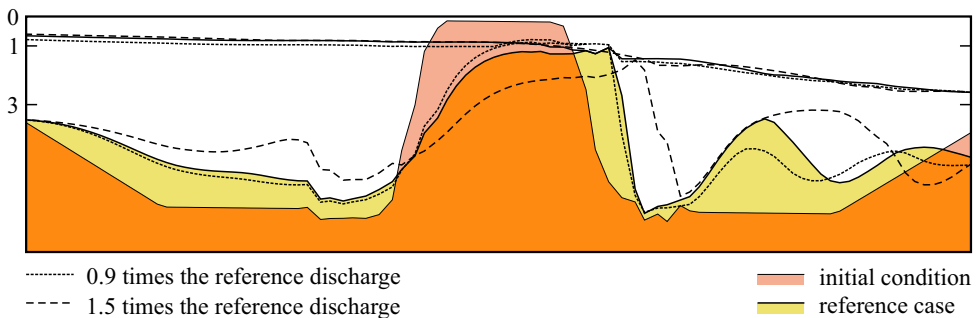


Figure 7.8: Bed and water levels along section AA (see Figure 7.5) for simulations with a 10% reduced and a 50% increased discharge relative to the reference simulation, respectively.

increases (between $\Delta Q = -25\%$ and $+50\%$) approximately linearly as a function of ΔQ , and thus of Q . The sudden increase in migration distance for the last simulation ($\Delta Q = +100\%$) may, at least partially, be attributed to the flow convergence in the downstream reach, which locally increases the sediment transport capacity. Based on the y_x values, one may conclude that there is a slight tendency for the cutoff channel to straighten for small and large discharges. Even though topographic steering (at low discharges) and flow momentum (at high discharges) could explain this behaviour, one must be careful to draw definite conclusions from the variation in y_x since this quantity is clearly influenced by the coarseness of the grid.

Most other results are plotted in Figure 7.7 against the natural logarithm of the multiplication factor α_q of the discharge: $\alpha_q = 1 + (\Delta Q/100)$. The discharge dependency of the quantities plotted can be approximated by linear functions of $\ln(\alpha_q)$, e.g. $\Delta z_x \approx 1.22 + 2.90 \ln(\alpha_q)$. Note that, for small discharge changes, i.e. $\alpha_q \approx 1$, $\ln(\alpha_q)$ can be approximated by $\Delta Q/100$, such that these relations become also linear in ΔQ , and thus Q . The quantity ΔA is characterised by a similar dependency on the discharge. Since the total volume of the pointbar is finite, these relations cannot be expected to hold for much larger discharges, although a higher discharge Q may result in a steepening of the channel and, thereby, lead to the erosion of the cutoff channel below the original base level. If, instead of the magnitude of the discharge, the duration of the flood peak would be increased, the maximum erosion depth would be determined by the equilibrium conditions for the highest discharge (see Section 7.3.5).

An increase of the discharge Q leads to an increase of the flow velocity u and associated shear stress τ on the pointbar. The relation between τ and Q depends on the shape and roughness of the flood plain (flow confinement). The resulting increase in sediment transport capacity, which depends on the transport relation, leads to an increase in the development rate of the cutoff channel. For the selected geometry, sediment transport relation and hydrograph the erosion turns out to depend linearly on the logarithm of the discharge. Finally, it should be noted that in all simulations the cutoff channel formed from the upstream side.

7.3.2 Downstream boundary: water level

The influence of the downstream water level has been investigated by carrying out two simulations with a lower downstream water level (-0.50 and -0.25 m, respectively) and two with a higher downstream water level ($+0.25$ and $+0.50$ m, respectively). Again, all other parameters remained unchanged during these simulations. It should be noted that the back-water effect of the downstream boundary influences a large part of the model. The initial water levels at the upstream boundary for the simulations with a 0.50 m raised and lowered downstream water level, respectively, differ by about 0.35 m. During the simulations this difference becomes smaller. The resulting planforms of all simulations are shown in Figure A.5. The quantitative results have been summarised in Table 7.2.

Inspection of the results shows that when the downstream water level is lowered, the cutoff development accelerates. A lower downstream water level leads to a smaller water depth on the point bar, which causes in an increase of the flow velocities on the pointbar. The change in downstream water level has less effect on the velocity in the main channel because the relative change in water depth in the main channel is smaller. The increased velocities on the flood plain accelerate the formation of the cutoff channel. Figure 7.10 shows the morphological development along section AA. From this plot one can conclude that the main difference

nr	Δz_w m	Δs m	ΔA 10^3 m^2	Δz_c m	y_x m	Δz_x m	Δz_{PB}		ΔV_{PB} 10^6 m^3
							μ m	σ m	
1	0.00	202	1.42	1.51	900	1.20	0.94	0.72	0.57
8	+0.50	131	1.15	1.25	900	0.89	0.72	0.66	0.46
9	+0.25	131	1.27	1.37	900	1.04	0.83	0.69	0.51
10	-0.25	202	1.54	1.62	900	1.36	1.04	0.75	0.63
11	-0.50	202	1.65	1.72	900	1.51	1.15	0.78	0.68

Table 7.2: Overview of the simulations carried out with increased/decreased downstream water level. All simulations use the same discharges as the reference case, a Manning's roughness coefficient of $0.02 \text{ s/m}^{1/3}$, and sediment transport parameters $\alpha = 16.77$, $c = 1.25$ and $\theta_{cr} = 0$.

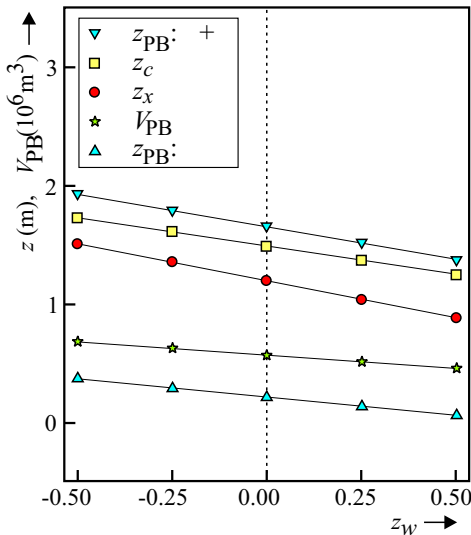


Figure 7.9: Graph of the data in Table 7.2. The magnitude of the erosion (quantified in different ways) depends linearly on the change in downstream water level Δz_w .

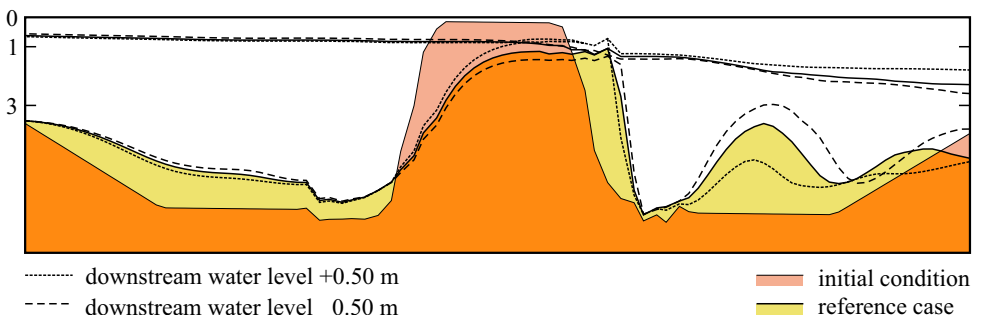


Figure 7.10: Bed and water levels along section AA (see Figure 7.5) for simulations with a 0.50 m higher and a 0.50 m lower downstream water level than the reference simulation, respectively.

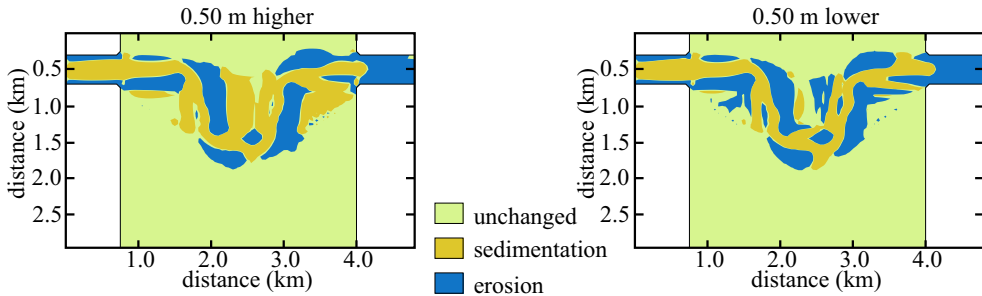


Figure 7.11: Net erosion and sedimentation pattern after the first 28 hours of simulation for a 0.50 m higher/lower downstream water level. In the case with a lower downstream water level erosion occurs initially at the downstream end of the pointbar.

regarding the cutoff development (i.e. considering differences in the area of the pointbar only) is remaining height of the pointbar; the downstream shift is similar for the two extreme cases (downstream water level 0.50 m higher/lower). Note that the water levels are now the same at the upstream boundary. Figure 7.9 shows that there is a linear relationship between the variation of the downstream water level and the erosion of the pointbar.

The lowering of the downstream water level causes an increased acceleration of the flow across the pointbar. This effect is not enough to trigger the cutoff process to start at the downstream side. The end results of the simulations do not show any tendency for such a switch: all shallow cutoff channels have formed from the upstream side. However, intermediate results indicate that some erosion did occur at the downstream side. In the case of a 0.50 m lower downstream water level erosion occurs initially at both the upstream and downstream side, whereas erosion occurs only at the upstream side when the downstream water level is raised by 0.50 m (see Figure 7.11).

Based on the results presented in this section, one can conclude that the cutoff channel formation is strongest for a low downstream water level. A lower downstream water level favours the formation of a cutoff from the downstream side, but this aspect did not play an important role in the simulations presented here. This effect can become more important if the downstream water level is lowered further. The influence of the downstream water level on the rate of cutoff development can be important in a tidal area or just upstream of the confluence with another river of similar magnitude. This is for instance the case near Aricha along the Jamuna River, just upstream of the confluence with the Ganges River, where the relative timing of the flood peaks of the two rivers influences the morphological changes (see Section 2.2.2).

7.3.3 Roughness

To investigate the influence of the bed roughness on the cutoff development, simulations have been carried using seven different roughness settings. Four simulations used a uniform Manning coefficient ($n = 0.015, 0.020, 0.025$ and $0.030 \text{ s/m}^{1/3}$, respectively) and the remaining three used a uniform Chézy coefficient ($C = 45, 60$ and $75 \text{ m}^{1/2}/\text{s}$, respectively). The simulation with a Manning coefficient of $0.020 \text{ s/m}^{1/3}$ corresponds to the reference simulation discussed in the previous sections. All other parameters remained unchanged during these

simulations. The resulting planforms are shown in Figure A.6. The quantitative results have been summarised in Table 7.3. The simulations indicate that an increase of the roughness (higher n , lower C) leads to more erosion of the pointbar and an increased development rate of the cutoff.

Table 7.3 shows that the results obtained for $C = 45$ and $60 \text{ m}^{1/2}/\text{s}$ are almost identical to those for $n = 0.020$ and $0.015 \text{ s/m}^{1/3}$, respectively. From this observation a characteristic water depth h of about 55 cm has been derived, which was used to convert between Chézy and Manning formulations using the relation $C = h^{1/6}/n$. It is not clear how this characteristic water depth is related to the actual water depth on the pointbar during the simulation since it is mostly larger than 1 m and the maximum water depth of about 2 m on the pointbar is maintained for about one third of the simulation. The results of all seven simulations have been plotted in Figure 7.12 as function of the (effective) Manning and Chézy coefficients. The dependence on the Manning's coefficient turns out to be almost linear although some deviations from this overall trend are visible; this implies also a linear dependence on the inverse of the Chézy coefficient. A comparison of Figures 7.9 and 7.12 shows that the effect of changing the bed roughness is — for the studied geometry — in the same order of magnitude as the effect of changing the downstream water level by at most 0.50 m up or down.

Figure 7.13 shows the computed bed levels (along section AA) for three cases: $C = 45 \text{ m}^{1/2}/\text{s}$, $n = 0.020 \text{ s/m}^{1/3}$ (reference case) and $n = 0.025 \text{ s/m}^{1/3}$, respectively. The figure shows the effect of the water depth dependence of the relation between the two considered roughness parametrisations: Manning's n and Chézy. The end result of the $C = 45 \text{ m}^{1/2}/\text{s}$ simulation agrees in the shallow pointbar area with the $n = 0.020 \text{ s/m}^{1/3}$ (reference) case, in the deeper downstream reach with the $n = 0.025 \text{ s/m}^{1/3}$ case and with a still higher value of n in the upstream reach. This indicates that the correspondence between simulations with different roughness formulations is not so well defined as the observations of only the pointbar area in Table 7.3 may suggest.

An increase of the bed roughness in a numerical model influences the hydrodynamics and sediment transport in three ways: it slows down the flow, it leads to flow redistribution in

nr	roughness $n \text{ s/m}^{1/3}$ $C \text{ m}^{1/2}/\text{s}$	Δs	ΔA	Δz_c	y_x	Δz_x	Δz_{PB}		ΔV_{PB} 10^6 m^3
		m	10^3 m^2	m	m	m	μ	σ	
1	$n = 0.020$	202	1.42	1.51	900	1.20	0.94	0.72	0.57
12	$n = 0.015$	131	1.09	1.18	900	0.91	0.73	0.60	0.44
13	$n = 0.025$	202	1.67	1.75	900	1.47	1.10	0.81	0.69
14	$n = 0.030$	262	1.86	1.94	850	1.71	1.23	0.86	0.78
15	$C = 75$	131	0.94	1.03	850	0.69	0.61	0.54	0.37
16	$C = 60$	131	1.13	1.23	850	0.87	0.75	0.61	0.44
17	$C = 45$	202	1.45	1.54	850	1.21	0.92	0.72	0.58
18*	$C = 75$	322	2.58	2.66	850	3.02	2.00	1.11	1.22
19	$C = 30\sqrt{h}$	202	1.95	2.02	950	1.93	1.33	0.95	0.83

Table 7.3: Overview of the simulations carried out with different roughness coefficients. All simulations use the same boundary conditions as the reference case and sediment transport parameters $c = 1.25$ and $\theta_{cr} = 0$. The calibration coefficient α of the sediment transport formula is equal to 16.77 for all simulations except nr. 18, which uses 60.37.

favour of shallow areas and it increases the bed shear stresses. Figure 7.12 shows that the combined effect is a net increase of the development rate of the cutoff channel. In the following the three effects are discussed individually.

1. *Slowing down the flow* Combining the continuity equation $q = hu$ (where q is the discharge per unit width: Q/B) and the Chézy relation $u = C\sqrt{hi}$ one can derive that under equilibrium slope conditions, the velocity is given by $u = q^{1/3}C^{2/3}i^{1/3}$ and the water depth is given by $h = q^{2/3}C^{-2/3}i^{-1/3}$. According to these relations, the velocity decreases and the water depth increases if the Chézy coefficient decreases, i.e. as the roughness increases. This is also true in our model (see Figure 7.14), although the equilibrium slope condition is not fulfilled. A lower velocity is generally associated with a smaller sediment transport rate. So, based on only this first effect, the overall morphological development rate should (at least initially) decrease as the roughness increases. One should note that the sediment transport rate reduction leads to upstream sedimentation and, therefore, to an increase of the slope which eventually may compensate for the increased roughness/resistance.
2. *Redistributing the flow* The second effect of the roughness is more subtle. The water level changes due to the first effect, which in turn results in a redistribution of the discharge over the cross-section. Flow in the shallow areas may, for instance, increase due to flooding as the water level rises. The discharge distribution will become more and more uniform as the water level rises further. This effect is amplified if a depth dependent roughness formulation like that of Manning is used: the roughness decreasing effect of a change Δh in water depth is larger in shallow areas. The redistribution of the discharge is accompanied by a redistribution of the sediment transport. So, an overall increase in roughness results, via the rise of the water level and the redistribution of

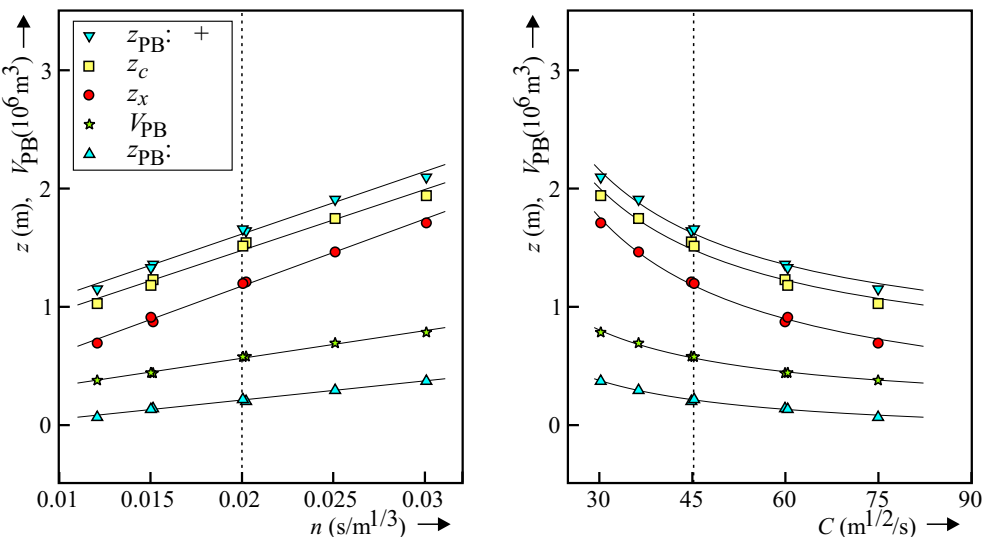


Figure 7.12: Graph of the data in Table 7.3. The magnitude of the erosion (quantified in different ways) depends approximately linearly on the effective Manning's roughness coefficient n (left plot). The same data is plotted as function of the Chézy coefficient in the right plot.

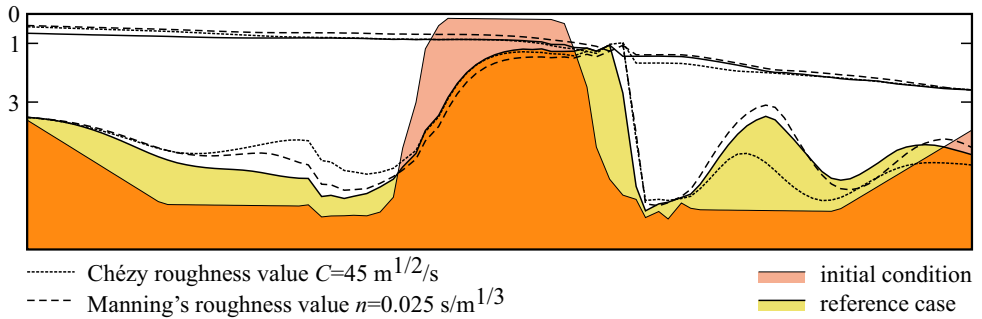


Figure 7.13: Bed and water levels along section AA (see Figure 7.5) at the end of the simulations with a roughness coefficient $n = 0.020 \text{ s}/\text{m}^{1/3}$ (reference case), $n = 0.025 \text{ s}/\text{m}^{1/3}$ and $C = 45 \text{ m}^{1/2}/\text{s}$, respectively.

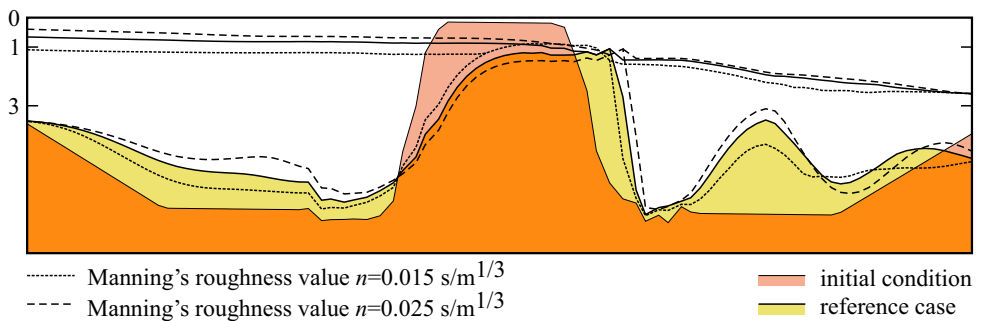


Figure 7.14: Bed and water levels along section AA (see Figure 7.5) for simulations with a Manning's roughness coefficient n of 0.015, 0.020 (reference case) and $0.025 \text{ s}/\text{m}^{1/3}$, respectively. A higher roughness is associated with a larger water depth.

the flow, in a relative increase of the sediment transport rates in the shallow areas: this favours cutoff development.

3. *Changing the bed shear stresses* Most sediment transport formulations in use today have been derived from flume experiments with an alluvial bed under equilibrium conditions. Under these conditions the the bed roughness (either grain roughness or bedform roughness, see Section 3.1) is the dominant factor determining the flow resistance. Under equilibrium conditions with only bed roughness, the bed shear stress τ_b is on average⁴ equal to $\rho_w g u^2 / C^2$. The bed shear stress, generally represented by the Shields parameter $\theta = u^2 / (C^2 \Delta D_{50})$, determines the sediment transport rate. This is the third influence of the roughness parameter: it directly influences the computed bed shear stress and, therefore, the sediment transport rate. A higher roughness is associated with a larger bed shear stress and thus a higher sediment transport rate.

All simulations described so far have been using the sediment transport relation given by Equation 7.2, which is proportional to $\theta^{1.25}$ and thus to $C^{-2.5}$. Therefore, an increase in roughness from $n = 0.015$ to $0.025 \text{ s}/\text{m}^{1/3}$, or from $C = 75$ to $45 \text{ m}^{1/2}/\text{s}$, results in a direct increase of the sediment transport rate by a factor of $(0.025/0.015)^{2.5} =$

⁴The average is taken over time (turbulent fluctuations) and space (perturbation due to bedforms).

$(75/45)^{2.5} \approx 3.6$. The results presented in Table 7.3 show, however, that the net increase in the cutoff development rate is limited to a factor of 1.6. So, the reduction of the flow velocities (effect 1) compensates a significant part of this third effect of a change in roughness.

If the change in roughness is not of alluvial origin — it may, for instance, represent the presence of vegetation — this third effect may not be realistic. It is possible to (partially) compensate for this effect by adjusting the calibration factor α in Equation 7.2. This approach has been studied qualitatively by repeating the simulation with a Chézy coefficient of $75 \text{ m}^{1/2}/\text{s}$ wherein α had been increased from 16.77 to 60.37. The results are shown in Figure 7.15. Whereas the net effect of a decrease in roughness (in the example from $C = 45$ to $75 \text{ m}^{1/2}/\text{s}$) is normally an decrease of the morphological activity on the pointbar (left plot), the effect — in absence of the effect on the bed shear stress computation — is an increase of the morphological activity on the pointbar (right plot). The presence of uniform vegetation on a pointbar may, therefore, reduce the probability of a cutoff channel formation. However, if there is a gap in the vegetation cover, the probability of channel formation at that location will be increased due to flow convergence.

The simulations indicate that the type of roughness formulation (i.e., Manning or Chézy) does not have a large influence on the formation of the cutoff. Only the effective average roughness of the pointbar is important. To study whether this conclusion holds if the roughness depends more strongly on the water depth, an extra simulation has been carried out using $C = 30\sqrt{h}$.⁵ The results of this simulation are shown in Figure 7.16. The changes are slightly larger than in the case of $n = 0.030 \text{ s/m}^{1/3}$, which may be explained by a slightly higher effective roughness. However, there is one planform feature that was not present in any of the previous simulations: the bar downstream of the pointbar (originating from flood plain area FP2 as defined in Figure 7.5) has an indentation at the upstream side. This suggests the formation of

⁵The relatively large exponent of 0.5 in this relation was applied in morphological studies on the Jamuna River and Ganges River (see Sections 3.4 and 4.3.2).

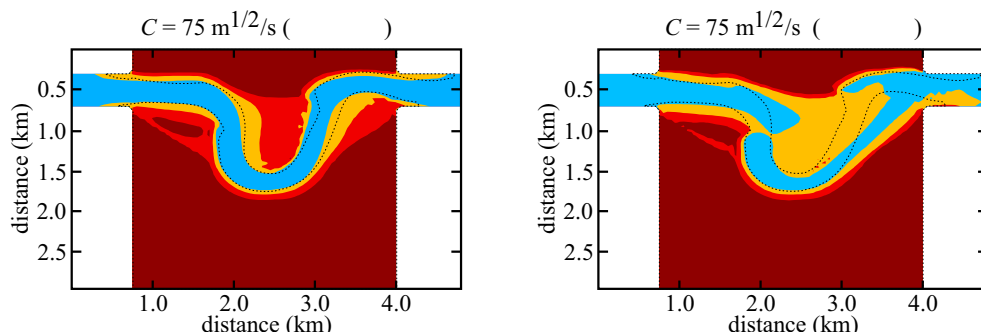


Figure 7.15: The effect of the roughness on the bed shear stress. Both plots show the results of simulations with $C = 75$ and $45 \text{ m}^{1/2}/\text{s}$ (continuous and dotted lines, respectively). The $C = 75 \text{ m}^{1/2}/\text{s}$ simulation in the left plot used the same transport formula as the $C = 45 \text{ m}^{1/2}/\text{s}$ simulation ($\alpha = 16.77$, $S(\theta)$ constant). The $C = 75 \text{ m}^{1/2}/\text{s}$ simulation in the right plot has been carried out using a calibration coefficient $\alpha = 60.37$ to compensate for the change in roughness from $C = 45$ to $75 \text{ m}^{1/2}/\text{s}$ ($S(u)$ constant).

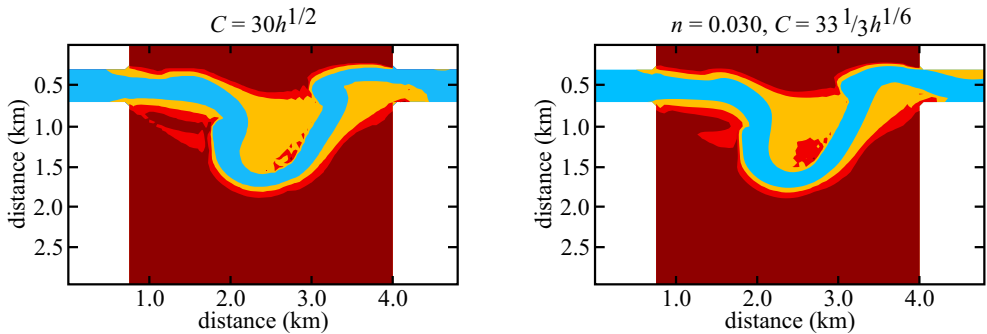


Figure 7.16: On the left the result of a simulation with a depth-dependent Chézy roughness given by $C = 30\sqrt{h}$. The result of a simulation with $n = 0.030 \text{ s/m}^{1/3}$, that is, $C = 33^{1/3}h^{1/6}$ is repeated for comparison on the right.

a second (smaller) cutoff downstream. So, the stronger depth-dependence of the roughness may result in a tendency to form more cutoffs and, possibly, even to form a more braided planform.

Based on the simulations reported in this section one may conclude that the net effect of an increase in (alluvial) roughness is an increase in the rate with which the cutoff channel forms. This is the result of three interacting effects: slowing down the flow, redistributing the flow in favour of the shallow areas and increasing the bed shear stress. The last effect is related to the assumption that the specified roughness represents only alluvial bed roughness. This basically limits the use of these numerical models (and the conclusions derived from them) to cases where vegetation plays only a minor role. Finally, it should be noted that in all simulations the cutoff channel formed from the upstream side.

7.3.4 Sediment transport relation

In the previous sections the discharge and the roughness formulation have been varied without influencing the direction of the cutoff formation. Although lowering the downstream water level did initially cause some erosion along the downstream edge of the pointbar, the cutoff channel still formed in all cases from the upstream end. So, none of the hydrodynamic aspects listed at the beginning of Section 7.3 on page 185 has had the desired effect. Will a change in sediment transport parameters be able to change the direction of cutoff formation?

Thus far we have not changed the nature of the sediment transport relation: Equation 7.1 has been used with $D_c = 200 \mu\text{m}$, $b = 0$, $\mu = 1$, $\theta_{\text{cr}} = 0$ and $c = 1.25$. The calibration coefficient α was generally equal to 16.77. In the following, seven simulations are presented and discussed in which the coefficients c (1.25, 1.83 and 2.5, respectively) and θ_{cr} (0.0, 0.25, 0.50 and 1.0) have been varied. It should be noted that these values for θ_{cr} are extremely high compared to the critical Shields parameter in, for instance, the Meyer-Peter and Müller formulation, i.e. 0.047. The higher values are considered here to investigate the possible effects of cohesion and vegetation cover. The calibration factor α has been adjusted such that the sediment transport rate remains the same for all simulations for a certain value of the Shields parameter θ . The quantitative results have been summarised in Table 7.4. Figure 7.17 shows all the sediment transport relations used for Shields parameter θ between 0 and 4.

nr	α	c	θ_{cr}	Δs	ΔA	Δz_c	y_x	Δz_x	Δz_{PB}		ΔV_{PB}
	-	-	-	m	10^3 m^2	m	m	m	μ	σ	10^6 m^3
1	16.77	1.25	0.00	202	1.42	1.51	900	1.20	0.94	0.72	0.57
20	15.00	1.83		322	2.19	2.21	850	2.12	1.40	0.97	0.85
21	13.19	2.50		322	3.01	3.02	800	4.06	1.95	1.42	1.19
22	8.70	1.83		202	1.31	1.38	850	1.00	0.81	0.68	0.48
23	4.08	2.50		131	1.19	1.25	850	0.82	0.69	0.64	0.40
24	27.00	1.25	1.00	131	1.22	1.27	750	0.85	0.73	0.66	0.41
25	20.96	1.25	0.50	131	1.36	1.43	850	1.03	0.88	0.69	0.51
26	18.45	1.25	0.25	202	1.37	1.45	850	1.08	0.90	0.70	0.53

Table 7.4: Overview of the simulations carried out with different roughness coefficients. All simulations use the same boundary conditions as the reference case and a Manning's roughness coefficient of $0.02 \text{ s/m}^{1/3}$.

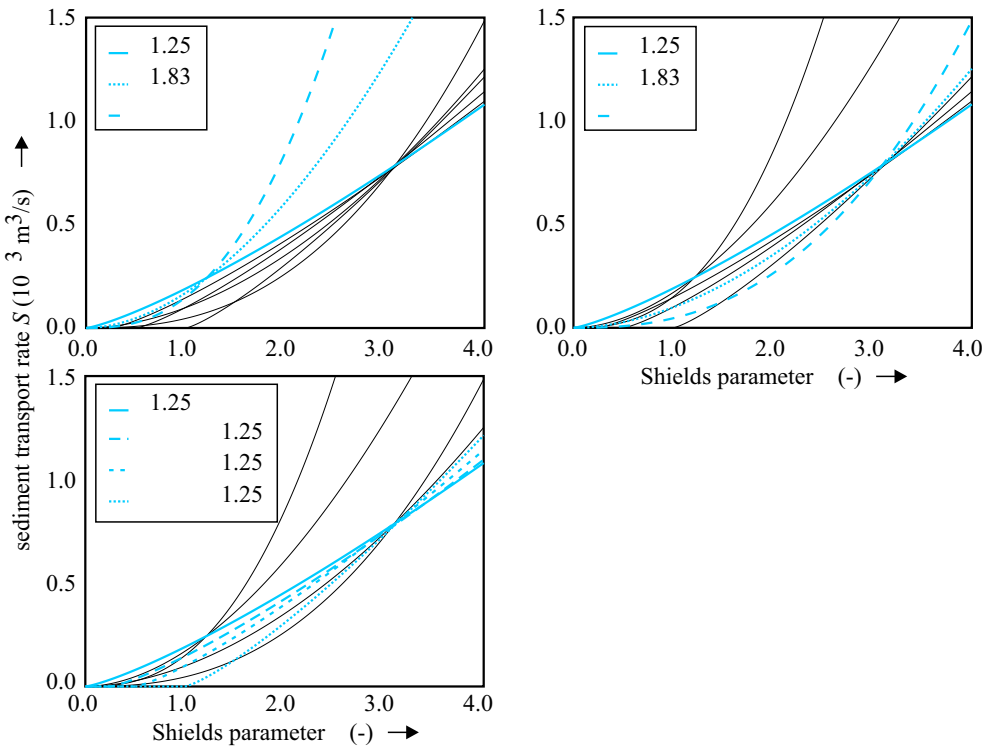


Figure 7.17: Sediment transport relations used in the simulations. Thin lines refer to transport relations in other subplots.

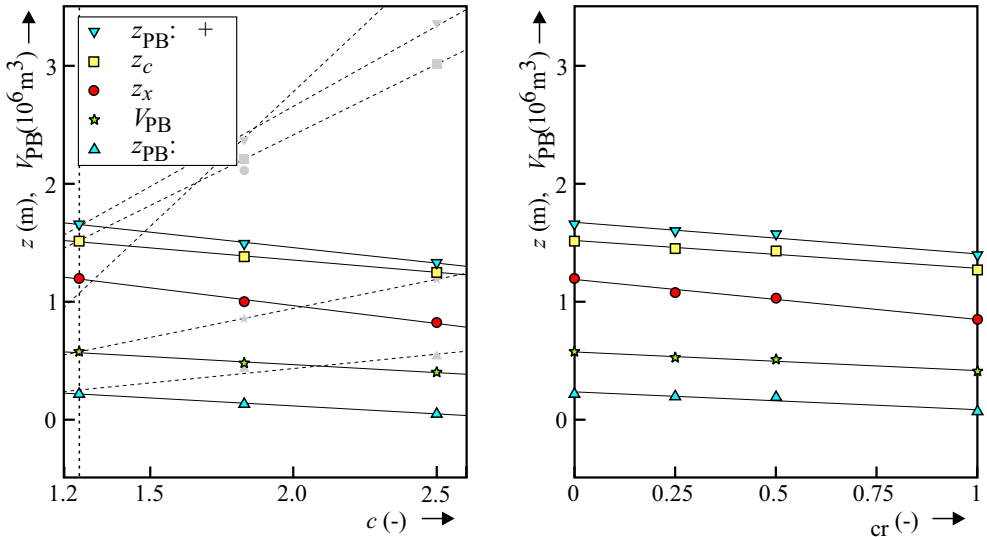


Figure 7.18: Graph of the data in Table 7.4. The magnitude of the erosion (quantified in different ways) depends approximately linearly on the exponent c (left plot) and the critical Shields parameter θ_{cr} (right plot). It should be noted that this includes an adaptation of the calibration factor α . The dotted lines and grey markers in the left plot refer to the first set of simulations.

In the first set of simulations the exponent c has been increased from 1.25 to 1.83 and 2.5. The exponent of 1.83 was actually based on measurements in the Jamuna River⁶, the other two values (among which the reference case of 1.25) were chosen to be smaller and larger, respectively. In this first set of simulations, the calibration coefficient α was adapted such that for a Shields parameter θ in the range of 1 to 1.4 the sediment transport capacity was similar for all three simulations. This range of Shields parameters corresponds, for a roughness of about $C = 60 \text{ m}^{1/2}/\text{s}$, to velocities between 1.1 and 1.3 m/s. The corresponding sediment transport relations have been plotted in the upper-left plot of Figure 7.17. Because the average velocity over the pointbar turned out to be much higher than 1.3 m/s (sometimes reaching 2 m/s) the total sediment transport rate increased significantly for increasing values of the exponent. This is visible in the planforms plotted in Figure A.7 and the plot along section AA in Figure 7.19. Because the newly formed channel in the case of $c = 2.50$ follows a slightly straighter course than section AA itself, the cutoff seems to be not complete in Figure 7.19. The results of these simulations have been plotted in Figure 7.18 using grey markers and dotted trend-lines. The rate of cutoff formation increases linearly or faster as c increases. It should be noted that this includes already a slight adjustment of the calibration factor α as indicated in Table 7.4.

Since the pivot value of θ was clearly too small in the first set of simulations, the simulations with $c = 1.83$ and 2.50 have been repeated using smaller calibration coefficients. This resulted in identical sediment transport rates for $\theta = 3.1$ (which corresponds to a velocity of about 1.9 m/s for $C = 60 \text{ m}^{1/2}/\text{s}$). The new transport relations are shown in the upper-right plot of Figure 7.17. The bed and water levels along section AA at the end of these simulations are plotted in Figure 7.20. The difference between the simulations are now much

⁶The value of 1.83 is based on slightly older information than the value of 1.82 used in Equation 3.1.

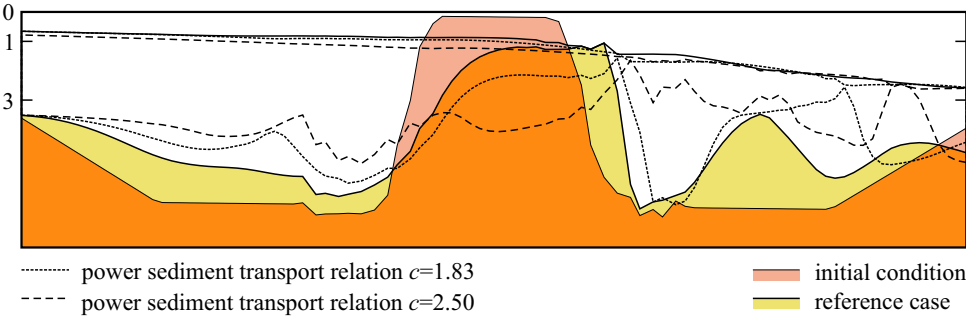


Figure 7.19: Bed and water levels along section AA (see Figure 7.5) for simulations with an exponent c in the sediment transport relation equal to 1.25 (reference case), 1.83 and 2.50, respectively. The calibration coefficient of the sediment transport relation was computed such that there is equal mobility for a Shields parameter of about 1.2.

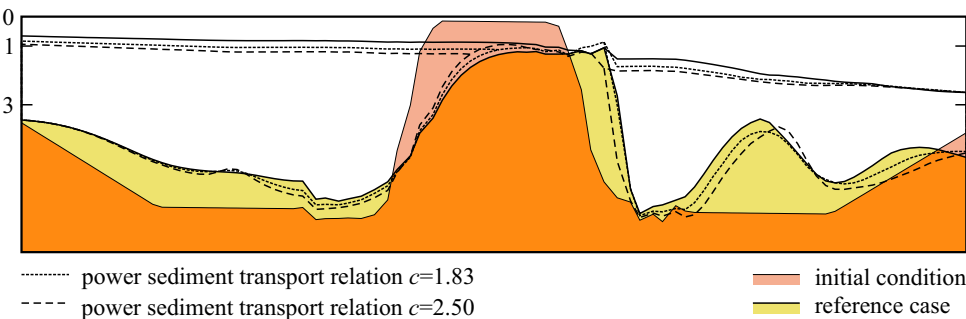


Figure 7.20: Bed and water levels along section AA (see Figure 7.5) for simulations with an exponent c in the sediment transport relation equal to 1.25 (reference case), 1.83 and 2.50, respectively. The calibration coefficient of the sediment transport relation was computed such that there is equal mobility for a Shields parameter of about 3.1.

smaller. The behaviour of the model for increasing c is similar to that for increasing values of the critical Shields parameter θ_{cr} . Both increasing the value of the exponent and increasing the critical shear stress result in a steepening of the sediment transport relation when the average sediment transport rate is kept constant (compare the upper-right and lower-left plots of Figure 7.17). The effect of an increase in θ_{cr} on the morphological development along section AA is shown in Figure 7.21 and the computed planforms are shown in Figure A.8. The steepening of the sediment transport relation (due to an increase of either c or θ_{cr}) leads to a decrease in the sediment transport rate at low velocities, which results in an overall slower cutoff development. The trend in the erosion of the pointbar is the same in both cases as shown by Figure 7.18.

During the simulation with $\theta_{cr} = 1$, the downstream edge of the pointbar becomes increasingly irregular (see the final planform plotted in Figure A.8). The irregular shape indicates that the morphological development is locally sensitive to small fluctuations in the velocity, i.e. the bed shear stress. Although the irregularities do not form straightaway and although they seem mostly to be related to selective sedimentation instead of selective erosion, they point to a sensitivity of the system that is related to the formation of headcuts. If the critical

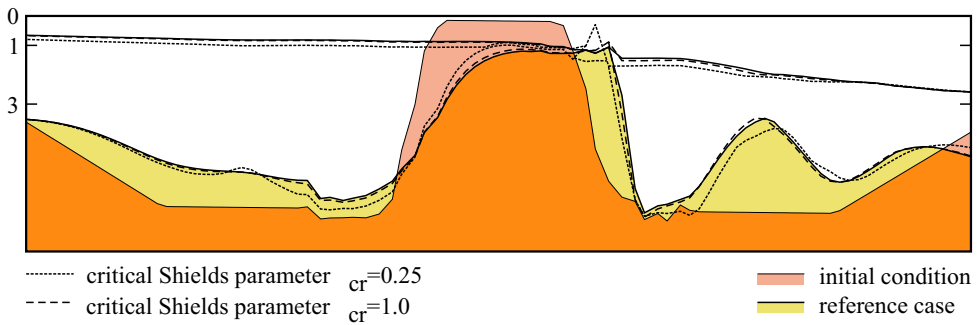


Figure 7.21: Bed and water levels along section AA (see Figure 7.5) for simulations with a critical Shields parameter of 0 (reference case), 0.25 and 1.0, respectively.

shear stress in an area subject to the possibility of erosion is very high, it is likely that the threshold is exceeded only at one or a small number of locations. The exceedance of the threshold may occur either due to locally slightly higher velocities or slightly lower threshold values. These high critical shear stresses may be related to the presence of vegetation/roots, cohesive properties of the sediment or a coarse imbrication layer. Once the protective top layer is erosion, more loosely packed non-cohesive layers of sediments may be exposed. When this occurs, the critical shear stress drops significantly and the erosion rate may increase accordingly. In this way an initial gully could develop which can grow further by attracting a larger part of the flow. The numerical model requires, however, that the same critical shear stress is applied everywhere throughout the simulation, which prevents us from investigating this topic any further in the standard program. Section 7.4.2 continues this line of research.

The simulation results presented in this section indicate that, after proper calibration, similar overall planform changes can be obtained using all sediment transport formulae. There are, however, two characteristics that seem to depend critically on the parameters c and θ_{cr} : the depth of the newly formed channel and the irregularity of the downstream pointbar edge. If both c and θ_{cr} are small, sediment is transported almost everywhere and the cutoff channel can easily form. An increase of either c or θ_{cr} results — in combination with an adjustment of the calibration coefficient α to keep the average sediment transport rate constant — in a steepening of the sediment transport curve. This causes a relative reduction in the sediment transport rates on the pointbar and the cutoff channel develops, therefore, relatively slowly. If the sediment transport curve is steep, small fluctuations in the flow velocity can result in large changes in the sediment transport rate. If such variations occur along the downstream edge of the pointbar, gullies may form. These gullies may initiate the formation of a cutoff channel from the downstream end.

7.3.5 Geometry

All simulations presented thus far have focused on the morphological development of a single geometry (i.e., the initial planform as presented in Figure 7.2). This geometry, in the following referred to as geometry 1, is characterised by a main channel with four 80 degree bends. Simulations have been carried out for three other geometries (geometries 2, 3 and 4).

nr	geometry - flow char.	Δs	ΔA	Δz_c	y_x	Δz_x	Δz_{PB}		ΔV_{PB} 10^6 m^3
		m	10^3 m^2	m	m	m	μ	σ	
1	1	202	1.42	1.51	900	1.20	0.94	0.72	0.57
27	2 0 h	262	0.87	1.14	850	1.12	0.25	0.48	0.40
28	2 100 h	322	1.34	1.75	850	1.87	0.40	0.75	0.65
29	2 200 h	443	1.65	2.14	850	2.40	0.52	0.94	0.85
30	3	60	0.75	0.66	1600	0.41	0.25	0.43	0.47
31	4	181	1.19	1.01	2150	0.64	0.46	0.56	0.83
32	4 rev.	50	0.22	0.45	2300	0.00	0.17	0.43	0.38

Table 7.5: Overview of the simulations carried out for different geometries. All simulations use the same boundary conditions as the reference case (except simulations 27 and 29, see main text), a Manning's roughness coefficient of $0.02 \text{ s/m}^{1/3}$, and sediment transport parameters $\alpha = 16.77$, $c = 1.25$ and $\theta_{\text{cr}} = 0$.

These simulations were based on the same sediment transport relation used in the reference simulation, that is, the general transport formula with $\alpha = 16.77$, $c = 1.25$ and $\theta_{\text{cr}} = 0$ as specified in Equation 7.2. The results are summarised in Table 7.5.

The bends in geometry 2 are longer than those in geometry 1: the main channel of geometry 2 turns at each bend over an angle of 110 degrees (80 degrees for geometry 1). The planform of geometry 2 can be characterised as a simplified meander just before a neck cutoff due to lateral migration (see Figure 7.22). The total size of the 'pointbar' is larger, but the inflow channel directs the discharge towards the narrowest part of it. Three simulations have been carried out for this geometry. The simulations differ in the length $T_{Q_{\max}}$ of the maximum discharge period: 0 (short flood), 100 (reference flood) and 200 hours (long flood), respectively. The hydrograph of the second case (100 hours) is identical to the reference case of geometry 1 (shown in Figure 7.3). Although the total amount of sediment eroded from the pointbar is about the same for simulations 1 and 28, the erosion occurred in a smaller area for geometry 2 (simulation 28) and, therefore, the final depth of the cutoff channel is larger in that case. Contrary to simulation 1, in which erosion occurred at every point on the pointbar, a significant part of the eroded sediment is deposited on the central part of the pointbar in simulation 28, while the remainder of the pointbar remains unaltered. The simulations 27 and 29 with the shorter and longer flood periods, respectively, show a similar behaviour. Furthermore, the results of those simulations confirm indicate that once the initial channel has formed, the cutoff formation slows down in agreement with the relaxation towards an equilibrium: $\Delta z = \Delta z_{\max}(1 - e^{-t/T_{\text{rel}}})$.

Geometry 3 is composed of bends of 90 degrees and the channel leading to the outflow boundary is shifted towards the left relative to the upstream channel. In the case of geometry 2 there is a well defined shortest path across the pointbar (other paths are significantly longer) that is almost the same as the overall shortest path for the flow. The distance across the pointbar of geometry 3 is less sensitive to deviations from the shortest path across the pointbar. Furthermore, the shortest path across the pointbar is not the same as the overall shortest path for geometry 3. Consequently, the flow across the pointbar is much more concentrated for geometry 2 than for geometry 3 (see Figure 7.23). This results in a lower transport capacity for geometry 3 and, thus, the cutoff channel has not completely formed by the end of simulation 30 for geometry 3 (see Figure 7.22).

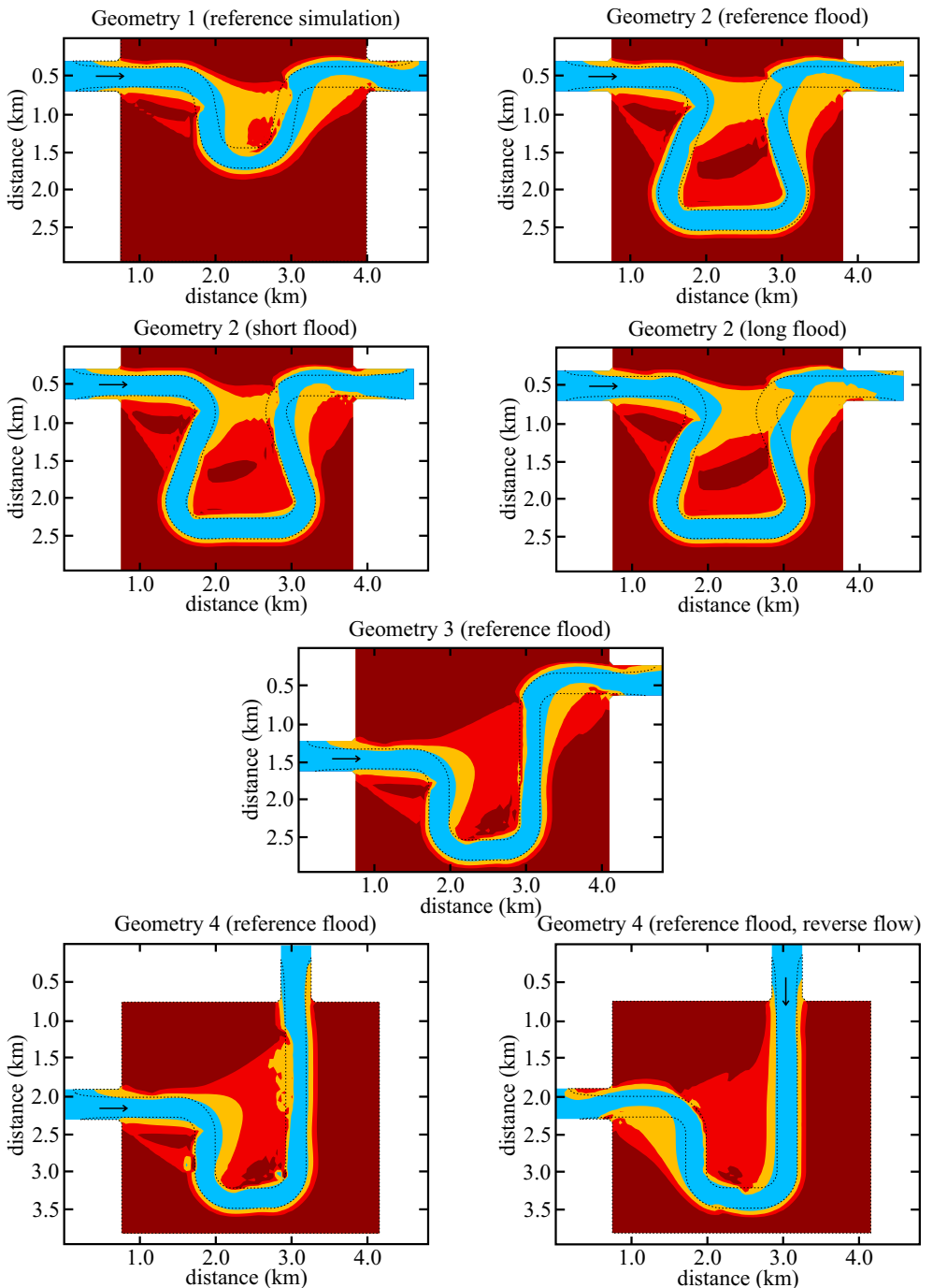


Figure 7.22: Results of simulations for various geometries and varying flooding period. The maximum flood height has been maintained for 100 hours during the reference flood, 0 hours for the short flood, and 200 hours for the long flood. The contour lines are drawn at 0, -1, and -3 m, the dotted line is the -3 m contour of the initial planform. The arrows indicate the flow direction.

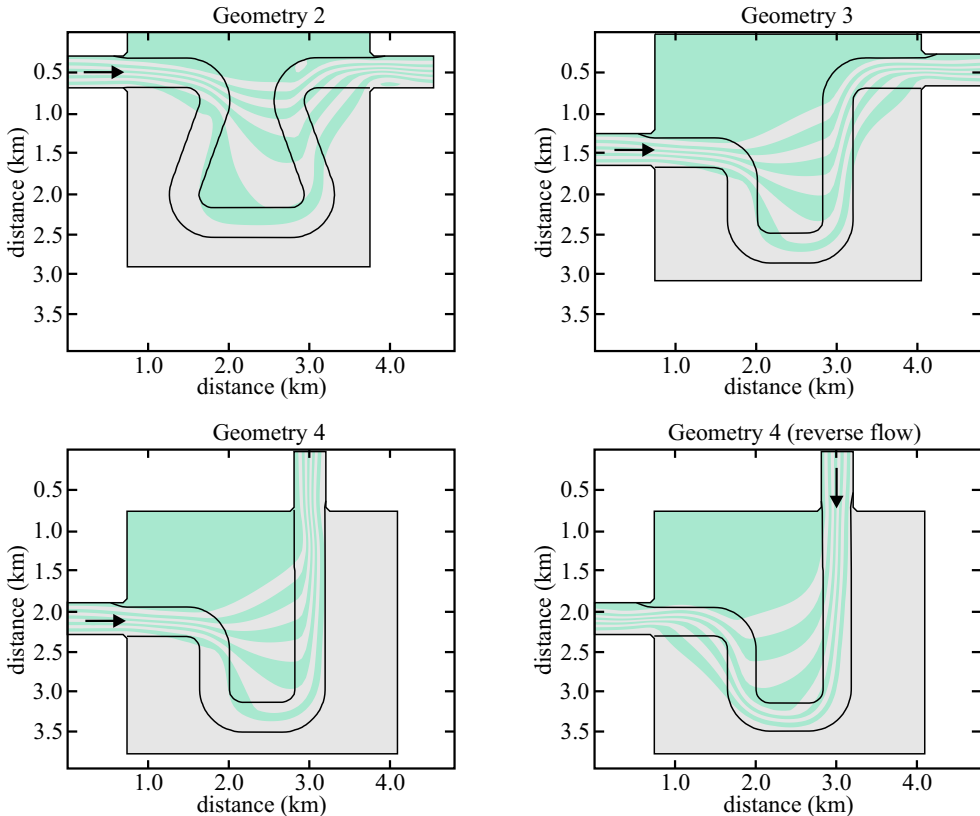


Figure 7.23: Streamlines at the end of the period of maximum discharge. The initial topography is indicated by a contour at -1 m .

Geometry 4 is identical to geometry 3 except for the location of the outflow boundary. The water levels are slightly lower for geometry 4, because the outflow channel is slightly shorter than for geometry 3. The flow across the pointbar is therefore, more concentrated and the velocities are higher, such that the overall erosion of the pointbar is somewhat higher for geometry 4 (simulation 31). Finally, the flow direction in geometry was reversed. Contrary to all other simulations, the inflow is now directed parallel to the pointbar and not perpendicular to the pointbar. In this case, the momentum of the flow does not carry the flow onto the pointbar and the flow through the existing, main channel remains much higher. Only a small amount of erosion occurs along the upstream edge of the pointbar. Some of the eroded sediments are deposited on the pointbar and the smallest amount of sediment was deposited at the location where the cutoff channel formed in the simulations with the normal (i.e., non-reversed) flow direction.

These simulations show that the bifurcation (or offtake) angle of the cutoff channel is an important parameter in the development of the cutoff. It did, however, not influence the direction of the channel formation process, since the erosion of the pointbar occurred again in all simulations at the upstream side. The total eroded volume of sediment and the flow confinement determine the timescale on which the cutoff forms.

7.4 Direction of channel formation

Most simulations described in the previous sections show a tendency for channel formation from the upstream side. This agrees with the observations from the Jamuna River (see Figures 6.15 and 6.16) on which the dimensions and average parameter settings were based. Erosion from the downstream side occurred if the downstream water level was low, or if the flow across the pointbar converges. The erosion led in both cases to a smoothing of the downstream slope, whereas in Chapter 6 it has been stated that cutoff channels that form from the downstream side do so via a headcut travelling in upstream direction. This raises the question in what respect the numerical model deviates from those prototype situations in which a headcut is formed. Two aspects seem to be most relevant: locally non-hydrostatic flows and spatially non-uniform erodibility (which may exist for several reasons). Both aspects will be discussed in the first subsection. Some first steps towards the inclusion of the characteristics of a headcut in a numerical model are presented in the second subsection.

7.4.1 Analysis of processes

Depending on the hydrodynamic and morphological conditions a step in the topography may cause upstream erosion and/or downstream sedimentation. If the water level at the downstream side of the pointbar (or flood plain), where the overbank flow joins the main channel, is sufficiently low, the overbank flow accelerates — in the absence of a backwater effect — due to an increase in the bed level gradient towards the river. The gradual increase in flow velocity (possibly even supercritical flow) causes a significant increase in the sediment transport capacity. This results in erosion of the river bank, but under alluvial, non-cohesive conditions not to steepening (Figure 7.24b). The gradient in the water level cannot be neglected and a gradual flattening of the river bank is the result. This corresponds to the textbook case of an alluvial river adjusting to the effects of a bend cutoff (Figure 7.24a) or a change in the downstream water level (for instance when flowing into a lake).

On the other hand, the dominant behaviour of the numerical model observed in the previous section corresponds to the textbook case of the response of a river to a short, shallow transverse hump or trench (Figure 7.24c, d). Subcritical flow leads to an expansion-wave at the flow contraction and a downstream migrating shock-wave at the flow expansion (assuming instantaneous adaptation of the sediment transport rate, i.e. bedload).

If the banks are sufficiently steep, that is, if there is already a step in the topography, flow separation may occur and the overbank flow will plunge back into the river (Figure 7.24e). In that case erosion will occur at the toe of the river bank due to either a helical flow towards the bank or by erosion of the plunge pool that leads to exceedance of the local angle of repose at the bank toe and subsequent failure of (a part of) the bank. Depending on the composition of the bank (and the associated failure type) this process will lead either to a gradual retreat of a steep bank or to a decrease of the bank slope.⁷ So, one may conclude that it is not the local surface flow itself that determines whether a headcut forms.⁸ From this analysis it is also clear that, extending the conclusion of the sensitivity analysis in Section D.1 regarding

⁷Related to this process of headward erosion is the retrogressive erosion caused by the process of breaching described by Van de Berg *et al.* (2002).

⁸Subsurface flow, on the other hand, may — as indicated in Section 6.2.1 — result in the initiation of a headcut channel due to collapsing cavities.

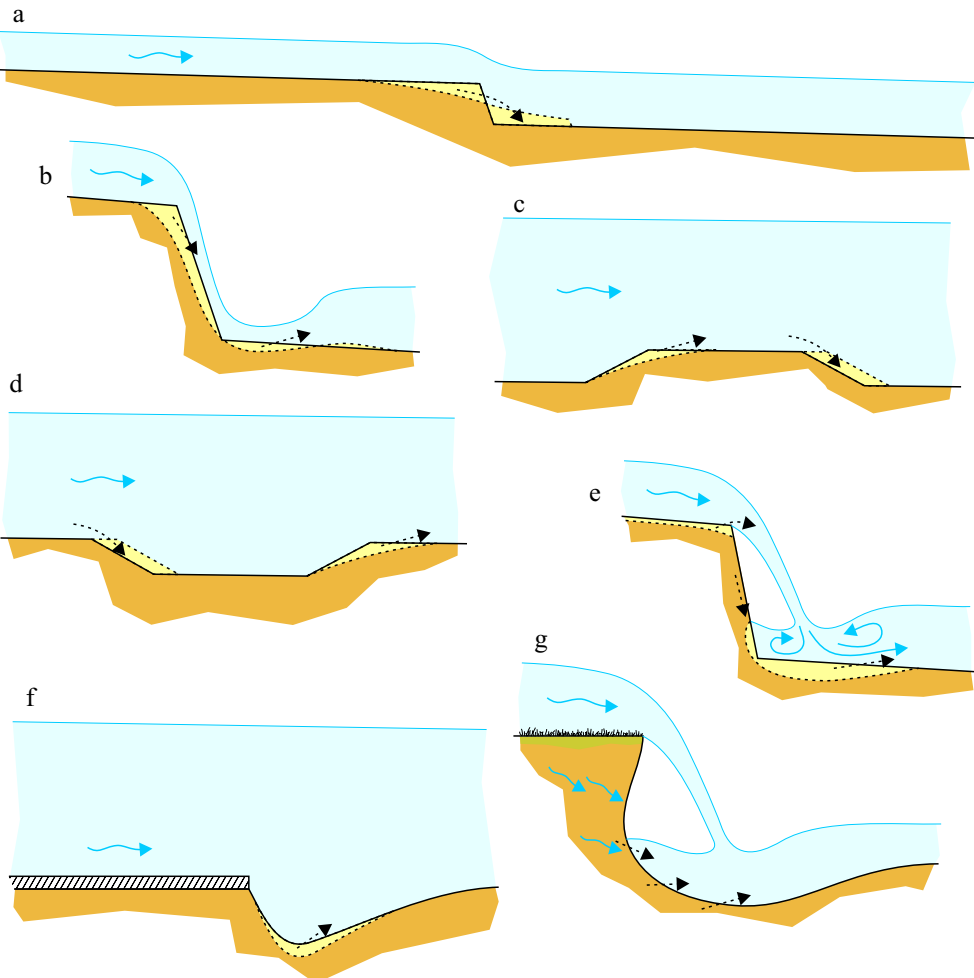


Figure 7.24: Erosion and sedimentation at steps in the topography: (a) regrading of an alluvial river after a cutoff, (b) slope reduction, (c,d) erosion and sedimentation at a transverse hump or trench under subcritical flow conditions, (e) flow separation and plunge pool erosion, (f) erosion downstream of non-erodible layer, and (g) undercutting of protective vegetation.

influence of the gridcell size on the simulation results, it is not just a matter of sufficiently refining the computational grid.

Spatially non-uniform erodibility can be caused by variations in sediment types and sizes (fine, cohesive clay, non-cohesive sand and gravel), presence of vegetation and protection works. Under the assumption of a sufficiently large sediment transport capacity, an increase of the erodibility will lead to an increase in sediment transport and thus to an abrupt increase of the erosion rate. The construction of a non-erodible layer to limit the erosion depth in the outer bend of a river leads to such a situation. Sediment transport in the outer bend is greatly reduced by the secondary flow sweeping the non-erodible layer clear of sediment. Downstream of and, to some extent, alongside the non-erodible layer scouring can occur that eventually can destabilise the layer (Figure 7.24f). This example shows how spatially varying erodibility can cause a large step in the topography to form. The formation of a migrating headcut requires a shifting threshold in erodibility.

Flood plains are generally covered by grass and other types of vegetation. In the photographs of headcuts shown in Figures 6.3b and 6.6 vegetation is present. The concave banks visible in Figure 6.6b and sketched in Figure 7.24g indicate effective protection by the vegetation/sod layer. Different types of vegetation influence the stability of the ground in different ways. Figure 6.6b suggests (and some other photographs by Gay *et al.* (1998) confirm) that, although some trees might have been uprooted, most of them remain standing; this suggests that in this case the tree roots have helped to stabilise the ground.⁹

That vegetation is not always the main factor determining the erodibility is shown by Figure 7.27a: the vegetation has been partly eroded whereas the underlying clays remain intact. In this case, there is a (non-cohesive) layer of gravel rich sediments at the base of the headcut. The cohesive clay layer determines the rate with which the channel can develop; the non-cohesive layer determines largely the height of the step. A naturally developed armour layer in a river or flume with graded sediments may, in a similar way, lead to the development of a headcut. The importance of cohesive sediments on the development of headcuts (or knickpoints) in flume experiments has also been reported by Brush and Wolman (1960).

The influence of the sediment and vegetation is also suggested by the observations of Gay *et al.* (1998) on the Powder River (see also Section 6.2.2). The flood plain deposits of the Powder River are characterised by a gravel layer on top of bedrock, overlain by an unconsolidated sand layer, protected by a toplayer of sod. Gay *et al.* (1998) indicate that, although the flooding that caused the headcut was the result of an ice jam in a river bend, the deposits were not frozen. Gay *et al.* (1998) observed three stages in the development of headcuts (see Figure 7.25). Initially the exposed gravel layer formed a convex surface, which soon straightened as the headcut evolved; this straight surface was maintained for some hours. As the headcuts progressed further upstream, where the sand layer was thinner, the exposed surface of the gravel layer became concave; the gully was deepest just downstream of the cutting face.

Within the active braid plain of the morphologically dynamic Jamuna River, which transports fine sand ($200 \mu\text{m}$), there are no significant concentrations of erosion-resistant sediments and vegetation is generally sparse. This lack of erosion resistance seems to be the key reason for

⁹An alternative explanation might be that the growth of the tree roots has locally elevated the ground surface and that these elevation differences have steered the erosive flows away from the trees.

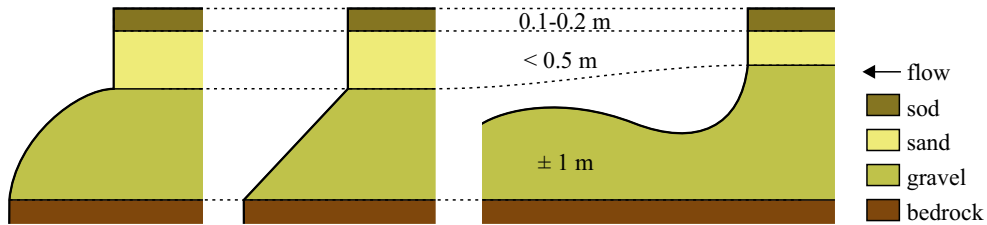


Figure 7.25: Types of headcut as observed by Gay et al. (1998).

the formation of new channels from the upstream side, under the influence of the momentum of the eroding flow. The same homogeneity forms the basis of the numerical models with uniform sediment. It also holds for morphologically active areas of the Western Scheldt estuary, where the channel incision starting from the upstream side has also been observed. Figure 7.26 shows the flow pattern and bed levels of a section of the Western Scheldt estuary between Terneuzen and Hansweert. Jeuken (2000) presents an extensive study on the morphologic behaviour of the tidal channels in the Western Scheldt estuary. More in general it has been observed that channels in estuaries in which the ebb-flow dominates have their shallowest point on the sea-side whereas flood-flows tend to follow channels with a shallow reach on the inland side (Van Veen, 1950). The basic appearance of this phenomenon is reproducible with Delft3D, as shown by Hibma *et al.* (2001).

Given a resistant top layer, there are two mechanisms conceivable by which a headcut can migrate:

- *Protection removed first.* In this case it is assumed that the top layer has a critical shear stress that, although it is much higher than that of the underlying material, can still be exceeded by the surface flow under natural conditions. Velocity fluctuations characteristic of turbulent flows may play an important role here (See Section 3.1). When a part of the protective top layer is removed by a sufficiently high shear stress, the underlying sand and gravel will be quickly eroded.
- *Underlayers removed first.* When the critical shear stress of the resistant top layer is so high that normal flow conditions cannot erode it (or only extremely slowly), the underlying erodible sediments will be removed first by plunge pool erosion or by groundwater flows. This will lead to steepening of the headcut (possibly to the point where undercutting occurs) until the stresses in the top layer become so high that it breaks down (see Section 3.3.3 for various bank failure types).

Based on the limited amount of the data reviewed in Chapter 6 and this section, the latter mechanism (where the underlayers are removed first) seems to be the dominant process for headward erosion. This mechanism is also claimed to cause the headward erosion of for instance the Niagara Falls (Hamblin and Christiansen, 1995).

7.4.2 Numerical modelling of headcuts

The analysis in the previous section indicates that headcut erosion can only occur due to erodibility variations in space *and* time: sediments upstream of the headcut are more difficult

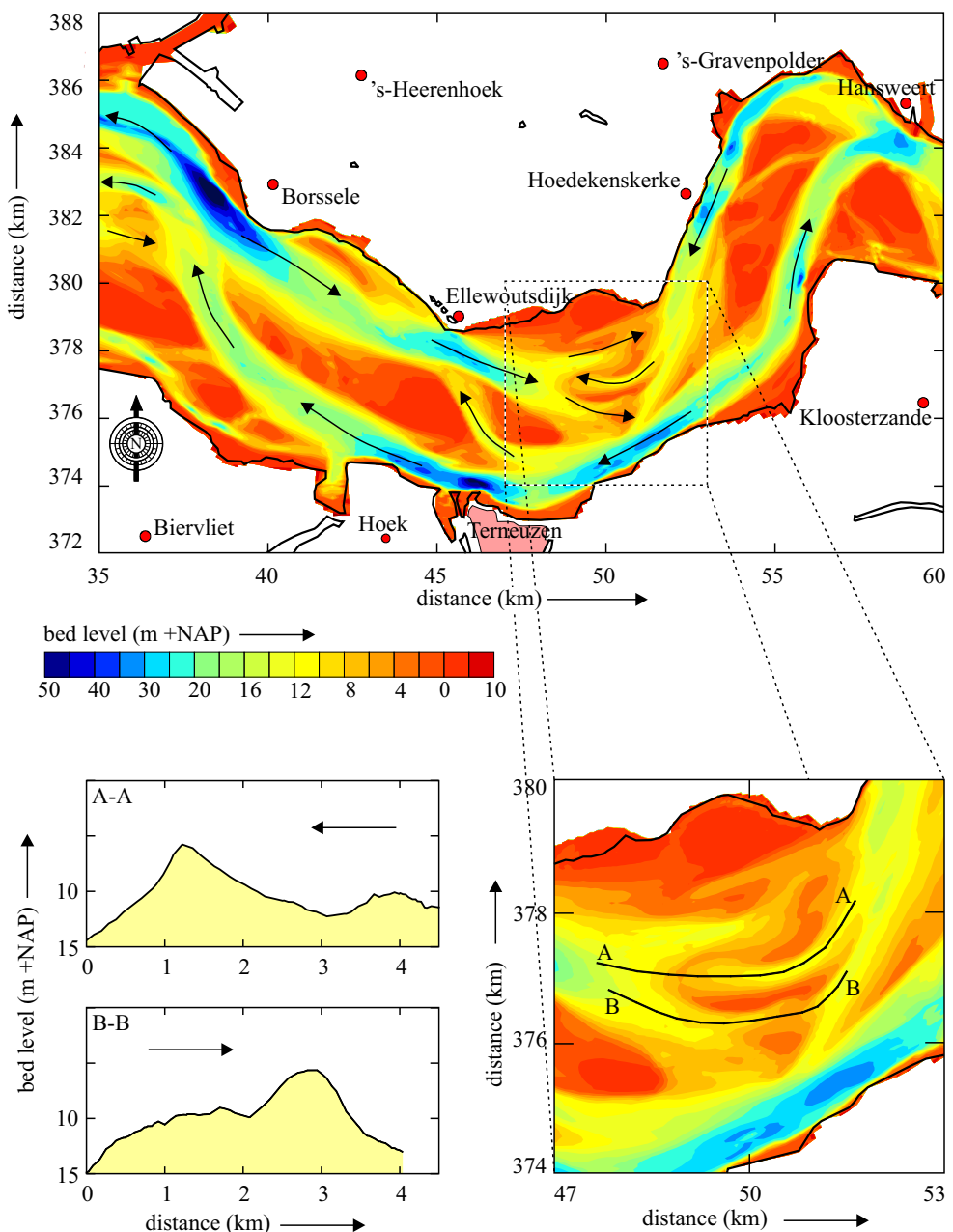


Figure 7.26: Flow pattern and bed levels of a section of the Western Scheldt estuary between Terneuzen and Hansweert (Jeuken, 2000).

to erode than sediments downstream of the headcut. It has been attempted to reproduce this phenomenon in Delft3D by making two dedicated transport formulae. Both adaptations are based on the general transport formula given by Equation 7.1. In both cases the exponent of the transport formula was selected to be 1.83, irrespective of the critical Shields parameter used.

The first adaptation is based on the assumption that the erosion-resistant top layer is removed first: once some critical threshold has been exceeded, the protective layer is broken and sediment transport becomes possible.

$$\theta_{\text{cr}}(x, y; t) = \begin{cases} \theta_{\text{cr},1}(x, y) & \text{while } \theta(x, y; t') < \theta_{\text{cr},1}(x, y) \text{ for all } t' \leq t \\ 0 & \text{afterwards} \end{cases} \quad (7.3)$$

For the testing of this concept a straight channel has been modelled using a 200×20 grid with cells of $10 \text{ m} \times 10 \text{ m}$. The channel bed is a superposition of

- a base slope of 10^{-4} ,
- a step of 0.5 m, and
- a periodic perturbation (amplitude 0.1 m, alongstream wavelength 150 m, and transverse wavelength about 130 m).

The step is located halfway the channel (at $x = 1 \text{ km}$ downstream of the inlet), except for a number of grid lines in the centre of the channel. At those grid lines, the step is located 200 m further upstream; this creates an initial straight headcut channel of 200 m, which attracts the flow and accelerates the development (see Figure 7.28a). Natural variations in the terrain height lead to convergence of the flow in the deepest areas. It is, therefore, assumed that the headcut migrates predominantly in the direction of the deepest areas, i.e., it is influenced by variations in the topography. To simulate this effect, a periodic perturbation has been added which causes spatial variations in discharge and flow velocity. The average upstream water depth is about 0.8 m and the downstream water depth is almost 1 m. The unit discharge at the upstream boundary is $0.25 \text{ m}^3/\text{m}$ and the roughness is $50 \text{ m}^{1/2}/\text{s}$ throughout the model. The initial value $\theta_{\text{cr},1}$ of the critical Shields parameter upstream of the step equals 1; downstream of the step, the bed is assumed to be alluvial with $\theta_{\text{cr}} = 0$.



Figure 7.27: Photographs of a headcut (of about 1.5 m high) in the Kerkeweerde near Stokkum, Belgium, along the Meuse River in March 2002.

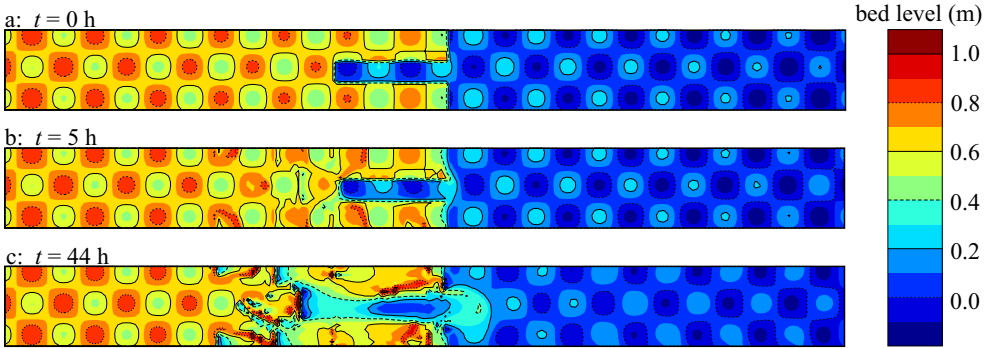


Figure 7.28: Initial channel topography (a) and the simulation results after 5 hours (b) and 44 hours (c) when using Equation 7.3.

Immediately after the start of the simulation, sediment starts moving in both the upstream and downstream reach. Sediment can easily be transported in the downstream reach because there the critical shear stress is zero. Sediment transport occurs in the upstream reach not only near the head of the imposed channel, but also at several local maxima of the periodic perturbation. The erosion at the local maxima was not anticipated and it complicates the simulation significantly. As indicated above, it had been expected that, from a viewpoint of topographic steering of the flow, the headcut would follow the shallow areas in the terrain. However, the influence of the perturbations on the flow pattern is relatively small and the perturbations lead to increased shear stresses at the highest points of the channel topography. Following the rule expressed in Equation 7.3, the exceedance of the critical Shields parameter at these locations leads to the break-up of the protective layer and θ_{cr} becomes equal to 0. Because no sediment arrives from upstream, the full transport capacity is available for transport and, thus, erosion occurs, which results in the formation of deep scour holes. The eroded sediment, however, is transported to other gridcells downstream where the critical Shields parameter is still equal to 1. Subsequently, most sediment is deposited immediately downstream of the scour hole. A better book-keeping system is needed to distinguish between the erodible and non-erodible sediments for this kind of situations. Although the overall behaviour of this simulation is not physically realistic, it is good to realise that under certain conditions somewhat elevated areas might be more sensitive to these threshold processes than the lowest areas.¹⁰

The second adaptation can be interpreted in two ways. Basically, it states that the critical Shields parameter reduces to zero below a certain threshold bed level.

$$\theta_{cr}(x, y; t) = \begin{cases} \theta_{cr,2}(x, y) & \text{while } z_b(x, y; t') > z_{b,2}(x, y) \text{ for all } t' \leq t \\ 0 & \text{afterwards} \end{cases} \quad (7.4)$$

where the bed level z_b has been defined positive up. When this approach was conceived of first, it was intended that the threshold level would represent the underside of the thin protective top layer: $z_b(x, y; 0) - \Delta z_{top}$ with Δz_{top} small. Once the top layer has been removed, the underlying sediments would become available for transport. However, it turned out that this

¹⁰High grounds that are close to (or above) the water level are subject to much lower shear stresses and will, therefore, be more stable.

interpretation was bound to fail, due to the way in which the various physical quantities are defined on the staggered grid of Delft3D. The bed level points are located at the corner points of the gridcells, whereas the bedload transport rates are computed at the water level points, which are located in the centres of the gridcells (see Figure 7.29a and Section C.3.3)). The bed level used to determine the sediment transport rate at a water level point is interpolated from the four surrounding bed level points. So, at the location of the step, both the upstream and downstream bed level play a role. This is explained in more detail in the following paragraph.

If we consider a case that is uniform in lateral direction, the one-dimensional situation sketched in Figure 7.29b arises. The bed levels indicated by the circles clearly define a step, where \circledast marks the upstream edge of a step with upstream bed elevation $z_{b,u}$ and downstream elevation $z_{b,d}$. The sediment transport rates are computed at the water level points, which are located halfway between the bed level points. The effective bed level at a water level point is given by the average of the upstream and downstream bed levels. So, the bed level at the water level point immediately downstream of \circledast equals $\frac{1}{2}(z_{b,u} + z_{b,d})$. If this lies below the threshold level $z_{b,2}(x,y)$ used in Equation 7.4, $\theta_{cr}(x,y;t)$ will be equal to zero and, thus, sediment will be transported and erosion will occur at \circledast . If the bed level at \circledast lowers by Δz , the bed levels at the water level points upstream and downstream of \circledast are lowered by $\frac{1}{2}\Delta z$ (indicated by the arrows). Sediment transport at the water level point upstream of \circledast will be activated as soon as the bed level at \circledast is lowered by $2\Delta z_{top}$, which for a thin protective layer is a relatively small change in bed level. Consequently, the step will almost disappear. Therefore, interpreting $z_{b,2}(x,y)$ as $z_{b,u} - \Delta z_{top}$ will not lead to the upstream migration of a headcut of a significant height.

A better definition of $z_{b,2}(x,y)$ is $z_{b,u} - \frac{1}{2}\Delta z_{step}$ where $\Delta z_{step} = z_{b,u} - z_{b,d}$ is the height of the headcut. With this definition it is assured that the bed level upstream of the step is only lowered if the bed level downstream of the step has been eroded to the base level $z_{b,d}$ of the step. In combination with a sufficiently high critical value for the Shields parameter such that erosion of the resistant top layer is impossible — in this case $\theta_{cr,2}(x,y) = 2$ has been used — this approach can be interpreted as an implementation of the mechanism that

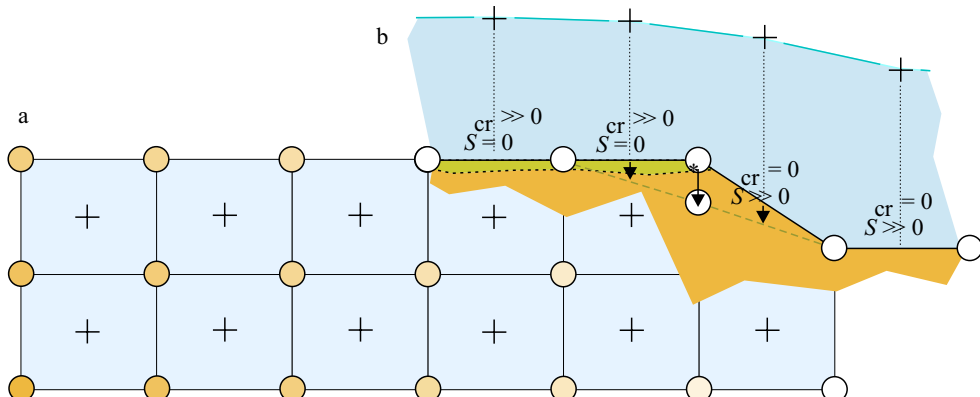


Figure 7.29: a) Staggered grid of Delft3D: the bed levels are defined at the locations marked with a circle whereas the water levels and bedload transport rates are computed at the locations marked with a cross. b) A side view of the for a quasi one-dimensional case of a step.

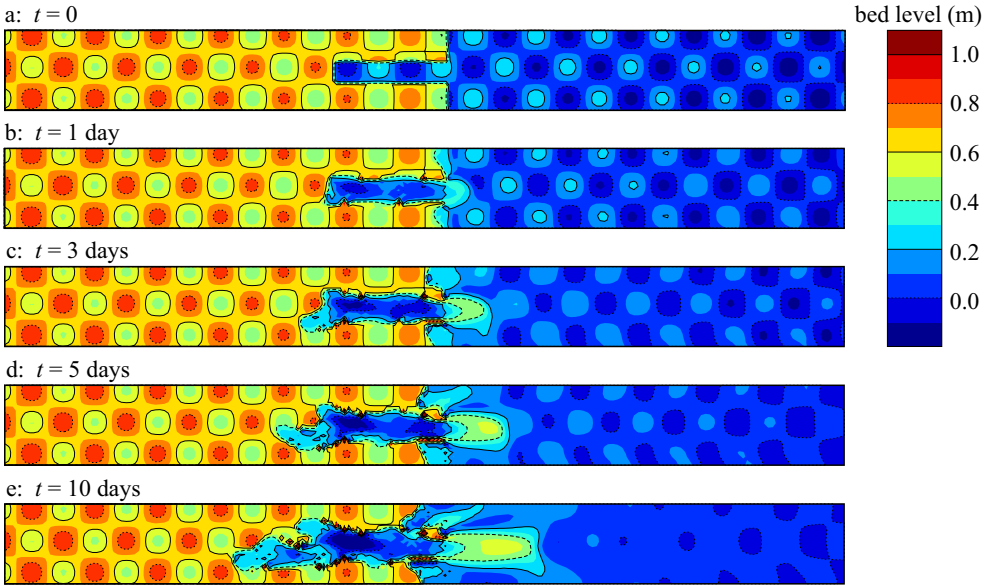


Figure 7.30: Initial channel topography and the simulation results after 1, 3, 5 and 10 days when using Equation 7.4.

removes the underlying sediments first. This modelling approach has been tested using the same geometry as above. The results, shown in Figure 7.30, are more realistic than those obtained with the first approach. The imposed perturbations on the initial topography cause the headward migration to follow the shallow areas of the terrain. Furthermore, there is a tendency for the channel to split and to form multiple heads. The main disadvantage of this method is that one needs to know the height of the step in advance. Again problems occur due to the lack of a book-keeping system for erodible and non-erodible sediments: sediment transported from gridcells with $\theta_{cr} = 0$ to cells with $\theta_{cr} > 0$ results in spikes in the topography along the deep channel. Further research is needed to determine whether this approach can be extended to a physics-based model concept.

7.5 Discussion

The results of the two-dimensional depth-averaged morphological simulations discussed in Section 7.3 indicate that cutoff formation is accelerated by

- a low water level downstream (a large gradient in the sediment transport rate),
- a large (alluvial) roughness (a major part of the discharge flowing across the pointbar),
- a low sediment transport threshold (easily erodible sediments on the flood plain), and
- a small value for the exponent c of the Shields parameter θ (or of the velocity u) in the sediment transport relation if the width-averaged sediment transport rate remains constant (relatively small depth/velocity dependence of the sediment transport rates).

The cutoff development is not sensitive to a modest depth-dependence of the roughness formulation. In all cases the cutoff channel started its formation at the upstream end. Only in the case of a relatively low downstream water level some erosion occurred initially at the downstream end of the channel, but this erosion was stopped by an increased sediment supply from upstream due to the erosion that occurred at the upstream end of the pointbar.

An additional sensitivity analysis, reported in Appendix D, has shown that the spatial discretisation was fine enough for the simulations with channel formation from the upstream side. Furthermore, the discretisation of the drying and flooding, the quasi-steady flow approximation and the details of the downstream boundary condition during the rising stage have been shown to be not decisive for the outcome of the simulations. The same holds even for the neglect of the spiral flow effect and all other 3D flow aspects covered by the 3D hydrostatic flow model.

Non-hydrostatic effects, vegetation and graded sediments are not covered by the numerical simulations. Especially the latter two aspects are important for the correct simulation of bend cutoffs via headcut erosion because they may cause spatial variations in erodibility. A first, simple model concept for simulating headward erosion has been proposed and tested in Section 7.4. Further analysis and validation are needed to improve the modelling of this type of erosion. Once a suitable way of describing the headcut erosion is found, local flow phenomena might become important to accurately estimate the erosion rate.

Before switching back to the larger picture of the overall morphodynamics of braided rivers, there is one feature in the numerical simulations that should be brought to the attention of the reader. In Section 3.5.2 four processes have been mentioned that lead to the onset of braiding: formation of a chute cutoff, growth of a mid-channel bar, dissection of a linguoid bar, and simultaneous growth of multiple bars. In the simulations, the material eroded from the cutoff channel progresses in downstream direction as linguoid bar. Figure 7.31 shows this migration for a simulation on a grid with gridcells of $25 \text{ m} \times 25 \text{ m}$ (see Section D.1). The bar, originating from the cutoff which forms just below the bottom of the figure, extends across the imposed deep main channel in the direction of the main flow. As the discharge decreases and the water level drops the flow bifurcates: one part of the flow through the cutoff continues to follow a straight line until it merges with the water flowing through the original channel (coming from the right), whereas the other part turns left and follows the deeper part of the

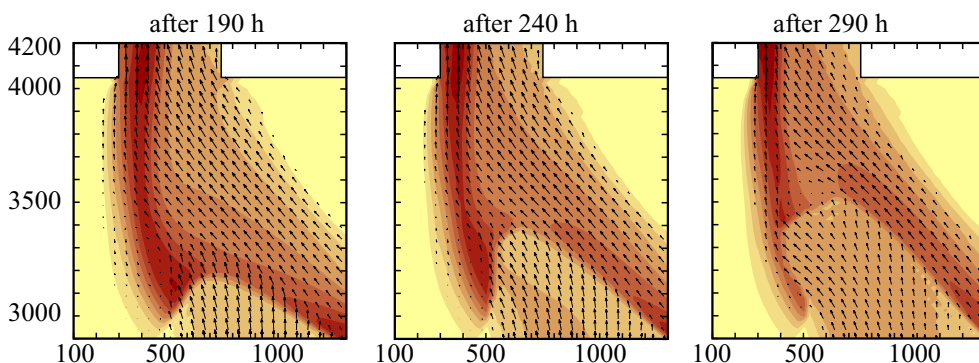


Figure 7.31: Splitting of the flow across the stalling sediment lobe.

imposed channel. An almost stagnant area forms in between these flows. Consequently, the sediment transport is characterised by a similar pattern, and the bar develops side lobes (becomes double-headed). In Section 3.5.2 it was indicated that, although the falling stage may speed up the process, it is not a necessary condition for the dissection process to occur. The example shows, however, that 2D numerical models may not only help to predict and understand the general trends in the braided river system, but that they can also be used to study the processes at smaller scales. The detailed description of morphological processes at the smaller scales, e.g., interaction of different sediment types and vegetation, should be improved for reliable results.

7.5.1 Adaptation of the branches model

Although the numerical simulations and the subsequent analysis have improved our understanding of cutoff processes, it has not directly led to a good modelling concept for channel formation to be included in the branches model. Too few geometries have been analysed to derive a relationship between geometrical parameters and rate of cutoff development. Furthermore, it should be noted that none of the physical parameters important for the development of a cutoff channel (discharge, water level, roughness, sediment transport relation, bed levels) is available in the branches model. Building on Equation 6.3, it is, therefore, advised to include the following procedure for the formation of new channels in the branches model.

For every point i the most likely course of a new channel is determined by selecting the point j — at which the new channel would rejoin the existing channel network — at which

$$P(i, j) = K_c R_c(i, j) [1 - P_{ij,ab}] [1 - \alpha_v f_{veg}(i, j)] \alpha_{vol} \alpha_{vel} \quad (7.5)$$

is maximised. Only those points that can be reached from point i via a straight line across land are included.¹¹ The term K_c is a calibration factor, and the other terms have the following meaning:

$R_c(i, j)$ gradient ratio, i.e. the distance reduction $L'_p(i, j) - L_c(i, j)$ divided by original distance via the existing channel network $L'_p(i, j)$. The latter distance is well defined in meandering rivers, namely the distance along the meandering channel from the upstream point i to the downstream point j , but in case of a braided river point j might not be located downstream of point i in the same branch. Therefore, the following definition is proposed. Let k be the first point downstream of both points i and j . The distance $L'_p(i, j)$ is defined as the distance $L_p(i, k)$ from point i to point k via the existing channels minus the distance $L_p(j, k)$ from point j to point k via the existing channels. The gradient ratio $R_c(i, j)$ will be assumed zero if $L_p(j, k) > L_p(i, k)$ or if there is no such point k . A more effective cutoff is more likely to form than a cutoff that barely reduces the length of the flow path.

$1 - P_{ij,ab}$ complement of the probability of abandonment $P_{ij,ab} = \alpha_c(\phi - \phi_c)$, constraint to values between 0 and 1. The bifurcation angle ϕ is the angle between the direction of the cutoff channel and the local flow direction in

¹¹Cutoffs can only form across point bars (i and j in same branch) and braid bars (i and j in different branches). The cutoff cannot cross other existing channels (i and j are not separated by a channel).

the existing channel at point i . ϕ_c and α_c are calibration constant identical to those used in the formulation used for channel abandonment (given in Section 5.3.1). A channel that is likely to be abandoned is not likely to form.

- $1 - \alpha_v f_{\text{veg}}(i, j)$ complement of the vegetation fraction $f_{\text{veg}}(i, j)$ defined as the fraction of the proposed cutoff channel that is covered by vegetation. The vegetation cover can be derived from the satellite data in the following way. Classify the pixels of the satellite image based on distribution of signal strength of the various spectral detection bands and identify the vegetated areas. Subsequently, determine the ratio $f_{\text{veg}}(i, j)$ of the number of vegetated pixels and the total number of pixels along the line from i to j . The calibration factor α_v (between 0 and 1) can be used to reduce the effectiveness of the vegetation with respect to erosion prevention. Vegetation generally protects sediment from erosion by reducing the near bed flow velocities. In the case of the Jamuna River, where vegetation plays only a minor role, this effect may (at least initially) be ignored, such that $\alpha_v = 0$.
- α_{vol} effect of the sediment volume to be eroded: $e^{-K_V \{L_c(i, j)(E(i, j) - E_0) - V_{\text{ref}}\}}$. In this expression, which should be restricted to values smaller than 1, the parameters have the following meaning:

- $E(i, j)$ the average elevation encountered along the line from i to j ,
- E_0 reference elevation (representing the average bed level of the channels),
- K_V calibration coefficients,
- $L_c(i, j)$ the distance between i and j along the cutoff,
- V_{ref} reference volume (note: $e^{K_V V_{\text{ref}}}$ is effectively only a multiplication factor and, therefore, indistinguishable from the general calibration factor K_c).

The larger the amount of sediment to be eroded during the formation of the cutoff, $L_c(i, j)(E(i, j) - E_0)$, the slower the cutoff develops. This requires information on the elevations of the bars. Since this formula only requires an average elevation, a rough estimate of the topography is sufficient. Such an estimate can, for instance, be obtained for the Jamuna River based on the land age using the relation shown in Figure 2.13 following work by EGIS (1997). The initially derived elevation data can be updated during the simulation to remember recently abandoned channels and, possibly, half-formed cutoff channels. If the elevation differences are relatively small, this expression effectively reduces to $K'_c e^{-K'_V L_c(i, j)}$, amplifying the effect of $R_c(i, j)$ that longer cutoffs are less likely to occur.

α_{vel} effect of the near bank excess velocity: $e^{K_u \max\{B_i/R_i - K_{br}, 0\}}$. Since no velocity information is available, the effect of high flow velocities near the outer bank is estimated using the relative curvature B_i/R_i of the channel. Here, B_i is the channel width and R_i the radius of curvature at point i ; this may be improved by including a weighted averaged of the upstream values (see Section 4.1.1). K_u and K_{br} are calibration coefficients. Note that this factor will be larger than 1: the probability of outer bank erosion is largest in sharp bends.

This procedure gives for every point i , a cutoff target point j_i and an associated probability $P(i, j_i)$. To take into account flow convergence and diverge (the former will accelerate cutoff formation, whereas the latter will slow it down), the probability is proposed to determine a corrected probability $P^*(i, j)$ of cutoff as

$$P^*(i, j) = \min\left\{1, P(i, j) \frac{2D_{\text{up}}}{D_{\text{up}} + D_{\text{down}}}\right\} \quad (7.6)$$

where $D_{\text{up}} = L_p(i-1, i) + L_p(i, i+1)$ is the distance between neighbouring points at the upstream end of the cutoff, and $D_{\text{down}} = L_p(j_{i-1}, j_i) + L_p(j_i, j_{i+1})$ is the distance between the end points of the cutoffs of points $i-1$, i and $i+1$. Again, $L_p(a, b)$ represents the distance along the channel network from point a to point b . The multiplication factor can vary between 0 (strong divergence) and 2 (strong convergence). This expression is not evaluated for bifurcation and confluences at which no additional bifurcation may occur. A cutoff should form at point i if a randomly selected number between 0 and 1 is smaller than $P^*(i, j)$.

This procedure represents events that occur during the flood period and should, therefore, be carried out in combination with the procedure for channel abandonment. In case the channel abandonment procedure is carried out after the channel formation procedure described above, a complete cutoff (i.e., formation of a new channel and subsequent abandonment of the existing channel) may occur during a single flood. The implementation, calibration and verification of this algorithm as part of the branches model is beyond the scope of this study.

Chapter 8

Conclusions

This study has been carried out to determine how and to what extent planform changes in large braided rivers, such as the Jamuna River, can be predicted. The sections of this chapter address the individual research questions formulated in Section 1.3. The research questions are grouped together into five sets relating to: the Jamuna River (description of the prototype example), the planform changes of braided rivers, the modelling of planform changes, the formation of new channels, and the formulation of a channel formation submodule for the branches model.

8.1 The Jamuna River

Two research questions have been formulated to define the context of this study.

- What are the general characteristics of the Jamuna River?
- What data are available for usage as input data for models of the Jamuna River?

These questions have been addressed in Chapter 2.

8.1.1 General characteristics

The Jamuna River is a large sand-bed braided river of 5–17 km wide. The width of individual channels during low flow can be over 1 km. During flood, when the discharge is 5–15 times larger than at low-stage, most islands are submerged. The long-term average migration direction of the whole river is westward. The river is influenced by tectonics: both directly (as shown by the alignment of individual braid channels with faultlines and the dramatic shift in recent history) and indirectly (due to variations in the sediment supply from upstream).

A large part (estimated at 90%) of the sediment load, mainly consisting of fine sands with a diameter of 0.16–0.25 mm, is transported as suspended sediment. The morphological changes

during a single monsoon/flood period cause low-stage channels to migrate laterally over distances up to 1 km. The backwater effect of the flood of the Ganges River causes sedimentation in the reach just upstream of their confluence.

8.1.2 Model input data

The collection of a consistent set of accurate and detailed model data for the Jamuna River is complicated by its magnitude and dynamic nature. Most data available originates, therefore, from two sources: satellite images and large-scale river surveys carried out as part of the Flood Action Plan studies.

Field surveys deliver detailed information on bed and flood plain topography and local flow characteristics. Their coverage is, however, limited to relatively small segments of the river for reasons of costs and data consistency (both related to the dimensions of the considered river). Furthermore, detailed data on flow and topography can be considered outdated for prediction purposes one year after their collection.

Satellite images form the most comprehensive source of data for the Jamuna River since 1973. Landuse classification methods based on this data source, provide spatial (two-dimensional) information on planform and vegetation cover with a resolution of 10–50 m. However, it is not yet possible to obtain sufficiently accurate topographic data from satellite observations for flat countries like Bangladesh. A rough estimate of the topography can be obtained from a relation between land age and elevation. Remote sensing data from airborne technology (e.g. laser altimetry) could provide sufficiently detailed information, but this technology has not yet been applied to this river. The lack of data on (submerged) bed topography is most restrictive for modelling this river.

8.2 Planform changes

Based on a series of satellite images of the Jamuna River, it has been concluded that six elementary planform changes can be distinguished: channel migration, channel width change, mid-channel bar growth, channel formation, channel abandonment and node deformation. Three research questions have been formulated to put these planform changes in a physical perspective.

- What basic physical processes are active in braided rivers?
- What are the primary sources for uncertainty and unpredictability given the current state of knowledge?
- What are the main types of planform changes observed in braided rivers?

These questions have been addressed in Chapter 3.

8.2.1 Physical processes in braided rivers

Hydrodynamics and morphology interact on several scales: from sediment grains, bedforms and turbulent flow, via bars and large-scale flow structures, until islands, bifurcations and

confluences. Based on a general overview of all relevant processes, the following conclusions can be drawn with respect to braiding:

- Braiding occurs on the same wide range of scales as the morphodynamic-hydrodynamic interaction: from small rainfall runoff streamlets to large rivers.
- Theoretical studies have shown that a fundamental instability of the flow leads to the formation of alternate bars in channels of moderate width-depth ratio, and to the formation of braid bars at high width-depth ratios. Multiple row bars develop if the width-depth ratio is very large. Flume experiments and field observations confirm these trends.
- Physically favourable conditions for the formation of a channel with high width-depth ratio are: (1) easily erodible banks, (2) over-abundant sediment load (leading to aggradation), and (3) decreasing discharge (dying river).
- Braiding may start due to: (1) the formation of a chute cutoff, (2) growth of a mid-channel bar, (3) dissection of a linguoid bar, (4) simultaneous growth of multiple bars.
- If braiding occurs predominantly due to the formation of chute cutoff across alternate bars, the river can be characterised as wandering or complete meandering. Lack of suspended sediment has been mentioned as one of the prerequisites for this type of behaviour.
- Although braiding may start off with the growth of a large number of braid bars, experiments have shown that the number of braid bars tends to gradually decrease to form larger channel and island complexes. This agrees with numerical simulations and field observations.

8.2.2 Sources of uncertainty

The sources of uncertainty in (conceptual, theoretical or numerical) model predictions can be lumped together in four categories.

1. *Boundary in space (large scale)*. Almost every model considers only a small part of a dynamical system. Most models in the field of river engineering concern only a small section of a river, coastal models focus on small parts of the seas and oceans, river catchment models include only (sub)surface processes. However, discharge from upstream, tidal and other large scale oceanic currents, and precipitation and evaporation are for these types of models important. Therefore, boundary conditions have to be applied. In the case of forecasts, assumptions must be made regarding the development of these boundary conditions. The locations of these boundaries result often from practical consideration concerning simulation time and data availability.
2. *Boundary in space (small scale)*. The larger the scale encompassed by the model, the more of the physics remains at the ‘subgrid’ level. This type of boundary cannot only be found in numerical models, which are based on a numerical grid, but also in theoretical models assumptions must be made about the dynamics on the smallest scales to obtain simple relations for the largest scales. For numerical models, this results in sub-grid

closure models. Also these boundaries generally result from practical consideration concerning simulation time and data availability.

3. *Boundary in knowledge.* Many dynamical processes are not yet fully understood.¹ Examples of morphological processes that require more research are the sorting of graded sediment, bank erosion and the interaction of morphology and vegetation.
4. *Boundary in time.* Dynamical models (contrary to equilibrium models) have also a boundary in time. Depending on the characteristics of the dynamical system, small errors in the description of the initial conditions may result in large or small differences at the end of the simulation (chaotic and dissipative systems, respectively).

A chaotic system will be sensitive to errors (uncertainty) originating from all four types of boundaries. For the prediction of large-scale planform changes of the Jamuna River, one should, therefore, take into account, amongst others, the uncertainty of the discharge hydrograph (type 1), the dynamics of small-scale channels and within channel morphology (type 2), uncertainty in the process formulations for bank erosion and channel formation (type 3) and the initial condition (type 4).

8.2.3 Planform changes in braided rivers

Six elementary planform changes have been identified for braided rivers.

1. *Channel migration.* The individual branches of a braided river migrate laterally due to the same processes that act in meandering rivers. Bank erosion and secondary flow are the dominant physical processes. During flood, the channels migrate as variations in bed topography in downstream direction similar to an oblique trench. In this case, the adaptation of the velocity profile due to flow acceleration and deceleration, or — depending on the steepness of the bank — erosion due to overbank flow with flow separation are important.
2. *Channel width change.* The width of a meandering channel changes little (in time) under quasi-equilibrium conditions. Although the braid plain as a whole may be in equilibrium with the hydrodynamic conditions and the associated equilibrium sediment transport, the width of individual channels of a braided river can vary in time as the main channel wanders through the braid plain. An increase in discharge will cause a widening of the channel, the reverse, a decrease in discharge, is associated with shallowing rather than narrowing. The bank erosion rate, the local sediment transport capacity and the sediment supply from upstream determine whether a channel will widen or aggrade.
3. *Mid-channel bar growth.* Mid-channel bar growth is generally proposed to be the most characteristic planform change of braided rivers. Flume experiments have shown that a braided planform may indeed be initiated by the formation of a mid-channel bar, but

¹Note that this may depend on the scale considered. The dynamics of fluids is, for instance, accurately described by the Navier-Stokes equations; however, for practical applications, it is impossible to model the fluid dynamics to the smallest (Kolmogorov) scales. Large-scale models require, therefore, a subgrid model to simulate the effect of the turbulent fluctuations. A lot of research is still going on in this field.

the comparison of a series of planform suggests that this process plays only a minor role in the dynamics of the low stage planform. The underlying physical instability is, however, important to keep the planform braided. Flow convergence and divergence are the dominant parameters here.

4. *Channel formation.* The length of a meandering river increases until a neck or chute cutoff straightens the channel and reduces the length of the river. In a braided river with multiple branches, new channels form not only across pointbars of individual channels but also between neighbouring branches. In an actively braiding river, new channels form continuously. Flood plain topography, erodibility and channel alignment are the main parameters in this process (see also Section 8.4).
5. *Channel abandonment.* Due to the migration of bars during flood and migration of channels during the low stage period, the conditions for water entering a certain channel may become unfavourable (large bifurcation angle). The abandonment of the channel may eventually result from sedimentation in the upstream reach due to a relatively high sediment load entering the channel, or from a migrating bar that closes the entrance to the channel during flood. A remnant of the channel will remain in the channel topography, which may be partly reused by a new channel formed years later. Sediment distribution (nodal point relation) at the upstream bifurcation and the flow pattern during flood are the decisive factors.
6. *Node deformation.* The list of planform changes could be assumed to be complete without the deformation of nodes (bifurcation and confluences) listed as a separate item, since one may argue that node deformation is the result of the migration of the channels that join at a node. Because bifurcations play an important role in the distribution of the discharge and sediment load over the downstream channels, which may eventually lead to the abandonment of either one, the deformation of these nodes needs extra attention. Migration of the upstream channel(s), the initial discharge distribution (during flood) and the erodibility and shape of the bifurcation point are the key parameters affecting the deformation of the nodal point.

8.3 Modelling planform changes

The process knowledge described in the previous sections should be combined with an appropriate modelling concept to give a model for predicting planform changes of braided rivers. After an initial investigation of modelling concepts in use for meandering and braided rivers, three different approaches were selected for a more detailed study: a neural network approach, a cellular approach, and an object-oriented approach. This phase of the research has been guided by the following research questions addressed in Chapters 4 and 5:

- Which models for predicting planform changes in (meandering and braided) rivers exist?
- How can a neural network be used to predict planform changes in braided rivers and how well does it perform?
- To what extent can the cellular model of Murray and Paola (1994) be used to predict planform changes in braided rivers?

- How can the approach of Klaassen *et al.* (1993) be used as an automated approach for the prediction of planform changes in braided rivers and how well does it perform?
- Which of the described models is best suited for predicting planform changes and what is needed to improve that model?

8.3.1 Existing models

Most of the research before 1990 was focused on the physical phenomena in meandering streams and as a result of this the largest amount of data is available for planform changes caused by channel migration of meandering rivers. The models for meander development vary from kinematic formulations, via dynamic one-dimensional models using linearised equations for flow (and morphology), to two-dimensional non-linear models using adaptive grids. Recent developments have focused on the relatively simple, yet physically sound, one-dimensional models: spatial variations in flood plain erodibility, flood plain tilting and sediment sorting have been included. The dynamics of a braided river is, however, much more complex than that of a meandering river: the channel bifurcations and the large morphological changes during flood (associated with larger erodibility of the flood plains of braided rivers) significantly complicate the modelling.

Until 1994 numerical models dedicated to braided rivers have been limited to static random walk models. With the development of generic two- and three-dimensional process-based morphological models and simplified cellular models (see Section 8.3.3), the research on the numerical modelling of braided rivers has accelerated. These generic models are relatively well suited for modelling braided rivers during flood, but problems arise if a significant part of the morphological development occurs during low-flow.

- The application of these generic morphological models is time-consuming. Therefore, most schematisations are relatively coarse, which can cause problems during low flow (too few gridcells to correctly represent individual channels).
- Bank erosion (either at the outer banks or at emerged bars/islands) is not included in most generic models. Since bank erosions is also the dominant planform changing process in meandering rivers, the simulation of the medium- to long-term development of untrained meandering rivers using the generic models is also impossible.

Sensitivity of the braided system to initial and boundary conditions limit the predictability. Furthermore, process knowledge is still incomplete for many processes, such as sediment transport characteristics (magnitude, mechanism, direction), sediment sorting, bedform development (alluvial roughness), and interaction with vegetation. Without proper topographic data, this type of model can only be used for qualitative, phenomenological studies. This is the case for most of the Jamuna River (see Section 8.1.2)

8.3.2 Neural network

Multi-layer feed-forward neural networks have been trained to correlate the state (i.e., land or water) of a pixel of a satellite image to a number of local planform characteristics derived from the satellite image of the preceeding year. The local planform has been characterised

using: the distance to the nearest channel, the direction in which the nearest channel is encountered, the local width of the nearest channel, and the amount of water near the point of interest. Ten neural networks with 1 to 7 hidden neurons have been trained; the convergence behaviour was similar for all configurations. The performance of a network with 3 hidden neurons has been analysed in depth. The trained neural network was able to reproduce three simple rules of thumb.

1. Points close to a channel are more likely to be eroded than points further away.
2. Channels tend to migrate down-valley.
3. Erosion is more likely to occur along wide channels.

This shows that this neural network approach basically works. Even though the trained neural network is fast, provides probabilistic information and requires only a satellite image as input, this approach is not very rewarding because it helps little to increase the understanding of the physical processes (black box model), and may not be applied to other rivers without recalibration.

8.3.3 Cellular model

Murray and Paola (1994) have formulated a cellular model for braided streams. The dynamics of this model is given by a simple water routing scheme and formulations for streamwise and lateral sediment transport. Although the model is based on significantly simplified physical formulations, the resulting braided planform and its morphodynamic development agree well with observations of actual braided rivers. However, due to the simplifications, this model is not suitable for predicting planform changes of an actual river. An alternative scheme is presented that solves the anisotropy of the flow routing at the expense of a significant increase in simulation time. This alternative approach is not better suited for predicting purposes than the original approach. Recent adaptations of the original model by Thomas *et al.* (2002) seem to provide more realistic results. The application of this model is, however, hampered by the same restriction as the generic two-dimensional model: lacking topographic data.

The cellular model is based on a simplified water routing scheme, formulae for alongstream and lateral sediment transport, and mass conservation for water and sediment. The model is able to reproduce the general behaviour of braided rivers, but suffers from an oversimplified water routing scheme. An alternative scheme is presented that solves some of the problems at the expense of a significant increase in simulation time. Both water routing schemes are too simplified to be of use for predicting planform changes of actual rivers. Furthermore, the model relies on topographic data that, as indicated above, may not be readily available.

8.3.4 Branches model

Klaassen *et al.* (1993) formulated the conceptual framework for predicting planform changes of braided rivers in which the low-flow branches play a central role. The planform observed at low discharges is subdivided into separate (meandering) single threaded branches. The behaviour of the individual branches and their interaction is governed by empirical relations

formulated for the elementary planform changes summarised in Section 8.2.3. This conceptual model has been converted into a numerical model in which:

- Channel migration was given a kinematic meander migration model augmented with a formulation for down-valley migration during to flood.
- Channel width change was modelled using a stochastic process.
- Mid-channel formation was represented by a stochastic model influenced by the local width-depth ratio.
- The probability of channel abandonment was determined by the bifurcation angle.

Node migration resulted from the migration of the composing branches. The formation of new channels has been left to the modeller.

The performance of the model has been assessed using the same data set as used for the neural network. The predictions obtained from the branches model are of similar quality or slightly better than those obtained from the neural network. The advantage of the branches approach is, however, that the individual physical processes can be identified and improved if necessary. The simulations indicate that the mid-channel bar growth process plays a relatively minor role, whereas the lack of a physical description for the channel formation process results in an important role for the modeller.

8.3.5 Model comparison: suitability

The neural network approach, the branches model and the conventional 2D approach have been compared with respect to handling uncertainty, speed, physical basis, general applicability, detail of prediction, extendability with new knowledge, and input requirements. This has led to the following conclusions:

- The neural network approach provides an indication of the likelihood of erosion based on a single model execution. The other modelling approaches require a large number of simulations. The 2D approach is less suited for this purpose.
- The neural network approach and the branches model require relatively little computer time compared to the 2D approach.
- Physical knowledge forms basis of the process-based 2D approach and the branches model. The neural network is a black box approach.
- Due to elementary nature of the physics in the process-based 2D, this model can be applied confidently to other rivers. The other two approaches require (at least) recalibration.
- The 2D (possibly extended to 3D) approach can provide very detailed answers, whereas the other model concepts are only suited for large scale changes.
- The branches model and the 2D approach can be extended with new submodules for new processes. This is easiest for the 2D approach. It is not possible to add new knowledge to the neural network without extensive retraining.

- The 2D approach cannot be applied without accurate elevation data. This type of data is, however, not readily available for the Jamuna River. The other approaches have been developed to deal with this restriction.

The 2D approach is the best suited modelling approach if (1) new data collection techniques become available for faster acquisition of accurate elevation data and (2) computational speed continues to increase for some time. As long as these conditions are not met, the branches model is the most attractive model concept for predicting planform changes in the Jamuna River over periods of 1 to 3 years. Or, phrased in more general terms: the branches model is currently the most suitable modelling technique for predicting planform changes in braided rivers for periods encompassing 1 to 3 floods. However, its conceptual framework — based on a low stage channel network — needs to be extended with respect to the modelling of flood related processes, such as the interaction of overbank flow and low-stage channel alignment in general and the formation of new channels (cutoffs) in particular.

8.4 Channel formation

One of the most important events in the dynamics of a braided river is the formation of a new channel by incision. A physical or empirical description of this process lacks, however, in the branches model. Therefore, the process of channel formation has been studied in more detail in Chapters 6 and 7 based on the following research questions:

- What information is available in literature on the physical processes involved in channel formation?
- How are cutoffs dealt with in the existing numerical models?
- How sensitive are the results of 2D morphological simulations of bend cutoffs for changes in roughness, boundary conditions and sediment transport formula?

8.4.1 Processes

Channel incision results from erosion caused by an alongstream increase in the sediment transport rate (a function of sediment transport capacity and sediment availability). Such an increase may initially occur at the upstream or downstream end of the channel to be formed. This determines the direction of the channel forming process: headward erosion (or backcutting) from downstream or gradual incision from the upstream. The former process is encountered on hillslopes where discharge and shear stresses increase downslope due to an increase in rainfall runoff. New channels across a mature part of the flood plain during flood are generally also formed by this process. Headward erosion has also been observed in flume experiments of gravel-bed streams and under various circumstances in prototype streams (e.g., purely erosional cyclic steps of cohesive beds). The incision from the upstream side has, however, been observed in the Jamuna River.

8.4.2 Modelling concepts

Although there are several models for the formation of channels on hillslopes, there are none for the formation of new channels in rivers. The submodel for chute cutoffs in the numerical model of meander development by Howard (1996) comes closest. Others have addressed the stability of a bifurcation based on empirical relations or simplified physical models. A phase-plane stability analysis has shown that the distribution of sediment over the two downstream branches is decisive for the stability of the bifurcation. The sediment distribution is determined by the mode of transport, the relative dimensions of the channels downstream, and the geometry of the bifurcation point. The analysis shows that if the sediment distribution is approximately proportional to the discharge distribution (uniform distribution of suspended sediment), the bifurcation is unstable for any sediment transport formula $S = mu^n$ with a power n larger than 3. A similar analysis has shown that under such conditions the formation of a cutoff can be triggered by a flood period.

8.4.3 2D simulations

Depth-averaged flow and morphological simulations have been carried out using Delft3D-MOR for a schematised bend of the Jamuna River. The planform of the bend was suitable for a cutoff during flood. The formation of the cutoff channel was initiated in all simulation, but the extent of the erosion varied. The simulations show that the erosion (measured either as total eroded volume or as characteristic bed level lowering) increases — in the parameter range covered by the simulations: linearly — as a function of the discharge, the downstream water level lowering, and the roughness expressed in Manning. Furthermore, it decreases for increasing exponent c or critical Shields parameter θ_{cr} in the sediment transport relation $S = \alpha'(\theta - \theta_{cr})^c$ if the calibration coefficient α' is adjusted such that the width-averaged sediment transport rate remains the same. The simulation results are most sensitive for variations in discharge, roughness magnitude, and the exponent of the sediment transport relation (without adjustment of the calibration coefficient). The effect of the roughness is particularly large due to its presence in the sediment transport formula. Due to a relatively large water depth and relatively high velocities, the influence of the downstream water level and the critical Shields parameter was small.

In all cases the cutoff formed from the upstream end, which agrees with the observations of cutoffs in the Jamuna River. Only in simulations with a relatively low downstream water level, some initial erosion occurred at the downstream end of the cutoff channel. Similar results were obtained for a limited number of simulations for other planform geometries (with similar characteristic dimensions). These simulations indicate that the bifurcation angle is important for the rate of the cutoff formation.

Based on the simulations, it is concluded that none of the investigated physical parameters determines whether the cutoff formation starts at the upstream end (as in the case of the Jamuna River and the numerical model) or at the downstream end (headcut process). The simulation program has been adjusted to allow for spatial and temporal variations in the critical shear stress. With this adapted program it was possible to qualitatively reproduce the process of backcutting. This indicates that variations in the erodibility of sediment layers can be the cause of this erosion process.

8.5 Cutoff submodel for the branches model

Finally, there remains one research question:

- How can the knowledge on channel formation be incorporated in the branches model?

At the end of Chapter 7 an algorithm has been presented that can be implemented as part of the branches model. The actual implementation, calibration and testing of the algorithm was beyond the scope of the present study. The new submodule is conceptually similar to the model of Howard (1996) for cutoffs in meandering rivers. It is based on the following geometric parameters: cutoff ratio, bifurcation angle, vegetation cover, and relative curvature. Furthermore, the effect of flow convergence/divergence is included based on geometric properties of the cutoff channel. If topographic steering must be taken into account, a rough estimate of the flood plain elevations is required.

Bibliography

- Alabyan, A. M. and R. S. Chalov, 1998. “Types of river channel patterns and their natural controls.” *Earth Surface Processes and Landforms* 23: 467–474.
- Allen, J. R. L., 1965. “A review of the origin and characteristics of Recent alluvial sediments.” *Sedimentology* 5 (2): 89–191.
- Allison, M. A., 1998. “Historical changes in the Ganges-Brahmaputra Delta front.” *Journal of Coastal Research* 14 (4): 1269–1275.
- Anderson, R., 1994. “Eolian ripples as examples of self-organization in geomorphological systems.” *Earth Science Review* 28 (29): 77–96.
- Ashmore, P., F. Varkaris, J. Chandler, M. Stojic and J. Luce, 2000. “Animation of a sequence of DEMs of a braided river physical model.” In Nolan and Thorne (2000).
- Ashmore, P. E., 1982. “Laboratory modelling of gravel, braided stream morphology.” *Earth Surface Processes and Landforms* 7: 201–225.
- , 1985. *Process and form in gravel braided streams: Laboratory modelling and field observations*. University of Alberta, Canada. Ph.D. thesis.
- , 1988. “Bed load transport in braided gravel-bed stream models.” *Earth Surface Processes and Landforms* 13: 677–695.
- , 1991. “How do gravel-bed rivers braid?” *Canadian Journal of Earth Sciences* 28: 326–341.
- , 1993. “Anabranch confluence kinetics and sedimentation processes in gravel-braided streams.” In Best and Bristow (1993), pages 129–146.
- Ashmore, P. E., R. I. Ferguson, K. L. Prestegaard, P. J. Ashworth and C. Paola, 1992. “Secondary flow in anabranch confluences of a braided, gravel-bed stream.” *Earth Surface Processes and Landforms* 17: 299–311.
- Ashmore, P. E. and G. Parker, 1983. “Confluence scour in coarse braided streams.” *Water Resources Research* 19 (2): 392–402.
- Ashworth, P. J., 1996. “Mid-channel bar growth and its relationship to local flow strength and direction.” *Earth Surface Processes and Landforms* 21: 103–123.

- Ashworth, P. J., S. J. Bennet, J. L. Best and S. J. McLelland, eds., 1996. *Coherent Flow Structures in Open Channels*. John Wiley & Sons, Chichester etc.
- Ashworth, P. J., J. L. Best, J. O. Leddy and G. W. Geehan, 1994. "The physical modelling of braided rivers and deposition of fine-grained sediment." In Kirkby (1994), pages 115–139.
- Ashworth, P. J., R. I. Ferguson and D. M. Powell, 1992. "Bedload transport and sorting in braided channels." In Billi *et al.* (1992), pages 497–513.
- Babakaiff, C. S. and E. J. Hickin, 1996. "Coherent flow structures in Squamish River estuary, British Columbia, Canada." In Ashworth *et al.* (1996), pages 321–342.
- Bagnold, R. A., 1941. *The physics of blown sand and desert dunes*. Methuen, London. Reprinted by Chapman & Hall, London).
- Baptist, M. and E. Mosselman, 2002. "Biogeomorphological modelling of secondary channels in the Waal river." In Bousmar and Zech (2002), pages 773–782.
- Bendegom, L. van, 1947. "Some considerations on river morphology and river training." *De Ingenieur* 59 (4): B1–B12. In Dutch (Enige beschouwingen over riviermorphologie en rivierverbetering). An English translation appeared as National Research Council Canada (1963), *Technical Translation 1054*.
- Berg, J. H. van de, A. van Gelder and D. R. Mastbergen, 2002. "The importance of breaching as a mechanism of subaqueous slope failure in fine sand." *Sedimentology* 49: 81–95.
- Berlekamp, E. R., J. H. Conway and R. K. Guy, eds., 1982. *Winning Ways for Your Mathematical Plays*, vol. 2. Academic Press, New York.
- Best, J. L., 1986. "The morphology of river channel confluences." *Progress in Physical Geography* 10 (2): 157–174.
- , 1987. "Flow dynamics at river channel confluences: implications for sediment transport and bed morphology." In Ethridge *et al.* (1987), pages 27–35.
- , 1988. "Sediment transport and bed morphology at river channel confluences." *Sedimentology* 35: 481–498.
- , 1996. "The fluid dynamics of small-scale alluvial bedforms." In P. A. Carling and M. R. Dawson, eds., *Advances in Fluvial Dynamics and Stratigraphy*, pages 67–125. John Wiley & Sons, Chichester, etc.
- Best, J. L. and C. S. Bristow, eds., 1993. *Braided Rivers*. No. 75 in Geological Society Special Publication. The Geological Society, London.
- Best, J. L. and A. G. Roy, 1991. "Mixing layer distortion at the confluence of channels of different depths." *Nature* 350: 411–413.
- Best, J. L., A. G. Roy and B. De Serres, 1991. "Recent advances in the dynamics of river channel confluences: towards more complete flow models." *Eos* 72 (17): 138. Abstract book of the AGU/ASM 1991 Spring Meeting.

- Bhatnager, P., E. P. Gross and M. K. Krook, 1954. "A model for collision process in gases. I. Small amplitude processes in charged and neutral one-component systems." *Physics Review* 94 (3): 511–525.
- Bian, C., 1998. "Scientific exploration of Yarlung Zangbo River grand canyon." *Beijing Review* Apr.
- Biglari, B., 1989. *Cut-offs in curved alluvial rivers*. Master's thesis, IHE Delft, Delft, The Netherlands.
- Billi, P., R. D. Hey, C. R. Thorne and P. Tacconi, eds., 1992. *Dynamics of Gravel-Bed Rivers*. John Wiley, Chichester etc.
- Blom, A., 2003. *A vertical sorting model for rivers with non-uniform sediment and dunes*. University of Twente, Enschede, The Netherlands. Ph.D. thesis.
- Blom, A. and J. S. Ribberink, 1999. "Non-uniform sediment in rivers: vertical sediment exchange between bed layers." In Proc. RCEM 1999, vol. I, pages 45–54.
- Blom, A., J. S. Ribberink and H. J. de Vriend, 2003. "Vertical sorting in bed forms: Flume experiments with a natural and trimodal sediment mixture." *Water Resources Research* 39 (2).
- Blondeaux, P., P. Scandura and G. Vittori, 1999. "A lagrangian approach to describe sediment dynamics over a rippled bed: preliminary results." In Proc. RCEM 1999, vol. I, pages 185–194.
- Blondeaux, P. and G. Seminara, 1985. "A unified bar-bend theory of river meanders." *Journal of Fluid Mechanics* 112: 363–377.
- Boghosian, B. M., 1999. "Lattice gases and cellular automata." *Future Generation Computer Systems* 16 (2–3): 171–185.
- Booij, M., 2002. *Appropriate modelling*. University of Twente, Enschede, The Netherlands. Ph.D. thesis.
- Boothroyd, J. C. and G. M. Ashley, 1975. "Process, bar morphology and sedimentary structures on braided outwash fans, northeastern Gulf of Alaska." In Jopling and McDonald (1975), pages 193–222.
- Boothroyd, J. C. and D. Nummedal, 1978. "Proglacial braided outwash: a model for humid alluvial-fan deposits." In A. D. Miall, ed., *Fluvial Sedimentology*, Canadian Society of Petroleum Geologists, pages 641–668. Calgary, Canada.
- Bousmar, D. and Y. Zech, eds., 2002. *River Flow 2002, Proceedings of the International Conference on Fluvial Hydraulics, Louvain-la-Neuve, Belgium, 4–6 September 2002*. Balkema, Rotterdam.
- Bridge, J. S., 1993. "The interaction between channel geometry, water flow, sediment transport and deposition in braided rivers." In Best and Bristow (1993), pages 13–71.
- Bridge, J. S. and Bennett, 1992. "A model for the entrainment and transport of sediment grains of mixed sizes, shapes and densities." *Water Resources Research* 28: 337–363.

- Bridge, J. S. and S. L. Gabel, 1992. "Flow and sediment dynamics in a low sinuosity, braided river: Calamus River, Nebraska Sandhills." *Sedimentology* 39: 125–142.
- Bristow, C. S., 1987. "Brahmaputra River: Channel migration and deposition." In Ethridge *et al.* (1987), pages 63–74.
- Brush, L. M., Jr and M. G. Wolman, 1960. "Knickpoint behavior in noncohesive material: A laboratory study." *Geological Society of America Bulletin* 71: 59–74.
- Cane, M. A., 1983. "Oceanographic events during the El Niño." *Science* 222: 1189–1195.
- Carson, M. A., 1986. "Characteristics of high-energy "meandering" rivers: the Canterbury plains, NZ." *Geological Society of America Bulletin* 97: 886–895.
- Chalov, R. S. and A. M. Alabyan, 1994. "Channel processes and river ecosystems." In *Proceedings of the International Symposium East-West North-South Encounter on the State-of-the-Art in River Engineering Methods and Design Philosophies, 16-20 May 1994, St. Petersburg, Russia*, vol. I, pages 34–42. State Hydrological Institute, St. Petersburg, Russia.
- Chase, C. G., 1992. "Fluvial landsculpting and the fractal dimension of topography." *Geomorphology* 5: 39–57.
- Chein, N., 1961. "The braided stream of the Lower Yellow River." *Scientia Sinica* 10 (6): 734–754.
- Chopard, B., A. Dupuis, A. Masselot and P. Luthi, 2002. "Cellular automata and lattice Boltzmann techniques: An approach to model and simulate complex systems." *Advances in Complex Systems* 5 (2–3): 103–246.
- Church, M., 1972. "Beffin Island sandurs: a study of arctic fluvial processes." *Geological Survey of Canada Bulletin* 216.
- , 1985. "Bed load in gravel-bed rivers: observed phenomena and implications for computation." In *Annual Conference and the 7th Canadian Hydrotechnical Conference, 27-31 May 1985, Saskatoon, Saskatchewan*, vol. 1B - Hydrotechnical, pages 17–38. Canadian Society for Civil Engineering.
- , 1996. "Space, time and the mountain — How do we order what we see?" In B. L. Rhoads and C. E. Thorn, eds., *The scientific nature of geomorphology*, pages 147–170. John Wiley & Sons, Chichester.
- Church, M. and R. Gilbert, 1975. "Proglacial fluvial and lacustrine environments." In Jopling and McDonald (1975), pages 22–100.
- Church, M. and D. Jones, 1982. "Channel bars in gravel-bed rivers." In Hey *et al.* (1982), pages 291–324.
- Coleman, J. M., 1969. "Brahmaputra River: channel processes and sedimentation." *Sedimentary Geology* 3 (2–3): 129–239.
- Collinson, J. D. and J. Lewin, eds., 1983. *Modern and Ancient Fluvial Systems*. No. 6 in Special Publication of the International Association of Sedimentologists. Blackwell Scientific, Oxford.

- Colombini, M., G. Seminara and M. Tubino, 1987. "Finite-amplitude alternate bars." *Journal of Fluid Mechanics* 181: 213–232.
- Crosato, A., 1990. *Simulation of meandering river processes*. Communications on Hydraulic and Geotechnical Engineering, report 90-3. Delft University of Technology, Delft, The Netherlands.
- Cui, Y. and G. Parker, 1997. "A quasi-normal simulation of aggradation and downstream fining with shock fitting." *International Journal of Sediment Research* 12 (2).
- Darby, S. E. and I. Delbono, 2002. "A model of equilibrium bed topography for meander bends with erodible banks." *Earth Surface Processes and Landforms* 27: 1057–1085.
- Davoren, A. and M. P. Mosley, 1986. "Observations of bedload movement, bar development and sediment supply in the braided Ohau River." *Earth Surface Processes and Landforms* 11: 643–652.
- DHI, 2001. "Jamuna Bridge Bangladesh 95/96." <http://www.dhi.dk/dhiproj/Country/Bangla/Jamuna/bridge/bridge.avi>.
- DHI and SWMC, Jan. 1997. *Mathematical Morphological Model of Jamuna River, Jamuna Bridge Site, Draft Final Report*. Government of Bangladesh, Jamuna Multipurpose Bridge Authority, The World Bank.
- Dhondia, J. F. and G. S. Stelling, 2002. "Application of one dimensional – two dimensional integrated hydraulic model for flood simulation and damage assessment." In Hydroinformatics 2002, pages 265–276.
- Dietrich, W. E. and T. Dunne, 1993. "The Channel Head." In K. Beven and M. J. Kirkby, eds., *Channel Network Hydrology*, pages 175–219. John Wiley & Sons, Chichester etc.
- Doolen, G., ed., 1990. *Lattice Gas Methods for Partial Differential Equations*. Addison-Wesley.
- Dupuis, A., 2002. *From a lattice Boltzmann model to a parallel and reusable implementation of a virtual river*. 3356. University of Geneva, Switzerland. Ph.D. thesis.
- Dupuis, A. and B. Chopard, 2000. "Lattice gas simulation of sediment flow under submarine pipelines with spoilers." In Hydroinformatics 2000.
- Egiazaroff, I. V., 1965. "Calculation of nonuniform sediment concentration." *Journal of the Hydraulics Division, ASCE* 91 (4): 225–246.
- EGIS, 1997. *Morphological dynamics of the Brahmaputra-Jamuna River*. Tech. rep., EGIS, Dhaka, Bangladesh.
- , 2002. *Developing and updating empirical methods for predicting morphological changes of the Jamuna River*. Tech. Rep. 29, EGIS II, Dhaka, Bangladesh.
- Einstein, A., 1926. "Die Ursache der Meandebildung der Flussläufe und des sogenannten baerschen Gesetzes." *Die Naturwissenschaften* 14: 223.
- Elliot, C. M., ed., 1984. *River Meandering, Proc. Conf. Rivers, New Orleans, 1983*. American Society of Civil Engineers.

- Engelund, F., 1974. "Flow and bed topography in channel bends." *Journal of the Hydraulics Division, ASCE* 100 (11): 1631–1648.
- Engelund, F. and E. Hansen, 1967. *A monograph on Sediment Transport in Alluvial Streams*. Teknisk Forlag, Copenhagen.
- Engelund, F. and O. Skovgaard, 1973. "On the origin of meandering and braiding in alluvial streams." *Journal of Fluid Mechanics* 57: 289–302.
- Enggrob, H. G. and P. H. von Lany, 1994. "An application of 2-D mathematical modelling on the Brahmaputra River." In W. R. White and J. Watts, eds., *2nd International Conference on River Flood Hydraulics, 22-25 March 1994, York*, pages 117–130. John Wiley & Sons, Chichester etc.
- Enggrob, H. G. and S. Tjerry, 1999. "Simulation of morphological characteristics of a braided river." In Proc. RCEM 1999, vol. I, pages 585–594.
- Erskine, W., C. McFadden and P. Bishop, 1992. "Alluvial cutoffs as indicators of former channel conditions." *Earth Surface Processes and Landforms* 17 (1): 23–37.
- Erskine, W. and M. D. Melville, 1982. "Cutoff and oxbow lake. (a) On a straight-simulating river." *Australian geographer* 15: 174–177.
- Ethridge, F. G., R. M. Flores and M. D. Harvey, eds., 1987. *Recent Developments in Fluvial Sedimentology*. Society of Economic Paleontologists and Mineralogists, Special Publication 39.
- FAP21/22, 1994. *Technical report No. 2: Morphological predictions for test areas, Bank protection and river training pilot project FAP21/22*. FAP21/22, Dhaka, Bangladesh.
- , 2001. *Final report*. FAP21/22, Dhaka, Bangladesh.
- FAP24, 1994. *Study report No. 3: Morphological studies phase 1, Available data and characteristics*. FAP24, Dhaka, Bangladesh.
- , 1996. See River Survey Project (1996).
- Ferguson, R. I., 1984a. "Kinematic model of meander migration." In Elliot (1984), pages 942–951.
- , 1984b. "The threshold between meandering and braiding." In K. V. H. Smith, ed., *Proceedings of the 1st International Conference on Hydraulic Design*, pages 615–629. Springer Verlag, Berlin.
- Ferguson, R. I. and P. J. Ashworth, 1992. "Bedload and channel change in braided rivers." In Billi *et al.* (1992), pages 477–492.
- Fergusson, J., 1863. "Delta of the Ganges." *The Quarterly Journal of the Geological Society of London* 19: 321–354.
- Flokstra, C., 1985. *The influence of nodal relations on the bed levels at bifurcations*. Tech. Rep. R2166, Delft Hydraulics, Delft, The Netherlands. In Dutch (De invloed van knooppuntrelaties op de bodemligging bij splitsingspunten).

- Foody, G. M., 1996. "Approaches for the production and evaluation of fuzzy land cover classifications from remotely-sensed data." *International Journal of Remote Sensing* 17 (7): 1317–1340.
- Forrest, S. B. and P. K. Haff, 1992. "Mechanics of wind ripple stratigraphy." *Science* 255: 1240–1243.
- Foufoula-Georgiou, E. and V. B. Sapozhnikov, 1998. "Anisotropic scaling in braided rivers: An integrated theoretical framework and results from application to an experimental river." *Water Resources Research* 34 (4): 863–867.
- Fredsøe, J., 1978. "Meandering and braiding of rivers." *Journal of Fluid Mechanics* 84 (4): 609–624.
- Frisch, U., D. d'Humières, B. Hasslacher, P. Lallemand, Y. Pomeau and L.-P. River, 1987. "Lattice gas hydrodynamics in two and three dimensions." *Complex Systems* 1: 649–707. Reprinted in Doolen (1990).
- Frisch, U., B. Hasslacher and Y. Pomeau, 1986. "Lattice-gas automata for the Navier-Stokes equation." *Physical Review Letters* 56 (14): 1505–1508.
- Fujita, Y., 1989. "Bar and channel formation in braided streams." In Ikeda and Parker (1989), pages 417–462.
- Gagliano, S. M. and P. C. Howard, 1984. "The neck cutoff oxbow lake cycle along the Lower Mississippi River." In Elliot (1984), pages 147–158.
- Galay, V. J., E. K. Yaremko and M. E. Quazi, 1987. "River bed scour and constriction of stone riprap protection." In Thorne *et al.* (1987), pages 353–383.
- Gallapatti, G. and C. B. Vreugdenhil, 1985. "A depth-integrated model for suspended sediment transport." *Journal of Hydraulic Research* pages 359–377.
- Gay, G. R., H. H. Gay, W. H. Gay, H. A. Martinson, R. H. Meade and J. A. Moody, 1998. "Evolution of cutoffs across meander necks in Powder River, Montana, USA." *Earth Surface Processes and Landforms* 23 (7): 651–662.
- Gilvear, D., S. Winterbottom and H. Sichingabula, 2000. "Character of channel planform change and meander development: Luangwa River, Zambia." *Earth Surface Processes and Landforms* 25 (4): 421–436.
- Goff, J. R. and P. E. Ashmore, 1994. "Gravel transport and morphological change in braided Sunwapta River, Alberta, Canada." *Earth Surface Processes and Landforms* 19: 195–212.
- Goodbred, S. L. and S. A. Kuehl, 2000a. "Enormous Ganges-Brahmaputra sediment discharge during strengthened early Holocene monsoon." *Geology* 28 (12): 1083–1086.
- , 2000b. "The significant of large sediment supply, active tectonism, and eustasy on margin sequence development: Late Quaternary stratigraphy and evolution of the Ganges-Brahmaputra delta." *Sedimentary Geology* 133: 227–248.
- Gorycki, M. A., 1973a. "Hydraulic drag: a meander-initiating mechanism." *Geological Society of America Bulletin* 84: 175–186.

- , 1973b. "Reply: Hydraulic drag: a meander-initiating mechanism." *Geological Society of America Bulletin* 84: 3119–3122.
- Goswami, D. C., 1985. "Brahmaputra River, Assam, India: Physiography, basin denudation, and channel aggradation." *Water Resources Research* 21: 959–978.
- Griffiths, G. A., 1993. "Sediment translation waves in braided gravel-bed rivers." *Journal of Hydraulic Engineering* 119 (8): 924–937.
- Guala, M., G. Zolezzi, A. Branca and G. Seminara, 1999. "Preliminary experimental observations of upstream overdeepening." In Proc. RCEM 1999, vol. II, pages 131–140.
- Hagerty, D. J., 1991a. "Piping/sapping erosion I: Basic considerations." *Journal of Hydraulic Engineering* 117 (8): 991–1008.
- , 1991b. "Piping/sapping erosion II: Identification-diagnosis." *Journal of Hydraulic Engineering* 117 (8): 1009–1025.
- Halcrow, DHI, EPC and DIG, 1991. *River Training Studies of the Brahmaputra, Second Interim Report*. FAP1, Bangladesh.
- Hamblin, W. K. and E. H. Christiansen, 1995. *Earth's Dynamic Systems*. Prentice Hall, Englewood Cliffs, New Jersey.
- Hansen, E. A., J. Fredsøe and R. Deigaard, 1994. "Distribution of suspended sediment over wave generated ripples." *Journal of Waterway Port, Coastal and Ocean Engineering* 120 (1): 37–55.
- Hardisty, J., H. L. Rouse and N. E. Highes, 1996. "On the origin and effects of large-scale longitudinal flow structures in the Outer Humber Estuary." In Ashworth *et al.* (1996), pages 681–703.
- Heijden, F. van der, 1994. *Image Based Measurement Systems, Object Recognition and Parameter Estimation*. John Wiley & Sons, Chichester etc.
- Hein, F. J. and R. G. Walker, 1977. "Bar evolution and development of stratification in the gravelly, braided, Kicking Horse River, British Columbia." *Canadian Journal of Earth Sciences* 14 (4): 562–570.
- Hertz, J., A. Krogh and R. G. Palmer, 1991. *Introduction to the theory of neural computation*, vol. 1 of *Santa Fe Institute studies in the sciences of complexity. Lecture Notes*. Addison-Wesley, Redwood City (CA, USA), etc.
- Hey, R. D., J. C. Bathurst and C. R. Thorne, eds., 1982. *Gravel-bed rivers*. John Wiley & Sons, Chichester etc.
- Hibma, A., H. J. de Vriend and M. J. F. Stive, 2001. "Channel and shoal formation in estuaries." In Proc. RCEM 2001, pages 463–471.
- Hickin, E. J., 1979. "Concave-bank benches on the Squamish River, British Columbia, Canada." *Canadian Journal of Earth Sciences* 16: 200–203.
- Hickin, E. J., ed., 1995. *River Geomorphology*. John Wiley & Sons, Chichester etc.

- Hicks, D. M., M. J. Duncan, J. M. Walsh, R. M. Westaway, S. N. Lane and D. A. Jonas, 2000. "The braided Waimakariri River: new views of form and process from high-density topographic surveys and time-lapse imagery." In Nolan and Thorne (2000). Online image resource: <http://www.niwa.cri.nz/cam-era/sites/waimaka/about-waimakariri.htm>.
- Higuera, F. and J. Jiménez, 1989. "Boltzmann approach to lattice gas simulations." *Euro-physics Letters* 9 (7): 663–668.
- Higuera, F., S. Succi and R. Benzi, 1989. "Lattice gas dynamics with enhanced collision." *Europhysics Letters* 9 (4): 345–349.
- Hirst, Maj. F. C., 1916. *Report on the Nadia Rivers 1915*. The Bengal Secretariat Book Depot, Calcutta.
- Hjulström, F., 1935. "Studies of the morphological activity of rivers as illustrated by the River Fyris." *Bulletin of the Geological Institute University of Uppsala* 25: 221–527.
- Hoey, T. B. and A. J. Sutherland, 1991. "Channel morphology and bedload pulses in braided rivers: a laboratory study." *Earth Surface Processes and Landforms* 16: 447–462.
- Hoffmans, G. J. C. M. and H. J. Verheij, 1997. *Scour manual*. Balkema, Rotterdam.
- Horton, R. E., 1945. "Erosional development of streams and their drainage basins; hydrophysical approach to quantitative morphology." *Geological Society of America Bulletin* 56: 275–370.
- Hossain, M. M., 1992. "Total sediment load in the Lower Ganges and Brahmaputra." *Journal of the Institution of Engineers, Bangladesh* 20 (1–2): 1–8.
- Hou, S., J. Sterling, S. Chen and G. D. Doolen, 1988. "A lattice Boltzmann subgrid model for high Reynolds number flows." *Fields Institute Communications* 6: 151–166.
- Howard, A. D., 1984. "Simulation model of meandering." In Elliot (1984), pages 952–963.
- , 1992. "Modeling Channel Migration and Floodplain Sedimentation in Meandering Streams." In P. A. Carling and G. E. Petts, eds., *Lowland Floodplain Rivers: Geomorphological Perspectives*, pages 1–41. John Wiley & Sons, Chichester, etc.
- , 1994. "A detachment-limited model of drainage basin evolution." *Water Resources Research* 30 (7): 2261–2285.
- , 1996. "Modelling channel evolution and floodplain morphology." In M. G. Anderson, D. E. Walling and P. D. Bates, eds., *Floodplain processes*, pages 15–62. John Wiley & Sons, Chichester etc.
- Howard, A. D., M. E. Keetch and C. L. Vincent, 1970. "Topological and geometrical properties of braided streams." *Water Resources Research* 6: 1674–1688.
- Howard, A. D. and T. R. Knutson, 1984. "Sufficient conditions for river meandering: a simulation approach." *Water Resources Research* 20: 1659–1667.
- Hydroinformatics 2000, 2000. *Hydroinformatics 2000, Proceedings of the fourth international conference on hydroinformatics, Iowa, USA, 2000*.

- Hydroinformatics 2002, 2002. *Hydroinformatics 2002, Proceedings of the fifth international conference on hydroinformatics, Cardiff, UK, 2002.*
- Ikeda, S. and G. Parker, eds., 1989. *River Meandering*. American Geophysical Union, Water Resources Monograph 12.
- Ikeda, S., G. Parker and K. Sawai, 1981. "Bend theory of river meanders. Part 1: Linear development." *Journal of Fluid Mechanics* 112: 363–377.
- Imran, J. and G. Parker, 1999. "A nonlinear model of flow in meandering submarine and subaerial channels." *Journal of Fluid Mechanics* 400: 295–331.
- Inglis, C. C., 1938-39. "The relationship between meandering belts, distance between meanders on axis of streams, width and discharge of rivers in flood plains and incised rivers." In *Annual Report (Technical)*, page 49. Central Board of Irrigation, New Delhi, India.
- , 1947. *Meanders and their bearing on river training*. Maritime and Waterways, Paper no. 7. Institution of Civil Engineers.
- Izumi, N. and G. Parker, 1995. "Inception of channelization and drainage basin formation: upstream-driven theory." *Journal of Fluid Mechanics* 283: 341–363.
- , 2000. "Linear stability analysis of channel inception: downstream-driven theory." *Journal of Fluid Mechanics* 419: 239–262.
- Jackson, R. G., 1976. "Sedimentological and fluid-dynamic implications of the turbulent bursting phenomenon in geophysical flows." *Journal of Fluid Mechanics* 77 (3): 531–560.
- Jagers, H. R. A., 1999. "Numerical analysis of cutoff development." In Proc. RCEM 1999, vol. I, pages 553–562.
- , 2001. "A comparison of prediction methods for medium-term planform changes in braided rivers." In Proc. RCEM 2001, pages 713–722.
- Jansen, P. Ph., ed., 1979. *Principles of River Engineering*. Pitman Publishing Ltd. and London, Great Britain.
- Jeuken, M. C. J. L., 2000. *On the morphologic behaviour of tidal channels in the Westerschelde estuary*. No. 279 in Netherlands Geographical Studies. KNAG/Netherlands Geographical Studies, University of Utrecht, Utrecht. Ph.D. thesis.
- Joglekar, D. V., 1971. *Manual on river behaviour, control and training*. No. 60 in publication. Central Board of Irrigation and Power, New Delhi, India.
- Johannesson, H. and G. Parker, 1988. *Inertial effects on secondary and primary flow in curved channels*. No. 208 in External Memo. St. Anthony Falls Hydraulics Laboratory, University of Minneapolis, Minneapolis.
- , 1989. "Linear theory of river meanders." In Ikeda and Parker (1989), pages 181–213.
- Johnson, R. H. and J. Paynter, 1967. "The development of a cutoff on the River Irk at Chadderton, Lancashire." *Geography* 52 (1): 41–49.

- Jopling, A. V. and B. C. McDonald, eds., 1975. *Glaciofluvial and Glaciolacustrine Sedimentation*. Society of Economic Paleontologists and Mineralogists, Special Publication 23.
- Karpeta, W. P., 1993. "Sedimentology and gravel bar morphology in an Archaean braided river sequence: the Witpan Conglomerate Member (Witwatersrand Supergroup) in the Welkom Goldfield, South Africa." In Best and Bristow (1993), pages 369–388.
- Kellerhals, R., M. Church and D. I. Bray, 1976. "Classification and analysis of river processes." *Journal of the Hydraulics Division, ASCE* 102: 813–829.
- Kennedy, J. F., 1963. "The mechanics of dunes and antidunes in erodible-bed channels." *Journal of Fluid Mechanics* 16 (4): 521–544 plus 2 plates.
- Kilian, M., 1999. "Explorers say area discovered in Tibet is lush with life and glorious waterfalls." *World Tibet Network News* Also printed as: "'Shangri-la' found deep in Tibetan gorge", *Chicago Tribune*, Jan. 8, 1999.
- Kinoshita, R. and H. Miwa, 1974. "River channel formation which prevents downstream translation of transverse bars." *Shinsabo* pages 12–17. In Japanese.
- Kirkby, M. J., ed., 1994. *Process Models and Theoretical Geomorphology*. John Wiley & Sons, Chichester etc.
- Klaassen, G. J., 1992. "Experience from a physical model for a bridge across a braided river with fine sand as bed material." In *5th International Symposium on River Sedimentation, April 1992, Karlsruhe*, pages 509–520.
- Klaassen, G. J. and G. Masselink, 1992. "Planform changes of a braided river with fine sand as bed and bank material." *5th International Symposium on River Sedimentation, April 1992, Karlsruhe* pages 459–471.
- Klaassen, G. J., E. Mosselman and H. Brühl, 1993. "On the prediction of planform changes in braided sand-bed rivers." In S. S. Y. Wang, ed., *Proceedings 1st International Conference on Advances in Hydro-Science and -Engineering, 7-10 June 1993, Washington*, pages 134–146. University of Mississippi, University, Mississippi.
- Klaassen, G. J. and K. Vermeer, 1988. "Confluence scour in large braided rivers with fine bed material." In *Proceedings of the International Conference on Fluvial Hydraulics, Budapest, Hungary*, pages 381–394.
- Klaassen, G. J., K. Vermeer and N. Uddin, 1988. "Sedimentological processes in the Jamuna (lower Brahmaputra) River." *Proceedings of the International Conference on Fluvial Hydraulics, Budapest* pages 381–394.
- Klaassen, G. J. and B. H. J. van Zanten, 1989. "On cutoff ratios of curved channels." In *23rd Congress of the International Association on Hydrological Research, 21-25 August 1989, Ottawa*, vol. B, pages 121–130.
- Klees, R. A. P., R. F. Hanssen and S. Usai, 1997a. "SAR-interferometry (1), a new geodetic technique for determining elevations and elevation changes." *Geodesia* 1997 (4): 155–162. In Dutch (SAR-interferometrie (1), een nieuwe geodetische techniek voor het bepalen van hoogten en hoogteveranderingen).

- , 1997b. "SAR-interferometry (2), the interferometric creation of digital elevation models." *Geodesia* 1997 (12): 547–552. In Dutch (SAR-interferometrie (2), de interferometrische vervaardiging van digitale hoogtemodellen).
- Kleinhans, M. G., 2002. *Sorting out sand and gravel: sediment transport and deposition in sand-gravel bed rivers*. No. 293 in Netherlands Geographical Studies. KNAG/Netherlands Geographical Studies, University of Utrecht, Utrecht. Ph.D. thesis.
- Klis, H. van der, 2000. "Stochastic modelling of river morphology: A case study." In Z.-Y. Wang and S.-X. Hu, eds., *Stochastic Hydraulics 2000*, pages 109–116. Balkema, Rotterdam. Proceedings of the Eighth International Symposium on Stochastic Hydraulics, Beijing, China, 25–28 July 2000.
- , 2001. "Uncertainty analysis of a river morphological model." In Proc. RCEM 2001, pages 801–809.
- Knighton, D., ed., 1998. *Fluvial Forms & Processes: A New Perspective*. Arnold, London (co-published by John Wiley & Sons, New York).
- Koch, F. G. and C. Flokstra, 1980. "Bed level computations for curved alluvial channels." In *Proceedings of the XIXth congress of the International Association for Hydraulic Research, 2-7 Feb. 1981, New Delhi, India*, vol. 2, pages 357–364.
- Kostaschuk, R. A. and S. A. Ilersich, 1995. "Dune geometry and sediment transport: Fraser River, British Columbia." In Hickin (1995), pages 16–36.
- Krigström, A., 1962. "Geomorphological studies of sandur plains and their braided rivers in Iceland." *Geografiska Annaler* 44: 328–346.
- Krumbein, W. C. and A. R. Orme, 1972. "Field mapping and computer simulation of braided-stream networks." *Geological Society of America Bulletin* 83: 3369–3380.
- Kuehl, S. A., T. M. Hariu and W. S. Moore, 1989. "Shelf sedimentation off the Ganges-Brahmaputra river system: evidence for sediment bypassing to the Bengal fan." *Geology* 17: 1132–1135.
- Ladd, A. J. C., 1994a. "Numerical simulations of particulate suspensions via a discretized Boltzmann equation. Part 1. Theoretical foundation." *Journal of Fluid Mechanics* 271: 285–309.
- , 1994b. "Numerical simulations of particulate suspensions via a discretized Boltzmann equation. Part 2. Numerical results." *Journal of Fluid Mechanics* 271: 311–339.
- Lane, S. N., K. F. Bradbrook, K. S. Richards, P. M. Biron and A. G. Roy, 2000. "Secondary circulation cells in river channel confluences: measurement artefacts or coherent flow structures?" *Hydrological Processes* 14 (11–12): 2047–2071.
- Larson, R., 1999. "Fabled waterfall found near roof of the world." *Insight on the News* 15 (6): 42.
- LaTouche, T. H. D., 1910. "Relics of the great Ice Age in the plains of northern India." Reprinted in *Report on the Hoogly River and its Headwaters*, vol. 1. Bengal Secretariat Book Depot, Calcutta, 1919, pages 21–22.

- Ledden, M. van and Z. B. Wang, 2001. "Sand-mud morphodynamics in an estuary." In Proc. RCEM 2001, pages 505–514.
- Leopold, L. B. and M. G. Wolman, 1957. "River Channel Patterns, Braided, Meandering, and Straight." *United States Geological Survey, Professional Paper 282-B* pages 45–62. Reproduced in Schumm, S. A. (ed.), River morphology, Benchmark papers in geology, Hutchinson & Ross. and Dowden, 1972, pp.283–300.
- Lesser, G. R., J. A. Roelvink, J. van Kester and G. S. Stelling, 2003. "Development and validation of a three-dimensional morphological model." *Coastal Engineering* Submitted for publication.
- Lewis, G. W. and J. Lewin, 1983. "Alluvial cutoffs in Wales and the Borderlands." In Collinson and Lewin (1983), pages 145–154.
- Liverpool, T. B., R. C. Ball and S. F. Edwards, 1995. "A lattice model of the meandering river." *Europhysics Letters* 20 (3): 181–186.
- Lorenz, E. N., 1963. "Deterministic non-periodic flow." *Journal of Atmospheric Science* 20: 130–141.
- Lowe, C. P., J. G. M. Eggels and S. W. d. Leeuw, 1996. "Van statistische naar toegepaste natuurkunde via de rooster-Boltzmannvergelijking." *Nederlands Tijdschrift voor Natuurkunde* 62 (15): 327–331.
- Makaske, B., 1998. *Anastomosing rivers: Forms, processes and sediments*. No. 249 in Netherlands Geographical Studies. KNAG/Netherlands Geographical Studies, University of Utrecht, Utrecht. Ph.D. thesis.
- Martin, J. H., 1993. "A review of braided fluvial hydrocarbon reservoirs: the pretroleum engineer's perspective." In Best and Bristow (1993), pages 333–367.
- Masselot, A. and B. Chopard, 1998. "A lattice Boltzmann model for particle transport and deposition." *Europhysics Letters* 42: 259–264.
- , 1999. "The lattice Boltzmann method: a new approach to computational fluid dynamics and particle transport." *Future Generation Computer Systems* 16: 249–257.
- Matthes, G. H., 1948. "Mississippi River cutoffs." *American Society of Civil Engineers Transactions* 113: 1–39.
- McEwan, I., J. Heald and D. Goring, 1999. "Discrete particle modelling of entrainment from a mixed grain size sediment bed." In Proc. RCEM 1999, vol. I, pages 75–84.
- McNamara, G. R. and G. Zanetti, 1988. "Use of the Boltzmann equation to simulate lattice-gas automata." *Physical Review Letters* 61 (20): 2332–2335.
- Meyer-Peter, E. and R. Müller, 1948. "Formulas for bed load transport." In *Proceedings of the 2nd Congress IAHR, Stockholm*, vol. 2, pages 39–64.
- Molnar, P. and P. Tapponier, 1977. "The collision between India and Eurasia." *Scientific American* Apr.: 30.

- Montgomerie, T. G., 1885. "Report of a route survey made by Pandit Nain Sigh." *Proceedings of the Royal Geographical Society* 7: 188 pp.
- Montgomery, D. R. and W. E. Dietrich, 1994. "Landscape Dissection and Drainage Area-Slope Thresholds." In Kirkby (1994), pages 221–246.
- Morgan, J. P. and W. G. McInitire, 1959. "Quaternary geology of the Bengal basin, East Pakistan and India." *Geological Society of America Bulletin* 70: 319–342.
- Mosley, M. P., 1976. "An experimental study of channel confluences." *Journal of Geology* 84: 535–562.
- Mosley, M. P., ed., 2001. *Gravel-bed rivers V*. New Zealand Hydrological Society, Wellington.
- Mosselman, E., 1991. *Modelling of river morphology with non-orthogonal horizontal curvilinear coordinates*. No. 91-1 in Communications on hydraulic and geotechnical engineering. Delft University of Technology, Delft, The Netherlands.
- , 1992. *Mathematical modelling of morphological processes in rivers with erodible cohesive banks*. No. 92-3 in Communications on hydraulic and geotechnical engineering. Delft University of Technology, Delft, The Netherlands. Ph.D. thesis.
- Mosselman, E., M. Huisink, E. Koomen and A. C. Seymonsbergen, 1995. "Morphological changes in a large braided sand-bed river." In Hickin (1995), pages 235–247.
- Mosselman, E. and T. Martin, 1993. *Software system for river planform changes JAMUNA; Definition study and functional design*. Tech. rep., Joint project FAP21/22 and FAP19. Working document.
- Mosselman, E. and K. Sloff, 2002. "Effect of local scour holes on macroscale river morphology." In Bousmar and Zech (2002), pages 767–772.
- Murray, A. B. and C. Paola, 1994. "A cellular model of braided rivers." *Nature* 371: 54–57.
- , 1996. "A new quantitative test of geomorphic models, applied to a model of braided streams." *Water Resources Research* 32: 2579–2587.
- , 1997. "Properties of a cellular braided-stream model." *Earth Surface Processes and Landforms* 22: 1001–1025.
- Nanson, G. C. and E. J. Hickin, 1983. "Channel migration and incision on the Beatton River." *Journal of Hydraulic Engineering* 109: 327–337.
- Nanson, G. C. and A. D. Knighton, 1996. "Anabranching rivers: their cause, character and classification." *Earth Surface Processes and Landforms* 21: 217–239.
- Nanson, G. C. and K. Page, 1983. "Lateral accretion of fine-grained concave benches on meandering rivers." In Collinson and Lewin (1983), pages 133–143.
- NASA, 1988. "Photo STS027-033-079: Tibetan highlands." Featured in Strain and Engle (1992).

- , 1990. "Photo STS038-082-021: Brahmaputra River, Northeast India." <http://earth.jsc.nasa.gov/printinfo.cgi?PHOTO=STS038-082-021>.
- , 1996. "Photo STS075-705-057: Brahmaputra and Ganges Rivers." <http://earth.jsc.nasa.gov/printinfo.cgi?PHOTO=STS075-705-057>.
- , 2001a. "Photo ISS003-E-6632: Tibetan braid, Oct. 13, 2001." <http://visibleearth.nasa.gov/cgi-bin/viewrecord?10829>.
- , 2001b. "Terra/MODIS image of the valley of the Brahmaputra, India, and Mouths of the Ganges, Bangladesh on Oct. 23, 2001." <http://visibleearth.nasa.gov/cgi-bin/viewrecord?10722>.
- National Geographic, 1999. "Lost waterfall discovered in remote Tibetan gorge." Press Release Jan. 9, <http://www.geomag.com/events/releases/pr990111.html>, articles by among others Larson and Kilian.
- Nishimori, H., M. Yamasaki and K. H. Andersen, 1998. "A simple model for the various pattern dynamics of dunes." *International Journal of Modern Physics B* 12: 256–272.
- Nolan, T. J. and C. R. Thorne, eds., 2000. *Gravel-bed Rivers 2000 CD-ROM, Gravel-bed Rivers workshop, 28 August – 3 September 2000, Christchurch, New Zealand*, Special Publication. New Zealand Hydrological Society.
- Nykanen, D. K., E. Foufoula-Georgiou and V. B. Sapozhnikov, 1998. "Study of spatial scaling in braided river patterns using synthetic aperture radar imagery." *Water Resources Research* 34 (7): 1795–1807.
- Odgaard, A. J., 1981. "Transverse bed slope in alluvial channel bends." *Journal of the Hydraulics Division, ASCE* 107 (12): 1677–1694.
- Olsen, N. R. B., 2000. "Unstructure hexahedral 3D grids for CFD modelling in fluvial geomorphology." In *Hydroinformatics 2000*.
- , 2001. "CFD modelling of a self-forming meandering channel." <http://www.bygg.ntnu.no/ivb/forskn/prosjekt/nils-r/meander/>.
- , 2002. "Estimating meandering channel evolution using a 3D CFD model." In *Hydroinformatics 2002*, pages 52–57.
- Paola, C., 1996. "Incoherent structure: turbulence as a metaphor for stream braiding." In Ashworth *et al.* (1996), pages 705–723.
- , 2001. "Modelling stream braiding over a range of scales." In Mosley (2001), pages 11–46.
- Paola, C. and E. Foufoula-Georgiou, 2001. "Statistical geometry and dynamics of braided rivers." In Mosley (2001), pages 47–71.
- Paola, C., G. Parker, R. Seal, S. K. Sinha, J. B. Southard and P. R. Wilcock, 1992. "Downstream fining by selective deposition in a laboratory flume." *Science* 258: 1757–1760.
- Parker, G., 1975. "Meandering of supraglacial melt streams." *Water Resources Research* 11: 551–552.

- , 1976. “On the cause and characteristic scales of meandering and braiding in rivers.” *Journal of Fluid Mechanics* 76: 457–480.
- , 1978. “Self-formed straight rivers with equilibrium banks and mobile bed. Part 2. The gravel river.” *Journal of Fluid Mechanics* 89: 127–146.
- , 1984. “Theory of meander bend deformation.” In Elliot (1984), pages 722–732.
- , 1996. “Some speculations on the relation between channel morphology and channel-scale flow structures.” In Ashworth *et al.* (1996), pages 423–458.
- Parker, G., K. Sawai and S. Ikeda, 1982. “Bend theory of river meanders. Part 2: Nonlinear deformation of finite-amplitude bends.” *Journal of Fluid Mechanics* 115: 303–314.
- Pendick, D., 1996. “Himalayan high tension.” *Earth* Oct. Kalmbach pub., <http://www.kalmbach.com>.
- Pinet, P. R., ed., 1992. *Oceanography, an introduction to the planet oceanus*. West Publishing Company, St. Paul, Minnesota.
- Pittaluga, M. B., B. Federici, R. Repetto, C. Paola, G. Seminara and M. Tubino, 2001. “The morphodynamics of braiding rivers: experimental and theoretical results on unit processes.” In Mosley (2001), pages 143–181.
- Poddar, M. C., 1952. “Preliminary report of the Assam earthquake, 15th August, 1950.” *Bulletin Geological Survey India* 2: 11–13.
- Press, F. and R. Siever, eds., 1994. *Understanding earth*. W. H. Freeman and Company, New York.
- Proc. RCEM 1999, 1999. *Proceedings of the I.A.H.R. Symposium on River, Coastal and Estuarine Morphodynamics, 6–11 September 1999, Genova*, vol. I & II. University of Genova, Genova, Italy.
- Proc. RCEM 2001, 2001. *Proceedings of the I.A.H.R. Symposium on River, Coastal and Estuarine Morphodynamics, 10–14 September 2001, Obihiro*.
- Qian, Y. H., D. d’Humières and P. Lallemand, 1992. “Lattice BGK models for Navier-Stokes equation.” *Europhysics Letters* 17 (6): 470–484.
- Qian, Y. H., S. Succi and S. A. Orszag, 1996. “Recent advances in lattice Boltzmann computing.” In D. Stauffer, ed., *Annual Reviews of Computational Physics III*, pages 195–242. World Scientific.
- Rachocki, A. H., 1981. *Alluvial Fans, An attempt at an empirical approach*. John Wiley & Sons, New York.
- Rashidi, M., 1997. “Burst-interface interactions in free surface turbulent flows.” *Physics of Fluids* 9 (11): 3485–3501.
- Repetto, R. and M. Tubino, 1999. “Transition from migrating alternate bars to steady central bars in channels with variable width.” In Proc. RCEM 1999, vol. I, pages 605–614.

- Richardson, W. R. and C. R. Thorne, 1998. "Secondary currents around braid bar in Brahmaputra River, Bangladesh." *Journal of Hydraulic Engineering* 124 (3): 325–328.
- Richardson, W. R. R., C. R. Thorne and S. Mahmood, 1996. "Secondary flow and channel changes around a bar in the Brahmaputra River, Bangladesh." In Ashworth *et al.* (1996), pages 519–543.
- Rijn, L. C. van, 1984a. "Sediment transport, Part I: bed load transport." *Journal of Hydraulic Engineering* 110 (10): 1431–1456.
- , 1984b. "Sediment transport, Part II: suspended load transport." *Journal of Hydraulic Engineering* 110 (11): 1613–1640.
- , 1984c. "Sediment transport, Part III: bed form and alluvial roughness." *Journal of Hydraulic Engineering* 110 (12): 1733–1754.
- , 1989. *Handbook sediment transport by currents and waves*. Tech. Rep. H461, Delft Hydraulics, Delft, The Netherlands.
- , 1993. *Principles of sediment transport in rivers, estuaries and coastal seas*. Aqua Publications, Amsterdam.
- River Survey Project, 1996. *FAP24 Final report*. Delft Hydraulics, Delft, The Netherlands. For detailed information see Table A.1.
- Rozovskii, I. L., 1961. *Flow of water in bends of open channels*. Israel Program for Scientific Translations, Jerusalem, Israel. Translation of И.Л. Розовский, 1957. Движение Воды на Повороте Открытого Русла, Академия наук Украинской ССР(Academy of Sciences of the Ukrainian SSR), Киев (Kiev).
- Rundle, A., 1985. "Mechanisms of braiding." *Zeitschrift für Geomorphologie Suppl.-Bd* 55: 1–14.
- Sapozhnikov, V. and E. Foufoula-Georgiou, 1996. "Self-affinity in braided rivers." *Water Resources Research* 32 (5): 1429–1439.
- , 1997. "Experimental evidence of dynamic scaling and indications of self-organized criticality in braided rivers." *Water Resources Research* 33 (8): 1983–1991.
- Sapozhnikov, V., A. B. Murray, C. Paola and E. Foufoula-Georgiou, 1998. "Validation of braided-stream models: Spatial state-space plots, self-affine scaling, and island shapes." *Water Resources Research* 34 (9): 2353–2364.
- Sarker, M. H., 1996. *Morphological Processes in the Jamuna River*. Master's thesis, IHE Delft, Delft, The Netherlands.
- Schielen, R., A. Doelman and H. E. de Swart, 1993. "On the nonlinear dynamics of free bars in straight channels." *Journal of Fluid Mechanics* 252: 325–356.
- Schielen, R. M. J., 1995. *Nonlinear stability analysis and pattern formation in morphological models*. University of Utrecht, Utrecht, The Netherlands. Ph.D. thesis.

- Schijndel, S. A. H. van and H. R. A. Jagers, 2003. "Complex flow around groynes: Computations with Delft3D in combination with HLES." In *Proceedings Shallow Flows, Delft, 16–18 June 2003*. Balkema. Submitted for publication.
- Schmuck-Widmann, H., 2001. *Facing the Jamuna River: Indigenous and engineering knowledge in Bangladesh*. BARCIK, Bangladesh Resource Centre for Indigenous Knowledge, Dhaka, Bangladesh. Ph.D. thesis at the Institute of Sociology, Free University of Berlin, Germany, 2000.
- Schumm, S. A. and H. R. Khan, 1972. "Experimental study of channel patterns." *Geological Society of America Bulletin* 83: 1755–1770.
- Seminara, G. and M. Tubino, 1989. "Alternate bars and meandering: free, forced and mixed interactions." In Ikeda and Parker (1989), pages 153–180.
- Shields, A., 1936. "Application of similitude mechanics and the research on turbulence to bedload movement." *Mitteilungen der Preussischer Versuchsanstalt für Wasserbau und Schiffbau* 26. In German (Anwendung der Ähnlichkeitsmechanik und der Turbulenzforschung auf die Geschiebebewegung).
- Shimizu, Y., 2002. "A method for simultaneous computation of bed and bank deformation of a river." In Bousmar and Zech (2002), pages 793–801.
- Shock, R., S. Mallick, H. Chen, V. Yakhot and R. Zhang, 2002. "Recent results on two-dimensional airfoils using a lattice Boltzmann-based algorithm." *Journal of Aircraft* 39 (3): 434–439.
- Silva, W., F. Klijn and J. Dijkman, 2000. *Ruimte voor Rijntakken. Wat het onderzoek ons heeft geleerd*. Rijksinstituut voor Integraal Zoetwaterbeheer en Afvalwaterbehandeling (RIZA) and WL | Delft Hydraulics.
- Simons, D. B. and E. V. Richardson, 1961. "Forms of bed roughness in alluvial channels." *Journal of the Hydraulics Division, ASCE HY* 3: 87–105.
- Simons, D. B. and R. K. Simons, 1987. "Differences between gravel- and sand-bed rivers." In Thorne *et al.* (1987), pages 3–15.
- Slingerland, R. and N. D. Smith, 1998. "Necessary conditions for a meandering-river avulsion." *Geology* 26 (5): 435–438.
- Sloff, C. J., H. R. A. Jagers, Y. Kitamura and P. Kitamura, 2001. "2D morphological modelling with graded sediment." In Proc. RCEM 2001, pages 535–544.
- Smith, C. R., 1996. "Coherent flow structures in smooth-wall turbulent boundary layers: facts, mechanisms and speculation." In Ashworth *et al.* (1996), pages 1–39.
- Smith, D. G. and N. D. Smith, 1980. "Sedimentation in anastomosed river systems: examples from alluvial valleys near Banff, Alberta." *Journal of Sedimentary Petrology* 50: 157–164.
- Smith, N. D., 1974. "Sedimentology and bar formation in the upper Kicking Horse River, a braided meltwater system." *Journal of Geology* 82: 205–223.
- Smith, S. A., 1987. "Gravel counterpoint bars: examples from the River Tywi, South Wales." In Ethridge *et al.* (1987), pages 75–81.

- Smith, T. R. and F. P. Bretherton, 1972. "Stability and the Conservation of Mass in Drainage Basin Evolution." *Water Resources Research* 8 (6): 1506–1529.
- Southard, J. B., N. D. Smith and R. A. Kuhnle, 1984. "Chutes and lobes: newly identified elements in braiding in shallow gravelly streams." In E. H. Koster and R. J. Steel, eds., *Sedimentology of Gravels and Conglomerates*, Memoir 10, pages 51–59. Canadian Society of Petroleum Geologists.
- Stojic, M., J. Chandler, P. Ashmore and J. Luce, 1998. "The assessment of sediment transport rates by automated digital photogrammetry." *Photogrammetric Engineering and Remote Sensing* 64 (5): 387–395.
- Stølum, H.-H., 1996. "River meandering as a self-organization process." *Science* 271: 1710–1713.
- Strain, P. and F. Engle, 1992. *Looking at Earth*. Turner Publishing, Inc., Atlanta. Also appeared as *De aarde in beeld*, Natuur & Techniek, Maastricht, 1993.
- Struiksma, N., 1980. "Recent developments in design of river scale models with mobile bed." In *IAHR symposium on River Engineering and its Interaction with Hydrological and Hydraulic Research, Belgrado*. Wiley, Chichester, etc.
- , 1999. "Mathematical modelling of bedload transport over non-erodible layers." In Proc. RCEM 1999, vol. I, pages 89–98.
- Struiksma, N. and A. Crosato, 1989. "Analysis of 2-D bed topography model for rivers." In Ikeda and Parker (1989), pages 153–180.
- Struiksma, N. and G. J. Klaassen, 1988. "On the threshold between meandering and braiding." In *International Conference on River Regime, Wallingford, 18–20 May 1988*, pages 107–120. Wiley, Chichester, etc.
- Struiksma, N., K. W. Olesen, C. Flokstra and H. J. de Vriend, 1985. "Bed deformation in curved alluvial channels." *Journal of Hydraulic Research* 23 (1): 57–79.
- Sun, T., P. Meakin and T. Jøssang, 2001a. "A computer model for meandering rivers with multiple bed load sediment sizes, 1, Theory." *Water Resources Research* 37 (8): 2227–2241.
- , 2001b. "A computer model for meandering rivers with multiple bed load sediment sizes, 1, Computer simulations." *Water Resources Research* 37 (8): 2243–2258.
- , 2001c. "Meander migration and the lateral tilting of floodplains." *Water Resources Research* 37 (5): 1485–1502.
- Sun, T., P. Meakin, T. Jøssang and K. Schwarz, 1996. "A simulation model for meandering rivers." *Water Resources Research* 32: 2937–2954.
- Sun, T., C. Paola, G. Parker and P. Meakin, 2002. "Fluvial fan deltas: linking channel processes with large-scale morphodynamics." *Water Resources Research* 38 (8).
- Sundborg, A., 1956. "The River Klarälven: A study of Fluvial Processes." *Geografiska Annaler* 38 (2): 127–316.

- Talmon, A. M., N. Struiksma and M. C. L. M. van Mierlo, 1995. "Laboratory measurements of the direction of sediment transport on transverse alluvial-bed slopes." *Journal of Hydraulic Research* 33 (4): 495–517.
- Tetzlaff, D. and J. Harbaugh, eds., 1989. *Simulating Clastic Sedimentation*. Van Nostrand Reinhold, New York.
- Thomas, R., A. P. Nicholas and T. A. Quine, 2002. "Development and application of a cellular model to simulate braided river process-form interactions and morphological change." In Bousmar and Zech (2002), pages 783–791.
- Thorne, C. R., 1982. "Processes and mechanisms of river bank erosion." In Hey *et al.* (1982), pages 227–271.
- Thorne, C. R., J. C. Bathurst and R. S. Hey, eds., 1987. *Sediment Transport in Gravel-Bed Rivers*. John Wiley & Sons, Chichester etc.
- Thorne, C. R. and A. P. G. Russel, 1993. "Geomorphic study of bankline movement of the Brahmaputra River in Bangladesh." In *5th annual seminar of Scottish Hydraulics Study Group on sediment transport processes and phenomena, 2 April 1993, Edinburgh, U.K.*
- Thorne, C. R., A. P. G. Russel and M. K. Alam, 1993. "Planform pattern and channel evolution of the Brahmaputra river, Bangladesh." In Best and Bristow (1993), pages 257–276.
- Tillotson, E., 1951. "The great Assam earthquake of August 15, 1950." *Nature* 167: 128–130. Followed by 'Notes on the Assam earthquake' by Kingdon-Ward, Capt. F., 130–131.
- Tubino, M., 1991. "Growth of alternate bars in unsteady flow." *Water Resources Research* 27: 37–52.
- Tubino, M. and G. Seminara, 1990. "Free-forced interactions in developing meanders and suppression of free bars." *Journal of Fluid Mechanics* 214: 131–159.
- Umitsu, M., 1993. "Late quaternary sedimentary environments and landforms in the Ganges Delta." *Sedimentary Geology* 83: 177–186.
- Veen, J. van, 1950. "Ebb and flood channel systems in the Netherlands tidal waters." *Tijdschrift Koninklijk Nederlands Aardrijkskundig Genootschap* pages 303–325. In Dutch (Eb- en vloedschaar systemen in de Nederlandse getijwateren).
- Verwey, A., 2001. "Latest developments in floodplain modelling – 1D/2D integration." In *6th Conference on Hydraulics in Civil Engineering, 28–30 Nov. 2001, Hobart, Tasmania, Australia*. The Institute of Engineers Australia.
- Vriend, H. J. de, 1981a. *Steady flow in shallow channel bends*, vol. 81-3 of *Communications on Hydraulics*. Delft University of Technology, Delft, The Netherlands. Ph.D. thesis.
- , 1981b. "Velocity redistribution in curved rectangular channels." *Journal of Fluid Mechanics* 107: 423–439.
- , 1987. "2DH mathematical modelling of morphological evolutions in shallow water." *Coastal Engineering* 11: 1–27.

- Vriend, H. J. de and N. Struiksma, 1983. "Flow and bed deformation in river bends." In *Proceedings of the Conference, Rivers '83*, page 810. New Orleans, Louisiana.
- Vuren, S. van, H. van der Klis and H. J. de Vriend, 2002. "Large-scale floodplain lowering along the River Waal: a stochastic prediction of morphological impacts." In Bousmar and Zech (2002), pages 903–912.
- Wan, Z. H., 1983. "Some phenomena associated with hyperconcentrated flow." In B. M. Sumer and A. Müller, eds., *Euromech 156: Mechanics of Sediment Transport, Istanbul, 12–14 July 1982*, pages 189–194. Balkema, Rotterdam.
- Wang, Z. B., R. J. Fokkink, M. de Vries and A. Langerak, 1995. "Stability of river bifurcations in 1D morphodynamic models." *Journal of Hydraulic Research* 33 (6): 739–750.
- Warburton, J. and T. R. H. Davies, 1994. "Variability of bedload transport and channel morphology in a braided river hydraulic model." *Earth Surface Processes and Landforms* 19: 403–421.
- Wasson, R. J. and R. Hyde, 1983. "Factors determining desert dune type." *Nature* 304: 337–339.
- Webb, E. K., 1994. "Simulating the three-dimensional distribution of sediment units in braided stream deposits." *Journal of Sedimentary Research* B64: 219–231.
- , 1995. "Simulation of braided channel topology and topography." *Water Resources Research* 31: 2603–2611.
- Wilcock, P. R., 1992. "Experimental investigation of the effect of mixture properties on transport dynamics." In Billi *et al.* (1992), pages 109–140.
- Willgoose, R., R. L. Bras and I. Rodriguez-Iturbe, 1991. "A coupled channel network growth and hillslope evolution model, 1, theory." *Water Resources Research* 27 (7): 1671–1684.
- Williams, P. F. and B. R. Rust, 1969. "The sedimentology of a braided river." *Journal of Sedimentary Petrology* 39: 649–679.
- Winterwerp, J. C., 1999. *On the dynamics of high-concentrated mud suspensions*. Delft University of Technology, Delft, The Netherlands. Ph.D. thesis.
- WL | Delft Hydraulics, 1999. *Delft3D-FLOW v.3.05 manual*.
- , 2001. *Delft3D-MOR v.3.00 manual*.
- Xu, J.-X., 1996. "Wandering braided river channel pattern developed under quasi-equilibrium: an example from the Hanjiang River, China." *Journal of Hydrology* 181: 85–103.
- Zhang, D. D., 1998. "Geomorphological problems of the middle reaches of the Tsangpo River." *Earth Surface Processes and Landforms* 23: 889–903.
- Zolezzi, G. and G. Seminara, 2001. "Downstream and upstream influence in river meandering. Part I - General theory and application to overdeepening." *Journal of Fluid Mechanics* 438: 183–211.

Appendix A

Tables and figures

A.1 Overview FAP24 reports and data

The FAP24 project was carried out by Delft Hydraulics and the Danish Hydraulic Institute in association with Osiris, Hydroland and Approtech. The final report consists besides the main volume of five annexes, 24 special reports and 20 CDs of data:

Annexes	
1 Surveys	4 Sedimentology
2 Sustainable survey techniques	5 Morphological characteristics
3 Hydrology	
Special Reports	
1 Validation of staff gauge benchmarks	12 Optimization of sediment measurements
2 Water level gauging stations	13 Sediment transport predictors
3 Bathymetric surveys	14 Mineralogical and physical properties of river sediments
4 Stage-discharge relationship for the Jamuna at Bahadurabad	15 Overland flow and flood plain sedimentation
5 Qualitative impact assessment of FAP implementation	16 Study of secondary currents and morphological evolution in a bifurcated channel
6 Flood plain levels and bankfull discharges	17 Spatial representation and analysis of hydraulic and morphological data
7 Channel dimensions and geomorphological controls	18 Sediment rating curves and balances
8 Bed material sampling in Ganges, Padma, Old Brahmaputra and Jamuna	19 Joint measurements BWDB/RSP, hydrology
9 Bedforms and bar dynamics in the main rivers of Bangladesh	20 Joint measurements BWDB/RSP, morphology
10 Morphology of Gorai off-take	21 Guide to RSP databases
11 Optimization of hydraulic measurements	22 River data book, June 1993 - March 1995
	23 River data book, April 1995 - May 1996
	24 Morphological processes in the Jamuna River

Table A.1: General overview of the contents of the FAP24 report

Year	1993	1994
Quarter	Jan–Mar Apr–Jun Jul–Sep Oct–Dec	Jan–Mar Apr–Jun Jul–Sep
<i>Hydrological year</i>		
Flood season	=====	=====
Dry / lean season	=====	=====
<i>Water level gauging</i>		
Bahadurabad	=====
<i>Bahadurabad area</i>		
Gabgachi	=====	=====
Char Parul	=====	
Thantania Para	=====	
North Katiamari	=====	=====
North Horindhara		=====
Belgacha		=====
Kabilpur (Ratanpur)		=====
Shanki Bhanga		=====
Bhagir Chaow		=====
Bhuyanpur		=====
Sirajganj		
Aricha (Teota)		=====
<i>Routine transect gauging</i>		
Bahadurabad	* * * * *	* * * * *
Sirajganj	* * * *	* * * *
Aricha (Teota)	*	*
<i>Special surveys</i>		
Flow meas. at Bah'bad		*** *** ***
<i>Bedform inventory</i>		
Bah'bad–Sirajganj		***
Sirajganj–Aricha		***
Other special surveys		* *** * *
<i>Bathymetric surveys</i>		
Kamarjani		*
Bahadurabad	*	
Dhaleswari offtake	*	
Hurasagar outlet	*	
Jamuna/Ganges confl.	*	*

Table A.2: An overview of the FAP24 measurements along the Jamuna River from January 1993 until June 1996. Continued on next page.

1994	1995			1996			Year
Oct–Dec	Jan–Mar	Apr–Jun	Jul–Sep	Oct–Dec	Jan–Mar	Apr–Jun	Quarter

			<i>Hydrological year</i>
-----	-----	-----	Flood season
-----	-----	-----	Dry / lean season

		Water level gauging
		Bahadurabad
		<i>Bahadurabad area</i>
		Gabgachi
		Char Parul
		Thantania Para
		North Katiamari
		North Horindhara
		Belgacha
		Kabilpur (Ratanpur)
		Shanki Bhanga
		Bhagir Chaow
		Bhuyanpur
		Sirajganj
		Aricha (Teota)

Special surveys									
* * * * *	* * *** * * * **							Flow meas. at Bah'bad	
								<i>Bedform inventory</i>	
* * * * *	* * * * * * * * *							Bah'bad–Sirajganj	
* * * * *	* * * * * * * * *							Sirajganj–Aricha	
*1 * * *	* * * * * 22*3 * * * * 34					*		Other special surveys	

<i>Bathymetric surveys</i>					
*	*	*	*	*	Kamarjani
*	*	*	*	*	Bahadurabad
*	*	*	*	*	Dhaleswari offtake
*	*	*	*	*	Hurasagar outlet
*	*	*	*	*	Jamuna/Ganges confl.

Table A.2 continued: The Other special surveys were done at Bahadurabad, except for 1 Bahadurabad to Aricha, 2 Sirajganj, 3 Kamrajani, and 4 Jamuna/Ganges Confluence.

A.2 Results of Delft3D simulations

The tables and figures in this appendix summarise the results of all morphological Delft3D simulations reported on in Chapter 7 and Appendix D. Table A.3 lists the results of the simulations described in Chapter 7; selections of the data in this table have been presented in Tables 7.1 (discharge variation), 7.2 (downstream water level variation), 7.3 (roughness variation), 7.4 (variation of c and θ_{cr}) and 7.5 (various geometries). Table A.4 lists the results of the simulations that were carried out as part of the verification study described in Appendix D. The last column of the tables refers to the location of simulation results on the accompanying CD. The CD contains a dedicated version of QuickPlot that allows you to interactively inspect these results.

nr	ΔQ %	Δz_w m	roughness $n \text{ s/m}^{1/3}$ $C \text{ m}^{1/2}/\text{s}$	α -	c -	θ_{cr} -	geometry - flow char.	Δs m	ΔA 10^3 m^2	Δz_c m
1	0	0.00	$n = 0.020$	16.77	1.25	0.00	1 100 h	202	1.42	1.51
2	-25							131	0.78	0.86
3	-10							131	1.16	1.25
4	+10							202	1.62	1.71
5	+25							262	1.90	1.98
6	+50							322	2.28	2.34
7	+100							1004	2.70	2.76
8		+0.50						131	1.15	1.25
9		+0.25						131	1.27	1.37
10		-0.25						202	1.54	1.62
11		-0.50						202	1.65	1.72
12			$n = 0.015$					131	1.09	1.18
13			$n = 0.025$					202	1.67	1.75
14			$n = 0.030$					262	1.86	1.94
15			$C = 75$					131	0.94	1.03
16			$C = 60$					131	1.13	1.23
17			$C = 45$					202	1.45	1.54
18			$C = 75$	60.37				322	2.58	2.66
19			$C = 30\sqrt{h}$					202	1.95	2.02
20				15.00	1.83			322	2.19	2.21
21				13.19	2.50			322	3.01	3.02
22				8.70	1.83			202	1.31	1.38
23				4.08	2.50			131	1.19	1.25
24				27.00	1.25	1.00		131	1.22	1.27
25				20.96	1.25	0.50		131	1.36	1.43
26				18.45	1.25	0.25		202	1.37	1.45
27							2 0 h	262	0.87	1.14
28							2	322	1.34	1.75
29							2 200 h	443	1.65	2.14
30							3	60	0.75	0.66
31							4	181	1.19	1.01
32							4 rev.	50	0.22	0.45

Table A.3: Overview of the simulation parameters and results. Continued on next page.

Figure A.1 shows for every simulation a histogram of the erosion/sedimentation values on the pointbar PB defined in Figure 7.6. The mean μ and standard deviation σ of the Δz_{PB} distribution and the total eroded volume $\Delta V_{PB} = \sum_{\Delta z_{PB} < 0} \Delta x \Delta y \Delta z_{PB}$ given in the tables are based on the plotted data. Figure A.2 shows for every simulation the initial and final bed levels along cross-section BB (for the reference geometry defined in Figure 7.5). Based on the plotted data, the location y_x of maximum erosion and the amount of maximum erosion Δz_x have been determined. Finally, Figure A.3 shows for every simulation the initial and final bed levels along section AA (for the reference geometry defined in Figure 7.5). Based on the plotted data the total eroded area ΔA , the average erosion Δz_c over the eroded reach, and the downstream displacement Δs of the pointbar have been determined from these plots. The remaining figures show contour plots of the final planforms of simulations 1–17 and 20–26.

nr	y_x m	Δz_x m	Δz_{PB}		ΔV_{PB} 10^6 m^3	location on CD
			μ m	σ m		
1	900	1.20	0.94	0.72	0.57	Data/01_geo1
2	850	0.43	0.43	0.50	0.26	Data/02_geo1_0.75Q
3	900	0.88	0.74	0.64	0.45	Data/03_geo1_0.90Q
4	900	1.49	1.11	0.79	0.68	Data/04_geo1_1.10Q
5	900	1.87	1.28	0.91	0.83	Data/05_geo1_1.25Q
6	850	2.41	1.59	1.04	1.05	Data/06_geo1_1.50Q
7	800	3.24	2.03	1.15	1.40	Data/07_geo1_2.00Q
8	900	0.89	0.72	0.66	0.46	Data/08_geo1_z+0.50m
9	900	1.04	0.83	0.69	0.51	Data/09_geo1_z+0.25m
10	900	1.36	1.04	0.75	0.63	Data/10_geo1_z-0.25m
11	900	1.51	1.15	0.78	0.68	Data/11_geo1_z-0.50m
12	900	0.91	0.73	0.60	0.44	Data/12_geo1_n.0.015
13	900	1.47	1.10	0.81	0.69	Data/13_geo1_n.0.025
14	850	1.71	1.23	0.86	0.78	Data/14_geo1_n.0.030
15	850	0.69	0.61	0.54	0.37	Data/15_geo1_C75
16	850	0.87	0.75	0.61	0.44	Data/16_geo1_C60
17	850	1.21	0.92	0.72	0.58	Data/17_geo1_C45
18	850	3.02	2.00	1.11	1.22	Data/18_geo1_C75_CalAdapted
19	950	1.93	1.33	0.95	0.83	Data/19_geo1_C30sqrtH
20	850	2.12	1.40	0.97	0.85	Data/20_geo1_gf1.83_Cal1
21	800	4.06	1.95	1.42	1.19	Data/21_geo1_gf2.50_Cal1
22	850	1.00	0.81	0.68	0.48	Data/22_geo1_gf1.83_Cal2
23	850	0.82	0.69	0.64	0.40	Data/23_geo1_gf2.50_Cal2
24	750	0.85	0.73	0.66	0.41	Data/24_geo1_gf1.25thc1.00
25	850	1.03	0.88	0.69	0.51	Data/25_geo1_gf1.25thc0.50
26	850	1.08	0.90	0.70	0.53	Data/26_geo1_gf1.25thc0.25
27	850	1.12	0.25	0.48	0.40	Data/27_geo2_peak0h
28	850	1.87	0.40	0.75	0.65	Data/28_geo2_peak100h
29	850	2.40	0.52	0.94	0.85	Data/29_geo2_peak200h
30	1600	0.41	0.25	0.43	0.47	Data/30_geo3
31	2150	0.64	0.46	0.56	0.83	Data/31_geo4
32	2300	0.00	0.17	0.43	0.38	Data/32_geo4_ReverseFlow

Table A.3 continued: Overview of the simulation parameters and results.

nr	roughness $n/\text{sm}^{1/3}$ $C\text{ m}^{1/2}/\text{s}$	α	c	θ_{cr}	Δs m	ΔA 10^3 m^2	Δz_c m	y_x m	Δz_{cr} m	μ m	Δz_{PB} σ m	ΔV_{PB} 10^6 m^3	location on CD
1	$n = 0.020$	16.77	1.25	0.00	202	1.42	1.51	900	1.20	0.94	0.72	0.57	Data/01-geo1
33		15.00	1.83		267	2.27	2.35	850	2.31	1.46	1.17	1.12	Data/33-geo1.gf1.83.cal1.FineGrid
34				1.00	202	1.20	1.27	750	0.86	0.73	0.67	0.40	Data/34-geo1.gf1.25thc1_00_NoUpw
35		15.00	1.83		322	2.24	2.25	850	2.17	1.42	0.98	0.86	Data/35-geo1.gf1.83.cal1.ContZ
36				1.09	131	1.09	1.19	850	0.82	0.69	0.62	0.42	Data/36-geo1.C60.ContZ
37		15.00	1.83		262	2.06	2.29	900	2.08	1.38	1.03	0.84	Data/37-geo1.gf1.83.cal1.SpirEq
38		15.00	1.83		322	2.33	2.35	900	2.22	1.47	1.05	0.88	Data/38-geo1.gf1.83.cal1.SpirNonEq
39		0.077	Van Rijn	131	0.65	0.71	750	0.28	0.30	0.47	0.19	Data/39-geo1.vRijn_0.077	
40		0.154	Van Rijn	131	1.22	1.28	750	0.81	0.64	0.67	0.38	Data/40-geo1.vRijn_0.154	
41		1.000	Van Rijn	554	4.09	3.73	800	5.68	1.62	1.99	1.02	Data/41-geo1.vRijn_1.000	
42			Van Rijn	*	1.87	3.40	700	9.66	1.53	2.76	0.89	Data/42-geo1.vRijn	
43			Van Rijn	*	3.25	4.58	750	9.95	2.00	2.95	1.07	Data/43-geo1.3DMor_5Layers	

Table A.4: Overview of the simulation parameters and results. * indicates values not determined.

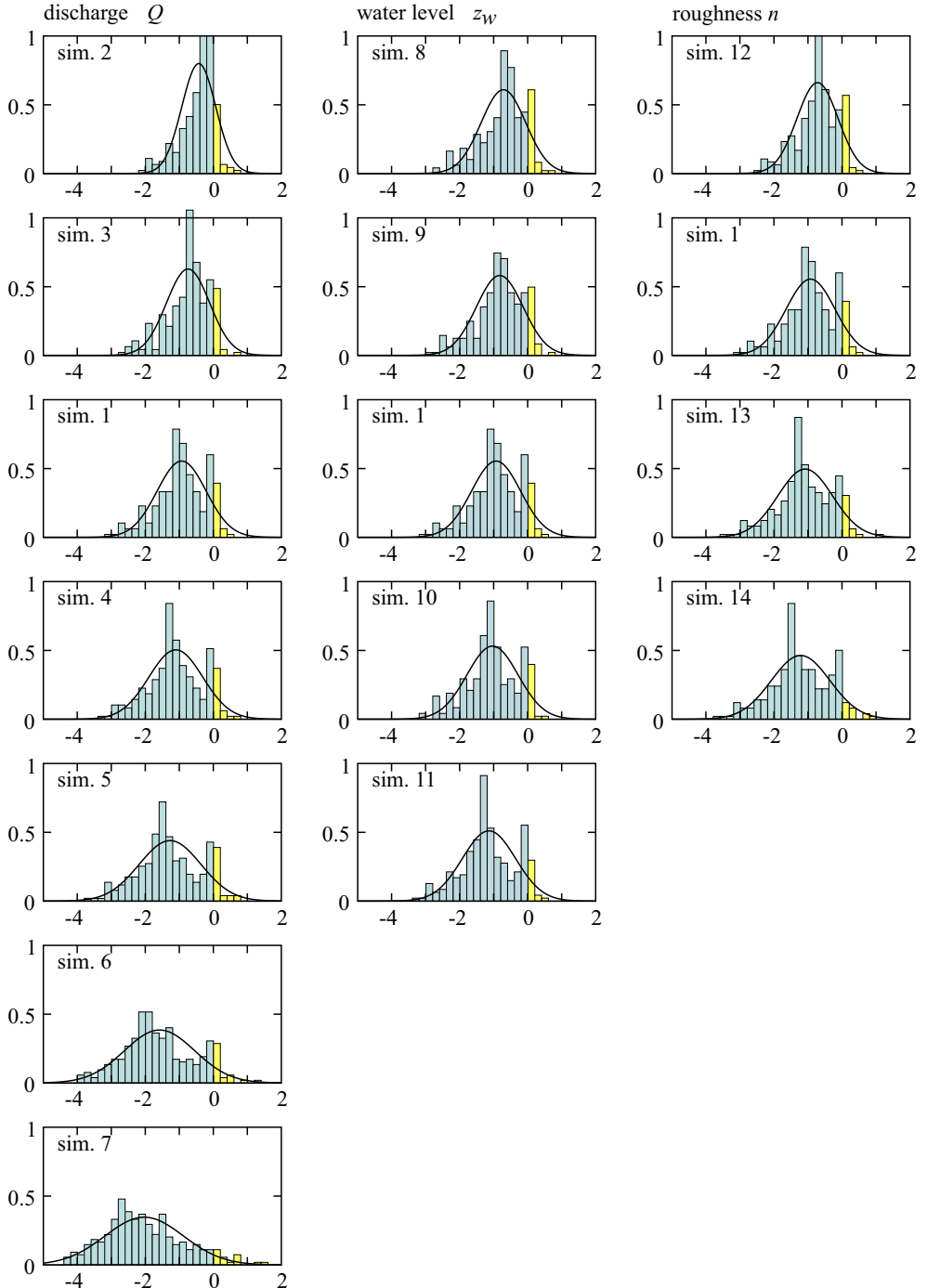
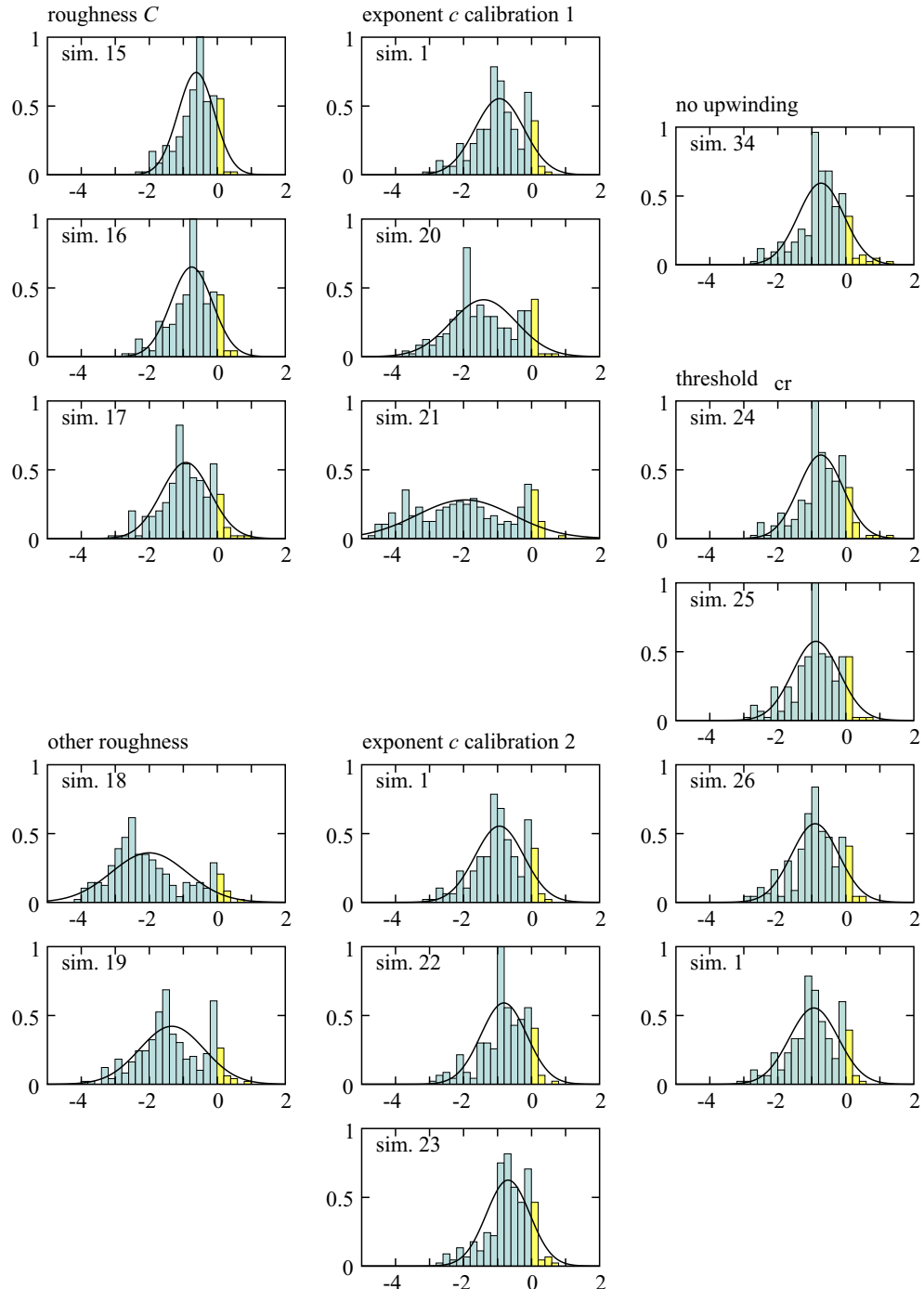


Figure A.1: Distribution of the amount of erosion on the pointbar Δz_{PB} . Gaussian fit based on the values of μ and σ given in Table A.3.



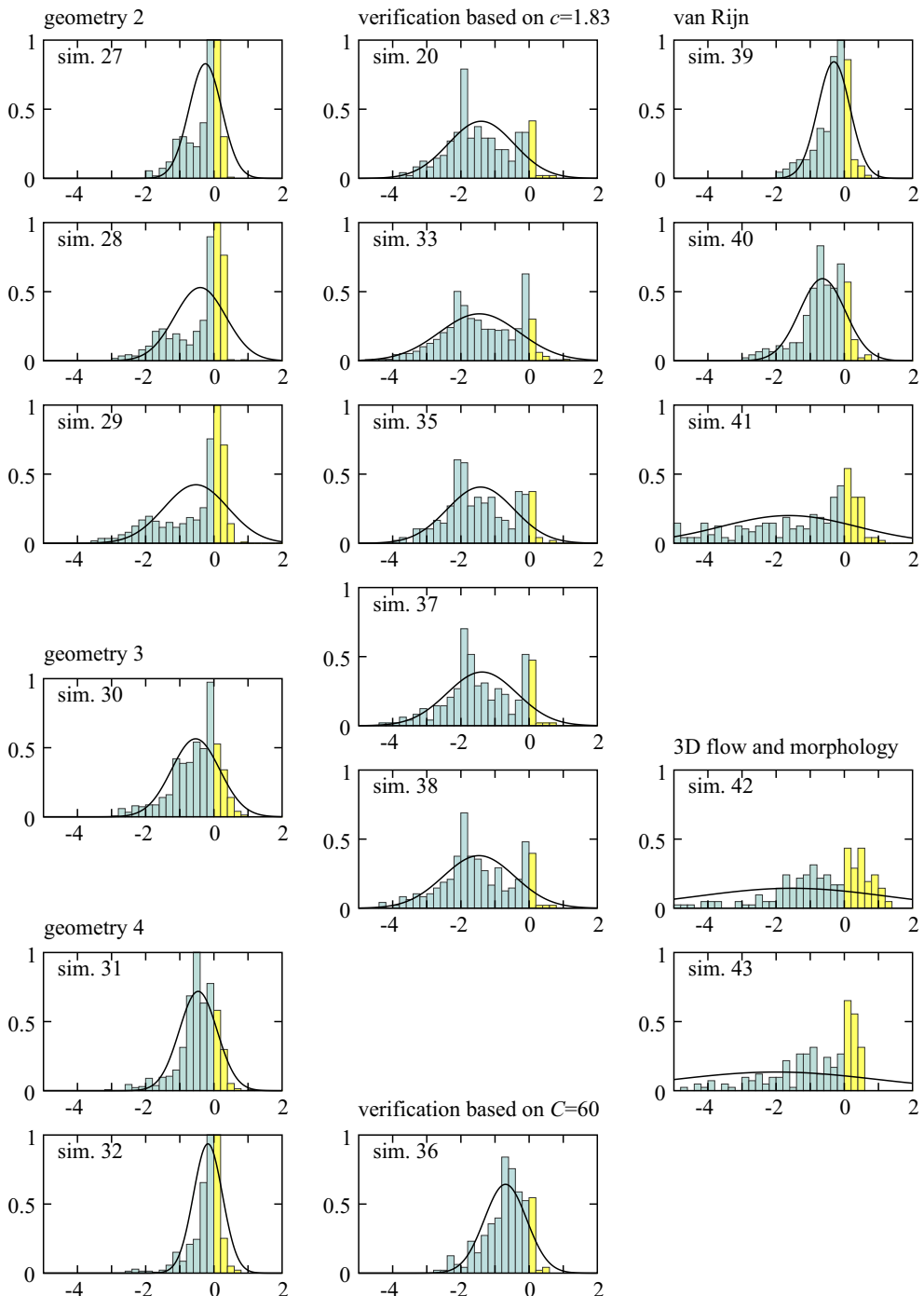


Figure A.1 continued: Distribution of the amount of erosion on the pointbar Δz_{PB} .

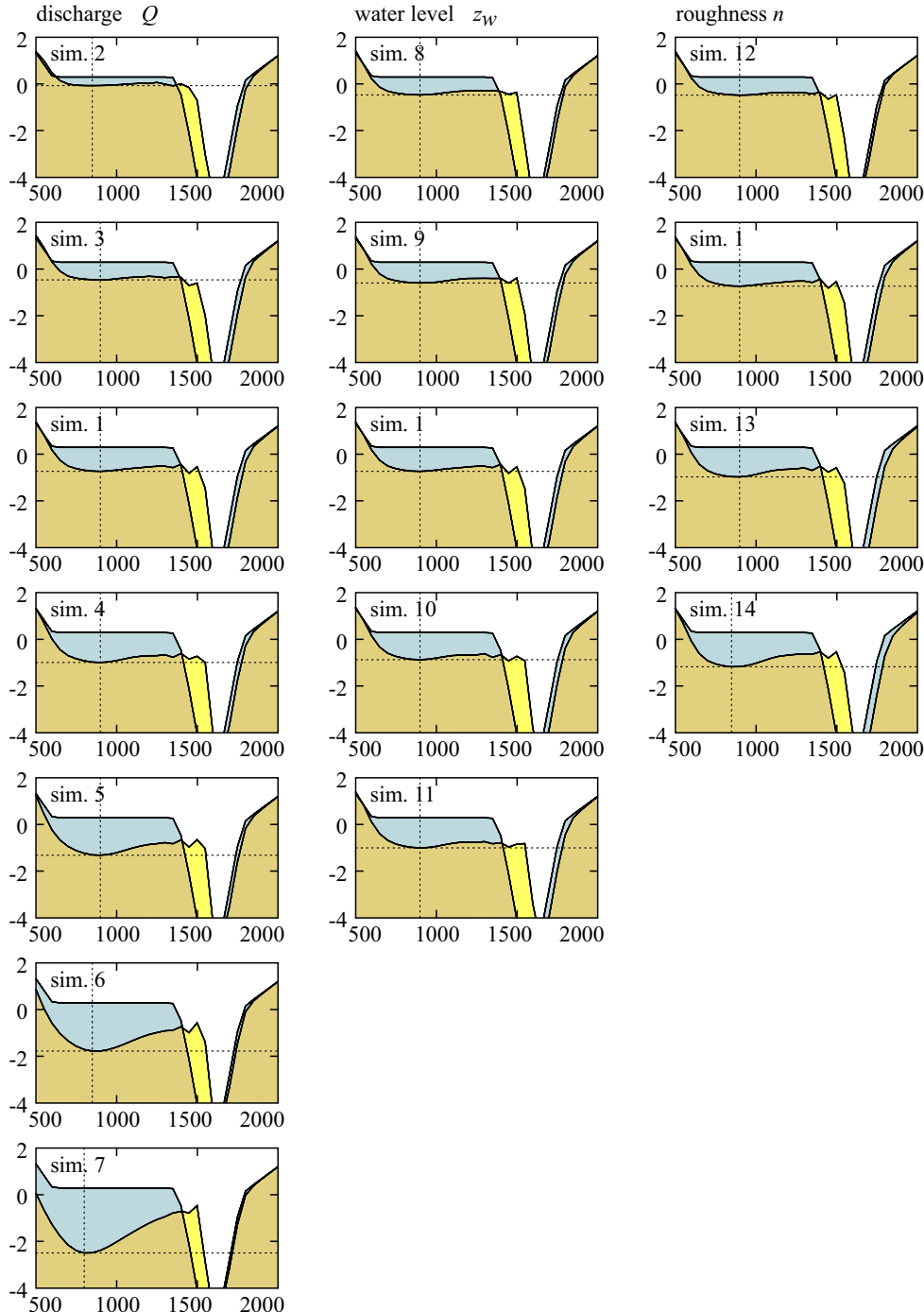


Figure A.2: Initial and final bed levels along section BB (see Figure 7.5) used to determine y_x and Δz_x summarised in Table A.3.

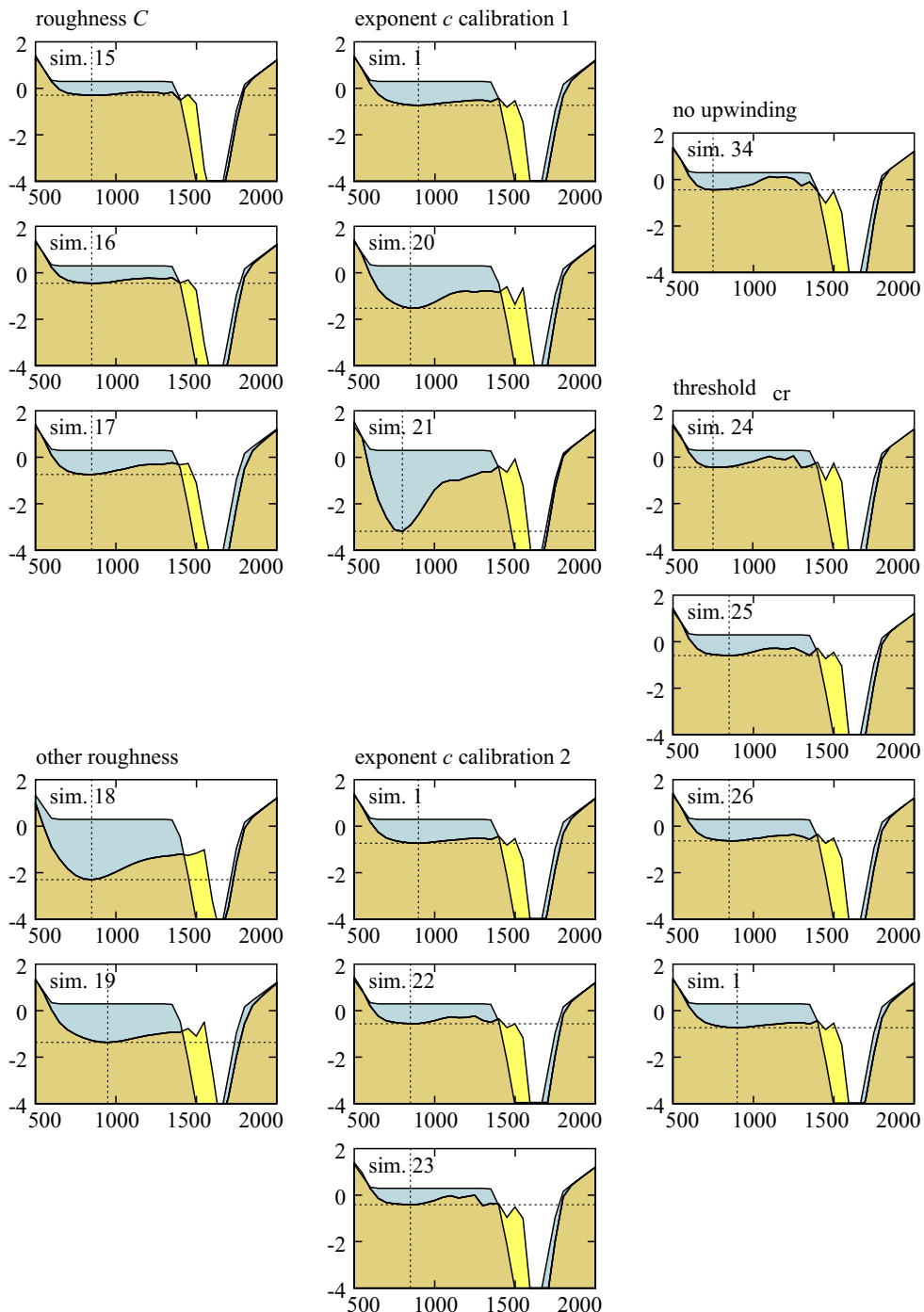


Figure A.2 continued: Bed levels along section BB.

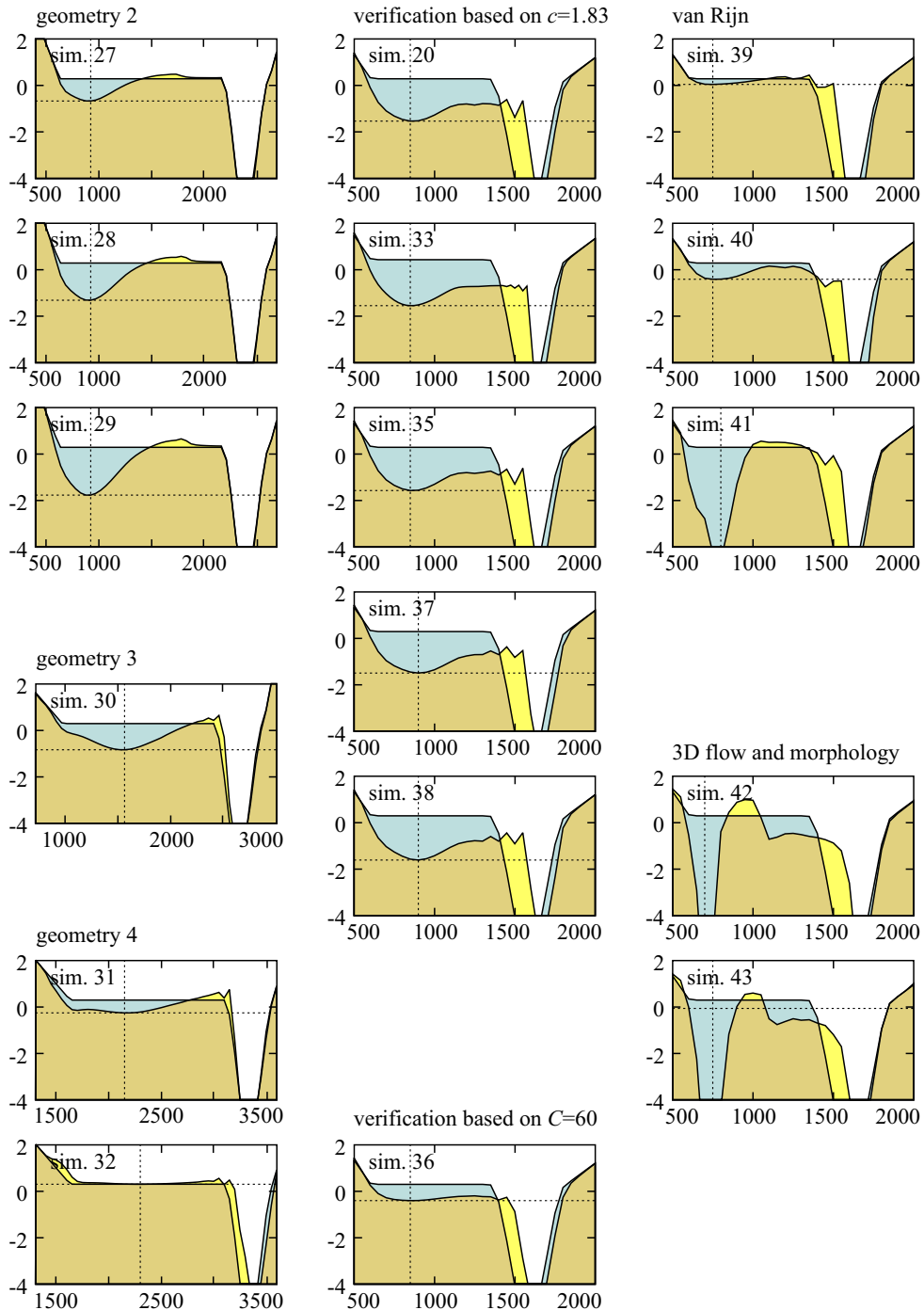


Figure A.2 continued: Bed levels along section BB.

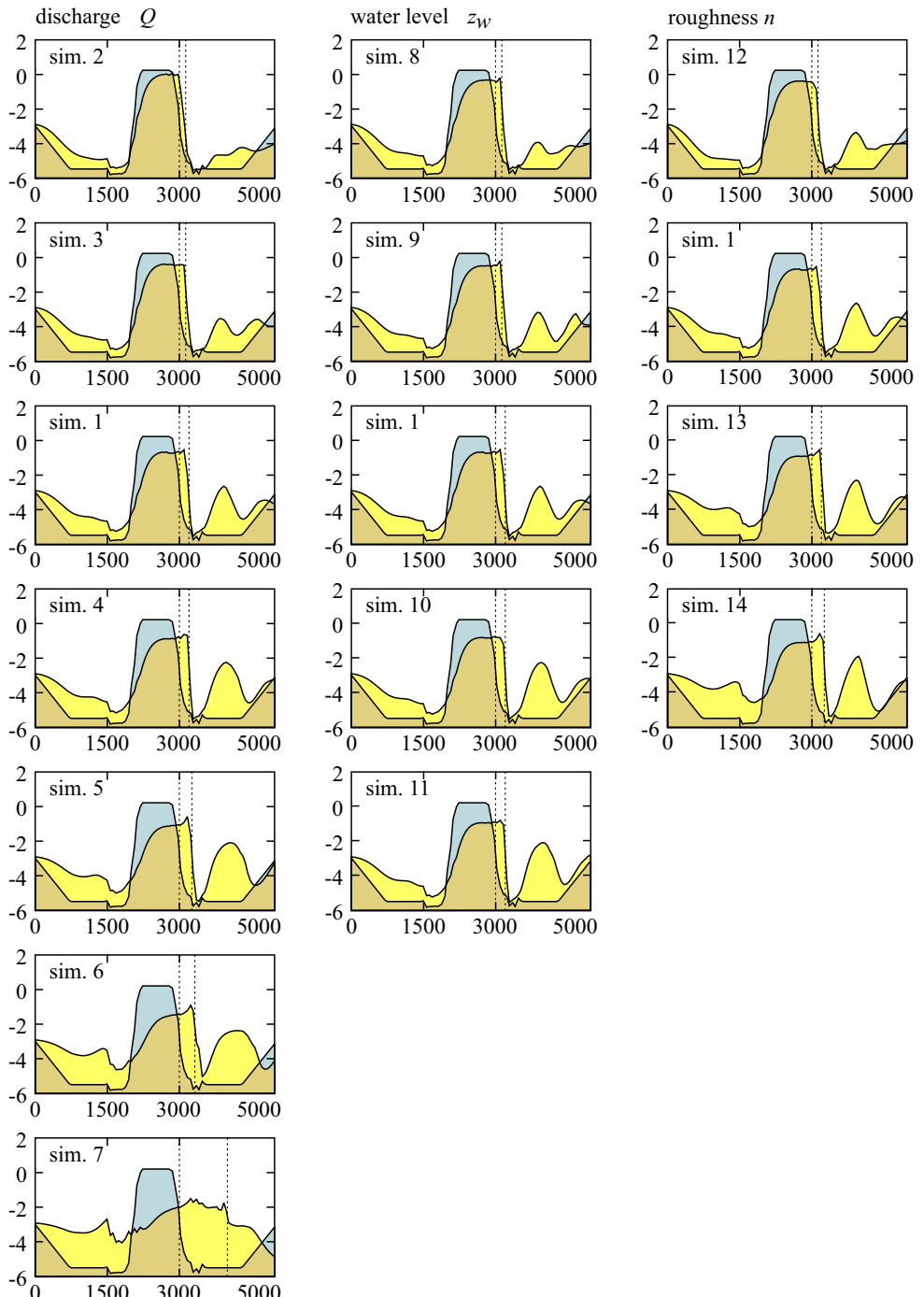


Figure A.3: Initial and final bed levels along section AA (see Figure 7.5) used to determine Δs , ΔA and Δz_c summarised in Table A.3.

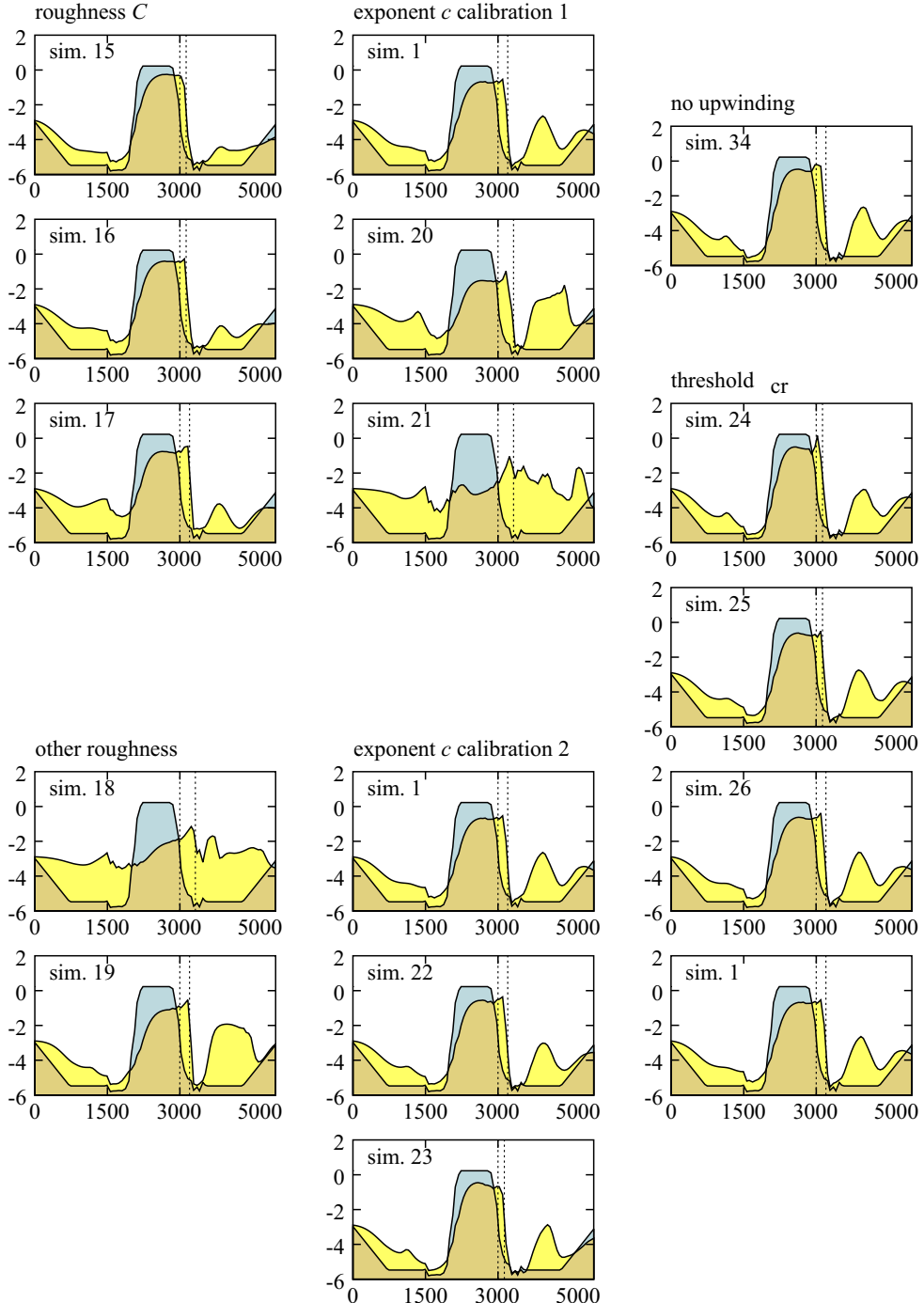


Figure A.3 continued: Bed levels along section AA.

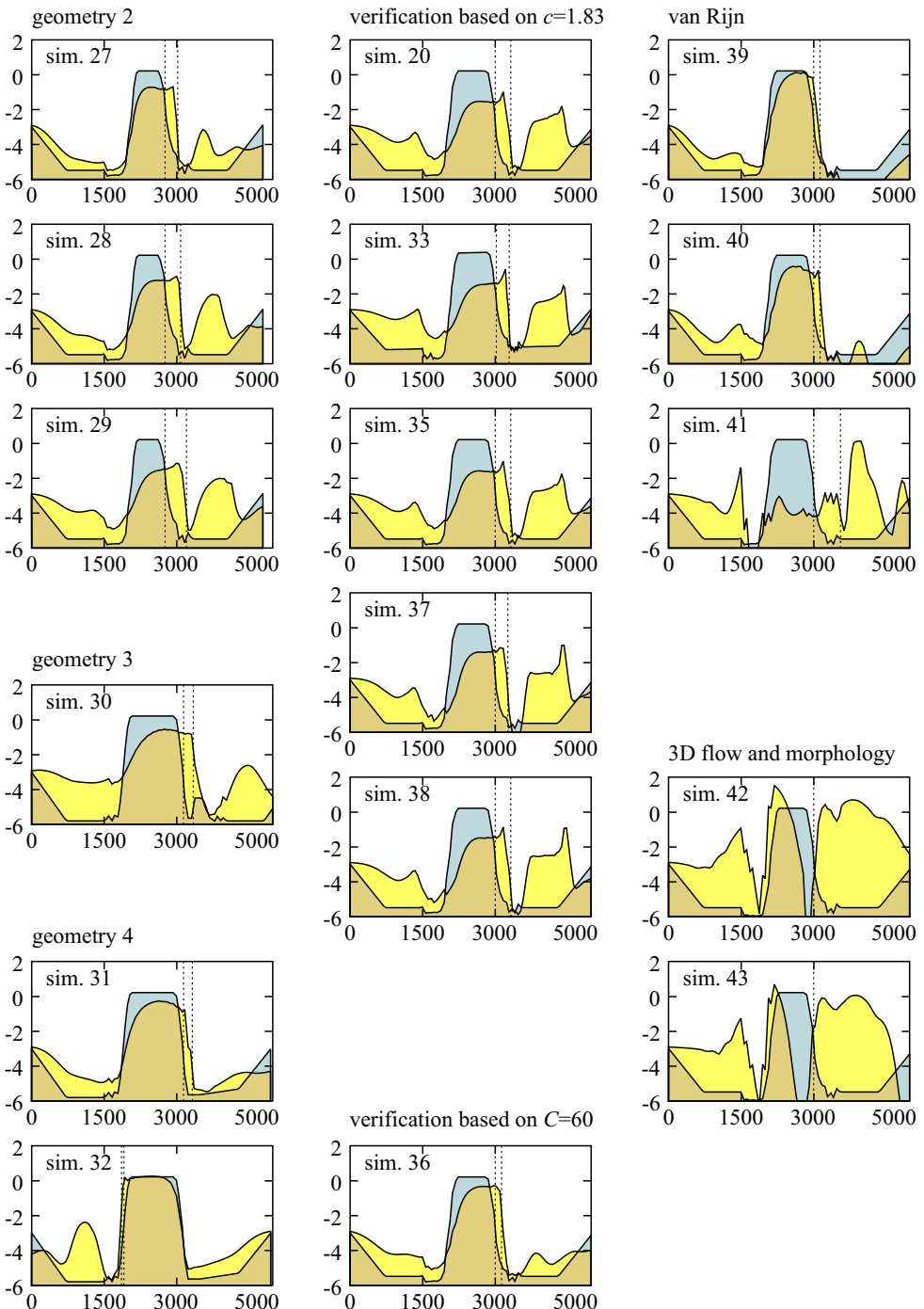


Figure A.3 continued: Bed levels along section AA.

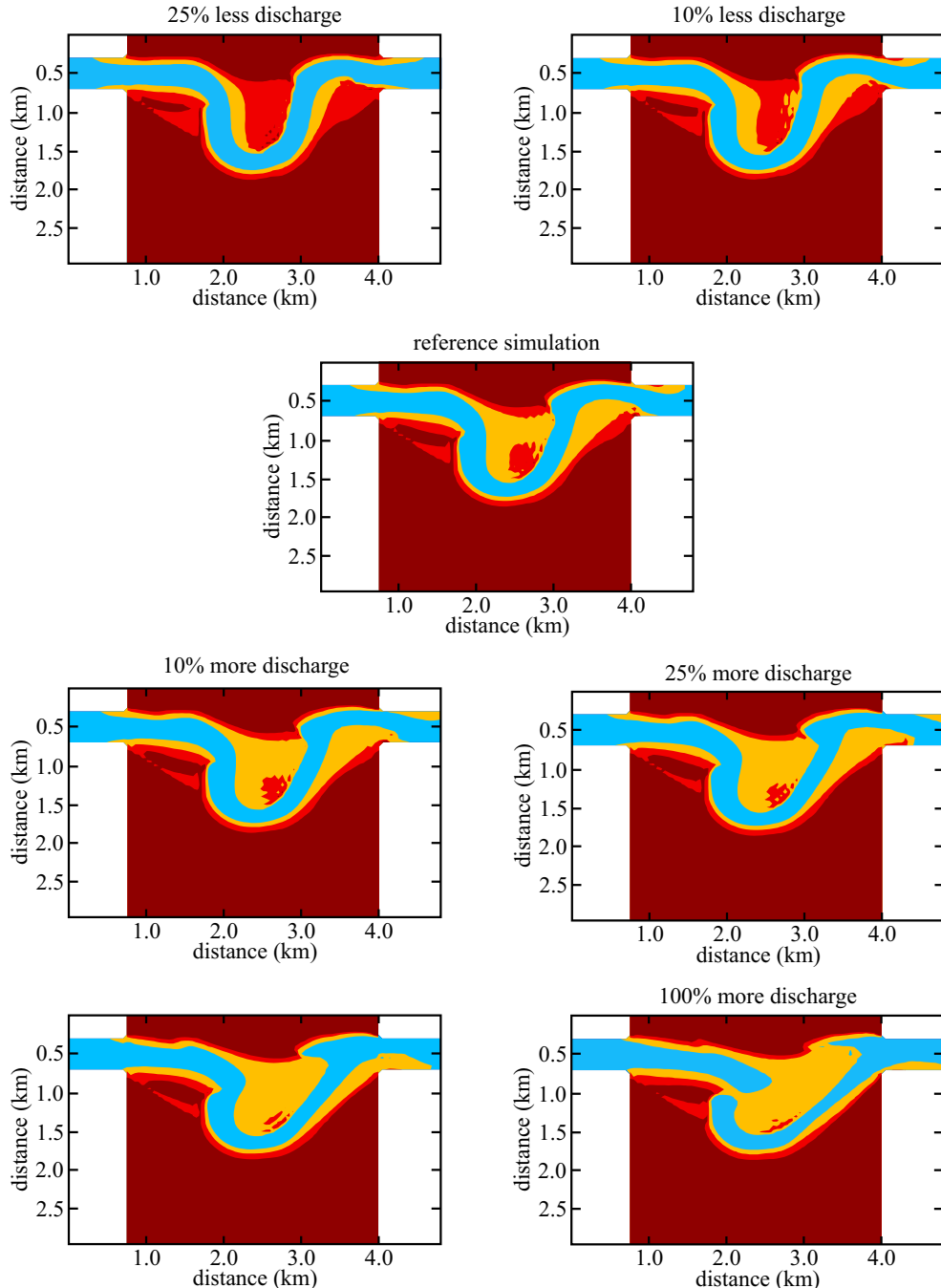


Figure A.4: Planforms for different discharges (downstream condition not changed). The contour lines are drawn at 0, -1, and -3 m. Flow is from left to right. If the discharge is reduced by 25% or more, little morphological change occurs. At twice the reference discharge the cutoff forms almost completely within the same simulation period of 320 hours. See also Section 7.3.1.

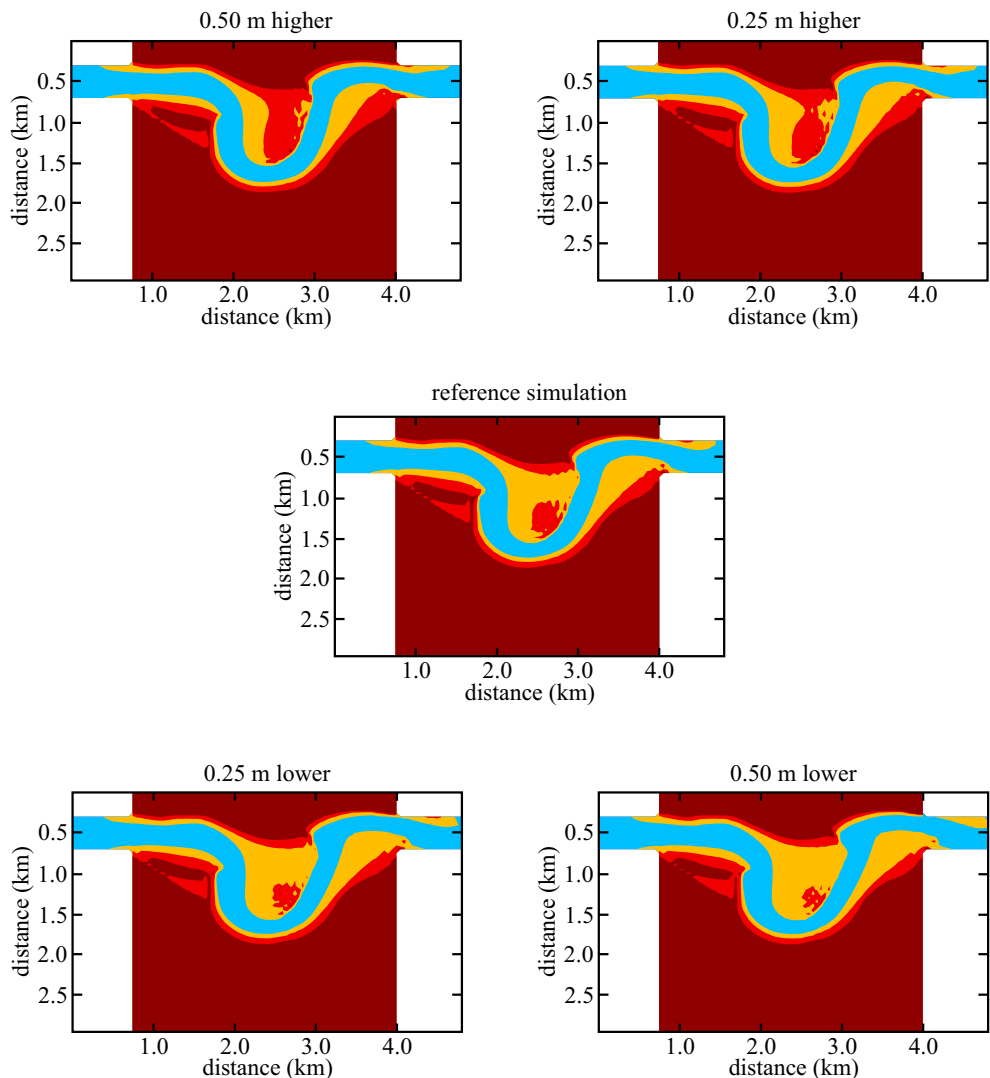


Figure A.5: Planforms for different downstream boundary conditions. The contour lines are drawn at 0, -1, and -3 m. Flow is from left to right. A shallow cutoff channel develops further if the downstream water is lower. See also Section 7.3.2.

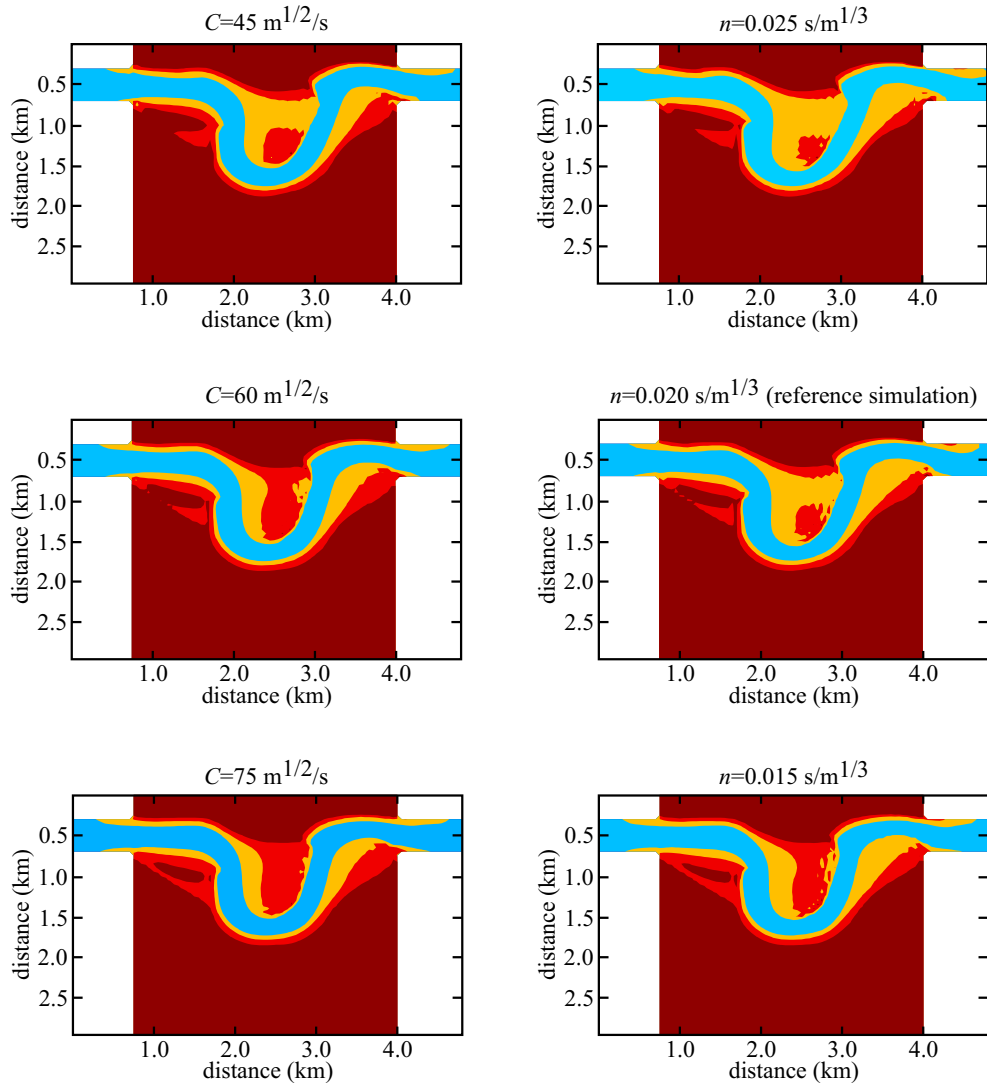


Figure A.6: Planforms for different settings of the roughness parameter. The contour lines are drawn at 0, -1, and -3 m. Flow is from left to right. Wide and shallow cutoff channels develop in case of a large roughness (i.e. high n or low C). See also Section 7.3.3.

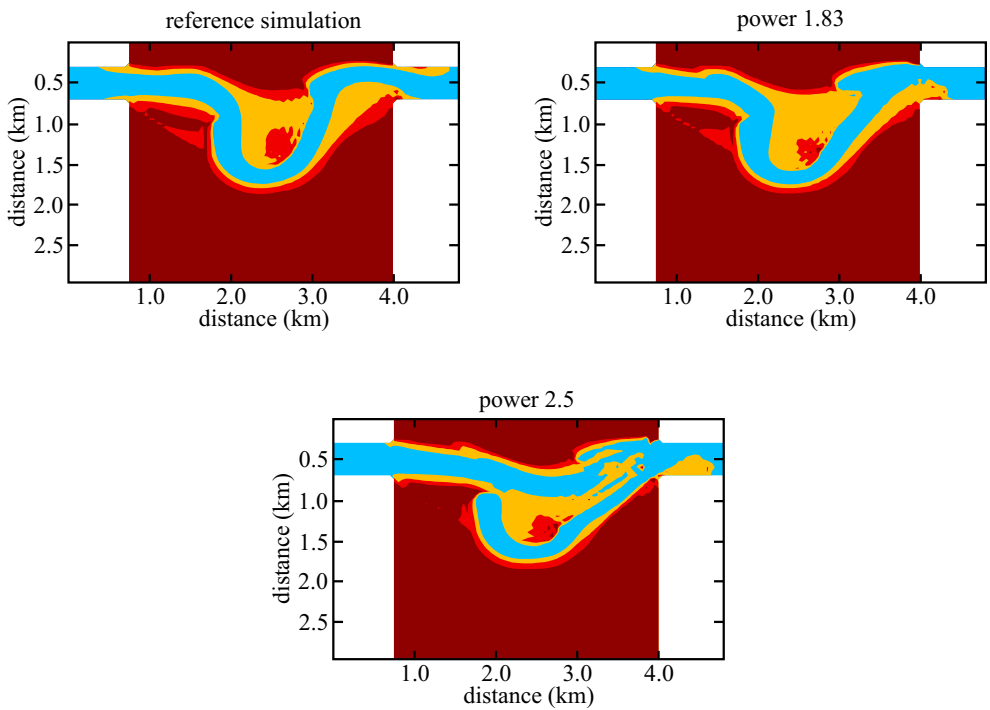


Figure A.7: Planforms for varying exponents c . The contour lines are drawn at 0, -1, and -3 m. Flow is from left to right. A larger value for the exponent in the sediment transport relation increases the cutoff development rate significantly. See also Section 7.3.4.

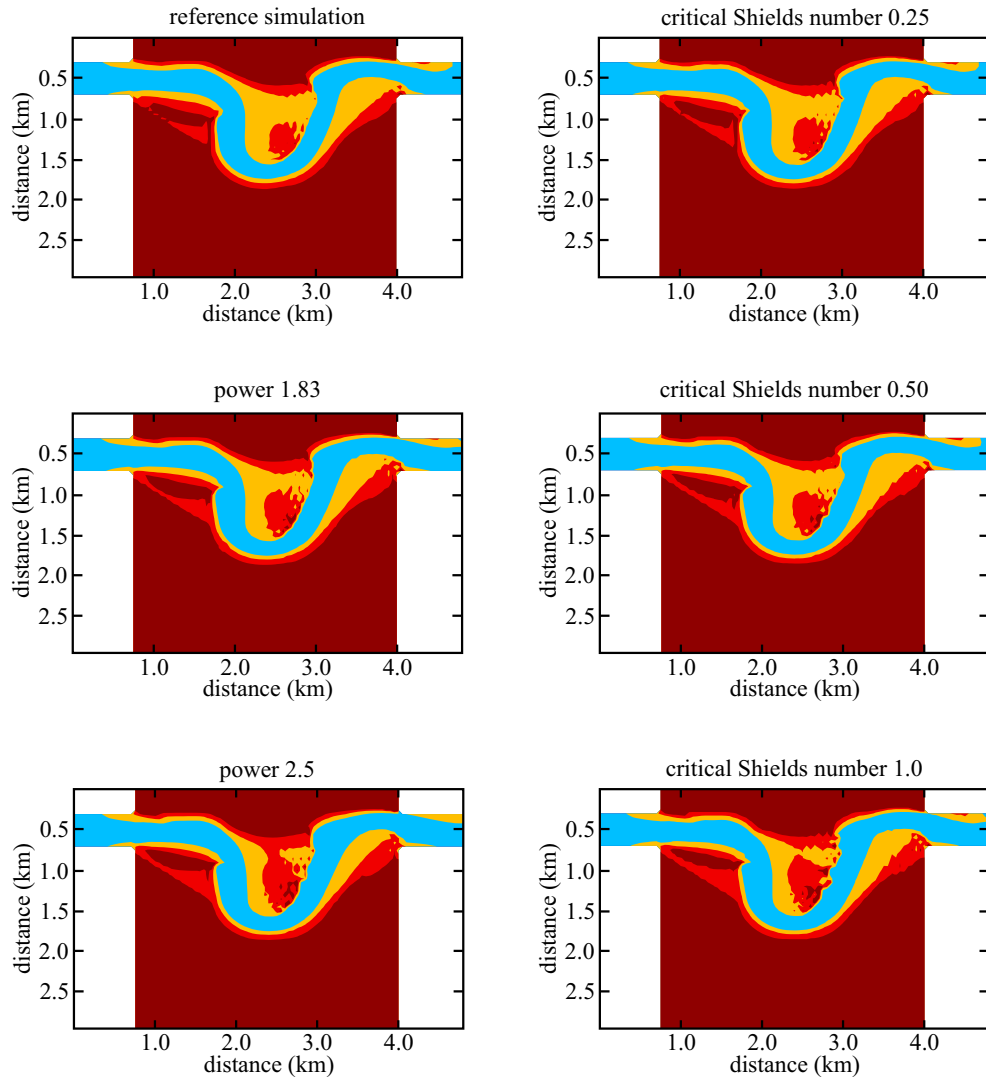


Figure A.8: Planforms for different sediment transport relations. The contour lines are drawn at 0, -1, and -3 m. Flow is from left to right. If the average sediment transport rate remains constant, the development of the cutoff slows down if either the exponent c or the critical shear stress θ_{cr} increases. See also Section 7.3.4.

Appendix B

Program details

B.1 Programs related to neural network

Two programs were used for the neural network approach:

1. a dedicated pre-processing program to derive the input parameters from a classified satellite image, and
2. a program for training and applying the neural network.

The first program is described in Section B.1.1. The second program, which has been developed by Dr. Van den Boogaard at WL | Delft Hydraulics, is not described in this thesis. However, Section B.1.2 gives a short introduction into the concept of neural network training.

B.1.1 Pre-processing

For the preparation of the input data for the neural network and for the derivation of the extraction of the channel network from the satellite image, a program has been constructed that can perform a number of image processing operations. All algorithms have been implemented in such a way that in each step of the operation the routine requires at most 3 lines of the satellite image. Each step consists of

- requesting one or more lines from one or more dataset from the data manager,
- performing the actual action required for the data processing,
- storing processed data to the data manager.

The transfer of data between the processing routine and the data manager may slow down the execution of the program, but it allows for both memory and disk based data processing. If the available memory space permits, the data manager loads the whole satellite image in memory, otherwise the individual lines are read from and written to file.

The program is command-driven and accepts the following commands:

1DM	create an input file for branches model pre-processing (see Section B.3)
ADD	add the values of two data sets
ANG	determine the angle of the direction to the nearest water point (uses reference)
AVG	average over a specified area around each point
CHANGE(3)	determine differences between two or three binary data sets
CHN_TH	remove water segments smaller than a specified size (e.g. ponds)
CHW	determine the channel width (at skeleton points)
CNT_CHN	number the water segments in the data set
CNT_ISL	number the land segments in the data set
COS	determine the sine and cosine of the direction to the nearest water point (uses reference)
EXT	extract water class from 8-bit BMP file
ISL_TH	remove land segments smaller than a specified size (i.e. small islands)
MIN_LAND	compute the distance to the nearest land point (uses reference)
MIN_WATER	compute the distance to the nearest water point (uses reference)
NCW	determine the width of the nearest channel (uses reference)
NOD	identify type of skeleton point: boundary point, normal point, node point
NPS	determine the nearest point on the skeleton (creates reference)
NST_LAND	determine the nearest land point (creates reference)
NST_WATER	determine the nearest water point (creates reference)
SKE	perform a skeletonise operation on the water segments
XLE	determine distance to water on the left
XRI	determine distance to water on the right
YAB	determine distance to water above
YBE	determine distance to water below

Together these commands provide enough flexibility for generating the input of the neural network and a basic channel schematisation for the branches model (flow directions and complex nodes have to be edited manually).

B.1.2 Back-propagation algorithm

The fit of the network on a set $M = \{\underline{\xi}^\mu, \underline{\zeta}^\mu | 1 \leq \mu \leq m\}$ is generally measured by the cost function E given by

$$E[w, \theta] = \frac{1}{2} \sum_{\substack{i \in L_N \\ 1 \leq \mu \leq m}} (\zeta_i^\mu - o_i^\mu)^2 \quad (\text{B.1})$$

where the summation of residual errors — that is, differences between the output o_i^μ of output neuron i given the input vector $\underline{\xi}^\mu$ and network parameters $w_{i,j}$ and θ_i and the target value ζ_i^μ — is taken over all input-output combinations in the set M and all output neurons i . The gradient-descent methods commonly used to optimise the values of the parameters $w_{i,j}$ and θ_i (that is, to minimise the cost E) require the computation of the partial derivative of the cost E with respect to each parameter. These derivatives are determined using the (error) back-propagation method, which as the name suggest computes these derivatives in reverse order: from the output layer to input layer. This method is described in all textbooks on neural networks and summarised here for reference.

The derivative of E with respect to the weight $w_{i,j}$ can be related to the derivative of E with respect to the resulting state variable s_i as

$$\frac{\partial E}{\partial w_{i,j}} = \frac{\partial E}{\partial s_i} \frac{\partial s_i}{\partial w_{i,j}} = \frac{\partial E}{\partial s_i} o_j \quad (\text{B.2})$$

where o_j is equal to $g(s_j)$. The derivative of E with respect to the offset θ_i can also be related to the derivative of E with respect to the resulting state variable s_i as

$$\frac{\partial E}{\partial \theta_i} = \frac{\partial E}{\partial s_i} \frac{\partial s_i}{\partial \theta_i} = -\frac{\partial E}{\partial s_i} \quad (\text{B.3})$$

To determine the gradient vector of E, an algorithm is needed to compute the derivates of E with respect to the state variables s_i . For this purpose a recursive formulation is used. For a neuron i in the output layer L_N , one obtains

$$\frac{\partial E}{\partial s_i} = \frac{\partial E}{\partial o_i} \frac{\partial o_i}{\partial s_i} = -2(\zeta_i - o_i)g'(s_j) \quad (\text{B.4})$$

for any other neuron j lower in the multi-layer network, one can derive

$$\frac{\partial E}{\partial s_j} = \sum_{i \in L_n} \frac{\partial E}{\partial s_i} \frac{\partial s_i}{\partial s_j} = g'(s_j) \sum_{i \in L_n} w_{i,j} \frac{\partial E}{\partial s_i} \quad (\text{B.5})$$

where the summation is taken over all neurons i in layer L_n when neuron j is located in layer L_{n-1} . This last equation forms the heart of the back-propagation algorithm.

The equations given above are based on a single input-output combination ξ^μ, ζ^μ in the training set M_{train} . This represents the case in which the weights are updated after each individual input-output combination μ (so-called incremental updating). And, formally, the cost function E should in these equations be replaced by E^μ which is identical to E except for the summation over μ . The algorithm used here was based on batch updating, which means that the weights are updated after the network has been applied to all elements μ of the training set. In this case Equations B.2 through B.5 should be evaluated for all input-output combinations ξ^μ, ζ^μ in the training set and summed.

B.2 Implementation branches model

This section describes some implementation details of the branches model described in Section 5.3. The execution of the program is indicated schematically in Figure B.1. The outermost loop is the Monte Carlo loop, which makes it possible to run multiple scenarios during one execution of the program. Each single simulation starts by loading the planform from disk. Subsequently, a limited check on the planform consistency is performed (check node connections, remove coincident channel points) and the simulation is started. The floods are assumed to occur once a year, so two further loops are distinguished. An outer loop (representing the years) comprising all processes and an inner loop (representing the low stage periods) comprising channel migration only.

As a first step in the yearly cycle, the planform may be smoothed to eliminate possible irregular configurations that may lead to instabilities in the planform development. The first

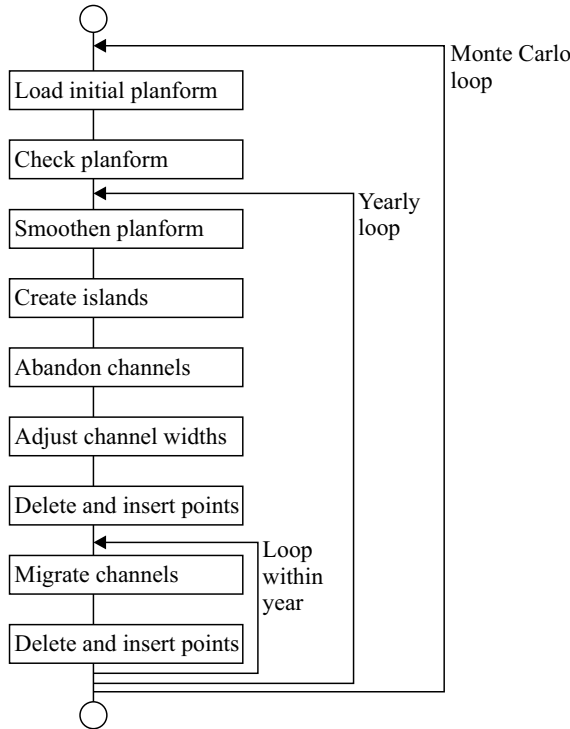


Figure B.1: Schematic representation of the program of the branches model.

process is island creation by mid-channel bar/island growth. Subsequently, branches may be abandoned. Note that this could include branches that have just been formed by the island creation process, this will in general only happen to channels at the inside of a bend. This process is followed by the process of width adjustment, which if it results in widening may lead to the formation of new islands in the next year. The remainder of the year — the low stage period — consists of a loop of channel migration and associated adding and deleting of points. The timestep used in this period is adjusted such that an integer number of timesteps fits into one year.

Input, output and data storage

The program requires two input files: a parameter definition file, called `def`, and a planform input file, called `prp`. The parameter definition file contains per parameter one line with its name followed by an equal sign and its value (see Table B.1). In the parameter definition file also the time scale (step dt and end time T_{end}), spatial discretisation (minimum distance Δs_{min} and maximum distances Δs_{max} between points) and maximum array dimensions (maximum number of branches $N_{\text{br,max}}$ and maximum number of points per branch $N_{\text{p,br}}$) have to be specified. The variables may occur in the file in any order. The planform input file should have the following format

- The first line contains the number of branches.

- The second line is skipped, normally it will contain the text BRANCH DATA.
- Subsequently, for each branch a line containing the following data will be expected:
 - the numbers of the branches that flow into the upstream node: either two positive integers if the upstream node is a confluence, or a positive integer and a zero if the upstream node is a bifurcation, or two zeroes if the upstream end of the branch is an end point (inflow boundary),
 - the numbers of the branches that flow out of the downstream node: either two positive integers if the downstream node is a bifurcation, or a positive integer and a zero if the downstream node is a confluence, or two zeroes if the downstream end of the branch is an end point (outflow boundary),
 - the number of points representing the branch,
 - length of the branch (value will be overruled by internal computation),
 - bifurcation angles ϕ_1 and ϕ_2 if the upstream node is a bifurcation (values will be overruled by internal computation),
 - modifiers for the bifurcation angles $\Delta\phi_{1,c}$ and $\Delta\phi_{2,c}$ if the upstream node is a bifurcation.
- After the branch data one line is skipped, normally it will contain the text POINT DATA.
- Subsequently, for each point in the network a line containing the following data will be expected (points should be specified in the same order as the branches, the point within a branch should be specified starting at the upstream end): x and y coordinates of the point, channel width at that location, channel depth at that location, erodibilities of the left and right banks.

Although the nodes and endpoints are identified as separate objects in the automatic extraction process described in Section 5.3.2 and Appendix B.3, they are not explicitly stored in the branches program itself. The internal storage format of the data matches the format of the file. Two record arrays are created for the points and branches respectively. The maximum space available for storing points $N_{p,max}$ and branches $N_{br,max}$ has to be specified by the user in the parameter definition file. If the program tries to exceed the allocated space, the program stops.

keyword	var.	keyword	var.	keyword	var.
DT	dt	AV_ISLE	L_{av}	CHI	χ
ENDTIME	T_{end}	ALPHA_PHI	α_ϕ	K1	k_1
MIN_DIST	Δs_{min}	PHI_C	ϕ_c	K2	k_2
MAX_DIST	Δs_{max}	C1	α_1	K3	k_3
SMTH_FAC	γ	P1	β_1	SIGMA_MG1	σ_{mg1}
MAXBRANCH	$N_{br,max}$	C2	α_2	SIGMA_MG2	σ_{mg1}
MAXPOINT	$N_{p,br}$	P2	β_2	LAMBDA_A	λ_a
P_CR	P_{cr}	ALPHA_HM	α_{hm}	SM_FAC_ADJ_BMR	γ_{abmr}
BETA_C	β_c	EROSION_REF	E_{ref}		

Table B.1: Keywords in the parameter definition file and corresponding variables

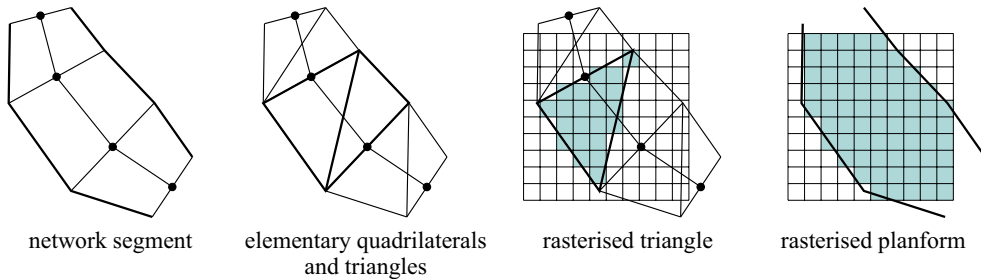


Figure B.2: The planform is subdivided into elementary triangles for transfer onto the grid to determine the spatial uncertainty in the planform after the prediction period.

The program generates two output files: one file containing the final planform (of the last run in case of a Monte Carlo simulation with multiple runs), called `out`, and a log file, called `log`. The former file has basically the same format as the planform input file `prp`, however, for each point also the radius of curvature is exported.¹ Intermediate planforms (after each N_{dt} migration steps) and final planforms of all Monte Carlo runs are stored in the log file. The first line of the log file lists the maximum number of branches $N_{br,max}$ and points $N_{p,br}$ per branch — as specified by the user in the parameter definition file — followed by the number $N_{log} \approx T_{end}/(N_{dt}dt)$ of (intermediate and final) planforms per simulation run and the number of runs N_{MC} . The remainder of the file consists of the $N_{MC}N_{log}$ planforms formatted in the same way as the `out` file.

A post-processing program is created that can overlay the final planforms of all the runs in the log file to obtain a spatial distribution for the chance that a certain point will be part of the channel system after the prediction period. The spatial distribution is determined on a rectangular grid. This is done by counting the number of simulations for which a point corresponds to water — that is, it lies within the area covered by the final planform. Whether or not a certain point corresponds to water for a given planform has been implemented as an analogy of a very basic graphics routine: the planform is reduced to elementary triangles, each of which is transferred on to the grid by marking the gridcells that have their centre inside the triangle. This process is illustrated in Figure B.2. The marking is done by setting the sign bit of the counting integer. When all triangles have been processed (which will overlap at nodes), for all marked points the sign bit is unset and counter is increased by one.

Physical subprocesses

The width change is a straightforward local change in local channel width. Island creation by mid-channel island formation leads to an increase in the number of branches by three. The two branches to the left and right of the island and the new branch downstream of the island are added to the end of the list of branches. The abandonment of branch results in the renumbering of all branches with a higher branch identification number. When a branch is abandoned all channels strictly downstream of the original branch are also abandoned. A

¹Two values are written to the file. For normal points the first will be the radius of curvature and the second one will be zero. If the point is a node (bifurcation or confluence) a radius of curvature is exported for both connections. The two extra values are skipped when the output file is reused as input file.

channel a is called strictly downstream of another channel b if there are only bifurcation nodes between the channels a and b , that is all the water flowing in channel a must have flowed through channel b .

Channel migration requires determining the channel curvature. To prevent unnecessary numerical errors, the curvature in a point p_2 is done using a local coordinate system with the origin in p_2 . The radius of curvature is defined as the radius of the circle through point p_2 and the upstream and downstream points p_1 and p_3 , respectively. Using the definition that $x_{ij} = x_i - x_j$ (and similarly for the y coordinate) the radius of curvature equals the distance between the crossing of the lines normal to the two channel segments (the centre point p_c of the circle) and point p_2 as indicated in Figure B.3:

$$R = \sqrt{x_{c2}^2 + y_{c2}^2} \quad (\text{B.6})$$

with the local coordinates of the centre point p_c of the circle given by

$$x_{c2} = \frac{1}{2}x_{12} - \frac{\lambda}{2}y_{12} \text{ and } y_{c2} = \frac{1}{2}y_{12} + \frac{\lambda}{2}x_{12} \quad (\text{B.7})$$

where

$$\lambda = \frac{x_{23}x_{31} + y_{23}y_{31}}{x_{12}y_{23} - y_{12}x_{23}} \quad (\text{B.8})$$

The Equations B.6 and B.7 have been combined into

$$R = \frac{1}{2} \sqrt{(x_{12}^2 + y_{12}^2)(1 + \lambda^2)} \quad (\text{B.9})$$

The sign of the curvature, which is taken positive for a bend to the right when facing downstream, is the opposite of the sign of the denominator of the λ definition given above

$$c = \text{sign}(x_{23}y_{12} - y_{23}x_{12}) \frac{1}{R} \quad (\text{B.10})$$

Given the local channel curvature the nominal bend migration rate can ζ_n be determined. Subsequently, the adjusted bend migration rate ζ_a is computed as an exponentially weighted

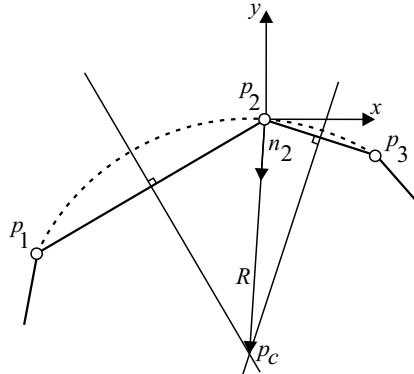


Figure B.3: Sketch indicating the derivation of the radius of curvature using the crossing of two normals.

upstream average of the nominal bend migration rates. The average is determined recursively by starting at the most upstream branches and extending the computation in downstream direction when the adjusted migration rates have been determined for all upstream branches. For a confluence the adjusted migration rate is computed as an average of the two migration rates immediately upstream weighted using the discharges of the two upstream channels:

$$\zeta_a = [(B_1 h_1^{3/2})\zeta_{a1} + (B_2 h_2^{3/2})\zeta_{a2}] / (B_1 h_1^{3/2} + B_2 h_2^{3/2}) \quad (\text{B.11})$$

whereby it has been assumed that roughness and slope are equal for the two channels ($C_1 = C_2$, $i_1 = i_2$). Assuming a linear transition in the nominal migration rate between two successive points, the adjusted migration rate can be determined for any other point p_2 from the nominal and adjusted migration rates $\zeta_{n,1}$ and $\zeta_{a,1}$ in the upstream point p_1 and the local value $\zeta_{n,2}$ of the nominal migration rate as

$$\zeta_{a,2} = \alpha \zeta_{a,1} + \zeta_{n,2} - \alpha \zeta_{n,1} + (1 - \alpha) \frac{\lambda_a}{\Delta} (\zeta_{n,1} - \zeta_{n,2}) \quad (\text{B.12})$$

where $\alpha = \exp(-\Delta/\lambda_a)$ and $\Delta = \sqrt{(x_2 - x_1)^2 + (y_2 - y_1)^2}$.

Given the adjusted migration rate and the normal direction n_2 indicated in Figure B.3, the channels migrate and the distance between successive points increases. When the distance between two points becomes larger than Δs_{\max} , one (or more) points are inserted. Especially during the initial step multiple points may be included. Given two points p_1 and p_2 with radii of curvature R_1 and R_2 two circle segments can be defined. These segments, which are indicated by the dotted lines in Figures B.4a and b, satisfy the following equation

$$y_i(x) = \sqrt{R_i^2 - (x - \frac{\Delta}{2})^2} - \sqrt{R_i^2 - (\frac{\Delta}{2})^2} \quad (\text{B.13})$$

in a local coordinate system with the x direction coincident with the chord through the two points and the origin halfway between the two points as indicated in Figure B.4a. Hereby is i equal 1 or 2 and Δ equals the distance between the two points p_1 and p_2 . The new points are inserted at equal intervals in the local x direction while the local y coordinates follow the transitional curve

$$y(x) = y_1(x) + (y_2(x) - y_1(x)) \frac{x}{\Delta} \quad (\text{B.14})$$

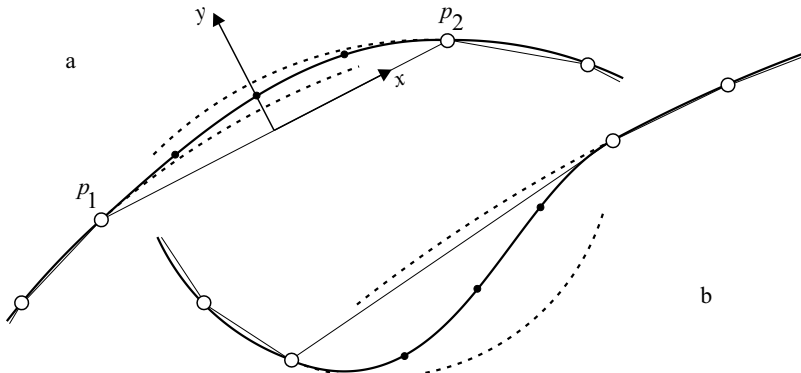


Figure B.4: Points are inserted based on a linear transition between two circle segments.

This curve provides a relatively smooth transition from one curvature to the next, even when the curvatures have opposite sign as in Figure B.4b.

B.3 Extract channel network from satellite image

The model that was described in the previous section requires a channel network. A pre-processor has been developed that can automatically extract a channel network (comprising centreline, channel width, and node point information) from a satellite image of which each pixel has been classified as representing either land or water. This thematic satellite image can be obtained by supervised or unsupervised classification from the original satellite image. The automated process consists of eight steps that are described below. The process is illustrated in Figure B.5 using a 1994 satellite image of a river section upstream of Bahadurabad.

Step 1. Either by supervised or unsupervised classification of a satellite image one obtains a thematic image. In a thematic image each pixel is assigned one label (number) taken from a limited set. Each label represents a certain class of pixels that all have a certain property (often the spectral distribution in the original satellite image) in common. In the example four classes have been distinguished: 1 - water, 2 - sand, 3 - vegetated land, and 4 - other types of landuse (indicated by black, white, light grey, and dark grey in image 1 of Figure B.5).

Step 2. From the thematic image one selects all classes that correspond to water areas. All pixels in those classes are assigned the value one and all other pixels are become zero. When the image satisfies the following three conditions this step can be automated:

- the classification has resulted in a sufficiently patchy classification of the land area,
- all water pixels belong to one class, and
- the river runs from the top of the image to the bottom.

Under these conditions the water class will be the only class containing an uninterrupted sequence of pixels connecting top and bottom of the image, and it can as such be selected automatically. This is true for our example.

Step 3. The set of all water pixels selected in the previous step contains in general besides the river itself, all kinds of small ponds, (oxbow) lakes, partially dry channels, and possibly even some pixels incorrectly classified as water. These areas are not relevant for the extraction of the channel network and should be removed. This can be done by selecting only the largest body of water, which is the main channel. This procedure requires the determination of the size of each group of interconnected water pixels. This procedure is implemented in three steps.

- (a) The first step makes a top to bottom sweep through the image; it starts by assigning a unique identification number to each set of connected water pixels on the first line of the image. The next rows are processed one by one, where for each set of connected water pixels on row i determine whether it is connected to any set of water pixels on the previous row $i - 1$. If it is connected to one or more of these sets, then the pixels are assigned the lowest identification number

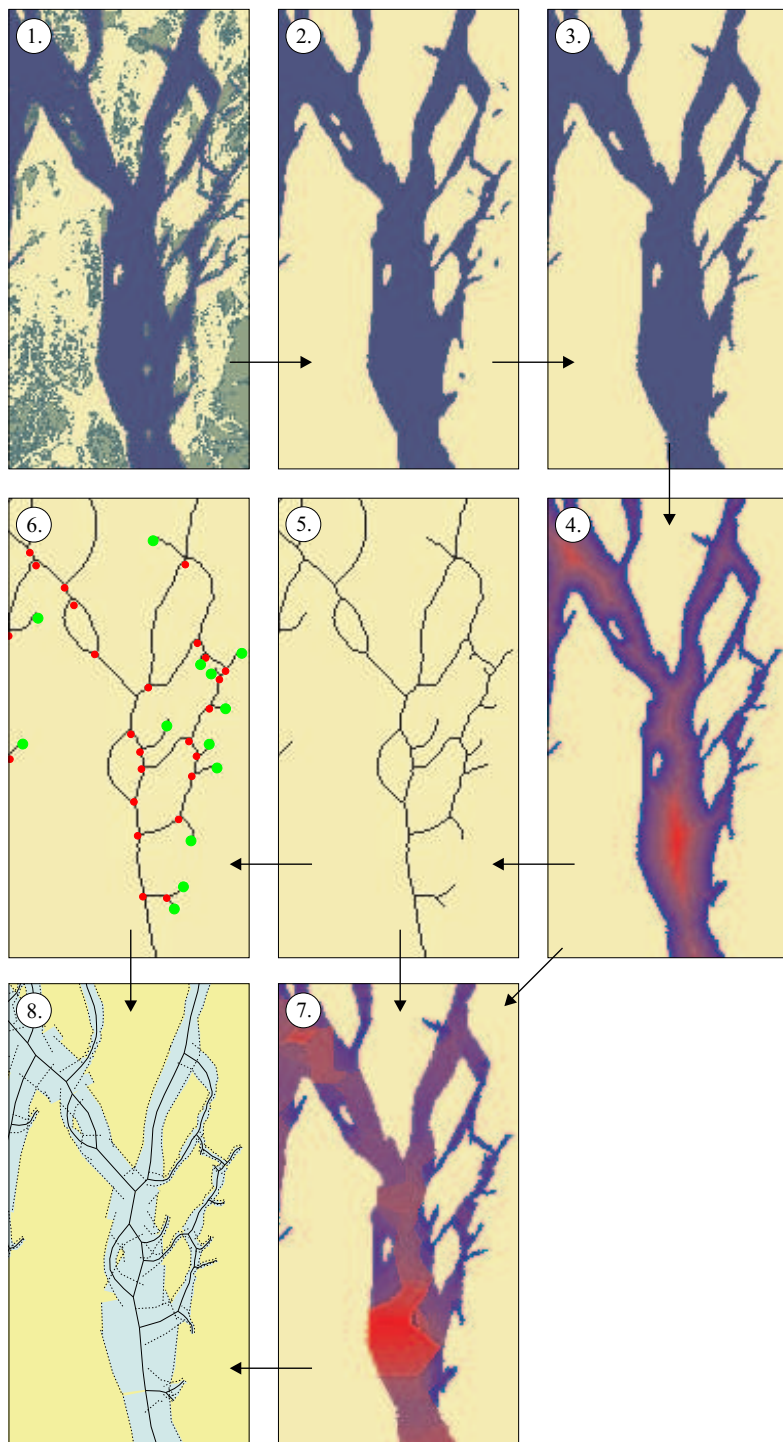


Figure B.5: Example of the steps in the extraction of a channel network from a satellite image (details of Figures 5.17 and 5.12).

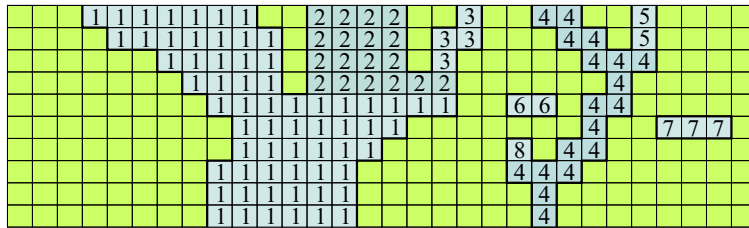


Figure B.6: First sweep through the image to determine the size of the various groups of interconnected water pixels: initial numbering of pixel clusters and cluster matching (1 and 2, 2 and 3, 4 and 5, 4 and 8).

of these sets. If it is not connected to a set of water pixels on the previous row, a new identification number is assigned to the pixels. The end result of this step is indicated in Figure B.6.

- (b) In the second step the algorithm determines the interconnections of groups with different identification numbers and determines the number of pixels belonging to each set. All interconnected groups are assigned the lowest identification number of their set. In the example shown in Figure B.6 this results in the merging of classes 2 and 3 with 1 (68 pixels in total), and of 5 and 8 with 4 (19 pixels in total). An additional renumbering causes the numbers 1 to n_{groups} (here 4) to be used.
- (c) And finally, all pixels are assigned their new group identification number and the corresponding group size. All pixels belonging to groups of water pixels smaller than a certain threshold (for example not belonging to the largest group) can be removed.

One should note that by removing all small ponds also all separate water segments are removed that might contain clues about channels that have (temporarily) been abandoned. In a similar way small islands can be removed.

- Step 4. The next step is to determine the distance of all water pixels to the nearest bankline, i.e. the distance to the nearest non-water pixel. The nearest non-water pixel can be found for all pixels in two sweeps: one from top left to bottom right, covering all directions to the left and above, and one in the reverse direction covering all pixels in the remaining directions. Once for every pixel the nearest non-water pixel is known, the distance can be calculated.
- Step 5. From the distance image obtained in step 4 one can determine the centrelines by selecting the pixels locally furthest from the banks and 'similar' points. If one takes only those pixels that are at least as far away from the banks as their immediate neighbours, one obtains only the centrelines of channels of constant width and pixels corresponding to local maxima in channel width. The other centreline pixels which connect these local maxima and the pixels leading to a dead end of a channel are more difficult to characterise. Therefore, we use a different approach, namely carefully removing all non centreline pixels from the outside in. This process is similar to the skeletonise operation in image processing (Van der Heijden, 1994), which removes pixels while keeping the topology of the image unchanged. The procedure is,

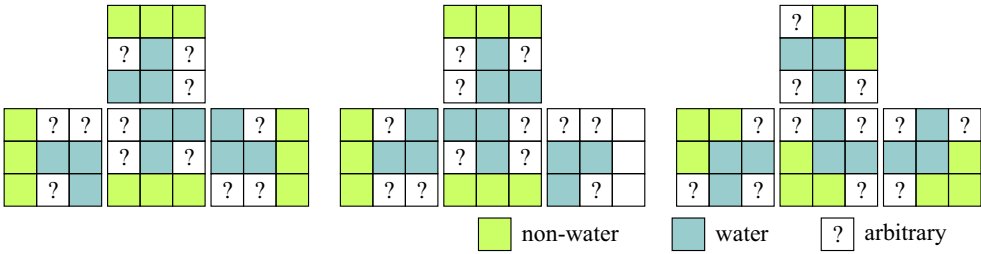


Figure B.7: The three skeletonising masks (and their rotated variants) used in step 5 for determining the centrelines.

however, quite sensitive to local irregularities in the bankline, which can lead to spurious side branches. The algorithm is used in such a way that the formation of these spurious branches was minimised and in the investigated cases none were formed. The algorithm repeatedly removes all water points which lie at a distance d from the banks and of which the neighbourhood matches one of the structure elements shown in Figure B.7. Black pixels should match water, striped pixels should match non-water pixels, and pixels with a question mark may be of both types. The process is repeated as long as a water pixel at a distance d from the banks can be removed. If no water pixel at that distance can be removed the process continues with points of distance $d + 1$. This is the most time-consuming part of the extraction process.

- Step 6. The node pixels of the channel network can be separated from the normal channel centreline pixels as those centreline pixels that have more than two neighbouring (centreline) pixels. End points, on the other hand, have only one neighbouring (centreline) pixel. A node will always be a cluster of pixels; in general its shape will be a cross, triangle or square. Each interconnected cluster of pixels that remains after the node pixels have been removed represents one branch of the network.
- Step 7. Subsequently, the local channel width can be determined as the smallest distance between two bankline pixels for which the distance to the centreline pixel is smaller than their mutual distance. Only the bankline pixels closest to the centreline pixel are used in this procedure. By this definition the channel width B is in general about twice the distance b from the centreline pixel to one bank, but it gives a lower value for pixels near nodes where it can become about $\sqrt{3}b$.
- Step 8. Now all nodes, endpoints, and branches have been marked in the image, it is possible to trace the courses of the individual branches. The traced courses are combined with the information from the channel width dataset and the channels courses are resampled such that the distance between points in the branch is of the same order as the local channel width. This resampling not only reduces the number of points in the network, but it also smoothes the channel centreline. Finally, the connections between the nodes, endpoints and branches are derived from the image. Thereby the automatic extraction process of a channel network is completed.

The channel network thus automatically extracted does not satisfy the requirements of the branches model with respect to two points. First, the numbering of the points making up a branch should start at the upstream end of the branch. For most branches the flow upstream

end corresponds to the upper end point in the image (when as in our example the river flows from top to bottom). However, there are a small number of branches for which this is not the case. Second, on several occasions more than three branches meet at a node — thereby forming a confluence of multiple branches, a bifurcation into multiple branches, or a combination of a confluence and a bifurcation. These complex nodes have to be converted into closely spaced simple confluentes and bifurcations. Both the detection of incorrectly assigned flow directions and the conversion of the complex nodes require a visual inspection of the network by the user. For this purpose the network is written to an ASCII file. The format of that file deviates from the standard file format used by the branches program because the artefacts in the geometry that cannot be represented in that format. The format is as described below:

- The first line contains the number of branches, number of nodes, number of endpoints.
- The first part of the file contains the data of the branches. For each branch a line can be found in the file containing: the branch number, the coordinates² of the rectangle tightly fitting the branch in the image, the coordinates of the upstream end, the number of associated node or endpoint (negated in case of an endpoint), the coordinates of the downstream end, and the number of the associated node or endpoint (negated in case of an endpoint). The next line contains the number of points forming that branch. Subsequently the coordinates of these points and the channel widths at these points are listed.
- After all branches and their points have been listed, a data block for the nodes is encountered. For each node one line lists all properties: the node number, the coordinates of the rectangle tightly fitting the node in the image, the selected, average coordinates for the node, the number of branches connected to the node (three or more), the number of inflowing branches, the number of outflowing branches, the branch numbers (three or more numbers).
- Finally, for each endpoint one line lists its endpoint number, its coordinates, and the branch connected to it.

This file can be read into a program that allows the user to interactively change the flow direction in branches, delete branches, smoothen branch coordinates, shift channel confluentes, and perform coordinate transformations. An example of the interface is presented in Figure B.8. When the network satisfies all the conditions of the branches program, the network is saved in the input format of that program described in Appendix B.2.

²All coordinate mentioned here are pixel coordinates.

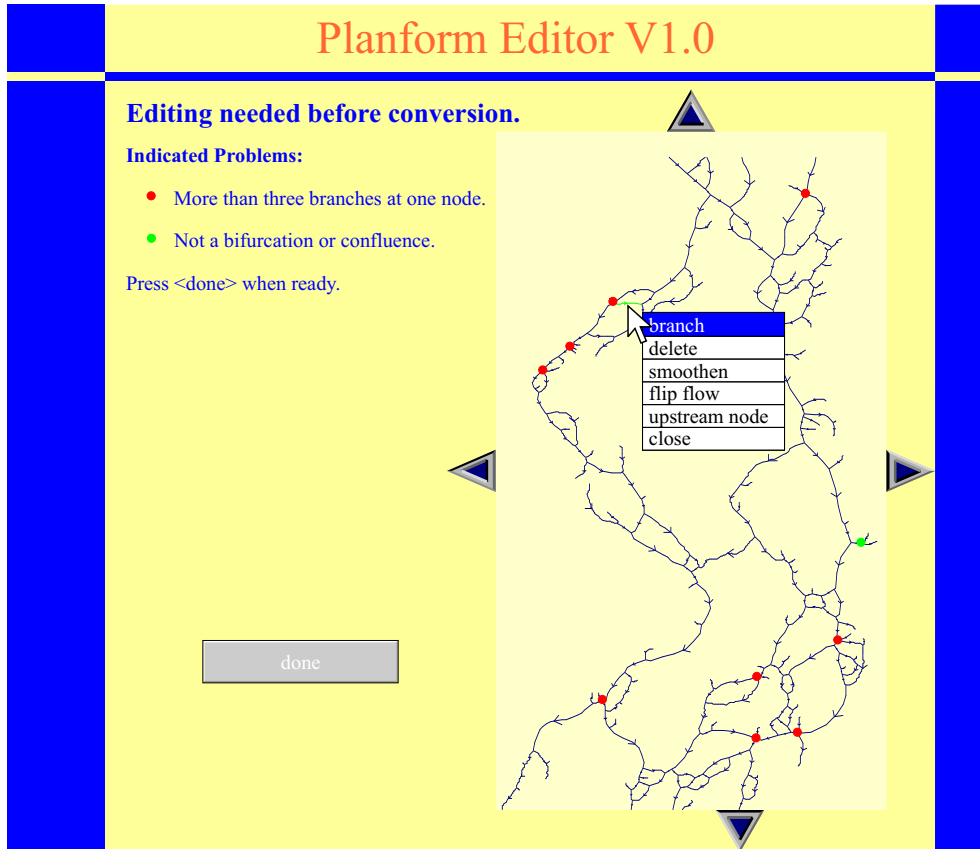


Figure B.8: User interface for interactively solving the complications in the channel geometry.

Appendix C

Model details

C.1 Analytical cutoff criterion

Klaassen and Van Zanten (1989) analytically derived a criterion for the occurrence of a cutoff in meandering channels, assuming the idealised situation of a clearly defined but small cutoff channel as indicated in the sketch in Figure C.1; this analysis was extended by Biglari (1989). The highlights of the latter analysis are presented here with some modifications. It is assumed that the width B , roughness C , and the constants m and n of the sediment transport relation mu^n are uniform along the main channel. The same is assumed to be true initially for the water depth H and the slope i . The ratio Ω of the discharge following the cutoff and the original bend respectively can — under the assumption of normal depth at the bifurcation — be expressed using the depth, slope, roughness, and width ratios of the two channels as

$$\Omega = \frac{Q_{\text{cutoff}}}{Q_{\text{bend}}} = \beta \gamma \eta^{3/2} \lambda^{1/2} \quad (\text{C.1})$$

where

- β width ratio $B_{\text{cutoff}}/B_{\text{bend}}$,
- γ roughness ratio $C_{\text{cutoff}}/C_{\text{bend}}$ in general less than 1,
- η depth ratio $H_{\text{cutoff}}/H_{\text{bend}} < 1$,

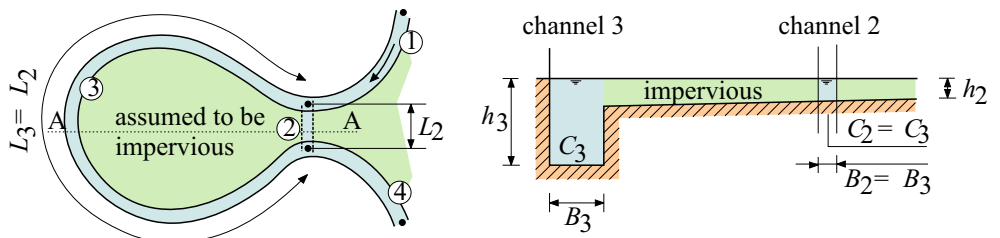


Figure C.1: Schematised cutoff of Klaassen and Van Zanten (1989).

λ cutoff ratio $L_{\text{bend}}/L_{\text{cutoff}} > 1$ equal to the slope ratio $i_{\text{cutoff}}/i_{\text{bend}}$.

The ratio q of the unit discharges is given by

$$q = \frac{q_{\text{cutoff}}}{q_{\text{bend}}} = \frac{\mathfrak{Q}}{\beta} = \gamma \mathfrak{m}^{3/2} \lambda^{1/2} \quad (\text{C.2})$$

The distribution of sediment over the cutoff channel and the original meander bend is — inspired by the relation used by Wang *et al.* (1995) — taken to be

$$\frac{S_{\text{cutoff}}}{S_{\text{bend}}} = \frac{1}{\sigma} \left(\frac{Q_{\text{cutoff}}}{Q_{\text{bend}}} \right)^k \left(\frac{B_{\text{cutoff}}}{B_{\text{bend}}} \right)^{1-k} \quad (\text{C.3})$$

for some constants σ and k . Klaassen and Van Zanten (1989) and Biglari (1989) assumed that if most of the sediment is transported as suspended load, the distribution of sediment over the cutoff and the original meander bend can be assumed in first approximation¹ proportional to the distribution of the discharge, which results in the above mentioned relation with $k = 1$. Wang *et al.* (1995) assume a symmetrical relationship, in which case σ should be 1. From this expression for the distribution of sediment it follows that

$$S_{\text{cutoff}} = \frac{\mathfrak{Q}^k \beta^{1-k}}{\mathfrak{Q}^k \beta^{1-k} + \sigma} S_{\text{upstream}} = \frac{q^k \beta}{q^k \beta + \sigma} S_{\text{upstream}} \quad (\text{C.4})$$

where S_{upstream} is the amount of sediment in transport just upstream of the bifurcation. The sediment transport capacity of the cutoff channel is estimated as

$$\begin{aligned} S_{\text{cutoff}}^{\text{cap}} &= m_{\text{cutoff}} B_{\text{cutoff}} (u_{\text{cutoff}})^n \\ &= m_{\text{cutoff}} B_{\text{cutoff}} (C_{\text{cutoff}})^n (H_{\text{cutoff}} i_{\text{cutoff}})^{n/2} \\ &= \frac{m_{\text{cutoff}}}{m_{\text{upstream}}} \frac{B_{\text{cutoff}}}{B_{\text{upstream}}} \left(\frac{C_{\text{cutoff}}}{C_{\text{upstream}}} \right)^n \left(\frac{H_{\text{cutoff}}}{H_{\text{upstream}}} \frac{i_{\text{cutoff}}}{i_{\text{upstream}}} \right)^{n/2} S_{\text{upstream}}^{\text{cap}} \\ &= \mu \beta^n \alpha^{-n/2} \mathfrak{m}^{n/2} \lambda^{n/2} S_{\text{upstream}}^{\text{cap}} \end{aligned} \quad (\text{C.5})$$

where

α depth ratio $H_{\text{upstream}}/H_{\text{bend}} > 1$, which assuming normal depths in all channels equals

$$\alpha = (1 + \mathfrak{Q})^{2/3} = (1 + \beta q)^{2/3} \quad (\text{C.6})$$

μ ratio of the linear coefficient in the sediment transport relation ($m_{\text{cutoff}}/m_{\text{upstream}}$) may depend on one or more of the other ratios.

For erosion to take place in the cutoff channel, the incoming sediment transport must be less than the transport capacity, which — assuming the original channel was (and for some distance upstream still is) in dynamic equilibrium ($S_{\text{upstream}} \approx S_{\text{upstream}}^{\text{cap}}$) and using Equations C.4

¹The sediment concentration varies in space, which results in deviations from this approximation. Depending on the situation the water flowing into the cutoff channel may contain a higher or lower sediment concentration than the main channel. Based on a characteristic distribution of sediment over the vertical Slingerland and Smith (1998) propose that a shallow side channel may receive water with a relatively low sediment concentration (see Section 6.3).

and C.5 — leads to the following condition

$$\mu\beta\gamma^n\alpha^{-n/2}\eta^{n/2}\lambda^{n/2} > \frac{\eta^k\beta}{\eta^k\beta + \sigma} \quad (\text{C.7})$$

This can also be written as

$$\frac{\mu\eta^{n-k}}{\eta^n} > \frac{\alpha^{n/2}}{\eta^k\beta + \sigma} \quad (\text{C.8})$$

or, after expansion of α using Equation C.6, as

$$\frac{\mu\eta^{n-k}}{\eta^n} > \frac{(1+\beta\eta)^{n/3}}{\eta^k\beta + \sigma} \quad (\text{C.9})$$

For the Engelund-Hansen transport formula ($\mu = \gamma^{-3}$, $n = 5$) this becomes

$$\frac{\eta^{5-k}}{\gamma^3\eta^5} > \frac{(1+\beta\eta)^{5/2}}{\eta^k\beta^{1-k} + \sigma} \quad (\text{C.10})$$

If one expands all occurrences of η using Equation C.2, one obtains

$$\gamma^{2-k}\eta^{(5-3k)/2}\lambda^{(5-k)/2} > \frac{(1+\beta\eta^{3/2}\lambda^{1/2})^{5/3}}{\sigma + \beta\gamma^k\eta^{3k/2}\lambda^{k/2}} \quad (\text{C.11})$$

For small β this can be simplified to

$$\gamma^{2-k}\eta^{(5-3k)/2}\lambda^{(5-k)/2}\sigma > 1 \quad (\text{C.12})$$

which reduces for $k = 1$ to

$$\gamma\lambda^2\sigma > 1 \quad (\text{C.13})$$

which was also derived by Klaassen and Van Zanten (1989) and agrees for $\gamma = \sigma = 1$ with the empirically derived criterion given by Joglekar (1971). For the general transport formula one obtains from Equation C.9

$$\mu\gamma^{n-k}\eta^{(n-3k)/2}\lambda^{(n-k)/2} > \frac{(1+\beta\gamma^{3/2}\lambda^{1/2})^{n/3}}{\sigma + \beta\gamma^k\eta^{3k/2}\lambda^{k/2}} \quad (\text{C.14})$$

and if β is small

$$\mu\gamma^{n-k}\eta^{(n-3k)/2}\lambda^{(n-k)/2}\sigma > 1 \quad (\text{C.15})$$

or, when keeping the ratio of unit discharges,

$$\mu\eta^{n-k}\sigma > \eta^n \quad (\text{C.16})$$

From this analysis one can conclude that the larger the values of γ , η , and λ the higher the probability on a cutoff is. This means that a relatively smooth flood plain, a high flood, and a long bend are favourable conditions. Furthermore, the criterion is rather sensitive to the exponent n in the sediment transport relation.

If μ , γ and σ are constants, that is stage-independent, and for simplicity we assume them all to be equal to 1, Equation C.15 can be simplified to

$$\eta^{(n-3k)/2}\lambda^{(n-k)/2} > 1 \quad (\text{C.17})$$

During a cutoff the ratio λ of the two channel lengths will remain approximately constant. Now, let us assume that at a certain moment η has such a value that the product on the left hand side is indeed larger than 1. In that case the cutoff will start eroding and the ratio η will change. If the exponent of η in Equation C.17 is larger than zero, the left hand side will become larger and, therefore, it will remain larger than 1: the cutoff will continue through to completion. If the exponent is less than zero, however, the left hand side will become smaller and will eventually become equal to 1. In that case the condition for the cutoff is no longer satisfied. The result is a system with two open branches. The condition for this stable situation is $n - 3k < 0$, i.e. $k > n/3$. This is exactly the same result as that obtained by Wang *et al.* (1995). A summary of their analysis of bifurcation dynamics can be found in Appendix C.2. One should, however, note that this derivation is only valid as long as the formation of the cutoff channel has a negligible influence on the dynamics of the main channel, i.e. only during the initial stages of the cutoff.

If the threshold of motion cannot be neglected, for instance in case of coarse or cohesive sediments, the sediment transport relation becomes

$$S = m_1 B(\theta - \theta_{\text{cr}})^{n_1}$$

using the Shields parameter θ and critical Shields parameter θ_{cr} , or — similar but not equivalent — by

$$S = m_2 B(u - u_{\text{cr}})^{n_2}$$

using a critical velocity u_{cr} as suggested by Biglari (1989). The threshold value prevents us from carrying out a similar analytical study for this case, because the sediment transport capacity $S_{\text{cutoff}}^{\text{cap}}$ can no longer be expressed as a combination of the ratios β , γ , η and λ times the sediment transporting capacity upstream. Neglecting the amount of sediment entering the cutoff channel, the condition for erosion (and, therefore, for cutoff enlargement) becomes $\theta > \theta_{\text{cr}}$, or $u > u_{\text{cr}}$ (Biglari, 1989).

C.2 Dynamics of bifurcations

Wang *et al.* (1995) studied the dynamics of a simple model of one channel splitting into two parallel branches ending in a lake. They assume that the sediment distribution at the bifurcation varies as specified by the following, symmetrical nodal point relationship

$$\frac{S_1}{S_2} = \left(\frac{Q_1}{Q_2} \right)^k \left(\frac{B_1}{B_2} \right)^{1-k} \quad (\text{C.18})$$

in which k is a constant and S_j for $j = 1, 2$ are the sediment transport rates entering the two downstream branches, in which the discharge is Q_j ($j = 1, 2$) and the width is B_j ($j = 1, 2$), respectively. Furthermore, equilibrium flow conditions are assumed in all branches, such that

$$Q_j = B_j C_j h_j^{3/2} i_j^{1/2} \quad (\text{C.19})$$

where C_j , h_j and i_j are the Chézy roughness, water depth and slope of branch j , respectively. The sediment transport capacity $S_{j,\text{cap}}$ is assumed to be given by

$$S_{j,\text{cap}} = B_j m \left(\frac{Q_j}{B_j h_j} \right)^n \quad (\text{C.20})$$

with constant m and n . Wang *et al.* (1995) continue by assuming that the bed levels in each branch can be represented by a single depth value, even if the system is not in equilibrium. This results in the following equation for the depth

$$\frac{dh_j}{dt} = \frac{S_{j,\text{cap}} - S_j}{B_j L_j} \quad (\text{C.21})$$

where L_j equals the length of branch j . Because the two downstream branches have the starting point (bifurcation) and the end point (lake) in common, the following geometric relation holds: $i_1 L_1 = i_2 L_2$. Combining this relation with Equation C.19 and mass conservation at the bifurcation $Q_0 = Q_1 + Q_2$ gives the discharges in the two downstream branches as functions of the water depths:

$$Q_1 = \frac{\beta_1 h_1^{3/2}}{\beta_1 h_1^{3/2} + \beta_2 h_2^{3/2}} Q_0 \text{ and } Q_2 = \frac{\beta_2 h_2^{3/2}}{\beta_1 h_1^{3/2} + \beta_2 h_2^{3/2}} Q_0 \quad (\text{C.22})$$

where $\beta_j = B_j C_j L_j^{-1/2}$. Note that Equations C.19 and C.22 imply that

$$i_j L_j = Q_0 / (\beta_1 h_1^{3/2} + \beta_2 h_2^{3/2}) \quad (\text{C.23})$$

Substitution of the normal flow formulation given by Equation C.19 into the nodal point relation given by Equation C.18 gives

$$\frac{S_1}{S_2} = \frac{B_1 C_1^k L_2^{k/2}}{B_2 C_2^k L_1^{k/2}} \left(\frac{h_1}{h_2} \right)^{3k/2} = f(h_1/h_2) \quad (\text{C.24})$$

Combining this relation with the conservation of sediment at the bifurcation gives

$$S_1 = \frac{f(h_1/h_2)}{1 + f(h_1/h_2)} S_0 \text{ and } S_2 = \frac{1}{1 + f(h_1/h_2)} S_0 \quad (\text{C.25})$$

whereas the equilibrium sediment transport leaving branch j is obtained by substituting Equations C.22 into Equation C.20 giving

$$S_{j,\text{cap}} = \frac{\gamma_j h_j^{n/2} Q_0^n}{(\beta_1 h_1^{3/2} + \beta_2 h_2^{3/2})^n} \quad (\text{C.26})$$

where $\gamma_j = m B_j C_j^n L_j^{-n/2}$. Combined with Equation C.21 Wang *et al.* (1995) obtain the following two coupled differential equations

$$\frac{dh_1}{dt} = \frac{Q_0^n}{B_1 L_1} \left(\frac{\gamma_1 h_1^{n/2}}{(\beta_1 h_1^{3/2} + \beta_2 h_2^{3/2})^n} - \frac{f(h_1/h_2)}{1 + f(h_1/h_2)} \frac{m_0}{B_0^{n-1} h_0^n} \right) \quad (\text{C.27})$$

$$\frac{dh_2}{dt} = \frac{Q_0^n}{B_2 L_2} \left(\frac{\gamma_2 h_2^{n/2}}{(\beta_1 h_1^{3/2} + \beta_2 h_2^{3/2})^n} - \frac{1}{1 + f(h_1/h_2)} \frac{m_0}{B_0^{n-1} h_0^n} \right) \quad (\text{C.28})$$

The qualitative behaviour of these equations is shown in the phase diagrams in Figures C.2a and b for a symmetric case with $B_1 = B_2 = B_0/2 = 50$, $C_1 = C_2 = C_0 = 50$, $L_1 = L_2 = 10^4$,

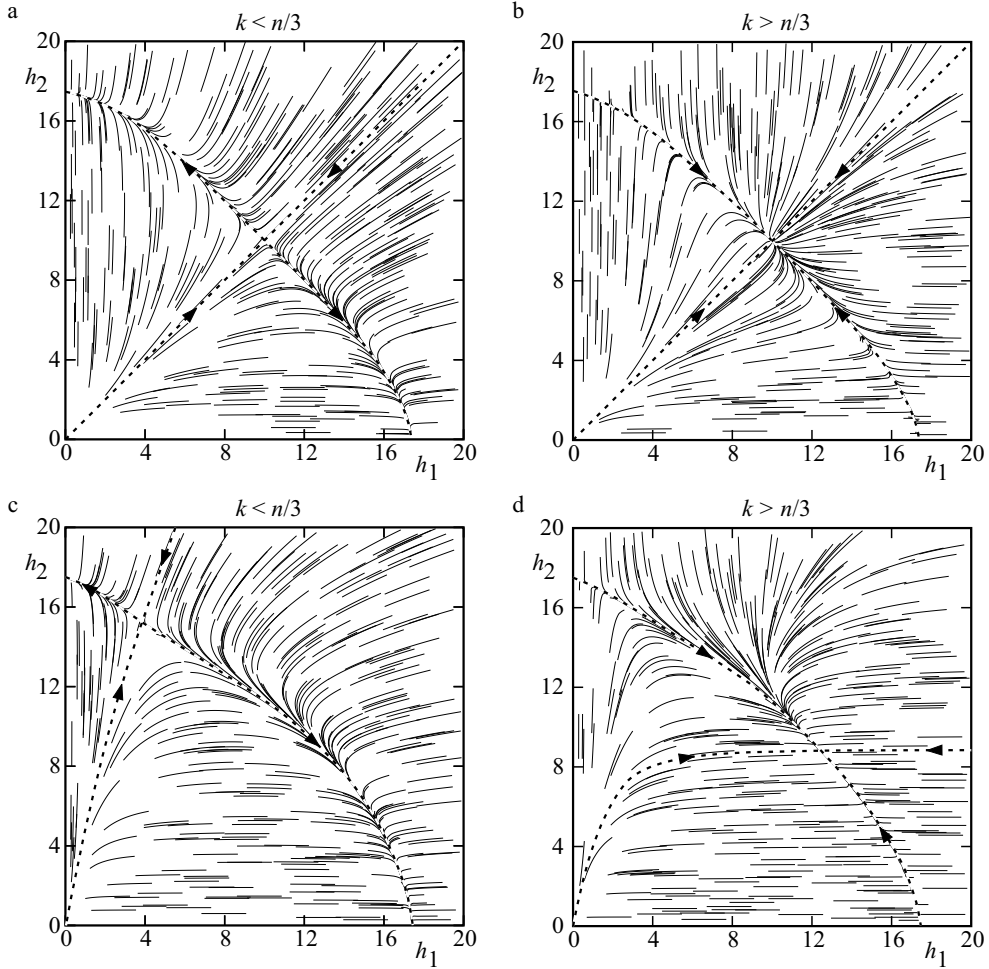


Figure C.2: Phase diagrams of the differential equations for h_1 and h_2 . The equilibrium with both branches open is unstable if $k < n/3$. a, b: symmetric case, c, d: asymmetric case with the length of branch 2 twice the length of branch 1.

$i_0 = 4 \cdot 10^{-5}$, $n = 5$ and $k = 1$ and 3 respectively. The stability of the equilibrium with both branches open turns out to depend on the values of k and n . If $k < n/3$ the equilibrium is unstable, if $k > n/3$ it is stable. For the equilibria with just one branch open the reverse holds; they are stable if $k < n/3$. As indicated in Appendix C.1 the same condition could have been obtained using the approach followed by Klaassen and Van Zanten (1989) and Biglari (1989). A more detailed analysis of the dynamics is given by Wang *et al.* (1995). Figures C.2c and d show the asymmetric case with the same settings except for L_2 which equals $2 \cdot 10^4$ (and therefore $i_2 = i_1/2$). In the asymmetric case with the unstable equilibrium with both branches open shown in Figure C.2c one can see that the basin of attraction for the situation with only the shortest branch (branch 1) open covers the largest part of the phase space. In the asymmetric case with the stable equilibrium with both branches open phase space becomes significantly distorted; the state with only the longest branch open clearly

being much more unstable than the state with only the shortest branch open. The ratio of the water depths in the two branches in the equilibrium with both branches open is given by

$$\frac{h_1}{h_2} = \left(\frac{C_1^2 L_2}{C_2^2 L_1} \right)^{(k-n)/(n-3k)} \quad (\text{C.29})$$

which results in a ratio h_1/h_2 of $\sqrt{2}$ for the stable asymmetric case and $1/4$ for the unstable asymmetric case with $L_2 = 2L_1$. One should note that the ratio does not depend on the ratio of the channel widths or the total discharge.

C.3 Delft3D description

This section describes the part of Delft3D that has been used in this study. The first section describes the basic flow equations (simplified to a formulation on a rectangular grid with 2D depth averaged flow). The second paragraph deals with the morphological equations. The equations in these two sections deviate little from those given by Struiksmma *et al.* (1985). The final paragraph deals with the spatial discretisation of the various variables.

C.3.1 Flow equations

Water motion in a river is, neglecting Coriolis and non-uniform atmospheric pressure forces, governed by the following depth-averaged equations in rectangular coordinates

$$\frac{\partial \zeta}{\partial t} + \frac{\partial hU}{\partial x} + \frac{\partial hV}{\partial y} = 0 \quad (\text{C.30})$$

$$\frac{\partial hU}{\partial t} + \frac{\partial hU^2}{\partial x} + \frac{\partial hUV}{\partial y} = -\frac{\tau_x}{\rho} - gh \frac{\partial \zeta}{\partial x} + hF_{sx} \quad (\text{C.31})$$

$$\frac{\partial hV}{\partial t} + \frac{\partial hUV}{\partial x} + \frac{\partial hV^2}{\partial y} = -\frac{\tau_y}{\rho} - gh \frac{\partial \zeta}{\partial y} + hF_{sy} \quad (\text{C.32})$$

where $h = \zeta - z_b$ and

ζ water level with respect to the reference level,

τ_x, τ_y shear stress components,

F_{sx}, F_{sy} correction terms for secondary flow,

g gravitational acceleration,

U depth averaged velocity component in x direction,

V depth averaged velocity component in y direction,

z_b bed elevation with respect to the reference level.²

The shear stress components τ_x and τ_y are modelled using the Chézy roughness coefficient C as

$$\tau_x = \frac{\rho g U \sqrt{U^2 + V^2}}{C^2} \text{ and } \tau_y = \frac{\rho g V \sqrt{U^2 + V^2}}{C^2}. \quad (\text{C.33})$$

²As everywhere else in this report, z_b is defined with the positive direction upward. Delft3D, however, uses the bathymetric convention of defining z_b positive downward.

The correction terms F_{sx} and F_{sy} for the secondary flow are given by

$$F_{sx} = \frac{1}{h} \left(-2 \frac{\partial \beta h U V}{\partial x} + \frac{\partial \beta h (U^2 + V^2)}{\partial y} \right) \quad (\text{C.34})$$

$$F_{sy} = \frac{1}{h} \left(\frac{\partial \beta h (U^2 + V^2)}{\partial x} + 2 \frac{\partial \beta h U V}{\partial y} \right) \quad (\text{C.35})$$

where

$$\beta = \beta_c (5\alpha - 15.6\alpha^2 + 37.5\alpha^3) \frac{h}{R_s^*} \quad (\text{C.36})$$

where

- R_s^* equals $\max(10, \sqrt{U^2 + V^2}/I)h$, the effective radius of curvature where I is the spiral motion intensity defined below,
- α equals $\min(0.5, \sqrt{g}(\kappa C)^{-1})$ where κ is the Von Kármán's constant,
- β_c correction factor.

The mass and momentum equations are solved using an ADI solver. The spiral motion intensity I due to curvature of the streamlines is obtained by solving

$$\frac{\partial hI}{\partial t} + \frac{\partial hIU}{\partial x} + \frac{\partial hIV}{\partial y} = h \left[\frac{\partial}{\partial x} \left(D_h \frac{\partial I}{\partial x} \right) + \frac{\partial}{\partial y} \left(D_h \frac{\partial I}{\partial y} \right) \right] - \frac{h(I - I_{be})}{T_a} \quad (\text{C.37})$$

where

- D_h horizontal diffusion coefficient,
- I_{be} equals $h\sqrt{U^2 + V^2}/R_s$,
- T_a equals $L_a/\sqrt{U^2 + V^2}$ for $L_a = [1/(2\alpha) - 1]h/\kappa^2$.

C.3.2 Morphological equations

Two sediment transport formulae were used in the computations, namely a general total load formula and the formula of Van Rijn (1984a,b, 1989). For the convenience of the reader, both formulae are given at the end of this section. In case of the Van Rijn transport formula, the sediment transport rate is split into a bedload component and a suspended load component. The sediment transport rate given by the simpler, total load formula is treated as a bedload transport rate. Local variations in the bedload and suspended load transport rates result in bed level changes, which are computed using

$$(1 - \epsilon) \frac{\partial z_b}{\partial t} = - \frac{\partial S_{b,x}}{\partial x} - \frac{\partial S_{b,y}}{\partial y} - E + D \quad (\text{C.38})$$

where ϵ is the bed porosity.

- ϵ bed porosity,
- D deposition of suspended sediment,
- E entrainment of suspended sediment, and
- $S_{b,x}, S_{b,y}$ components of the bedload transport in x and y direction.

This equation is solved using a first-order Lax scheme. The bedload transport components $S_{b,x}$ and $S_{b,y}$ are computed from the bedload transport magnitude S_b and the transport direction, indicated by an angle α_s relative to the x direction, as

$$S_{b,x} = S_b \cos(\alpha_s) \text{ and } S_{b,y} = S_b \sin(\alpha_s) \quad (\text{C.39})$$

The sediment transport rate S'_b , given by transport formula used, is corrected using two multiplication factors to give the applied transport rate S_b :

$$S_b = \left(1 - \alpha_{bs} \frac{\partial z_b}{\partial s}\right) \left(1 - \alpha_{mn} \frac{\partial z_b}{\partial s}\right) S'_b \quad (\text{C.40})$$

The two terms have the same appearance, but their meaning is different. The first term represents the physical effect of the bed slope on the magnitude of the bedload transport rate. The second term is included for increasing numerical stability of the first-order scheme or for increasing the accuracy for this scheme to second order using a Lax-Wendroff approach (WL | Delft Hydraulics, 2001).

The direction of the bedload transport, α_s , deviates from $\arctan(V/U)$, the depth-averaged flow direction, as a result of spiral flow and bed slope effects. The flow direction near the bed, and thus the bed shear stress direction, deviates in a river bend from the depth-averaged flow direction due to spiral flow. This effect is modelled using

$$\tan(\alpha_\tau) = \frac{V - \alpha_I \frac{U}{|U|} I}{U + \alpha_I \frac{V}{|U|} I} \quad (\text{C.41})$$

where $|U|$ is the depth-averaged velocity magnitude and α_I is given by

$$\alpha_I = \frac{2}{\kappa^2} E_s \left(1 - \frac{1}{2} \frac{\sqrt{g}}{\kappa C}\right) \quad (\text{C.42})$$

where E_s is a calibration coefficient. The influence of the bed slope on the bedload transport direction is modelled using the formulation by Koch and Flokstra (1980):

$$\tan(\alpha_s) = \frac{\sin(\alpha_\tau) - \frac{1}{a_s \theta^{b_s}} \frac{\partial z_b}{\partial y}}{\cos(\alpha_\tau) - \frac{1}{a_s \theta^{b_s}} \frac{\partial z_b}{\partial x}} \quad (\text{C.43})$$

where a_s and b_s are calibration coefficients.

The suspended sediment component (here, only non-zero in case of the Van Rijn transport formula) is computed using an advection diffusion equation for the depth-averaged concentration c with local erosion and sedimentation (Gallapatti and Vreugdenhil, 1985):

$$\frac{\partial c}{\partial t} + u \frac{\partial c}{\partial x} + v \frac{\partial c}{\partial y} - \frac{\partial}{\partial x} \left(D'_h \frac{\partial c}{\partial x} \right) - \frac{\partial}{\partial y} \left(D'_h \frac{\partial c}{\partial y} \right) = \frac{c_e - c}{T_a} \quad (\text{C.44})$$

where

c_e local equilibrium depth-averaged sediment concentration,

D'_h (horizontal) diffusion coefficient,

T_a adaptation time (in the order of h/w_s , where h is the water depth and w_s the fall velocity of the suspended sediment).

From the concentration field c the suspended sediment transport rates in x and y direction are determined as

$$S_{s,x} = uhc - hD'_h \frac{\partial c}{\partial x} \text{ and } S_{s,y} = vhc - hD'_h \frac{\partial c}{\partial y} \quad (\text{C.45})$$

The entrainment and deposition term $-E + D$ in Equation C.38 is equal to h times the right hand side of Equation C.44 or, if the change in sediment concentration c is neglected, it is equal to the divergence of suspended sediment transport

$$-E + D = \frac{\partial S_{s,x}}{\partial x} + \frac{\partial S_{s,y}}{\partial y} \quad (\text{C.46})$$

General formula

$$S_t [= S_b + S_s] = \alpha D_{50} \sqrt{\Delta g D_{50}} \theta^b (\mu \theta - \theta_{cr})^c \quad (\text{C.47})$$

where

b user specified calibration factor,

c user specified calibration factor,

D_{50} median particle diameter,

g gravitational acceleration,

α user specified calibration factor,

Δ relative density of the sediment with respect to water,

μ ripple factor for weighting the shear stress relative to critical shear stress,

θ dimensionless shear stress or Shields parameter, equal to $(u/C)^2 / (\Delta D_{50})$, where u is the local velocity and C is the local Chézy value,

θ_{cr} critical dimensionless shear stress required for the initiation of sediment motion.

The ripple factor μ and the θ^b term have been dropped in the analysis in Section 7.3.4 for simplicity.

Van Rijn (1984a,b, 1989)

The bedload component S_b of the sediment transport rate is given by

$$S_b = \begin{cases} 0.053 \sqrt{\Delta g D_{50}^3} D_*^{-0.3} T^{2.1} & \text{if } T < 3 \\ 0.1 \sqrt{\Delta g D_{50}^3} D_*^{-0.3} T^{1.5} & \text{if } T \geq 3 \end{cases} \quad (\text{C.48})$$

where

- D_{50} median particle diameter,
 D_* dimensionless particle diameter given by $D_* = D_{50} \sqrt[3]{\Delta g/v^2}$ where v is the kinematic viscosity of clear water,
 g gravitational acceleration,
 T transport stage parameter given by

$$T = \frac{\mu_c (u_*)^2 - (u_{*,\text{cr}})^2}{(u_{*,\text{cr}})^2} \quad (\text{C.49})$$

- where u_* , $u_{*,\text{cr}}$ and μ_c are defined below,
 Δ relative density of the sediment with respect to water.

The ripple factor μ_c is defined as $(C/C')^2$ where the overall Chézy coefficient C and the Chézy coefficient C' related to grains are given by

$$C = 18^{10} \log \left(\frac{12h}{k_s} \right) \text{ and } C' = 18^{10} \log \left(\frac{12h}{3D_{90}} \right) \quad (\text{C.50})$$

with h the water depth, k_s the equivalent Nikuradse roughness for the bedforms, and D_{90} the 90th percentile of the sediment diameter. Using the overall Chézy coefficient C the overall bed-shear velocity u_* can be computed from the depth averaged flow velocity u as $u_* = u\sqrt{g}/C$. The critical bed-shear velocity $u_{*,\text{cr}}$ for the initiation of motion is given by $\sqrt{\Delta g D_{50} \theta_{\text{cr}}}$ where the dimensionless critical bed-shear stress θ_{cr} is determined using the following approximation of the Shields curve

$$\theta_{\text{cr}} = \begin{cases} 0.240 D_*^{-1} & \text{if } D_* < 4 \\ 0.140 D_*^{-0.64} & \text{if } 4 \leq D_* < 10 \\ 0.040 D_*^{-0.10} & \text{if } 10 \leq D_* < 20 \\ 0.013 D_*^{-0.29} & \text{if } 20 \leq D_* < 150 \\ 0.055 & \text{if } D_* \geq 150 \end{cases} \quad (\text{C.51})$$

The suspended component S_s of the sediment transport rate is given by

$$S_s = f_{\text{cs}} u h c_a \quad (\text{C.52})$$

where

- c_a reference concentration at a height a above the bed given by

$$c_a = 0.015 \alpha_1 D_{50} T^{1.5} a^{-1} D_*^{-0.3} \quad (\text{C.53})$$

- where α_1 is a constant, normally equal to 1,
 f_{cs} current related friction factor for suspended transport given by

$$f_{\text{cs}} = \begin{cases} \frac{(a/h)^{z_c} - (a/h)^{1.2}}{[1 - (a/h)]^{z_c} (1.2 - z_c)} & \text{if } z_c \neq 1.2 \\ -\frac{\ln(a/h)}{[(h/a) - 1]^{1.2}} & \text{if } z_c = 1.2 \end{cases} \quad (\text{C.54})$$

where z_c is defined below.

The reference level a for the concentration c_a will in general be equal to k_s although Van Rijn (1984b) suggests a minimum value of at least 1% of the water depth for accuracy reasons. In Delft3D-MOR, a is always equal to k_s . The modified suspension parameter z_c (indicated by Z' by Van Rijn (1984b)) is defined as

$$z_c = \min(20, \frac{w_s}{\beta \kappa u_*} + \varphi) \quad (\text{C.55})$$

where

w_s fall velocity of a single sediment particle,

β influence of turbulence fluctuations on suspended sediment transport given by

$$\beta = \min(1.5, 1 + 2 \left(\frac{w_s}{u_*} \right)^2) \quad (\text{C.56})$$

κ Von Kármán's constant, being 0.4,

φ correction factor for the concentration profile given by

$$\varphi = 2.5 \left(\frac{w_s}{u_*} \right)^{0.8} \left(\frac{c_a}{c_0} \right)^{0.4} \quad (\text{C.57})$$

with $c_0 = 0.65$, the maximum concentration.

C.3.3 Staggered definition of variables

Delft3D uses a staggered discretisation for the hydrodynamic and morphological equations. Four sets of points can be distinguished as indicated in Figure C.3: bed level or depth points (z_b), water level points (ζ) and velocity points in two directions (u and v). Water depth, sediment concentration and sediment transport rates are all determined in the water level points. The staggering becomes important when specifying the boundary conditions, and when interpreting the results in detail. Velocity vectors are computed and plotted in water level points by combining the velocities from the four surrounding velocity points. For the cross-section plots of Chapter 7, the bed levels were interpolated to the water level points.

In the lower half of Figure C.3 a small piece of a curvilinear grid is shown enlarged. The discretisation of the sediment transport rates is also indicated in this sketch. The bedload and total load sediment transport rates are computed at the water level points based on interpolated bed levels. The (combination of advective and diffusive) suspended load transports, on the other hand, are computed at the velocity points in Delft3D-MOR. The discretisation of these quantities is reversed in the new Delft3D-FLOW version (of which some results are shown in Section D.6). The sediment concentrations are computed at the water level points.

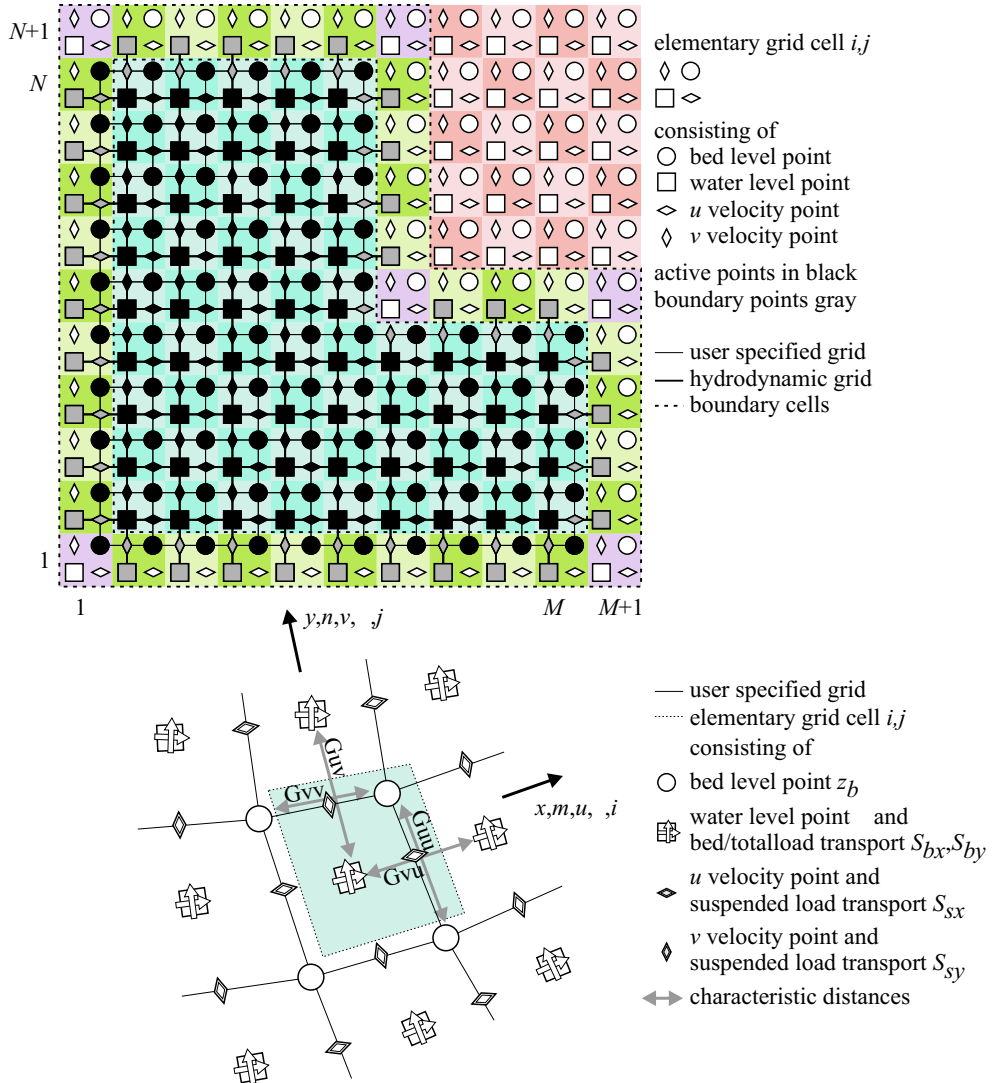


Figure C.3: Spatially staggered definition of the variables

Appendix D

Simplifying assumptions of the 2D simulations: a verification study

Numerical modelling introduces inaccuracies into the prediction by discretisation in time and space and by the simplification and neglect of physical processes. In this section we try to establish how important some of the assumptions are that were made to do the simulations described in the previous section. The following assumptions are addressed in the various subsections: spatial discretisation using gridcells of $50\text{ m} \times 50\text{ m}$, hydrodynamics near drying and flooding, quasi-steady flow approximation (stepped hydrograph), neglect of spiral flow effects, total load transport modelling, and 3D flow modelling and direct coupling between flow and sediment transport.

D.1 Gridcell size

When using a numerical model, one should be aware of the possible effects of the dimensions chosen for the gridcells. All simulations described in the main text were carried out on a

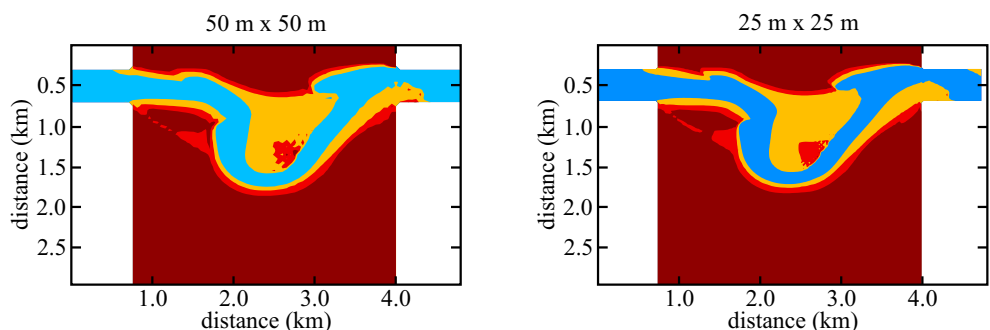


Figure D.1: Planforms of simulations using different gridcell sizes. The contour lines are drawn at 0, -1, and -3 m. Flow is from left to right.

rectangular grid with gridcells of $50\text{ m} \times 50\text{ m}$. To study the effects that this gridcell size has had on the simulations, one simulation has been repeated with a grid with gridcells of $25\text{ m} \times 25\text{ m}$. For this purpose the first simulation with $c = 1.83$ described in Section 7.3.4 (the simulation without the fully adapted calibration coefficient) has been used. This simulation was selected because of the relatively large morphological changes.

The resulting planform after 320 hours is shown in Figure D.1 together with the planform obtained from the original simulation. The results of the two simulations are similar, indicating that the gridcell size of 50 m is fine enough for this simulation. A larger gridcell size is not recommended since the number of cells in the main channel would become very small. The same conclusion is expected to hold for the other simulations, most of which are characterised by less morphological development. Although some grid dependency can be expected for the simulations that are sensitive to small fluctuations (for instance the one with a critical Shields parameter of 1.0), the results will not be significantly altered.

D.2 Hydrodynamics of drying and flooding

An important aspect of the model is the adaptive growing and shrinking of the active model area during drying and flooding of the pointbar and the flood plains. Correct mathematical treatment of drying and flooding is not simple in itself, but it is further complicated by the staggered definition of the variables on the grid (see Section C.3.3). To resolve problems encountered during the overtopping of dikes, an option has been added to the flow module that allows the module to switch from a central schematisation of the water level in velocity points to an upwind schematisation when the water depth drops below a certain threshold (WL | Delft Hydraulics, 1999). The two approaches are illustrated in Figure D.2. During all the simulations the upwind schematisation was used throughout the model area. The morphological module, however, does not have this option and uses always the central schematisation. Although problems may result from combining these two approaches, none have been spotted during the simulations.

To check whether this approach has had any influence on the simulations, one simulation has been repeated without using the upwind scheme in the flow module. The simulation with a critical Shields parameter of 1.0 has been selected for this purpose because it is assumed that this simulation is the most sensitive to this change in discretisation. Three reasons underpin this assumption.

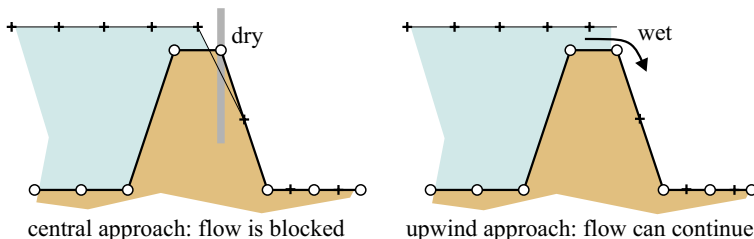


Figure D.2: The effect of upwind or central schematisation of the water level at the velocity point at the downstream side of a dike. The approach used by the flow module depends on the parameter DCO.

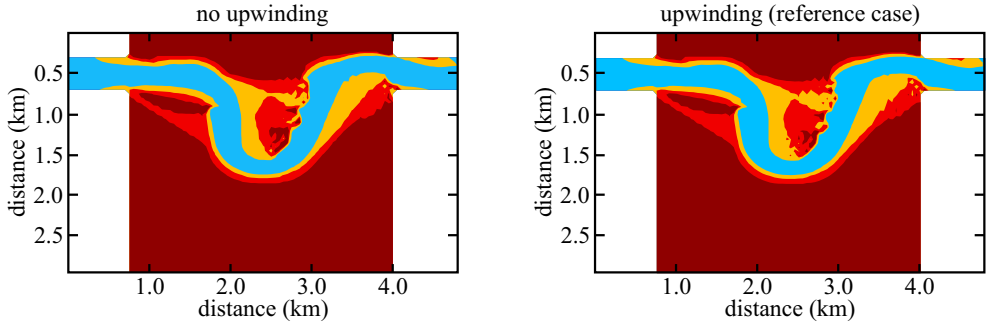


Figure D.3: Planforms of two identical simulations with different schematisations for the water levels at the velocity points. The contour lines are drawn at 0, -1, and -3 m. Flow is from left to right.

- As illustrated by the example shown in Figure D.2, the largest effect of upwind schematisation of the water level is at locations with strong downhill gradients.
- The initial simulations for this study indicated that instabilities occurred first at the downstream edge of the pointbar.
- Of all simulations (with upwind scheme on) it was the one with the critical Shields parameter of 1.0 that showed the largest remaining irregularities at the downstream side.

The planform at the end of two simulations with and without the upwind schematisation switched on are shown in Figure D.3. The results indicate that — although the shape of the downstream edge of the pointbar is sensitive to the schematisation used — two planforms have the same general characteristics. So, the handling of drying and flooding has not significantly influenced the outcome of the simulations.

D.3 Boundary conditions

The simulations have been carried out using the boundary conditions shown in Figure 7.3. Two aspects stand out.

- The discrete nature of the boundary conditions.
- The large jump in the downstream water level during the rising stage.

Both aspects originated from problems encountered with the model during the initial simulations. Various improvements to the modelling system have made it possible to determine what influence these schematisations have had.

The step-wise schematisation of the flood wave was accompanied by a process tree (described in Section 7.2 and shown in Figure 7.4) that consists of two branches. The first branch was used to establish an equilibrium flow condition after each step in the boundary conditions. The simulation with $c = 1.83$ has been repeated using a continuously varying discharge and

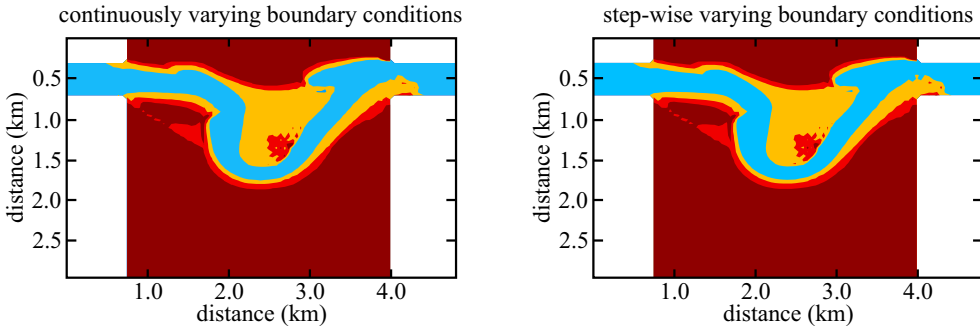


Figure D.4: Planforms of one simulation with a continuously varying boundary condition and one simulation with a step-wise schematisation of the flood wave (as shown in Figure 7.3). The contour lines are drawn at 0, -1, and -3 m. Flow is from left to right. There are no significant differences.

downstream water level.¹ The first branch of the process tree has been removed for this simulation since no adjustment period is needed anymore. Figure D.4 shows the end result of this simulation and that of the reference case with a step-wise schematisation. There are no significant differences. So, the step-wise schematisation of the flood wave has not had a significant effect on the outcome of the simulations.

The simulation with a Chézy roughness of $60 \text{ m}^{1/2}/\text{s}$ has been repeated with the downstream boundary condition during the rising period (hours 20–90) replaced by the same gradual (but step-wise) variation as was used during the falling period (hours 210–280). This simulation with a constant Chézy value was chosen to prevent changes in roughness from interfering with the interpretation of the simulation results. The planforms of the original simulation (with the large jump in the water level at $t = 20$ hours) and the new simulation are shown

¹The downstream boundary condition still included the large jump between $t = 20$ and 30 hours.

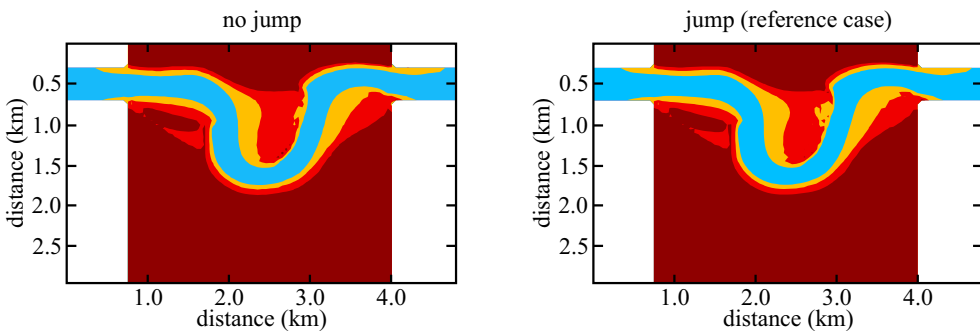


Figure D.5: The results of two simulations with different downstream boundary conditions during the hours 20–90 in the simulations. The simulation on the left had a gradual (yet, step-wise) increase of the downstream water level. The reference simulation on the right was carried out using the boundary conditions shown in Figure 7.3, that is with a large jump in the boundary condition at $t = 20$ hours. The contour lines are drawn at 0, -1, and -3 m. Flow is from left to right.

in Figure D.5. The latter simulation has slightly more erosion at the downstream side of the pointbar. At first this seems rather remarkable since one might expect higher flow velocity and, therefore, higher sediment transport and erosion rates when the downstream water level is kept low. However, the jump in the downstream water level causes earlier and, therefore, longer flooding of the pointbar. The higher water levels cause a redistribution of discharge resulting in a relatively larger discharge across the pointbar. This increase in discharge during a longer period causes the larger amount of erosion during the simulation with the jump in the downstream water level. Although the jump in the water level has had influence on the simulations, it is likely that the effect is similar for all simulations and that the differences between the simulation results are not significantly influenced by the downstream boundary condition applied.

D.4 Spiral flow

Another important aspect that we have neglected so far is the 3-dimensional structure of the flow. In particular, it is well known that bends induce secondary or spiral flow: the water at the surface is flowing to the outside of the bend, while the water near the river bed is flowing to the inside. The flow near the bed directs the near-bed sediment transport towards the inner bend, which results in the build-up of the pointbar. When simulating the morphological developments in meandering rivers, one cannot neglect the effects of the spiral flow, since it forces the sediment transport to be directed towards the inner bend. Although the topography includes a main channel with four bends, the spiral flow effect has not been included. Although numerical problems were the main reason for excluding the secondary flow, it was assumed that the secondary flow was not very important for the outcome of these simulations. This assumption was based on the consideration that the main element in the simulations is the possible formation of a cutoff channel during the flood event. Firstly, the cutoff channel would be much straighter, so the spiral flow intensity in the new channel would be small. Secondly, during a flood period (which covers the main part of the simulations) the flow is not confined to the main channel and secondary flow components are likely to be less important.

Two simulations have been carried out using the latest version of Delft3D to assess whether these assumptions were correct. The results of these simulations are shown in Figure D.6. The two simulations differ in the way in which the spiral flow intensity is estimated. The first simulation is based on an equilibrium flow condition, with the intensity computed from the local streamline curvature. The second simulation is based on a non-equilibrium situation in which an advection-diffusion equation (given by Equation C.37) is solved for the secondary flow, i.e. lag effects are included. The results of the two simulations with spiral flow included are almost identical. The differences between two simulations and the reference simulation without the spiral flow effect are also limited. The most striking difference is the shape of the upstream side of the pointbar, which is much more curved in the simulations with the spiral flow effect included. This difference may indeed be attributed to the flow within the main low-stage channel during the initial stages of the flooding. The net effect on the outcome of the simulation is, however, too small to invalidate the results of this study.

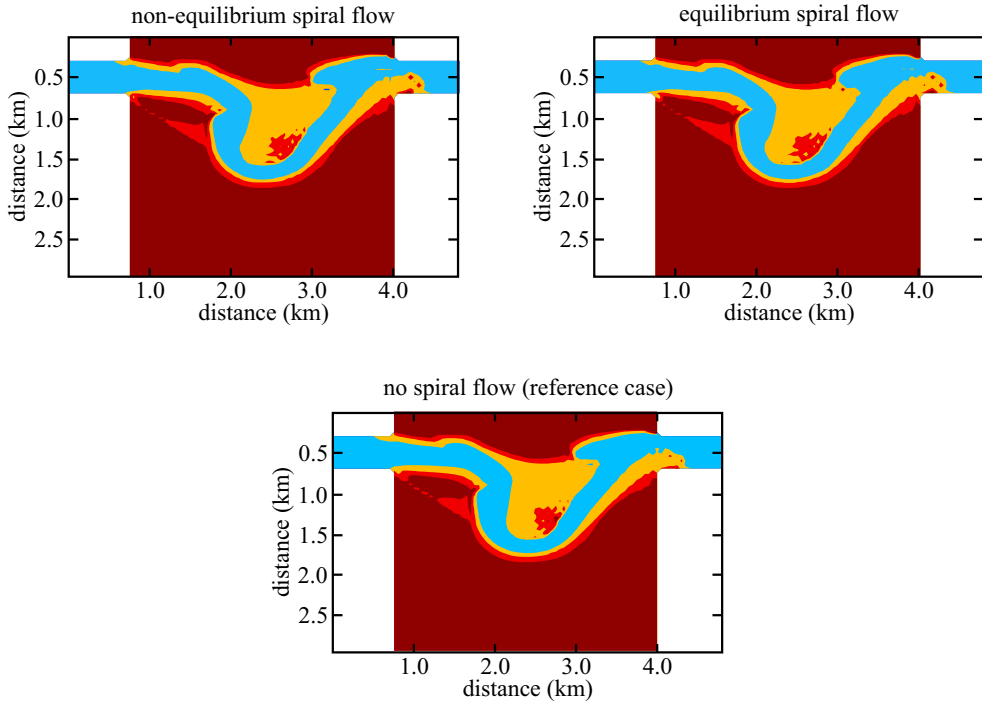


Figure D.6: Planforms of two simulations with spiral flow included (one based on an equilibrium condition, one based on a non-equilibrium description) and one simulation without (reference case). The simulations are based on the simulation with $c = 1.83$ described in Section 7.3.4. The drawn contour lines are at 0, -1, and -3 m. Flow is from left to right.

D.5 Suspended sediment

All simulations reported in the main text were carried out using the total load sediment transport relation given by Equation 7.1. They all resulted in the (partial) formation of a cutoff channel. The total load approach is a simplification of a suspended load approach since in the former case it is assumed that the adaptation length L_a of the sediment transport rate is small relative to the size of the gridcells used. Although most braided rivers are characterised by coarse sand or gravel, the bed of our prototype example, i.e. the Jamuna River, consists of fine sand and silt (see Section 2.2.2). The average sediment size is about 0.2 mm, which according to Van Rijn (1993), corresponds with a settling velocity w_s of about 0.0257 m/s. The adaptation length can be estimated as the horizontal distance travelled by a settling particle originally located near the water surface, i.e.

$$L_a \approx \frac{hu}{w_s} \quad (\text{D.1})$$

where h equals the water depth and u is the magnitude of the flow velocity in the plane parallel to the bed. Based on a characteristic flow velocities on the pointbar in the order of 1–2 m/s and a water depth of 2–3 m, we arrive at an adaptation length in the range of 78–233 m. Since the gridcell dimensions are 50 m × 50 m, the lag effect of the suspended load may influence

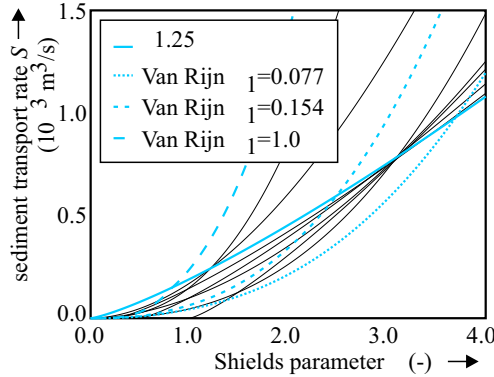


Figure D.7: Sediment transport relation by Van Rijn (1984a,b) for a water depth of 3 m, a roughness height of 0.02 m and a settling velocity of 0.0257 m. Thin lines refer to the transport relations used in the other simulations (see Section 7.3.4 and Figure 7.17).

the morphological development. Therefore, some simulations have been carried out using a depth-averaged advection diffusion equation for the suspended sediment concentration c with local erosion and sedimentation (Gallapatti and Vreugdenhil, 1985) based on the sediment transport relation given by Van Rijn (1984a,b). The reader is referred to Section C.3.2 for an overview of the equations involved. For comparison with the transport formulae used before, the transport relation by Van Rijn is plotted in Figure D.7 for the parameter settings used in the final set of simulations.

The first simulations carried with the suspended load approach and the sediment transport relation by Van Rijn displayed a completely different behaviour than the simulations based on the total load approach and the general formula: sedimentation occurred on the upstream half of the pointbar (see the upper left plot of Figure D.8). This behaviour was initially assumed to be related to the properties of the suspended fraction of the sediment transport (Jagers, 1999). Because the sediment carrying capacity is much lower in shallow areas, it seemed plausible that deposition could occur where the sediment rich waters from the main channel flowed onto the pointbar. Since the sediment transport rate in the main channel was very high, it seemed plausible that deposition could occur as these sediment rich waters flowed onto the pointbar because the sediment carrying capacity is much lower in shallow

nr	α -	c -	θ_{cr} -	Δs m	ΔA 10^3 m^2	Δz_c m	y_x m	Δz_x m	Δz_{PB}		
									μ m	σ m	
1	16.77	1.25	0.00	202	1.42	1.51	900	1.20	0.94	0.72	0.57
27	0.077	Van Rijn		131	0.65	0.71	750	0.28	0.30	0.47	0.19
28	0.154	Van Rijn		131	1.22	1.28	750	0.81	0.64	0.67	0.38
29	1.000	Van Rijn		554	4.09	3.73	800	5.68	1.62	1.99	1.02

Table D.1: Overview of the simulations carried out with suspended sediment following the formulation by Van Rijn (1984a,b). All simulations use the same boundary conditions as the reference case and a Manning's roughness coefficient of $0.02 \text{ s/m}^{1/3}$.

areas. The sedimentation on the edge of the pointbar could be explained by referring to the formation of levees by the Jamuna River (see page 27) and other suspended load carrying rivers.

Although these results seemed completely acceptable initially, they turned out to be incorrect. This was caused by erroneous values for two of the input parameters of the sediment transport formula by Van Rijn, namely, the settling velocity w_s and the effective roughness height k_s . During the first simulations, w_s had been set to 0.015 m/s, which was too small, and k_s had been set to about 1 m. The latter value was chosen because it is the average height of the bedforms (dunes) in the Jamuna River (see Figure 3.6). However, it does not represent

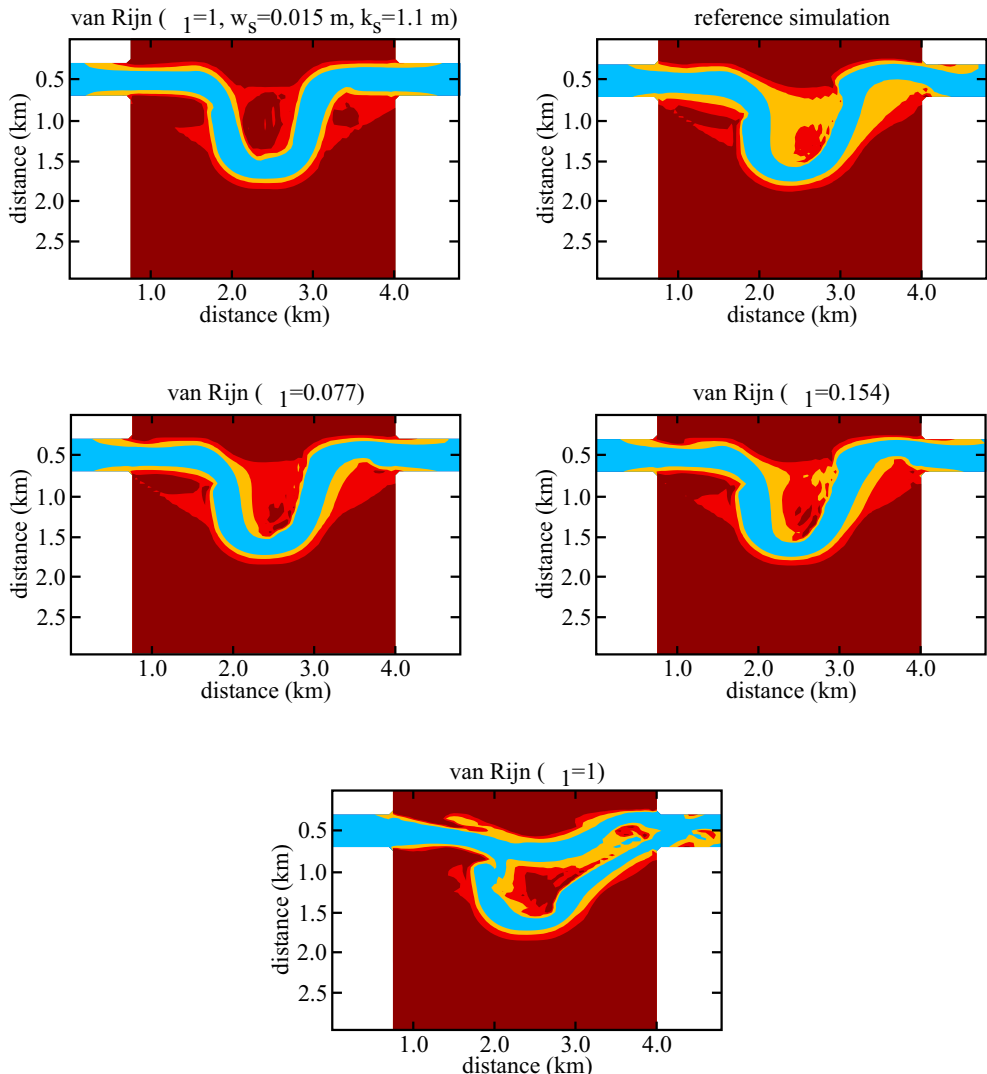


Figure D.8: Planforms for simulations using the sediment transport relation by Van Rijn (1984a,b). The contour lines are drawn at 0, -1, and -3 m. Flow is from left to right.

the shallow areas well, and even for the main channel it does not represent the generally low effective roughness of the Jamuna River. Therefore, it has been reduced to a more appropriate 0.02 m in the final simulations. Because the reference height for the suspended sediment concentration in Delft3D-MOR is coupled to the roughness height (see Section C.3.2), a reduction of the roughness height leads to an increase in the suspended sediment transport rates. The combined effect of the changes in the settling velocity and the roughness height is a general increase in the sediment transport rate. More importantly, however, the depth-dependence of the sediment transport rate is much smaller for the new, correct value of k_s : using the old settings the sediment transport capacity reduced by about a factor of 4 if the water depth decreased from 7 to 3 m, using the new settings the reduction is just a few percent.

These adaptations led to a significant increase in the sediment transport rate, which resulted in the formation of a complete cutoff as shown in the last plot titled ‘Van Rijn ($\alpha_1 = 1$)’ in Figure D.8. This result is quite the opposite of the earlier results. The effective sediment transport relation used in this simulation is similar to the general formula with $\alpha = 13.19$ and $c = 2.50$ (see Section 7.3.4), and the extent of the morphological development is also comparable (see Figure A.7). Therefore, the overall sediment transport rate has been reduced. Because a linear calibration factor has not been implemented for this transport formula, another approach had to be used. The reduction was achieved by lowering the coefficient α_1 in the expression for the reference concentration (see Equation C.53). For α_1 in the range between 0.077 and 0.154, the Van Rijn sediment transport relation becomes (given a water depth of 3 m, a roughness height of 0.02 m and a settling velocity of 0.0257 m) similar to the general formulae used in the simulations presented in Chapter 7. Consequently, the resulting planform changes are also similar. Based on these observations, it is concluded that the *general pattern* of developments is not affected by the neglect of the adaptation length of the suspended sediment.

D.6 Integrated model

Given the consistent picture of the bend cutoff outlined in Section 7.3 and the previous sections, the verification of the basic assumptions has been extended one step further, namely, to a fully 3D approach. Recently, a new version of the Delft3D-FLOW module has been developed which includes a 3D morphology module (Lesser *et al.*, 2003) based on the sediment transport formulation by Van Rijn (1984a,b). The new integrated model is intended to be used if the hydrodynamics is not well represented by a 2D approach, or if high sediment concentrations significantly affect the hydrodynamics. In Section D.4 it has been concluded that the morphological changes were not significantly influenced by the (parametrised) spiral flow intensity. Since all bed gradients were relatively small, no significant effect are expected from other 3D flow structures, either. Sediment concentrations were relatively low, whence density effects are not anticipated. It is therefore to be expected that the new, integrated 3D model will result in similar morphological changes as the 2D model.

Two simulations have been carried out using this integrated program: one simulation with 5 layers in the vertical and one with 10 layers. The resulting planforms are shown in Figure D.9. Since these simulations have been carried out using the Van Rijn formulation for

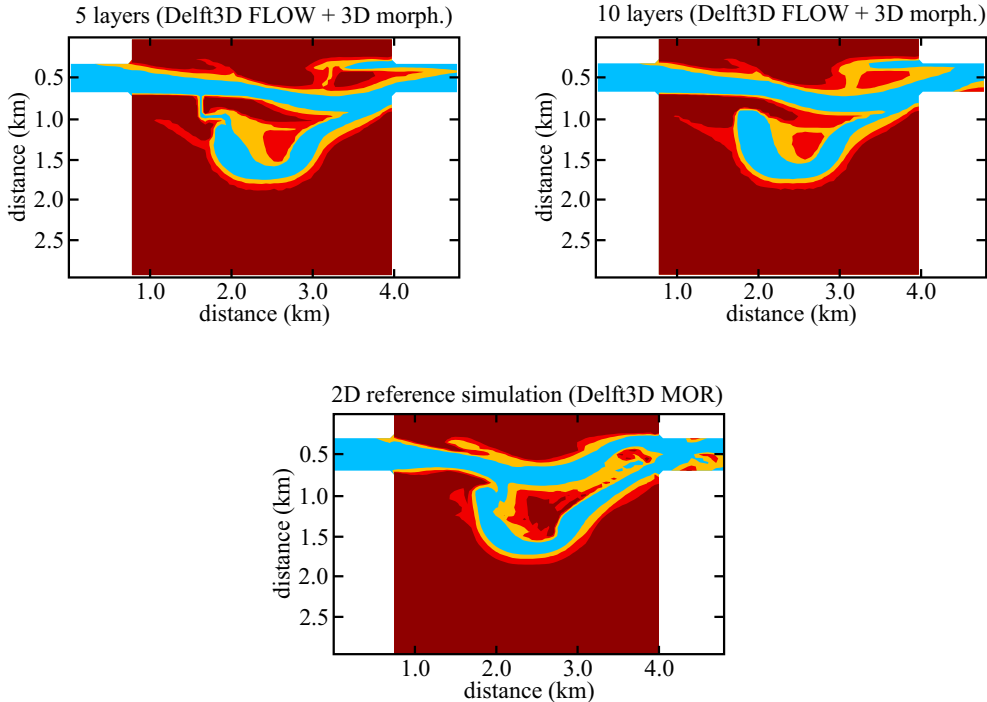


Figure D.9: Planforms of two simulations with the recently developed version of Delft3D-FLOW and one simulation with Delft3D-MOR (reference case). The simulations are based on the Van Rijn transport formula. The contour lines are drawn at 0, -1, and -3 m. Flow is from left to right.

sediment transport, the planform of the 2D simulation using this same formulation (see previous section) is shown for reference. In all cases (2D and 3D) the cutoff is formed completely. Also the sedimentation in the downstream reach is of the same magnitude. Yet, there are a number of differences between the results of these three simulations.

1. The results of simulations using the integrated 3D model are smoother than the result of the Delft3D-MOR simulation. This is probably related to the difference in the numerical schemes used.
2. Most sediment eroded from the pointbar is deposited on the left side of the downstream channel in the 3D simulations, and to the right side in the 2D simulation. Although this difference dominates the downstream morphology, it is important to note that the selection of either sedimentation pattern occurs early on in the simulation when the sediment lobe originating from the cutoff formation moves either slightly to the left or to the right of the main flow. At that time the difference is small, and the selection is very sensitive to the local direction of sediment transport. The difference in the sediment transport pattern may result from differences in the treatment of the bedslope effect and the computed flow directions.
3. The initial channel has been completely abandoned in the simulation with 10 layers, whereas at the end of the simulation with 5 layers a small connection channel remains

(which is clearly influenced by the underlying spatial discretisation). A substantial opening remains in the 2D case. The difference between the simulations may be attributed to differences in the lateral sediment transport, which is, again, governed by the treatment of the bedslope effect and the computed flow directions near the bed.

Based on these results it cannot be concluded with complete certainty that the 3D flow structure does not have a significant influence on the formation of the cutoff channel. Development of the 3D model continues and results have changed substantially between different versions. Therefore, it is preliminary assumed that, since there is currently no clear physical reason why the flow field should significantly deviate from 2D, the 3D structure of the flow is not important for the formation from the upstream end. However, further research is needed to study the effect of different formulations for, for instance, the bedslope effect on the sediment transport (magnitude and direction) and, thus, on the morphological development of the system.

Index

- Allier River, 64
anabranching, *see* planform types, anabranched
- bank erosion, 62–64, 84, 87, 91, 94, 104–105, 119–121, 127, 134–136, 138
bars, 53–60
 migration, *see* migration, bar
 stability, *see* stability, bar
bed composition, 62–64, 66, 205, *see* graded sediment
bedforms, 40–53
 migration, *see* migration, bedform
bifurcations, *see* channel nodes
 stability, *see* stability, bifurcation boundary
 ~ in knowledge, 10, 69
 ~ in space, 66–68, *see* boundary conditions, *see* model detail
 ~ in time, 69, *see* initial condition
boundary conditions, 181, 186–190, 301–303
braid bar formation, 57–60, 75, 80, 81, 136–137, 157
braided, *see* planform types, braided
branches model, 132–147, 150, 213–215, 273–284
- Calamus River, 70
cellular model, 125–132
channel abandonment, 79, 82, 139
channel formation, 81, 140, 157–215
 direction of ~, 203–206
channel incision, 158, 160–165, 203–206, 208–211
- channel network, 132, 140–143, 279–284
channel nodes, 61, 152
 deformation, 78–79, 82, 152
 migration, *see* migration, node
channel width change, 62, 81, 134–136
confluences, *see* channel nodes
critical shear stress, 50, 195–199, 208–211, 301
- cutoff
 bend flattening, 160
 chute ~, 73, 74, 86, 159, 162–165
 mobile bar ~, 160, *see* dissection
 linguoid bar
 neck ~, 86, 158–159, 166, 200
 stability, *see* stability, cutoff
- dissection linguoid bar, 76–77, 160
- erodibility, 62–64, 203–206
- flood, 2, 26, 28, 147, 180
- Froude number, 44, 126
- Ganges River, 2, 18, 26, 28, 65, 190
graded sediment, 52–53, 56, 205
- headcut, 161–163, 203, 206–211
human influence, 1, 66, 148–151
- initial condition, 180
- Jamuna River, 1–4, 17–38, 45, 46, 50, 73, 106, 119, 145, 169, 174–176, 180
- kinematic model, 84–87, 132–140
- lattice gas model, 106–108
levee building, 27, 158

- meandering, *see* planform types, meandering
- Meuse River, 208
- migration
 - bar ~, 54, 212
 - bedform ~, 45, 53, 78
 - channel ~, 80, 137–139, 143, *see* bank erosion
 - node, 79, 82, 139, 152
- Mississippi River, 1, 159, 165, 167
- model detail, 10, 148–151
 - gridcell size, 299–300
- multiple bar growth, 77
- neural network, 112–125, 148–149, 271–273
- object-oriented model, *see* branches model
- one-dimensional model, 84–94, 96–98, 100–103
- planform types, 4–8
 - anabranching, 146
 - braided, 96–101, 111–155
 - meandering, 83–96, 99, 143
- Powder River, 163–165, 205
- prediction, 1, 148–151
- roughness, 45, 67, 190–195
- satellite image, 28–33, 39, 114–115, 119, 140–142, 145, 279–282
- secondary flow, 59, 64, 89, 182, 303–304
- sediment transport, 48–53, 127, 179, 195–199, 304–307
- sediment transport, fluctuations, 51, 78
- sedimentary deposits, 53, 99
- sensitivity, 11, 69, 185, 299
- spiral flow, *see* secondary flow
- stability
 - bar, 54–56, 79–80
 - bifurcation, 170–173, 288–291
 - cutoff, 165–173, 285–291
 - staggered grid, 210, 296–297
 - stochastic model, 96–103, 132–140, 213–215
- stratigraphy, *see* sedimentary deposits
- tectonics, 18–23, 33
- three-dimensional model, 108, 307–309
- trachytote, 67, *see* roughness
- turbulence, 46–48, 51
 - analogy, 100
- two-dimensional model, 94–96, 103–106, 150–151, 177–213, 254–270, 291–297, 299–307
- uncertainty, 1, 10, 66–69, 118–121, 143–146, 148–151, 213
- vegetation, 60, 194, 205, 214
- Waimakariri River, 7
- Western Scheldt, 206, 207

About the author



The author was born and raised in Enschede, The Netherlands. From 1983 to 1989 he received secondary education at the Ichthus College there. After graduation in 1989, he started with M.Sc. studies on Applied Mathematics and Applied Physics at the University of Twente.

In the field of mathematics he specialised in systems and control theory. During a traineeship he worked at Goudappel Coffeng in Deventer on the prediction of waiting times for cyclists at vehicle dependent traffic lights. In the field of physics he specialised in low temperature physics (superconductivity). His master's project combined these two specialisations and concerned the estimation of the number of independent sources of brain activity based on electro- and/or magnetoencephalogram data. He graduated in March 1995 cum laude in Applied Mathematics and in June 1995 also cum laude in Applied Physics.

At the beginning of July 1995, he started his Ph.D. study on braided rivers at the University of Twente. The research was carried out at WL | Delft Hydraulics, initially in 'De Voorst' and since fall 1996 in Delft. During this study he visited the FAP21/22 and FAP24 projects in Bangladesh in the spring of 1996 and gave presentations at conferences in The Hague (1996), Cape Town (1997), and Genova (1999).

In 1999 he interrupted his Ph.D. study for half a year to work at WL | Delft Hydraulics on graded sediments. Since the beginning of 2000, he has been working full-time as researcher/advisor on morphology and numerical modelling in the River Engineering department of WL | Delft Hydraulics. Since that time he has been working on the morphological modules for the one-, two- and three-dimensional simulation programs Sobek and Delft3D. Furthermore, he has been working on research related to graded sediment, alluvial and vegetation roughness, spiral flow, bank erosion, bottom vanes, large eddy simulation, ship motion and non-hydrostatic flow.

